

PROCEEDINGS OF THE
ISSMGE TECHNICAL COMMITTEE 207
INTERNATIONAL CONFERENCE
ON GEOTECHNICAL ENGINEERING

**SOIL-STRUCTURE INTERACTION,
UNDERGROUND STRUCTURES
AND RETAINING WALLS**

Russia, Saint Petersburg, 16-18 June 2014

Volume 1

Edited by V.M. Ulitsky, M.B. Lisyuk and A.G. Shashkin

Saint Petersburg
2014

Proceedings of the International geotechnical conference “Soil-Structure Interaction. Underground Structures and Retaining Walls”.

In 1st volume of the Proceedings the lectures and papers presented by the authors in English are published.

In 2nd volume of the Proceedings the papers presented by the authors in Russian are published.

The text of the various papers in this volume was set individually by typists under the supervision of each of the authors concerned.

All rights reserved. No part of this publication may be reproduced, stored or transmitted in any form without the written permission of the Publisher.

Published by: “Georeconstruction” Institute
190005, 4 Izmaylovsky prosp., St. Petersburg, Russia

ISBN 978-5-9904956-5-4

© “Georeconstruction” Institute, 2014

Printed in Russia



TC207 ISSMGE
Soil-Structure Interaction
and Retaining Walls
 tc207ssi.org



National Mineral
Resources University
(University of Mines)
 spmi.ru



Georeconstruction
Engineering Co.
 georec.spb.ru



Petersburg State
Transport University
 pgups.ru

ORGANIZED BY

- International Society for Soil Mechanics and Geotechnical Engineering (ISSMGE)
 Technical Committee 207 “Soil-Structure Interaction and Retaining Walls”
- “Georeconstruction” Institute (Russia)
- National Mineral Resources University (Russia)
- Petersburg State Transport University (Russia)

ORGANIZING COMMITTEE

V.M. Ulitsky, Chairman of TC207, Head of Petersburg Branch of RSSMGFI,
 St. Petersburg

M.B. Lisyuk, Co-Chairman of TC207, Deputy Director of “Georeconstruction” Institute,
 St. Petersburg

A.G. Shashkin, General Director of “Georeconstruction” Institute, St. Petersburg

CONFERENCE SCIENTIFIC COMMITTEE

Ö. Bilgin (USA)
W. Bilfinger (Brazil)
J.-L. Briaud (USA)
R.E. Dashko (Russia)
Fang Liu (China)
R. Finno (USA)
C. Haberfield (Australia)
H. Hazarika (Japan)
R. Katzenbach (Germany)
M. Mets (Estonia)
I. Sokolić (Croatia)
C. Shashkin (Russia)
V. Paramonov (Russia)
W. Van Impe (Belgium)
Yasser El-Mossallamy (Egypt)

CONFERENCE SECRETARIAT

E. Dubinin, “Georeconstruction” Institute, St. Petersburg
E. Ukhina, “Georeconstruction” Institute, St. Petersburg
N. Steklyannikova, Petersburg State Transport University (Russia)

G.P. Tschebotarioff Address

Technical Committee 207 ISSMGE "Soil-Structure Interaction and Retaining Walls", of which I have been honoured to be the Chairman since 2005, has organized eight conferences and special sessions in Saint Petersburg, Ghent, Moscow, Rostock, Dubrovnik and Paris.

This conference which is taking place during the white nights in Saint Petersburg is dedicated to the memory of an outstanding geotechnical expert Gregory Porphyryevich Tschebotarioff.

Gregory Porphyryevich Tschebotarioff is mentioned in all encyclopaedias as a Russian-American scholar, a specialist in soil mechanics and foundation engineering. He was born in February 1899 in Pavlovsk. His parents owned a splendid residential house in Tsarskoe Selo, a suburb of St. Petersburg.

In light of several inconsistencies in his subsequent biography I would like to clarify certain moot points based on archive materials found in St. Petersburg and specifically in the library of Saint Petersburg University of Transport, formerly known as Alexander I Institute of Transport, founded in 1809. In 2014 Saint Petersburg University of Transport regained its association with the name of that benevolent Russian Emperor Alexander I, known by many to have been its founder. This oldest establishment of education in the field of technology is also inherently connected with the name of Gregory Porphyryevich Tschebotarioff.

Gregory Porphyryevich Tschebotarioff was born not simply in the family of a Cossack officer. His father was especially close to the Russian Emperor's family, as can be now stated unequivocally, whereas his wife and mother of G.P. Tschebotarioff served as a lady-in-waiting to the Empress. Prior to the October Revolution of 1917 his father was in the rank of lieutenant-general serving in the Guards of the River Don Cossack Regiment. And one more interesting touch: G.P. Tschebotarioff's godmother was the Dowager Empress, the mother of Tsar Nicholas II, who was deposed after the 1917 uprising.

Gregory Tschebotarioff's first wife was Lydia Fyodorovna Krasnova, who prior to their marriage was a young friend of Tschebotarioff's mother and resided in Detskoe Selo (currently a town of Pushkin, a suburb of St. Petersburg mentioned above). She was close to the emperor's family even through the location of her house. It was natural that generals true to the emperor, like Tschebotarioff or Krasnov, Grigory's father in law, as well as the historic River Don ataman Kaledin, felt it a call of duty to preserve Russia's integrity by being victorious both against Germany and inside Russia itself, at the time embroiled into Bolshevik revolts, which the remaining army tried very hard to quell. Those included the well-known mass uprising on the River Don. Subsequently the forces of the so-called "Volunteers" or the White Army were fighting battles with the Red Army Corps, initially victorious but later largely unsuccessful. The last stronghold of the whites on the River Don was the city of Novochoerkassk. Allegedly, it was there that Grigory Porphyrievich ended his military career. Here I would like to mention several interesting moments from the highly eventful revolution months of 1917–1918. The young Gregory Porphyryevich, having barely turned 18, was appointed a personal aide to general Krasnov, one of the combatants against the Reds in 1917–1918 in Russia. Being an expert German translator, having legal, albeit secondary education, Gregory took part in the famous talks between Krasnov, Trotsky and seaman Dybenko, which were attended also by the German military.

Now let's move to a bit of historical data, establishing the fact that his legal education began at the age of 12 when he joined the Imperial Law School. It was already during the war that he finished a concise course at Mikhailovsky Artillery School and graduated in 1916 in the rank of corporal. It was thus impossible for him to have been one of the leaders of the Whites' opposition neither in St. Petersburg nor on the River Don, as is sometimes believed. He doubtless must have felt deeply for them, but his chosen career at that turbulent time for Russia was that of a civil or transport engineer.

Here I have in front of me a copy of G.P. Tschebotarioff's inscription and signature on a book on soil mechanics published in the USA and presented in 1973 to professor Vladimir Petrovich Sipidin at the Department of subsoils and foundations of St. Petersburg Transport University (Figures 1 and 2). Therein Gregory Tschebotarioff designates himself a student who entered the Transport University in 1918. The inscription states that the book is being presented to be read and subsequently donated to the university library.

The full title of the book is «Foundations, retaining and earth structures». I am a member of the international community of geotechnical engineers united today by the ISSMGE, and I am really happy about the fact that G.P. Tschebotarioff had chosen his professional career at our Transport University and that amongst his colleagues, professors of soil mechanics, to whom he would subsequently present his books, were representatives of our department at St. Petersburg. Moreover, he held Russian specialists, and particularly geotechnical engineers, in high regard. Having worked in the USA for a long time he condemned politically engaged distortions of Russian history published by the USA media during the McCarthy era at the time of the so-called «cold war». It is officially known that during exchange of scientific delegations between the USA and the USSR Professor Tschebotarioff declined certain advances on the part of the CIA. Moreover, as a sign of protest he turned down the Professor Emeritus rank at Princeton. Another reason for that reaction were cases of persecution of professors of Slavic nationalities, particularly those teaching the Russian language and literature. This gives us a man of a very broad range of attention in the areas of both science and humanities.

All this does not quite endorse the image of a leader of Whites' opposition to the Reds on the river Don. At the age of 19 in 1918 he opted to come to St. Petersburg and enter the University of Transport which he could not graduate from for purely political reasons, being a member of a family close to the Russian Emperor, who were at the time being persecuted by the Soviet law enforcement agencies.

Having spoken to my senior colleagues from the field of soil mechanics and construction I confidently can bring to your attention the following moments from Gregory Tschebotarioff's youth. After entering the University of Transport he understood quite clearly that his social origins could lead to quite dramatic consequences. He was aware of what was being done to his colleagues – officers from famous St. Petersburg families, but the wish to become a professional civil engineer prevailed over the sense of self preservation danger. According to the famous professor of St. Petersburg University of Architecture and Construction (St. Petersburg Institute of Civil Engineering) and St. Petersburg Transport University Vladimir Alexeevich Gastev and professor Victor Anatolievich Florin, Gregory Tschebotarioff was interested in soil testing research in the Laboratory of Soil Mechanics at the Transport University. At that time the laboratory supervisor was the famous Russian and subsequently American professor S.P. Timoshenko. I am convinced that their ways crossed whilst still in St. Petersburg: it was in that oldest mechanical laboratory that N.M. Gershevanov conducted his pile tests (a graduate of the Transport University of 1902 and son of the rector of the University who served in that capacity for more than 25 years). Subsequently,

the leading and one of the largest specialized underground construction and foundation engineering institutes in Russia was named after N.M. Gersevanov (known today as Moscow NIIOSP). Among his student contemporaries there were N.N. Maslov and V.A. Florin who subsequently having become leading geotechnical specialists of world renown served as translators of papers and monographs by G.P. Tschebotarioff published in the USA. One can say quite confidently that since the very first days of his study at the University of Transport, being in contact with a constellation of future geotechnical gurus (S.P. Timoshenko, V.A. Gastev, N.N. Maslov, N.M. Gersevanov), he could not help getting engaged into geotechnical science which was at the time at the breaking point in terms of its importance for construction practice, and not only in Russia. He continued to maintain his ties with those bright minds also in his late years. The present writer was not spared the «geotechnical bug» that tied him to the circles of people engaged in soil mechanics after attending lectures by professor N.N. Maslov in 1957 in St. Petersburg. I was at the time a cadet of the military faculty at the University of Architecture and Construction (former Institute of Civil Engineers, later known as LISI).

According to Prof. N.N. Maslov young G.P. Tschebotarioff arrived to Berlin Technical School with notes on lectures by S.P. Timoshenko on theory of elasticity and books including publications by the Transport University Press preserved in his personal library. He profoundly impressed the examination board having presented to them his Russian knowledge in the German and English languages. According to his own testimony, Gregory Tschebotarioff had free and lengthy conversations in those languages with the members of the board and the invited leading civil engineers from the Berlin Technical School.

Sadly, fear for his life never left G.P. Tschebotarioff during the war years after the October Revolution in 1917, even after his departure to the south of Russia. Those fears were especially reinforced after he found out that some people known to him were imprisoned after their arrests and the military officers arrested in those years were loaded on ferry boats and drowned in the Gulf of Finland. This information is contained in his memoirs. I read about a lot of similar facts in Tschebotarioff's book entitled «Russia, My Native Land» published in New York in 1964 by McGraw-Hill Book Company. From this book I learned that his grandfather, whose name was also Gregory Tschebotarioff, was of Cossack stock and, a graduate of the Paris Institute of Technology, was in charge of railway construction in the South-East of Russia connecting the cities of Rostov and Voronezh in late 19th – early 20th centuries, whereas his mother Valentina Ivanovna during the war was a nurse in the military hospital at Tsarskoe Selo, where at this time the Empress Alexandra Fyodorovna was also engaged in a similar capacity. Gregory Tschebotarioff doubtless was in contact with them – his mother and his god-mother, during his sojourn while on leave in 1917 at Tsarskoe Selo, where his family resided at the time.

Initially it was with a certain degree of reluctance that I read sections on G.P. Tschebotarioff's life not connected to soil mechanics and foundation construction. But those five chapters read like an adventure story resembling «The Road to Calvary» by Alexey Tolstoy. G.P. Tschebotarioff was frequently arrested in the south of Russia but he was lucky «not to have been shot» as he himself put it in the book. Once he was mistaken by the Reds' patrol to be a «Whites' guerrilla fighter» due to a typical white officer's knapsack he was wearing, but he was spared by the timely benevolent intervention of a high-ranking official of the Reds who happened to be a former officer of the Imperial Russian Army, and a native St. Petersburger. He quietly talked to Gregory Tschebotarioff and in spite of violent protests from the blood-thirsty revolutionaries let him go. The second arrest was even more dangerous but he had time to conceal himself from the arresting brigade in the huge crowd of pro-

revolutionary populace greeting the arrival of the Red Leaders to the city of Novorossiysk. In such environment of constant threats the only solution left for him was emigration. He was evacuated to Egypt together with the College of the Don Cadets where he worked as instructor since 1921, acting as an aide to the Artillery Inspector of the Don Army. We will not be far from the truth supposing he instructed his officers in the matters of construction science because construction was the only practical field where disciplined Russian officers were in high demand, organizing and conducting building activities – there were simply no other activities ongoing in Egypt at that time.

After graduating as a civil engineer in Berlin, Gregory Tschebotarioff worked in Egypt. Demanding ground conditions of that country alerted him to the issue and importance of soil mechanics in general, and to complicity and responsibility of foundation construction in particular. He served as a consultant in these areas for some time in France, Germany and the USA. As of 1937 he became a full-time professor at Princeton, holding a tenure in the art of construction. It is interesting to point out that directions connected to soil mechanics and foundations, including stability of retaining structures were quite rightly regarded as construction art. Gregory Tschebotarioff was involved in projects related to construction of bridges, high dams, tunnels and other civil and military structures, some of them being unique.

I would like to point out the following moments from Gregory Tschebotarioff's notes which infused our work in ISSMGE TC 207 «Soil-Structure Interaction and Retaining Walls» for eight years (2005–2013):

- he alerted the scientific community to instances of serious discrepancy between results of large-scale and expensive *in situ* tests and calculations, including those behind recommended values in design standards and construction codes;
- he objectively reviewed hypotheses and theories propounded by various authors and prevalent at the time openly challenging instances of inconsistency and obsolescence;
- he reinforced understanding of soil mechanics as the theoretical foundation for calculation and computation paying specific attention to soil tests as capable of clearer representations of stressed-strained conditions in soils and structures of any degree of responsibility;
- in his book «Soil Mechanics, Foundations and Earth Structures» Prof. Tschebotarioff provides a lot of numerical data and gives a large number of numerical examples as compared to calculations according to various theories.

Below follow some highlights from a section of his book entitled «Interaction between structures, foundations and subsoils». Here is a direct quotation: «The bearing soil beneath a foundation, the foundation itself and the superstructure form a connected system and must therefore be always viewed as a unified whole». This premise was in the past too often ignored and is still sometimes overlooked by individual authors. All of it is largely connected to the complicity of the actual problem, which was impossible to calculate efficiently with the old mathematical toolbox, that is to say without the computerized numerical modelling capabilities. Even today, theoretical background lags somewhat behind the actual contemporary construction practice, in which we have witnessed mega-deep underground structures and super-tall skyscrapers over 1000 meters tall.

Reviewing his quotes about calculations and *in situ* measurements one may conclude that Gregory Tschebotarioff was and has remained an ideologist for the activities of our contemporary Technical Committee №207 (Soil-Structure Interaction and Retaining Walls) of

ISSMGE, which I was fortunate enough to head for eight years (2005–2013), and which was hosted by Russia and the Transport University.

Without looking down on the SSI related research of my contemporaries, it is important to point out the significance of Prof. Tschebotarioff's ideas which he even in his day and age communicated to colleagues whilst a delegate to almost all congresses and conferences of ISSMGE (whose abbreviation certainly changed a number of times over the years), starting from the first 1936 congress in the USA. He frequently chaired sessions and sections, as well as working committees on stability of retaining walls and underground structures.

In 1958 the USA and the USSR exchanged delegations of scientists and engineers. As member of the American delegation Gregory Tschebotarioff visited Moscow, Leningrad, Kiev and Stalingrad. He summarized his impressions in the following words: «I was leaving with a happy feeling that my motherland – Russia – was alive and recovering after the terrible ordeals which it had had to suffer».

Concluding my account of the life of a world-famous geotechnical specialist Gregory Tschebotarioff, who started his career as a student of the St. Petersburg Transport University in 1918, and developed into a great specialist at Princeton in the USA, it is relevant to address a possible question from my geotechnical colleagues as to why it was that the members of TC 207 “Soil-Structure interaction and retaining walls” suggested a lecture dedicated personally to Prof. Gregory Tschebotarioff. I believe that soil-structure interaction was the leading element in his works and, additionally, extensive systems of monitoring on large scale projects in the USA assisted his evaluation of integrity of calculations and in situ tests.

The two sessions allowed to TC 207 “Soil-Structure Interaction and Retaining Walls” at the 18th International Conference on Soil Mechanics and Geotechnical Engineering in Paris in 2013 hosted about 1350 conference delegates, which demonstrates importance of our field to the geotechnical community. We enjoyed record attendance figures, which was pointed out in the concluding speech by the newly elected ISSMGE President Roger Frank (France). All significant construction projects over the last 10 years have broadly implemented systems of mathematical modelling in design, during construction and in subsequent monitoring. This was conducive to unification of «the three elephants» who serve as foundation for our profession both in new construction and in reconstruction. The three elephants in question are the architect, the superstructure engineer, and the geotechnical engineer. The reports at TC207 SSI sessions in Paris presented bold achievements implemented in design of super-tall structures (over 1000 m) constructed in Dubai, as well as in other unique structures using state-of-the-art software engineering solutions and contemporary construction codes (Proceedings of the TC207 workshop on soil-structure interaction and retaining walls – September 2013, Paris – www.paris2013-icsmge.org).

The geotechnical engineers of the new century have reached a new stage in numerical calculations using advantages of contemporary computing, i.e. such as were simply not there before. This disadvantaged level of calculation methods troubled Professor Gregory Tschebotarioff and burdened him greatly, which he openly wrote and spoke about.

In conclusion I would like to quote our newly elected ISSMGE President Professor Roger Frank: «The perspective of contemporary codes for geotechnical design will be grounded in three words: «SOIL-STRUCTURE-INTERACTION»!

Table of contents

Volume 1

Key-note lectures

<i>V.M. Ulitsky, A.G. Shashkin, K.G. Shashkin, M.B. Lisyuk</i> Soil-structure interaction calculations of a high-rise building and subsoil consisting of sedimentary strata.....	3
<i>Jean-Louis Briaud, Alireza Mirdamadi & Mojdeh Asadollahi</i> Modeling Single Piles under Lateral Impact	11
<i>J. Gniel & C. Haberfield</i> Design, construction and performance of a tied-wall embankment supported on concrete column ground improvement.....	18
<i>R. Katzenbach, S. Leppla, W. Krajewski</i> Numerical analysis and verification of the soil-structure-interaction in the course of large construction projects in inner cities	28
<i>C.F. Leung, D.E.L. Ong</i> Effects of deep excavations on adjacent foundations	35
<i>W.F. Van Impe & P.O. Van Impe</i> Comments on crushable sand stiffness relevant to soil structure interaction issues.....	52
<i>Y. El-Mossallamy</i> Pile group action under vertical compression loads	66

Session 1. Soil-structure interaction

<i>A. Akhtarpour, M. Damghani</i> The Study of Replacing the Central Clay Core with the Plastic Concrete cut-off Wall in the Body of Soombar Reservoir Dam.....	81
---	----

<i>K. Ch. Avellan</i> Application of Soil-Foundation-Pile Interaction Design Method for Strengthening Foundations of St. John's Church in Tartu, Estonia Using Sustainable Manual Calculation.....	88
<i>T. Awwad, B.E. Al-Asali</i> Efficiency of improving the specifications of soil lenses, that are formed near the tunnel during the stages of its investment.....	96
<i>G. Baykal</i> Three techniques for the study of soil structure interface properties; 3D roughness parameter; contact stress mapping; artificially manufactured sand.....	105
<i>C. Jacquard</i> Foundations by prestressing anchors of the “Villa Méditerranée” in Marseille: from design to monitoring	113
<i>H. Hazarika, T. Hara, S. Kuroda, K. Kuribayashi, T. Nishi, H. Furuichi, K. Takezawa, T. Ohsumi</i> Effect of Ground Motions and Tsunami Impact Force on the Performance of a Damaged River Dike	118
<i>H. Hashimoto, T. Yamanashi, H. Hayashi, M. Yamaki</i> Influence of Thermal Condition on the Extraction Characteristics of Steel Strip Reinforcing Members	126
<i>O. Z. Khalimov</i> Methods of Research on Frost Heave of Soil and Foundation – Freezing Soil Bulk Interaction in Terms of Seasonal Deep Frost Penetration including Areas of Pressure Migration	133
<i>F. Liu, M. Jiang</i> Oblique pullout capacity of a single drilled pile in sandy grains cemented by methane hydrates: DEM analyses.....	142
<i>P.V.S.N Pavan Kumar, M. R. Madhav, M. Kumar</i> Modeling of interaction of polymeric sheet reinforcement and backfill	148
<i>D. Lombardi, V. Nappa, A. Flora</i> Soft grouting for the seismic protection of existing buildings.....	156
<i>L. de Moraes Pereira da Rosa, E. Maria Lopes Carvalho, Bernadete Ragoni Danziger</i> Soil Structure Interaction: An analysis of the effect of creep and shrinkage of concrete....	163
<i>E. Osman, M. Abdelmonem</i> Beneficial and Detrimental Effects of Seismic Soil Structure Interaction (SSI) Analysis of High Rise Buildings	171

<i>N. Phienwej, K. Amornfa, W. Cheang</i> Comparative analysis of piled foundation design of a highrise building in Bangkok subsoils.....	180
<i>S. Sadek, S. Hasan</i> Foundation System Design for a Tall Structure on Mortar–Column-Improved Ground	186
<i>H. F. Shehata</i> Soil, Foundation, and Superstructure Interactions of Two-Bay by Two-Bay Frames with Isolated Footings on Sand.....	194
<i>I. Sokolić, B. Vukadinović</i> Design of pile group system for “Most Sava – Zeleni” railway bridge in Zagreb.....	201
<i>E. Turk, S. Oguzhan Akbas, O. Tufenkci</i> Estimation of the Undrained Bearing Capacity of Footings Using Random Finite Element Method: Application in Ankara Clay.....	207
<i>M. Vaniček, I. Vaniček</i> Soil-structure interaction analyses for the study of nuclear power plant foundation alternatives under static and seismic loading.....	213
<i>S. Varaksin, B. Hamidi</i> Analysis of soil-structure interaction by Ménard pressuremeter tests and ground improvement case histories.....	219
<i>N. Vyal'tsev</i> Monitoring based analysis of interaction between an integral bridge and GSY-reinforced embankment	226
<i>L. Vollmert, J. Schlee</i> Piled embankments in soft estuary clay – Experience from design and field measurements for redevelopment of harbour areas in Northern Germany.....	231
<i>Youpele O. Beredugo</i> Vibration of dynamically loaded foundations partially embedded in an elastic stratum.....	239
<i>Zhuang Haiyang, Yu Xu, Zhu Chao</i> An efficient method for estimating the dynamic response of base-isolated structure with SSI effect	247
<i>A.Zh. Zhussupbekov, N.T. Alibekova, I.O. Morev, Ye.B. Utepov</i> Determination of bearing capacity of the precast piles by dynamic cone penetration test (DCPT).....	255

Session 2. Underground structures and retaining walls

C.W. Ong, Su Thiri, K.Y. Yong, Ariaratnam Kulaindran

Understanding of Soil Responses due to Tunnelling – 3D Numerical Analysis
and Case Study of Bendemeer Station (DTL-3), Singapore.....262-1

A. Adekunle

An investigation into the vertical axial capacities and groundwater
cut-off capabilities of secant pile walls..... 263

Ö. Akçakal, T. Durgunoğlu, B. Koçak, T. Tari

3D Modelling in Deep Excavations – Case Studies 271

Bruno Becci & Marco Carni

Pseudo-static analysis of flexible retaining structures including seismic thrust
dependency on wall deformation 277

Ö. Bilgin

Soil-structure interaction for sheet pile walls considering ground surface
and sub-wall soil conditions 285

C. Jurado Cabañes

Seismic Soil-Interaction on Earth Retaining Structures.
Performance-based seismic design of a Retaining Wall..... 291

T. Chernova, Ö. Bilgin, N. Tsimbelman

Overview of Shells with Infill used in Geotechnical Engineering Applications 297

A. Edinçliler & Y. S. Toksoy

Investigation on Effects of Tire Crumb Cushion
on Seismic Performance of Retaining Wall..... 305

H. Elahi, M. Sabermahani, H. Vahidifard

Shoring-structure interaction in stabilization of excavation
adjacent to historic buildings – A Case Study 310

D.S. Kim, S.Y. Park

Design and construction of reinforced retaining wall in the railway of Korea..... 316

C.E.M. Maffei, H.H.S. Gonçalves, M.C. Guazzelli

A bold constructive method for the retaining structures of the excavation
of the underground parking Clinics, in Brazil 320

C.E.M. Maffei, H.H.S. Gonçalves, M.C. Guazzelli, J.P. Ciriades,

P.E.M. Maffei & R.A. Simoni & C. Goulart

Deepening of some Brazilian quays using the technique of reinforced jet-grouting..... 328

S. Melentijevic & J.L. Fernández

Comparison of finite element and limit equilibrium methods
in analysis of soil nail walls..... 334

<i>M.A. Putera Agung, S. Pramusandi, A. Ardianto, B. Sunaryo</i> Assessment Analysis of Lateral Movement of Gate Shaft Structure on Fractured Rock Mass, Jatigede Dam Area, West Java, In-donesia	342
<i>L. A. Estevez Rey & N. A. Daza Rodríguez</i> A case study of a Deep Excavation on aSoft Lacustrine Clay of Bogota, Colombia, with emphasis between Predicted and Measured deformations	350
<i>G. Russo, S. Autuori, M.V. Nicotera</i> San Pasquale station of the Linea 6 in Napoli: dewatering field tests, measurements and back-analyses	358
<i>A. Sato, T.Yamanashi, T. Suzuki, N. Tatta, K. Yoshida</i> Frost Protection for Geotextile-reinforced Soil Walls in Service.....	366
<i>S.V. Sivapriya, S.R.Gandhi</i> Evaluation of pile behaviour on sloping clayey soil in supporting a diaphragm wall for building excavation	374
<i>H.F. Shehata, T.M. Sorour</i> Effect of Base Soil Stiffness on the Earth Pressure of Cantilever Retaining Walls	379
<i>J.C. Solis Tito, C. Romanel</i> Numerical Analysis 3D of a Deep Circular Excavation in the City of Rio de Janeiro.....	385
<i>A. Soroush, & M. Hashemzadeh</i> Finite element analysis of the soil type effect on buried pipelines under strike-slip faulting.....	392
<i>P. Tanseng & V. Namwiset</i> Performance of soil-cement column retaining wall used with top-down construction method for basement construction in Bangkok subsoil	399

Session 3. Site investigation as source of input parameters for soil-structure interaction

<i>M. Abu Sadeque, Partha Saha, A.R.M. Farid Uddin</i> Standard Penetration Test and Its Discrepancies in Bangladesh Perspective: A Comparative Study Between Automatic Trip Hammer And Donut Hammer	409
<i>A. El Khoury, Imad Esta, Jean B. Esta</i> Test for Determining Mechanical Characteristics of Any Rocky.....	413
<i>C. L. Zenti, A. Bellocchio, D. Sterpi</i> Laboratory and In-Situ testing for the identification of bonding parameters of GFRP pipes and soil nailing systems	415

Key-note lectures

Soil-structure interaction calculations of a high-rise building and subsoil consisting of sedimentary strata

Ulitsky V.M., Shashkin A.G., Shashkin K.G., Lisyuk M.B.
“Georeconstruction” Institute, St. Petersburg

ABSTRACT: Soil-structure interaction calculations constitute a basis for design decision making on a structure of any building even an ordinary housing. The importance of soil-structure interaction calculations largely increases when unique structures are designed for which construction there is no experience in geotechnical conditions of a given area. Special interest is placed on calculations of a high-rise building on soft subsoil where there is a necessity to estimate soil strains caused by application of unusually high loads.

There is an example of design of a 400-m-high skyscraper consisting of 78 above ground and 3 underground storeys, it was planned to erect the building on more than 200-m-thick bulk of sedimentary deposits.

The skyscraper represented a spiral screwing cone, a pentagon in plan composing of 5 square “petals” connected with a central round core. With building height increasing square “petals” turned counter-clockwise around the building axis and reduced in size, their center moving towards the axis of the round central core of the building.

In terms of structure the building followed a core and frame scheme. Its general stability was ensured by joint work of a central monolith reinforced-concrete core and 15 metal columns located along the perimeter and united by metal beam carcasses, which discs of floorings rested upon, and special outrigger beams installed at three levels of technical storeys providing significant increase of total horizontal rigidity of the building against wind loads. Outriggers represented metal console beams with one end being fixed in the central reinforced concrete core and the other linked with exterior metal columns. An outrigger beam has up to 50 mm-thick wall of altering section with a system of rigidity ribs.

The core served the main element which provided transfer of vertical and horizontal load components in the given structural scheme. The central reinforced concrete core diameter reduced with height. At the level of lower floors up to the level of the 61st storey it comprised

24.5 m, beginning with the 61st storey it decreased down to 18.6 m, from the 71st storey – down to 12.1 m.

The thickness of outside wall of the core made of reinforced concrete (concrete class B80) changed from 2 m in the lower part down to 0.4 m in the upper part of the building. Internal bearing reinforced concrete walls of the core of at least 300 mm thickness ensured additional rigidity of the core structures.

Due to a spiral screwing form of the building there emerged horizontal loads applied to floorings and the beam carcass which tended to turn floorings around the core axis. In order to take these horizontal loads creation of rigid discs of floorings was required. It was envisaged to make floorings of the above part in office floors of reinforced concrete, concrete class B60, thickness 180 mm, in technical floors the thickness comprised 250 mm.

Exterior metal columns represented an important element of the core and frame system of the building. Steel columns were located along the building perimeter and provided resting for the system of beams of floorings in the span from the central reinforced concrete beam to exterior walls of the building. The columns had a box-shape cross section with exterior planes of 850×850 mm and wall thickness from 140 to 100 mm. At the level of the last flooring loads from metal structures of approximately 76-m-high spire were applied to metal columns of the main frame.

The structural scheme of the building foresaw considerable concentration of loads transferred to subsoil near the central part – the core.

One of the important principles of constructing a high-rise building on soft soil is installation of a developed underground part which has two functions: 1) load distribution from a high-rise building to a large area; 2) reduction of pressure on soil by a weight value of soil extracted from a volume of an underground part. For an underground part of a high-rise building to be able to fulfill the function of load redistribution it should have the required spatial rigidity. It means that underground spaces should be crossed by radial rigidity diaphragms providing even transfer of forces from the core and exterior columns (connected with outrigger beams in technical storeys of the above ground part) throughout a square of underground space of the building. Certainly this underground space becomes uncomfortable for utilization: rigidity diaphragms, for example, significantly reduce an amount of parking places. But construction of skyscrapers on sedimentary soils *a priori* is not economically well-grounded investment; it is more likely to reflect ambitions of a developer.

Since interaction of architects, structural and geotechnical engineers designing the considered high-rise building started at the stage of development of an architectural concept, an optimum structural solution for the underground space providing the required spatial rigidity was found at design stage. It was envisaged to install 800-mm-thick radial traverse wall at the level of underground floors. At the level of underground floors the load from exterior metal columns of the building was carried by reinforced concrete columns of 1350×1350 mm in cross section. Vertical reinforced concrete bearing structures of the underground part were supposed to be made of concrete of B80 class, B60 – for floorings.

Installation of barrettes (of B60 class concrete) to the depth of 105 m from the ground surface was envisaged to transfer loads of the high-rise building to subsoil. On the top barrettes were united by a 3.6-m-thick powerful monolith raft made of B60 concrete.

According to investigation data the geotechnical profile of the site within the drilling depth

of 170.0 m consists of quaternary deposits of various origin and venda bedrock.

Upper Proterozoic Kotlin sediments (Vkt2) are characterized by comparative permanency of cross section. In the given site venda bedrock deposits were found at absolute benchmarks of minus 43.80 m – minus 50.09 m BS. From the depth of 45.0 m to the depth of 53.0 m the profile composes of layered clays with thin seams (up to 1 mm) of poorly dislocated sandstone. A dislocated area is characterized by excessive fracturing, distribution, moulding of subhorizontal layering and excessive hydration of deposits.

From the depth of 53.0 to the depth of 127.5 m the section is represented by layered clays with thin seams (up to 1 mm) of sandstone. In the depth range of 65.0...89.0 m investigators found a seam of dislocated clays having low values of mechanical properties. Below the depth of 127.5 m there is a siltstone-clay assise of the upper subset of Kotlin set represented by a bulk of uneven over-layering of consolidated clays, fine-grained and silty sands, poorly cemented sandstones, solid argillites.

In hydro-geological terms the territory was characterized by presence of several aquifers. Aquifer I is non-pressure, aquifers II, III and IV – pressure ones. Statistical level of aquifer I is fixed at the benchmarks of 0.8...1.8 m BS; for aquifer II – at the benchmarks of 0.5...1.7 m BS; for aquifer III – at the benchmarks of 0.1...0.4 m BS; for aquifer IV – at the benchmarks of 0.1...0.6 m BS.

In order to obtain accurate distribution of forces in barrettes structures and account of their interaction with soil simulation of barrettes and the piled raft was carried out with a help of volumetric finite elements. Massive external walls of the core were also modeled as volumetric finite elements, internal walls of the core were simulated as shell elements (interaction between external and internal walls of the core was modeled with a help of special contact elements allowing to set different shear rigidity in contact zones). Floorings in the internal volume of the core were simulated as shell elements, steel frame columns and reinforced concrete columns of the underground part – as spatial rod elements, the beam carcass beyond the rigidity core was set by spatial rod elements (rigidity of reinforced concrete slabs of above

ground floorings beyond the core was not taken for safety factor, slabs were modeled with flexible load), simulation of outrigger beam behavior was made by shell elements with equivalent rigidity.

Fig. 1 shows the general view of the computation scheme for the problem of soil-structure interaction computation. 1, the general view of structures of the designed building is given in fig. 2.

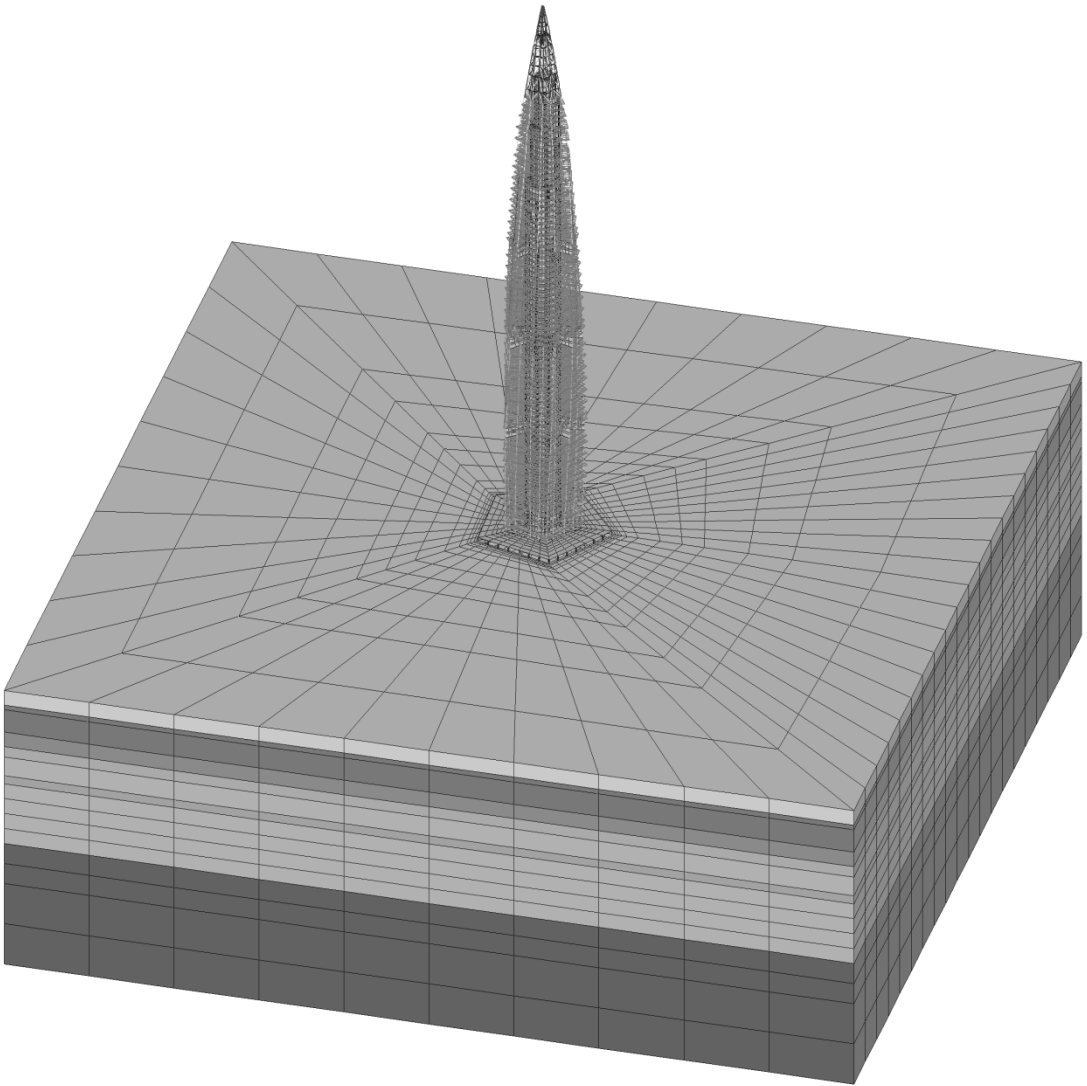


Fig. 1. The general view of the computation scheme.
The designed high-rise building and subsoil. Soil-structure interaction calculation

The design company proposed barrettes of 105 m depths from the ground surface based in the layer of venda hard soil as a foundation for the high-rise building. This option was selected

by designers in order to limit the expected settlement by the value of about 10 cm. Limiting the value of absolute settlements the project authors tried to restrict their difference as well.

Soil-structure interaction computation included 3 steps: 1 – definition of natural stresses of dead load of soil; 2 – installation of retaining walls for the pit to the depth down to 40 m from the surface and further excavation of soil within the underground structure; 3 – construction of structures of the designed high-rise building.

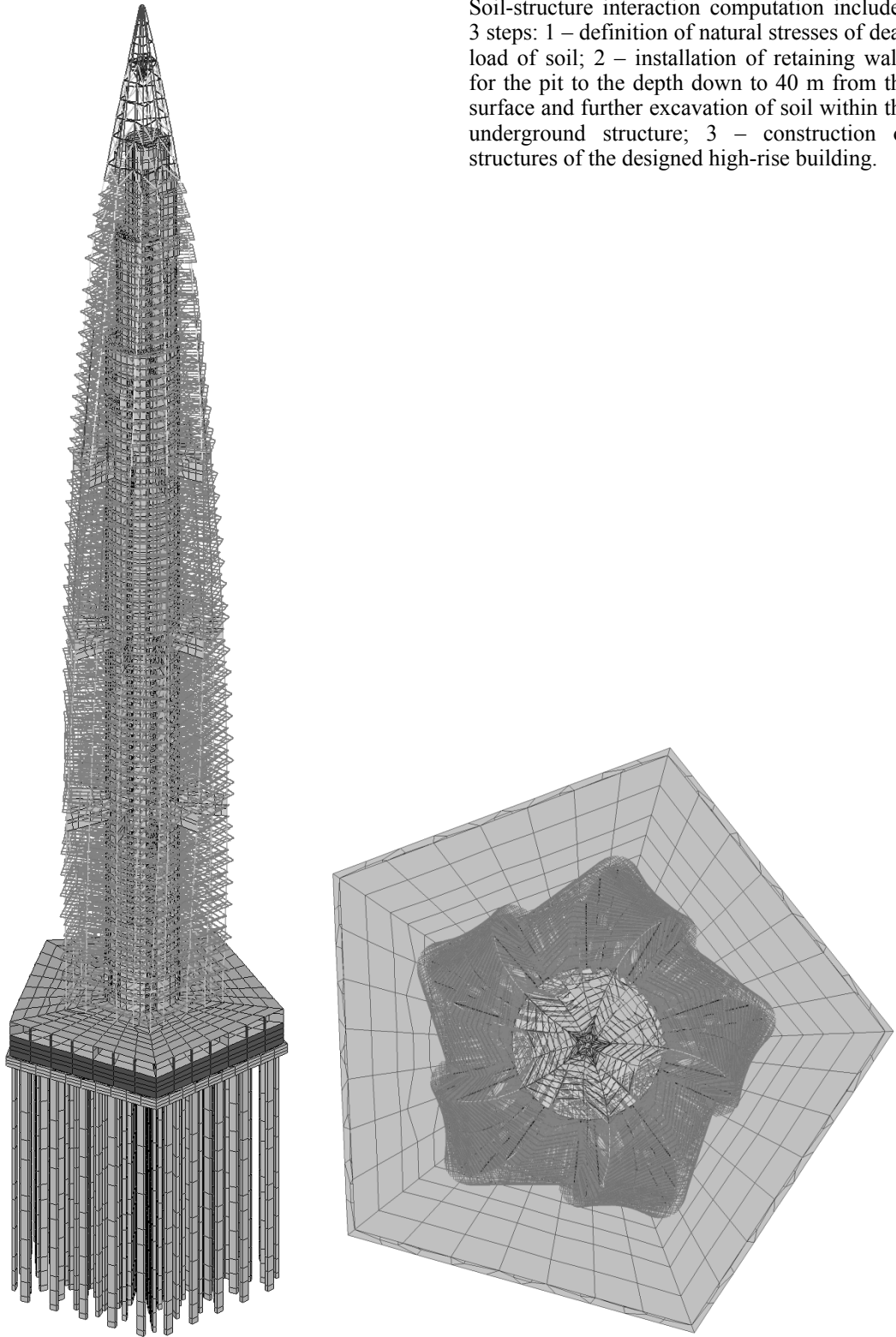


Fig. 2. The general view of structures of the designed building

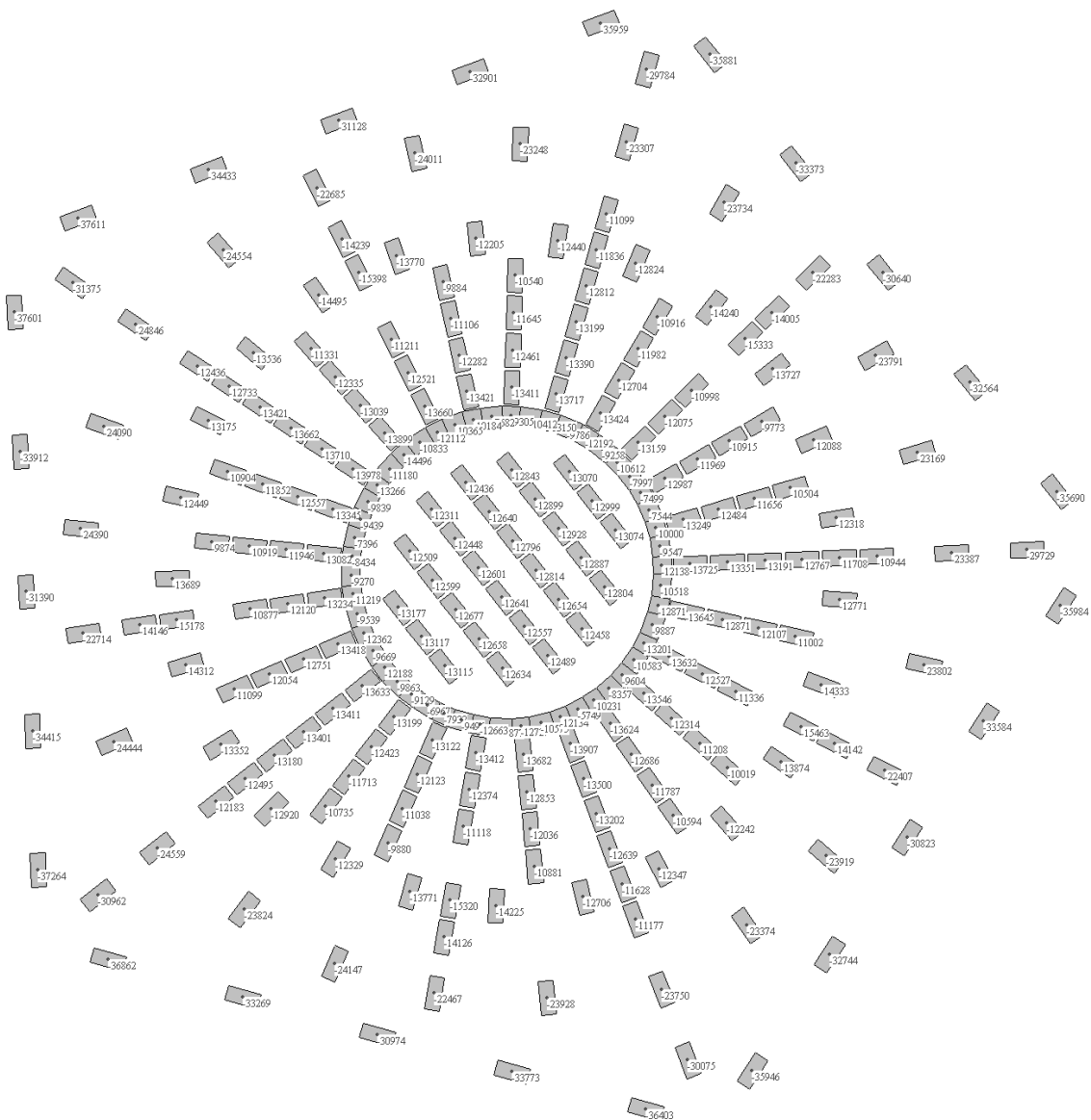


Fig. 6. Forces (kN) in barrettes (normative) based on results of calculation of the building taking into account non-linear behavior of the soil according to visco-plastic model

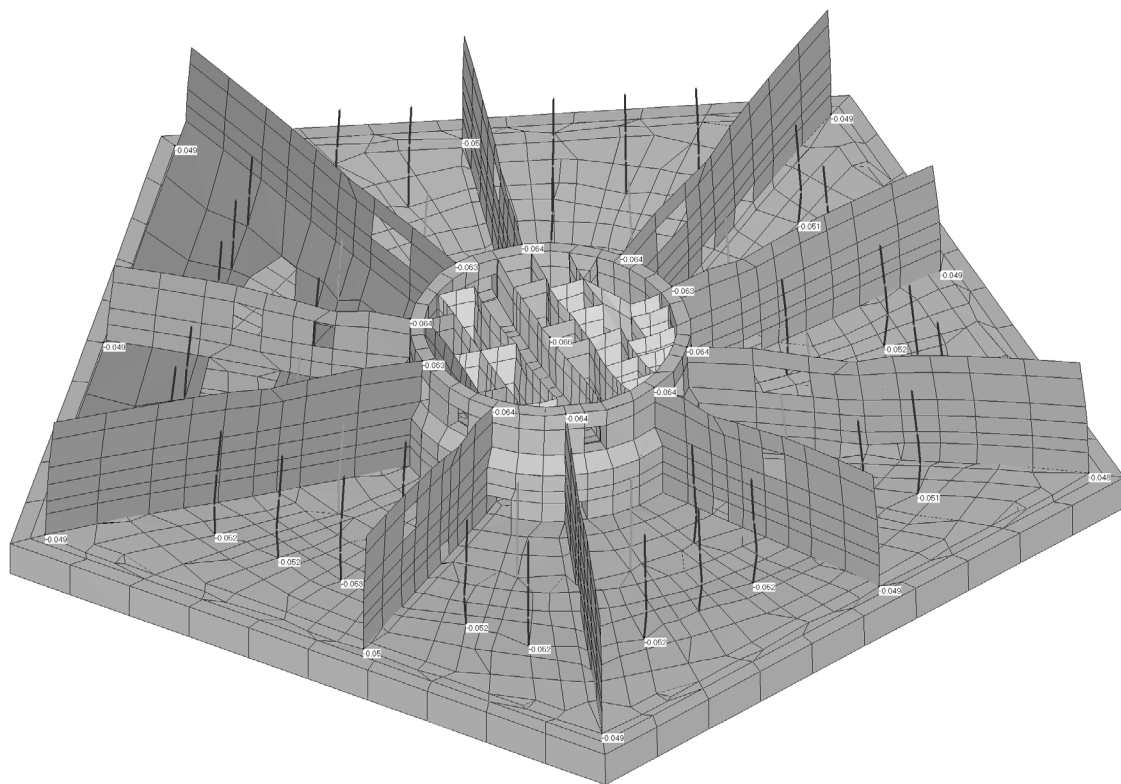


Fig. 7. The deformation scheme of the underground part of the designed high-rise building based on non-linear subsoil according to visco-plastic model. There are given values of vertical displacements (m)

Calculation analysis of the high-rise building- subsoil interaction allowed to find out that the limitation of settlements by the value of about 10 cm which constituted the basis for structural solution of foundations is extremely restrictive. Relative difference of settlements has turned out to be four times as low as the value which structural designers found admissible for the designed buildings. Soil-structure interaction calculations showed that to provide long-term mechanical safety of the high-rise building it was sufficient to install barrettes to the depth of about 65-70 m, using which the skyscraper would settle to maximum 15 cm, the value of differential settlements would reach up to 0.002. The experience of the given calculations of the high-rise building and soft soil has served the purpose when making a design decision on development of underground space and pile foundation of the first skyscraper in St. Petersburg.

Modeling Single Piles under Lateral Impact

Jean-Louis BRIAUD

Dpt. of Civil Engineering, Texas A&M University, College Station, TX, USA

Alireza MIRDAMADI & Mojdeh ASADOLLAHI

Dpt. of Civil Engineering, Texas A&M Univ., College Station, TX, USA

ABSTRACT: In this paper the behavior of single piles under lateral impact is investigated by using the performed pendulum and bogie tests. Three types of soil deposits were used in the experimental tests including hard clay, loose sand and crushed lime-stone. The acceleration and displacement of the striking mass are measured. The results show that the soil response to impact is a function of soil stiffness; however the inertia and damping resistance are also important contributors. In order to model the system, a Single Degree of Freedom (SDF) model with two different basic materials is used to find the best simple model to predict the behavior of piles under impact. Finally an advanced model with multi degree of freedom is used to analyze a single pile under the pickup truck impact with 60 miles per hour. The results of the simple model and the experimental tests are compared with the LS-DYNA simulations.

1. INTRODUCTION

Piles may be designed to resist lateral impact loads in different situations such as: motor vehicles collision with highway guardrails and bridge pier or posts around critical and important infrastructure locations. Berthing foundations, river bridge piers, and dolphins structures are also exposed to the horizontal impact from ships. The system resisting the impact contains two major components: pile as a structural element and soil as a support element. Note that soil has a more complex behavior than the pile. In order to analyze and then design the pile or group of piles for this situation, soil-structure interaction, soil behavior under high strain rate, and load properties are the most important issues that need to be considered.

Using a simple model to analyze the pile under lateral impact can help us to perform the simulations with fewer numbers of parameters and also in shorter time, so the user can get the reasonable results with minimum soil properties parameters. In order to simulate the problem a finite element program called LS-DYNA can use both explicit and implicit method, but it is complicated, expensive, time consuming. For example, simulating an ordinary impact model with LS-DYNA may take about 40 to 60 hours and the number of input parameters is about 15.

The analysis of a single pile under the static lateral load has been developed by different methods (Briaud 1997) (Broms 1964) (Evans 1982). There are a number of studies have been

done for dynamic lateral load which are generally related to earthquake loads (Gazetas 1984, Blaney et al 1976, Barghouthi 1984, Boulanger, Kutter et al 1999). In most methods for dynamic analysis, soil is modeled with springs and dashpots and sometimes lump masses (which are representative of stiffness, damping, and inertia effects, respectively). In the case of impact, there are only a few studies performed on piles and also few experimental results of lateral loading are available to verify these methods.

Smith (1960) developed a simple solution for pile-driving analysis by using the wave equation and a simple model for soil in order to estimate the pile drivability and capacity. In the case of lateral dynamic load the modeling of pile and soil is more complicated. Ghazzaly et al (1975) introduced an approximate, rational approach to analyze a vertical pile subjected to low-amplitude, surface, lateral vibrations. The concept of beam on elastic foundation and the elastic half-space theory are used in the development of the proposed method.

In this study a Single Degree of Freedom (SDF) model is used to simulate the single pile and surrounding soil, the model is then calibrated against some scaled tests. If the analysis can match the test results material model, there is a good chance that the model can be used for soil in multi degree of freedom. First a number of scaled test were done with a pendulum and a bogie to provide a calibration for the SDF model.

2. EXPERIMENTAL TESTS

Three types of soil (loose sand, dense crushed limestone and hard clay) were used in a pit which was 3m by 1.5m by 1.8m deep (fig 1). Impact loads on posts are caused by vehicles, ships or sometimes by explosion (which is not discussed in this paper). So in these scaled tests a rigid mass strikes the pile with a specific velocity. The mass is a pendulum for the crush limestone and the sand, and a bogie for the clay. In all tests a single 15.2cm*15.2cm*0.95cm box section post embedded 1m was used as the pile.

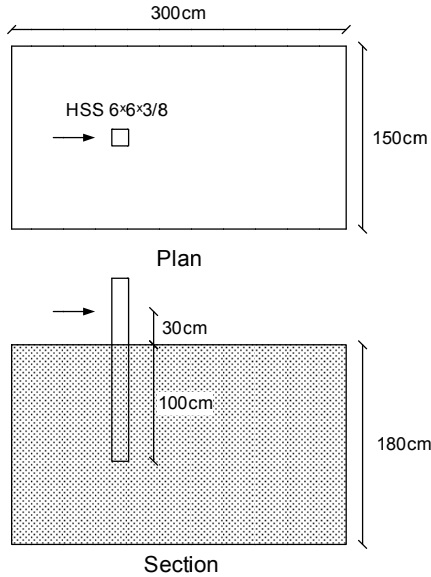


Figure 1: Plan and section of test

A Total number of eight tests were performed on single piles with different velocities and masses. The pile was installed by either driving or backfilling and the range of velocities and masses was between 2.5 m/s and 10 m/s and 250kg and 900kg. The list of tests is presented in table 1. For each test acceleration of mass was measured by a sensor on the pendulum or bogie and by using a high speed camera (1000 fps) and analyzing the movie frame by frame against a fixed target the displacement of the pile was determined. A photo of test P3 and B1 are shown in figure 2. In addition to the properties of each soil including the Pressuremeter Test (PMT) and the Standard Penetration Test (SPT) as in situ tests, and sieve analysis water content, unite weight and direct shear test as lab tests, series of static horizontal load tests were done.

Table 1. Details of single pile tests

Test	Soil	Striking mass	Velocity (m/s)	Mass (kg)	Pile installing method	Kinetic energy (KJ)
P1	Crushed limestone	Pendulum	4.65	862	Back-filled	9.3
P2	Crushed limestone	Pendulum	2.41	862	Back-filled	2.5
P3	Crushed limestone	Pendulum	9.97	862	Back-filled	42.8
P4	Loose Sand	Pendulum	4.94	249	Driven	3.0
P5	Loose Sand	Pendulum	2.5	249	Driven	0.8
P6	Loose Sand	Pendulum	10.1	249	Driven	12.7
P10	Loose Sand	Pendulum	9.83	249	Back-filled	12.0
B1	Clay	Bogie	4.56	903	Driven	9.4

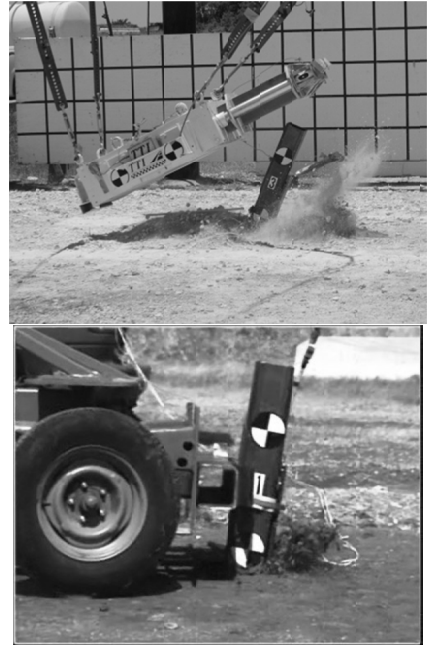


Figure 2. Pendulum and Bogie tests

3. TEST RESULTS AND DISCUSSION

The acceleration of the striking mass and the displacement of the pile are two major outputs of each test. It is also possible to obtain the rotation of the pile head from the high speed movies. By multiplying the acceleration of the pendulum or the bogie by the mass, the load-time history on the pile is obtained. The dis-

placement and the acceleration for all eight impact tests are presented in Figure 3. The static lateral load test results for each soil type are also shown in figure 4.

As it is seen from the acceleration output, for all of tests there are three steps: 1- a peak at the beginning, 2- a flat part in the middle, 3- a drop at the end of the impact.

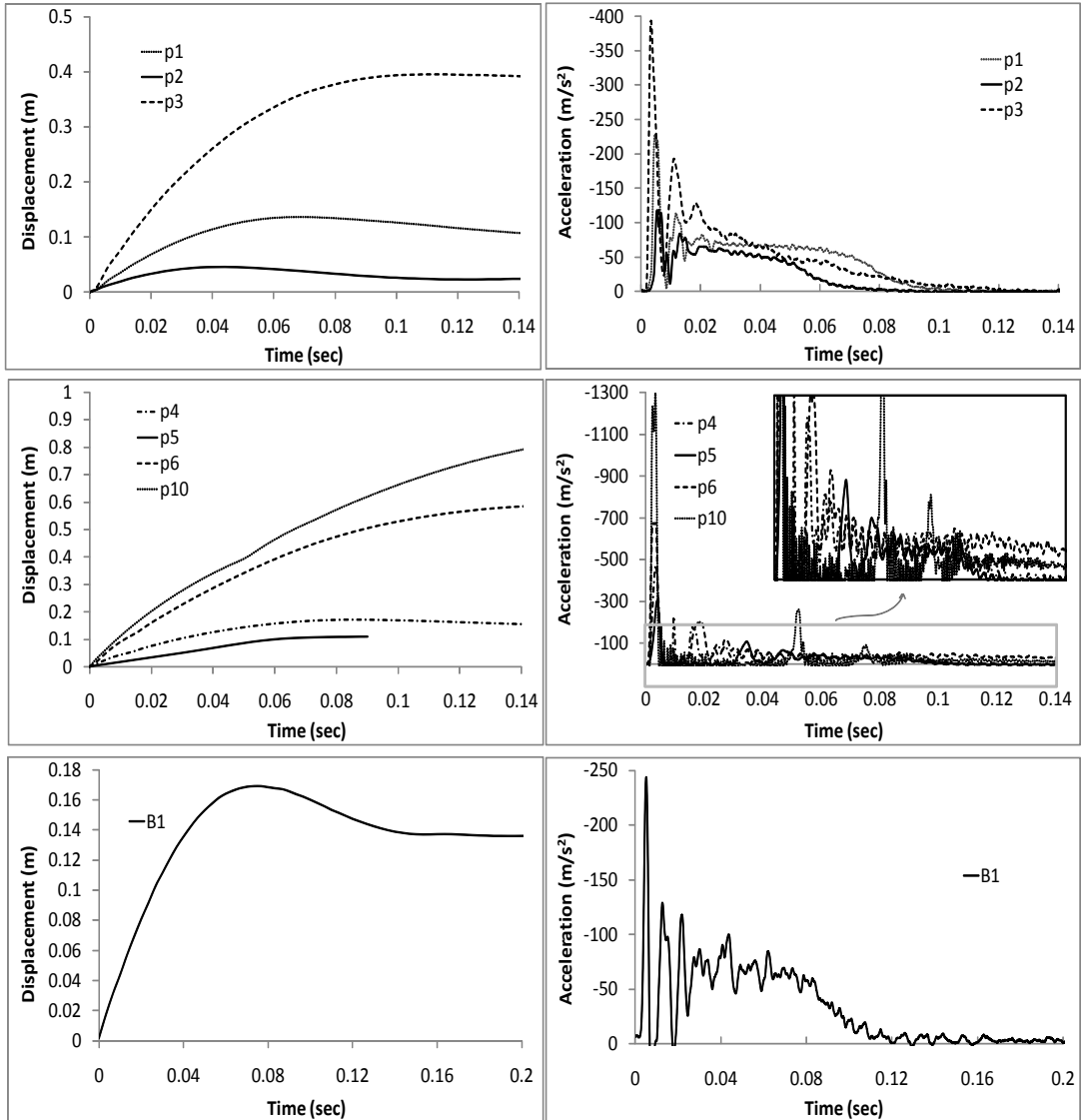
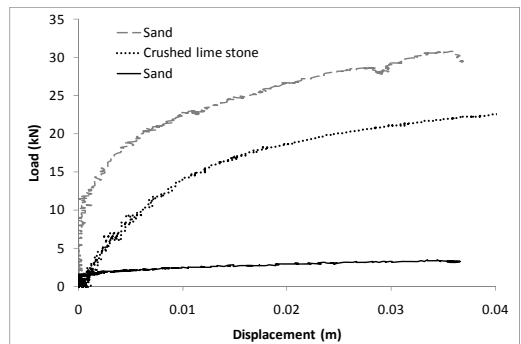


Figure 3. Measured displacement and acceleration results

Figure 4. The static lateral load test results for each soil type



4. MODELING

Due to the permanent deformations after impact and the viscous behavior of soil, the suitable dynamic model for this problem will be a viscoplastic model. There are several material models that can simulate viscoplasticity; all of them are combinations of stiffness (E), viscosity (E^*) and inertia (M) parameters. Two simple and basic models are the Kelvin-Voigt and Maxwell models (Fig 5). For both of these models the inertia effect is added in the equations, which is shown by a mass in the diagram. The stiffness of soil in this study is assumed elastic-perfectly plastic.

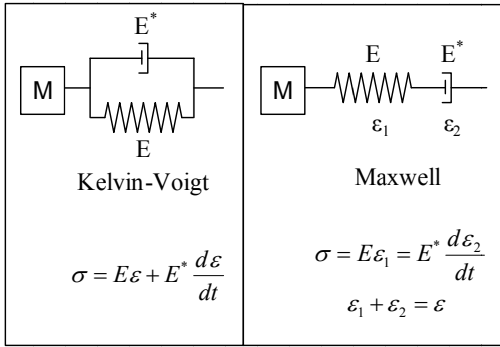


Figure 5. Kelvin- Voigt and Maxwell material model

Applying the governing equation for each model gives the Partial Differential Equation (PDE) which cannot be solved with ordinary methods. The Finite Difference method with the explicit approach is one of the simplest methods to solve this PDE. By using central difference formulas and applying boundary conditions (initial velocity of the striking mass) a step forward solution is proposed for the equation. This method is simple enough that it can be coded in Microsoft Office Excel.

Model parameters are evaluated from soil properties especially pressuremeter test and static analysis results. The results from the single degree of freedom of two material models are compared with test P1 in Figure 6 and Figure 7. As can be seen from the outputs the Kelvin-Voigt model shows a better prediction than the Maxwell. The Maxwell model cannot generate the peak in the acceleration; also the maximum load from this model is equal to the minimum resistance of the damper and the spring. Therefore this resistance is at most equal to the static resistance. For the Kelvin Voigt

model on the other hand the resistance from the damper and the spring sum up, so the model gives more resistance than the static one.

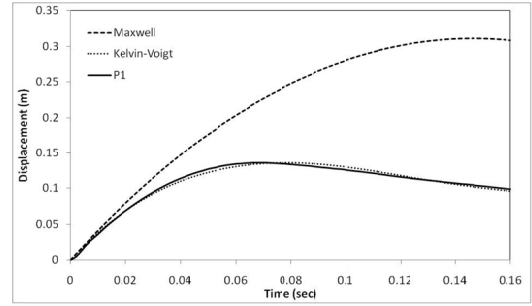


Figure 6. Displacement result from the Maxwell and the kelvin-Voigt model and comparison with P1 test

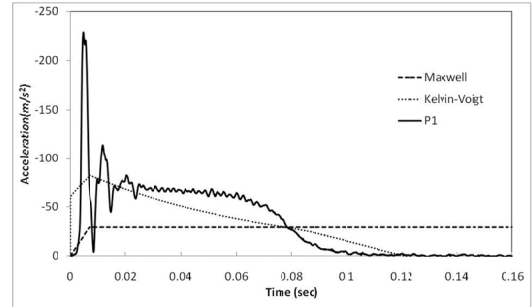


Figure 7. Acceleration result from the Maxwell and the kelvin-Voigt model and comparison with P1 test

5. HORIZONTAL IMPACT LOADING FROM VEHICLE

In the case of road side safety, embassy defense against unrestricted trucks, ship berthing, piles are impacted horizontally. To predict the behavior of piles subjected to horizontal impact, it is possible to use 4D programs (x, y, z, t) such as LSDYNA (2006). This is expensive and time consuming. The problem can be simplified by using a P-y curve approach generalized to include the effect of time. In this case the governing differential equation is:

$$EI \frac{\partial^4 y}{\partial z^4} + M \frac{\partial^2 y}{\partial t^2} + C \frac{\partial y}{\partial t} + Ky = 0 \quad \text{or} \quad Eh y'''' + M \ddot{y} + C \dot{y} + Ky = 0$$

where E (N/m^2) is the modulus of elasticity of the pile, I (m^4) the moment of inertia of the pile against bending around the horizontal axis perpendicular to impact, y (m) the pile horizontal displacement at a depth z and a time t , M

(kg/m) the mass per unit length of pile (mass of pile M_p plus mass of associated soil M_s), C ($N.s/m^2$) the damping of the system per unit length of pile, and K (N/m^2) the soil spring stiffness per unit length of pile. Note that the soil horizontal resistance is limited to P_u (kN/m^2). The boundary conditions are zero moment and zero shear at the point of impact, and zero moment and zero shear at the bottom of the pile. The initial condition is the displacement of the impact node during the first time step; this displacement is equal to $V_0 \times \Delta t$ where V_0 is the velocity of the vehicle and Δt the time step. Other inputs include the mass and velocity of the impacting vehicle, and the parameters in governing differential equation for the soil and the pile. The differential equation is then solved by the finite difference method and it turns out that the parameter matrix is a diagonal matrix so that no inversion is necessary. As a result, the solution can be provided in a simple Excel spread sheet (Mirdamadi, 2014).

Since the problem concerns a horizontal load on a pile, the PMT is preferred to obtain the soil data. The PMT in this case is a mini PMT called the Pencil (Fig. 8) which is driven in place or driven in a predrilled slightly smaller diameter hole if the soil is hard. As a result of many static and impact horizontal load tests at various scales (Lim, 2011, Mirdamadi, 2014).



Figure 8: Pencil pressuremeter equipment and the test in the field

Fig. 9 shows a photo sequence of an impact test where a 2300kg pickup truck impacted a pile at 97.2 km/h. The pile was a steel pipe with a 356mm diameter and a 12.7mm wall thickness. It was embedded 2 m into a very stiff clay which gave the PMT parameters shown in Table 2. PMT tests were performed with a Pencil pressuremeter by first driving a slightly smaller diameter rod in the very stiff clay and then driving the Pencil probe in the slightly under-sized hole. A comparison between the movement measured and calculated behavior of the pile is presented in Fig. 10. The calculations were based on the simple Excel program (TAMU-POST, Mirdamadi, 2013) and a 4D FEM simulation using LS-DYNA (2006).

Table 2: Pressuremeter test results in hard clay

Depth(m)	E(MPa)	ER1(Mpa)	ER2(Mpa)	pL(kPa)
1	27.8	40	92	1400
1.8	16.7	27	74	1200



1



2



3



4



5



6



7



8

Figure 9: Pickup truck impact test (PU60)

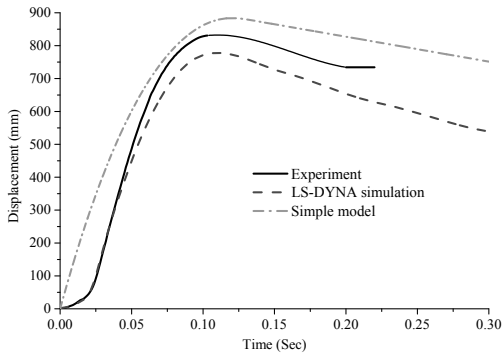


Figure 10: PU60 impact displacement-time results from experiment, LS-DYNA simulation, and simple model

6. CONCLUSION

Although studies have been conducted on piles subjected to lateral loads, few of them have addressed the problem of lateral impact load. In this study eight impact tests were performed on a single pile. The results show that in order to model the behavior of the system a viscoplastic model is required.

Test results reveal different ratios between dynamic and static load (amplification factor) for each soil type. Moreover three steps dynamic results can be observed in all tests.

A Single Degree of Freedom (SDF) system with two basic models, Kelvin-Voigt and Maxwell, is investigated to simulate the pile behavior under lateral impact. The Finite Difference method with an explicit approach is used to solve the governing differential equations of these models. Both proposed model and solution are simple enough that can be developed in a basic coding program (e.g. Microsoft Office Excel). The Kelvin-Voigt model shown to be preferable in this case compared with the Maxwell model.

By upgrading the SDF model to Multi Degree of Freedom (MDF) with the same material model for soil, the prediction of model will be improved considering the benefit of easy use of model. The comparison of the simple MDF model with a full scale pickup truck impact test proves that the model is capable of analyzing a single pile behavior under lateral impact as good as LS-DYNA simulation.

7. REFERENCES

- Barghouthi, (1984). "Pile response to seismic waves," thesis presented Univ. of Wisconsin, at Madison, Wisconsin.
- Blaney, G. W., Kausel, E., and Roesset, J. M. (1976). "Dynamic stiffness of piles." Proc. Second Int. Conference Numerical Meth. in Geomech., ASCE, 1001-1012.
- Boulanger, R.W., Curras, C.J Boulanger, R.W., Curras, C.J., Kutter, B.L., Wilson, D.W., Abghari, A. (1999). "Seismic soil-pile-structure interaction experiments and analyses" Journal of Geotechnical and Geoenvironmental Engineering, 125 (9), pp. 750-759.
- Kutter, B.L., Wilson, D.W., Abghari, A. (1999). "Seismic soil-pile-structure interaction experiments and analyses" Journal of Geotechnical and Geoenvironmental Engineering, 125 (9), pp. 750-759.
- Briaud, J-L., (1997). "SALLOP: Simple Approach for Lateral Loads on Piles" Journal of Geotechnical and Geoenvironmental Engineering, October, P 958-964
- Broms, B. B. (1964). "Lateral resistance of piles in cohesive soils." *J.Soil Mech. Found. Div.*, 90(2), 27-64.
- Evans, Leonard Thomas.(1982). "Simplified analysis of laterally loaded piles" dissertation, University of California at Berkeley
- Gazetas, G. (1984). "Seismic response of end-bearing piles." *Int. J. Soil Dynamics Earthquakes Engrg.*, 3(2), 82-93.
- Ghazzaly, O.I. , Hwong, S.T., O'Neill, M.W., (1976). "Approximate analysis of a pile under dynamic, lateral loading" *Computers and Structures*, vol. 6, n 4-5, p 363-
- Mirdamadi A., 2013, "Deterministic and Probabilistic Simple Model for Single Pile Behavior under Lateral Truck Impact", PhD dissertation, Zachry Dpt. of civil engineering, Texas A&M University, College Station, Texas, USA.
- Smith E.A.L., (1960). "Pile driving analysis by wave equation". *Journal of Soil Mechanics and Foundation Division*, ASCE 86, pp. 35-61.

Design, construction and performance of a tied-wall embankment supported on concrete column ground improvement

J. Gniel & C. Haberfield

Golder Associates, Melbourne, Australia

ABSTRACT: A 5 m high earth fill embankment comprising vertical side-walls constructed from precast concrete wall panels tied together using steel straps was constructed on a 10 m thick deposit of soft clay. Due to the relatively small specified settlement tolerances of the embankment/wall structure, ground improvement in the form of drilled displacement columns (unreinforced concrete columns) was used to improve the engineering properties of the embankment foundation. This paper discusses the design and construction of the embankment and foundation system and compares the predicted settlements with those measured after construction. Discussion on the quality control measures adopted during construction is also provided.

1. INTRODUCTION

Areas of inner city Melbourne, Australia are underlain by a relatively thick layer of soft, compressible silty clay known as Coode Island Silt (CIS). The properties of this soil unit are well documented (Neilson 1992, Ervin 1992, Day 2007 and Srithar 2010).

CIS may be present in thicknesses of up to about 30 m. It has traditionally posed a constraint to development due to its tendency to experience a large change in void ratio (high primary consolidation) under a relatively small increase in vertical effective stress and significant creep.

As part of a recent large transport project, several existing embankments founded on CIS have been widened or duplicated. The subject of this paper is a 200 m long section of duplicated embankment up to 5 m high, founded on a layer of CIS approximately 10 m thick.

Based on laboratory testing and data from nearby sites, it was estimated that CIS underlying the new embankment would undergo primary consolidation ranging between 500 mm and 1000 mm if the CIS was left untreated. This process was estimated to take approximately 3 years to occur ($t_{95} = 3$ years). Creep of the untreated CIS was expected to range between 5 mm and 10 mm per year following the end of primary consolidation. It must be noted that conventional creep theory observed in many soft clay deposits, comprising a logarithmic

reduction in creep settlement over time, is often not observed in CIS.

Although not subject to particularly onerous total settlement tolerances, differential settlement was a key constraint in design of the new embankment. In addition, due to the narrow corridor of land available in which to construct the embankment, side-batters were not feasible. A tied-wall design was therefore adopted comprising vertical wall panels on either side of the embankment formation, tied together with steel straps. The arrangement is similar to that of a conventional reinforced soil structure (RSS) wall in terms of panel arrangement and strap frequency but does not rely on the frictional properties of the soil fill behind the wall face to provide passive support in the same way an RSS wall does. In fact, tying the wall panels together enabled lower quality fill to be reused on site, providing significant savings for the project. A sketch of the typical tied-wall arrangement is presented in Figure 1.

Full-height wall panels were adopted in the design which limited the amount of total allowable settlement at the edge of the embankment to approximately 100 mm with differentials of about 5 mm/m length of wall over the 50 year design life. Due to construction program constraints, removal, or at least a significant reduction in time-dependent settlement was also required. A semi-rigid form of ground improvement was therefore needed to stiffen the CIS and meet the design settlement tolerances. Options considered included a fully-piled

structure or semi-rigid inclusions such as soil mixed columns or drilled displacement columns (DDCs).

Piling and soil mixing are both well-established forms of ground support and are not further discussed in this paper. DDCs are not as widely known but were ultimately used to improve the strength and stiffness of the embankment foundation. They are described in greater detail below.

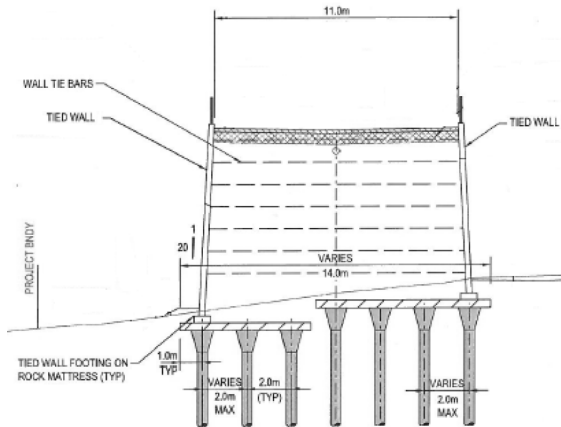


Figure 1. Typical tied-wall arrangement

1.1. Background to construction and design using DDCs

DDCs typically comprise 450 mm diameter columns constructed from unreinforced concrete. They are generally installed with an “Omega” auger using a full-displacement technique. They are often referred to by other names including “Controlled Modulus Columns (CMCs)”, “Concrete Injected Columns (CICs)” and “Drilled Displacement Piles (DDPs)”. However, these terms are considered to be confusing or inappropriate. Firstly, the term CMC is linked to a proprietary product. Secondly, the authors consider the use of the term “pile” to be confusing in an industry where piles are traditionally designed as structural elements and therefore need to satisfy structural design requirements. This typically involves factoring up loads and factoring down design soil strengths. If a ground improvement column was required to satisfy traditional pile design requirements, the comparatively cheap technique would lose its competitive advantage. The authors therefore consider the generic term

“Drilled Displacement Columns”, “DDCs” or “geotechnical elements” to be a more appropriate description when applied to ground improvement.

In saying this, it is also recognised that columns are correctly designed as structural elements on many projects. It is therefore essential that a designer knows when it is appropriate to consider columns as ground improvement, thereby designing them economically as geotechnical elements, or when they should be considered as structural elements (i.e. as piles).

Some of the clearest guidance on this matter is provided by Wong and Muttevel (2012). They suggest that, for the case where the columns act semi-rigidly by sharing load with surrounding soil as a result of (a) column compressibility, (b) yielding of the column toe, and (c) the use of a load-transfer platform (they also postulate that a load transfer platform is not always warranted depending on embankment height and fill quality), they may be treated as geotechnical elements. This is also the authors’ experience.

Treatment of columns as structural elements is more likely to be applicable where (a) column spacing exceeds a maximum of about 2.5 m, or more simply where a foundation support system transitions from high redundancy to low redundancy, i.e. there is potential for the performance of a single column to detrimentally impact the performance of the overall embankment / structure, or (b) bending, shear or tensile stresses are high and overall stability of the embankment may be compromised or lateral displacements cannot be controlled, resulting in the need for steel reinforcement. In either of these cases, adopting a ground improvement approach to design rather than a structural approach should be undertaken with due caution and appropriate engineering judgment.

1.2. Use of DDCs in Australia

The use of DDCs is becoming increasingly popular in Australia due to the ability to install columns quickly, effectively and with minimal generation of spoil material. This is particularly important for soils such as CIS, which have a high acid-sulphate potential and spoil can be prohibitively expensive to dispose of off-site. Contractors are also becoming more proficient at using the technique, particularly testing and implementing quality control.

1.3. Application to current project

As set out previously, DDCs were adopted for this project and used to reinforce the CIS as part of the embankment foundation treatment.

Construction of the embankment in question is now complete. The remainder of this paper describes the subsurface conditions, design of the embankment foundation using DDCs, testing and quality control of the DDCs and post-construction monitoring of the structure.

2. SUBSURFACE CONDITIONS

The subject site falls within a complex geological sequence of Quaternary age deposits overlying Silurian age siltstone of the Melbourne Formation. Paleo channels and buried river terraces within the sequence were encountered. Typically the subsurface conditions at the site comprise up to about 5 m of fill overlying 10 m of CIS, overlying silts and sands to about 40 m depth, overlying siltstone bedrock. The generalized subsurface profile is presented in Table 1.

Table 1. Generalized subsurface profile

Soil Unit	Material Type	Surface RL (m AHD)	Thickness (m)
Fill	Mix of medium dense gravel and firm to stiff clay	2 to 5	1 to 6
Coode Island Silt (CIS)	Soft clay	1 to -2	7 to 13
Quaternary aged Alluvium (QA - Including Fishermans Bend Silt and Moray Street Gravel)	Stiff to very stiff clay at surface becoming hard with depth with sub-units of dense to very dense sand	-8 to -15	18 to 32
Melbourne Formation (MF)	Extremely weathered siltstone	-34 to -42	-

Groundwater was typically encountered between RL 0.5 m and 1.0 m (AHD), or roughly 4.5m below ground surface level.

3. DESIGN

The geotechnical component of design was divided into two components. The first was an assessment of the ground improvement required

to support the embankment. The second was an assessment of the load transfer platform (LTP).

3.1. Parameter Selection

Design of the DDC improved foundation was undertaken using finite element modelling (PLAXIS 2D 2011). Limit equilibrium modelling (SLOPEW) was also used to compliment this analysis.

Initially, the untreated soil stratigraphy and proposed embankment geometry were modelled using the parameters and soil models presented in Table 2.

Table 2. Soil unit parameters adopted for analysis

Soil Unit	γ (kN/m ³)	c' (kPa)	ϕ' (°)	Model Type	E/E ₅₀ (MPa)	μ
Fill	19	5	28	HS	30	-
CIS	16	1	25	HS	1.5-2.5	-
QA	18-20	3-5	28-38	MC	30-80	0.2-0.3
MF	22	50	30	MC	500	0.15

Where:

γ = unit weight of soil

c' = effective cohesion

ϕ' = effective angle of internal friction

HS = hardening soil model

MC = Mohr-Coulomb model

E/E₅₀ = Young's Modulus (MC Model) / Secant Modulus (HS Model)

μ = Poissons Ratio

3.2. Modelling of DDCs

Once the response of the untreated foundation to embankment loading had been modelled, DCCs were then incorporated. The model geometry is presented in Figure 2 along with shaded contours of calculated settlement.

DDCs were modelled in 2D as individual rows of columns using plate elements with an axial stiffness consistent with a cracked column and with little to no bending stiffness. An LTP was modelled above the columns (described later in this paper), followed by the embankment and tied-wall. The effect of varying bending stiffness was investigated by initially using stiffness consistent with the section moment capacity of the unreinforced 450 mm diameter concrete column. This was steadily decreased from 100%, to 30%, to 10% then 1% of the section moment capacity. The effect was significant, with lateral displacement (spreading) of the DDC supported foundation steadily

increasing with reducing bending stiffness. However, as movements were considered acceptable when using 1% of the bending capacity, further assessment of the most appropriate parameters to use in the analysis were not undertaken. This being said, if relying on bending stiffness in a DDC model, an appropriate level of engineering judgment is required. This is discussed in more detail below.

Columns ranging in spacing from 2 m to 2.2 m, installed on a square grid, were ultimately adopted.

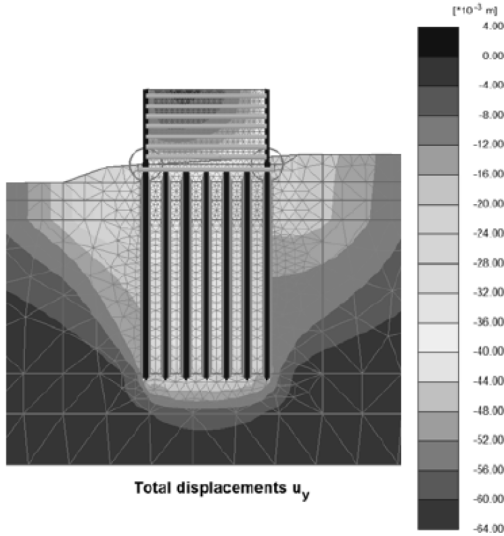


Figure 2. Settlement calculated using the adopted finite element model

The use of plate elements in design did not correctly model the shear resistance that the column cross-section obviously provides, nor was it needed in the analysis because the tied-wall provided most of the resistance to lateral thrust and therefore shear stresses produced in the founding material were quite low.

In the event that column shear resistance does need to be included in a model, it can be accounted for in a 2D model by modelling the plate element at the centre of a strip of frictional material. The strip should be assigned properties (modulus and effective strength parameters) consistent with cracked concrete. This requires engineering judgment, but as a rough guide, for concrete with a compressive strength of 32 MPa, the effective strength parameters of $c' = 100$ kPa and $\phi' = 35$ degrees may serve as a useful starting point for this strip.

The width of the strip can be calculated by equivalent area, using the diameter and spacing of the columns. Care should be taken when undertaking this analysis as strips are often very narrow and numerical errors may result if a suitably fine mesh is not adopted.

Since undertaking the analysis described above, Wong and Muttuvel (2012) have provided additional design guidance in the form of a “new design approach”. Many components of the work presented in this paper are consistent with the approach proposed by Wong and Muttuvel (2012). Subsequent work undertaken by the authors of this paper suggest that the “new design approach” appears reasonable and appropriate although would benefit from further research and verification.

3.3. DDC toe level

In the interest of providing an economical design and to promote load sharing between the columns and surrounding soil, a penetration of 2 m into the stiff to hard clays of the QA unit was modelled. This meant that columns behaved semi-rigidly, rather than with full rigidity as would be expected from a piled alternative. It is worth noting that a conventional pile design utilizing driven concrete precast piles would require piles to be driven roughly 10 m into the QA unit.

As a guide, and assuming most of the embankment load is supported by columns rather than soil, the factor of safety on ultimate bearing capacity is calculated to be between 1.0 and 1.5 but sometimes less than 1.0. This was confirmed in modelling by the generation of localized plastic zones beneath individual columns, indicating that columns were punching into the founding material. This would obviously be a concern for a structure with strict settlement tolerances, such as a building or bridge abutment. However, in this instance the settlement tolerances were not as severe. Also, the parameters used to define the Mohr-Coulomb failure criteria were considered reasonably conservative, along with the adopted soil modulus at founding level.

After investigating the impact of punching on settlement behavior using a parametric study in the finite element model, the state of plastic equilibrium developed at the toe of the columns was considered to be acceptable. Obviously, design using this approach relies on appropriate engineering judgment and review.

3.4. Calculated Settlements

The results of finite element modelling indicated that total settlement of the embankment surface would be in the range of 50 mm to 70 mm with up to 30 mm settlement at DDC toe level. Post-construction settlements were expected to be minimal, that is, the majority of settlement was calculated to occur as the embankment was being constructed.

3.5. Stability Analysis

As a final check of the design, slope stability analysis of the embankment was performed using a limit equilibrium approach. Effective stress parameters were adopted for this analysis and a lateral shear resistance/force was applied to the model at the location of each row of DCCs. Shear resistance was calculated by assuming less than half the embankment load (normal force) was supported by the columns and the column material had a friction angle of roughly 35 degrees.

Engineering judgment must again be exercised appropriately in this process. If the majority of the embankment load is supported by the columns then it follows that the surrounding soil supports a relatively small load. Using a limit equilibrium approach, the full-height embankment cannot then be modelled in conjunction with columns that support the majority of the embankment load without some form of correction or strength reduction being applied to the model. Nor can a bulk strength approach (which models the columns and soil as a single unit with strength properties proportional to the strength and area supported by both) be used. In each case, the shear resistance along the plane of failure would typically be overestimated, along with the factor of safety against global instability.

For the subject embankment, the assessment of stability was less critical due to the support provided by the tied walls. Even so, a correction was applied to the analysis by assuming a small normal load in the columns and adopting conservative effective strength parameters for the cracked concrete.

To model global stability more accurately, finite element approaches that model DDCs as individual geotechnical elements (incorporating a strip of surrounding frictional material) are considered the most theoretically robust, albeit more time consuming.

The discussion above, which highlights some of the pitfalls of limit equilibrium approaches, may provide a reason for the differences between limit equilibrium and finite element approaches reported by Wong and Muttevel (2012) and others.

3.6. Load Transfer Platform (LTP)

An LTP is typically designed to transfer load from the embankment more evenly to the semi-rigid or rigid elements supporting it. It generally comprises granular material up to about 1 m thick, with a maximum particle size of up to about 150 mm in diameter. Geogrid reinforcement is used to provide tensile strength to the LTP and, in particular, support soil located between columns and below the arched zone. Design standards including EBGeo (2010) and BS8006 (2010) provide background and further guidance to the design of the LTP, including thickness and geogrid reinforcement.

Due to the presence of up to 5 m of insitu fill overlying the CIS through which the DDCs would be installed, the authors postulated that much of the soil arching that would typically occur within the LTP would instead occur within the insitu fill underlying the LTP. Further to this, given the thickness of embankment fill overlying the columns, any differential settlement between the column head and surrounding soil would not be realized at the embankment surface some 5 m above this level. This phenomenon was confirmed using 2D and 3D finite-element modelling. It is also addressed by Wong and Muttevel (2012).

Unfortunately, due to an extremely rigorous review process involving numerous consultants and stakeholders, this theory could not be tested. An LTP, designed in accordance with BS8006 (2010) was ultimately adopted. This comprised a geogrid with a biaxial long-term tensile strength of 200 kN/m. A reduction in the thickness of the LTP (from 600 mm to 350 mm) and strength of the geogrid was made by designing DDCs with enlarged heads measuring 1 m x 1 m in plan area and 0.6 m deep.

3.7. Further Research

Partly from opportunity and partly in response to a lack of published information for design of LTPs on sites with thick layers of insitu fill, the authors are currently supervising postgraduate research in this area. The research is being undertaken by Monash University. An instru-

mented embankment has been installed on a foundation supported by DDCs. One of the aims of the research is to investigate the behaviour of an LTP on a site with up to 2 m of fill overlying 15 m of CIS. Twelve months of monitoring data has currently been collected with plans to record data for the next few years.

It is hoped that the research will lead to a better understanding of LTP behaviour, particularly on sites where thick layers of insitu fill overlies the highly compressible material. A photograph of the instrumentation being installed as part of this research is presented in Figure 3.



Figure 3. Instrumented embankment footprint as part of postgraduate research aimed at better understanding LTP behavior over DDCs

4. CONSTRUCTION, TESTING AND QUALITY CONTROL

Roughly 600 DDCs were installed as part of strengthening the embankment footprint. The aim of testing was to ensure that each and every column performed as it was designed. This involved testing of pre-production columns (trial columns), provision of an installation specification and geotechnical review of electronic rig data from each and every DDC installed. The program of testing and monitoring adopted is described in the following sections.

4.1. Pre-production testing (Trial DDCs)

The aims of pre-production testing on trial DDCs were to confirm that each rig could construct columns as per the design, that the methodology was repeatable and that columns demonstrated an appropriate load-settlement response.

Prior to design, a series of cone penetration tests (CPTs) and boreholes were undertaken across the site. These were then used to test the accuracy of the rig instrumentation.

Two trial columns were installed for each rig used on site (six in total). For each trial column, the rig was positioned over a previously completed CPT or borehole and the column was drilled. An engineer monitored the rig instrumentation (mainly torque) and confirmed that the instrumentation was sensitive enough to detect the changes in stratigraphy identified in the CPT and critically, that the DDC founding layer could be identified so that a minimum 2 m penetration could be confirmed.

An example of the rig instrumentation data is presented in Figure 4, where fill (higher torque) is observed in the upper 5 m to 6 m, underlain by CIS (lower torque). The QA unit is encountered at about 19 m depth, as inferred from a spike in torque and comparison to CPT data at a similar depth.

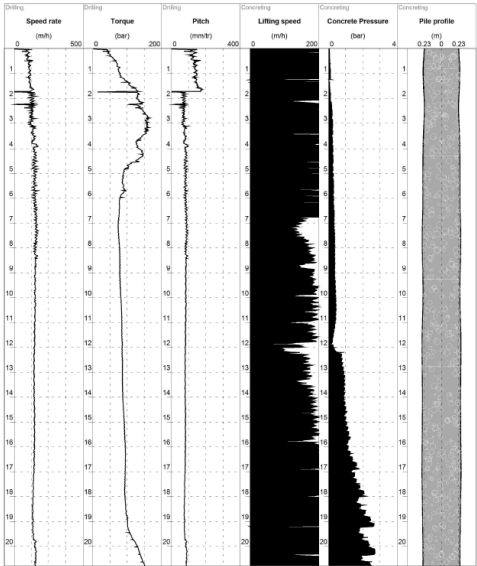


Figure 4. Rig instrumentation data obtained from installation of a DDC

Once it was shown that rigs could detect the DDC founding layer and confirm a minimum

penetration of 2 m, proof load testing of the trial columns was undertaken to confirm an acceptable load-settlement response at this minimum penetration. Proof load testing comprised Pile Driving Analyser (PDA) and Case Pile Wave Analysis Program (CAPWAP) analysis. This required reinforcing the column and building up the head so that PDA gauges could be attached aboveground. The column then needed to cure for at least one week to achieve the required test strength. This process added significant cost to testing. The end result was that fewer tests were undertaken than for conventional piling but a greater reliance was placed on rig instrumentation data and site supervision.

A photograph of the built-up head of a DDC within a test frame (awaiting PDA testing) is presented in Figure 5.



Figure 5. Built-up head of DDC in test frame awaiting PDA testing

For each trial column, the PDA test results indicated the section of column shaft (and base) located below the CIS was capable of supporting a load of at least 700 kN (maximum working load calculated using finite element methods) at a displacement of no greater than 5 mm. A typical load-settlement response inferred from this testing is presented in Figure 6.

When group effects were accounted for, the potential embankment settlement inferred from the PDA results was calculated to range between 30 mm and 50 mm, which was less than

the settlement calculated using finite element modelling. The results of testing were therefore considered to validate the design and provide confirmation that the rigs were capable of installing columns that met the design intent.

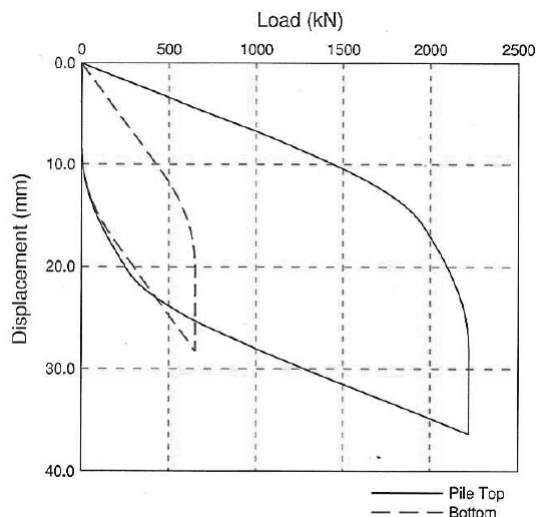


Figure 6. Typical load-settlement response inferred from PDA test

The size and power of each rig utilised on site was different, as was their instrumentation. The more powerful rigs were generally observed to have greater difficulty detecting changes in soil stratigraphy and stiffness, possibly due to higher hydraulic pressures required to power the drill stem. The result was that these rigs typically needed to penetrate the QA unit by a greater amount (up to 5 m rather than 2 m) to register an observable increase in torque.

One of the rigs that was set up to measure crowd (or down pressure) on the drill stem had greater success in detecting the founding layer and constructing shorter and therefore more economical DDCs. The conclusion the authors drew from this exercise was that all DDC rigs should be set up to measure drill crowd.

4.2. Production DDCs

As part of installing production DDCs, the following was generally undertaken:

- A work method statement was provided by the contractor to the design engineer for approval prior to commencing.
- Columns were installed on a “hit 1 miss 1” basis with columns installed no closer than about 7D (where D is the column diameter)

in a 24 hour period. This distance was based on the results of inclinometer testing undertaken near driven precast piles and DDCs as part of another component of ongoing research, and observations of concrete heave from adjacent wet DDCs that suggested squeezing of the column cross-section occurred at closer spacing.

- The drill stem was not to be lifted at any stage during the drilling process to avoid necking of columns.
- The concrete pumps were not to be shut-off until the base of the drill stem was above base of enlarged head level to avoid necking or contamination of the column shaft.
- The base of the enlarged head had to be cleaned and then the enlarged head poured while the shaft concrete was still wet.

In addition to this, the contractor provided the design engineers with the following information within 48 hours of each DDC being installed:

- i. DDC name, date and grid reference or identification
- ii. Penetration rate vs. depth
- iii. Torque vs. depth
- iv. Crowd vs. depth
- v. Pitch vs. depth
- vi. Lifting speed during concreting vs. depth
- vii. Concrete volume vs. depth
- viii. Total depth and total volume of concrete injected, including concrete dockets showing volume of concrete delivered to site

This information was reviewed for each and every column installed.

An allowance was also made for geotechnical engineers to make regular visits to observe DDC installation throughout the duration of the project. This supervisory role was considered critical to ensuring consistency during the construction period.

Where defects or discrepancies were observed, such as column necking, insufficient toe penetration or conflicting information regarding the volume of concrete installed or delivered to site, additional measures were implemented. These ranged from Pile Integrity Testing, used to investigate whether a reduction in column cross-section had occurred, or more significant measures such as installation of replacement columns. The latter was not a simple task as the impact of a localised increased in stiffness needed to be assessed numerically before additional columns could be installed.

4.3. Outcome of quality control

In the authors' opinion, the adopted approach of (a) PDA testing trial columns installed at locations with known stratigraphy, (b) reviewing rig instrumentation data for each and every CMC installed, and (c) regular site supervision throughout construction, provided a robust approach to quality control. A photograph of the completed embankment footprint prior to construction of the LTP is presented in Figure 7. The enlarged heads of the DDC are evident.



Figure 7. Completed embankment footprint prior to placement of LTP

5. SETTLEMENT MONITORING

One end of the embankment supported on DDCs transitions into an untreated foundation which coincides with the edge of the CIS deposit. A roughly 15 m wide transition zone comprising DDCs with steadily decreasing length (but same spacing) was adopted to reduce differential settlement across the transition. Although not the subject of this paper, the transition zone provides useful settlement data for comparison to the DDC treated zone.

The section of untreated foundation is underlain by CIS of 3 m maximum thickness. This area was not treated with stiffening elements but had been surcharged by a large, monitored stockpile for several months. Estimates of total settlement in this zone, as a result

of embankment construction, were in the order of 100 mm. Approximately half of this was expected to occur during construction with the remainder occurring in the following six to twelve months.

5.1. Construction Phase Settlement

Settlement was not monitored as the embankment was constructed. Monitoring commenced immediately after the last layers of fill were placed. Therefore it is not possible to confirm the amount of settlement that occurred during construction, except that it was likely to be significantly less than 100 mm based on the level of wall panels compared to the design level.

5.2. Post-construction settlement

As noted above, post-construction monitoring commenced immediately after construction was completed. The results of this monitoring is presented in Figure 8, which shows the results of seven (7) monitoring points located at various points along the length of the tied-walls.

With reference to Figure 8, points 100, 300 and 500 are positioned above the section of DDC improved embankment footprint. Not surprisingly, post-construction settlements measured in the 6 months following construction are a maximum of 5 mm and do not show signs of ongoing creep. This is consistent with design.

Points 600 and 900 are located at either end of the transition zone (point 600 being closest to the full-depth DCCs). They show maximum post-construction settlements of 18 mm and 28 mm respectively. The rate of settlement appears to be slowing but is ongoing.

Points 1100 and 1200 are located above the section of untreated embankment footprint and show maximum settlements of 26 mm and 28 mm, respectively. The rate of settlement appears to be slowing but some ongoing settlement is expected, which is consistent with design.

On the basis of this data, it is apparent that DDCs are very effective in reducing post-construction settlement when used in the manner described in this paper.

6. CONCLUSIONS

Using a case study of a tied-wall embankment founded on a significant thickness of soft clay, DDCs are shown to provide an effective and economic option for reinforcing the foundation. Importantly, the technique can be used to reduce post-construction settlements to acceptable limits.

Design using finite element methods can be used to reliably model DDC behavior by considering columns as geotechnical elements (surrounded by soil strips) with very low bending stiffness. The approach requires considerable engineering judgment and would benefit from further research and modelling, some of which is currently being undertaken. Design using limit equilibrium approaches should be treated with caution.

A method for controlling the quality of DDCs is discussed, which involves PDA testing of trial columns installed over the location of known CPTs or boreholes (undertaken in advance of the trial). Comparison of the rig data, including torque and crowd, to the CPT/borehole data can be used to confirm that the rig can detect changes in stratigraphy and, most importantly, can detect the DDC founding layer.

Due to time and costs constraints associated with building up DDC heads for PDA testing, fewer dynamic tests are undertaken on DDCs than might be undertaken on a conventional pile-supported embankment. This can be supplemented by reviewing the rig instrumentation data for each and every DDC installed and by the design engineer undertaking regular site visits throughout the construction phase to ensure consistency with design.

Further research is currently being undertaken that investigates the role of the LTP in the overall performance of a DDC supported embankment. In particular, the research looks at the impact of insitu fill overlying the highly compressible soil unit.

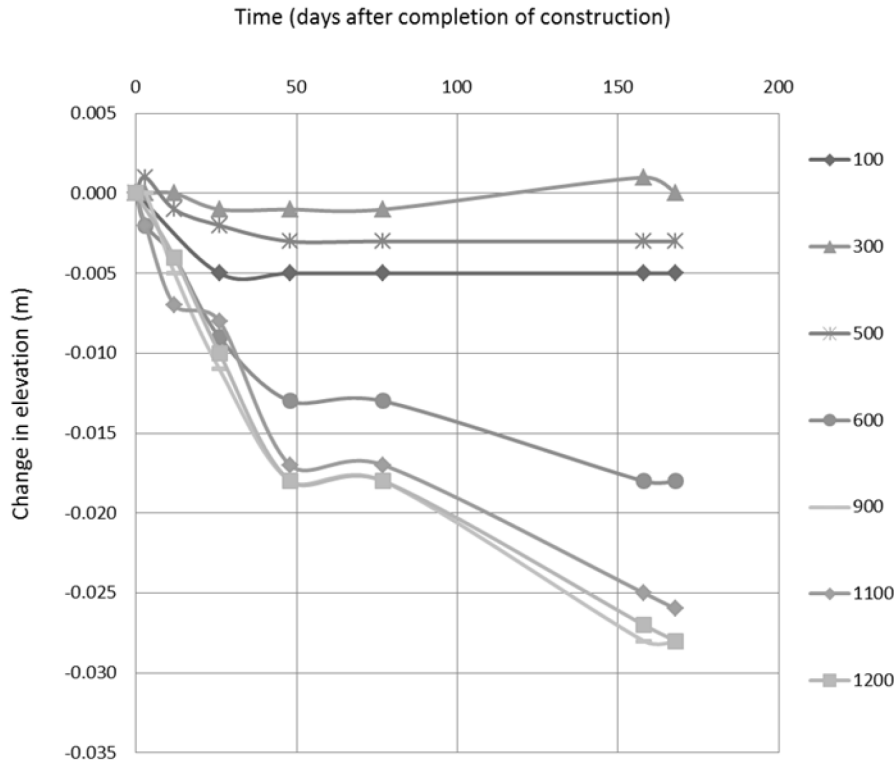


Figure 8. Post-construction settlement of the tied-all at various locations

7. REFERENCES

- British Standard, BS8006-1, 2010. Code of practice for strengthened/reinforced soils and other fills.
- Day R.A. and Woods P. – Verification of consolidation parameters of a near-normally consolidated clay by back-analysis of an instrumented, wick-drained reclamation. *Common Ground Proceedings 10th Australia New Zealand Conference on Geomechanics* Brisbane, Australia.
- EBGEO, 2010. Recommendations for design and analysis of earth structures using geosynthetic reinforcements – *EBGEO*. German Geotechnical Society. Translated English version of 2nd edition of EBGEO. Ernst & Sohn.
- Ervin, M.C. 1992. Engineering properties of Quaternary aged sediments of the Yarra Delta. *Engineering Geology of Melbourne*, Olds and Seddon (editors).
- Neilson, J.L. 1992. Geology of the Yarra Delta. *Engineering Geology of Melbourne*, Olds and Seddon (editors).
- Srithar, S.T. 2010. Settlement characteristics of Coode Island Silt. *Australian Geomechanics*, Vol. 45 no. 1 p. 55-64
- Wong, P.K. and Muttuvel, T. 2012. Economic Design of Controlled Modulus Columns for Ground Improvement. *Proceedings of 11th Australian and New Zealand Conference on Geomechanics (ANZ2012)*, Melbourne, Australia.

Numerical analysis and verification of the soil-structure-interaction in the course of large construction projects in inner cities

Rolf Katzenbach, Steffen Leppla

Technische Universität Darmstadt, Institute and Laboratory of Geotechnics, Germany

Wolfgang Krajewski

University of Applied Sciences Darmstadt, Germany

ABSTRACT: The analysis of the soil-structure-interaction is a very important part during all stages of planning, design and construction. Large urban construction projects create an impact not only on neighbouring structures but also on existing, sensitive underground structures, like metro and street tunnels. But not only new constructions have an effect on existing structures. Deconstruction projects may cause enormous displacements as well. For the analysis of the soil-structure-interaction in most cases numerical methods are necessary. For verification of the numerical simulations geodetic and geotechnical measurements according to the observational method have to be carried out. An outstanding large urban construction project on existing underground structures of the metro of Frankfurt am Main, Germany, is presented in this paper.

1. INTRODUCTION

Large construction projects with a distinct soil-structure-interaction and a distinct influence on neighbouring structures are categorized by the Geotechnical Category GC 3 according to the technical regulations and standards. The Geotechnical Category GC 3 is the category for construction projects with the highest complexity factor (CEN 2008a, 2008b).

A current large project is under construction in the historic city centre of Frankfurt am Main, Germany.

Due to the urban development the area between the historic church Kaiserdom and the city hall (Römer) is under construction. To get space for new structures the Municipal Technical Administration, built in the 1970s, was deconstructed down to the basement.

The Municipal Technical Administration and the underground parking cover directly the metro station Dom/Römer and the metro tunnels. Due to this fact the Municipal Technical Administration and the underground parking transfer the loads directly into the underground structures. A complex deformation and float problematic occurs caused by the difficult soil and groundwater situation and the unloading due to the deconstruction. In addition and for verification of the comprehensive analysis regarding stability and serviceability of the remaining structures a geodetic and geotech-

nical monitoring program is installed. One main aspect is the integrity of the sealing systems of the basements and the tunnel structures.

2. EXISTING STRUCTURES, SOIL AND GROUNDWATER CONDITIONS

The historic center of Frankfurt am Main between the historic church Kaiserdom and the city hall (Römer) was totally destroyed in World War II. In this area the Municipal Technical Administration was built at the beginning of the 1970s (Gravert & Buch 1974). The Municipal Technical Administration was a high-rise building complex consisting of three towers with up to 14 storeys, a connecting structure and an underground parking with two sublevels. The project area is shown in Figure 1 and 2.

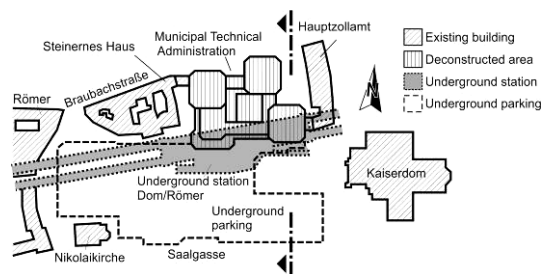


Figure 1. Overview of the project area.

The two levels of the underground station, the tunnels and the superstructures of the high-rise building have been constructed simultaneously. The underground station has been constructed in an open excavation pit. The eastern tunnels have been constructed by a tunnel boring machine (TBM). The western tunnels have been constructed by using the shotcrete method. It was the first time in the world that the shotcrete method was used in an inner city under existing structures (Laufer 2010).

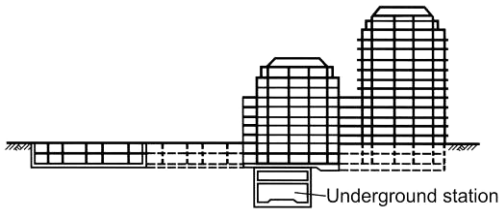


Figure 2. Cross section of Figure 1.

The sealing of the sublevels and of the underground structures consists of several bitumen layers and copper sheets, located on the outside of the reinforced concrete structures. Figure 3 shows the sealing detail of the underground structures and the sublevels of the Municipal Technical Administration. It has to be guaranteed that the sealing of the structures is not damaged during the deconstruction of the Municipal Technical Administration and the construction of the new structures.

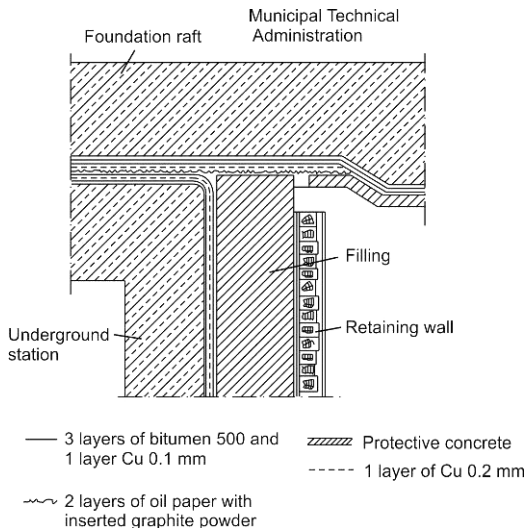


Figure 3. Detail of the sealing system.

The soil and groundwater conditions at the project area are as follows:

- fillings down to a depth of 8 m
- quaternary sands and gravel down to a depth of 15 m
- tertiary Frankfurt Clay down to a depth of 30 m
- Frankfurt Limestone

The sublevels of the Municipal Technical Administration, the underground parking, the underground station and the tunnels are below the groundwater level. The groundwater level is strongly influence by the river Main, which is about 180 m south of the project area.

3. NUMERICAL ANALYSIS OF THE DEFORMATION

For the evaluation of the effect of the deconstruction of the Municipal Technical Administration and the construction of the new structures the uplift and the settlements have to be predicted. For the prediction three dimensional numerical simulations were used.

For the correct prediction of the deformations the complex geometries and the stress and time dependent deformation behaviour of the Frankfurt Clay (Breth & Stroh 1974, Reul & Krajewski 2010, Katzenbach et al. 2011a, Kolembach 2012, Katzenbach & Leppla 2013a) have to be considered in the numerical models.

In the last decades the development of numerical models focused on the simulation of the stress and deformation behaviour of the soil and the structures, e.g. foundations systems, retaining systems or tunnels. The experiences from different projects show, that the numerical analysis using the Hardening-Soil-Model (HS-Model) produce true results. The HS-Model is an elasto-plastic constitutive equation with an isotropic double hardening. The elastic sphere with stress dependent, non-linear elastic behaviour is covered by two yield surfaces. In the principle stress sphere these two yield surfaces are a cone, closed by a cap (Figure 4). The sphere of the permitted stress is defined by the the limit condition of Mohr-Coulomb. If the stress level reaches one of the yield surfaces elastic and plastic deformations occur. The yield surface is expanding and causes a plastic solidification. The direction of the plastic deformation is defined by a flow rule.

The numerical material parameters for the Frankfurt clay are shown in Table 1. Generally these parameters lead to good results.

Regarding the current project it is important to consider the difference between the construction of new structures and the deconstruction of existing structures. The stress path is extremely different. The stress path of the described project is influenced by the primary loading, the unloading and the reloading.

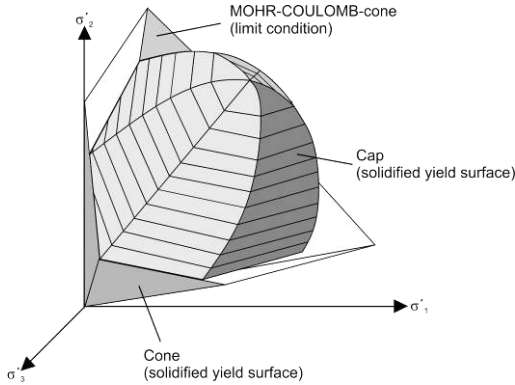


Figure 4. Yield surface of the Hardening-Soil-Model.

Table 1. Parameters of the HS-Model of Frankfurt Clay.

Angle of friction	$\varphi' [^\circ]$	20
Cohesion	$c' [\text{kN/m}^2]$	20
Angle of dilatancy	$\psi [^\circ]$	0
Triaxial stiffness of strain	$E_{50} [\text{MN/m}^2]$	35
Elastic modulus	$E_{\text{oed}} [\text{MN/m}^2]$	35
Triaxial stiffness of release	$E_{\text{ur}} [\text{MN/m}^2]$	105
Poisson's ratio	$\nu [-]$	0.2
Coefficient for stress level	$m [-]$	1.0

For the analysis of the deformation the designing geotechnical consulting office used the Finite-Element-System PLAXIS for the numerical simulations. According to the building permission and the 4-eye-principle the analysis were checked by an independent geotechnical expert with own numerical simulations. Figure 5 shows the three dimensional numerical model including the main parts of the foundation and underground structures. The walls and the columns were modeled with special plane

elements. The raft and slabs were modeled with continuum elements. All construction parts consisting of reinforced concrete are modeled with elastic deformation behaviour. The expansion gaps between the tunnel blocks were modeled as well.

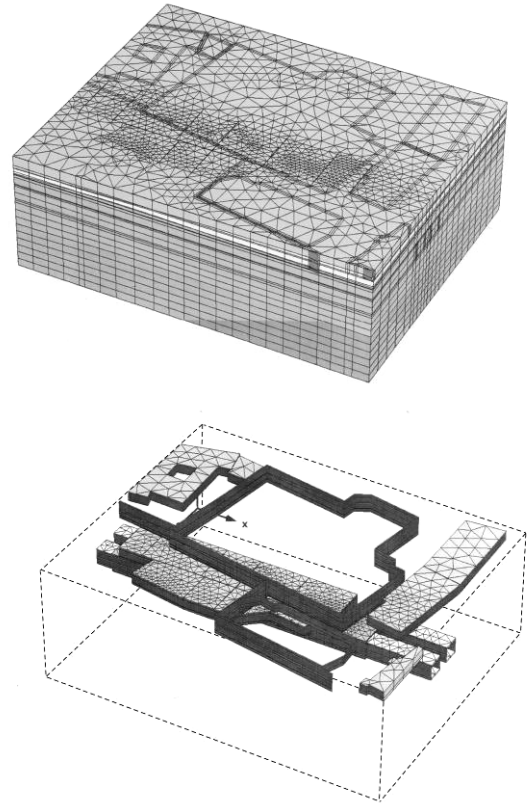


Figure 5. 3D-numerical system.

The results of the three dimensional simulations of the first analyzing phase were an uplift of the remaining structures up to 3 cm and a tilting of about 1:2,500, as displayed in Figure 6. According to the observational method a geodetic and geotechnical measurement program was installed. In the first phases of deconstruction these measurements showed, that the uplift will be much bigger than the results of the first analyzing phase. The maximum of the uplift did not occur in the centre of the project area, but in the northern part (Figure 6).

The investigations show that the realistic modeling of the stiffness of the structures is very important. The walls in the underground structures and in the remaining sublevels avoid deflexions of the foundation rafts. However, in the present case the three dimensional model

requires strong simplifications in modelling the remaining building structures. By these simplifications the flexural stiffness of the structures could only be reproduced unsatisfactorily.

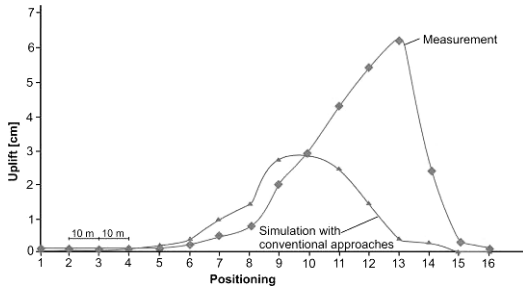


Figure 6. Comparison of measured and calculated uplift (3-D calculation, cross section of Figures 1 and 2, material parameters of Table 1).

For a better agreement between the results of practice and analytical model additional two dimensional simulations have been carried out, where the stiffness of the structures could be considered more realistically. A typical result of the Finite-Element-analysis is given in Figure 7. The biggest uplift deformations amount is more than 5 cm. That is a difference of more than 70 % compared to the results of the three-dimensional calculations (Figure 6). The uneven deformation curve, which is measured in reality can be reproduced qualitatively. However the total deformations are still too small compared to the measurements of more than 6 cm (Figure 6).

The investigations lead to the knowledge that the material parameters in Table 1 do not lead to correct results, if unloading effects dominate the present geotechnical problem. Moreover it can be stated, that the proved material sets allow satisfactory predictions for example foundation problems or construction pits. In the case that the effects of the deconstruction of high or heavy buildings are to comprehend additional reflections are necessary. In advance to chapter 4 it has to be pointed out that the uplift due to unloading is nearly the same as the former settlement due to loading. For this reason, the numerical analysis of the uplift of Frankfurt Clay requires the same approach of stiffness as for analysis of settlements of new structures. The common distinction for the Young's Modulus for loading and unloading like shown in Table 1 is not useful. This awareness is qualitative and is based on the new experiences. Further research is needed for the development of a new constitutive law under consideration of the stress path including preloading and unloading and the overconsolidation of the Frankfurt Clay.

Additional to the analysis of the deformations analysis for buoyancy were carried out. The analysis showed that the safety against buoyancy of the sublevels is not given, when the Municipal Technical Administration is totally deconstructed. For this case a temporary loading was installed and an emergency plan was developed.

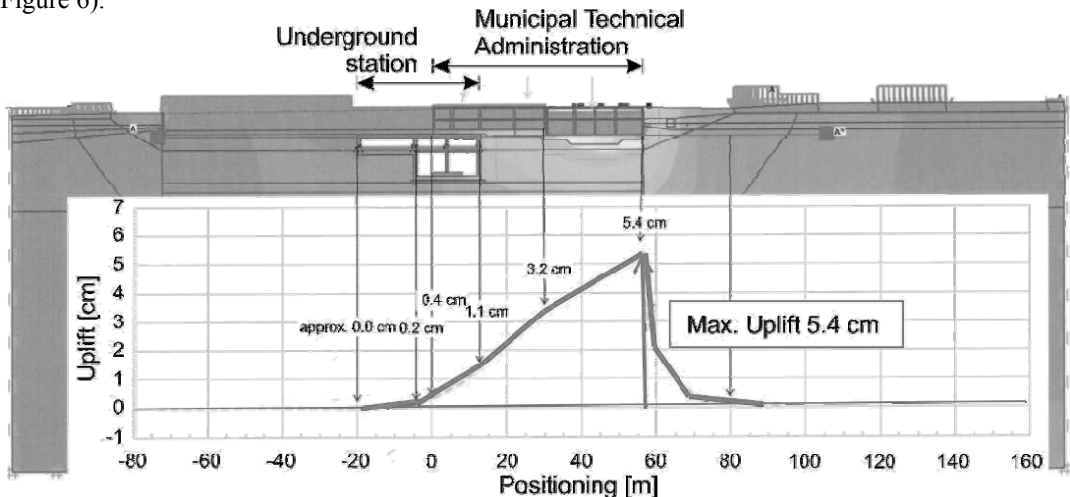


Figure 7. Calculated uplift deformations (2-D-FEM calculation, cross section of Figures 1 and 2, material parameters of Table 1).

4. GEODETIC MEASUREMENTS

Regarding the classification of the project into the Geotechnical Category GC 3 and the principles of the observational method the developed geodetic measurement program consists of 580 measuring points:

- 220 at the surface of the project area around the Municipal Technical Administration
- 110 in the underground parking and the sublevels
- 30 in the underground station
- 220 in the metro tunnels

The observation area at the surface is about 50 m around the Municipal Technical Administration. The observation area in the metro tunnels is about 80 m from the Municipal Technical Administration. During the deconstruction and the consolidation time the time interval of the measurements is two weeks. The time interval is adapted to the measured deformation rates. Up to now it was between one week and 8 weeks depending on the project phase.

To guarantee the water tightness of the metro tunnels and of the underground station the STUVAtec (Cologne, Germany) was involved.

For example of the occurred deformation the measurement results of decisive geodetic points are presented. Figure 8 shows the position of these points.

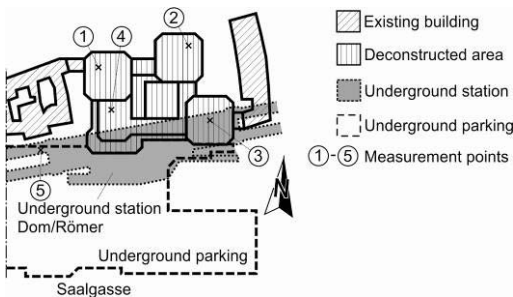


Figure 8. Position of selected measurement points.

The measuring points 1 to 4 are in the sublevels of the Municipal Technical Administration located in the area of the high-rise towers (measuring points 1 to 3) and in the area of the connecting component (measuring point 4). The measuring point 5 is at the transition of the underground station to the north-western metro tunnel. The reduction of the floors of the

Municipal Technical Administration and the measured deformations related to this deconstruction are shown in Figure 9.

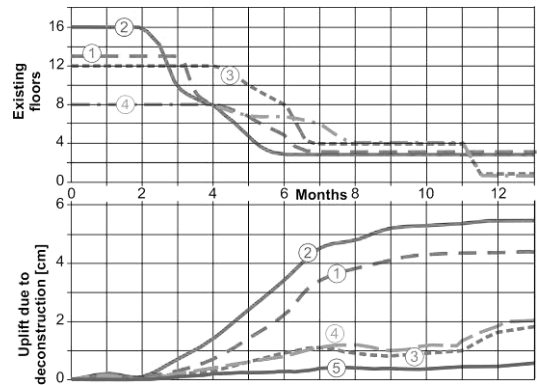


Figure 9. Measured uplift of points 1 to 5.

At the measuring points 1 to 4 an uplift between 1 cm and 5 cm was detected in the deconstruction time (March to December 2010).

After the deconstruction down to the sublevels in December 2010, the modification of the sublevels began. In that phase the loads only were changed insignificantly. The uplift of the whole project area and the neighborhood in October 2012 is drawn in Figure 10.

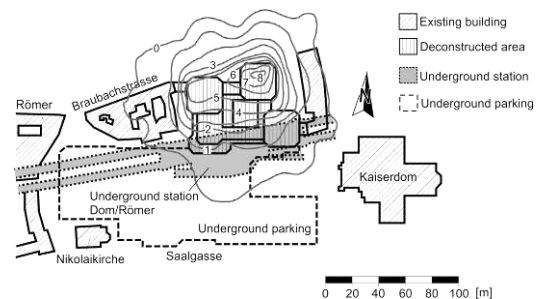


Figure 10. Measured uplift of the whole project area [cm].

The uplift caused by the reduced stress level and the time related deformation behaviour of the Frankfurt Clay is continuously raising due to the consolidation process. A maximum uplift of 8.5 cm was measured in the area where the most floors were deconstructed. The maximum uplift of the underground station and the metro tunnels is less than 2 cm. The uplifts fade down related to the distance very quickly. So no dangerous deformations of the neighbourhood were detected.

Since October 2012 the loads were not changed. The further construction of the new structures will start in 2014 when the building permission is finished.

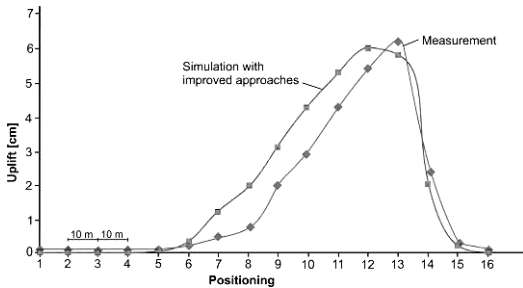


Figure 11. Comparison of measured and calculated uplift (2-D-FEM calculation, cross section of Figures 1 and 2, material parameters of Table 1).

Under consideration of the stiffness of the structures and an improved approach for the deformation behaviour of the Frankfurt Clay the numerical simulations show a good accordance to the measurement results. For example the calculated and measured deformations of the cross section of the Figures 1 and 2 are drawn in Figure 11. The comparison shows that for difficult analysis of the soil-structure-interaction the stiffness of the structures and of the soil have to be modeled close to reality.

5. CONCLUSIONS

The presented soil deformation of the current large construction project show, that the uplift due to the deconstruction are nearly as big as the settlements occurred due to the construction. The uplifts cannot be avoided.

To guarantee the stability and the serviceability of large construction projects in difficult soil and groundwater conditions in the area of underground structures the following aspects have to be considered:

- For the precise determination of the soil deformation comprehensive numerical analysis covering the non-linear deformation behaviour are necessary (Wörner & Pfeiffer 1998).
- Regarding the observational method a geodetic and geotechnical measurement program has to be developed and installed (Katzenbach et al 2010 and 2013b, Paul 1998, Ulitsky 2003).

- For indemnification of the 4-eye-principle an independent, publicly certified geotechnical expert has to be involved in an early planning stage (Fuchs & Haugwitz 2009, Katzenbach et al. 2011b).
- For extreme situations an emergency plan has to be developed considering the stability and the serviceability.
- For the correct simulation of the time dependent deformation behaviour of soils due to reduced stress levels further research is necessary. The verification of constitutive laws describing the time dependent deformation behaviour due to reduced stress levels has to consider measurement data of real construction projects or load tests.

6. REFERENCES

- Breth, H.; Stroh, D. 1974. Das Verformungsverhalten des Frankfurter Tons beim Aushub einer tiefen Baugrube und bei anschließender Wiederbelastung durch ein Hochhaus. *13. Baugrundtagung der Deutschen Gesellschaft für Geotechnik in Frankfurt am Main*, 10.-12. September, Germany, 51.70.
- CEN European Committee of Standardisation 2008a. *Eurocode 7: Geotechnical design – Part 1: General rules*.
- CEN European Committee of Standardisation 2008b. *Eurocode 7: Geotechnical design – Part 2: Ground investigation and testing*.
- Fuchs, B.; Haugwitz, G. 2009. Duty to check and to report problems: Practical geotechnical experiences. *Darmstadt Geotechnics No. 17*, Technische Universität Darmstadt, Institute and Laboratory of Geotechnics, Germany, 165-181.
- Gravert, F.W.; Buch, G. 1974. Probleme bei der Gründung der Dom-Römerberg-Bebauung in Frankfurt am Main. *Bautechnik 51*, Heft 2, Ernst & Sohn Verlag, Berlin, 52-58.
- Katzenbach, R.; Bachmann, G.; Leppla, S.; Ramm, H. 2010. Chances and limitations of the observational method in geotechnical monitoring. *14th Danube-European Conference on Geotechnical Engineering*, 2.-4. June, Bratislava, Slovakia, 13 p.
- Katzenbach, R.; Leppla, S.; Seip, M. 2011a. Das Verformungsverhalten des Frankfurter Tons infolge Baugrundentlastung. *Bauingenieur*, Band 86, Heft 5/2011, Springer VDI Verlag, Düsseldorf, Germany, 233-240.
- Katzenbach, R.; Leppla, S.; Weidle, A.; Werner, A. 2011b. Das Vier-Augen-Prinzip in der Geotechnik: Der Prüfsachverständige für Erd- und

- Grundbau. *Geotechnik-Kolloquium anlässlich 60. Geburtstag von Prof. Dr.-Ing. Dietmar Placzek*, Universität Duisburg-Essen, 26. May, Essen, Germany, 255-267.
- Katzenbach, R.; Leppla, S. 2013a. Deformation behaviour of clay due to unloading and the consequences on construction projects in inner cities. *18th Conference of the International Society for Soil Mechanics and Geotechnical Engineering*, 2.-6. September, Paris, France, Vol. 3, 2023-2026.
- Katzenbach, R.; Vogler, M.; Kurze, S. 2013b. Lösungen zur Akzeptanz großer Infrastrukturprojekte. *Bauingenieur*, Band 88, Heft 9/2013, Springer VDI Verlag, Düsseldorf, Germany, 358-367.
- Kolembach, K. 2012. Time dependent deformation behaviour of Frankfurt Clay and the relevance on large construction projects in urban areas. *International Conference „Topical Issues of Rational Use of Natural Resources“*, 24.-27. April, St. Petersburg State Mining University, Russia, 96-98.
- Lauffner, H. 2010. The development of the NATM – a historical review. *Geomechanics and Tunneling* 3, Heft 6, Ernst & Sohn Verlag, Berlin, 763-772.
- Paul, T. 1998. Soil-structure-interaction in urban environments: some issues for planners. *Darmstadt Geotechnics No. 4, Vol. 2*, Technische Universität Darmstadt, Institute and Laboratory of Geotechnics, Germany, 511-517.
- Reul, O.; Krajewski, W. 2010. Foundation design for the extension of existing high-rise buildings. *International conference on geotechnical challenges in megacities*, 7.-10. June, Moscow, Russia, Vol. 2, 446-453.
- Ulitsky, V.M. 2003. Geotechnical Challenges in Reconstruction of Historical Cities. *International Geotechnical Conference “Reconstruction of Historical Cities and Geotechnical Engineering”*, St. Petersburg, Vol. 1, 13-29.
- Wörner, J.-D.; Pfeiffer, R. 1998. Importance of the development of stiffness and load during the construction period for the soil-structure-interaction. *Darmstadt Geotechnics No. 4, Vol. 2*, Technische Universität Darmstadt, Institute and Laboratory of Geotechnics, Germany, 383-396.

Effects of deep excavations on adjacent foundations

C.F. Leung

National University of Singapore, Singapore

D.E.L. Ong

Swinburne University of Technology Sarawak Campus, Malaysia

ABSTRACT: With rapid development in metropolitan areas, deep excavation and tunnelling are often carried out close to existing buildings or infrastructure. The soil movement due to excavation may cause damages to adjacent foundation, worse for shallow foundations as compared to deep foundations. In this keynote paper, the latest development and understanding of soil-structure interaction involving foundation subject to adjacent excavation are presented; with references to successfully implemented projects or research work based on finite element modelling, centrifuge experiments and field monitoring, observations and interpretations. The novel concept of limiting soil pressure due to excavation stress relief is also presented.

1. INTRODUCTION

With the phenomenal increase in population in urban areas, construction works are now often carried out in close proximity to existing buildings and geotechnical structures. As such, many soil-structure interaction problems exist and examples of such problems include the effects of deep basement or tunnel excavation on foundations of adjacent buildings. Nowadays, the problems have become more complex as new structures are often constructed in grounds consisting of very soft soils within very congested sites as the choices of ‘good’ sites have rapidly diminished in the ever-growing large urban cities.

The soil movements due to nearby excavations may induce additional loading and movement on adjacent foundations. The effect is worse on shallow foundations as compared to piled foundations. In general, when large soil movements are anticipated in the course of excavation, the construction process would be extensively monitored. Despite extensive instrumentation and monitoring, a good number of foundation damages caused by excavation-induced soil movements have been reported, see for example, Poulos (1997) and Ong et al. (2010). Such damages are often due to much thicker soft soil deposits or considerably lower shear strength of soft soil, which are unforeseen and unexpected at the design stage.

Failures often cause significant human, financial and time loss and are also very difficult to remedy. One major design concern is that the behaviour and mechanism of complex soil-structure interaction problems are still not well understood. Very few design methods are currently available to evaluate these problems in practice.

The use of sophisticated finite element computer program would substantially help the design process of such complex soil-structure interaction problems as long as the validity of the soil models, parameters employed and boundary conditions are

justifiable. Alternatively, physical modelling can offer an attractive method to further understand the behaviour and mechanism of complex soil-structure interaction problems. However, the results of conventional laboratory small-scale model tests cannot be extrapolated to prototype scale as the behaviour of soils is stress dependent. The use of centrifuge modelling technique would overcome this shortcoming. In his Rankine Lecture, Schofield (1980) highlighted the useful applications of centrifuge modelling technique to study geotechnical problems.

In this keynote paper, the latest development and understanding of soil-structure interaction caused by adjacent excavation are presented with references to successfully implemented projects or research work based on finite element modelling, centrifuge experiments and field monitoring, observations and interpretations.

The following soil-structure phenomena are addressed in this paper:

- (i) Effects of limiting soil pressure due to excavation
- (ii) Effects of soil-structure interaction adjacent to deep foundations
- (iii) Effects of soil-structure interaction adjacent to shallow foundations
- (iv) Effects of excavation / tunnelling on building damage assessment

2. EFFECTS OF LIMITING SOIL PRESSURE DUE TO EXCAVATION

2.1 Concept of limiting soil pressure

Piles embedded in soils undergoing increasing lateral movements would experience increasing horizontal soil pressures which in turn induces additional loadings. For piled foundations, this

would translate to bending moment and deflection. Horizontal limiting soil pressures are important because they define the maximum magnitude of soil pressures that can effectively act on a pile. Beyond this maximum soil pressure magnitude, there would be no further increase in the induced pile bending moment and deflection. Such scenario is particularly prevalent in piles embedded in soft soils and loose sand.

During design stage, the post-excavation undrained shear strength profiles are not available. In view of this, Leung et al. (2006) back-analyzed P_n values with respect to the pre-excavation undrained shear strength profiles for the three centrifuge tests depicting a case of wall failure thus inducing large lateral soil movement. P_n is defined as the ratio of limiting soil pressure (p_y) to the undrained shear strength (c_u). The development of P_n is shown in Figure 1(b).

As expected, the back-analyzed P_n values are much lower than the theoretical P_n values shown in Figure 1(a), calculated based on the pre-excavation c_u . An envelope of limiting P_n values is hence plotted and indicated by the dash line in Figure 1(b). The maximum back-analyzed P_n value is about 6.

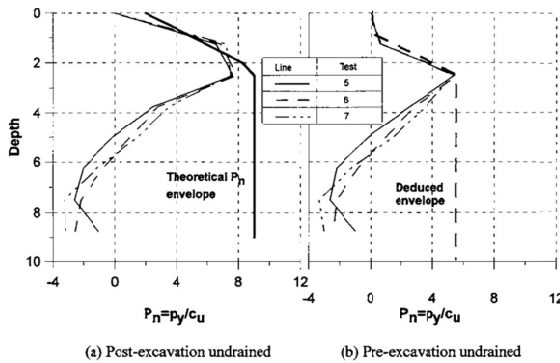


Figure 1: Variation of P_n value with depth using (a) post-excavation and (b) pre-excavation undrained shear strength (Leung et al., 2006)

Figures 1(a) and (b) show that P_n is positive in magnitude above 5 m depth and becomes negative below 5 m depth. This change of sign physically means that above 5 m depth, the soil moves more than the pile while below 5 m depth, the pile moves more than the soil. This can be verified by comparing the free-field soil movement profiles shown in Figures 2(a) against pile deflection profiles shown in Figures 2(b), 3(b) and 4(b). The above finding illustrates that the reduction of P_n from a value of 9 for conventional laterally loaded piles to a lower value of 6 for piles subject to excavation-induced soil movements is attributed to the lateral stress release with a reduction in the undrained shear strength upon excavation.

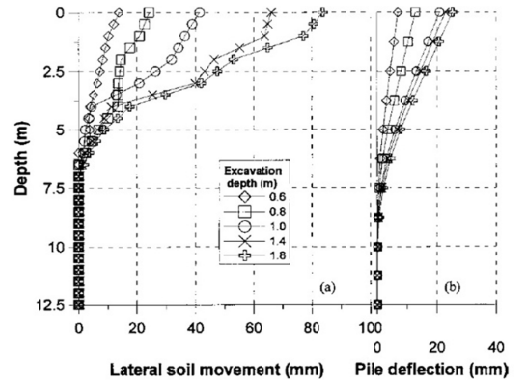


Figure 2: (a) Measured lateral soil movement profile (b) calculated pile deflection profile for Test 5 (Leung et al., 2006)

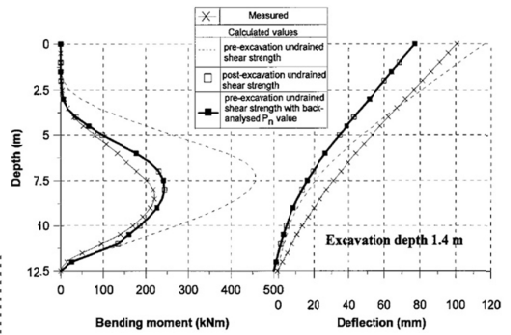


Figure 3: Comparison of measured and calculated pile (a) bending and (b) deflection profiles for Test 6 at excavation depth of 1.4 m (Leung et al., 2006)

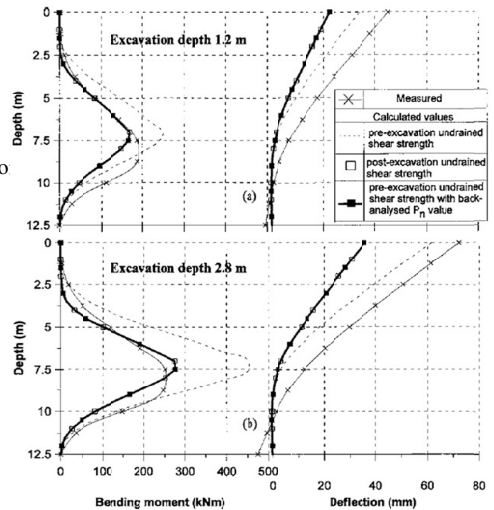


Figure 4: Comparison of measured and calculated pile bending moment and deflection profiles for Test 7 at excavation depth of (a) 1.2 and (b) 2.8 m (Leung et al., 2006)

Although this value of 6 was derived based on back-analysis of the centrifuge results, it may be applicable for situations where the soil has undergone large movement due to stress relief during excavation or landslide. Some evidence of the latter may be seen in the work of Maugeri (1994) and Leung et al. (2006).

2.2 Case Study 1: Centrifuge study in soft clay

Details of a test involving a failed excavation in clay has been reported in Ong et al. (2004). Figure 5 shows the centrifuge model set-up for the study. In this test, much of the retaining wall is embedded in the soft kaolin clay layer. The maximum excavation depth is 1.8 m. The single pile is located 3 m behind the wall. In-flight bar penetrometer tests were performed to quantify the undrained shear strength (c_u) profile of the clay before the test. The shear strength profile shown in Figure 6 reveals that a 2.5 m thick overconsolidated crust exists above the normally consolidated clay.

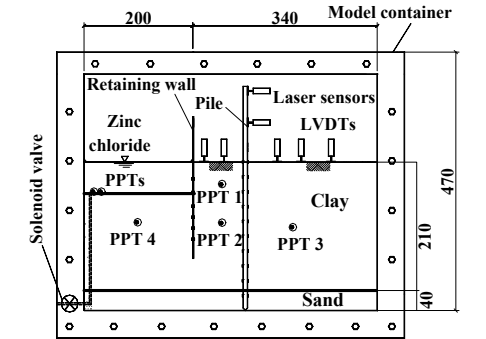


Figure 5. Centrifuge model set-up (all dimensions in mm) (Ong et al., 2003)

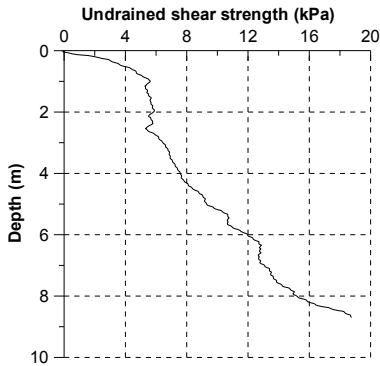


Figure 6. Undrained shear strength profile of clay (Ong et al., 2004)

Figure 7 shows the wall deflection profiles during and after excavation. The tilted wall causes the clay behind the wall to settle and the ground settlement continues to increase over time after the completion

of excavation, as shown in Figure 8. The long term time dependent wall deflection and settlement troughs have been further investigated in detail by Ong et al. (2003, 2004).

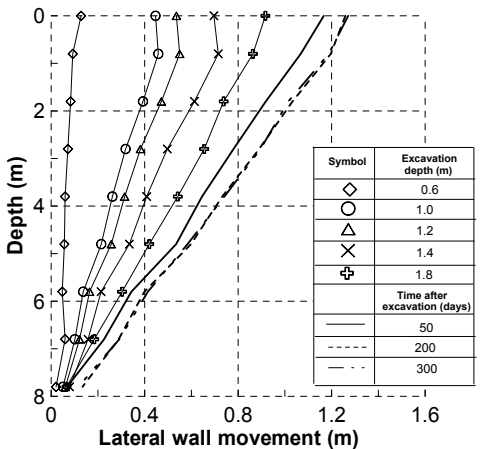


Figure 7. Wall deflection profiles during and after excavation (Ong et al., 2004)

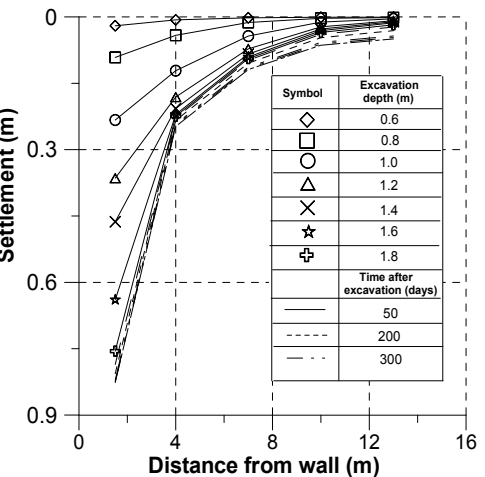


Figure 8. Ground settlement profiles during and after excavation (Ong et al., 2004)

Figure 9 shows that the maximum induced pile bending moment is located at 8.75 m below the ground level. The induced bending moment initially increases with increase in excavation depth. A maximum value of 236 kNm is recorded at an excavation depth of 1.2 m. The bending moment then decreases with increase in excavation depth. At the maximum excavation depth of 1.8 m, the bending moment reduces to 185.8 kNm. Thereafter, the bending moment profile is found to decrease further over time.

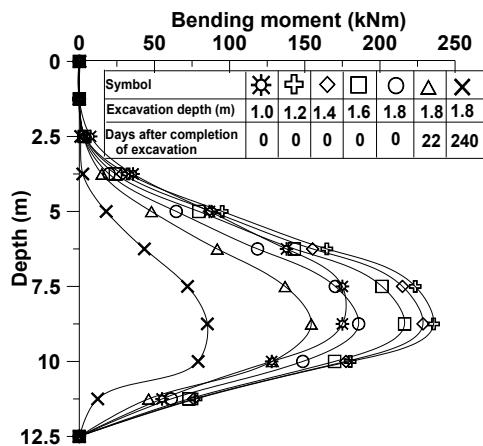


Figure 9. Development of pile bending moment profile over time (Ong et al., 2004)

High-resolution photographs were taken during various excavation stages of the test, as shown in the left-hand side photographs of Figure 10. It is evident that tension cracks have developed when the excavation depth exceeds 1.0 m.

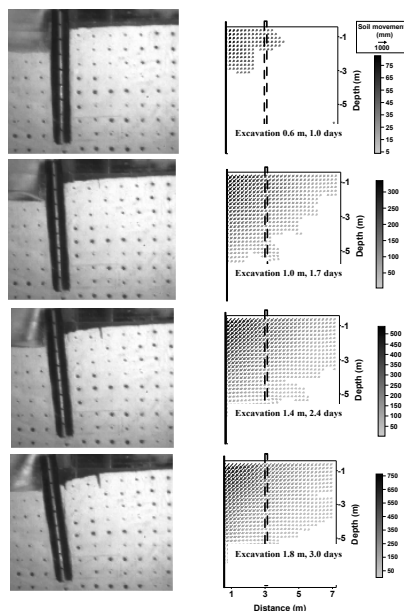


Figure 10. Pictures and vectors showing development of tension cracks and corresponding soil movements, respectively (Leung et al., 2006)

These cracks cause the loss of contact of clay in front of the pile and may have prevented the transmission of additional soil pressures onto the pile. The vectors of soil movement shown in the right-hand side plots of Figure 10 indicate that the size of considerable soil movement zone increases as excavation progresses, but the shape does not

alter. This observation is consistent with that observed by Bolton et al. (1987).

The variations of pile head deflection and free field soil movement at different depths at the pile location with time are shown in Figure 11. The free field soil movement is measured by using a commercial image processing software to track the movement of beads placed on the side surface of the clay.

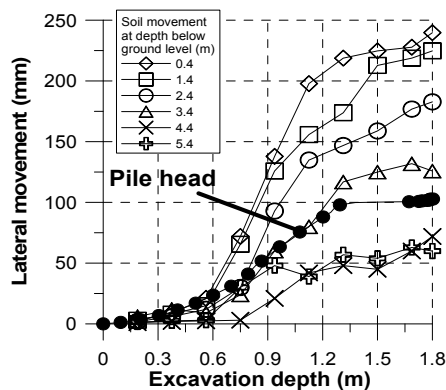


Figure 11. Variations of pile head deflection and soil movement (Ong et al., 2004)

It is observed that the soil starts to move ahead or “flow” past the pile at a relatively shallow excavation depth of 0.6 m. After which the difference between the soil and pile movements becomes more significant with increasing excavation depth. The movement is expected to be reasonably large during excavation due to the low undrained shear strength profile of the clay as shown in Figure 6. As expected, greater soil movement is observed to occur nearer to the ground surface.

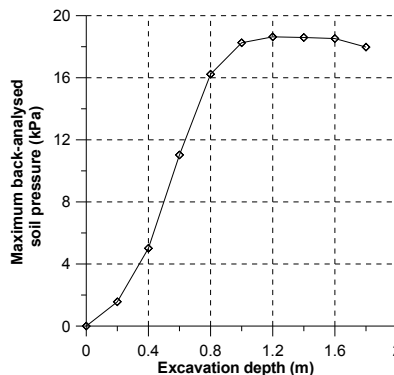


Figure 12. Variation of maximum back-analysed soil pressure with excavation depth (Ong et al., 2004)

In order to verify this finding, the soil pressure profiles are obtained by differentiating the measured pile bending moment profiles twice using

a 7th order polynomial. Figure 12 shows the development of the maximum soil pressure deduced from the corresponding bending moment profiles shown in Figure 9. It is evident that the limiting maximum soil pressure values have been reached at an excavation depth of 1.2 m.

Thereafter, the soil pressures do not increase further with increasing excavation depth. This observation further reinforces the postulation that when the soil flows past the pile. In addition, with the presence of the tension cracks in front of the pile as described earlier, the soil could not transmit its full pressure onto the pile, resulting in a drop in induced pile bending moment as shown in Figure 9.

2.3 Case study 2: Centrifuge study in sand

Leung et al. (2000) examined the pile behaviour behind a failed excavation in sand. The test set-up is essentially similar to that shown in Figure 5, except that the clay is replaced by sand. In Test WC1, the pile is located 2 m behind the wall. As sand is much stiffer than clay, a maximum excavation depth of 6.0 m was necessary to induce the failure of the retaining wall.

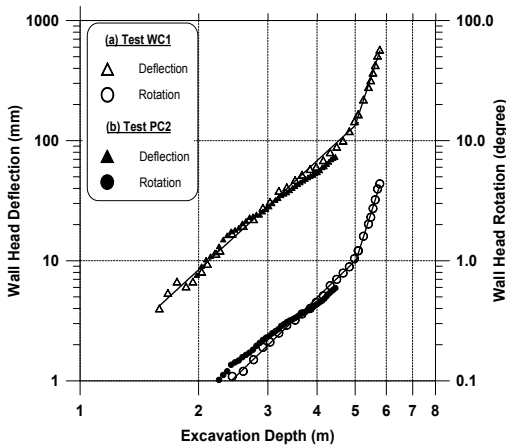


Figure 13. Wall deflection and rotation versus excavation depth (Leung et al., 2000)

The pile would be located within the active pressure rupture zone behind the wall when the excavation failed. The variations of wall deflection and rotation with excavation depth are shown in a log-log scale in Figure 13. It is evident that an approximate bi-linear relationship exists. The interception of the two straight lines denotes the occurrence of wall failure. As such, the excavation had failed at an excavation depth of approximately 5.0 m.

Figure 14 shows the induced pile bending moment profiles of Test WC1. The location of maximum pile bending moment is noted to be about 7.5 m below the ground surface.

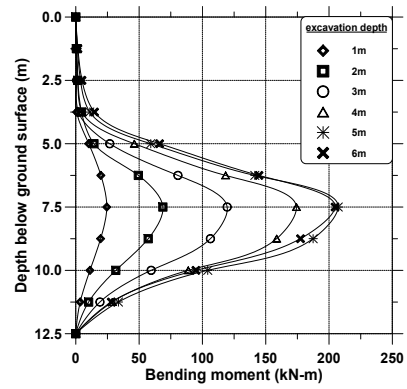


Figure 14. Induced pile bending moment profiles (Leung et al., 2000)

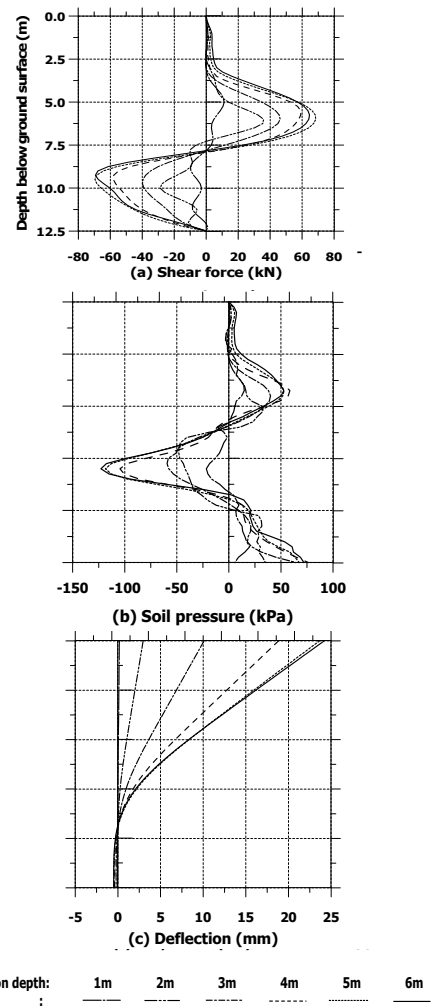


Figure 15. Induced pile (a) shear force, (b) soil pressure and (c) deflection profiles (Leung et al., 2000)

The induced shear force, soil pressure and deflection profiles derived from the measured pile bending moment profiles are shown in Figures 15 (a), (b) and (c), respectively.

It is observed that after the wall collapses at excavation depth of 5 m, the induced pile bending moment, shear force, soil pressure and deflection do not increase further. Video pictures reveal that at this stage, the sand flows past the pile resulting in no further increase in loading on the pile.

The results of the centrifuge model studies revealed that the wall movement due to excavation would cause soil movements behind the wall and this would induce deflection and bending moment on adjacent piles. For clay, the pile responses are noted to be time dependent, i.e. the pile bending moment and deflection continue to change after completion of excavation.

For a failed excavation in clay, the development of tension cracks at the ground surface may have prevented the full transmission of soil pressure on the piles and hence the induced pile bending moment and deflection decrease after failure. For piles in sand, the sand is noted to “flow” past the pile and no further increase in pile bending moment and deflection is noted after failure.

2.4 Case study 3: Field study in soft clay

Ong et al. (2004, 2011) reported a case study where a proposed 7-storey industrial building with one-level basement car park was to be constructed at a congested site in the city. In order to construct an underground storage facility, a temporary open-cut excavation of a 1V:2.5H slope was proposed. Owing to some unforeseen situations, excessive soil movement had taken place during the slope excavation and caused failure of the instrumented pile group. The post-failure pile behaviour has provided valuable field data for back-analysis.

To facilitate the building basement construction, an unsupported 5-m high slope excavation was carried out in front of the capped 4-pile group of 900-mm diameter cast-in-situ concrete bored piles. Unfortunately, during the course of excavation, the slope failed as a result of heavy rainfall as shown in Figure 16.

The effect of large-strain soil movement or soil flow on pile group responses is analysed. Figure 17(a) shows that the measured inclinometer readings where the magnitudes of lateral soil movement are much larger than the measured pile deflection (in-pile inclinometer), thus suggesting that soil flow around the pile has taken. As the pile has experienced lateral movement of more than 100mm, it could have cracked severely, thus raising another parameter that requires careful consideration.

Table 1 shows the various analysis cases performed so as to simulate the understanding level of a designer when confronted with such a case study.

Method 1 considers application of 2D FE analysis by smearing of 3-D pile properties (Ong et al. 2007, 2011), while Method 2 involves the use of an established numerical method described in detailed in Leung et al. (2006).

Table 1. Various analysis cases performed

Analysis cases	I_g of I_{cr}	p_y
Case 1 (Method 1): simulates ignorance of soil flow phenomenon	I_g	Not considered
Case 2 (Method 2): simulates available knowledge on I and p_y	I_{cr}	$p_y=6c_u$
Case 3 (Method 2): simulates available knowledge on p_y but not on I	I_g	$p_y=6c_u$
Case 4 (Method 2): simulates absence of knowledge on I and p_y	I_g	$p_y=K_h$

Note: I_g =gross moment of inertia, I_{cr} =fully cracked moment of inertia, p_y =limiting soil pressure, c_u =undrained shear strength, K_h =soil spring stiffness

Figure 16(a) shows the outcome of the pile responses for Case 1 based on Method 1. The front pile is located nearer to the slope than the rear pile. In this case, the natural behaviour of soil deformation is negated by the presence of the ‘equivalent wall’ (no longer a pile) in a 2-D environment, resulting in relatively smaller magnitudes than measurements taken on site. Consequently, the predicted pile responses (bending moment and deflection) are both very much under-predicted, leading to inappropriate design of pile to resist lateral soil movement.

In Case 2, if both I_{cr} and p_y are correctly adopted, Figure 17(b) shows that the prediction of pile responses is very reasonable. This simulates the available and appropriate level of understanding of the back-analysis carried out considering the development on site.

Case 3 simulates the situation where knowledge on limiting soil pressure is available but not on the pile moment of inertia, I . In such a case, the pile bending moment tends to be over-predicted, but the deflection is under-predicted as shown in Figure 17(c).

This is due to the pile being assumed to be uncracked (much stiffer) thus attracting high bending moment and low deflection. The above does not simulate the behaviour on site where the pile has experienced lateral movement of more than

100mm. This highlights the importance of knowing the condition of the pile on site when performing back-analysis.

In Case 4, if the back-analysis is carried out without having prior knowledge of estimating limiting soil pressure and transformed pile moment of inertia, I on site due to cracking, the predicted

pile bending moment will be grossly over-predicted as shown in Figure 17.

However, in this case, the 'reasonable' estimation of pile deflection is merely a coincidence.

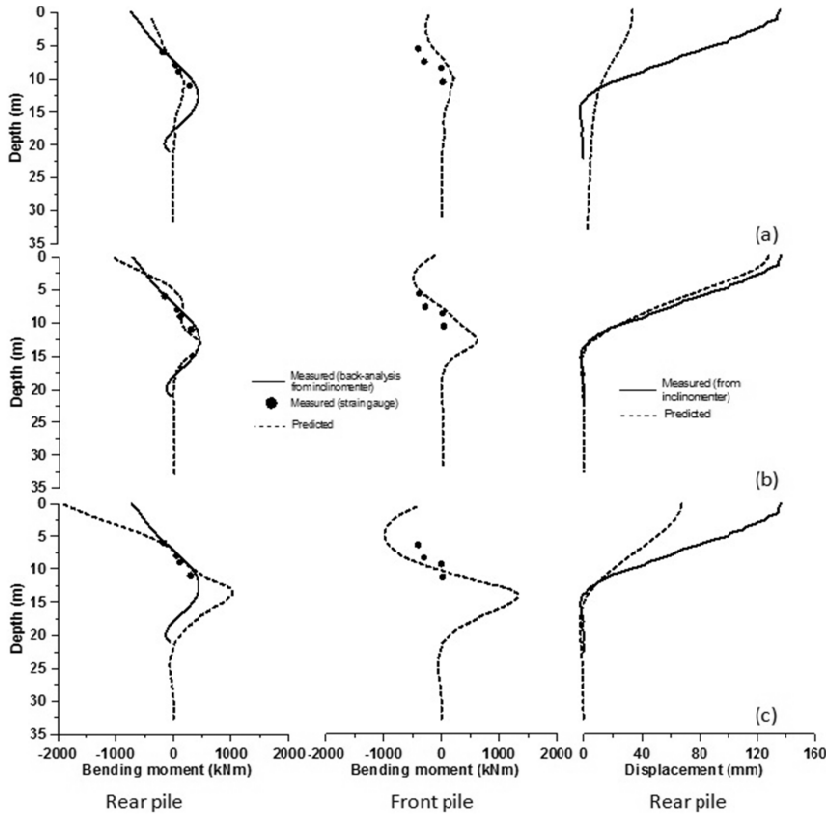


Figure 16. Profiles of measured and predicted rear and front pile bending moment and rear pile deflection (Ong et al., 2010)

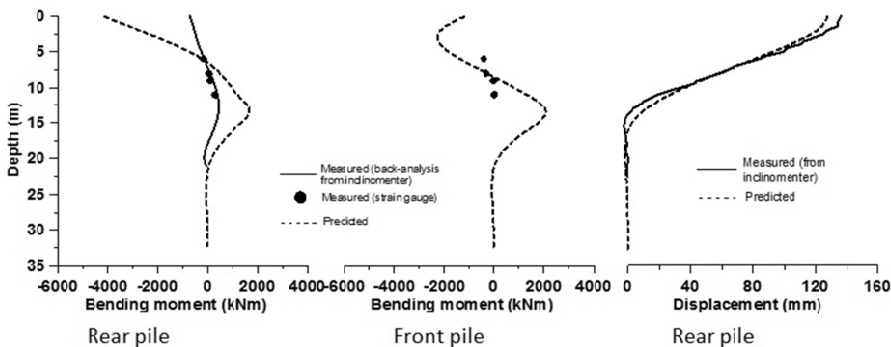


Figure 17. Profiles of measured and predicted rear and front pile bending moment and rear pile deflection (Ong et al., 2010)

3.0 EFFECTS OF SOIL-STRUCTURE INTERACTION ADJACENT TO DEEP FOUNDATIONS

3.1 Case study 1: Field study of failure of building due to excavation in soft clay

A well-documented field case study on the effects of excavation on nearby pile foundations was presented by Poulos (1997). It reported the failure of piles supporting a building due to excessive ground movement arising from an uncontrolled and unsupported excavation close to one corner of the building.

The project involved the construction of three buildings; namely, an office block, a hotel and a shopping centre in Indonesia. A nearby building had to be demolished due to the continual increase in settlement that caused it to tilt. Poulos (1997) summarized the available geotechnical and foundation data for the project and evaluated the various possible causes of settlement. The foundations for the buildings consisted of cast-in-situ piles, 0.5-m nominal shaft diameter and 20 m in length. Vertical and lateral load tests were carried out and the piles generally performed satisfactorily.

Both the office and hotel buildings were completed and no undue settlement was noted. Subsequently, piling work for the shopping centre building was undertaken between the two completed buildings. At the same time, an excavation adjacent to the shopping centre was carried out for the placement of a ground tank. The excavation was unsupported and extended to depth of 4 m. Before the excavation was completed, massive ground movement was observed. The contractor decided to stop the excavation and subsequently backfilled the excavated ground.

The backfilling process took about three months. During backfilling, the soil was merely dumped into the excavated ground without proper compaction. Consequently, the nearby ground continued to move towards the excavation over a period of two months. This resulted in a large area (approximately 36 m by 22 m) surrounding the excavated area being affected by soil settlement. The office building was found to have tilted towards the shopping centre site with a maximum settlement of about 900 mm. The horizontal movement at the top of the building was reported to be about 1.2 m.

In view of this, grouting was carried out to arrest the settlement but this remedial action was unsuccessful. Eventually, it was decided to demolish the office building in order to prevent possible collapse. Nevertheless, no substantial movement was observed at the hotel site where the

ground was undisturbed. However, substantial movement was observed for the newly installed free head piles for the shopping centre. The piles, which were located about 2 to 3 m from the line of excavation, had moved more than 1 m towards the excavation. Besides that, settlement of about 50 to 60 mm was also noted for these piles.

Numerical analysis was also carried out to further study the effects of excavation on the piles. The analysis revealed that the pile head movement increased with increasing soil movement until the soil movement reached about 200 mm. It was postulated that at this stage, the soil might have just flowed past the pile and thus the pile did not experience any further movement.

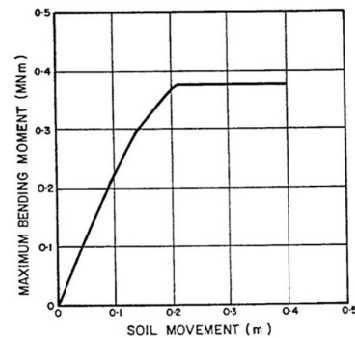


Figure 18. Maximum pile bending moment (Poulos, 1997)

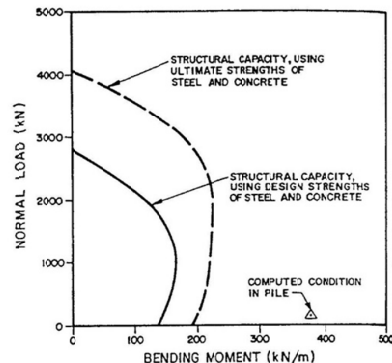


Figure 19. Structural capacity of shopping centre piles (Poulos, 1997)

Figure 18 shows the maximum bending moment induced on the pile due to soil movement. A maximum bending moment of about 380 kNm had developed. For these piles having an unrestrained head, the maximum deflection occurred at the pile head while the maximum bending moment and shear occurred at a pile shaft elevation near the base of the soft soil layer. The maximum bending moment calculated from the numerical analysis was

then compared with the structural capacity of the pile section.

Figure 19 shows the computed axial force and bending moment in the pile and clearly reveals that the structural capacity of the pile section is far exceeded, even for the case where ultimate steel and concrete strengths are used.

Figure 20 compares the maximum bending moment and axial load computed from the horizontal soil movement acting on the capped pile of the office building with the structural capacity of the pile section. Again, the pile capacity was found to have been far exceeded.

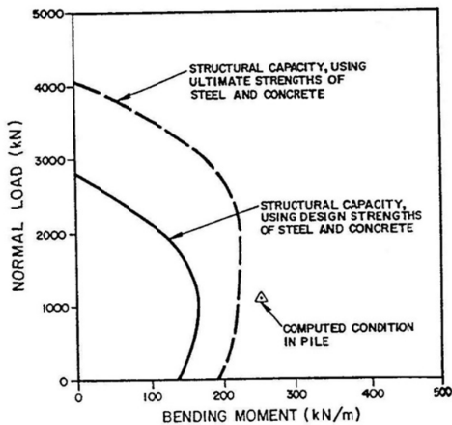


Figure 20. Structural capacity of office building piles (Poulos, 1997)

There was sufficient evidence to suggest that the failure of the pile foundations was directly associated with attempts made to carry out an unsupported excavation near the existing office building and shopping centre. It was also suggested that horizontal movement caused by such excavation could have caused overloading and eventual structural failure of the piles supporting the building.

3.2 Case study 2: Pile group study in soft clay behind a stable retaining wall

Ong et al. (2009, 2011) presented a series of 8 centrifuge tests for free and capped heads of 2-, 4- and 6-pile groups adjacent to an excavation in very soft clay behind a wall that remains stable after excavation. Therefore, limiting soil pressure is not expected to be reached. In these cases, soil-pile interactions such as shadowing, reinforcing and soil arching effects are studied in detail. The centrifuge pile group test set-ups are identical to the single pile set-ups as reported by Ong et al. (2006) except that structural pile caps are introduced to tie the

individual pile heads for cases with capped pile head conditions.

It is found that the induced maximum bending moment is always smaller than that of a corresponding single pile (Ong et al., 2006) at an identical location. If the free-head piles are located at the same distance, the measured bending moment is higher for the front pile as opposed to the rear pile of the pile group. In a pile group, each individual front pile (3m behind the wall) will provide shadowing and reinforcing effects to the other the rear piles (5m behind the wall), thus reducing the magnitudes of pile deflection and bending moment. This is evident from Figures 21 and 23.

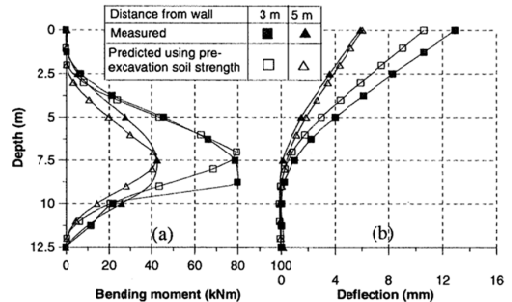


Figure 21. Predicted and measured pile (a) bending moment and (b) deflection profiles for free-head 4-pile group (Test 12) (Ong et al., 2009, 2011)

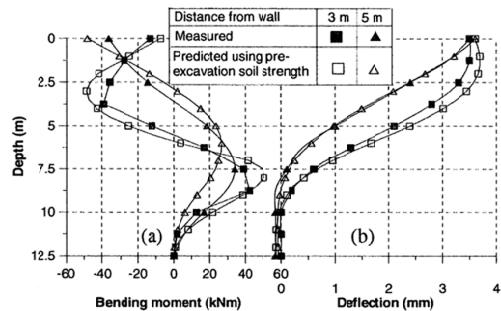


Figure 22. Predicted and measured pile (a) bending moment and (b) deflection profiles for capped-head 4-pile group (Test 13) (Ong et al., 2009, 2011)

The degree of shadowing experienced by each individual pile depends on its relative position with its surrounding piles. It is observed that the induced bending moment for the front peripheral pile is greater than that of the front centre pile at the same distance behind the wall. Similarly, the bending moment developed at the rear peripheral piles is also greater than that of the rear centre pile at the same distance behind the wall. As the number of piles in a group becomes larger, the shadowing and reinforcing effects become more prominent.

The immediate effect of pile shadowing and reinforcing effect is to reduce the detrimental effects of excavation-induced soil movement on the pile group. By capping a pile group, the individual pile heads are forced to act in unison when subject to different magnitudes of soil movement, depending on the distance of the piles from the wall.

The induced bending moment of the front pile, which experiences a greater soil movement, is moderated by the rear pile through the pile cap. The interaction between the front and rear piles induces negative bending moment at the pile head, but reduces the magnitude of bending moment developed along the pile and the pile group deflection as observed in Figure 22.

Soil arching and “separation” of soil as shown in Figure 23, have been observed to occur between the front piles of a pile group when the soil moves upon excavation, in the 4-pile group. The arch is formed between the rows of piles when the yielded soil gets detached from its surrounding. The detached soil is then forced to squeeze between the row of piles but without significantly increasing the pressure acting on the piles.

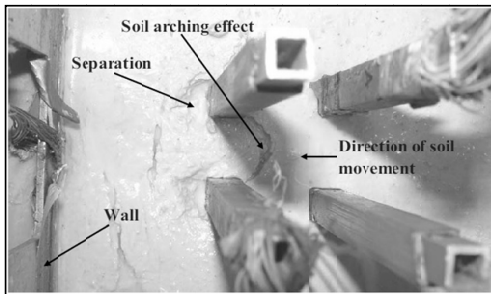


Figure 23: Soil arching and separation observed in Test 12 (Leung et al., 2006)

Generally, the observed long term maximum positive bending moment would increase after excavation until about 50 days later and subsequently reduce with time. It is believed that progressive wall and soil deformations are the reasons for such observed time dependent pile behaviour. On the contrary, the maximum negative bending moment generally reduces slightly over time after excavation. This behaviour could be the result of pile-pile cap interaction as the maximum negative pile bending moment is located nearer to the pile cap.

To account for the pile group shadowing and reinforcing effects, an empirical soil moderation factor k_s was introduced to “correct” the measured free-field soil movements. By back-analysis, the magnitude of soil moderation factor k_s is established to be 0.8 for a 2-pile group, 0.7 for a 4-pile group and 0.5 for a 6-pile group in clay as

compared to 0.9 for a 2-pile group, 0.8 for a 4-pile group and 0.6 for a 6-pile group in sand as reported by Leung et al. (2003).

3.3 Case study 3: Pile behaviour subjected to excavation stress relief

Ng et al. (2014) performed centrifuge model tests to determine the capacity and deformation of a single pile, a 3 x 3 pile group and a piled raft foundation, with and without stress relief effects. The behaviour of piles in non-dilatant (soft clays) and dilatant soils (stiff clay or dense sand) were assessed so as to have a better understanding on the fundamental mechanisms controlling the pile capacity when subjected to stress relief. This study is analogous to a top-down construction method consisting piles which are designed from pile load tests carried out at the ground surface and installed before excavation.

Discrete element modelling (DEM) was also used to explore the shearing mechanisms at the pile-soil interface and to estimate the normal stress increment contributing to pile shaft resistance, when a pile undergoes stress relief due to deep excavation.

For piles installed in soft clay (non-dilatant soil), it was observed that the reduction in shaft resistance is proportional to the normal stress acting on the pile shaft and hence the depth of excavation. As shown in Figures 24 (a) and (b), the shaft resistance has been fully mobilised at 11.1 MN (without stress relief) and 5.0 MN (with stress relief), respectively, as validated by the constant slope of the measured axial load distribution profiles along the entire pile shaft in the soft clay.

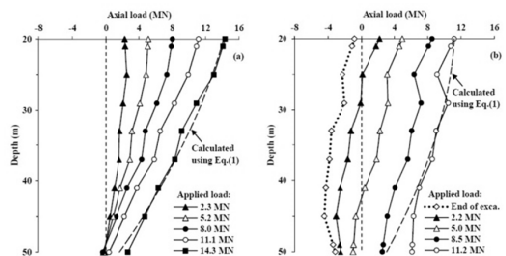


Figure 24: Shaft resistance fully mobilised at 11.1 MN (without stress relief) and 5.0 MN (with stress relief) respectively (Ng et al., 2014)

After the respective shaft resistances have been fully mobilised, the pile toe which is founded on dense sand starts to mobilise its toe resistance in the tests. It can thus be concluded that the shaft resistance of the low friction piles was proportional to the normal stress on the pile shaft as validated by theoretical calculation of shear stress, $\tau = \sigma_n' \tan \delta'$, where σ_n' is the effective normal stress and δ' is the

interface friction angle. The reduction in shaft resistance due to stress relief led to a lower capacity of the pile subjected to excavation.

For a pile installed in stiff clay or dense sand (with a dilatant pile-soil interface), the increase in pile capacity was attributed to soil dilation at the soil-pile interface, resulting in an increase in the normal stress ($\Delta\sigma'_n$) acting on the pile shaft and hence the pile capacity. The contribution of dilation was more significant for a pile subjected to stress relief since dilation was more pronounced at lower stress. The DEM study showed that an unloading of normal stress from 400 to 100 kPa can lead to a 30% increase in $\Delta\sigma'_n$.

It has also been found that due to excavation stress relief, tensile force can occur at 70% to 83% section of the shaft length from the pile head, as a result of the upward movement of soil due to stress relief. Therefore, a pile should be reinforced appropriately to resist the induced tensile force during deep excavation. As loads were applied at the pile head gradually, positive shaft resistance was mobilized along the entire pile length, as well as toe resistance.

4.0 EFFECTS OF SOIL-STRUCTURE INTERACTION ADJACENT TO SHALLOW FOUNDATIONS

4.1 Case study 1: Deep excavation next to the Frances Xavier Warde School, Chicago

Finno et al. (2002) described the performance of a support excavation system in Chicago and its effects on adjacent building supported on individual pad footings as shown in Figure 25. The Frances Xavier Warde School was located within 1.3m of the wall supporting the excavation. The excavation was conducted in soft to medium clays to a depth of 13 m supported by a 900 mm thick secant pile wall, one level of steel-pipe bracing and subsequent two levels of tiebacks.

Field data consisted of lateral soil movements, building settlement markers and measured loads in the support system. Figure 26 shows the development of lateral soil movements and building settlement during excavation process. The main contribution of this case study is that distortions under an adjacent building can be estimated using inclinometer data when excavating through soft clay, at least when the movements are small and the retaining system was sufficiently stiff.

It was found that minor damage occurred to non-load bearing portions of the building. The prediction of maximum lateral soil movements and

building settlements were both approximately 32 mm as shown in Figure 27.

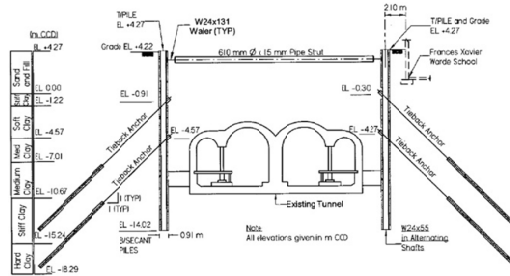


Figure 25: Excavation support system in Chicago (Finno et al., 2002)

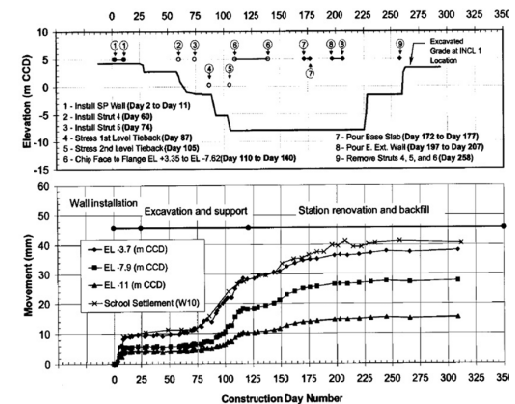
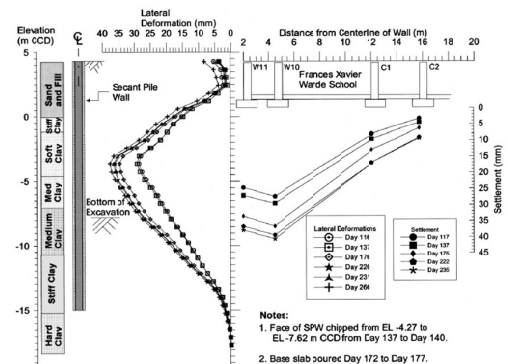


Figure 26: Development of lateral soil movements and building settlement during excavation process (Finno et al., 2002)



larger settlements within the affected zone but not expanding along its width.

The distortion was obtained from the extensive settlement data obtained from the inclinometer data. Inclinometer data can be used to assess the distortion of adjacent structures. Damage starts to be apparent in non-load bearing portions of the building when the distortion exceeds approximately 1/960.

4.2 Case study 2: Deep excavation supported by flexible, tied-back retaining wall

Ground deformations affected by corner effects were observed during a 12.8 m deep excavation in Chicago as reported by Finno et al. (2005). The excavation was supported by sheet-piles and regrowable ground anchors which were carried out through soft to medium clays. Field monitoring data consists of lateral, vertical optical survey and lateral inclinometer data.

The construction stages include wall installation, caisson construction, excavation and installation of tied-back anchors on ground movements. Figure 28 shows the field measured ground settlements and lateral movements, respectively. The maximum settlements behind the wall were about 80% of the maximum lateral movements when the excavation was within the soft to medium clay.

Figure 29 illustrates the direction of the soil movements determined from the two axes of the inclinometers at the final excavation level. The data is presented incrementally for each excavation stage and thus illustrates the overall behaviour of lateral soil movements. It was observed that most movements occurred perpendicular to the sheet pile retaining wall with rather limited out-of-plane movement.

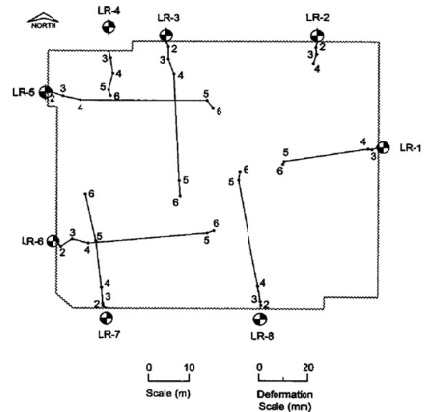


Figure 29: Direction of soil movements determined by two axes of inclinometers at final excavation level (Finno et al., 2005)

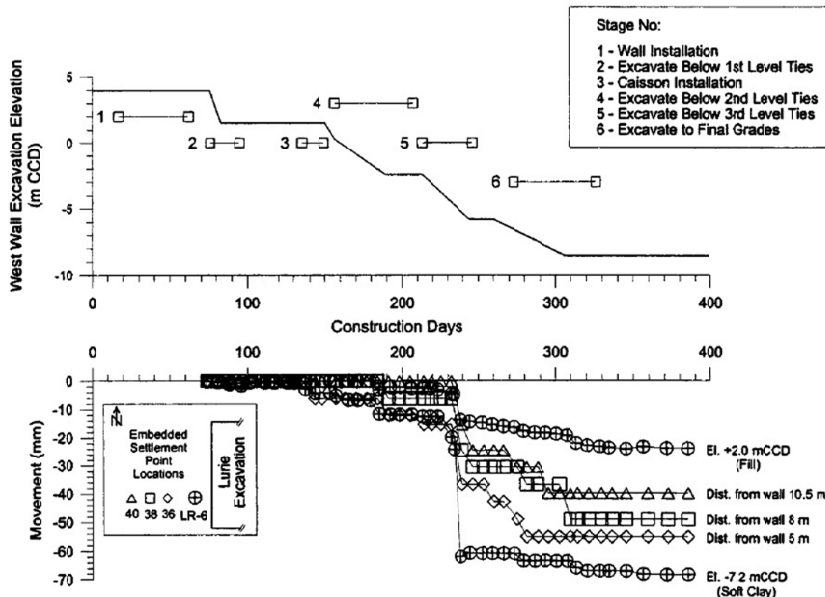


Figure 28: Field measured ground settlements and lateral movements (Finno et al., 2005)

As shown in Figure 30, a performance based relationship was established to estimate the maximum ground movements for the flexible wall system, which is a function of the factor of safety against basal heave and excavation depth.

An empirical approach was proposed to estimate the distribution of ground movements parallel to a supported wall. Maximum incremental movements were largest at the final excavation level and where factor of safety against basal heave was lowest. Where factor of safety against basal heave was at least 1.7, reasonably small lateral movements were observed.

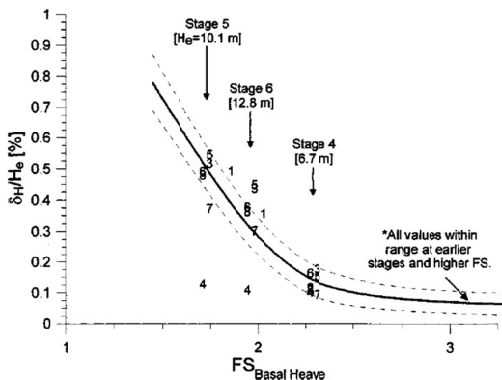


Figure 30: Performance based relationship to estimate maximum ground movements for flexible wall system (Finno et al., 2005)

At the final excavation level, contour plot of lateral movements at the western part of the excavation was obtained by optical survey and shown in Figure 31.

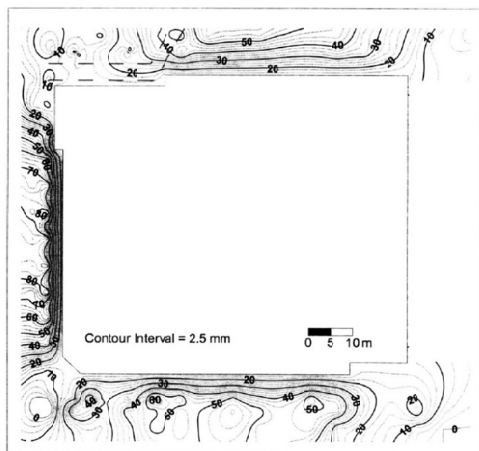


Figure 31: Contour plot of lateral movements at the western part of excavation (Finno et al., 2005)

It is observed that the lateral soil movements indicate 'bowl-shaped' patterns. The maximum

lateral movement occurred in the middle portion with much smaller lateral movements occurring at the corners due to 3-D corner effect.

By the end of the excavation, significant distortions developed at both the perpendicular and parallel to the excavation. According to existing damage criteria, these distortions were large enough to cause cracking in non-structural elements of framed buildings and supported on shallow foundations. However, at this project site, no damage was reported on the infrastructure such as utilities that paralleled the excavation or in the floating floor slab of the adjacent caisson-supported building.

5.0 EFFECT OF EXCAVATION / TUNNELLING ON BUILDING DAMAGE ASSESSMENT

5.1 Case study 1: Effect of building stiffness on building damage assessment

Tensile strains, which are obtained using deflection ratios and horizontal strains under 'greenfield conditions', is usually used for assessment of building damage. This approach eliminates the building stiffness and is considered to be more conservative and sometimes, not realistic.

In view of the above, Goh et al. (2011) studied the behaviour of building stiffness in relation to the response of excavation-induced settlements, by comparing the settlement results obtained from the Singapore Art Museum case study. Figure 32 shows the schematic of the Bras Basah Station next to the Singapore Art Museum.

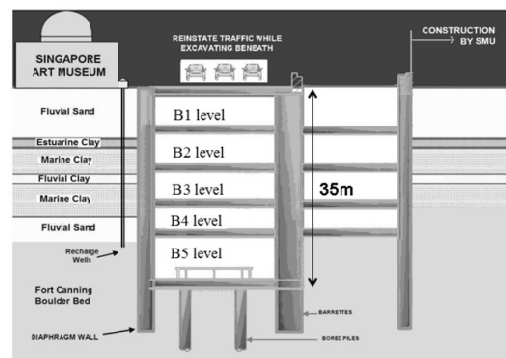


Figure 32: Schematic of the Bras Basah Station next to Singapore Art Museum (Goh et al., 2011)

Finite element method was used to conduct a numerical study on the building response to ground movements induced by an adjacent deep excavation in soft clay. Using similar properties of the marine clay, the soft clay was modelled in Abaqus using

the Modified Cam Clay and the building using an elastic beam with bending and axial stiffness properties.

Based on the case study, it was found that the Singapore Art Museum building stiffness will influence its response due to excavation-induced movements, thus rendering the ‘greenfield’ assessment very conservative. Apart from bending stiffness, other factors such as building length and location on the settlement trough would affect the foundation response subject to excavation-induced settlements. The proposed modification factors for deflection ratio for this case study are shown in Figure 33.

It can be seen that when the relative bending stiffness is less than 10^{-4} , the corresponding modification factor is close to unity. Therefore, the building is expected to behave like a fully flexible one, having deflection ratio close to that of Greenfield condition.

Nonetheless, when the relative bending stiffness is more than unity, the modification factor is close to zero, depicting a fully rigid structure. In between the two values, the modification factor decreases rapidly from unity to zero.

By including the influence of building stiffness, the design guidance can be used to estimate a more realistic building response and to assess the reduction in deflection ratio from the Greenfield condition. The composite bending stiffness of a building is the sum of the individual stiffness contributions from the plane walls, floor slabs and the structural framing action.

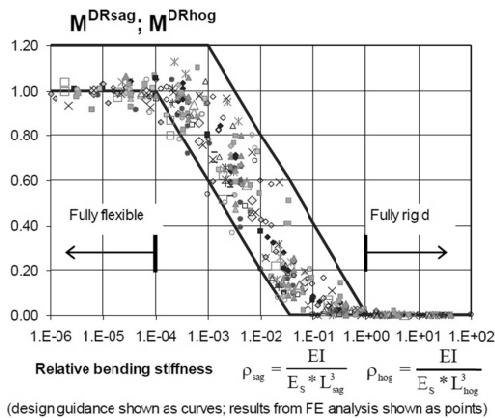


Figure 33: Proposed modification factors for deflection ratio (Goh et al., 2011)

Goh et al. (2011) pointed out that the estimation of building stiffness is still a challenge to designers, especially for masonry structures where the influence of wall openings and differences in

sagging and hogging deformation should be included.

5.2 Case study 2: Responses of building supported on continuous footings to movements induced by deep excavations in soft clays

Goh et al. (2012) used finite element code PLAXIS to perform a total stress analysis for a 20 m deep excavation in soft clay. The building was modelled as a weightless elastic beam with axial and bending stiffness properties. With high axial and bending stiffness, a building tends to rotate and act as a rigid body. For low axial and bending stiffness, the building is flexible and follows the Greenfield ground deformations.

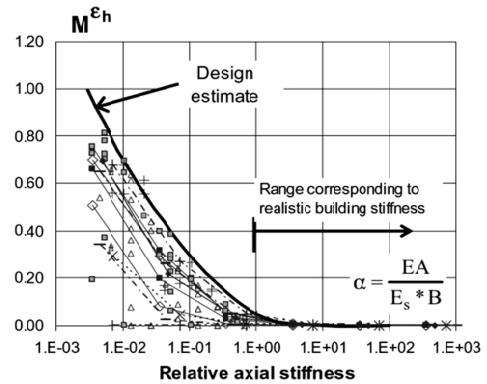


Figure 34: Horizontal strain modification factors plotted against the relative axial stiffness of a typical building (Goh et al, 2012)

It was found that building response depends on its bending stiffness whereas the horizontal displacement depends on its axial stiffness. Figure 34 shows the horizontal strain modification factors plotted against the relative axial stiffness of a typical building. An upper-bound limit can be developed to estimate the horizontal strain modification factors for building on continuous footings. For example, for a 100mm thick reinforced concrete slab that is 100m long and continuous and for E_s around 20MPa, the relative axial stiffness is in the order of 10^0 .

Therefore, similarly, a building with high bending and axial stiffness results in a lower deflection ratio and horizontal strain. Hence, considering the building stiffness for estimating the deflection ratio and horizontal strains, a lower risk of building damage can be obtained from the reduction of maximum tensile strains induced by the building.

Although having the same elastic stiffness in bending, Goh et al. (2012) reported that a shorter building will have a stiffer deflection compared to a taller building. Thus, from the understanding, by having the same elastic and geometric properties, a building adjacent to a deeper excavation will have

higher modification factors for the deflection ratio and horizontal strains compared to a shallower excavation, thus reflecting the nature of soil-interaction effect.

5.3 Case study 3: Responses of building supported on individual footings to movements

Goh et al. (2012) examined the interaction between horizontal strains in buildings and individual footings. A case study of a Singapore framed building subjected to bored tunnelling is presented, whereby remarkable horizontal strains were noted.

The case study involved shop houses along the Pasir Panjang Road, Singapore, being two-storey, reinforced-concrete framed buildings supported on shallow foundations. The shallow foundations consist of individual footings supported by timber bakau piles, having an average length of 8m.

Along the Pasir Panjang Road, the geology mainly consist of fluvial and marine deposits of the Kallang Formation over-lying the soils and rocks of the Jurong formation which has varied sedimentary origins but having evidence of metamorphism.

During the tunnelling works, ground and building settlement markers and tape extensometers were used to monitor the settlement response. Venkta et al (2008) reported that the building settlement for one shop house reached 100 mm. The tape extensometer measurements were categorised as transverse and longitudinal horizontal strains due to the orientation of the framed buildings with respect to the tunnelling drive.

Using finite element method, the frame building was modelled where the frame columns were unconnected at the footing level for a 20 m depth excavation in an undrained condition. The frame was modelled as a weightless structure. The outcome shows that the horizontal strains are mostly compressive. Although cracks were initiated due to the settlement on the brick walls and column brick wall interface, the structural integrity of the building was not affected.

It is well-established that for most buildings with continuous footings, the horizontal strains are significantly reduced. However, for buildings supported on individual footings such as this case study, the approach assumes horizontal strains in the Greenfield condition, which is shown to be reasonable. Therefore, based on this understanding, a new frame stiffness factor, as shown in Figure 35, was developed to characterise the horizontal strain modification factor derived from a rigidly-connected frame structure on individual footings, using a simple pin-support portal-frame structural analysis.

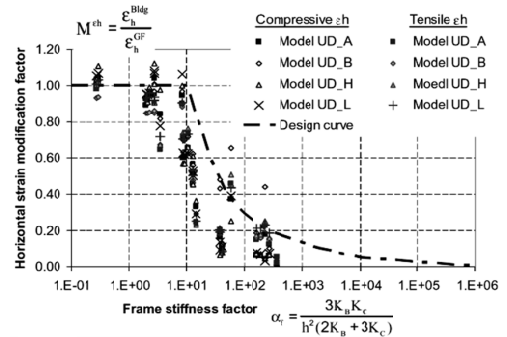


Figure 35: New frame stiffness factor developed to characterise horizontal strain modification factor (Goh et al, 2012)

6.0 CONCLUSIONS

In this keynote paper, the latest development and understanding of soil-structure interaction caused by adjacent excavation are presented with references to successfully implemented projects or research work based on finite element modelling, centrifuge experiments and field monitoring, observations and interpretations.

It is important that the concept of limiting soil pressure due to excavation stress relief is well-understood as it provides a fundamental understanding that has been observed in excavation works performed in soft clay or loose sand. If a pile is positioned within the active wedge failure zone of an adjacent excavation, it will experience a maximum pressure when the soil movements are sufficiently large to cause limiting soil pressures to manifest the behaviour of the surrounding soils. However, as further soil movements take place beyond this threshold situation, no additional soil pressures could further act on the pile, which in turn would not result in any further increase in pile bending moment and deflection.

The effects of soil-structure interaction adjacent to shallow foundations are more pronounced and thus more detrimental as compared to deep foundations. This is naturally so because shallow foundations are founded on shallower embedment thus limiting the soil from the beneficial confining or overburden pressure. Differential shallow foundation settlement is the main parameter that needs to be addressed in this case. Therefore, it is expected that stiffer retaining systems ought to be employed for adjacent buildings or infrastructure supported on shallow foundations so as to limit possible damages due to differential settlements. Such strategy has been successfully employed by Finno et al. (2002).

The effects of soil-structure interaction adjacent to buildings supported on deep foundations could perhaps take more 'punishment' from the detrimental effects associated to excavation works.

This is so due to the ability of the installed piles to transfer building loads to deeper and thus more competent soil layers, besides benefitting from the much larger soil confining pressures to mobilise greater soil strength. However, designers have to be aware that lateral soil movements and stress relief due to excavation will cause detrimental pile responses such as additional bending moment and deflection (Ong et al., 2004, 2006, 2009, 2010, 2011 and Leung et al., 2000, 2003, 2006) and to some extent reduction (in non-dilatant soils) and increment (in dilatant soils) in vertical pile capacity (Ng et al., 2014).

Effects of excavation are often associated to the development of tensile strains in buildings due to differential movements. Tensile strains are computed based on data obtained from tape extensometer and building settlement markers that indicate the magnitude of 'squeeze' or 'relaxation' experienced by a building. The associated parameters are deflection ratios and horizontal strains. Through extensive experience developed by the Land Transport Authority (LTA) of Singapore as well as the recent works by Goh et al. (2011, 2012), it has been observed that a framed building supported on individual pad footings or old timber 'floating' piles may not necessarily behave under 'greenfield' condition, which usually provide a more conservative estimate. In fact, if building bending and axial stiffness are considered, appropriate modification factors can be assigned to the building such that a more realistic condition can be achieved. However, the estimation of building stiffness is still a challenge to designers, especially for masonry structures where the influence of wall openings and differences in sagging and hogging deformations should be included.

7.0 ACKNOWLEDGMENT

The authors would like to thank Mr. Irfaan M. Peerun and Mr. Chung-Siung Choo for their time spent on data collection and editorial work of this paper. Their contribution is hereby gratefully acknowledged.

8.0 REFERENCES

- Bolton, M. D. and Powrie, W. (1987). The collapse of diaphragm walls retaining clay. *Geotechnique*, Vol. 37, No. 3, pp. 335-353.
- Chen, L.T., and Poulos, H.G. (1997). Piles subjected to lateral soil movements. *Journal of Geotechnical and Geoenvironmental Engineering, American Society of Civil Engineers (ASCE)*, Vol 123, No. 1, pp. 802-811.
- Finno, R.J, Bryson, S, and Calvello, M. (2002). Performance of a stiff support system in soft clay. *Journal of Geotechnical and Geoenvironmental Engineering, American Society of Civil Engineers (ASCE)*, Vol. 128, pp. 660-671.
- Finno, R.J, and Roboski, J.F. (2005). Three-dimensional response of a tied-back excavation through clay. *Journal of Geotechnical and Geoenvironmental Engineering, American Society of Civil Engineers (ASCE)*, Vol. 131, pp. 273-282.
- Goh, K.H, and Mair, R.J. (2011). Building damage assessment for deep excavations in Singapore and the influence of building stiffness. *Geotechnical Engineering Journal of the SEAGS & AGSSEA*, Vol. 42, No. 3, pp. 0046-5828.
- Goh, K.H, and Mair, R.J. (2012). The response of buildings to movements induced by deep excavations. *Geotechnical Aspects of Underground Construction in Soft Ground-Viggiani(ed)*, Taylor & Francis Group, London.
- Goh, K.H, and Mair, R.J. (2012). The horizontal response of framed buildings on individual footings to excavation-induced movements. *Geotechnical Aspects of Underground Construction in Soft Ground-Viggiani(ed)*, Taylor & Francis Group, London.
- Leung, C. F., Chow, Y. K. and Shen, R. F. (2000). Behaviour of pile subject to excavation-induced soil movement. *Journal of Geotechnical and Geoenvironmental Engineering*, Vol. 126, No. 11, pp. 947-954.
- Leung, C.F., Lim, J.K., Shen, R.F., and Chow, Y.K. (2003). Behavior of pile groups subject to excavation-induced soil movement. *Journal of Geotechnical and Geoenvironmental Engineering, American Society of Civil Engineers (ASCE)*, Vol. 129, No. 1, pp. 58-65.
- Leung, C.F., Ong, D.E.L. and Chow, Y.K. (2006). Pile behaviour due to excavation-induced soil movement in clay: II: Collapsed wall. *Journal of Geoenvironmental and Geotechnical Engineering, American Society of Civil Engineers (ASCE)*, Vol. 132, No. 1, pp. 45-53.
- Maugeri, M., Castelli, F. and Motta, E. (1994). Analysis of piles in sliding soil. *Proc. 3rd Int. Conf. on Deep Foundation Practice Incorporating Piletalk*, Singapore, pp. 191-196.
- Ng, C.W.W and Peng, S.Y. (2014). Three-dimensional centrifuge and numerical investigation of the performance of piled foundations subjected

to deep excavation. *Advanced in Foundation Engineering*.

- Ong, D.E.L., Leung, C.F. and Chow, Y.K. (2003). Time-dependent pile behaviour due to excavation-induced soil movement in clay. *Proc. 12th Pan-American Conference on Soil Mechanics and Geotechnical Engineering*, Massachusetts Institute of Technology, Boston, U.S.A., Vol. 2, pp. 2035-2040.
- Ong, D.E.L., Leung, C.F. and Chow, Y.K. (2004). Pile behaviour behind a collapsed wall. *Proc. International Conference on Structural and Foundation Failures, Singapore*, pp. 410- 421.
- Ong, D.E.L., Leung, C.F. and Chow, Y.K. (2006). Pile behaviour due to excavation-induced soil movement in clay: I: Stable wall. *Journal of Geoenvironmental and Geotechnical Engineering, American Society of Civil Engineers (ASCE)*, Vol. 132, No. 1, pp. 36-44.
- Ong, D.E.L., Leung, C.F., and Chow, Y.K. (2007). Effect of Horizontal Limiting Soil Pressures on Pile Behaviour. *16th South-East Asian Geotechnical Conference (SEAGC)*, 8-11 May 2007, Kuala Lumpur, Malaysia. pp. 427-437.
- Ong, D.E.L., Leung, C.F. and Chow, Y.K. (2009). Behaviour of Pile Groups Subject to Excavation-Induced Soil Movement in Very Soft Clay. *Journal of Geoenvironmental and Geotechnical Engineering, American Society of Civil Engineers (ASCE)*, Vol. 135, No. 10, pp. 1462-1474.
- Ong, D.E.L., Leung, C.F. and Chow, Y.K. (2010). Effect of limiting soil pressure on pile group adjacent to a failed excavation. *Proc. of International Conference on Geotechnical Challenges in Megacities*, Vol. 3, pp. 785-792, 7-10 June 2010, Moscow, Russia.
- Ong, D.E.L., Leung, C.F. and Chow, Y.K. (2011). Behaviour of Pile Groups Subject to Excavation-Induced Soil Movement in Very Soft Clay. *Discussion by F. Castelli & Closure, Journal of Geoenvironmental and Geotechnical Engineering, American Society of Civil Engineers (ASCE)*, Vol. 137, No. 1, pp. 110-113.
- Poulos, H.G., (1997). Failure of a building supported on piles. *Proc. Int. Conf. on Foundation Failures, Singapore*, pp. 53-66.
- Schofield, A.N. (1980). Cambridge geotechnical centrifuge operation. *Geotechnique*, 30, 3, 227-268.
- Venkta, R., Hoblyn, S., Mahatma, S. & Lim, H.C. (2008). EPB tunnelling under 2-storey shophouses in mixed face conditions. *Proceedings of International Conference on Deep Excavation*, 10-12 Nov 2008, Singapore.

Comments on crushable sand stiffness relevant to soil structure interaction issues

W.F. Van Impe & P.O. Van Impe
AGE consulting, University Ghent-Belgium

ABSTRACT: The lecture will cover mainly the importance of stiffness parameters of crushable type of foundation sands in the perspective of the state of the art of soil testing and its new developments.

Any soil structure interaction model (SSI) can be deployed successfully or can fail depending on the reliability of the estimations of the soil structure interaction stiffness parameters. The stiffness evaluation of the engineered materials' structural elements and their combined role in the structure itself, commonly can be evaluated rather easily. However, the key issue and the much more problematic interaction parameters in any successful SSI analysis are linked to the soil stiffness, at the relevant strain levels, of the specific interacting soil layers under the corresponding structural loading conditions.

1. INTRODUCTION

The difficulty of developing a reliable SSI prediction, or even of a type C-verification, indeed remains high, because of the unknown details of the influencing soil stiffness.

This can be very simply illustrated by the example of 3 oil tanks (fig 1) containing each 33000m³, positioned in a triangular pattern and each supported by about 430 end bearing soil displacement screw piles of the Omega-type (fig 4), carrying structural allowable loads of about 1000 kN/screw pile, including the expected negative skin friction due to auto-consolidation of the upper soft hydraulically deposited layers (fig 2).

The loading conditions transferred by a flexible steel tank filled with oil, resting on a relatively thin (flexible) concrete slab (0.6m), and supported by a regular pattern of a large group of end bearing, cast on site, soil displacement screw piles, cannot pose any difficulty to the required assumptions for the structural stiffness itself. One simply can state that in such case there is a very uniformly spread equally distributed overburden top load to be carried by the end bearing pile group.

However, predicting, or even back calculating the monitored real load-deformation pattern (type C- calculation), of the 3 interacting tanks under full loading (fig 3a,b) cannot be done without the extensive testing of the soil and its layering and the advanced evaluation of the soils' stiffness parameters as function of time

(changing consolidation coefficients of the relevant layers, etc...) and developing strain levels.

To the reliability and usefulness of each SSI method, it is consequently of utmost importance to evaluate, with an as high a precision as possible, the stiffness characteristics of the most relevant of the SSI elements: the soil. The value of the shear stiffness modulus as a function of the effective stress level, void ratio and developing strain level has to be well understood and measured in lab and in situ, before one can start to use reliably any SSI technique. This becomes even more problematic when dealing with non-traditional soil material, such as cemented soils, expansive soils, crushable soils, etc...

In the lecture, one focuses on crushable sand material as one of the most difficult soil materials in this respect, because the soil material continuously changes its index properties as such with varying stress and strain conditions.

2. INTRODUCTION ON THE STIFFNESS CHARACTERISTICS OF SANDS

The stiffness of sands depends on the sand type, its granulometric curve, the grain shape, the grain crushability, but mainly as well on the relative density of the skeleton and its stress state history.

The sand layer deformations relevant to each SSI analysis are physically governed by a combination of sand particle rolling, particle sliding and particle crushing. Temporary excess

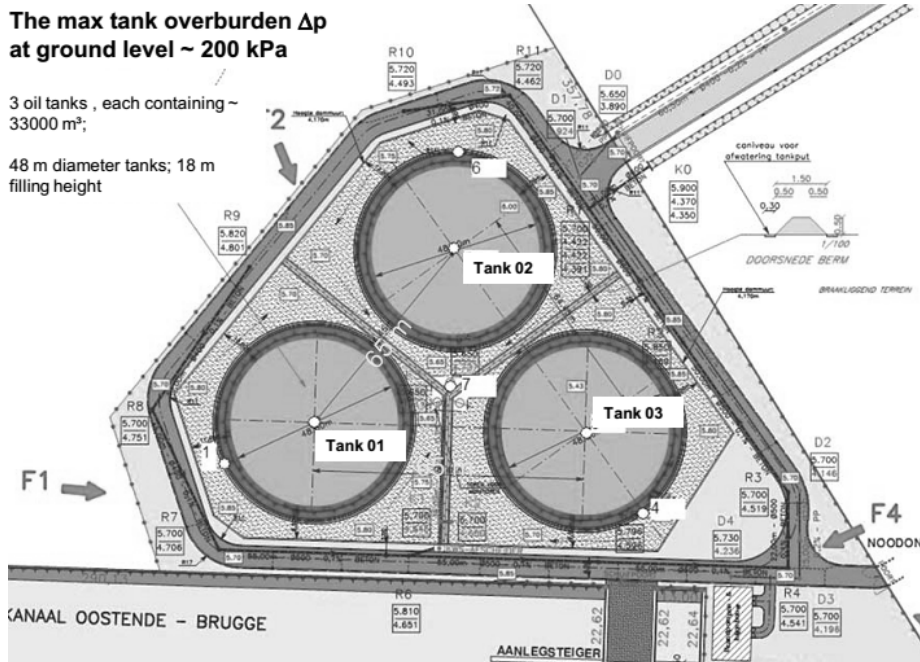


Fig. 1. The site and location of the 3 oil tanks at Ostend – Belgium.

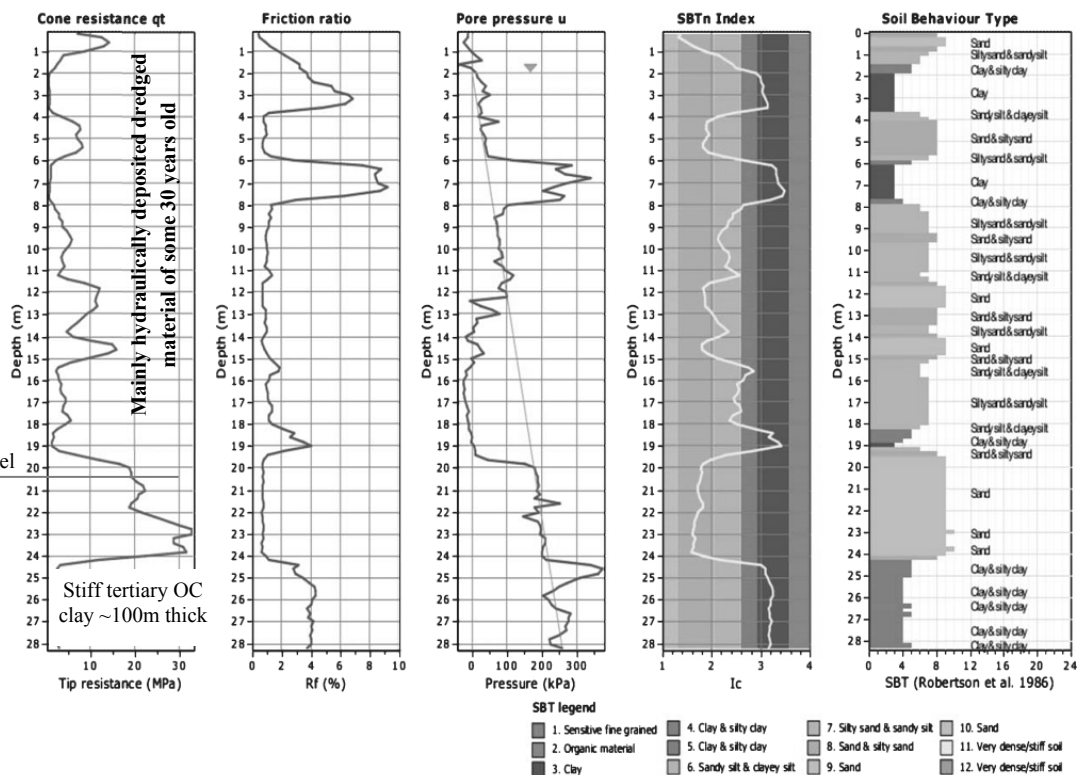


Fig 2 Characteristic CPTU result at the site of the oil tanks in Ostend [3, 4].

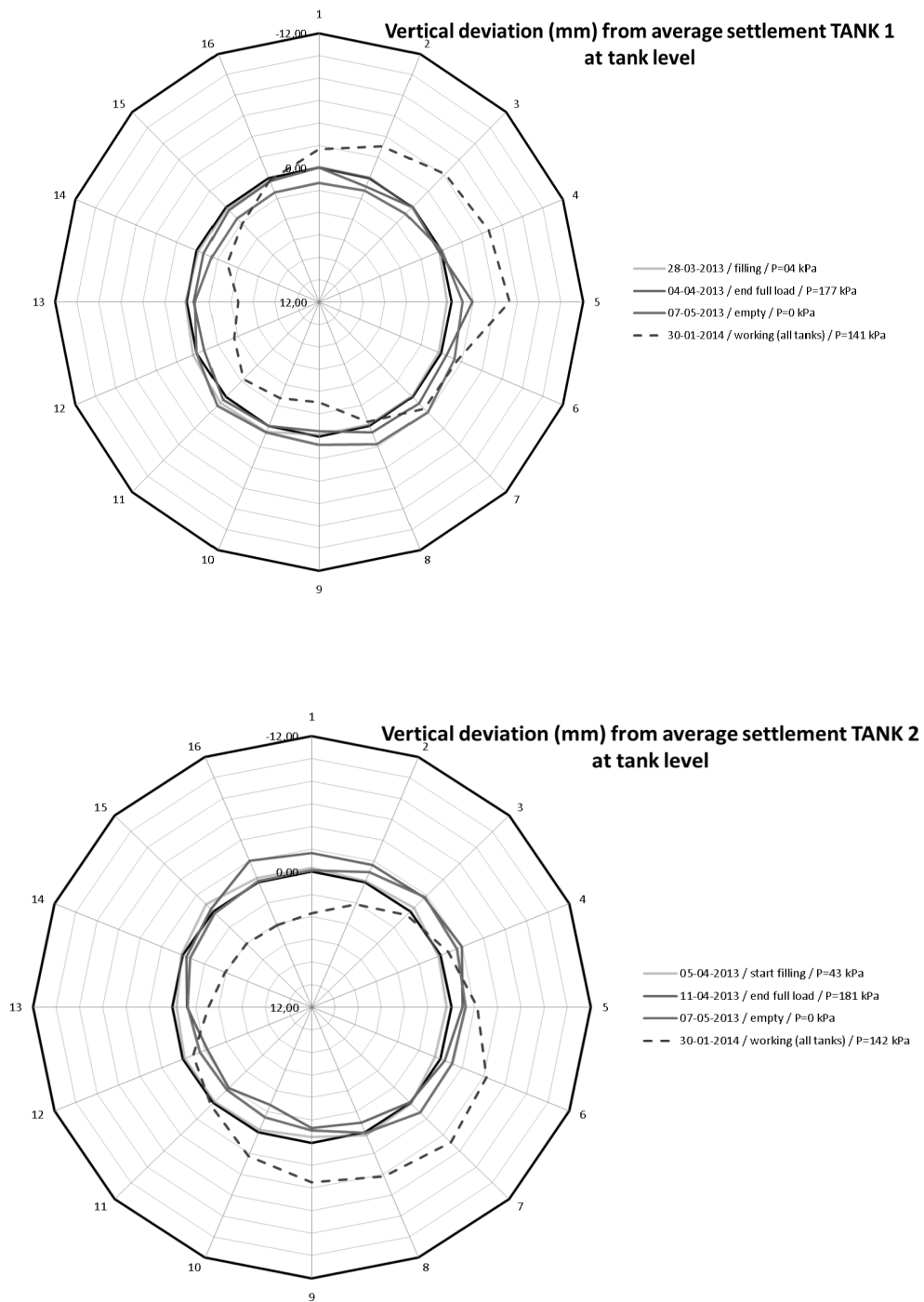


Fig3a settlement increase pattern of the tanks nr 1 and 2, in the phases of the water testing and after the full load oil filling

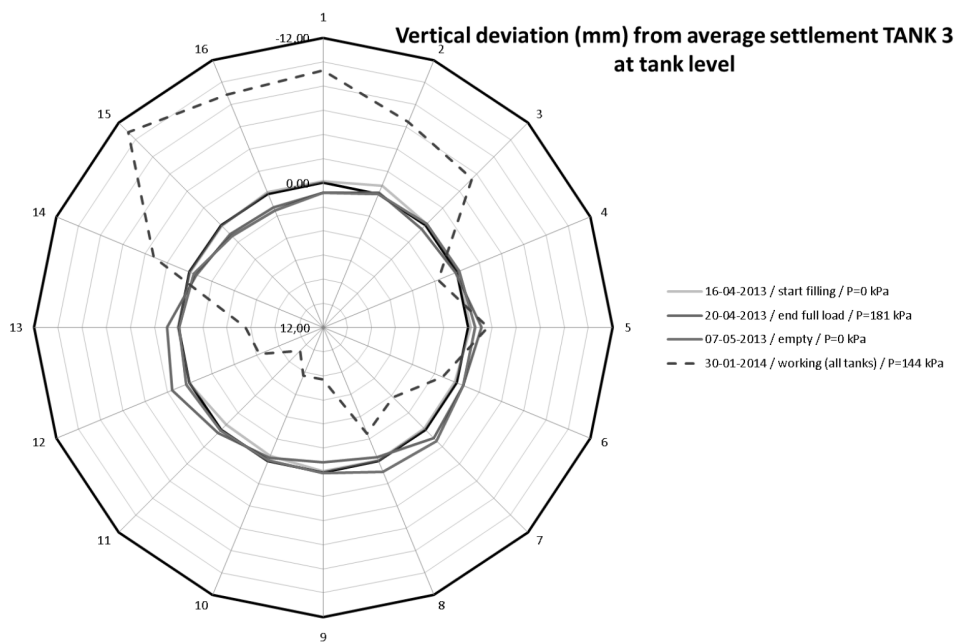


Fig3a settlement increase pattern of the tank nr 3 in the phases of the water testing and after the full load oil filling

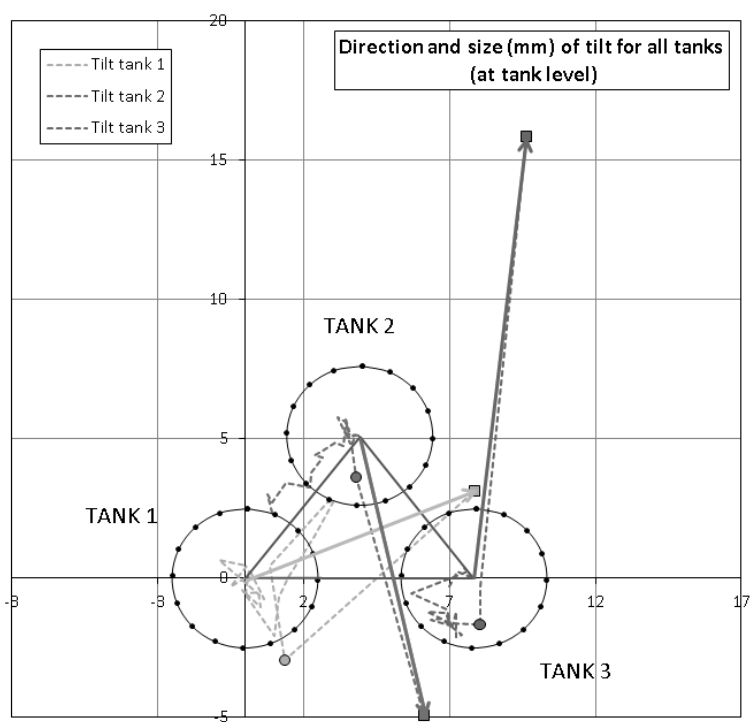


Fig 3b Direction and magnitude of the tanks rotational movements

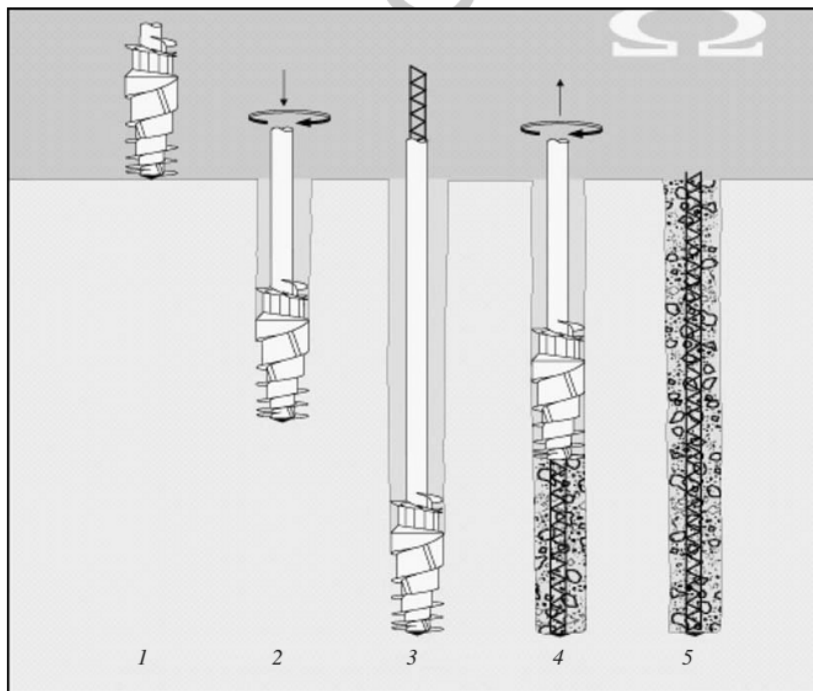


Fig. 4. The Omega screw pile type in Belgium [1, 2].

pore water pressures due to the required squeezing out of the pore fluid does exist, but is of no meaning in practice because of the extremely short time frame linked to such “consolidation” effects.

In carbonate sands, due to crushing of the particles and increasing the fines%, this phenomenon of consolidation will become more important. It also means that ageing of a carbonate deposit will lead to continuously changing c_v -values. It however will always remain negligible as compared to any soft layer consolidation behavior which might come into the picture of the SSI analysis on such construction sites.

Relevant sand particle crushing usually should be considered for the long term deformation behavior, as soon as the mean stress level of the soil-structural interaction element does rise above a certain threshold value. For quartz sands it means: above a value of the order of some 15 MPa; minor crushing of quartz soil grains might already appear from a mean stress level of some 5 to 8 MPa. But generally this type of crushing is not influencing the overall settlement behavior of the deposit too strongly.

The level of 15 MPa is of course a mean effective stress level; the real interparticle contact stress levels do rise easily up to 4 to 10 times higher (depending on the soil skeleton fabric), fig. 5.

In carbonate sands however, this threshold mean stress level triggering the relevant crushing already starts at far lower values and so well within the common geotechnical SSI-engineering mean unit loading ranges (1 to 8 MPa), fig 5.

Particle breakage in crushable sands is a progressive process, ongoing for a long time, even under constant mean stress levels, because of the wide dispersion of the real inter-particle contact stresses. Such inter-particle contact stresses in the sand are varying as well all the time, due to local crushing and subsequent particle displacement. The secondary deformation curves are therefore no longer continuous smooth curves, but do show rather stepwise decaying shapes.

An increase for example of not more than 10% of fines in an embankment (either due to crushing or due to varying grain size of the “various sands” deposited on site), leads easily to an increase of the volumetric strain level of around 10% – 12% of carbonate sand layers.

Such secondary deformation behavior in principle may be described through effective stress based models such as the one associated with the Taylor rheological set up. This model is probably for this type of crushable material more appropriate. Indeed, in the Taylor approach, the secondary stress strain behavior keeps to be uncoupled and is not linked to the stress level at the end of the primary consolidation period. For sands this might be a better approach, (fig. 6).

For silica sands the long-term stress strain curve at common SSI stress level increments is depending on all the above mentioned parameters, up to mean stress levels of about 15 MPa.

From that level on, in practice only the particle strength is left as the governing parameter for the deformations. All other parameters become irrelevant. Similarly, in case of carbonate sands, (fig 7) parameters of the changing sand granulometry, the relative density, particle shape, etc... could become irrelevant as well from a much more moderate mean effective stress level (for example 5 to 8 MPa).

However, the degree of saturation will continue to play all over its predominant role when it comes to influencing the stiffness of crushable sands. Indeed, from many data in our own past years' lab research – mainly on Middle East carbonate sands (bio-clastic origin), the pres-

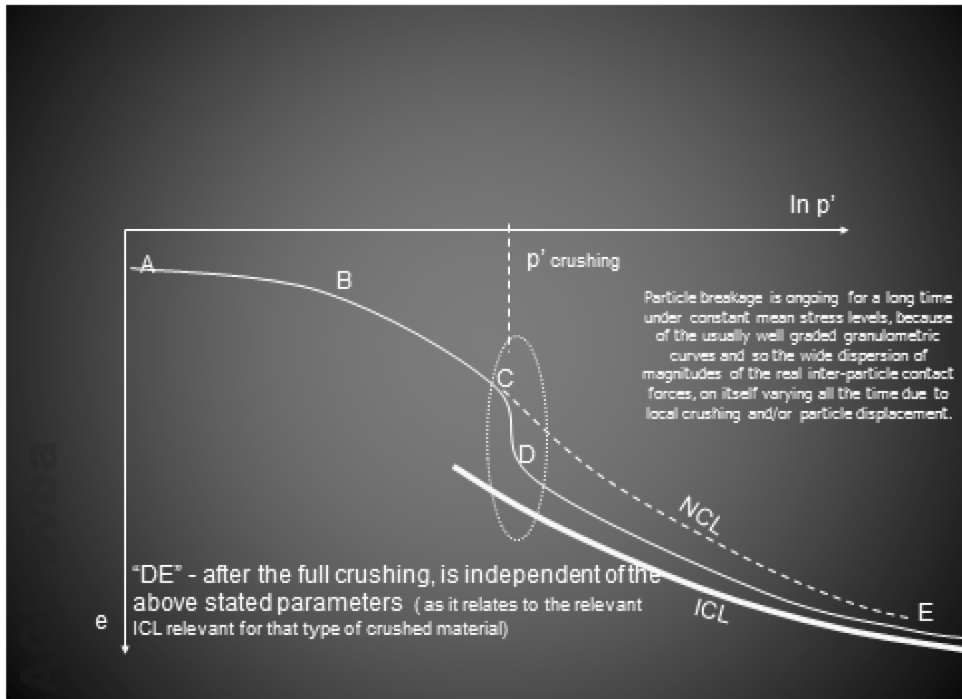


Fig 5

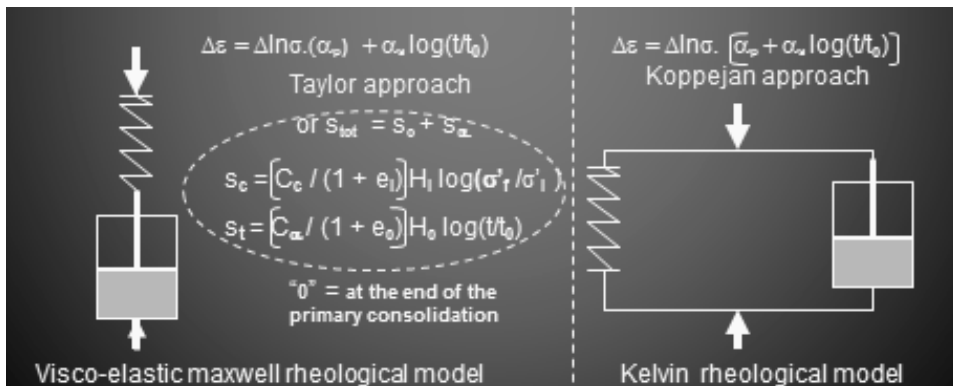


Fig 6

ence of pore water clearly promotes unexpected additional crushing of particles!

Bio-clastic sands contain particles of skeletal origin, such as shells, coral reefs or similar, together with broken organic material fragments (pictures, fig. 7a,b). Such particles are structurally weak due to their shape and the weakness of the composing carbonate materials. It results for calcareous sands (fig 8a,b).

It's obvious (cfr Been et al 1985) that due to the fines content, increasing during the crushing of particles process, the secondary sand matrix stiffness is decreasing.

We therefore would recommend to very carefully (in small steps) draw the “e – ln p’ ”

curve as well as the tangent constrained modulus:

$Moed = \Delta \sigma'_v / \Delta \epsilon_v$, on the vertical axis versus $\ln p'$ on the horizontal axis.

At the “yield point” of the “e – ln p’ ” graph, one might expect a minimum value of the Moed to correspond with this yield point level. The “e” is commonly linked to the relative density D_r from conventional lab testing. The concept of a relative density D_r has been developed to allow for comparing the behavior of different materials at equivalent “density”.

However, the parameter of relative density D_r is not an inherent soil property. It depends on the determination of the minimum and maxi-

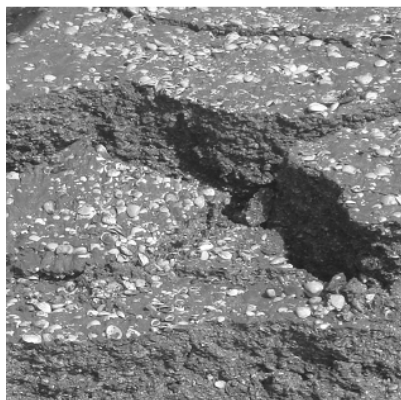


Fig 7a. South American

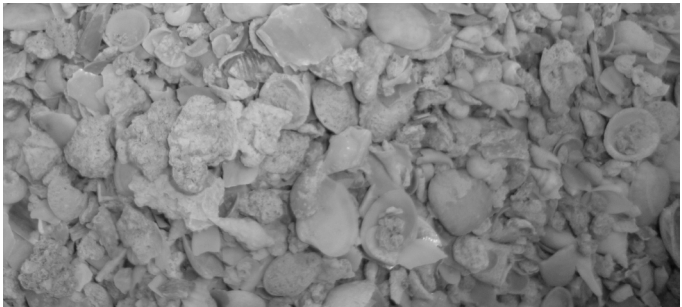


Fig 7b. Middle East

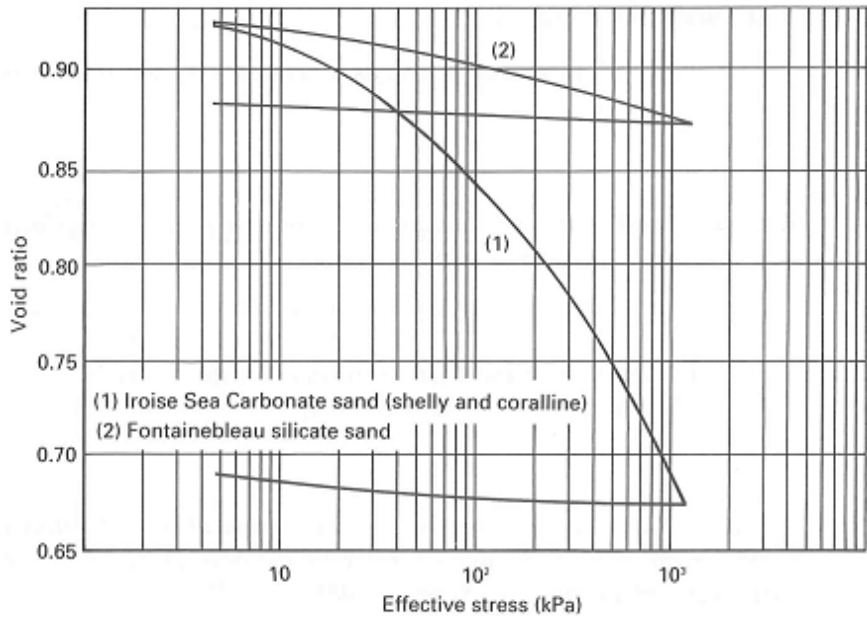


Fig 8a

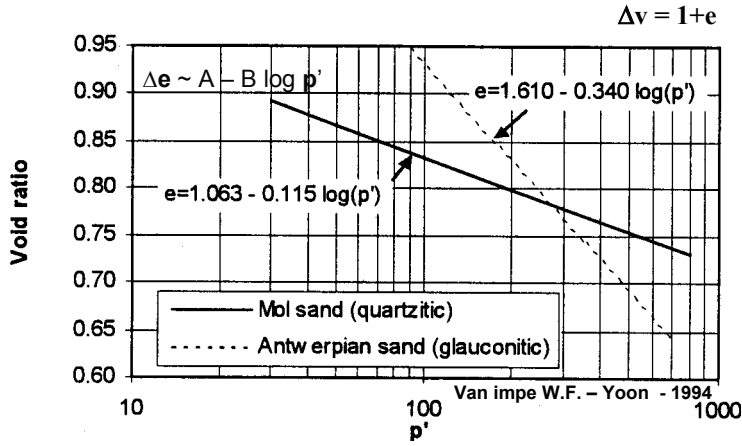


Fig 8b

imum density of the soil, which themselves are the result of index tests, very sensitive to the methodology applied for the input energy.

3. RELEVANCE OF RELATIVE DENSITY

The accuracy at which D_r can be determined is considerably low. We need to consider errors on the determination of the minimum, maximum and actual sample density. Any small error in either of these values leads to disproportionate errors in the calculated value of D_r (e.g. a 1 % error in the minimum density could lead to more than 10 % error in the value of D_r).

From our own research over the last 5 years, in carbonate Middle East sands, (fig 14a), it became clear that we should try to deal more directly with “void ratio” (e) related to the elastic wave velocities measurements on site and the corresponding effective stresses involved.

In this respect, a proposal of such possible correlations (P.O. van Impe -2013), for the Middle East sands (fig 14a) in hydraulically deposited vibro-compacted sand masses, extensively tested, is:

$$\bar{V}_s = C_s (\sigma'_v/p_a)^{nv} (\sigma'_h/p_a)^{nh} e^{-d}$$

$$\bar{V}_p = C_p (\sigma'_v/p_a)^{mv} (\sigma'_h/p_a)^{mh} e^{-f}$$

with the correlation coefficients:

$$C_s = 248; \quad d = 0.291;$$

$$nv = 0.164; \quad nh = 0.142;$$

$$C_p = 1661; \quad f = 0.1753;$$

$$mv = 0; \quad mh = 0.0323$$

The on-site measured data analysed (P.O. Van Impe -2013), using the indicated correlations mentioned, (fig 9a,b), were showing very

good reliable correspondence with the predicted values according to the equations above.

In the case of crushable soils, we encounter the additional problem of the validity and the much stronger influence of the test-method to determine maximum density. Values of maximum density depend very much on the chosen densification method (densification energy). High densification energy will lead to higher maximum density, but will induce more important crushing. This means that we are actually never dealing with identical soil material, and a value of maximum density becomes irrelevant.

As reported by P. Main et al (2009) (fig. 10); from related to calibration chamber testing, a very general mean conversion factor would be around $F = 2.3$. This is of course a very much oversimplified approach. In the past three decades indeed, a number of studies have been developed to define a correlation factor between the cone resistance measured in silica (or quartz) sand and later on as well calibration chamber type of centrifuge tests were performed as well for crushable sands such as the calcareous sands.

As shown in the table below, for each carbonate sand tested, one assumes the lower and upper bounds of a type of conversion factor F defined as:

$$F = \frac{q_{c,silica}}{q_{c,crushable}}$$

when comparing
crushable sands
with silica sands

$$F = \frac{q_{c,quartz}}{q_{c,crushable}}$$

when comparing
crushable sands
with quartz sands

Table: Conversion factors F for crushable sands

Sand	Lower Bound F	Upper Bound F	Note	Reference
Quiou calcareous and Ticino Silica sand	1.3	2.2	Depending on D_r	Bellotti/Jamiolkowski (1991)
Quiou calcareous and Ticino Silica sand	1.8	2.2	Depending on D_r	M.Almeida et al (1992)
Patrn island calcareous and quartz sand	1.5	1.7	Depending on D_r	G.Gudehus, Cudmari (2004)
Dogs Bay calcareous and Mol quartz sand	4.0	8.0	Depending on D_r	Yasufuku et al. (1995)
Quiou calcareous and Mol quartz sand	2.0	4.0	Depending on D_r	Bellotti (1991)
Bioclastic calcareous (Banco Archimedes Uruguay-an) and Mol quartz sand	1.4	2.3	at depths < 7m under water to 4 m above water	Van Impe (2010)
Abu Dhabi (S_1) Bioclastic calcareous sand and Mol sand	Estimate 1.8		$D_r \sim 60\%$	Van Impe (2012)

It's important to notice that most stiffness correlations appear to show a very weak dependency on relative density D_r . There is moreover hardly any connection between the actual stress-strain behavior at the site and the determined so-called D_r parameter. Such stress-strain behavior is indeed strongly controlled by the stress-state, particle shape, particle mineralogy, stress history etc., which are not (fully) reflected in the value of D_r nor in the cone resistance q_c . The SCPT results on the test site of our research areas clearly do support this statement.

Since the determination of relevant correlations to the D_r parameter remains a long and expensive lab testing process, while the final result is not at all accurate enough to make any kind of relevant prediction of the sand stiffness and so of the deformation behavior of the site.

For this reason, it is in our opinion much more efficient to measure these stiffness related parameters directly on the site. The quality control procedure would then consist of checking the measured parameters (e.g. shear wave velocity V_s and derived small-strain shear modulus G_0 from SASW combined with SCPT) to see if they can fit the relevant design requirements (settlement, bearing capacity, liquefaction).

4. THE ESTIMATION OF THE SAND STIFFNESS

The Moed, mentioned before as the tangent oedometric (constrained) stiffness, or even the simple young stiffness modulus E_y , can also be derived from on-site-test results such as the CPT data; based on empirical correlations such as : Moed (either $E_y = \alpha \cdot q_c$; with the values of $\alpha = f(D_r, \text{ stress history})$, decreasing with rising relative density D_r of the sand, (for example – fig 11), and increasing remarkably with more pronounced O.C. and ageing.

From empirical q_c - σ'_v - D_r relationships, varying obviously with increasing depth, (fig 12a,b), lots of commonly used approaches for various sand type are suggested in literature. From research on the corresponding sand type, lab test based correlations (ex. Fig 13 for Quiou sands) of the D_r and Moed at increasing stress levels, consequently would allow the geotechnics expert designer to also make use of in situ CPT measurements to evaluate reliable q_c -Moed correspondences at that site, for that type of sand. The above mentioned values “ α ” are actually the outcome of such approach.

The reliability of the empirical relationships of such stiffness parameters when starting from non-crushable sand material has proven to be high and fully reliable for common geo-engineering practice and modeling such as required for the SSI approaches.

From extensive research, it however became clear in the last couple of years, that the same reliability cannot be reached when dealing with crushable, carbonate, sands.

From a large number of centrifuge test campaigns, TX-bender element tests, and large scale oedometer tests on carbonate sands from the Middle East, on the one hand and extensive on site testing (CPT, CPTU, SCPT, large scale plate load tests, ...) of hydraulically deposited carbonate sand masses, on the other hand, the necessity of a different approach to the evaluation of the carbonate sand stiffness, became evident.

parameter	unit	Sand type –extreme boundaries “-S1”	
D_{50}	[mm]	0.23	0.57
% smaller than 75µm	[%]	3	3
CaCO ₃ content	[%]	93.0	98.0
min dry density	[kN/m ³]	10.92	11.65
max dry density	[kN/m ³]	14.08	15.12

5. A NEWLY PROPOSED METHODOLOGY FOR ANALYZING THE CARBONATE SAND STIFFNESS BEHAVIOR – AN ILLUSTRATING EXAMPLE

From advanced lab testing research, one can obtain for the crushable sand at stake, the

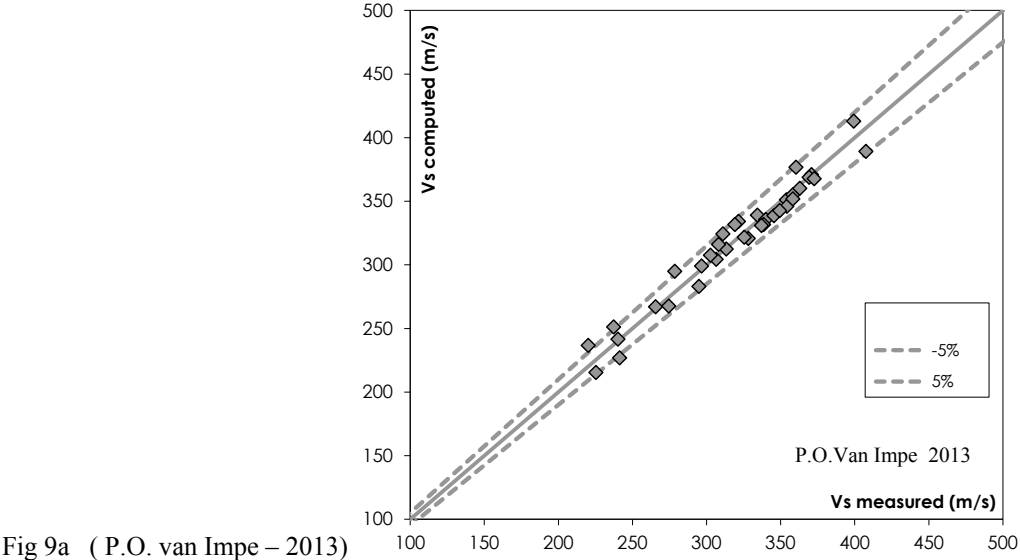


Fig 9a (P.O. van Impe – 2013)

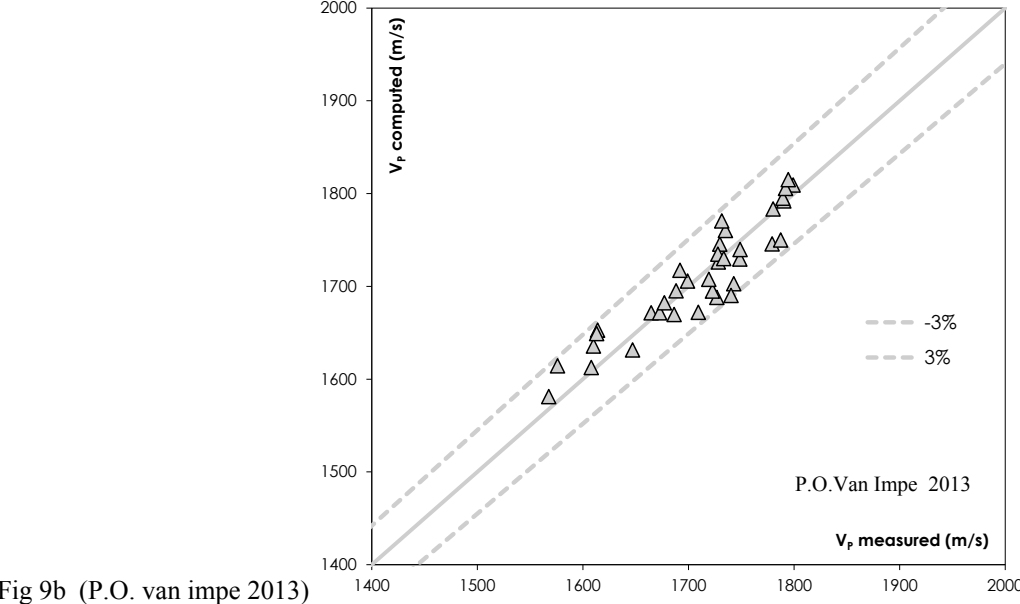


Fig 9b (P.O. van impe 2013)

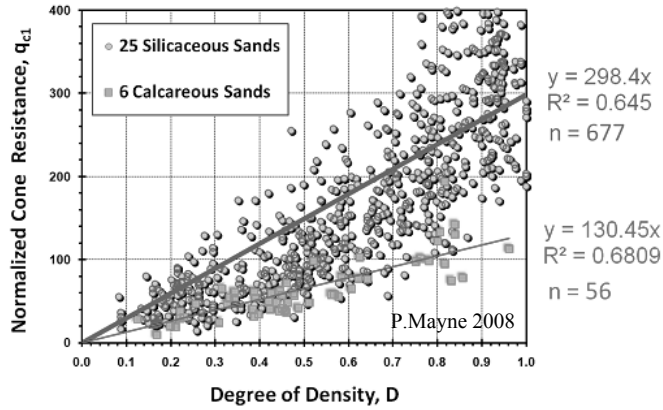


Fig 10, (after P. Mayne-2008)

$$F_{c\text{mean}} = q_{c\text{ silica}}/q_{c\text{ calcareous}} \sim 2.3 \text{ with } Dr = D \cdot \frac{\gamma_{d,\text{max}}}{\gamma_{d,\text{situ}}} \text{ and } q_{c1} = (q_c/p_{\text{atm}}) / (\sigma'_{v,0} / p_{\text{atm}})^{0.5}$$

Sand- stiffness from CPT
at “foundations”-strain level $\sim 0.1\%$
 $E_{\text{or } M} = \alpha q_c$

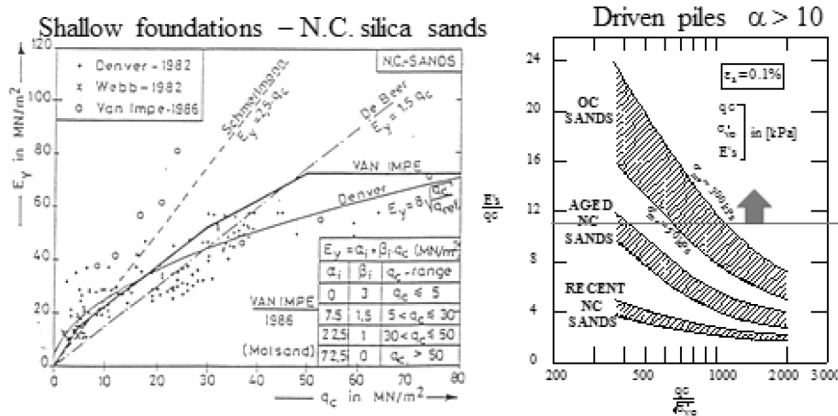


Fig 11

following interacting soil parameter relations:

- $q_c - D_r - \sigma'_v$ from calibration chamber tests in centrifuge K_0 conditions
- ϕ' as a function of the strain levels measured in careful strain controlled TX
- $V_s - \sigma'_v - \sigma'_h - e$, as well as $G_0 - \sigma'_v - \sigma'_h - e$ correlations based on bender element TX and resonant column tests, in the adapted lab test stress conditions (K_0)

- G – decay curve, based on the Bender element, the resonant column and the strain monitored TX test results.

This should allow the geo-engineering expert, on the basis of CPT results on site, to derive the following parameters:

- $q_c - D_r$ as a function of depth, on site
- G_0 as a function of depth (from i'), (from iii) at corresponding K_0 (from ii)
- G and so the constrained stiffness at the various strain levels, from (iv).

The analysis (P.O. Van Impe 2012), for this type of highly carbonatic Middle East sand (and going out from a series of K_0 centrifuge calibration chamber tests) has allowed to establish the correlation between CPT cone resistance q_c , relative density D_r and the vertical effective stress level σ'_v for the specific soil materials used at the hydraulically deposited sand site, (cfr also fig 12b).

$\forall \sigma'_v > 50 \text{ kPa}$

$$\frac{q_c}{p_a} = e^{D_r \cdot C_{2,avg}} \cdot C_{0,avg} \cdot \left(\frac{\sigma'_v}{p_a}\right)^{C_{1,avg}} \quad (1)$$

$\forall \sigma'_v \leq 50 \text{ kPa}$

$$\frac{q_c}{p_a} = \left(\frac{\sigma'_v}{50}\right)^{0.5 + C_{1,avg}} \cdot e^{D_r \cdot C_{2,avg}} \cdot C_{0,avg} \cdot \left(\frac{50}{p_a}\right)^{C_{1,avg}} \quad (2)$$

where the values of the correlation coefficients $C_{i,avg}$ are given in the table below. These correlations

are significantly different from what can be expected for silica sands. The deviation from the “typical” silica sand behavior becomes more significant for higher stress levels and higher relative densities.

In the middle East carbonate sands under investigation, at the test site and based on the results of CPT tests, values of the relative density D_r were determined along a CPT profile using the above correlations.

Parameter	Above GWT	Below GWT
C_0	25.410.375	12.95
C_1	2.265	0.27
C_2		2.76

We could link these parameters to the void ratio e and the parameters σ'_h and σ'_v , of the sample. Following correlations were established

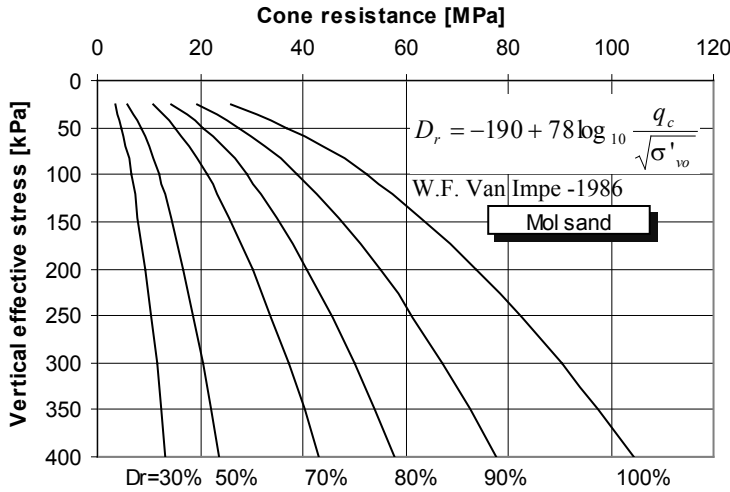


Fig 12a (Van Impe -1986) silica Mol sand in very large Calibration chamber and CPT(M)

• Jamiolkowski (2003) :

$$D_r = \frac{1}{3.10} \ln \left[\frac{q_c^{quartz}}{17.68 (\sigma'_{v,0})^{0.5}} \right]$$

• Baldi et al.(1986) :

$$D_r = \frac{1}{2.41} \ln \left[\frac{q_c^{quartz}}{157 (\sigma'_{v,0})^{0.55}} \right]$$

• Lancelotta (1983)
and Garizio (1997) :

$$D_r = -1.292 + 0.268 \ln \left[\frac{q_c^{quartz}}{(\sigma'_{v,0})^{0.5}} \right]$$

• Jamiolkowski (2003)

$$q_{c,quartz}^{corr} = [1 + 0.015(D_r - 20)] \cdot q_{c,calcareous}^{measured \text{ on site}}$$

• Gudehus/Cudmani (2004) :

$$q_{c,quartz}^{corr} = [1.3629 + 0.0046 \cdot D_r] \cdot q_{c,calcareous}^{measured \text{ on site}}$$

for P-wave velocity V_p , shear wave velocity V_s and small strain shear stiffness G_0 , with the proposal:

$$V_s = A_s \left(\frac{\sigma'_v}{p_a} \right)^{B_{sv}} \left(\frac{\sigma'_h}{p_a} \right)^{C_{sh}} e^{-D_s} \quad (3)$$

$$V_p = A_p \left(\frac{\sigma'_v}{p_a} \right)^{B_{pv}} \left(\frac{\sigma'_h}{p_a} \right)^{C_{ph}} e^{-D_s} \quad (4)$$

$$G_0 = A_g \left(\frac{\sigma'_v}{p_a} \right)^{B_{gv}} \left(\frac{\sigma'_h}{p_a} \right)^{C_{gh}} e^{-D_s} \quad (5)$$

Where p_a is the reference atmospheric pressure (100 kPa). The A, B, C and D parameters for each equation are fitted to the data of the BE

test in the laboratory triaxial equipment. Additionally, local strain measurements during triaxial tests have allowed to determine the degradation of the stiffness as a function of strain-level (stiffness degradation curve). It was found that the values for the small-strain shear modulus G_0 were significantly higher than those expected for silica sands at similar conditions, while – on the other hand – the stiffness degradation is more pronounced. These findings confirm the general trend presented in the literature.

It moreover was derived from all on site testing results that the performing series of CPT

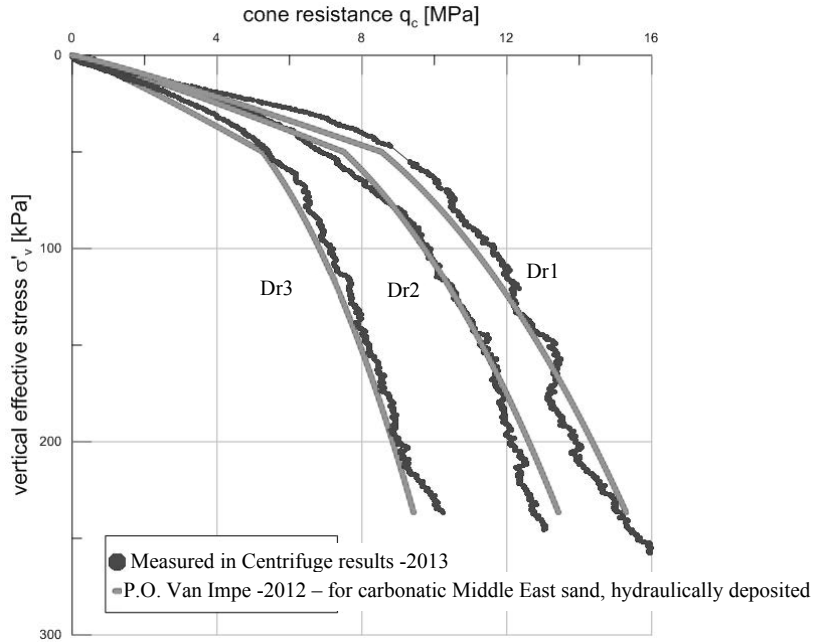


Fig 12 b - P.O. Van Impe-2013

$$M = K_M \cdot (1 - D_r)^{-0.97} \cdot \left(\frac{\sigma'_v}{p_a} \right)^{0.42}$$

being

$$K_M = 14.5 \text{ Mpa}$$

$$\Delta s = \frac{\Delta \sigma}{M} \cdot \Delta h$$

Δs = settlement

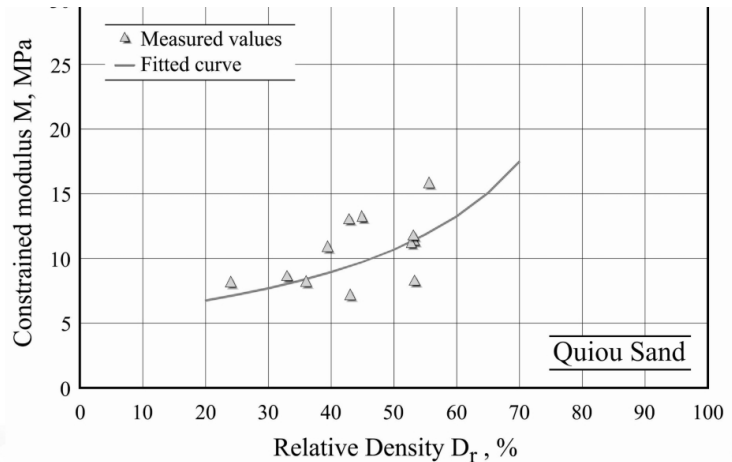


Fig 13 (after Jamiolkowski 1998)

as a stiffness controlling test in deposits of carbonate sand masses is not a recommendable methodology, for not really reliable at all. As we argued at several occasions, our recommendation on the contrary would go out from the carbonate sand testing on site by means of SCPT(u), combined on site with SASW and DMT.

For understanding the behavior of the carbonate sands, the depth versus D_r , G_0 and V_s prediction curves, derived from well elaborated testing programs, with lots of data of SCPT cone values is not enough; it is also becoming unavoidable to dispose of a reliable estimate of the on-site stress conditions (σ'_v and σ'_h). This has been briefly mentioned here above under i/ to iv/ and the equations 1/ to 5/.

Once below the mechanically OC upper zones of hydraulically deposited sand embankments, the predictions on the basis of the earthquake K_0 -steered equations proposed, are very well matching the stiffness data predicted for common carbonate sand deposits out of the testing highlighted above.

In any case, geo-engineering quality control of such densified carbonate sand mass proves that hydraulic clapping energy or/and vibro-compaction ground improvement technique in such crushable sand material, actually do not lead to a densification as such, but are actually only leading to a ground improvement, because of the very strongly changing stress field conditions (from K_0 to very O.C. range).

6. SUMMARISING CONCLUSIONS

In carbonate sand masses, in situ quality control testing should at least start from a series of (seismic) SCPTu (measuring the standard CPT cone resistance, friction angle and pore water pressure, combined with the shear wave velocity V_s) and zone load tests.

Based on the SCPT result and the $q_c - D_r$ correlations from laboratory tests, the relative density profile can be determined for each SCPT profile. Additionally, one can try to correlate the measured shear wave velocity V_s and the corresponding cone penetration resistance q_c . From this, it became clear that, in carbonate sands, there is absolutely no correlation between these two parameters. The same conclusion can be reached when comparing the measured shear wave velocity V_s and the corresponding relative density D_r (derived from the local q_c value). One only can conclude that

the relative density D_r does not reflect the actual behavior of the material and is therefore irrelevant as a quality control parameter.

Attempts were made to predict the in situ stiffness profile based on the common CPT test, using the correlations determined during the laboratory testing campaigns. It is shown that, although our predictions were significantly better than those based on "typical" correlations for silica sands, in some cases the carbonate sand, the soil stiffness was significantly underestimated. This is due to the fact that the reliability of such "qc-stiffness" correlations are strongly depending on the parameters (K_0 , OCR,...) which cannot be "measured" on site, but have to be estimated, with the appropriate geo-engineering judgment.

Certainly at sites where various densification techniques were applied and so do lead to a very complex stress history in the soil, adequate in situ testing is the only way to obtain relevant information on the relevant stress-strain parameters (like V_s), and so on the corresponding relevant sand stiffness characteristics. In our opinion, a combined on-site use of SCPT(u) testing, coupled to DMT and SASW testing profiles, would be the most appropriate way to deal with the evaluation of the deformation behavior of such crushable sand fills and embankments.

It is the greatest challenge for an advanced SSI methodology to model such stress conditions influences in connection to the deformations to derive from the full soil-structure interaction approach.

Pile group action under vertical compression loads

Y. El-Mossallamy

Ain Shams University, Cairo, Egypt

ABSTRACT: Piles are powerful geotechnical foundation elements which are suitable for most subsoil conditions where structure loads should be transmitted to deeper layers either to fulfill the required bearing capacity or to control the deformation to acceptable values regarding the structural serviceability requirements. In most cases, the pile foundations consist of group of piles. Realistic considerations of the pile group action regarding both the ultimate bearing capacity as well as the deformation behavior of the pile group are necessary to achieve a reliable, efficient and economic design. This paper deals with performance of pile groups under vertical compression loads. Simple analytical methods to estimate the settlement of pile groups will be presented and compared with enhanced three dimensional numerical analyses. The field monitoring of a well documented pile group under vertical compression loads and the feed-back of this information into the analyses procedure of the same pile group applying different analytical models will be demonstrated and discussed.

1. INTRODUCTION

The load-settlement behavior of the piles in a pile group, in many cases, is completely different from the behavior of the corresponding single pile. The group action presents the behavior of the pile group in comparison with that of the single pile. Pile group action plays an important role for the behavior of piled foundation either under vertical tension and compression loads or under horizontal loads. This paper will deal only with the behavior of pile groups under vertical compression loads. The pile group action is considered either by adapting simple correlations or by relating the pile group to simplified foundation forms or by applying advanced numerical analyses. Comparison between different methods will be presented and discussed in the presented paper.

As it is almost impossible to take into account, in an adequate manner, all details of the soil disturbance caused due to pile installation by theoretical means, pile load tests on single piles are frequently carried out to determine the load-settlement behavior of a single pile. On the other hand, it is expensive and may be not possible to carry load tests on pile groups. Therefore, the utilized analytical tools and soil data in this research are first validated based on the results of pile load test before extrapolating the analysis to pile groups.

2. PILE GROUP ACTION

There are two types of pile group action which affect the pile group behavior. The first one considering the ultimate bearing capacity of the pile group in comparison with that of the corresponding single pile (pile group efficiency). The group efficiency is defined as the ratio of the ultimate load capacity of a pile group to the sum of the individual ultimate pile load capacities. The second type of pile group action considers the settlement of the pile group in comparison with that of the corresponding single pile under the same average load. Figure 1 illustrates schematically these two types of the pile group actions.

2.1. Pile group efficiency

There are two failure mechanisms that can be applied to estimate the ultimate load of a pile group (Kishida and Meyerhof, 1965). Failure of the individual piles in the pile group or a block failure of the whole pile group can occur depending on the soil conditions and on the pile spacing. In case of failure of individual piles, the ultimate load of a pile group is the sum of the ultimate load of the piles of a pile group and the pile group efficiency is equal to unity. In case of driven piles in sand, the pile efficiency may be larger than unity (Kézdi 1957, Fig. 2a). This increase of the bearing capacity is due to the densification of the sand by successive driving of the individual piles. Liu et al. (1985) conducted an extensive field test series on bored

pile groups in sandy soil with and without the cap being in contact with the soil. The results of these field tests showed that there is no evidence of a block failure. It can generally be concluded that in cases where effective stresses

control the pile group performance, failure of the individual piles govern the pile group capacity. A pile group efficiency of unity can be considered in such cases as a lower bound that lies in the safe side.

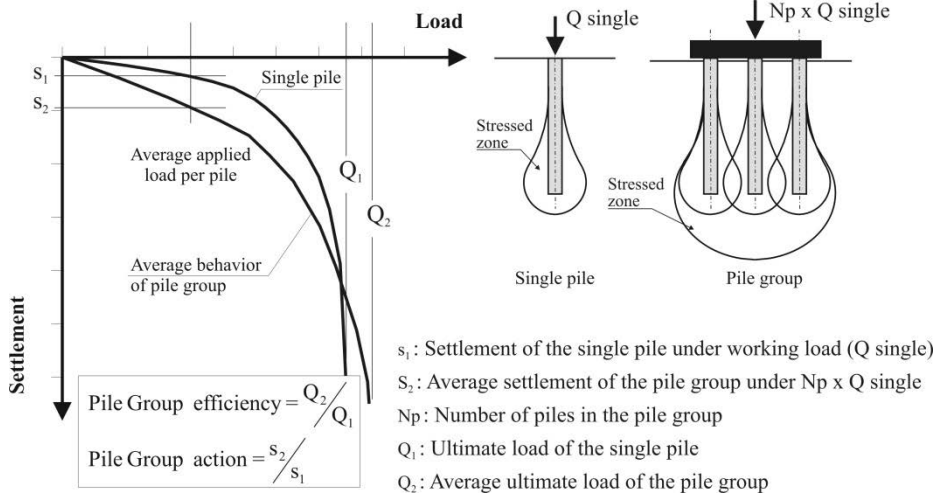
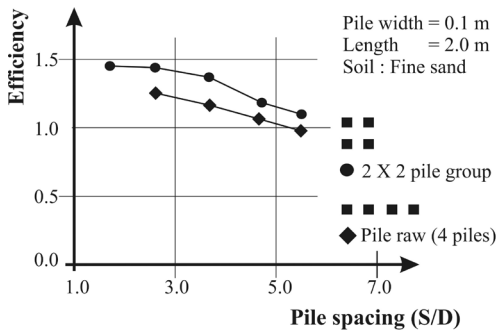
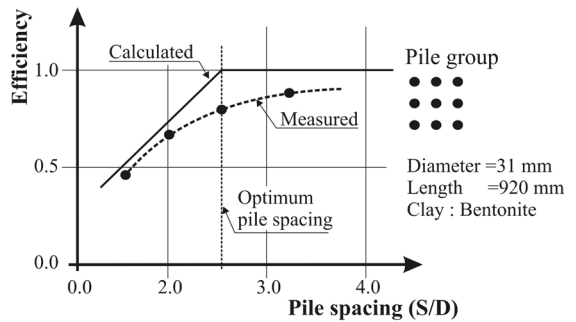


Fig. 1: Definition of pile group efficiency and pile group action



a- Pile group efficiency in sand (Kézdi 1957)



b- Pile group efficiency in clay (Sowers et. al 1961)

Fig. 2: Pile group efficiency

The second failure mechanism is the block failure of the pile group as a whole. In this case the ultimate load of a pile group can be determined by the following expression for pile groups in cohesive soil (Sowers et. al 1961):

$$Q_{\text{ultimate, group}} = (c_{ub} N_c B W) + (2 (B+W) L_p c_{us}) \quad (1)$$

where:

$Q_{\text{ultimate, group}}$ = Ultimate resistance due block failure

N_c : Bearing capacity factor ranging between 5 and 9 (according to Skempton, 1953)

c_{ub} = Undrained shear strength of clay at and below pile tips

c_{us} = Average undrained shear strength of clay along pile shaft

B = Breadth of group

W = Width of group

L_p = Length of piles

The calculated pile group efficiency applying equation 1, for pile groups in soft to firm clay with pile spacing larger than three times the pile diameter, is almost equal to unity. Therefore, the failure of the individual piles in a pile group governs the group behavior for these conditions. The measurements of the small scale load tests in soft clay (Sowers et al. 1961, Fig. 2b) agree well with these results. The calculated efficiency of the pile groups in stiff to hard clay is always greater than unity for all pile spacing. Therefore, for most practical applications, the bearing capacity of the individual piles in a pile group governs the whole pile group capacity and the pile group efficiency can be considered equal to unity. The block failure can only be a decisive design criterion in the case of pile groups in soft clay with smaller pile spacing (smaller than three times the pile diameter) or in cases where there is a relatively weak layer just beneath the pile tips causing punching of the whole pile group as a block.

2.2. Pile group action

In many cases, the absolute settlement as well as the differential settlement is the governing aspects of the foundation design. The load-settlement behavior of the pile group is totally different from the behavior of the corresponding single pile depending on the geometry of the foundation, the number of the piles within the pile group, the pile-pile spacing, the depth of compressible layer and the applied load level.

2.2.1 Factors affect pile group action

Numerical analyses can be utilized to study the pile group behavior and to evaluate factors affecting it. Three dimensional analyses applying the boundary element method (El-Mossallamy/Franke 1997, Franke et al. 2000

and El-Mossallamy 2002) are used to study the performance of pile groups under vertical compression loads.

The performance of pile groups of 2×2 , 3×3 and 4×4 with different pile length to pile diameter ratio and different pile spacing to pile diameter ratio were investigated applying a real three dimensional analyses. The depth of compressible soil is taken in all these analyses corresponding to twice the pile length. The effect of the depth of compressible layer was studied in separate analyses. In the first analyses stage, stress strain behavior of the soil as well as the pile-soil interaction is considered as linear elastic. The effect of soil and pile-soil nonlinear behavior at pile shaft and pile base is considered in a separate stage of analysis.

Figure 3 shows the results of the first stage of analysis. The pile group action is defined as the ratio between the settlement of the pile group connected with a rigid pile cap to the settlement of the corresponding single pile acting on the average load of the pile group. Increasing the pile spacing decreases the pile group action. The pile group action controls the group performance of floating piles in homogeneous soil even in case of large pile spacing. The number of piles in the pile group has a recognizable effect on the pile group action. The pile group action increases with increasing the number of piles in the pile group. This effect is more pronounced by small pile spacing than by large spacing.

Figure 4 shows the relation between the group action and the pile length to pile diameter. The pile group action increases with pile length to pile diameter ratio. The effect of pile length to pile diameter on the pile group action depends on the pile spacing and on the number of piles in the pile group. This effect is more pronounced with increasing the number of piles in the pile group.

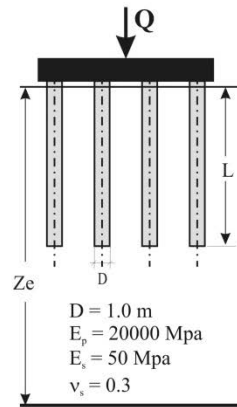
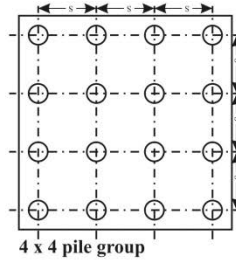
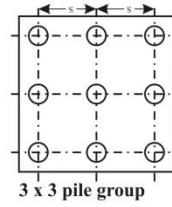
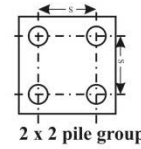
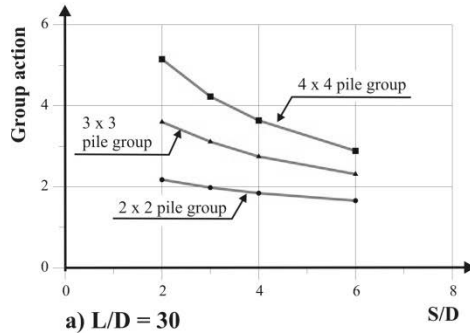
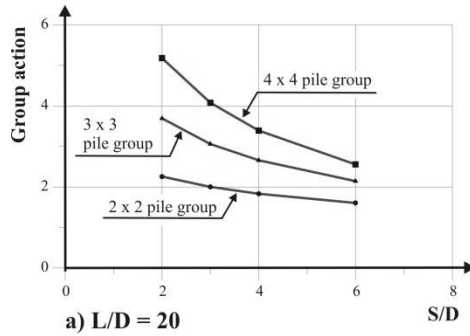
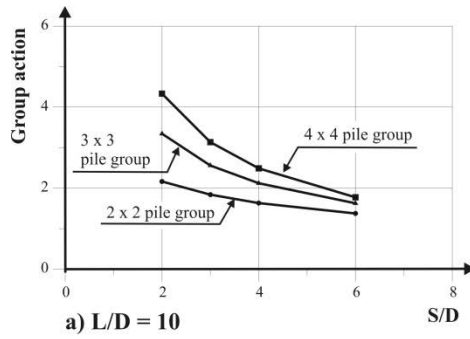


Fig. 3 Pile group action regarding pile spacing and number of piles

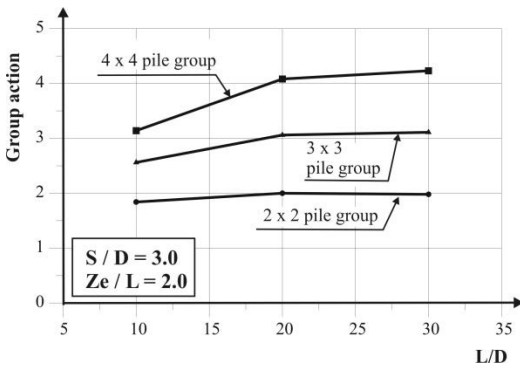


Fig. 4 Pile group action regarding pile length to diameter ratio

The 4x4 pile group was analyzed further using different thickness of the compressible layer to study its effect on the group action. Figure 5 shows the results of these analyses. It can be recognized that the pile group action increases with increase the depth of the compressible layer to some extent and has a certain convergence trend with very large thickness of the compressible layer. These results show that the thickness of the compressible layer is a decisive factor for calculating the pile group action. The depth of the compressible layer could be determined either according to the geological conditions of the site or considering the so called

small strain deformation modulus. In the later technique the deformation modulus of the soil depends on the strain level. At very deep layer below pile tip, the strain due to pile loading is too small and hence corresponding deformation modulus is too high. Applying such models can help to determine the effective depth in a more rational way. Alternatively, the effective depth

is estimated as a ratio either of the pile length or of the pile group breadth. It was found that the effective depth of the compressible layer could be taken in practical application in the range of 1.5 times the pile length or at least the smallest group width below the pile tip. It is apparent that this topic needs more research.

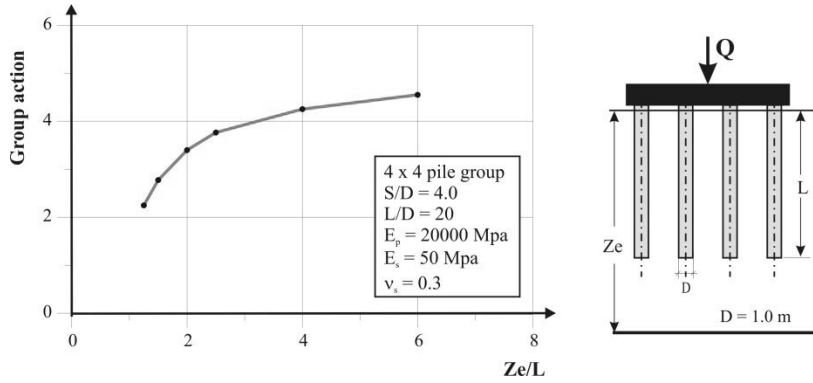


Fig. 5 Pile group action regarding depth of compressible layer

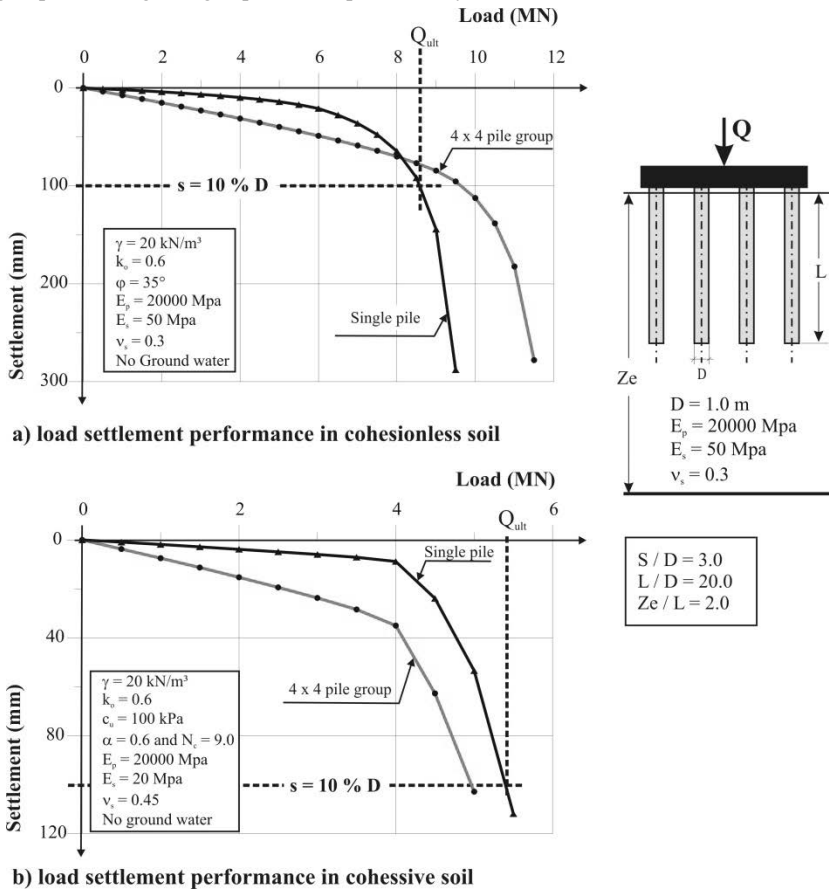


Fig. 6 Load settlement performance of single pile and the corresponding average behavior of the pile group in different soil types.

The effect of nonlinear response on the pile/pile interaction was studied in the case of 4×4 pile group with pile spacing to pile diameter of 3.0. The piles were connected with a relatively rigid pile cap and were assumed floating in homogeneous soil. Two extreme types of soil were studied. Pure cohesive stiff clay with undrained shear strength of 100 kPa as well as a pure cohesionless soil with angle of internal friction of 35° was considered in these analyses. The effective depth of the compressible soil was taken twice the pile length. The load-settlement behavior of the pile group and the corresponding single pile were calculated applying a nonlinear boundary element method. Figure 6 shows the calculated load-settlement behavior of the single pile compared with the average one of the pile group.

Figure 7 shows the effect of the pile group interaction on the load-settlement behavior of the 4 x 4 pile group depending on the load level (applied load related to the ultimate one). The ultimate load is defined as the load corresponding to settlement of 10% of the pile diameter as detected for single pile performance.

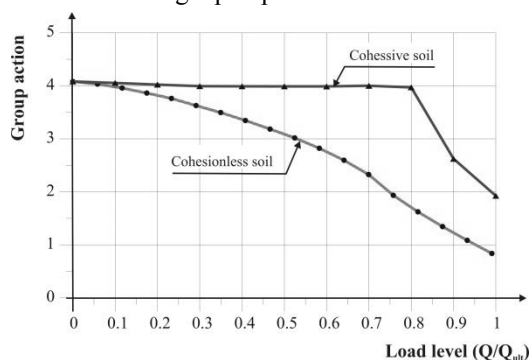


Fig. 7 Pile group action regarding the applied load level

The relation between pile group action and load level depends mainly on the soil type. In case of cohesive soil, the effect of nonlinear pile response is negligible at relatively low load levels (the elastic range) till complete slip takes place along the pile shaft. At higher load levels, the nonlinear pile response affects the pile/pile interaction considerably. Therefore, the pile group action decreases as the load approaches failure. On the other hand, in case of cohesionless soils, the pile group action depends on the stress level and decreases gradually with increasing the load level up to full mobilization of the skin friction. After that, the group action

decreases considerable as the load approaches the failure condition. Such a decrease affects the group settlement and leads to a more uniform distribution of load within the pile group when failure is approached. This example shows the importance of considering the nonlinear performance of the pile group in cases where the effective shear parameters govern the pile group performance or in cases where higher load levels are allowed to be mobilized within the pile group such as piled rafts.

2.2.2 Simplified methods to determine the pile group settlement

Simplified methods to predict the pile group action under working loads are very useful at least in the first design stage to give a quick estimation of the foundation dimensions (e.g. number of piles, pile lengths and diameters) that can fulfill the design serviceability requirements. Available simplified methods to predict the settlement of pile groups may be classified as follows:

Empirical correlations:

Correlations were developed based on small scale laboratory and in-situ tests (e.g. Skempton 1953, Meyerhof 1959 and Vesíć 1969, 1977). All these correlations should be used with caution and only in cases where the conditions are similar to those of the tests where these correlations are developed.

Equivalent raft

An equivalent raft is commonly used to transform the pile group to a simpler raft form, which can be solved by the currently available methods. The equivalent raft is still used to predict the settlement of a pile group due to its simplicity. Terzaghi (1943) has suggested imposing the foundation load at a level corresponding to the lower third point of the length of the piles (in the case of mainly friction piles) or at the pile base in case of end bearing piles. The additional stresses in the soil are then determined by the theory of elasticity (e.g. using the equation of Steinbrenner 1934) or by the 2:1 method for an equivalent raft at this level. This approach is used in many standards (e.g. DIN 1054) with some differences in the suggested procedure. However, the equivalent raft method does not take into consideration the number of piles which may have a significant effect.

Superposition technique based on theory of elasticity

Randolph and Wroth (1978, 1979) and Randolph (1983) suggested an approximate analytical model based on theory of elasticity to predict the vertical displacement of a single pile and a pile group. The vertical displacement of a rigid pile under axial load is given by:

$$s = \frac{P}{G r_0} \left[\frac{4}{\eta (1 - \nu)} + \frac{2 \pi L}{\zeta r_0} \right]^{-1} \quad (2)$$

$$\text{and } \zeta = \ln(r_m / r_0)$$

where:

P : The applied load,

r_0 : Pile radius,

L: Pile length

r_m : Influence radius at which the shear stresses become negligible. Randolph has suggested $r_m = 2.5 L (1 - \nu)$ based on a parametric study using an axisymmetric finite element analyses,

G, ν : Soil shear modulus and Poisson's ratio

η : represents the interaction of the upper layer of soil along the pile shaft with the lower layer beneath the pile base. Randolph and Wroth (1978) have suggested values of η ranging from 0.85 to 1.0.

The above mentioned equation may be modified to consider approximately the pile stiffness and the soil non-homogeneity (Randolph and Wroth 1978). Randolph and Wroth (1979) suggested an approximate analytical solution to calculate the vertical deformation of a rigid pile

group using the superposition technique. In a more convenient way, Fleming et al. 1985 suggested to relate the settlement of a group of piles to the settlement of the corresponding single pile by pile group action defined as a settlement ratio R_s as follows:

$$R_s = (N_p)^\omega \quad (3)$$

in which N_p is the number of piles in the group and ω is an exponent depending on pile slenderness ratio, pile/soil relative stiffness, group dimensions and soil properties. ω ranges for most practical conditions between 0.4 and 0.6.

3. CASE HISTORY: THE PILE FOUNDATION OF A HIGHWAY BRIDGE (ALLZEY, GERMANY)

In the last two decades, numerical analyses have been remarkably developed in both theory and applications. The more enhanced numerical analyses give the designer the possibility to determine the pile group action more accurately than the above mentioned simplified methods. The finite element, the finite difference as well as the boundary element methods are very powerful tools considering more complex constitutive laws, loads and boundary conditions. A case history will be back-calculated applying different methods to examine their validity determining the pile group action and the behavior of individual piles of the pile group.

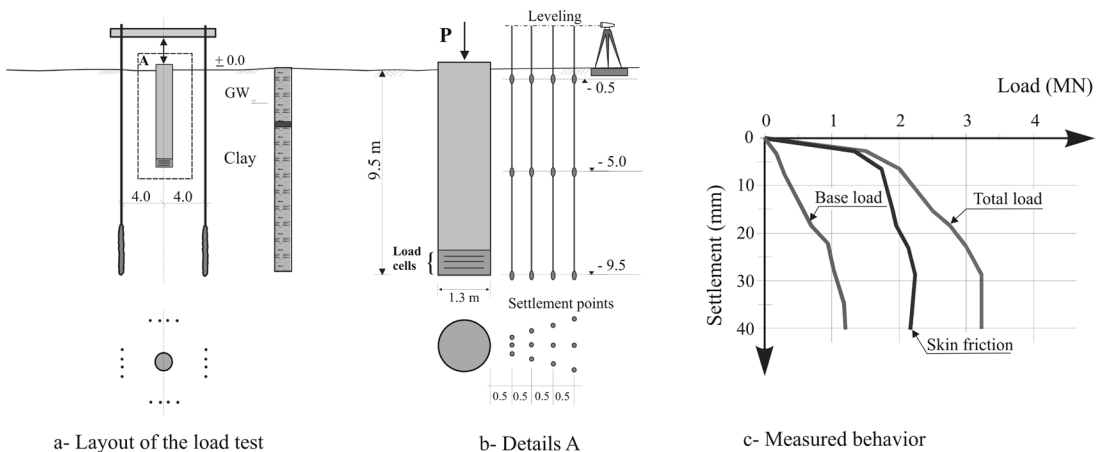


Fig. 8: Layout of the pile load test and the measured points (Sommer and Hambach, 1974)

An extensive research program related to large diameter bored piles in overconsolidated clay was conducted by Sommer and Hambach (1974) to optimize the foundation design of a highway bridge in overconsolidated clay (Allzey bridge, Germany). Special load cells were installed at the pile tip to measure the loads carried directly by pile base so that the behavior of pile skin friction and its base resistance can be separately recognized. Figure 8 shows the layout of the pile load test arrangement. The main subsoil consists of tertiary sediments down to great depths which are more or less overconsolidated stiff plastic clay. The groundwater table is about 3.5 m below the ground surface. The considered tested pile has a diameter of 1.3 m and a length of 9.5 m. It is

located completely in the overconsolidated clay. A complete three dimensional boundary element method (El-Mossallamy/Franke 1997 and El-Mossallamy 1999) as well as an axisymmetric finite element (program Plaxis) were applied to simulate the pile load test. The soil was idealized using different constitutive laws to check their reliability. An elastic-perfectly plastic analysis using the Mohr-Coulomb model and a double hardening model (Plaxis hardening soil model) were utilized to detect the sensitivity of a stress path dependent model. The required soil parameters of different applied constitutive laws were determined based on the conducted laboratory and in-situ tests as well as on experience gained in similar soil conditions. These parameters are given in Table 1.

Table 1: Geotechnical parameters of the different applied constitutive laws

a- BEM model and Mohr-Coulomb (MCM)			b- Hardening soil model		
Soil parameter		Overconsolidated clay	Soil parameter		Overconsolidated clay
E		60	E_{50}^{ref}		45
	[MN/m			[MN/m ²]	
2]			E_{ur}^{ref}		90
v				[MN/m ²]	
γ / γ'	[-]	0.3	v_{ur}	[-]	0.2
		20/10	m	[-]	0.5
	[kN/m ³		R_f	[-]	0.9
]			γ / γ'	[kN/m ³]	20/10
c'		20	c'	[kN/m ²]	20
	[kN/m ²		ϕ'	[°]	20
]			k_o	[-]	0.8
ϕ'	[°]	22.5			
k_o	[-]	0.8			
where:					
E	Elastic modulus				
v	Poisson's ratio				
E_{50}^{ref}	Primary loading stiffness				
E_{ur}^{ref}	Unloading/reloading stiffness				
v_{ur}	Unloading/reloading Poisson's ratio				
k_o	Coefficient of earth pressure at rest				
m	Power in stiffness laws				
R_f	Failure ratio				
c'	Cohesion				
ϕ'	Angle of Internal friction				
γ / γ'	Total / Effective unit weight of soil				

Figure 9 shows a comparison between observations, the results of the boundary element method (BEM) and the results of the finite element method (FEM). The good agreement between measurements and analysis can be recognized. The pile base load share of the total load ranged between 10% and 15% till the skin friction is fully mobilized and then it reached

35% at the end of the pile load test. Therefore, the pile under working loads can be considered mainly as a friction pile. The calculated settlement according to Randolph 1983 (equation 2) is added for comparison. It can be recognized that this simple equation gives good agreement with other sophisticated methods at low load level. In case of piles in clay the Randolph's

method gives reasonable results under working conditions due to the justified bilinear behavior of the pile. However, Randolph's method should be applied with caution in cases where the pile-load settlement behavior shows high nonlinear performance under working conditions.

The ultimate skin friction was determined from the results of the pile load test to be about 60 kPa. An allowable skin friction of 30 kPa is chosen for the foundation design. The measured settlement of the tested pile under load corresponding to 30 kPa skin friction was detected to be in the order of 3 mm. The bridge piers consisted of 2 pillars each founded on a separate pile group. The foundation piles had a diameter of 1.5 m and a length of 24.5 m with 6 piles under each pillar. The pile arrangement is shown in Figure 10a. Based on the pile load test results, the settlement of the whole foundation without considering the pile group action was

expected to be about 3 mm. The load-settlement behavior of the whole foundation was monitored during and after the construction to obtain information on the group action. The load-settlement relationship with time of one of the monitored pillars is shown in Figure 10b. The average measured settlement of the pier was about 9.0 mm. The difference between the expected settlement and the measured value demonstrates the importance of considering the pile group action to predict a reliable settlement of the whole foundation. Some of the above mentioned methods were applied to investigate their reliability in determining the pile group action. The results of the boundary element method as an enhanced three dimensional analyses were compared with the results of simple methods (the equivalent raft and the Randolph's method) as discussed below.

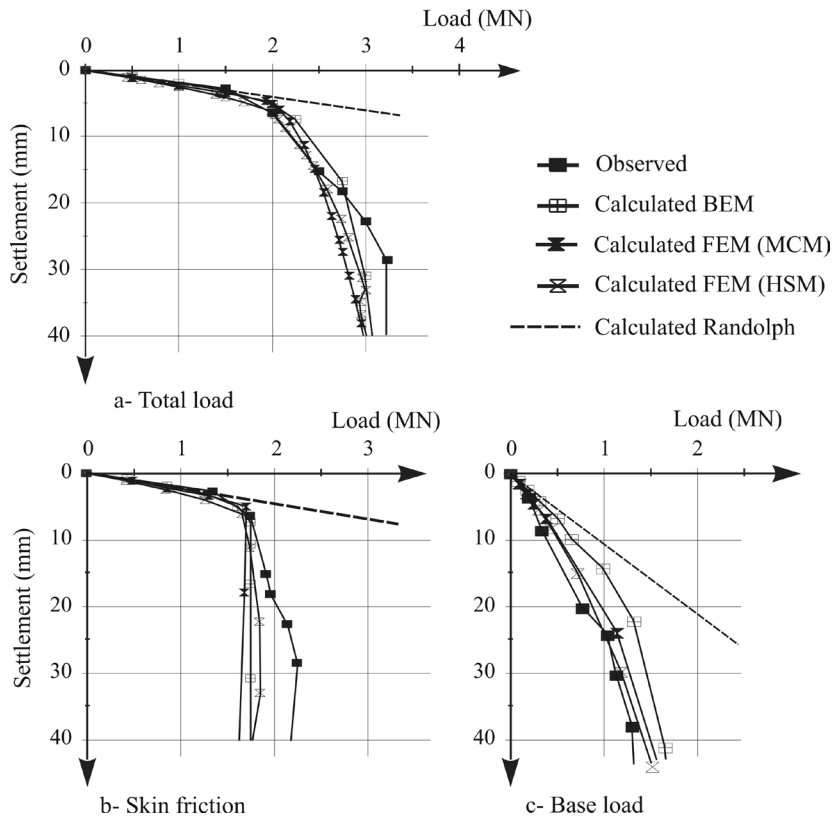


Fig. 9: Comparison between observed and calculated pile load settlement behavior

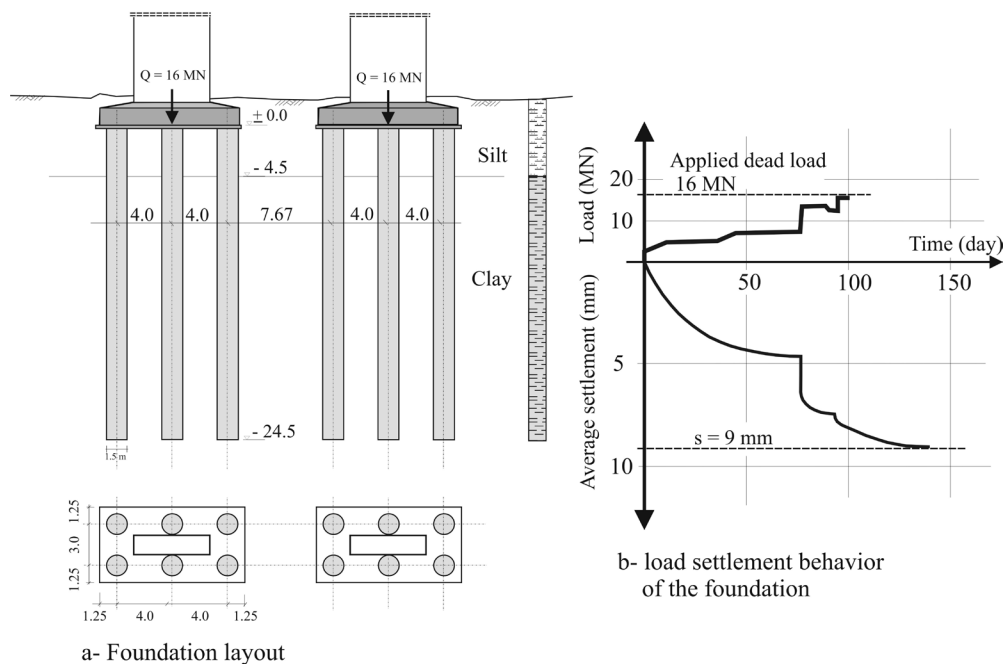


Fig. 10: Foundation layout and load settlement behavior (Sommer and Hambach, 1974)

The load-settlement behavior of a single foundation pile (pile length 24.5 m and pile diameter 1.5 m) was detected using both the BEM and Randolph's method (equation 2) applying the same soil parameters as described and validated by the analysis of the pile load test. The load-settlement relationship up to a working load of about 3 MN is mainly linear (Fig. 11). The good agreement between the results of the enhanced analysis using the BEM and the results of the simple method according to Randolph can be recognized. Figure 11a compares the behavior of the single pile with the average behavior of the pile group under the same average load. The calculated pile group action using the boundary element method can be determined to be in the order of about 3.0. This value agrees well with the results of the conducted measurements.

The pile group action was also determined applying both Randolph's method (equation 3) with ω value of 0.6. The ω value is calculated using the charts of Randolph (in Fleming et al. 1985). The equivalent raft method according to the German Standard DIN 1054 was also applied to determine the pile group action as shown in figure 11. These results demonstrate the ability of the simplified methods to predict

reasonably the pile group action under working loads corresponding to factor of safety of 2.0.

The illustrated comparison shows the good agreement between the different methods to detect the settlement of a pile group considering the pile group action. In cases of pile groups with limited number of piles and pile spacing in the order of two to three pile diameters, the pile group action can simply be calculated applying either the equivalent raft or the Randolph's method. There is still need for further research to check the ability of these simplified methods to predict the group behavior of pile groups with a large number of piles especially in cohesionless soil.

Figure 12 demonstrates the distribution of pile load and pile head settlement depending on pile position in the pile group based on the results of the three dimensional BEM analysis. The edge piles carry a higher load than the middle piles. The settlements of the inner piles are larger than that the ones of the outer piles due to the mutual interaction between the two pile groups. Therefore, an enhanced three dimensional analyses may be necessary in the final design stage of sensitive structures to determine the stiffness of the individual piles within the pile group.

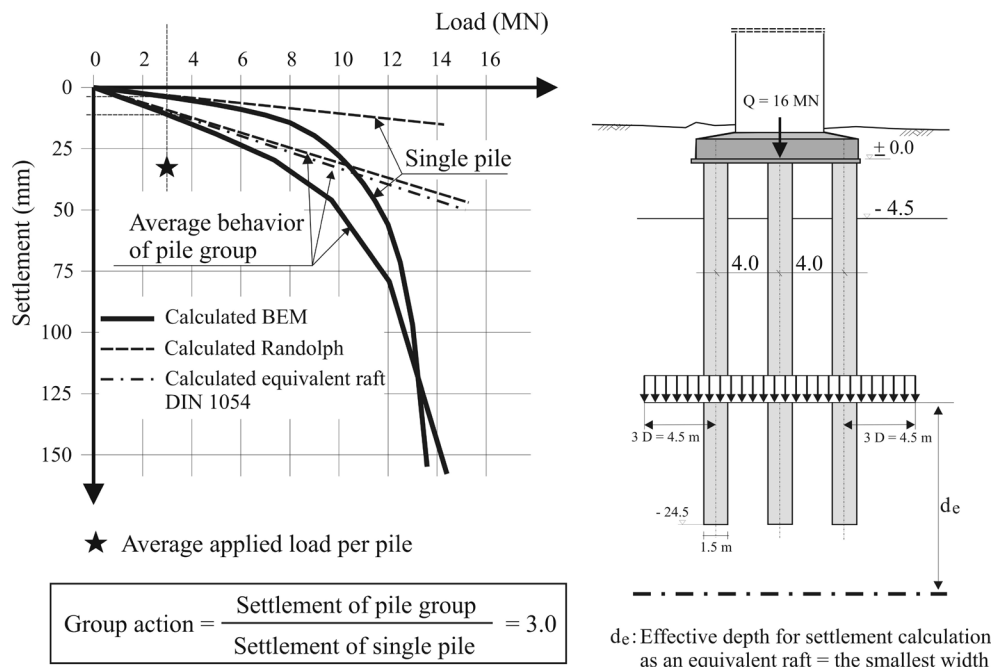


Fig. 11: Load settlement behavior of the pile group and the corresponding single pile (pile group action)

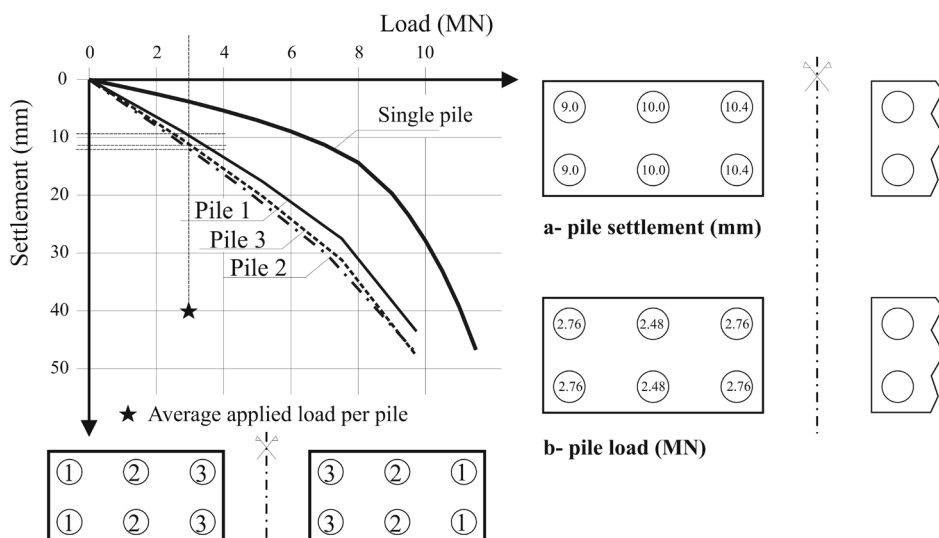


Fig. 12: Load distribution among the individual piles (BEM)

4. CONCLUSION

Considering the discussion on pile group efficiency given in this paper, it can be concluded that the pile group action regarding the foundation deformation, from the practical point of view, plays a more important role than the group action regarding the ultimate load (pile group efficiency).

The pile group action regarding the deformation of the whole piled foundation is an important design criterion in many practical cases. The simplified methods according to Randolph and the equivalent raft can be considered as suitable methods determining the group action at least for the first design stage. For more rigorous analyses (e.g. in the final design), a three dimensional analyses may be

necessary to determine the pile group behavior. The load-settlement behavior of the piles of a pile group is totally different from the behavior of the corresponding single pile depending on the geometry of the foundation, the position of the pile in the group and the applied load level.

The application of the results of a pile load test to the design of the actual foundation can only be done by using a suitable and calibrated analytical model. The presented boundary element as well as finite element methods proves their validity for such purpose.

5. REFERENCES

- DIN 1054-November 1976 "Zulaessige Belastung des baugrunds."
- El-Mossallamy, Y. und Franke, E. (1997) "Pfahl-Platten-Gründungen: Theorie und Anwendung." Bautechnik 74, Heft 11
- El-Mossallamy, Y (1999) "Load-settlement behavior of large diameter bored piles in over-consolidated clay". Proceeding of the 7th. International Symposium on Numerical Models in Geotechnical Engineering, Graz, Austria, September 1999
- El-Mossallamy, Y. (2002) "Innovative application of piled raft foundation in stiff and soft subsoil" ASCE Conference on Deep Foundations in February 2002
- Fleming, W.G., Welman, A.J. Randolph, M.F. and Elson, W.K. (1985) "Piling Engineering." Surrey University Press.
- Franke, E., El-Mossallamy, Y. and Wittmann, P. (2000) "Calculation methods for raft foundation in Germany." Design applications of raft foundation, edited by Hemsley, Thomas Telford, 283-322
- Kézdi, A. (1957) "Bearing capacity of piles and pile groups." Proc. 4th. ICSMFE, London, Vol. 2, pp. 46-51.
- Kishida, H. and Meyerhof, G.G. (1965) "Bearing capacity of pile groups under eccentric loads in sand." Proc. 6th. ICSMFE, Toronto, Vol. 2, pp. 270-274.
- Liu, J.L., Yuan, Z.L. and Zhang, K.P. (1985) "Cap-pile-soil interaction of bored pile group." Proc. 11th. ICSMFE., San Francisco, Vol. 3, pp. 1433-1436.
- Meyerhof, G.G. (1959) "Compaction of sands and bearing capacity of piles." ASCE, Vol. 85, No. SM6, pp. 1-29.
- Randolph, M.F. and Wroth, C.P. (1978) "Analysis of deformation of vertically loaded piles." ASCE, Vol. 104, No. GT12, pp. 1485-1488.
- Randolph, M.F., and Wroth, C.P. (1979) "An analysis of the vertical deformation of pile groups." Géotechnique, Vol. 29, No. 4, 423-439.
- Randolph, M.F. (1983) "Design of piled raft foundations." CUED/D-Soils TR. 143.
- Skempton, A.W. (1953) "Discussion contribution: Piles and pile foundations, settlement of pile foundations." Proc. 3rd. ICSMFE, Zurich, Vol. 3, pp. 172.
- Sommer, H. und Hambach, P. (1974) "Großpfahlversuche im Ton für die Gründung der Talbrücke Alzey." Der Bauingenieur, Vol. 49, pp. 310-317.
- Sowers, G.F., Martin, C.B., Wilson, L.L. and Fausold, M., 1961. The Bearing Capacity of Friction Pile Groups in Homogeneous Clay from Model Studies. Proceedings of the 5th International Conference on Soil Mechanics and Foundation Engineering, Vol. 2, pp. 155-159.
- Steinbrenner, W. (1934) "Tafeln zur Setzungsberechnung." Die Straße, Nr. 1, pp. 121-124.
- Vesić, A.S. (1969) "Experiments with instrumented pile groups in sand." Proc. Conf. on Performance of Deep Foundations, ASTM, Spec. Tech. Publ. No. 444, pp. 177-222.
- Vesić, A.S. (1977) "Design of pile foundations." Publication, National Research Council, Washington, D.C., No. 42.
- Terzaghi, K. (1943) "Theoretical soil mechanics", 510p. (Wiley, New York).

Session 1

SOIL-STRUCTURE INTERACTION

The Study of Replacing the Central Clay Core with the Plastic Concrete cut-off Wall in the Body of Soombar Reservoir Dam

Ali Akhtarpour

Assistant Professor, Ferdowsi University of Mashhad, Civil Engineering Department, Iran

Mahdis Damghani

Msc. Student of international branch of Ferdowsi University, Civil Engineering Department, Iran

ABSTRACT: Due to proper technical characteristics, economic and operating considerations, the clay core earth dams have such a special place in the world. In this kind of dams, the implementation of their core and adjacent filters are placed in the critical path of dam construction, while the coarse grain shells are performable easily and quickly. Considering this fact, the possibility of replacing the clay core with other appropriate sealing materials, has been studied. The discussed idea in this field is the implementation of plastic concrete in the center of the dam body with the stage drilling in coarse grain shells. The most concern are related to the rigidity of the plastic concrete wall in comparison with the dam's gravelly shells and also the pressure and tension/stress transfer to the wall in the dynamic and static conditions. In this paper, with a numerical method, the performance of the proposed cut-off wall in the body of a reservoir dam (Soombar reservoir dam). The static analyses show there is a possibility of developing cracks in cut-off wall, and due to technical issues this replacement is not possible for Soombar dam.

1. INTRODUCTION AND INTRODUCING THE DAM

Soombar River is under construction along the border of Iran and Turkmenistan in the north of North Khorasan province, in order to set the river's water for the agriculture usages. The primary plan of the dam includes a earth dam with a wide central clay core with a height of about 23.5 meters from the alluvial foundation, which is located on a weak saturated silty clay

alluvium with a maximum depth of 30 meters. Selection of large width for the clay core is first because of the existence of large volume of fine soil in the reservoir of the dam and also the limitations of volume in coarse grain materials in the plan region, and second because of compressibility of the alluvium. The sealing of the alluvium foundation is provided by a plastic concrete cut-off wall to a depth of 18 meters. In figure 1 you can see the cross section type of the dam body.

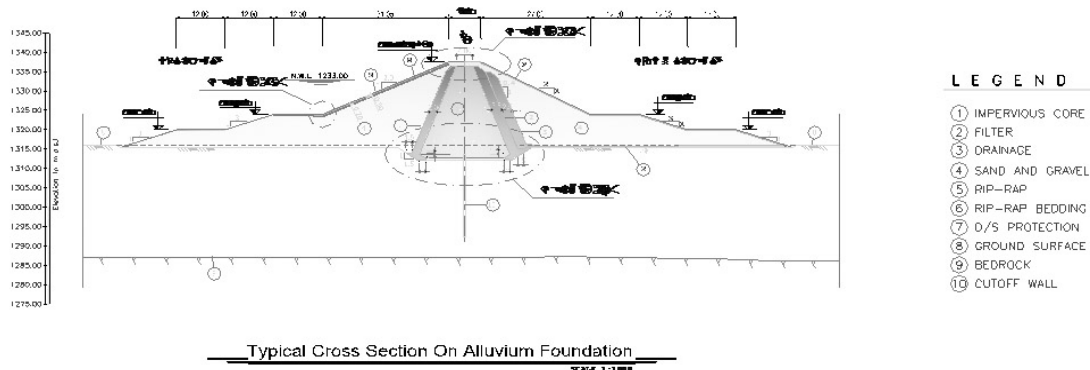


Figure 1- Cross Section Type Body of Soombar Dam

According to this fact that this project has been on the accelerated plans list of the management, the project review meetings were held in the form of value engineering. At the time of this review, major part of the cut-off wall in the dam foundation has been constructed, and also one part of the dam shells has been constructed

from the coarse grain materials in the upstream and downstream area of the body. The main problems of the contractor are filter material production, drainage, and also clay core process and implementation. Therefore, the option of replacing the central clay core in the dam body with the plastic concrete sealing wall has been

introduced with the aim of reducing or removing the filters and the core. In this paper, based on technical documentation and the parameters of the body and foundation materials in the approved technical report, the feasibility of this replacement is discussed.

2. STRESS-STRAIN ANALYSIS IN THE FINITE-ELEMENT METHOD

Evaluating the behavior of stress-strain and deformation of embankment dams is important and desirable from two perspectives of stability and reliable service. In analyzing the stress-strain, the highest cross section of the dam has been used. It's obvious that constructing the cut-off wall up to the dam crest will make some changes to the strain-stress distribution in the foundation cut-off wall. So the sealing wall

sustainability should be measured in both the foundation and the body. The stress-strain analysis has been done by Sigma/W, a computer program, which is a finite-element program for soil structures analysis from the program package of Geostudio 2007. The Elasto-plastic model was used for the numerical analysis, and in this model there is the possibility of stage loading and modeling the excavation and embankment. In the final stage of construction, the dam body will be constructed in 14 layers. In figure 2, you can see the finite-element grid which is used in the finite-element analysis.

Furthermore, a series of similar analyses has been done on the primary cross section of the dam (clay core), and the strains in foundation sealing wall has been measured. In figure 3, you can see the cross section which is used for analyzing this case.

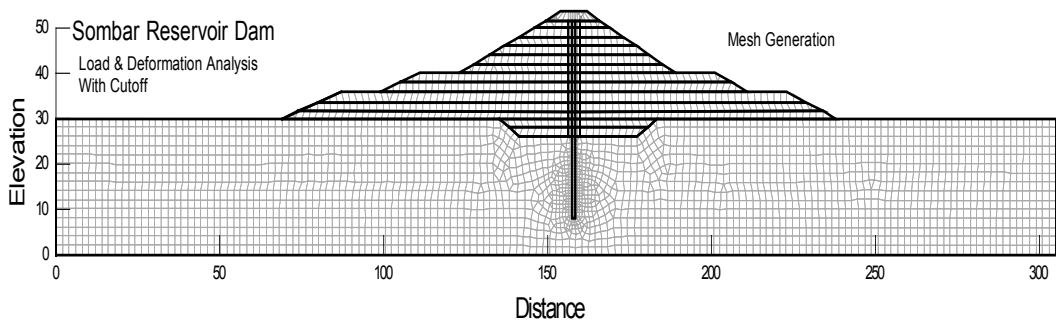


Figure 2- The Finite-Element Grid of Soombar Dam With Regard to the Sealing Wall Implementation up to the Crest Level

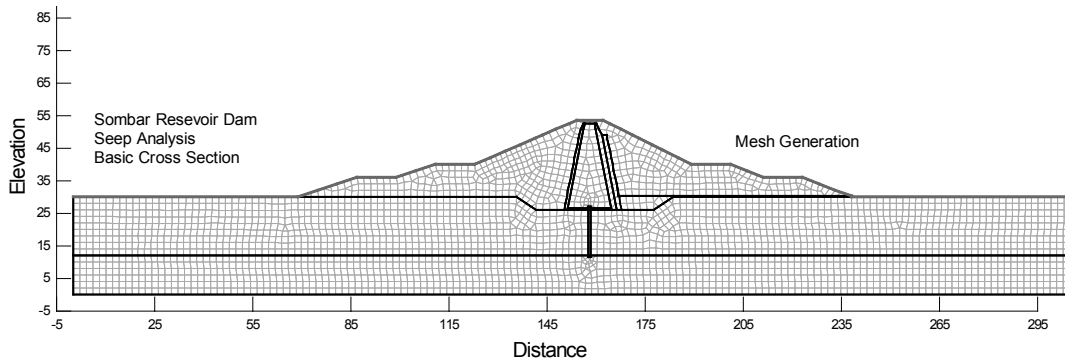


Figure 3- Finite-Element Grid of Soombar Dam Body (Clay Core)

The considered parameters for the Soombar dam body in the stress-strain analysis by the finite-element method are based on the studies of the detail stage studies which are shown in

table 1. Cut-off wall parameters are determined based on the quality control tests of the materials in the sealing wall construction of foundation dam.

Table 1- The Body and Foundation Material Characteristics of Soombar Dam in Stress-Strain Analysis in the Finite-Element Method

Material	$\gamma (KN / m^3)$	$E (Kpa)$	$C (Kpa)$	k_o	ν	(ϕ°)
Area 1 shell	22	40000	-	-	0.2	42
Area 2 alluvial foundation C.D	19	11800	50	0.5	0.3	20
Area 2 alluvial foundation C.U	19	14160	50	0.5	0.48	14
Area 3 transfer area	20	20000	-	-	0.3	33
Area 4 cut-off well	22	600000	600	-	0.2	35

3. STATIC ANALYSIS RESULTS IN THE FINITE-ELEMENT METHOD

3.1. Stresses

Total horizontal and vertical stresses in different parts of the foundation and dam body at the end of the dam construction have been shown in the figures 4 and 5. As you can see, the horizontal and vertical stress distribution in upstream and downstream of the body and foundation are almost symmetrical. The difference between the material characteristics of the sealing wall with the characteristics of its adjacent material leads to the transfer of stress from adjacent material to the wall. Due to the relative plasticity of alluvial foundation, this process somewhat continues in the alluvial foundation and causes the transmission of forces to the plastic concrete.

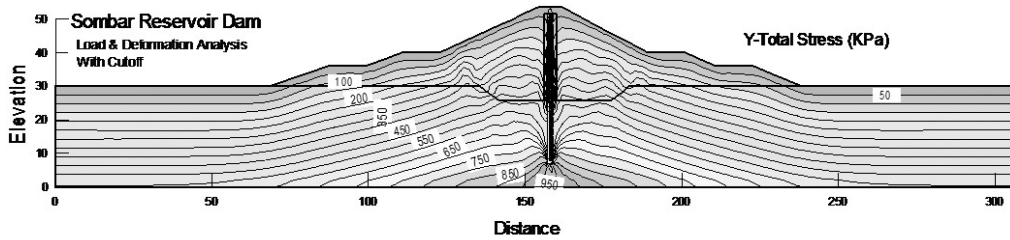


Figure 4- Total Vertical Stresses at the End of Construction Stage Considering the Sealing Wall Implementation up to the Crest Level

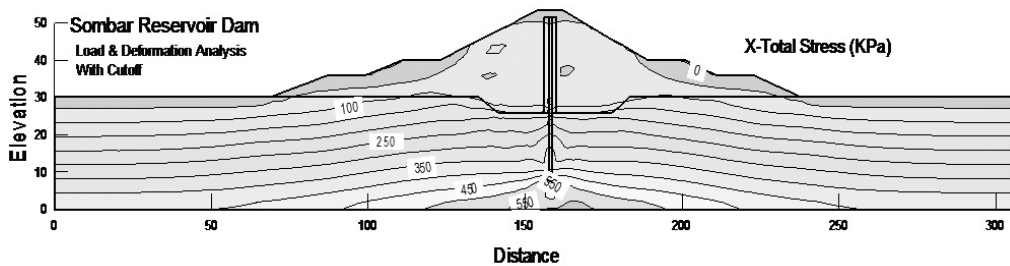


Figure 5- Total Horizontal Stresses at the End of Construction Stage Considering the Sealing Wall Implementation up to the Crest Level

In figure 6, you can see the total vertical stresses in different levels of the central plastic concrete sealing wall at the end stage of construction (crest level is 1237/5). It can be seen that the maximum horizontal stress has come to approximately 1200 (at the area of the alluvial foundation). Figure 7 shows the maximum shear stresses in the center of sealing wall in different levels at the end of the construction stage. Like

vertical stresses, the maximum shear stress has come to the level of 1200 and has happened in the upstream range of alluvial foundation.

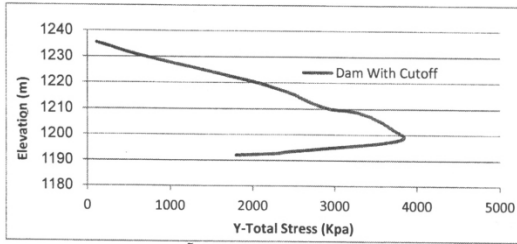


Figure 6_ Diagram of the Vertical Stress in the Sealing Wall

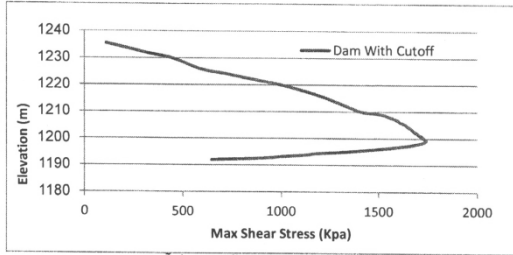


Figure7- Diagram of the Maximum Shear Stress at the Sealing Wall

3.2. Displacements

The vertical and horizontal displacements in this analysis are illustrated in figures 8 and 9. As you can see, upstream and downstream displacements of the dam are almost symmetrical. Maximum horizontal displacements in upstream are calculated as 12 centimeters and in downstream are calculated as 14 centimeters. The reason of this little difference in the horizontal displacements in downstream and upstream of the dam is the slope angle difference between the upstream and downstream shells. The vertical displacement in the center of dam reaches to maximum 84 centimeters. The above said displacements are compensated by the additional embankment at the end of the construction.

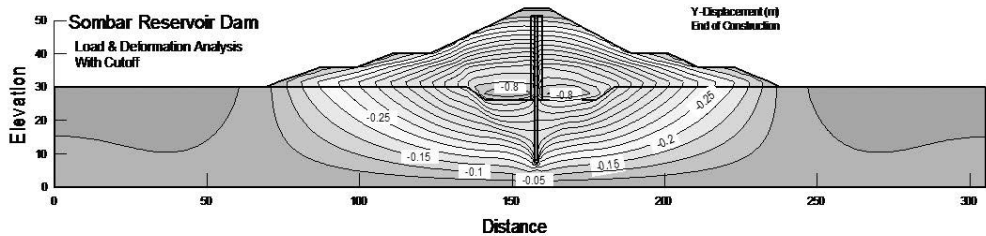


Figure 8_ Total Vertical Displacements at the End of Construction Stage Considering the Sealing Wall Implementation up to the Crest Level

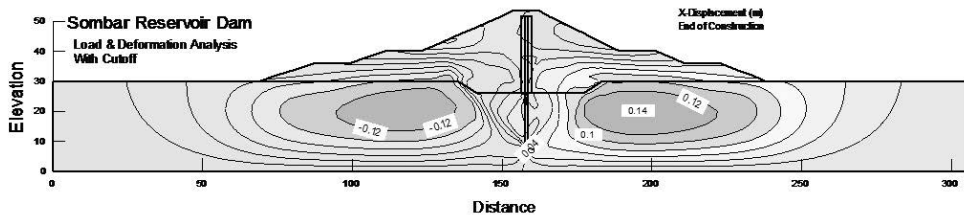


Figure 9_ Total Horizontal Displacements at the End of Construction Stage Considering the Sealing Wall Implementation up to the Crest Level

In figures 10 and 11, the shear and vertical strains in different levels of downstream area of the wall in the position of plan implementation of plastic concrete sealing wall up to crest level at the end stage are demonstrated. Again, it can be understood that constructing the sealing wall up to the dam crest can increase the strains in

sealing wall of the foundation area. The very important point is that at the end of construction state of the dam, the plastic concrete will experience vertical strains of about 1.7 percent which, based on the existing laboratory tests, cause the failure in the wall.

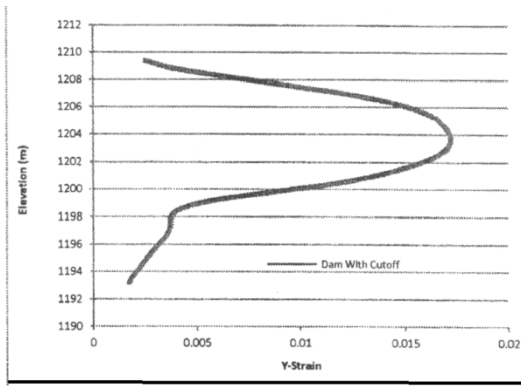


Figure 10- Diagram of the Vertical Strain for Both States

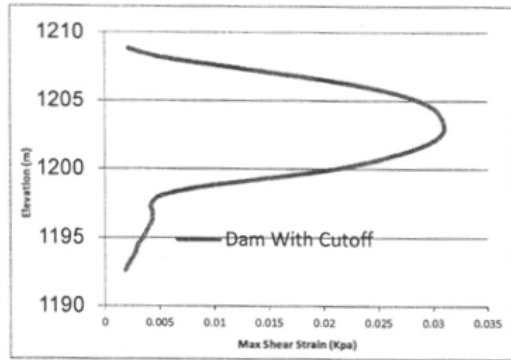


Figure 11- Diagram of the Maximum Shear Strain for Both States

4. EXAMINING THE FAILURE OF THE PLASTIC CONCRETE WALL

In order to evaluate the sustainability in plastic concrete wall in the static condition, stress Mohr circles has been studied in numerical analysis of three levels of sealing wall in the dam body, on the alluvium and in the alluvial foundation. The position of these points has been shown in figure 12.

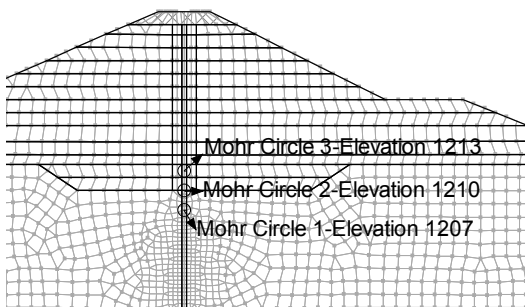


Figure 12- The Position of the Mohr Circles in the Direction of the Wall

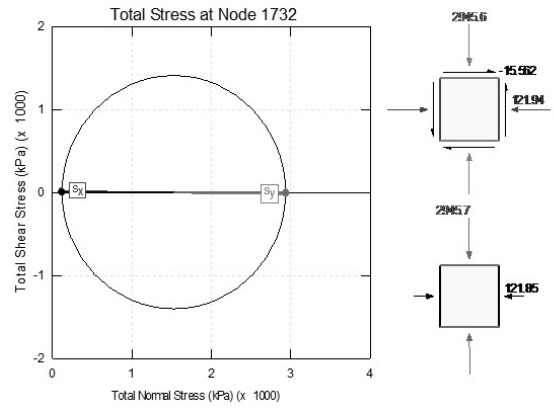


Figure 13- The Force Distribution in the 1213 Level Related to the Mohr Circle Number 1

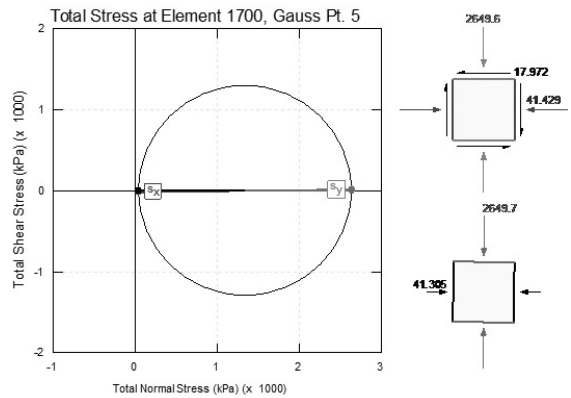


Figure 14- The Force Distribution in the 1210 Level Related to the Mohr Circle Number 2

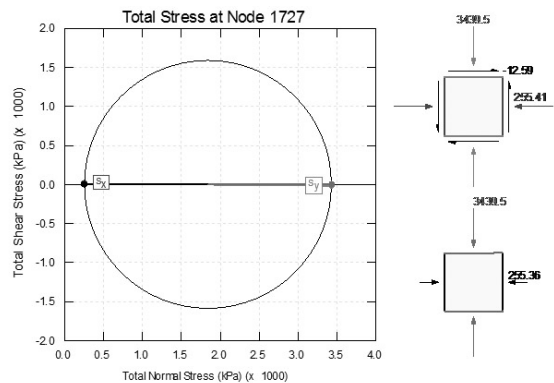


Figure 15- The Force Distribution in the 1207 Level Related to the Mohr Circle Number 3

Also in figures 13 to 15, you can see the stress Mohr circles in these points.

As a sample of related calculations of Mohr circle, figure 3 shows that the plastic concrete wall can't bear the force, and in the static condition, its failure is indispensable. The similar calculations show failure in all three points.

$$\sigma_1 = \sigma_3 \tan^2(45 + \frac{\phi}{2}) + 2C \tan(45 + \frac{\phi}{2})$$

$$IF, \phi = 35^\circ \text{ \& } C = 600KPa \text{ \& } \sigma_3 = 255KPa$$

$$\sigma_1 = 255 \tan^2(62.5) + 1200 \tan(62.5) = 3246KPa < \sigma_{1Max} = 3439KPa$$

In order to check the reliability of the obtained results from the Geostudio software, version 2007, similar analyses were performed with the Plaxis 8.2 software. Soombar dam body has been modeled in 15 layers and in numerical analysis the previous parameters have been used. Total, vertical, and horizontal subsidence in the dam body is similar to the analysis results of Geostudio whose presentation is avoided here.

The developed stress in the sealing wall and plastic points in it have been shown in figures 16 and 17. In figure 18, the vertical stress distribution of the wall has been demonstrated. Figure 16 clearly shows the concentration of the horizontal stress in the sealing wall especially in the alluvial foundation area. In view of figure 17, it can be understood that the concentration of the plastic points happens in the body and wall in the area on the alluvial foundation. Therefore, the shear failure of the sealing wall in this area is possible.

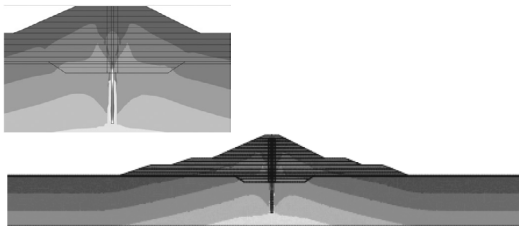


Figure 16- stress of the total vertical at the end stage of construction

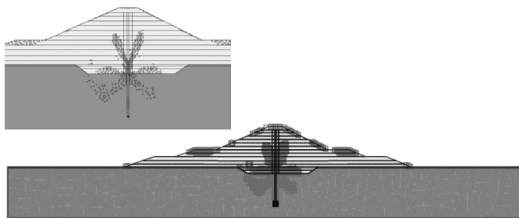


Figure 17- The Plastic Points in the Dam Body and cut-off wall

By observing figure 18 and comparing the vertical stress, it can be found that the major part of the wall in the dam body and foundation area reaches the plastic state and the received stress will pass the limits of the material resistance.

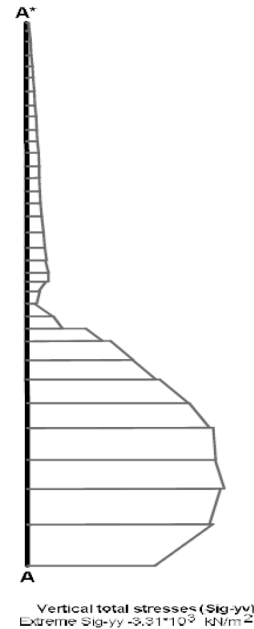


Figure 18- the horizontal stress distribution in the cut-off wall

5. CONCLUSIONS

The stress-strain analyses show that the failure in sealing wall happens in the dam body and foundation at the end of dam construction. So, with no more studies on loading conditions caused by the filling and earthquake conditions, this option is technically considered excluded. Furthermore, without any calculations and with a review of the dynamic analysis results of technical report of the plan's second stage, it can be said that in case of an earthquake, the instability in plastic concrete will also be noticed. Totally, the replacement of the clay core with the plastic concrete sealing wall for the constructed dams on the subsiding alluvial foundation is not advised.

Furthermore, for the dams constructed on the rock, it is needed to examine the static and dynamic loading conditions by considering the stiffness differences of the wall with its adjacent materials and also the brittleness of the plastic concrete (in comparison with the soil).

6. REFERENCES:

- Maharab Consulting Engineers CO. 2007. Soombar Reservoir Dam, Technical Report on alluvium Foundation. Mashhad, Iran.
- Maharab Consulting Engineers CO.2007. Soombar Reservoir Dam, Technical report on Dam Body Design. Mashhad, Iran.
- Stress-Deformation Modeling with sigma/W.2007. An Engineering Mannual,Vol.3.
- Kulhawy, F.H, Duncan, J.M, and SEED, H.B.1969. Finite Element Analysis of Stess and Movement in Em bankment during Construction.USAEWES Contract report S-69-8.

Application of Soil-Foundation-Pile Interaction Design Method for Strengthening Foundations of St. John's Church in Tartu, Estonia Using Sustainable Manual Calculation

D.Sc., CEng. Kari Christer Avellan, P.E.
KAREG Consulting Engineers, Helsinki, Finland

ABSTRACT: This article presents a developed design method applied in an actual structure (St John's Church, Tartu, Estonia) during the process of extensive underpinning. The article focuses on a practical theory of how to implement soil-foundation-pile interaction using pretested, end-jacked piles and how to design a strip foundation using only one method based on ultimate limit state (ULS) and serviceability limit state (SLS). The method takes the following into account as geotechnical requirements: contact pressure, total settlement and angular distortions. As far as structural requirements are concerned, the method considers admissible plastic rotations, end movements due to displacement angle, as well as control of cracking.

1. INTRODUCTION

Nowadays there are several software programs that evaluate the interaction between ground, foundations, and structures. There is, however, a lack of demonstrations of manual calculation methods that would complement such computerized calculations, verify their reliability, or could be used directly for assessment or estimating the soil-foundation interaction.

Because of the above-mentioned insufficiency, the author developed a simple design method based on his research work (Avellan 1992, 2011), and practical experience (Avellan & Maanas 2001, Avellan 2008).

1.1. Design method description

The method is based on the lower and upper bound sentence of plasticity theory, where a strip foundation lying on frictional soil can be designed geotechnically and structurally using ultimate limit state (ULS) and service limit state (SLS). This method uses separate parts of a strip foundation for practical calculations.

From the perspective of geotechnical requirements, the method takes into account the following: contact pressure, total settlement and angular distortions. The structural requirements are as follows: admissible plastic rotations end moments due to displacement angle, and control of cracking.

2. GEOMECHANICAL OVERVIEW

2.1. Design method overview

The method requires the value of foundation settlement. Depending on the soil or rock properties, the value of mean settlement can be estimated by settlement calculations, or settlement predictions.

2.2. Contact pressure distribution and safety factor

One of the important points to take into account is that the contact pressure distribution depends on safety factor against failure state and on the ground type (Figure 1).

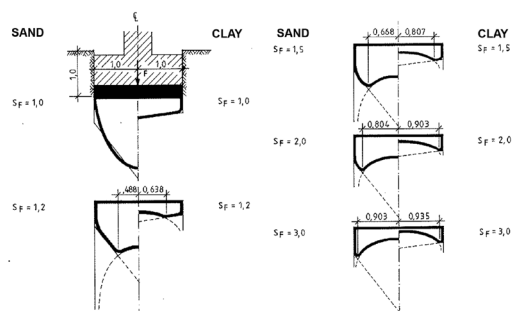


Figure 1. Distribution of ground contact pressure under a rigid strip foundation due to safety factor S_F and ground type (Schultze 1961).

In this article, the soil pressure at failure q_u (where q_u = ultimate base resistance pressure) divided by safety factor 1.6 (q_d) is used as design value of contact pressure from the substructure (ULS).

The author has used the same safety factor of 1.6 for estimating the soil settlement regardless SLS or ULS. According to the author's opinion, this satisfies standard cases when soil stratum is homogenous. If the soil stratum is not homogenous, the author's method may be used with a greater safety factor.

Essentially, the author's "separate foundations" method for soil-foundation interaction for strip foundations automatically takes care of ULS (Figure 2).

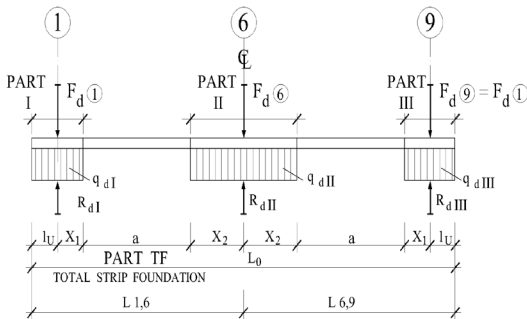


Figure 2. Total strip foundation and separated minimum parts I, II, and III. Forces acting in ULS (F_d) from the superstructure and opposing forces (R_d).

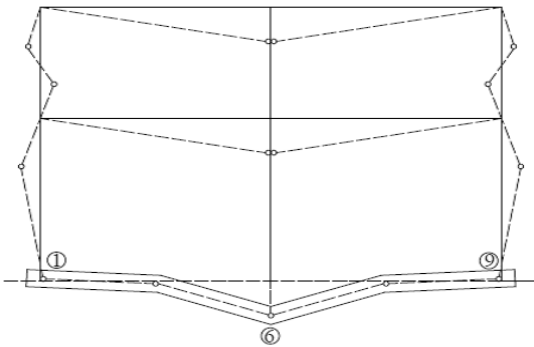


Figure 3. Two-storey structural frame founded on reinforced concrete strip foundation lying on the ground. The mechanism shown is one of the possible mechanisms of failure for the building frame and its foundation.

3. STRUCTURAL OVERVIEW

3.1. Plasticity theory of structures

The limit theories applied to foundations suggest that these structures perform adequately in the ULS, provided that the structural deformations remain within the acceptable limits in the state of serviceability. The design procedure may be started by presuming possible mechanisms for the structure and the foundations and also assuming that the soil is locally failing (Figure 3).

For simplicity it is presumed that only the structural foundation member and the respective ground the foundations, and also assuming that the ground is locally in the ULS (Figure 4).

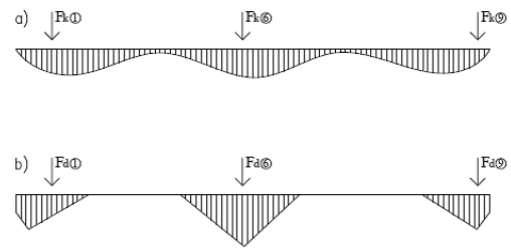


Figure 4. One distribution of contact pressure assumed for the strip foundation. a) In serviceability limit state, b) in ultimate limit state.

With reference to the theories of plasticity and elasticity the design may further be simplified by applying the lower and upper bound theorems for the limit load. In doing so, the deformations of substructure have to be estimated by means of elastic theory and based either on a loading specified particularly for this purpose, or on a loading derived from the ultimate mechanism including the partial safety factors. The plastic mechanism of a strip foundation used in the design calculations is demonstrated in Figure 5.

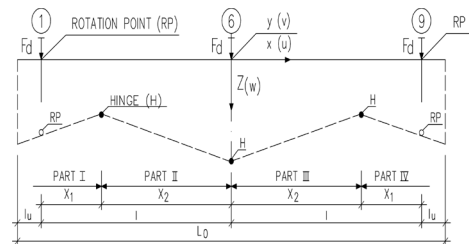


Figure 5. Plastic mechanism of strip foundation, plastic hinges (H), and rotation points (RP).

A practical example of the theory is explained in the former paper (Avellan 2008)

4. STRENGTHENING OF FOUNDATIONS OF ST. JOHN'S CHURCH OF TARTU

4.1. St. John's Church of Tartu overview

Strengthening of foundations for St. John's Church of Tartu was a project of historic significance which presented many challenges. In order to underpin the foundations of this massive structure, innovative solutions had to be delivered during work in progress.

The contour lines of the church are illustrated in Figure 6. The approximate thickness of the soil layers under the wooden rafts are shown in Figure 7.

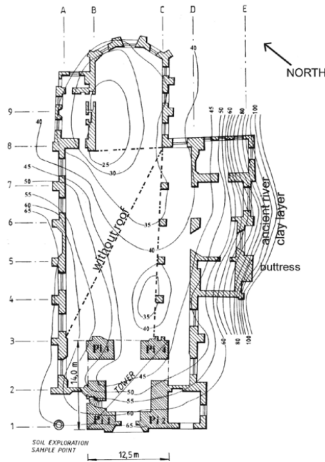


Figure 6. Contour lines of settlement (mm) in the area of the church during the years 1963-87 (Avellan & Lange 1997). Line A is on the left side without roof. line B, where the columns were destroyed, had to be completely rebuilt.

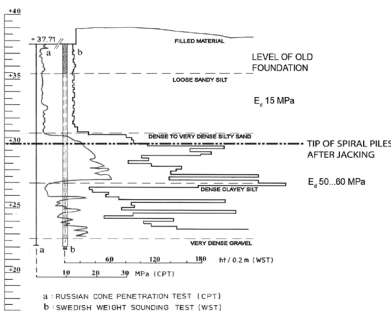


Figure 7. Russian cone penetration test (CPT) and Swedish weight sounding test (WST). Soil explorations results at sample point near the church wall

4.2. Soil-pile interaction

Soils and piles working together are illustrated in Figure 8.

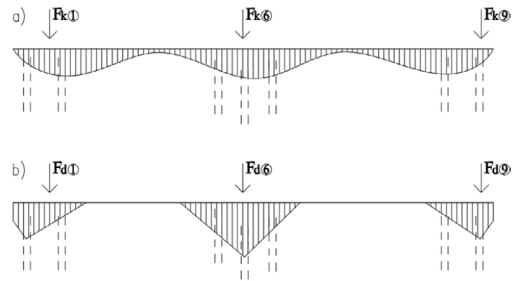


Figure 8. One assumed distribution of contact pressure applied to the piled floating strip foundation. a) In serviceability limit state. b) In ultimate limit state

Depending on the soil composition, the piles can be friction piles or tip bearing piles. In the author's method, the spring coefficient of the pile and the creep load of the pile must be predicted.

4.3. Underpinning lines A and B

The original, existing foundations of the church are on massive stones sitting on wooden rafts. During the process of strengthening, they were underpinned by piling using drilled spiral piles which were pretested by jacking. This pile type was installed as the structure was in a fragile state and would not tolerate the vibrations of driven piles.

Simple and practical equipment was designed and constructed by the author that enabled the assembly of the spiral drilled piles at a limited workspace. All parts of the equipment could be handled and carried by workmen.

4.3.1. Columns of line A

The outcome of the procedures in line A with special tested piles Nos. 220 and 222 suggests that using the same procedure for the piles in line B, the allowable maximum load in SLS according to DIN 1054 can be 400 kN. The safety factor is 1.56

The allowable load of 400 kN is less than the creep load $Q_c = 525$ kN (Figure 9). The safety factor of creep is then:

$$\gamma = \frac{525 \text{ kN}}{400 \text{ kN}} = 1.31 \quad (1)$$

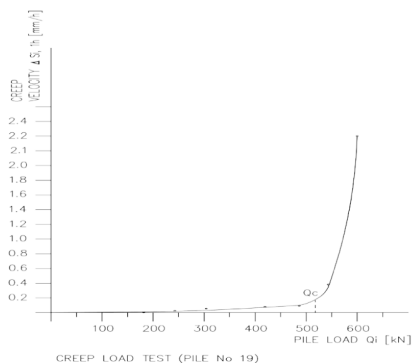


Figure 9. Creep velocity in the creep load Q_c is the load which the curvature of the diagram corresponds to the minimum radius of the curvature.

The maximum allowable load used on the installed spiral drilled piles was 375kN. The pretesting procedure is illustrated in Figures 10 and 11, including the end jacking procedure. The pressure was held constant for 15 minutes at each step and the settlement was measured at 3 intervals (5, 10, and 15 min). When the pressure of 450 bar (644 kN) decreased in 5 minutes by less than 50 bar (72 kN) to 400 bar (572 kN), the end jacking could start.

The sum of five steps was ≤ 10 mm then the pile was wedged against the structure.

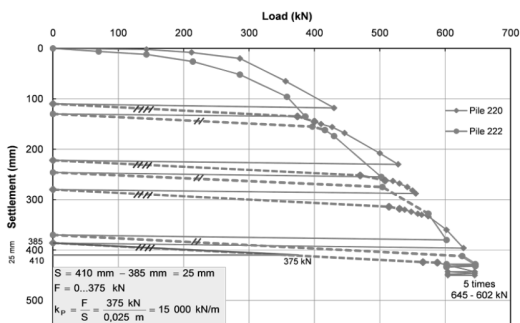


Figure 10. line A. Load-settlement diagrams of special tested drilled spiral piles Nos 220 and 222 showing the repeated load cycling between 645-602 kN and at the end of the pretesting procedure. A parallel line in the pretesting diagrams justifies the evaluation of the spring coefficient, k_p .

4.3.2. Columns of line B

The columns and the roof in line B of St. John's church were totally destroyed during World War II and had to be reconstructed.

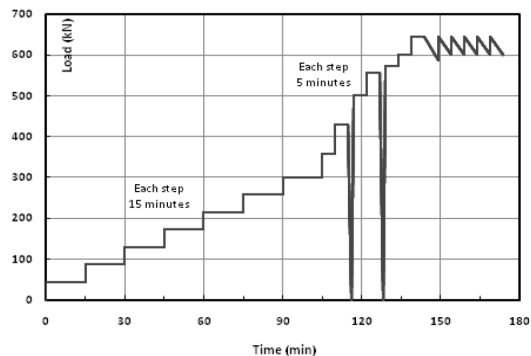


Figure 11. Time intervals for test loading of each of the drilled spiral piles in line A

Because of the lack of a sufficient counterweight of the spiral piles in line B, work had to be done using the piles as springs. Subsequently, the new columns and arches loaded the foundations. The load was eccentric because of the presence of one side arch.

The piles, foundations, and loads of line B are shown in Figures 12 and 13.

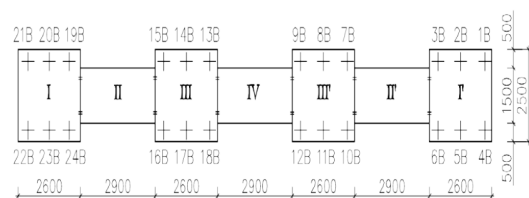


Figure 12. Line B in St. John's Church (overhead view) work joints and piles.

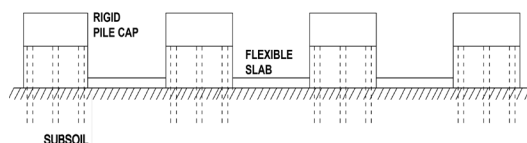


Figure 13. A) Section in direction x of line B in St. John's Church and piles.

Chapter 6, and in particular, subchapters 6.1 and 6.2 cover further in detail the soil-foundation-pile interaction and provide additional design calculations in ULS and SLS.

5. GEOTECHNICAL AND STRUCTURAL LIMIT STATE DESIGN OF STRIP FOUNDATION

The bearing resistance of a strip foundation resting on frictional soil makes a unique case of soil plasticity and a 3-dimensional passive pressure. The ultimate contact pressure q_u , the soil pressure with a safety factor $S_F = 1$ is a special ULS case. Thus the bearing capacity and ultimate contact pressure are functions of passive pressure.

5.1. Elastic-Plastic model

Horn (1970) found the relationship between the ratio $P_p(s) / P_p$ and S/S_f to be non-linear. He investigated the relationship between passive pressure and horizontal wall movements by test loading rigid wall parts ($h/b < 3.33$) against frictional soil. The elastic-plastic model according to the author is based on that the elastic-plastic pressure-settlement relationship implicates elastic behaviour up to the settlement ratio $S / S_f = 0.2$. For this settlement ratio the passive pressure $P_p(s)$ is 0.7 times the passive pressure at failure P_p (Figure 14).

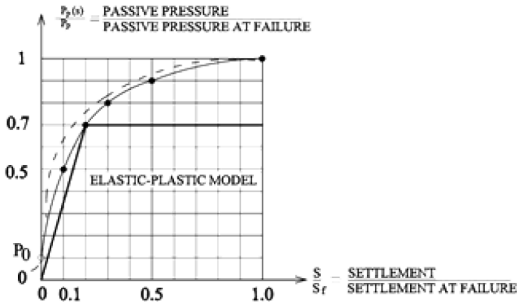


Figure 14. Elastic-Plastic model according to the author and based on the investigations of Horn.

The distribution of contact pressure for the ULS analysis can be taken into account by employing the lower bound theorem and choosing contact pressure according to these requirements. That ensures that the lower bound theorem becomes fulfilled in the ULS in the simplest manner for the minimally effective foundation, i.e. $p_d \leq q_d$. By means of the lower bound theorem, it is possible to choose such a distribution of contact pressure which shall satisfy the requirement of equilibrium in all

individual parts. The mean contact pressure due to loads (p_{0d}) shall not exceed the mean design contact pressure (q_{0d}) from substructure (Figure 15).

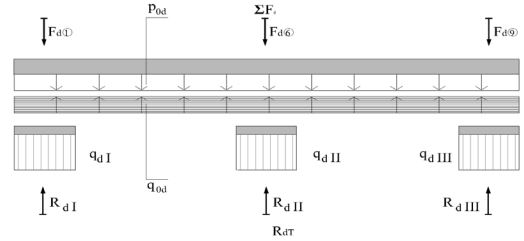


Figure 15. a) Strip foundation, design loads and design contact pressure of superstructure b) Separate parts, resistant contact pressures, and resistances of substructure

In addition, the distribution of the contact pressure $p_d(x)$ of superstructure must be applied in such a way that $p_{0d} \leq q_{0d}$, the mean resistant pressure and $p_d(x) \leq q_{di}$ (Figure 16).

The mean contact design pressure q_{0d} for the strip foundation length L_0 is determined for the whole strip foundation using the formula of Brinch Hansen (1961).

The design contact pressure distribution in direction y (B) depends on safety factor and the contact material (Schultze, 1961). The author used safety factor 1.6 which indicates uniform distribution on frictional contact material.

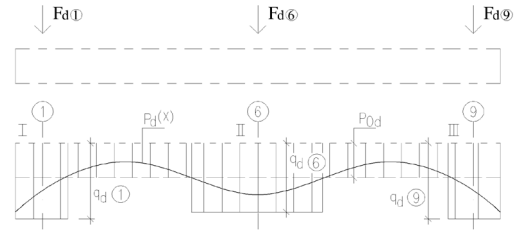


Figure 16. Balanced contact pressure $p_d(x)$.t material.

$$q_d = \frac{q_u}{1.6} \quad (2)$$

A strip foundation can be designed in geotechnical and structural ultimate limit states in accordance with the chart presented in Fig. 17.

Because the ratio p_{0d}/q_{0d} due to load from superstructure, p_{0d} , and design contact pressure of substructure, q_{0d} , correspond to the ratio of $P_p(s)/P_p$, the ratio of settlement S and settlement at failure, S_f , can be defined by the ratio p_{0d}/q_{0d} , which is marked as S_{sq} yielding thus:

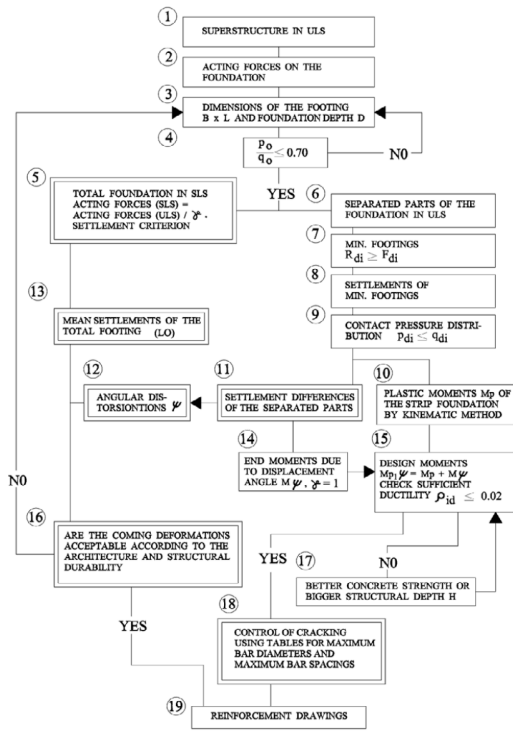


Figure 17. Geotechnical and structural design procedure in limit states for strip foundation. Double lines around boxes represent serviceability state.

$$S_{sq} = \frac{p_{0d}}{q_{0d}} = \frac{\frac{\Sigma F_d}{L_0 \cdot B}}{\frac{\Sigma R_d}{L_0 \cdot B}} \leq 0.70 \quad (3)$$

When S_{sq} is less or equal 0.70, then a settlement examination required for the feasibility of the strip foundation is carried out. As the contact pressure (q) is used, the design value is the design value is

$$q_d = \frac{q_u}{\gamma}, \quad (4)$$

where q_u = soil pressure at failure; γ = overall safety factor representing a combination of safety factors (in this case 1.6). The author used $\gamma = 1.6$ taking into consideration that $1/1.6 = 0.625 < 0.7$.

6. DESIGN CALCULATIONS IN ULS AND SLS IN LINE B

6.1. Soil-foundation-pile interaction in ULS

Characteristic loads in SLS (F_k) are multiplied by a safety factor, $\gamma = 1.4$, ($1.35 G + 1.5 Q$), to get design loads in ULS (F_d). The design load (for example on piles 22B...24B is 515.3 kN when the arch is finished. The allowable load is due the end jacking $415 \text{ kN}/1.3 = 319 \text{ kN}$. The pretesting and end-jacking process slightly differs compared to the process used in line A.

In line B, the pretesting process consisted of forces, load steps, and jacking times as in line A up to 415 kN then to zero and from 450 kN to zero. The end-jacking procedure consisted of forces of 450 kN and 415 kN, and the sum of settlement was the same, $\leq 10 \text{ mm}$.

Using the empirical correlation between the Swedish weight sounding test, we use $\varphi = 29^\circ$ as the frictional angle of the soil and a deformation modulus (E_d) of 15 000 kN/m² (Bergdahl & Eriksson 1983).

According to Brinch Hansen (1961), the contact pressure of the substructure $q_u = 173.4 \text{ kN/m}^2$. The breadth of the foundation (B_{eff}) due to the eccentricity of the arch to be built and vertical load is 1.71 m, and then:

$$q_d = \frac{q_u}{1.6} = \frac{173.4}{1.6} = 108.4 \text{ kN/m}^2, \quad (5)$$

Using the well-known formula of Schleicher (1926), and expanded by Gordunov-Posanov (Tsytoovich 1981), the settlement, S_{FI} is 9.7mm. The subgrade reaction (K_{FA}) and spring coefficient (k_F) are:

$$K_{FA} = \frac{q_d}{S_F} \quad (6)$$

$$k_F = K_{FA} \cdot A_F = 49\,685 \text{ kN/m} \quad (7)$$

A_F is the effective sub-area of the foundation (slab). The total spring coefficient (k_{PT}) for the three piles is:

$$k_{PT} = \Sigma k_p = 3 \cdot k_p \text{ and } k_p \text{ is } 15\,000 \text{ kN/m (Figure 10),}$$

$$\Sigma k_p = 3 \cdot 15\,000 \text{ kN/m} = 45\,000 \text{ kN/m.}$$

Compatibility:

$$\begin{cases} S_F = S_p \\ Q_F + \Sigma F_{dp} = V_{dp} \end{cases} \quad (8)$$

$$\begin{cases} S_F = \frac{Q_F}{k_F} \\ S_{dp} = \frac{\Sigma F_{dp}}{\Sigma k_p} \end{cases} \quad (9)$$

$$Q_F = V_{dp} - \Sigma F_{dp} \quad (10)$$

$$\frac{V_{dp} - \Sigma F_{dp}}{k_F} = \frac{\Sigma F_{dp}}{\Sigma k_p} \quad (11)$$

$$\frac{\Sigma k_p}{k_F} \cdot V_{dp} = \Sigma F_{dp} \cdot \left(1 + \frac{\Sigma k_p}{k_F}\right) \quad (12)$$

$$\Sigma F_{dp} = \frac{\frac{\Sigma k_p}{k_F} \cdot V_{dp}}{1 + \frac{\Sigma k_p}{k_F}} \quad (13)$$

Resistance of the piles, every pile is pretest-
ed and end-jacked.

$$F_{dp} = \frac{\Sigma F_{dp}}{3} = 244.9 \text{ kN} < \frac{415}{1.1} \sim 377 \text{ kN} \quad (14)$$

$< 400 \text{ kN}$

$$\Sigma F_{dp} = \frac{\frac{45\,000}{49\,685}}{1 + \frac{45\,000}{49\,685}} \cdot 1\,546.0 \text{ kN} = 734.8 \text{ kN} \quad (15)$$

The settlement of the piles is $S_p = 16.3 \text{ mm}$ and
the settlement of the foundation is:

$$S_F = \frac{V_{dp} - \Sigma F_{dp}}{k_F} = \frac{1\,546.0 - 734.8}{49\,685} = 16.3 \text{ mm} \quad (16)$$

From Figure jj 14, we see:

$$\frac{S_F}{S_f} = \frac{16.3 \text{ mm}}{54 \text{ mm}} = 0.30; q_{df} \sim 0.80 \cdot 173.4 \text{ kN/m}^2 = 138.7 \text{ kN/m}^2 \quad (17)$$

$$\gamma = \frac{173.4}{138.7} = 1.25 \quad (18)$$

6.1.1. Safety factor in SLS based on ULS calculations

The safety factor of piles in SLS:

-the calculated piled load in ULS is 244.9
kN

-the partial safety factor for the loads of the
superstructure is 1.4

-the real safety factor in SLS is:

$$1.4 \cdot \frac{1.3 \cdot 319.2 \text{ kN}}{244.9 \text{ kN}} = 2.37, \quad (19)$$

The safety factor of the bearing capacity of
the soil in SLS:

- the calculated safety factor is
 $1.4 \times 1.25 = 1.75$.

6.2. Soil-foundation-pile interaction in SLS

For the reason that the reader can compare the
results in SLS and ULS, the values used in SLS-
calculations are given as follows:

$$\begin{aligned} q_k &= q_d = 108.4 \text{ kN/m}^2 \\ S_F &= 9.7 \text{ mm} \\ k_F &= 49\,685 \text{ kN/m} \\ \Sigma k_p &= 45\,000 \text{ kN/m} \\ F_{kp} &= 174.9 \text{ kN} < 300 \text{ kN} = F_{adm} \end{aligned}$$

The settlement of the piles is $S_F = 11.7 \text{ mm}$
and the settlement of the foundation is:

$$S_F = \frac{V_{kp} - \Sigma F_{kp}}{k_F} = \frac{1104.3 - 524.8}{49\,685} = 11.7 \text{ mm} \quad (20)$$

Now we have to prove that the designed soil
pressure is smaller than q_u . We have used q_{kf} as
 $q_u/1.6 = 0.625 q_u$. We notice (Fig. 14) that the
calculated settlement 9.7mm is about 0.18 times
the settlement at failure (S_f), which means that
 S_f is about 54 mm. According to SLS, $S_F = 11.7$
mm and less than $S_f = 54 \text{ mm}$. The S_F/S_f ratio is
0.22 and then q_{kf} is 0.72 times q_u (Fig. 14, non-
linear line).

$$0.72 \cdot 173.4 \text{ kN/m}^2 = 124.8 \text{ kN/m}^2, \quad (21)$$

$$\gamma = \frac{173.4 \text{ kN/m}^2}{124.8 \text{ kN/m}^2} = 1.39. \quad (22)$$

The piles have enough resistance, but for limiting theoretical settlements we could also consider the effect of slabs.

7. SUMMARY

This article illustrates a simple design calculation method based on the lower and upper bound sentence of plasticity theory, where a strip foundation lying on frictional soil can be designed geotechnically and structurally using a single method based on the ultimate limit state (ULS) and service limit state (SLS). This method uses separate parts of a strip foundation for practical calculations.

For the soil-foundation interaction the spring coefficient of pile must be tested or predicted.

8. CONCLUSIONS

The author of this article is convinced that in order to leverage the technical advantage found in computerized systems and Eurocodes, it is important that manual design calculations be taken into consideration and implemented throughout the design process. For example, manual design calculations could be used as complementary tests to computerized design models to verify particular functionalities of software applications. In addition, they could also be used to compare the results with computerized calculations.

This consolidation would essentially contribute to integral quality of design methods and enhance the application and applicability of Eurocodes.

9. ACKNOWLEDGEMENT

The author would like to thank engineer Erika Belopotocanova M.B.A. for finalizing the text.

10. REFERENCES

Avellan, K. 1992. *Geotechnical and Structural Ultimate Limit State Design of Foundations Resting on Soil* (in Finnish). Licensiate thesis. Helsinki University of Technology, Faculty of Civil and Environmental Engineering.

Avellan K. 2008. *Ultimate Limit State Design of a Strip Foundation*. In *Development of Urban Areas and Geotechnical Engineering*. St. Petersburg 16-19 June 2008.

Avellan, K. 2011. *Limit state design for strengthening foundations of historic buildings using pretested drilled*

spiral piles with special reference to St. John's Church in Tartu. Doctoral thesis. University of Oulu, Faculty of Technology. Acta Universitatis Ouluensis, C Technica 392.

Avellan, K & Maanas, M. Strengthening the foundations of St. John's Church in Tartu, Estonia. *Proceedings of the Fifteenth International Conference on Soil Mechanics and Geotechnical Engineering*. Istanbul, 27-31 August 2001, pp. 1687-1690.

Bergdahl, U. & Eriksson, U. 1983. *Bestämning av jordegenskaper med sondering – en litteraturstudie*. Linköping. Statens Geotekniska Institut. Rapport 22. In Swedish.. Swedish Geotechnical Institute. Report 22.

Brinch Hansen J. 1961. *A general formula for bearing capacity*. Copenhagen. Akademiet for de tekniske videnskaber Geoteknisk institut. Bulletin no. 11:38-46

DIN 1054 1976. *Baugrund – Zulässige Belastung des Baugrunds*. German code, November 1976. Berlin, Beuth Verlag.

EN 1992. Eurocode 2. Design of concrete structures.

EN 1997. Eurocode 7. Geotechnical design.

FIP recommendations (1984) *Practical design of reinforced and prestressed concrete structures based on the CEB-FIP model code (MC78)*. London, Thomas Telford Limited.

Frank, R. 2006. *Some aspects of soil structure interaction according to Eurocode 7 – Geotechnical design*. Engenharia Civil. UM 2006/25, pp. 5-16.

Horn, A. 1970. *Sohlleibung und räumlicher Erdwiderstand bei massive Gründungen in nichtbindigen Böden*. Strassenbau und Strassenverkehrstechnik. Heft 110. Bonn. Bundesminister für Verkehr. Block 110. Federal Ministry of Transport, Building and Urban Environment.

Neal, B. 1970. *The plastic methods of structural analysis*. Great Britain, Norwich. Barnes & Noble Inc.

Schultze, E. 1961. *Distribution of stress beneath a rigid foundation*. Proc. 5th International Conference on Soil Mechanics. Paris, pp. 807-813.

Schleicher, F. 1926. Zur Theorie des Baugrundes. *Der Bauingenieur*. Heft 48: 931-935, Heft 49: 949-952. (The theory of the ground. The Civil Engineer. Block 48, pp. 931-935, Block 49, 949-952.)

Tsyтович, N. 1981. *Soil Mechanics*. Moscow. English translation Mir Publishers.

Efficiency of improving the specifications of soil lenses, that are formed near the tunnel during the stages of its investment

Talal Awwad

Higher Institute for Earthquake Researches and Studies (HIERS), Damascus University, Syria

Bader Eddin Al-Asali

Transport Department, Civil Engineering Faculty, Damascus University, Syria

ABSTRACT: The surrounding conditions of tunnel lining may be changed during the investment period, which lead to a redistribution of forces acting on the tunnel lining, and perhaps generate new forces that are not taken into account during the design. In this paper, a case study of Alsafkon tunnel is regarded, which is one of the Syrian Railway deep tunnels. The lining of this tunnel suffers from cracks, leakage, and other defects.

The results of numerical analysis are conformed to the current situation of the tunnel in terms of distributed cracks places in the concrete lining. The study showed also the importance of improving the lens properties to avoid the total fall down of the tunnel.

INTRODUCTION

The defects that appear on concrete tunnels lining through the stages of investment, vary widely from simple defects such as discoloration of the surface of the concrete, to severe, such as fragmentation and cracking and lamination... etc. Each of these defects has its reason. The factors that lead to these defects can be limited to three main categories: internal factors resulted from a defect in concrete components, factors related to errors in the design, implementation or investment, and external factors resulted from the change in the surrounding medium specifications of the lining through the stages of investment, such as changing in the ground water level which cause leaking into the tunnel, and the formulation of spaces behind the lining... etc. These factors lead to: - redistribution of the effective stresses acting on the lining, increasing in its values and changing in its nature. - Decreasing in the lining' strength.

The surrounding medium of the tunnels lining was the focus of many researchers; Bobet studied mutual influence between the soil and the lining of the circular tunnels, and gave an analytical solution to determine the stresses affecting the lining in the case of gaps left behind or without gaps, and for long or short-term investment periods [13]. Shin studied the effect of pore water pressure in the soil surrounding the lining of the tunnel, and found that this pressure can cause deformations that may lead to cracks formation, an increase in the

leakage rate, and a decrease in the bearing capacity of the lining [14]. Cheehan conducted experimental investigations to determine the effect of voids formation behind the lining on the distribution of stresses affecting it, and the study showed that the transmitted stresses are changed dramatically depending on the location of the formed gap, on the perimeter of the lining [15]. Thomas studied numerically the effect of the properties of the surrounding soil and injection materials on the behavior of the concrete lining of shallow tunnels. The results showed a significant impact of these properties on the tunnel behavior [16].

Due to the impact of change in the specifications of the surrounding environment on the behavior of the tunnel, it is necessary to study this change, and evaluate the performance of the tunnel during the period of investment, according to the field investigations that identifies these specifications.

1. TUNNELS IN SYRIA

There is a limited number of deep transportation tunnels in Syria, due to its high cost of construction. There is only eight concrete tunnels for Railways of Aleppo - Lattakia line, and five stone tunnels for Railways of Aleppo - Akbes field line, whereas traffic transportation deep tunnels are not existed [5].

2. ALSAFKON TUNNEL (EIGHT TUNNELS)

Alsfkon tunnel is one of the eight concrete tunnels used for rail transportation of Syrian railways (Figure 1). These tunnels were studied by Soviet company between 1962 – 1965, and executed by a Bulgarian company, 1971 [2].

The tunnel is located on the axis of the Aleppo-Lattakia near Alsfkon station. The length of the tunnel is 1600.6 m, and it contains 261 rings. The tunnel passes the curved path from ring 1 to ring 42 with a length of 400 m and radius of 260 mm from Aleppo, the rest is a straight path towards Latakia from ring 42 to ring 261 with length of 1340.6. Figure 2 shows a longitudinal section of the tunnel [3].

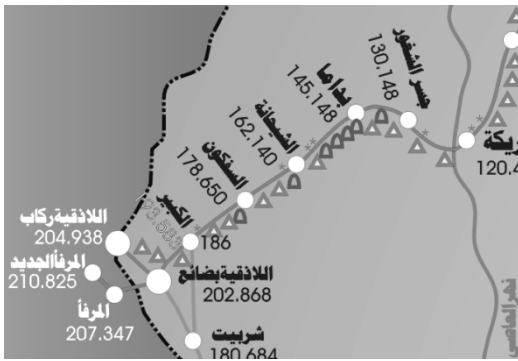


Figure 1.locations of railway tunnels on the axis of Aleppo, Lattakia

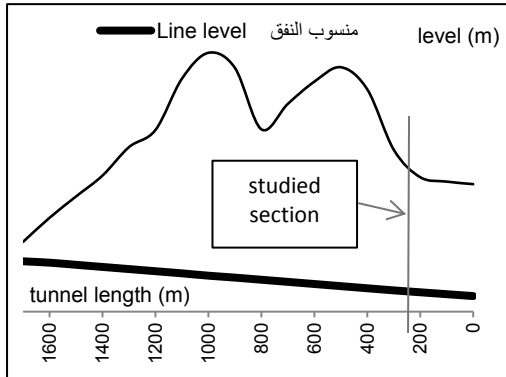


Figure 2.longitudinal section of Alsfkon tunnel [3]

Alsfkon tunnel lining was created from unreinforced concrete mass M-200 according to Russian specifications with a thickness of 60 cm, and there was no initial strengthen for the excavations, taking into consideration that the tunnel would be constructed within a rock structure. (Figure 3) shows the cross-section of the tunnel in a straight path [3].

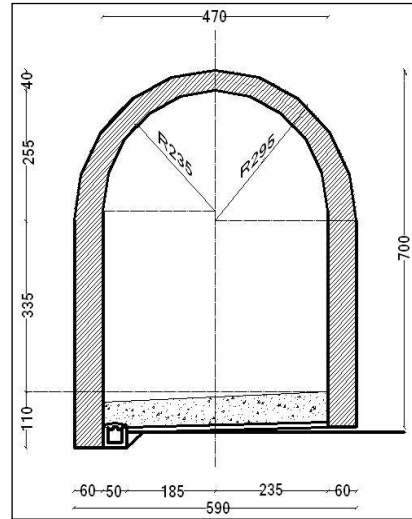


Figure 3.the cross-section of Alsfkon tunnel (dimensions in cm).

3. DEFECTS OF ALSAFKON TUNNEL

The tunnel lining is suffering of many disadvantages that appear as horizontal or inclined cracks with a width that reach 3 mm and lengths up to 30 meters (Figure 4), and other defects such as humidity or discolor (pink) in some areas (Figure 5). There is a water leakage of some cracks with a discharge of about 0.5 liter/hr. the quantity and condition of the defects in the lining, vary from a region to other along the tunnel. There are also white grey deposits in the drainage channels inside the tunnel that result from the transmitted soil particles with leakage water from behind the lining. These depositions block the drainage system inside the tunnel and prevent groundwater drainage (Figure 6).

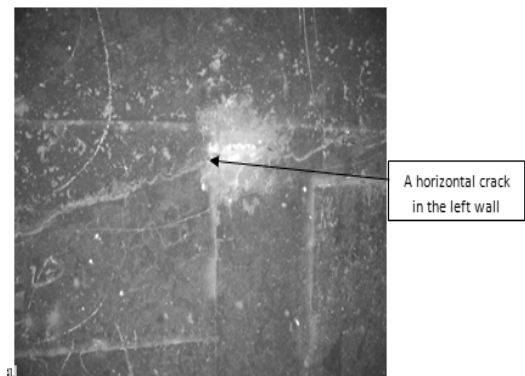


Figure 4. Gypsum label was removed in the cracking wall of Alsfkon tunnel

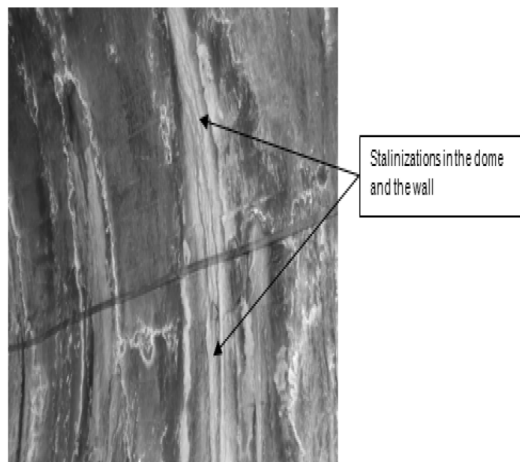


Figure 5. The humidity and salinity in the dome and the wall of Alsafkon tunnel

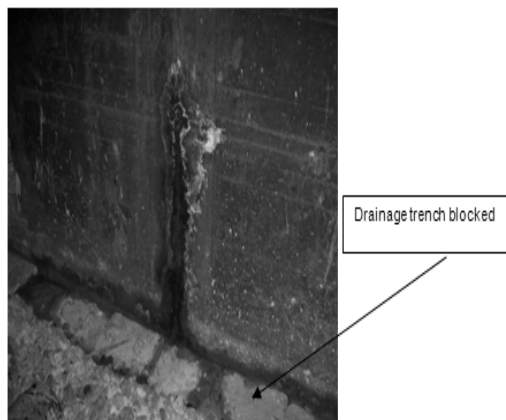


Figure 6. water leaking from the slit in the wall and clogged drainage ditch in Alsafkon tunnel.

4. TESTS CARRIED OUT ON TUNNEL LINING

In 2007, some tests were conducted by Russian experts from the University of St. Petersburg of roads and transport including in-situ observations that are reproduced as a plan of defects for the path of the tunnel. These works included also sampling of the lining of the tunnel and the surrounding soil in ten sections. The strength of the concrete were specified by testing the cores that are taken from the lining. The results show that the strength of concrete lining is conforming to the Russian standards M-200.

The work of this group also includes surveys by using Georadar to depths that reach 4 m on the tunnel perimeter. The survey showed soil

lenses in some areas on the path of the tunnel. Samples were taking from these lenses and characterized by the appropriate tests [4].

5. THE STUDY CASES

To study the impact of the changes in the condition of the lining during the stages of investment, a section from this lining at the ring (42) was selected where the lining suffers from cracks, water leakage, and where a lens is formed behind the concrete lining that may have a role in influencing the behavior of the lining [4].

To examine the condition of the tunnel lining since its creation, the following cases will be studied:

1. The reference case which is the design case of the lining with the adoption of the specifications design for concrete (M-200). The surrounding soil of the lining is considered as rarefied marl.
2. The case of ground water table rises to the middle height of the vertical wall of the lining, when the drainage system inside the tunnel is partially blocked.
3. The case of ground water table rises to fully submerge the tunnel. In this case a full blockage of drainage system occurred inside the tunnel. This case represents the long term investment conditions of the tunnel.
4. The case of lens formed behind the lining, which is revealed by Georadar survey that is conducted by the Russian team, which is also the case of the tunnel in investment conditions.
5. The case of the expected increasing in the size of the lens next to the lining, by 50% of the original size.

6. NUMERICAL MODELING

Numerical modeling is used to study and understand the behavior of facilities, because it has a low cost and allows for adjustments and recalculations, in comparing with empirical methods. There are many numerical methods such as the Finite elements method FEM [16, 17, 18] that was used in this research.

The numerical model was carried out using Phase2 that is based on finite element method, and can be used in the analysis of (2d) plane and solve a lot of geotechnical issues such as

determination of strains and stresses around tunnels [6].

A section from the eighth tunnel lining was selected. This section is located at the ring (42) where there are cracks, leakage, Efflorescence and a presence of a lens next to the lining. Modeling of tunnel lining was made at section 1-1, and was modeling in multiple stages that represent the long-term behavior of the tunnel since its construction and during the stages of investment (as indicated in paragraph 5). In the first modeling of the tunnel, the lining does not suffer of any defects, and then detect the emergence of the current cracks in the tunnel through numerical modeling results. Figure 7 shows the location of the cross section of the lining.

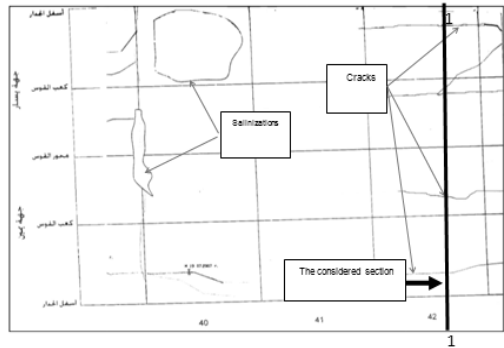


Figure 7.a map of defects from 40 – 42 in Alsafkon tunnel, and the position of the considered section

The Height of the coverage above the tunnel at the considered section is 43 m so the dimensions of the model were chosen to be sufficiently large as shown in figure (8) so the boundary conditions can't affect on the stresses and deformations arising in the lining of the tunnel [8], and it has been assumed that the studied issue is plane strain, and the boundary conditions were specified as a vertically sliding fixities at the sides and fixed restraints at the bottom [9, 12], the soil surrounding the lining is rarefied marl and has the following specifications: $\gamma = 0.018 \text{ MN/m}^3$, $\phi = 45^\circ$, $c = 0.5 \text{ Mpa}$. The soil is assumed to behave (elastic-plastic) behavior which is represented by the Saint-Venant model [1] and it is subject to the criterion of Mohr Coulomb. The analysis has been completed for the five cases previously listed as follows:

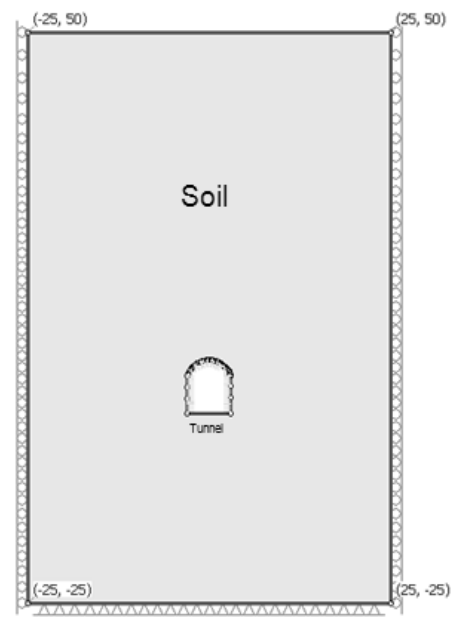


Figure 8.the model at the considered section

7.1 THE FIRST CASE: it's the reference case where tunnel lining was designed according to it and where no groundwater exists behind the lining. table (1) shows the specification of concrete lining and the surrounding soil.

Table (1) specification of the lining and the surrounding soil in the reference case [4]

Factors	Specification- sconcretelining	Thesurround- ingsoilspecification
Modulus of elasticity E(Mpa)	23E3	13E3
Poissonratio ν	0.3	0.35

Analysis was performed and also the value of the horizontal displacement in point A from the left wall, are monitored (where a change in the properties of the soil will happen near to it, because of formation of lens in the following phases) which is point A (-3, 2.68). The results showed that the lining of the tunnel did not show any defects or cracks, and the maximum value for the horizontal displacement at point A is $X_{disp} = 0.039 \text{ cm}$, the plastic area's radius was measured around the tunnel from the center of it, was $L = 3.8 \text{ m}$, as in figure (9):

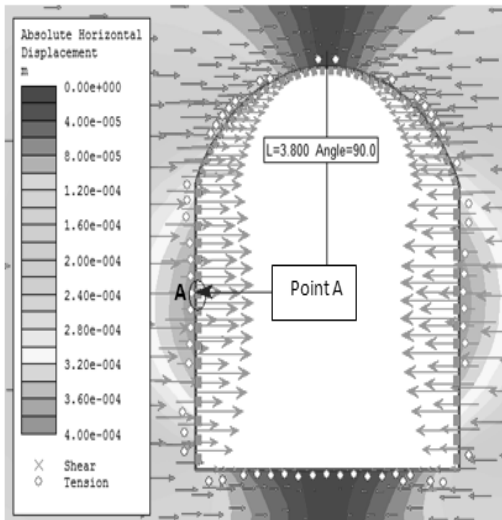


Figure 9.the horizontal displacement around the tunnel

7.2 THE SECOND CASE: the case of partially blocked drainage system inside the tunnel and the rising of the ground water level to the mid-high of the vertical wall of the tunnel lining. The analysis shows that the tunnel is stable and its lining does not show any defects and that the maximum value for the horizontal displacement at point A has not changed $XDisp = 0.042$ cm, and the plastic area's radius $L = 4.2$ m, as in figure (10):

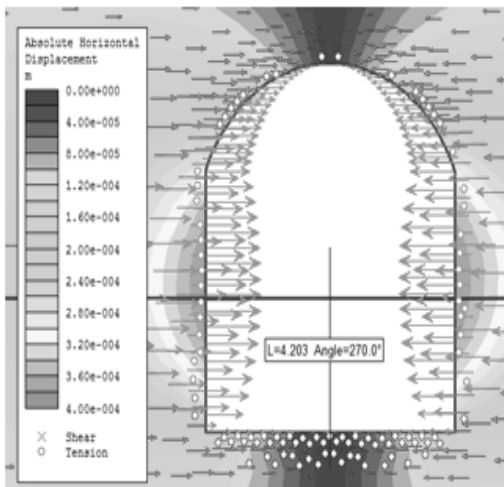


Figure 10.horizontal displacement for case 2

7.3 THE THIRD CASE: the case of inundation of the tunnel by groundwater, show that the maximum value of the horizontal displacement at point A is $XDisp = 2.1$ cm, and the plastic area's radius $L = 9.02$ m, as in figure (11):

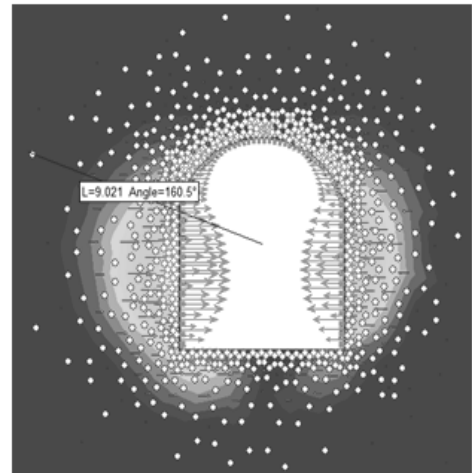


Figure 11.horizontal displacement for case 3

7.4 THE FOURTH CASE: the case when the lens is formed behind the left wall lining of the tunnel at the considered section. Georadar survey showed that this lens area is about 2 m^2 in the section and extend approximately to 15 meters along the tunnel, with the existence of ground water that submerge the tunnel entirely. The lens next to the tunnel was modeled with the same size and specifications established by the field investigations as shown in table (2):

Table (2) specification of the lining and the soil and the lens for phase 4 [4]

Factors	Specification- sofcon- cretelining	The sur- round- ingsoilspec- ifications	Specifica- tion- sof lenssoil
Modulus of elasticity E(Mpa)	23E3	13E3	0.15E3
Poissonra- tio ν	0.3	0.35	0.45

The analysis showed that the maximum value of the displacement is $XDisp = 9.48$ cm, and the plastic area's radius is $R_p = 9.5$ m, as in figure (12):

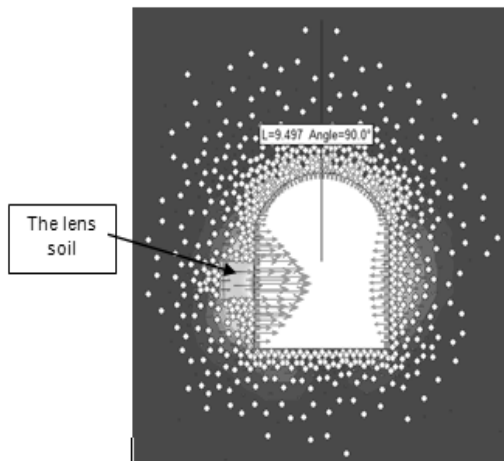


Figure 12. the horizontal displacement for the case 4

It is noticed that the cracks has been showed in the lining of the tunnel and concentrated mainly in the left wall adjacent to the location of the lens, and the junction of the left wall with bow top. Also two cracks showed on the opposite side of the lining, as in figure (13):

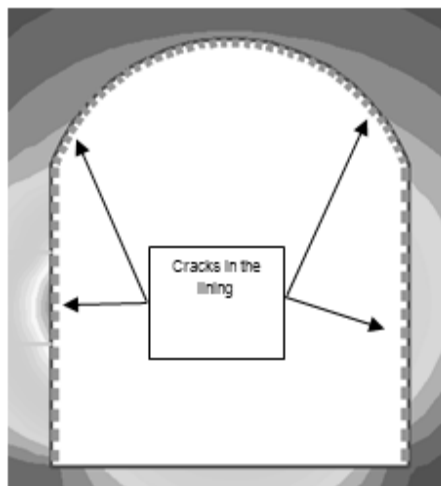


Figure 13. cracks positions in the lining of the tunnel at the considered section for case 4

Comparing (Figure 7), which represents the real defects in tunnel lining with (Figure 13), representing the places of cracks for the case 4, a match between the places of the cracks was observed, Which indicates that this is the actual situation in which the lining of the tunnel is.

7.5 THE FIFTH CASE: the case of expected increasing of the area of the lens by 50%, and we note that the maximum value of the horizontal displacement is $XDisp = 17.4$ cm, and the plastic area's radius is $L = 10.52$ m, as in figure (14):

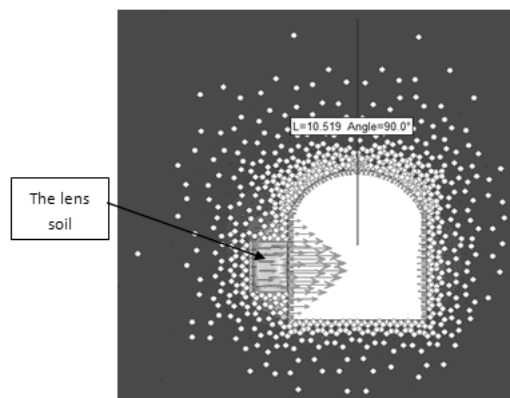


Figure 14. the horizontal displacement for the fifth case

Also we note the concentration of stresses in the lining along the lens and large cracks appearing on the left wall that is almost along the height so the wall is considered unable to bear the applied stresses, Figure 15:

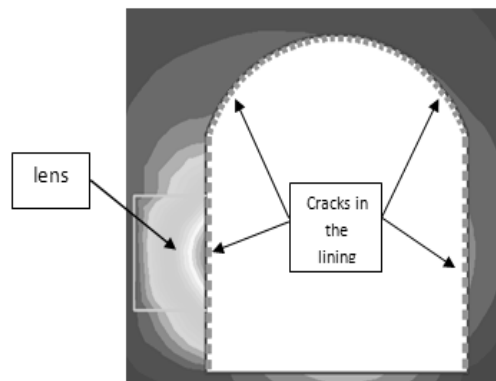


Figure 15. the tunnel lining cracks at the considered section – the fifth case

Figure (16), shows that the values of the horizontal displacement increase with the increase of the water table height and after the lens formed. the increase takes a maximum value in the case of increasing the size of the lens by 50% of its original size (the fifth case).

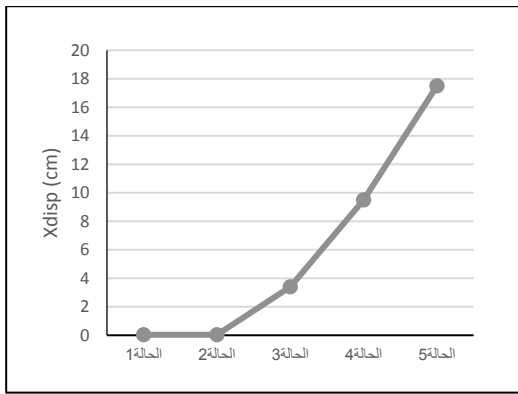


Figure 16. The values of the horizontal displacement at point A in accordance with study case.

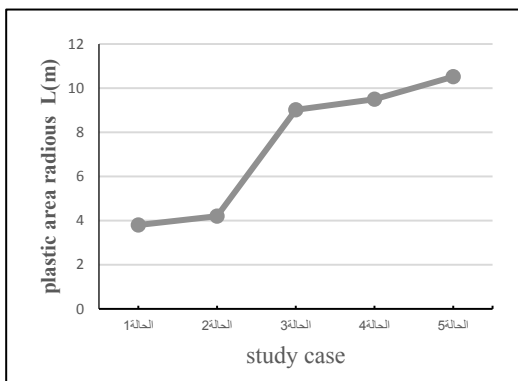


Figure 17. the number of elements in the soil that affected by tension stresses according to the study case.

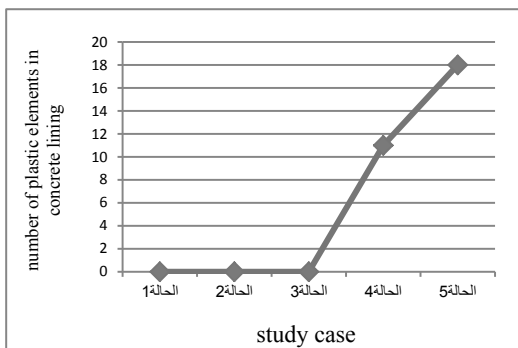


Figure 18. the number of plastic elements in the lining of the tunnel according to case study

As we note from the figures (17 and 18), increasing in the plastic area's radius around the tunnel with the increasing of the bad conditions around the tunnel, the cracks in the lining begin to appear in the studied fourth case where the

groundwater level inundates the tunnel, these cracks increase when lens exist and the left wall of the lining next to the lens, lining is almost completely cracked when the lens size become bigger by 50%, so it can't bear the applied stresses, therefore it is necessary to improve the lens's properties before getting to this condition.

8. THE PROPOSED TREATMENT OF THE CRACKS IN THE LINING OF THE TUNNEL

The results of previous analyses show that defects and cracks in the lining of the tunnel emerged as a result of the high water table due to blocked drainage system, changing soil conditions that surrounds the lining which is lens that appears next the wall lining. The best solution of this problem is to get rid of the reasons which led to the emergence of these defects, otherwise the problem will increase and no treatment will be effective. It must take care of drainage system inside the tunnel, clean it periodically from the substances that block the flow of water from behind the lining and improve the specification of the lens to reduce the stresses on the lining. This lens can be injected with a cement sand with the addition of bentonite to strengthen and raise the physical characteristics so that the properties of the treated lens is as follows [11]:

Factors	Specifications of concrete lining	The surrounding soils specification [5, 12]	Specifications of the lens after injection
Modulus of elasticity E(Mpa)	23E3	13E3	5E3
Poisson ratio ν	0.3	0.35	0.45

By re-analyzing, it is noted that the maximum value of horizontal displacement at point A has fallen to $XDisp = 3.3$ cm, as well as the plastic region's radius around the tunnel $Rp = 9.27$ m, as in figure (19).

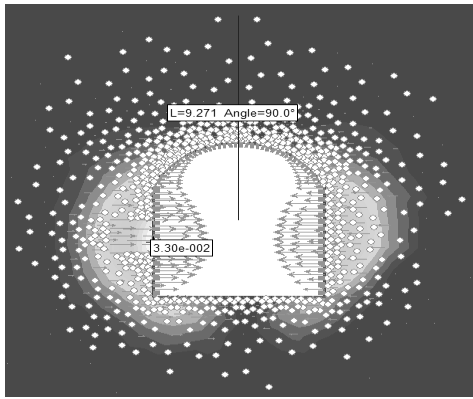


Figure 19. horizontal displacement in the lining of the tunnel, soil after processing the lens
Note from (figure 20) that no cracks have seen in the lining after injection.

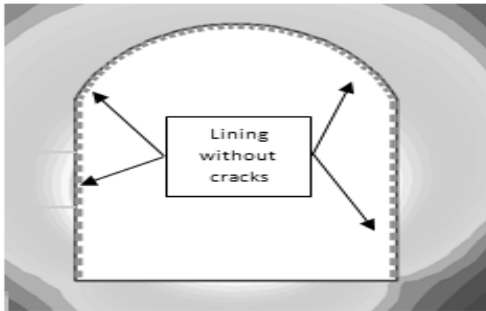


Figure 20. the non-appearance of cracks in the lining after injection.

9. RESULTS AND RECOMMENDATIONS

1. The results showed the existence of a consensus between the real condition of the Alsafkon tunnel and the model proposed, which confirms the validity of the proposed modeling method. This method can be applied to analyze other tunnels with different conditions, in order to verify other factors that may cause cracks developing in lining of tunnels through the stages of investment.
2. Groundwater level plays a negative role in cracks developing in concrete lining; therefore it is recommended to clean the drainage system inside the tunnel periodically to prevent this rise of water level.
3. Developing of Weak lens near the tunnel has an important role in increasing cracks in lining. If these lenses remain without treatment, the wall lining will deteriorate and the tunnel will becomes out of investment.

4. The properties of the lens can be improved by injecting mixture of cement, sand and bentonite. The results of analysis showed that the resistance of the lining is improved and no cracks will appear after injection process.

10. REFERENCES

1. Hamza, Mohammed Marwan, soil and rock mechanics, Directorate of books and publications, publications of the University of Aleppo, 2002.
2. Detailed report of the experts of the Bulgarian KOEHNE to RVP , Syria- Aleppo-Lattakia, Amhan Center for engineering consultation, Aleppo, 2004.
3. P. Yankov, K. Jiponov, G.Georgiev Measures for reconstructing of a part of tunelNo.8 Aleppo-Lattakia, Sofia 2003
4. A.P. Ledyayev, Yu.S. Frolov, Abdulfattah Mansur Design forUpgradingRailwayTunnelsNo.3 And No.8 In Aleppo-LattakiaLineIn Syrian Arab Republic, St. Petersburg2007
5. Sukkar, Naseem, Analysis for Syrian railways tunnels and rehabilitation, master, Aleppo, 2006.
6. RockscienceInc, Phase² User's Guide, Toronto, Ontario, Canada 2010.
7. Leca, E. Clough, W. Preliminary design for NATM tunnel support in soil. Journal of Geotechnical Engineering 118 (4), 558–575, 1992.
8. Matsuoka, S. M. Astudy on simulation of tunnel lining which involves cracks. Proceedings of Japan society civil engineers No.554/III-37. Tokyo, 1996.
9. Idris J. Al Heib M. Numerical modeling and mechanical behavior analysis of ancient tunnel masonry structures - Tunneling and Underground Space Technology, 2006.
10. Moeller, S.C., Vermeer, P.A. [On numerical simulation of tunnel installation](#). Tunneling and Underground Space Technology, Volume 23, Issue 4, Pages 461-475, July 2008.
11. Hoek, E. Practical Rock engineering. Rock Mass Properties. Rocscience.com on line, pp. 161–203 (Chapter 11), 2000.
12. Mollon, G. Dias, D. and Soubra A. Probabilistic analyses of tunneling-induced ground movements. ActaGeotechn. 8: 181-199, 2013.
13. Bobet, A. Analytical Solutions for Shallow Tunnels in Saturated Ground. Journal of Engineering Mechanics, 127(12), p 1258 – 1266, (2001).
14. Shin, H. Youn, D. Chae, S. and Shin, J. Effective Control of Pore Water Pressures on Tunnel Linings using Pin-Hole Drain Method. Tunneling and Underground Space Technology, 24, pp 555 – 561, (2009).

15. Cheehan, L. An Investigation of the Effect of Erosion Voids on Existing Tunnels. Department of Civil Engineering & Applied Mechanics McGill University, Montreal, Quebec, Canada Sept, 2009.
16. Thomas, K. Günther, M. A numerical study of the effect of soil and grout material properties and cover depth in shield tunneling, Institute for Structural Mechanics, Ruhr University Bochum, Denmark, 2006.
17. David, H. Fundamentals of finite element analysis, McGraw Co, New York, 2004.
18. David, R. Finite Element Analysis, Department of Materials Science and Engineering, Massachusetts Institute of Technology, Cambridge, MA 02139, 2001.

Three techniques for the study of soil structure interface properties; 3D roughness parameter; contact stress mapping; artificially manufactured sand.

Gökhan Baykal
Boğaziçi University, Turkey

ABSTRACT: Three techniques for the study of the soil structure interface properties will be presented. The first technique involves the development of a 3D surface roughness parameter to evaluate the skin friction. The second technique is used to map contact stress concentrations at the soil structure interface using sensitive films developed for medical profession. The third technique is manufacturing artificial crushable sand at the desired properties to study static and dynamic interface behavior of soil and concrete. All of the techniques presented have a potential to understand the interface behavior in more detail. The techniques presented are implementable and practical.

INTRODUCTION

Several studies have been published regarding laboratory interface testing. Most often, interface tests are performed to determine the soil-to-structure friction angle for design of geotechnical structures, such as retaining walls, buried culverts, piles, geosynthetics etc., and, in some cases, for the determination of parameters for constitutive modeling of the interface response. Determining the soil structure interface properties is a challenging task for the healthy assessment of the soil structure interaction behavior. New techniques are becoming available and they may be implemented to geotechnical engineering for better understanding of the interaction behavior. The three techniques presented here are; the development of a 3D surface roughness parameter to model the contact surface topography; contact stress mapping at the interface; manufacturing sand with varying crushing strength by cold bond pelletization to model calcareous sand. All of the techniques presented here are part of graduate theses conducted at Bogazici University.

CONTACT SURFACE TOPOGRAPHY: 3D ROUGHNESS COEFFICIENT

Egemen Danyıldız (2007) studied the interface between concrete and fly ash pellets. He has modeled the surface topography of the concrete

blocks by extending the 2D roughness coefficient to 3D using a simple algorithm.

1.1. 3D Roughness coefficient

The algorithms to model the contact surface topography are presented in Figure 1.

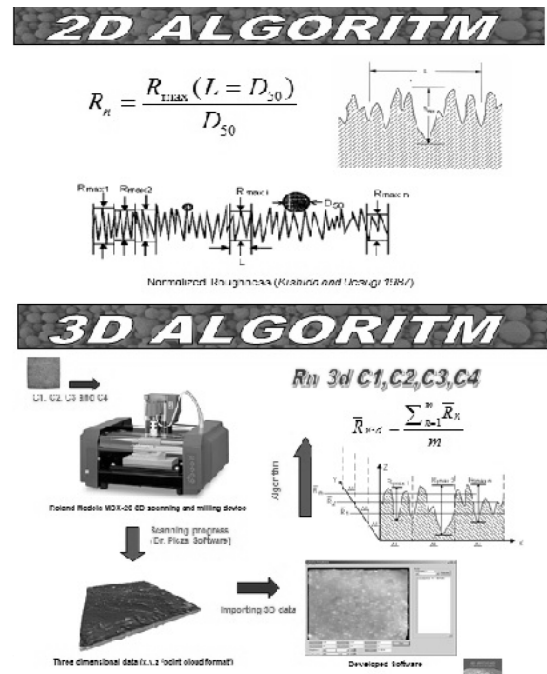


Figure 1. Contact surface topography modeling; 2d algorithm ; 3D algorithm.

The quantification of the surface roughness in terms of relative interface roughness R_n as reported by Uesugi and Kishida, 1986b, is defined by measuring R_{max} (vertical distance between the highest peak and the lowest trough) along a profile length L equal to the mean grain size D_{50} and then normalizing it by D_{50} as shown in Figure 1(2D algorithm). The surface roughness of each concrete block investigated is measured and digitized with a commercially available compact size 3D scanning and milling device Roland Modela MDX-20. The MDX-20 3D scanner is connected to the computer with an RS-232C cable. The scanner is capable of scanning objects at four to 15 mm per second with a resolution of up to 0.05 mm by contacting, mesh-point height-sensing. The scanning pitch was selected as 0.5 mm in order to have high resolution data which results in accurate information about the concrete surface topography. The 3D scanning software Dr. Picza is used in the scanning process. The scanning area is selected and each concrete block (C1, C2, C3 and C4) are placed on the table of the scanner and are scanned one by one. The scanning process takes approximately five hours for each block. Elevations on the surfaces are recorded in three dimensions which provides accurate information differently from other approaches where roughness characteristics are calculated from a set of intersecting or parallel 2D line segments. The obtained data are recorded as point cloud format which are the combination of coordinates (x, y and z) in three dimensional space.

An algorithm is developed to measure the normalized surface roughness parameter R_{n3d} of each concrete block in three dimensions. The main function (R_n) is identical with the one reported by Kishida and Uesugi, 1987 []. R_n can be defined by measuring R_{max} (vertical distance between the highest peak and the lowest trough) along a profile length L equal to the mean grain size D_{50} and then normalizing it by D_{50} as mentioned before. The average of normalized surface roughness parameter R_n along a profile in 2 dimensions can be given as;

$$\overline{R_n} = \frac{\sum_{i=1}^n \frac{R_{max\ i}}{L}}{n}$$

where R_n = average of normalized surface roughness along a line,
 R_{max} = vertical distance between the highest peak and the lowest trough,
 n = number of sections along the profile
 L = mean grain size D_{50}

Actually, the above equation represents a two dimensional approach where the other dimension is neglected. Since the data recorded in the scanning process are in three dimensions, there is a need of a three dimensional approach which can take into account the other direction. The addition of y dimension to the equation above, turns the profile into a three dimensional surface which is more representative. The illustration of the three dimensional approach and the three dimensional surface roughness parameter R_{n3d} are given in Figure 1 (3D algorithm).

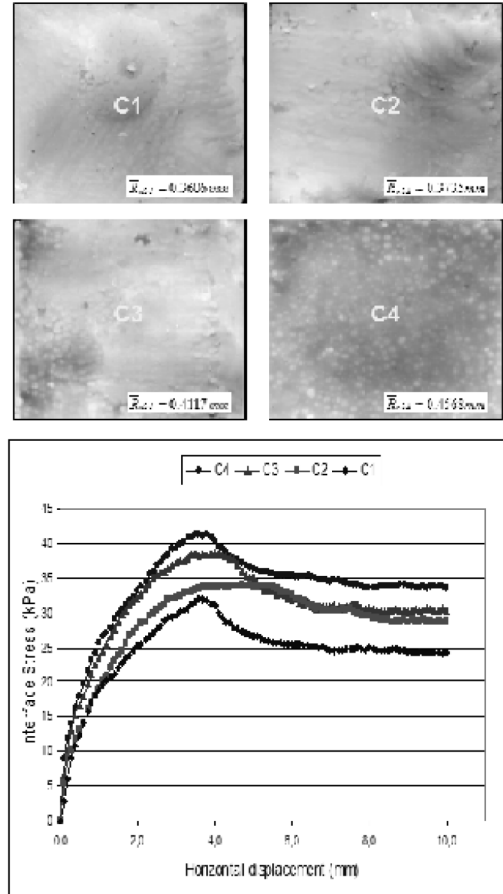


Figure 2. Concrete block surfaces with their 3D roughness coefficients and corresponding direct shear interface test results.

A user friendly standalone application is developed in order to evaluate the surface characteristics of the individual concrete blocks in three dimensions. The software is capable of previewing the surface roughness and magnifying z axis on the screen which allows being aware of surface texture prior to calculation of R_{n3d} . The supported format of the software is point cloud format which is very common in the industry. The three dimensional normalized surface roughness parameters (R_{n3d}) of C1, C2, C3 and C4 are computed by the algorithm (Figure 2 and Table 1).

Interface direct shear tests are performed on split samples of concrete and fly ash pellets. The results are analyzed in order to establish a relationship between R_{n3d} and the maximum interface stresses between pellets and concrete blocks. The interface tests are performed with pellets which consist of 20% cement and 80% fly ash in order to refrain from the effect of grain crushing under normal stress (Figure 2). Since the grain size distribution has considerable effect on interface stresses, only pellets that are retained between No4 (4.75 mm) and No10 (2.00 mm) are used in interface tests. The average diameter of pellets is assumed as 3.00 mm and the normal stress is chosen as 50 kPa. The interface friction angle values corresponding to four concrete surface topographies are presented in Table 1.

Table 1. 3 D roughness parameters and corresponding maximum interface shear stresses

Concrete Block No	Symbol	3D roughness coefficient	Max interface stress kPa
1	C1	0.36	32
2	C2	0.37	34
3	C3	0.41	38
4	C4	0.46	41

The magnitude of the interface shear stress measured is directly proportional to the magnitude of the measured and calculated 3D roughness coefficient. The 3D roughness coefficient may be used to estimate the variations in interface shear strength parameters. The measuring technique is practical and implementable for geotechnical soil structure studies.

CONTACT STRESS MAPPING

The contact normal stresses at the interface of soil and rock with concrete, geosynthetics, waste; or other construction materials are important design considerations to determine the engineering behavior of the interface. Conventional load cells measure the load over an area but do not provide details of the stress concentrations. Films developed for medical and biomedical stress mapping applications are good candidates to explore the stress distribution at the geosynthetic-material interface. The software developed for the special film has several useful tools to quantify the stress distribution with upto 200 dpi resolution. The film is composed of color microcapsules which explode under stress and the chemical released develops the companion film. The color density is related to pressure distribution. The interface between concrete blocks are fitted with the film and one MPa normal stress is applied. The maps of the contact stresses are obtained using the companion software provided by the film producer. The implemented stress mapping technique is a useful tool to help in understanding the mechanisms involved in the interface behavior of soil and construction materials.

The pressure value distribution measurement film is composed of two polyester bases. One is coated with a layer of microencapsulated color forming material and the other with a layer of the color development material (Figure 1). The thickness of the two sheet type film is composed of 75 μ m polyester base, 15 μ m microencapsule layer and 15 μ m of developer layer. The tensile strength of the film is measured as 21 kg/mm, and the elongation value of the film is 120 %. The coefficient of static friction is given as 0.40 (Fujifilm).

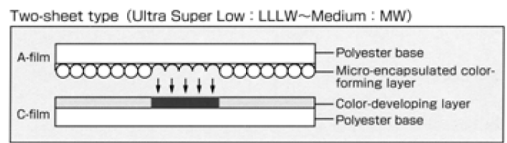


Figure 3. The composition of the Prescale Film.

The measurement ranges of the sensitive films are presented in Table 2. There are other films which can measure up to 300 MPa. For geotechnical applications the low range films are adequate. The high capacity films are

composed of one sheet only. The films are available in rolls with protected cover and must be cut to the desired size. Two sheet films are supplied with two rolls which are cut and fit on top of each other

Table 2. Properties of the Prescale Films

Pressure Range	Low MPa	High MPa
Extreme Low	0.05	0.2
Ultra Super Low	0.2	0.6
Super Low	0.5	2.5
Low Pressure	2.5	10.0

The color intensity ranges from 0.2 to 1.4. The contact pressure versus color intensity calibration curves are presented in Figure 4 for two temperature and relative humidity ranges.

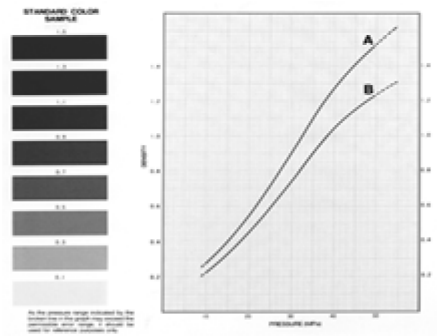


Figure 4. The color intensity range and corresponding stress levels for the prescale films (the gray scale real color is red).

Due to their sensitivity to pressure the films must be handled gently. The suitable range of the pressure measuring film is selected for the proposed study. Each sheet is cut to the size of the area to be measured. Two sheets are matched together and placed between the surfaces to be measured. The load is applied. There are two measurement types; momentary and sustained. For the momentary contact load application the load must be applied for 2 seconds and then removed. For the sustained measurement the duration of contact load application is for two minutes. The temperature and the relative humidity of the measurement

environment is recorded. This data is needed for the selection of the correct calibration chart for the color intensity-pressure relationship. The recommended measurement temperature values are between 20 and 35 °C (-20 to 180 °C is possible but the correlation is not guaranteed) and the relative humidity values are between 35 and 80 %. A special calibration sheet is provided for the software. A scanner cover is provided for the specified scanner. The calibration sheet must be scanned for each session. The films must be scanned within half hour. Once the scanning process is completed the stored image can be analyzed using several tools provided. The scanned image is analyzed with 2D. The pressure values are presented with a 200 dots per inch resolution (0.125mm).

Two 50 mm x 50 mm x 20 mm mortar blocks are used to sandwich the sensitive film under investigation. Odometer loading setup is used to load the mortar block to approximately 1MPa. 245.3 N load with a 10:1 mechanical advantage is applied imposing 2453 N on the sample. The pressure applied on the sample is 981 kPa. The load is sustained for 2 minutes for each application. The samples are then scanned and pressure maps are obtained.

The stress map of the sample studied is presented in Figure 5. The LLW pressure sensitive film has a measuring range of 0.5 to 2.5 MPa. The green color represents stress values below the operating range of this film and the yellow color shows the stress levels above the measurable range for the pressure film used. In certain cases two or three different range films can be used, provided that they are analyzed individually at their specified ranges. The concrete to concrete interface shows that the interface surface topography is not smooth causing stress concentrations.

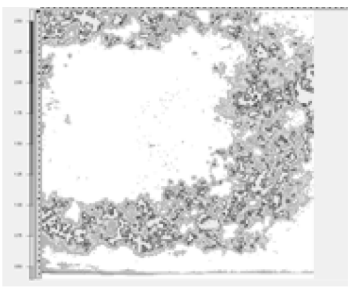


Figure 5. Contact stress map between two 50 mm by 50 mm concrete blocks.

The companion software has several functions which help to analyze the stress distribu-

tion at the interface in a detailed manner. The relative magnitudes of the stress levels may easily be detected using the software (Figure 6). The real stress values however require very thorough calibration and must be used with caution. The real stresses may be measured with other tactile sensors or pressure transducers but still they can only validate stress values on the points they are measured. There are calibration tools available to adjust the load level to the applied load. The larger the efficient contact area the more reliable are the results. For rough surfaces stress concentrations are easily detected by the software, however the magnitude of these high stresses are mostly out of range of the used film. A higher capacity film may be used together to determine the magnitude of these stress concentrations when needed.

The measurement data display shows the effective measurement rate which is an important tool to understand the reliability of the measurement. A high value is the sign of good contact and reliable measurement. Generally a rate of more than 80 per cent is needed. However with uneven topographies and rigid materials this is not an easy task to achieve. Maximum pressure values, average pressure values, calculated load and contact area are presented in the measurement data. All of the recorded data may be exported to Excel for further analysis.

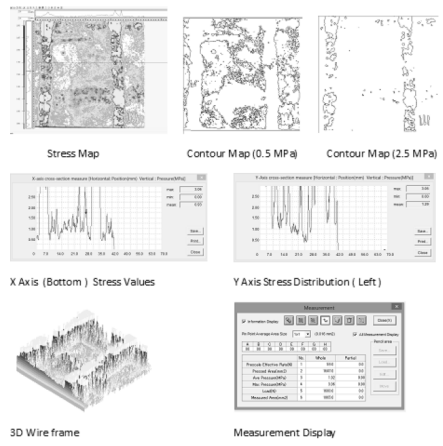


Figure 6. Typical output of pressure mapping software.

With a detailed and careful calibration, the software tool will become a powerful agent for understanding the behavior of the interface contact stress mapping. Pressure sensitive films are good and satisfactory tools to investigate the stress distribution at the soil structure interface.

Comprehensive calibration techniques must be developed for geotechnical applications. Even if the calibration of the films may not be adequate, the information about the distribution of the stresses, location of high stress concentrations and data about the contact areas are invaluable for researchers. The practicality of the films and ease of analysis with the provided software makes this method a good candidate for many geotechnical applications. The range of operating temperatures and relative humidity allows the use of these films in the laboratory and field conditions. The films must be scanned within half hour for further processing. If the films will be used in the field, the special scanner must be present in the field.

MANUFACTURED SAND

Artificial sand may be produced by crushing and screening of rock fragments or can be produced by pelletization of powder fines. Powder materials may be pelletized to form sand, gravel and aggregates. The geotechnical parameters of the pellets are production controllable parameters during the pelletization process such as roundness, sphericity, unit weight, porosity, water absorption, internal friction angle and crushing strength. Fly ash, fly ash with lime and fly ash with cement addition are pelletized into sand size and their engineering properties are measured. The addition of lime and cement helps to obtain any desired crushing strength. A typical collection of manufactured pellets is presented in Figure 7.

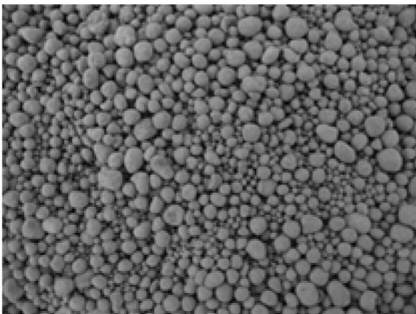


Figure 7. Manufactured fly ash pellets.

The manufactured pellets behave like calcareous sands found in the nature. The source and shape difference of the natural

calcareous sands do not exist in the manufactured pellets having nearly perfect sphericity and roundness. The crushing behavior of the manufactured soil is studied in detail. For potential applications like backfill for retaining walls, fill under the footings, pile installation in existing manufactured soil embankment, anchor installation in manufactured fills, the interface behavior and the influence of crushability on the interface behavior is also studied. Finally odometer tests, direct shear tests are conducted. By controlling the parameters during the pelletization process sands with desired crushability also can be produced. This type of manufactured sand may be used to study calcereous sand behavior at the soil structure interface.

Pelletization process is the agglomeration of moisturized fines in a rotating drum or disc. The product at the end of the process is called the “fresh pellet”. The crushing strength of the fresh pellet must be enough for hauling and stockpiling purposes. The pelletization technology is widely used in powder metallurgy engineering, and medicine industry.

The pelletization theory was developed in 1940's. The performance of the pelletization process is a function of; i) the engineering properties of the material pelletized; ii) the amount of moisture in the medium; iii) the mechanical process parameters such as the angle of balling drum or disc to the normal and the revolution speed. Observations and analysis performed on these parameters with respect to mechanic and kinetic laws formed the theory of pelletization process (Baykal and Doven 2000). The formation of capillary force between two grains is presented in Figure 8.

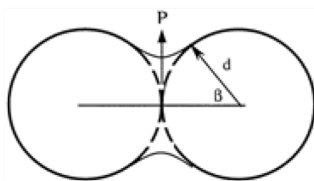


Figure 8. The formation of capillary force between two grains.

The grain diameter of the powder material influences the magnitude of the surface tension force; small grain diameter is necessary to

create enough pulling force to initiate agglomeration. Agglomeration can be achieved by drum or disc pelletizers (Figure 9).

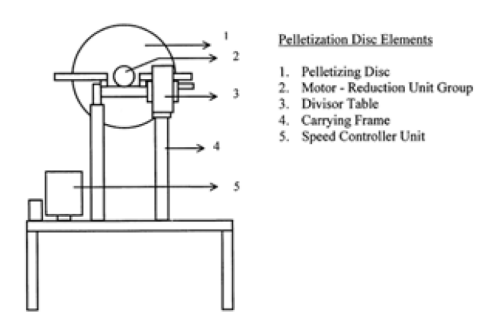


Figure 9. The disc pelletizer.

The revolution speed of the disc can be controlled between 0 and 70 rpm and the angle of the disc plane to the normal can be adjusted between 0 and 90 degrees. The diameter of the disc used in this study is 0.40 meters and scraping blades are placed from center to one edge at 0.06 m intervals. During the revolution of the disc the grains pulled by surface tension are compacted further. The agglomerated grains hit to the scraping blades, falling free to the bottom section of the disc. This free fall action compacts the agglomerated product more. This repeated revolving and free fall action densifies and makes the agglomerated product stronger for handling. To achieve the most suitable pelletization process; the revolution speed and the angle of disc plane to the normal should be set in a manner to avoid the dominance of gravitational or centrifugal forces. For various disc diameters the effect of operating angle and revolution speed on centrifugal and gravitational forces are presented in Figure 10.

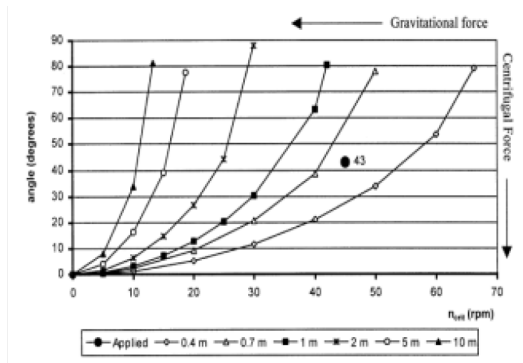


Figure 10. The effect of operating angle and revolution speed on centrifugal and gravitational forces.

Direct shear tests are conducted on manufactured fly ash pellet aggregates under 50, 100 and 200 kPa normal stress applications. Interface tests are conducted on split samples of fly ash pellets and concrete. The internal friction angle and interface friction angle plots are presented in Figure 11.

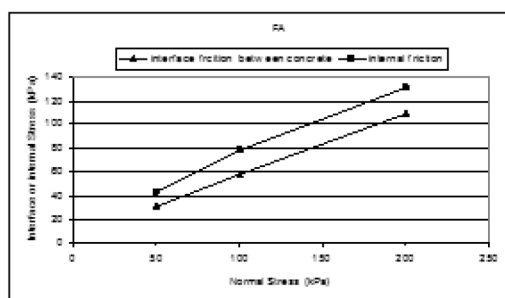


Figure 11. Internal and interface friction shear vs normal stress for fly ash pellets .

The shear stress vs. horizontal displacement and shear stress vs. vertical displacement values of fly ash pellet aggregates are presented in Figures 12 and 13 respectively. While dilation behavior is observed under 50 and 100 kPa, contraction behavior is seen under 200 kPa due to grain crushing.

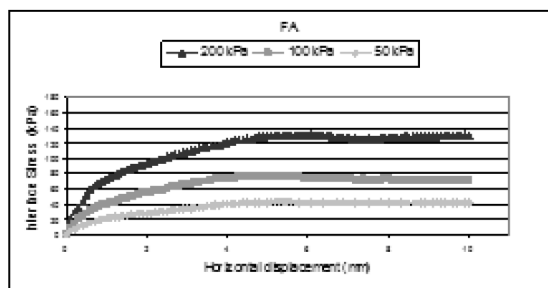


Figure 12. Shear stress vs horizontal displacement for fly ash pellets.

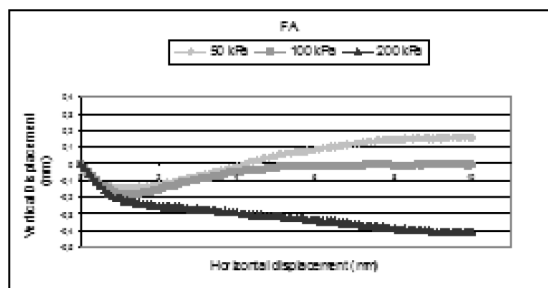


Figure 13. Vertical displacement vs horizontal displacement for fly ash pellets.

To demonstrate the effect of aggregate crushing sieve analyses are performed before and after direct shear testing of fly ash pellets at 50, 100 and 200 kPa normal stress. The change in grain size distributions before and after execution of the direct shear tests are given in Figure 14 (Danyıldız 2007). The fly ash pellets crushing behavior is similar to that of calcareous sands. The measured crushing behavior does not pose a threat for the engineering performance of the fly ash pellets for most geotechnical applications.

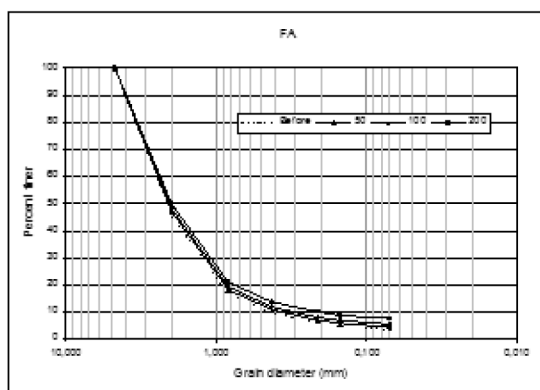


Figure 14. Grain size distribution curves of fly ash pellets before and after the direct shear test.

As demonstrated it is possible to manufacture sand sized pellets to the desired crushing strength to model calceraous sands. By eliminating one parameter at a time, parametric studies may be conducted to understand the behavior of calcerous sand at the interface.

CONCLUSIONS

The presented technologies are practical and easily implementable in geotechnical engineering research. If the soil structure interaction problem is handled in three different points of view; the structure, the soil and the loading conditions, the proposed techniques handle the first two.

The structure aspect of the interaction may be analyzed in more detail when the surface topography is quantified and the contact stresses are determined at the interface.

The soil behavior is harder to assess. The manufacture of sand or gravel sized pellets with pretargeted specifications (crushing strength, roundness, sphericity, surface roughness, grain size, unit weight, porosity etc) provides a new vision in conducting parametric studies related to calcerous sands which have great economical concerns for the offshore geotechnical research.

Although not presented here, a versatile laboratory interface shear device has been developed utilizing pneumatic muscles. The new equipment is able to apply both static and cyclic loads (compression and tension) and displacements. The loads are applied via pneumatic muscles while the displacement are applied with an additional step motor controlled linear drive.

With more technological advancements it will be easier for the geotechnical engineers to collect more information about the interface behavior between soil and structure leading to safer and more economic designs.

REFERENCES

- Arslan H. 2003. The effect of grain crushing on the behavior of granular materials. MSc Thesis. Bogazici University. Istanbul.
- Baykal G. And Doven A.G. 2000. Utilization of fly ash by pelletization process; theory, application areas and research results. *Resources Conservation and Recycling* 30, 59-77.
- Doven A.G. 1998. Lightweight fly ash aggregate production using cold bonding technique. PhD Thesis. Bogazici University, İstanbul.
- Erdurak M.C.2011. Artificial sand production for laboratory tests. MSc Thesis Bogazici University, Istanbul
- Danyıldız E.2007. The interface behavior between granular soils and concrete. MSc Thesis, Bogazici University. Istanbul.
- Fujifilm Corporation. “Operations Manual; Pressure Distribution Mapping System for Prescale”, Ver 2.
- Kishida, H. and Uesugi, M., “Tests of the Interface Between Sand and Steel in the Simple Shear Apparatus”, *Geotechnique*, Vol. 37, No. 1, pp 45-52.

Foundations by prestressing anchors of the “Villa Méditerranée” in Marseille: from design to monitoring.

Catherine JACQUARD
FONDASOL, France

ABSTRACT: The structure of the Villa Méditerranée is in an unstable position, which gives to four of its foundations a permanent traction load. Each of these foundations is stabilised by 4 to 6 active permanent anchors (149 to 349 Tonnes of load service each). In order to limit deformations due to elasticity of prestressing cables, a specific level of prestressing has been defined. The paper presents the design, the achievement and the monitoring of the prestressing anchors, in order to insure the stability of the structure.

1. INTRODUCTION

The Villa Méditerranée is a center of conference and exhibitions, built on the sea side of MARSEILLE by AREA PACA. Boeri, Manfredi and Di Pol are the architects designers of this metallic 36m cantilever structure, at 19 m high above the sea level (see fig.1 and 2). It is completely independent of the underground structure based at 15m under the sea level.

The construction area is around 60x60m, built from a platform at +1.7m NGF, earth-works have been carried out at -13.5m NGF, under cover of a diaphragm wall.



Figure 1. general view of the building.

Due to the cantilever structure, four of its foundations are in fact loaded with permanent traction (see fig.3, file 1). To maintain the

foundations, four to six prestressed nearly vertical anchors have been carried out.

This paper describes the design, the achievement and the monitoring of these anchors.

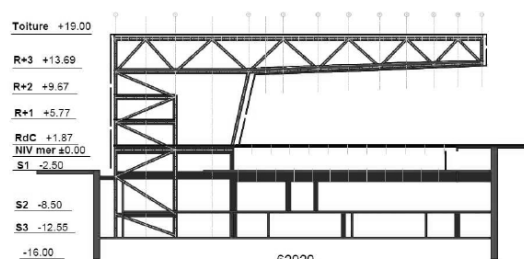


Figure 2. Cross section of the structure.

2. GEOLOGICAL CONTEXT

The site had previously a harbour activity, with old embankments, navigation channels.

Geotechnical investigations which have been carried out indicate the following lithology:

- Heterogeneous fills of 5 to 8 m thick,
- Alluvial sandy-gravelly to clayey silty soils,
- Tertiary Stampien formations, beginning from -7.5 to -12 m NGF, and constituted with pudding stone, cemented sands and sandy to clayey marls.

A 2 to 3m thick layer of relatively permeable gravely sand, was identified in the marls, between -20 to -25m NGF and is a captive aquifer. Fills and alluvial formations constitute a free surface aquifer. Both aquifers have nearly the same static water level.

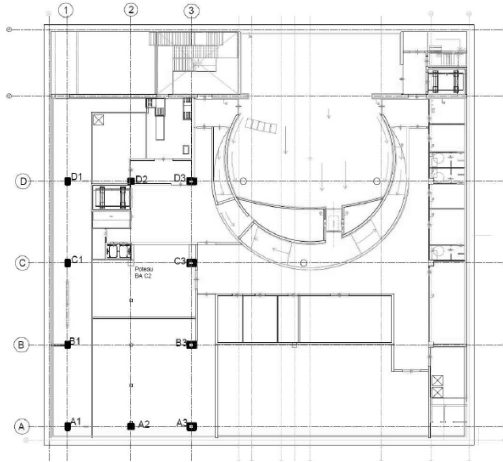


Figure 3. Foundations of the metallic structure.

3. GENERAL DESIGN OF FOUNDATIONS

3.1. Specific loads

The design of the cantilever metallic structure gives heavy compression loads up to 3500 tonnes (35 MN) on file 3 foundations, and traction loads on file 1 foundations of 500 and 2000 tonnes (5 to 20 MN).

3.2. Specific file 1 foundations

Each foundation of file 1 is designed to be maintained by 4 to 6 prestressed anchors. Reservations have been provided in the concrete of those bases, in order to be able to add new anchors, in case one anchor is defective (see fig. 4).

The anchors are in 0,18m or 0,20m diameter, bored vertically, or on slope to vertical line of 5°. Their free length is 11m, their grouted length is 9m (foundations B and C) or 20m (foundations A and D). They are equipped with cables of preconstraint respectively 10T15.7

and 26T15.7; their fixing length is injected with cement at low pressure from tubes with cuffs.

3.3. Procedure for injecting the anchors

The anchors are performed according french recommendations TA95 (1) procedure for global injection type of grouting.

First, drilling is carried out until the designed length; then the armature and the tube for grouting with cuffs are put in the hole. A first grout fills the hole from the bottom to the top of the whole length. After several hours, the injection of the fixing part is operated from the cuffs tube to a low pressure of 1 MPa.

3.4. Distortions

Considering that the stability of the whole structure is carried out on the anchors, it was decided to be more conservative than the Eurocode 7 for service situations load cases: The specific service limit state being considered gives up to 10 to 40% more load than usual characteristic service load.

The design of such foundations needs to estimate accurately the distortion to be expected in accordance with elasticity of the cables, and with different load cases, and to tight enough the cables, in order to limit the deformations to acceptable values for the long term behavior of the structure.

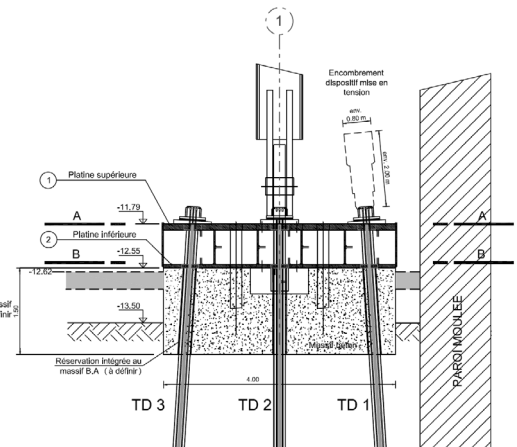


Figure 4. Cross-section of D foundation.

4. CHARACTERISTICS OF THE ANCHORS

4.1. Soil properties

The previous length of the anchors was calculated from pressiometric limit pressure values measured in marls ($Pl^* = 7 \text{ MPa}$), and using french recommendations TA95 (1) for global injection type of grouting. The ultimate friction in fixing length given by the abacus is $q_{su} = 400 \text{ kPa}$.

Preliminary test have been carried out (see 4.3 paragraph) and enabled to define a better ultimate friction of $q_{su} = 600 \text{ kPa}$, and to give the grouted length for each massif (see table 1) in conformity with situation loads.

Table 1. File 1 anchors specifications

	A1	B1	C1	D1
QELU (kN)	4173 (x6)	1990 (x4)	1830 (x4)	4512 (x6)
QELS CAR (kN)	2892 (x6)	988 (x4)	855 (x4)	3148 (x4)
QELS SPE (kN)	3148 (x6)	1368 (x4)	1190 (x4)	3588 (x6)
Free length (m)	11	11	11	11
Grouted length (m)	20	9	9	20

4.2. General stability

To verify the uploading general stability, we calculated a reduced volume of soil, associated to one anchor, in conformity with TA95 recommendations (see fig. 5). This condition gives the minimum length of the free length of the anchors.

4.3. Preliminary tests

At the beginning of works, three preliminary tests were carried out in order to define properly the ultimate friction to be considered in marls for global injection type of grouting.

In order to test the whole zone of embedding, the anchor tests were vertically drilled in 0.18m diameter, had a free length of respectively 26.5m, 31.5m, and 36.5m, and a fixing length of six meters.

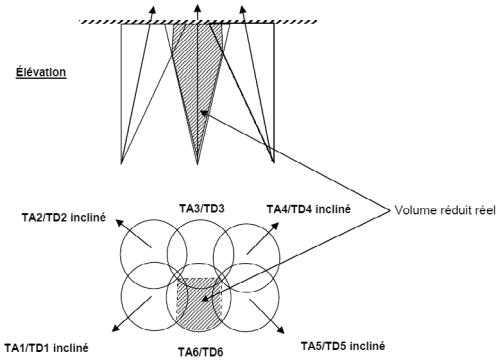


Figure 5. Reduced volume of soil associated to one anchor

Considering the equation (1), we can define that $QELS = 678 \text{ kN}$.

$$QELS = \frac{\pi D L q_{su}}{2}, \quad (1)$$

Where $D = 0.18 \text{ m}$ is the diameter of the drilling, $L = 6 \text{ m}$ the grouted length, and $q_{su} = 600 \text{ kPa}$, the ultimate friction.

The tests were carried out in conformity with french norma NF P94-153 (2) up to test traction $T_e = 2232 \text{ kN}$. This value is three times the theoretical load service value. Table 2 gives the main results of these tests. The ultimate value $q_{su} = 600 \text{ kPa}$, defined out of these tests, is 20% less than the lower measured value, in order to be conservative.

Table 2. Main results of preliminary tests

Anchor	T _c (kN)	T _c (kN)	T _u (kN)	T _s (kN)	q _{su} (kPa)
TR5	1688	1519	> 2232	1215	716
TR6	1825	1662	> 2232	1329	783
TR7	1925	1733	> 2232	1386	817

4.4. Creeping test

In order to check the risk of creeping in marls, one of the test (TR7) was carried out with a long time stage of 24 hours under the load of 1360 kN. On fig.6, it can be seen the results of the test, in term of a values of creeping, calcu-

lated according to formula 2, with gives the speed of the displacement of the anchor under the load. This speed is decreasing with time. Extrapolating these measures, it can be assumed that creeping becomes null after around 50 hours.

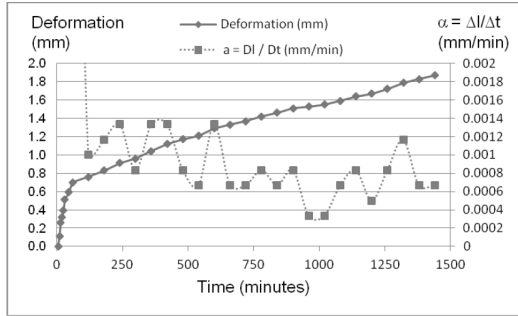


Figure 6. Deformation and creeping of the anchor TR7 24 hour test

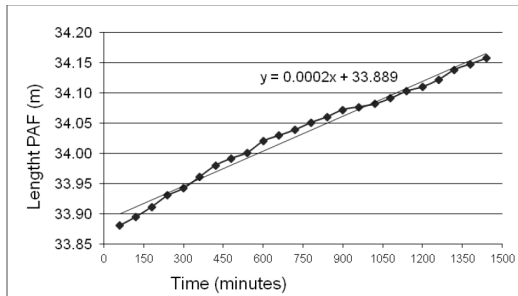


Figure 7. PAF of the anchor TR7 24 hour test

Moreover, the fictive anchor point (PAF) is calculated with formula (3), taking into account the extension of the anchor Δl , the elastic modulus of the steel $E=192500$ MPa, and the section of the cable $S=1500$ mm² (10T15.7).

When extrapolating the fictive anchor point graphic at 50 hours, we calculate a PAF of about 34.5m (see fig.7), which exactly corresponds to the sum of the free length ($L_f=31.5$ m) and half of the fixing length ($L_s=6$ m).

Under the load test of 1360 kN, the injected length is loaded at 50% of its capacity. The safety coefficient is then of 2 compared to the limit friction.

$$\alpha = \frac{\Delta l}{\Delta t} \quad (2)$$

$$PAF = \frac{ES\Delta l}{Te - T0} \quad (3)$$

During this test it has been measured:

$$\Delta l(60'-5') = 0.7 \text{ mm} < 1 \text{ mm}$$

$$\Delta l(2h-20') = 0.44 \text{ mm} < 1 \text{ mm}$$

$$\Delta l(24h-1h) = 1.17 \text{ mm}$$

These are criteria which also contribute to make the test satisfying.

5. PROCEDURES FOR TENSIONING ANCHORS

Each anchor is tight at a trial tension $Te=1,25Ts$, with Ts being the specific limit service state defined for the project. The tension is uploaded by five steps (0,1 Te - 0,2 Te - 0,4 Te - 0,6 Te - Te). The trial tension is maintained 30 minutes. If creeping conditions ($\Delta e5'-30' < 1$ mm) are not satisfied, the trial tension test is extended of 30 minutes, and it must be checked that $\Delta e30'-60' < 0.5$ mm. The tension is then downloaded to the service tension Ts .

To avoid an excessive rotation of the foundations, a procedure by steps of loading has been established: the first step consists of applying tension of 50% of final tension to all anchors of a foundation; the second step consists of applying the trial tension to each anchor and then to download it to the service tension Ts .

Fig.8 shows a foundation (D) with its anchors already in tension.



Figure 8. D foundation in tension

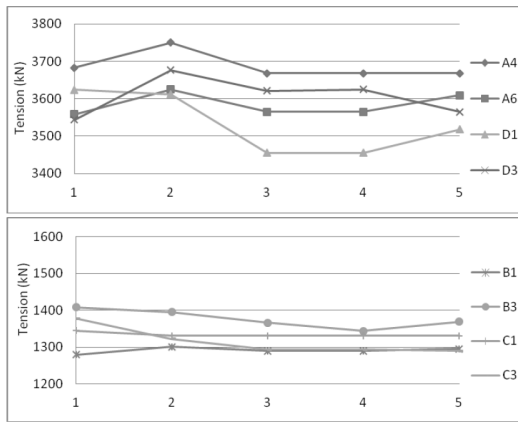


Figure 9. Tension control between 30th march and 2nd august 2011

6. MONITORING OF THE FOUNDATIONS

In order to control the behavior of the anchors with time, and to ensure the stability of the structure, two anchors of each foundation have been equipped with a control tension cell.

The fig.9 shows the tension of the anchors during the construction of the structure. Some relaxation occurs during the first months and then stabilizes. It is due to the settlement of the foundation in compression on the stiff marls under the tension of the anchors.

A protocol of periodic monitoring has been established and has to be maintained during the life of the structure, in order to make sure no problem is encountered. The procedure consists of automatic measurements of the tension of anchors; a system of alert is activated if the level of tension, defined for each foundation is overtaken.

7. ACKNOWLEDGEMENTS

The author thanks AREA PACA for his authorization to write this paper.

8. REFERENCES

- (1) Recommandations tirants d'ancrage : TA95 (1995), Eyrolles, 150 pages

- (2) Norme NF P94-153 (1993). Essai statique de tirant d'ancrage, 20 pages
- (3) Norme NF P94-282 (2009). Calcul géotechnique- Ouvrage de soutènement- Ecrans, AFNOR, 182 pages

Effect of Ground Motions and Tsunami Impact Force on the Performance of a Damaged River Dike

Hemanta Hazarika

Kyushu University, Fukuoka, Japan

Tadashi Hara

Kochi University, Kochi, Japan

Shunichi Kuroda & Kentaro Kuribayashi

EightJapan Engineering Consultants Inc., Osaka, Japan

Tsuyoshi Nishi

Construction Project Consultants, Tokyo, Japan

Hideo Furuichi

Giken Ltd., Tokyo, Japan

Koichiro Takezawa

Newjec Inc., Osaka, Japan

Tsuneo Ohsumi

National Research Institute for Earth Science and Disaster Prevention, Tsukuba, Japan

ABSTRACT: Many river dikes and embankments in the coastal region of Tohoku area were damaged due to strong ground motions of the 2011 Off the Pacific Coast of Tohoku Earthquake and subsequent attack by the tsunami. This paper analyzes the cause of damage to the Yoshihama river dike located in Ofunato city of Iwate prefecture based on past field investigations and numerical simulations. Analyses revealed that the dike body had low liquefaction resistance and the volume change after liquefaction was rather large. Due to main shock and aftershocks there is likelihood of liquefaction in dike body and the re-liquefaction possibilities are high even under small ground motions. Based on the series of analyses it could be confirmed that even though the dike body was covered with concrete panels, due to liquefaction induced settlement of the embankment, gaps developed between the embankment crown and the concrete covering. These gaps ultimately reduced the tsunami resistant characteristics of the dike, and thus resulting in the collapse of the dike

1. INTRODUCTION

Strong ground motions and resulting tsunami due to the 2011 Off the Pacific Coast of Tohoku earthquake ($M_w = 9.0$) led to the failure of many waterfront structures in the coastal regions of the Tohoku area (mainly Aomori, Iwate, Miyagi and Fukushima) of Japan. Geotechnical structures such as dikes and railway embankments in the vicinity of the eastern coasts suffered scouring and erosion due to overtopping of the highest ever tsunami which far exceeded the design head levels (JGS, 2011). According to investigation conducted in Aomori prefecture and northern part of Iwate prefecture (Hazarika et al., 2012), most of the damage of the river banks or coastal dikes were mainly due to scouring at the back of the structures. Scouring was found to be caused

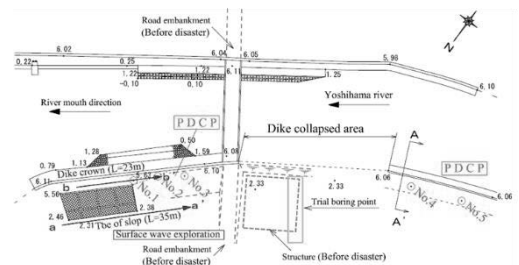
not only by the overtopping tsunami itself, but also the force of the backrush of tsunami. On the other hand, the investigation conducted by Hara et al. 2012 revealed that in southern central part of Iwate prefecture, the level of damage by the tsunami on river banks varies according to the structural forms, such as existence of surface covering, materials and topographical features.

According to investigation by the Ministry of Land, Infrastructure, Transport and Tourism (MILIT) of Japan, there were more than 1195 damage in the river bank that Tohoku district maintenance office directly manages (MILIT, 2011a). In the river mouth, the damage was mostly by the tsunami. In the other parts of river banks, the damage was mostly due to the subsidence by either earthquake motion or the liquefaction of soils in the dike body. Especially in those

areas under the jurisdiction of the Tohoku Regional Bureau of MILIT, extensive investigations were carried out to determine the damage characteristics. Based on those damage patterns and characteristics as well as analyses of the dikes due to the earthquake and tsunami, appropriate reconstruction measures were suggested (MILIT, 2011b). Many researchers conducted case study analysis of river dikes damaged due to liquefaction, and reported the damage patterns and the extent of deformation (Imai et al. 2013, Wakinaka et al. 2013).

2. OVERVIEW OF THE DAMAGE

Due to the 2011 Off the Pacific Coast of Tohoku Earthquake, several parts within 102.4 to 138.5 m of the upstream of both the right and left banks of the river were damaged and the dike revetments were tilted towards the river. The state of damage of the dike is shown in Fig. 1. The sea



Four surveys were conducted on the damaged dike after the disaster (Hazarika et al. 2013a, Hazarika et al. 2013b, Yamanaka et al. 2012). The following were four different surveying that were performed in accordance with various purposes: (1) VRSRTKGPS (using Sokkia : 1/J)

survey to determine the elevations after the earthquake (2) survey using total station (Laica Geosystems : TCR407S) to determine the cross section of the dike (3) Sounding (Portable Dynamic Cone Penetration (PDCP) test) and (4) Surface wave exploration method. The locations of the surveys are shown in Fig. 2. The surveys were conducted in three stages The first stage was after two months (May 2011), the second stage was after six months (September 2011) and the third stage was after almost two years and four months (July 2013).

Figure 3 shows the cross section of the Yoshihama dike along the AA' line shown in Fig. 2. The dike wall consists of a vertical buttress with 2 m wide crown with back slope (inclination of 1:1.2), which were covered with concrete. As of July, 2013, the crown height of the embankment was T.P. + 5.10 m. Wide area around the epicenter of the 2011 Off the Pacific Coast of Tohoku Earthquake suffered huge tectonic subsidence. According to the standard cross section used in design (1968) of Yoshihama dike (TDL 2011), the design crown height was T.P. + 6.15 m. Therefore, it can be inferred that in the concerned location, the crown subsided by about 1 m as compared to the original height at the time of completion of the embankment.

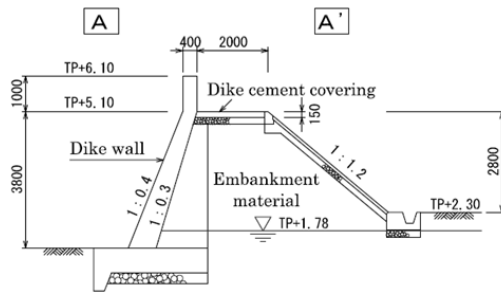


Figure 3. Cross section of the dike

3. NUMERICAL SIMULATIONS

In order to analyze the cause of damage of the embankment due to the strong ground motions and tsunami, numerical analyses were conducted for the damaged dike. The parameters used in the analyses were determined based on the in-situ and laboratory tests as described in Hazarika et al. 2013a. Simulations were performed for the damaged dike by considering the history of the main shock, aftershocks and the tsunami that at-

tacked the dike. In addition, stability of the embankment was evaluated based on the tsunami impact force experienced by the damaged cross section due to overtopping tsunami.

3.1. Numerical model

In order to simulate the influence of ground motions on the damaged embankment, two dimensional effective stress analyses were performed that can take into the account the post liquefaction settlement due to drainage (Oka et al. 1994). Here, attention was paid to the influence of long continuation time of the main quake and several aftershocks that followed within a short interval. In the analyses, timing of the concrete cover peeling off in the crown and back slope of the dike, subsidence of the embankment and the developed gap at the crown of the embankment, which were observed during the field surveys were evaluated in the time scale.

The numerical model is shown in Fig. 4. The target structure is the damaged part of the Yoshihama dike shown in Fig. 3. The bottom of analysis model was set where measured shear wave velocity (V_s) in the field survey (Hazarika et al, 2013a) was over 350 m/s. In the analyses, the bottom was taken as viscous boundary and the sides were set as equal displacement boundaries.

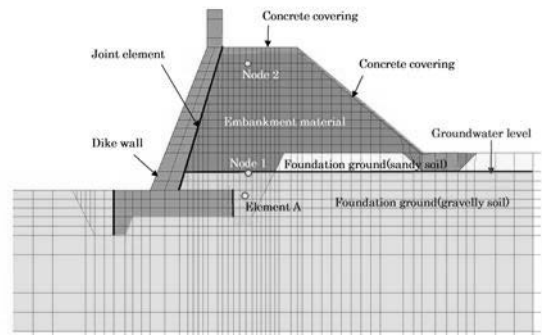


Figure 4. Numerical model of the dike

The input parameters are shown in Table 1, which were determined based on the undrained cyclic test of the materials collected from the surveyed site (Ueno et al. 2012), and using the simulations of the element tests. Embankment soils and foundations soils were modeled as elastoplastic materials. The retaining structures, concrete covers at the top and the back of the embankment were modeled as linear elastic materials. The interface between the structures and embankment were simulated using join elements.

The contact and separation between the structure and the embankment were carefully considered during the simulations. The ground water level was taken to be at T.P. + 1.78 m (Based on the field survey results).

Earthquake records of KiKnet recorded near the surveyed areas were adopted as the input ground motions. Ground motions observed at KiKnet Kamaishi (IWTH23), which has almost the same V_s as the base of analysis model, was used in the analyses. Figure 5 shows the synthesized input acceleration record used in the analyses. It is to be noted that the target area experienced main shock at 14:46 hours and two aftershocks at 15:06 hours and 15:09 hours (JMA 2011).

Table 1 Materials properties

	Elasto-plastic model		
	Embankment material	Foundation ground	
		Sandy soil	Gravelly soil
Unit weight, γ (kN/m ³)	14.31	14.00	20.00
Permeability, k (m/s)	7.0×10^{-6}	7.0×10^{-6}	1.0×10^{-4}
Initial void ratio, e_0	0.99	0.95	0.45
N-value	2.00	2.00	50.00
Fines fraction content, F_c (%)	20.50	15.50	-
S wave velocity, V_s (m/s)	175	155	350
Initial mean effective stress, σ'_m (kN/m ²)	98.00	98.00	66.67
Initial shear modulus, G_0 (kN/m ²)	45625	35022	255102
Cohesion, c' (kN/m ²)	0.00	0.00	0.00
Internal friction angle, ϕ' (°)	36.60	37.00	40.00
Bulk modulus, K_r (kN/m ²)	2200000	2200000	2200000
Compression index, λ	0.01610	0.02051	0.00142
Swelling index, κ	0.00151	0.00205	0.00014
Pseudo overconsolidation ratio, OCR*	1.000	1.000	1.000
Normalized initial shear modulus, G_0/B_0	466	357	3827
Phase transformation stress ratio, M^*_m	0.909	0.909	0.909
Failure stress ratio, M^*_f	1.215	1.229	1.336
Hardening parameter, B_0	1533	5000	11458
Hardening parameter, B_1	15	100	115
Hardening parameter, C_1	0.00	0.00	0.00
Reference value of plastic strain	0.0100	0.0070	-
Reference value of elastic strain	0.020	0.015	-
Parameter of dilatancy, D_0^*	1.000	3.000	-
Parameter of dilatancy, n	4.000	6.000	-

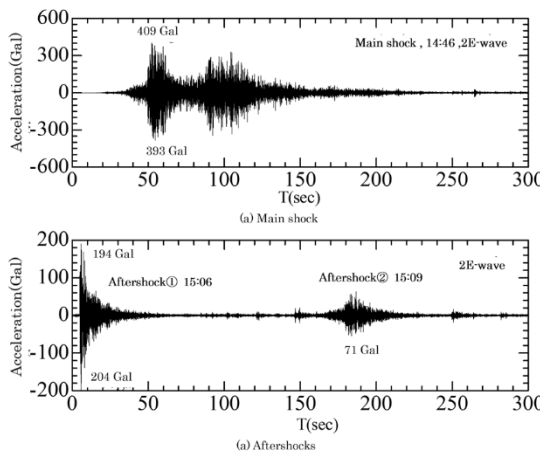


Figure 5. Input ground motion used in the simulations (KiKNet Kamaishi (IWTH 23)).

3.2. Simulation results

Figure 6 shows the deformation of the dike due to the ground motions. During the main shock and two aftershocks, the embankment subsided by about 0.67 m and the back slope was highly deformed resulting in the peeling off of the concrete covers as observed in the in-situ survey. However, near the toe of the embankment no large deformations were observed due to the ground motions.

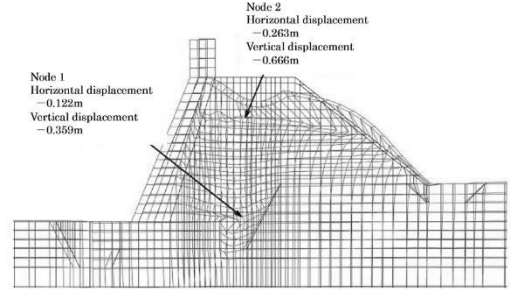


Figure 6. Deformation of the embankment due to main shock and aftershocks

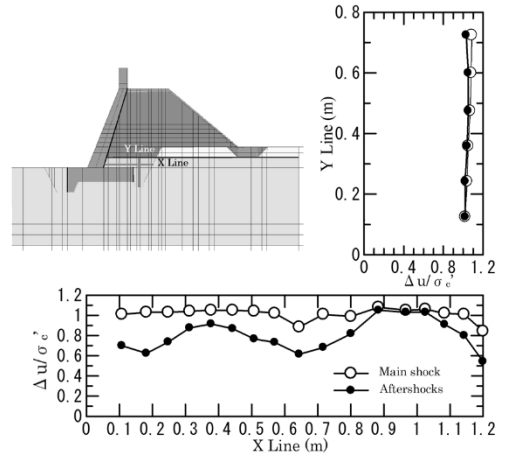


Figure 7. Distribution of maximum excess pore water pressures

Figure 7 shows the distribution of the maximum excess pore water pressures developed inside the embankment due to the main shock and aftershocks. The domain of the liquefied zone due to aftershocks is shown in the same figure. As seen in the figure, in Y Line the value of $\Delta u/\sigma'_e$ reaches 1.0, however, in X Line the value of $\Delta u/\sigma'_e$ reaches up to 0.6–0.8 without any liquefaction. It can be inferred from such phenomena that due to the main shock, the bottom parts

of the embankment located under the water table suffered local liquefaction. The excess pore water pressure dissipated in some cases, and in some cases not. Therefore, even though the after-shock ground motions are small as compared to the main shock, the excess pore water pressure built up again leading to re-liquefaction of the soils.

Figure 8 shows the development and dissipation of the excess pore water pressure due to the ground motions in the element A (refer to Fig. 4) within the embankment located below the ground water level. It can be seen that in spite of the sound bed rock that supports the dike, due to the maximum ground motion of about 400 Gal, almost whole of the bottom part of the embankment reached the excess pore water ratio of 1.0, and as result many locally liquefied zones were observed. However, within 20 minutes of the main shock (before the aftershock), the excess pore water pressure almost dissipated. During the first aftershock where the maximum acceleration was about 200 Gal, the excess pore water pressure inside the embankment built up again, and the $\Delta u/\sigma'_v$ value reached 1.0. The pore water pressure dissipated before the second after shock (maximum acceleration 70 Gal) and $\Delta u/\sigma'_v$ values came down to 0.4. However, the second aftershock brought the $\Delta u/\sigma'_v$ value again to 0.9, and as a result a part of the embankment experienced re-liquefaction.

Figure 9 shows the distribution of the volumetric strain inside the embankment due to dissipation of the excess pore water pressure. This figure reveals that during the main shock when $\Delta u/\sigma'_v$ attains 1.0, the volumetric strain becomes 2~5% . During the aftershocks, in the parts where $\Delta u/\sigma'_v$ attains 1.0 about the same amount of volumetric strains were generated. In parts where $\Delta u/\sigma'_v$ is 0.6 ~ 0.8 without any liquefaction, volumetric strain is 1~2%. This is consistent with the results from the reconsolidation test results conducted after the cyclic undrained test (Ueno et al. 2012).

Figure 10 shows the vertical deformation of the embankment at two points (nodal point 1 and nodal point 2 of Fig. 12) due to dissipation of the excess pore water pressure after the main shock and the aftershocks. The vertical deformations δv at the surface of the embankment were calculated to be 0.52 m after the main shock, 0.60 m after the first aftershock, and 0.67 m after the second aftershock

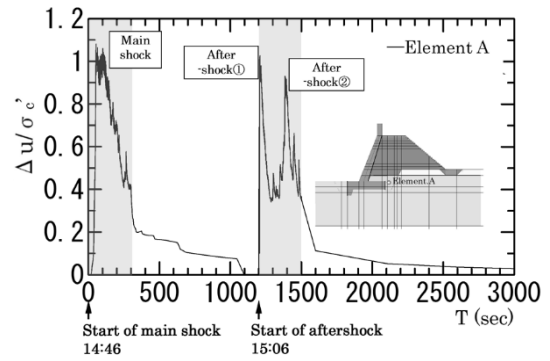


Figure 8. Time history of the excess pore water pressure (Element A of Fig. 4)

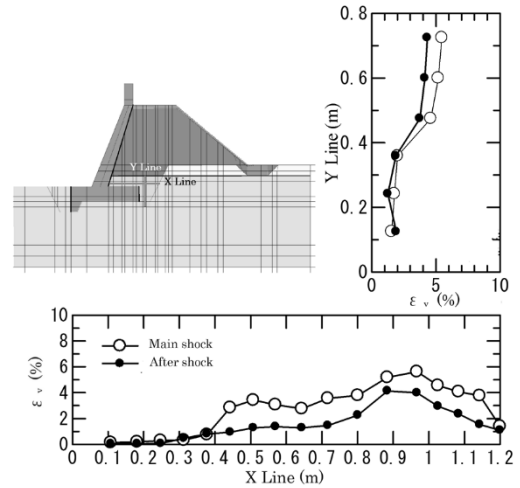


Figure 9. Distribution of volumetric strain due to dissipation of the water pressures

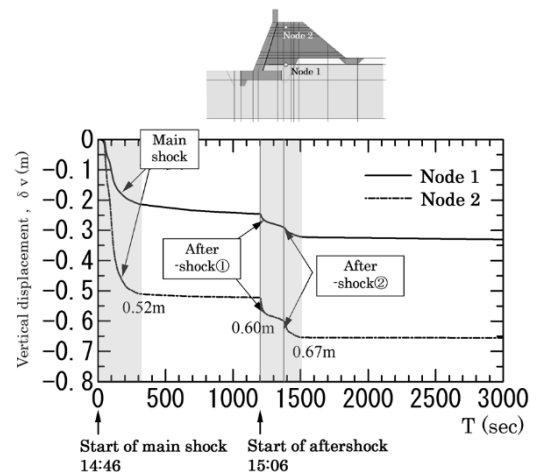


Figure 10. Subsidence of the embankment due to main shock and aftershocks

Based on the above results, it can be inferred that the subsidence of the embankment progressed due to repeated dissipation of the pore water pressures, and as a result even before the arrival of the tsunami, the embankment suffered huge deformation. It is to be noted that the subsidence at the end of the second aftershock calculated from the simulation agrees with the value recorded in the field survey (Hazarika et al. 2013a).

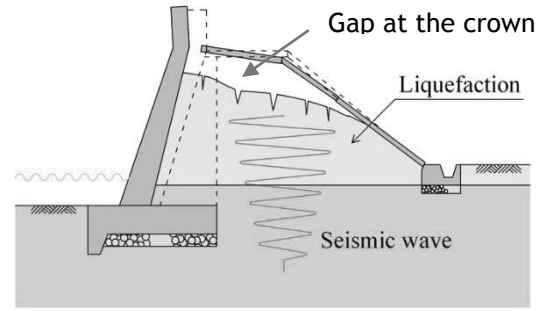
4. ANALYSIS OF DAMAGE AND FUTURE STRATEGIES FOR PROTECTION

In general, river damage is due mainly to the flood, erosion, seepage, earthquake etc. However, the surveyed area in Yoshihama was damaged due to the compound effect of liquefaction and tsunami overflow.

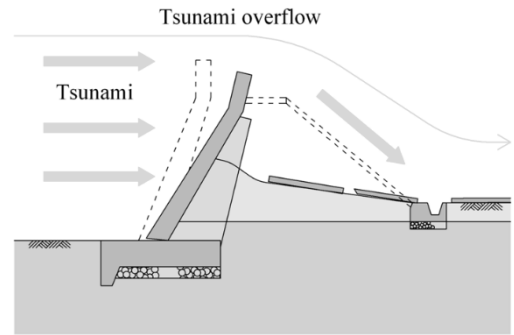
4.1. Mechanism of damage

Figures 11(a) – (c) show the damage to the embankment due to liquefaction induced settlement under the action of the main shock and aftershocks, and the collapse of the dike due to the tsunami attack. As shown in Fig. 11(a), due to action of the main shock and aftershocks, the embankment subsided resulting in the development of gap between the crown and the concrete covers. Since the durability of the concrete cover is due mainly to the amount of concrete or the connections of the blocks, there is a high possibility of the collapse due to the subsidence of the embankment and development of vertical cracks.

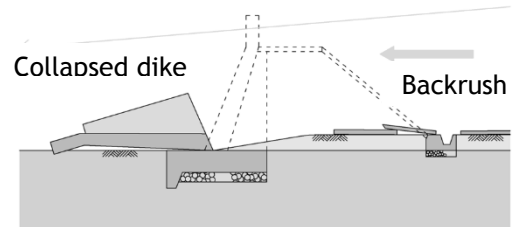
As compared to the other natural events such as typhoon, heavy rainfall etc., in the case of tsunami due to short interval within which the water level rises, the head level difference and the amount of overflow become very large. When the damage to the concrete covers is huge, as seen in Fig. 11(b), due to tsunami overflow at the crown, the dike body is swept away, and as a result the stability of the retaining structure is greatly affected. During the backrush, as seen the Fig. 11(c), the force of backrush acts as a force that made the already unstable retaining structure tilt and collapsed towards the river.



(a) Before the earthquake



(b) After the earthquake



(c) Effect of the tsunami and its backrush

Figure 11. Mechanism of collapse

4.2. Recommendation for countermeasures

Based on the series of analysis it can be concluded that it is necessary to develop resilient structure that can prevent the liquefaction induced damage of dikes not only during the main shock but also the aftershocks so that the structure can retain its strength before the arrival of tsunami. In addition to that, it is necessary that even under the action of the tsunami, the tsunami

overflow and the backrush, dikes need to preserve its water retention capacity and retain its function to prevent erosion and flow.

In order to adopt adequate seismic resistant and tsunami resistant measures for dikes, and proper design standard for the expected tsunami in the future, it is necessary that the tsunami run up does not cause much damage to the landside area beyond the dike (MILIT, 2011c). In principle, levee works materials used should be of proper standard, so that they do not undergo liquefaction. Such measure could maintain height of the design tsunami water level (Nakane et al. 2013). Especially, the filled soil used in the foundation needs to be compacted and stabilized well to prevent liquefaction.

It may be difficult to adopt the above mentioned techniques for existing structures. However, liquefaction of foundation soils still can be prevented by installing preventive piles or sheet piles in the riverside, landside as well as crown of the dike (Otsushi et al. 2011). Such structural measures would be able to preserve the water retention capacity of the dike by minimizing the vertical and horizontal deformation within the dike (Kochi Prefecture, 2013). Use of flexible structure behind the back of sea wall is another low cost approach which could be adopted to prevent scouring and erosion due to overtopping tsunami and its backrush (Hazarika et al, 2013c).

5. CONCLUDING REMARKS

(1) Embankment material in the dike body had low liquefaction resistance similar to those of alluvial soils and decomposed granite.

(2) The volume change due to dissipation of the excess pore water pressure at the end of the cyclic loading is larger than those of alluvial sand and decomposed granite with 50% relative density (Hara et al. 2004).

(3) When several ground motions from the main shock and the aftershocks act on the embankment, in the saturated zone of the foundation soils a large change of the excess pore water pressure develops. As a result even under small aftershocks, the foundation soils undergo re-liquefaction.

(4) The subsidence of the embankment due to dissipation of the excess pore water pressure after liquefaction increases due to repeated loads under main shock and aftershocks.

In this research attention was focused only on a particular site. It is, however, necessary to

collect data on more similar sites in order to develop adequate relationship amongst structural elements (such as dike materials, dike structures), topographical elements (such as nearby topography, rived shapes) and elements that contributes to compound disaster. It is also necessary to conduct simulations of undamaged flexible structures (Hazarika et al. 2013b), which may through light on the damage mechanism of conventional rigid structures.

ACKNOWLEDGEMENT

The authors greatly appreciate the contributions of the following individuals in the in-situ testing, field survey and data analysis of this research: Dr. Minoru Yamanaka, Kagawa University; Mr. Nozomu Kosaka, JAFEC USA, U.S.A.; Mr. Hiroshi Takenaka and Masaaki Fujii of Japan Foundation Engineering Co., Ltd., Sendai Branch, Japan.

REFERENCES

- Hara, T., Okamura, M., Uzuoka, R., Ishihara Y. and Ueno, K. 2012: Damages to river dikes due to tsunami in southcentral coastal area of Iwate Prefecture in 2011 off the Pacific Coast of Tohoku Earthquake, *Japanese Geotechnical Journal*, Japanese Geotechnical Society, 7(1), pp. 2536 (In Japanese).
- Hara, T., Kokusho, T. and Hiraoka, R. 2004: Undrained strength of gravelly soils with different particle gradations, *Proc. of the 13th World Conference on Earthquake Engineering*, Paper No. 144, pp.19.
- Hazarika, H., Kasama, K., Suetsugu, D., Kataoka, S and Yasufuku, N. 2012: Damage to geotechnical structures in waterfront areas of northern Tohoku due to the March 11, 2011 tsunami disaster, *Indian Geotechnical Journal*, Invited paper, Indian Geotechnical Society, 43(2), pp.137152.
- Hazarika, H., Hara, T., and Furuichi, H. 2013a: SoilStructure Interaction during Earthquake and Tsunami Two Case Studies from the Latest Disaster in Japan , *Proc. of the special workshop on challenges of soilstructure interaction and retaining walls*, 18th ICSMGE, Paris, pp.131142.
- Hazarika, H., Hara, T., Ohsumi, T., and Furuichi, H. 2013b: Time to Deviate from Wrong Perception – A Lesson Relearned from the 2011 Great East Japan Disaster , *Theme Lecture*, 5th International

- Geotechnical Symposium (IGS Incheon 2013), Incheon, Korea, CDRom.
- Hazarika, H., Etoh, I., Pradhan, K.H., Yasufuku, N., Ishikura, R., & Fukumoto, Y. 2013c: Fundamental Research on Tsunami Resistant Sea Wall using Low Carbon Material, 10th National symposium on Environmental Geotechnolgy, Tokyo, pp. 351354 (In Japanese).
- Imai, Y., Suzuki, A., and Tobita, T. 2013: Case Study Analysis of river embankment caused by the Great East Japan Earthquake, 48th Annual Meeting of the Japanese Geotechnical Society, Toyama, pp. 11291130 (In Japanese).
- Iwate Nippo 2011: Roads to Recovery Verification and Testimony of the Great East Japan Earthquake in Iwate, Part 6, Moving to Highland No.4, Ohfunato and Yoshihama, Lessons of our ancestors defended life, Morning newspaper article, Dec. 1, 2011 (In Japanese).
- Japanese Geotechnical Society (JGS) 2011: Joint Survey of Tohoku Branch, and Shikoku Branch Investigation Team: Damages in Southcentral Coastal Area of Iwate Prefecture in 2011 off the Pacific Coast of Tohoku Earthquake, Geotechnical Engineering Magazine, 59(6), pp. 3035, (In Japanese).
- Japan Meteorological Agency (JMA) 2011: 2011 Great East Japan Earthquake JMA Seismic IntensityMap, http://www.jma.go.jp/jma/en/2011_Earthquake/Information_on_2011_Earthquake.html
- Kochi Prefecture 2013: Report of The Nankai earthquake longterm flood Study Measures, Chapter 5, Water sealing method and Wastewater treatment method, pp. 5.15.54 (In Japanese).
- Ministry of Land, Infrastructure, Transport and Tourism (MLIT) 2011a: Restoration and Damage of Rivers and Coastal facilities in the Great East Japan Earthquake, Report of the River section of the Tohoku Regional Bureau (In Japanese).
- Ministry of Land, Infrastructure, Transport and Tourism (MLIT) 2011b: Kitakami River Dike Restoration, Technical Review Group Report, The Tohoku Regional Bureau (In Japanese).
- Ministry of Land, Infrastructure, Transport and Tourism (MLIT), 2011c: Proposal for the measures against tsunami in river (main part), The 1st river tsunami measure investigation commission, Document No.6 (In Japanese)..
- Nakane, H., Shimamoto, E., Tsunekawa, Y., Kuroda, S., Nakajima, N., Ishikawa, Y., Hara, T. and Okabayashi, K.: Consideration of river dike materials damaged by the 2011 Off the Pacific Coast of Tohoku Earthquake, Proc. of the 2013 JGS Shikoku Branch Annual Conference, pp. 5556, 2013. (In Japanese)
- Oka, F., Yashima, A., Shibata, T., Kato, M., and Uzuoka, R. 1994: FEMFDM coupled liquefaction analysis of a porous soil using an elastoplastic model, Applied Scientific Research, 52, pp. 209245.
- Otsushi, K., Koseki, J., Kaneko, M., Tanaka, H., Nagao, H., Experimental Study of Reinforcement of Dike by Steel Sheet Pile, Japanese Geotechnical Journal, Vol. 6, No. 1, pp. 114 (In Japanese)..
- Shikoku Regional Development Bureau, Ministry of Land, Infrastructure, Transport and Tourism (MLIT), 2013: Pamphlets for Earthquake Resistance and liquefaction countermeasure, Report of the Kochi Coastal Projects Run by National Government (In Japanese)..
- Tsunami Digital Library (TDL) 2011: http://tdl.civil.tohoku.ac.jp/TSUNAMI/TDL_top_e.html, http://tsunamidl.jp/docimg/080/chile80_125.jpg/medium.
- Ueno, M., Hara, T., Hazarika, H., Ohsumi, T., Yamanaka, M and Furuichi, T. 2012: Shear strength and deformation properties before and after liquefaction of the tsunamiaffected river dike, Proc. of the 67th JSCE Annual Meeting, III, pp. 3940 (In Japanese).
- Wakinaka, Y., Ishihara, M., and Sasaki, T. 2013: Case study analysis of River dike damage caused by liquefaction during the Great East Japan Earthquake, 48th Annual Meeting of the Japanese Geotechnical Society, Toyama, pp. 17011702 (In Japanese).
- Yamanaka, M., Hara, T., Hazarika, H., Ohsumi, T., Furuichi, H., Ueno, M., Yamazaki, T., Okada, H. 2012: Stability of Earth Structures against Overflow of Tsunami during the 2011 off the Pacific Coast of Tohoku Earthquake, Japan Association for Earthquake Engineering, 12(5), pp. 89101 (In Japanese).

Influence of Thermal Condition on the Extraction Characteristics of Steel Strip Reinforcing Members.

Hijiri HASHIMOTO, Takahiro YAMANASHI, Hirochika HAYASHI
& Masahiko YAMAKI

Civil Engineering Research Institute for Cold Region, PWRI, JAPAN

ABSTRACT: Cases of deformation in reinforced soil retaining walls have been reported in Hokkaido, Japan. Based on a survey of the deformed cases, the deformation was attributed to poor winter construction in which portions of the embankment soil froze and then subside during the thawing period, which resulted in bulging of the wall.

In this study, to clarify how the temperature acting on the ground affects the pulling resistance of the strip, pull-out tests were conducted under various embankment materials and curing conditions. The pulling resistance under the various construction conditions is discussed.

1. OUTLINE OF THE EXPERIMENT

1.1 Soil materials and strip

The soil materials used in this experiment were sandy soil and volcanic coarse-grained soil (here in after: "volcanic ash soil"). The physical characteristics of the soil materials are shown in Table 1. According to the manual, in principle, among soil materials with a maximum grain size of 75mm or smaller, materials with a fine fraction content F_c of 25% or lower, which are classified as [A1] material, are suitable for use as embankment materials. Materials whose F_c is greater than 25% but no more than 35% are classified as [B] materials; these are suitable for use as embankment materials provided that reinforcement measures are taken. The material used in our experiment was classified as [A1] material. Volcanic ash soil whose F_c exceeds 35% is unsuitable as a material for *terre-armee*

walls.

To understand the effect of soil material on the pulling characteristics of the strip under freeze-thaw with various degrees of frost heave, volcanic ash soil was selected as the experimental material. There are two types of strips: smooth, and ribbed. The experiment used a ribbed strip, which is frequently used in actual construction. The shape and dimensions of the ribbed strip are shown in Fig. 1. The material of the ribbed strip is hot-dip galvanized (JIS H 8641 HDZ35) rolled steel for welded structures (JIS G 3106 SM490A).

The width (60mm) and thickness (4mm) are the same as specified for strips used in actual construction. The length is 1,500mm.

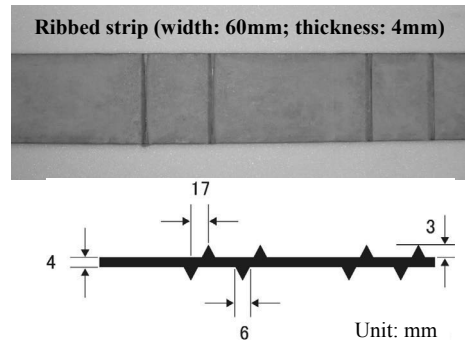


Fig.1 Ribbed strip

Table.1 Physical properties of the soil materials

Specimen		Sandy soil	Volcanic ash soil
Soil type		S-FG	SV-G
Soil particle density	ρ_s (g/cm ³)	2.720	2.498
Natural water content	W_n (%)	17.1	50.4
Maximum dry density	ρ_{dmax} (g/cm ³)	1.500	0.990
Fine-grain fraction content	F_c (%)	16.7	43.9
Silt	(%)	7.3	33.1
Clay	(%)	9.4	10.8
Liquid limit	W_L (%)	NP	NP
Plastic limit	W_p (%)		
Plasticity index	I_p		
Frost-heave velocity	U_h (mm/h)	0.10	0.74
Frost-heave potential		Medium	High

1.2 Experimental Set up

Fig. 2 shows the exterior view of the container used for the experiment. The dimensions are

11,500 × 2,280 × 2,230 mm(length × width × height).The container originally had hinged double dooronly. For this experiment, it was modified to provide facilities for all the workand experiments in the container. New door, windows, a ventilating opening, fluorescent lights (40W) and a power source (100, 200V) were installed.

Temperature adjustment was possible for the range of -30 to 25°C.The experiment was done in this modified container. The device for the pull-out test and the jig to close and shut the lid of the soil tank for the pullout test (here in after: "the experiment tank") were installed, and the soil materials were placed in the container.



Fig. 2 Container

1.3 The pull-out test device

Fig. 3 shows a cross-section of the pullout test device and a top view of the experiment tank.The pullout test device consisted of the experiment tank, a lid, a rubber membrane, load cells, a screw jack, a displacement meter and data loggers.

It is possible to pneumatically place an overburden stress of $\sigma_v=0 \sim 160\text{kPa}$ on the material in the experiment tank (1,200mm in length x 600mm in height x 600mm in width). It is possible to pull out the strip set in the soil material at a speed of 0.12mm - 1.20mm/min.

Insulating material (thermal conductivity specification value: $\lambda=0.028\text{W/mk}$) of 50mm in thickness was installed on the sides of the tank and that of 100mm was installed on the bottom of the tank. Use of the insulation material was to simulate actual embankment construction in winter. Only the uni-planar action of cold or warm air was used over the top surface of the density-adjusted soil in the experiment tank.The inside dimensions of the tank with the insulation layers installed were 1,100mm in length x 500mm in height x 500mm in width.

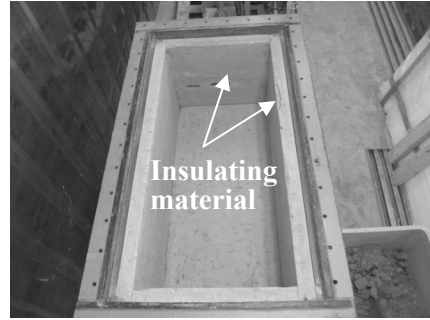
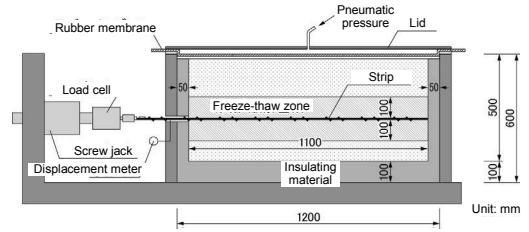


Fig. 3 The pull-out test device and the experiment tank

1.4 Experimental procedure

Fig. 4 shows the experiment procedure. Three thermal conditions were used: room temperature, low temperature and freeze-thaw.

The soil material kept in the experiment container was left for 24 hours at 20 °C for the room temperature test and at 2 °C for the low-temperature test and the freeze-thaw test (Table 1).After the temperature adjustment period, the experimental tank was filled with soil material to a depth of 150 mm.

Soil material with natural moisture content w_n was compacted to adjust its density to $D_c=90\%$. The strip was installed at this stage, and the soil material was placed over the strip up to the top of the experiment tank by following the same procedure as that for filling the soil before the strip was placed for the room temperature and the low-temperature conditions.

The temperature inside the container when the experimental embankment was prepared (i.e., when the experiment tank was filled) was 20 °C for the room temperature condition and 2°C for the low-temperature condition.

To secure the action of pneumatic pressure on the created embankment, a rubber membrane (a natural rubber sheet) was spread over the soil material and the lid was closed.For the freeze-thaw condition test, the process before the strip was installed was the same as that for the room

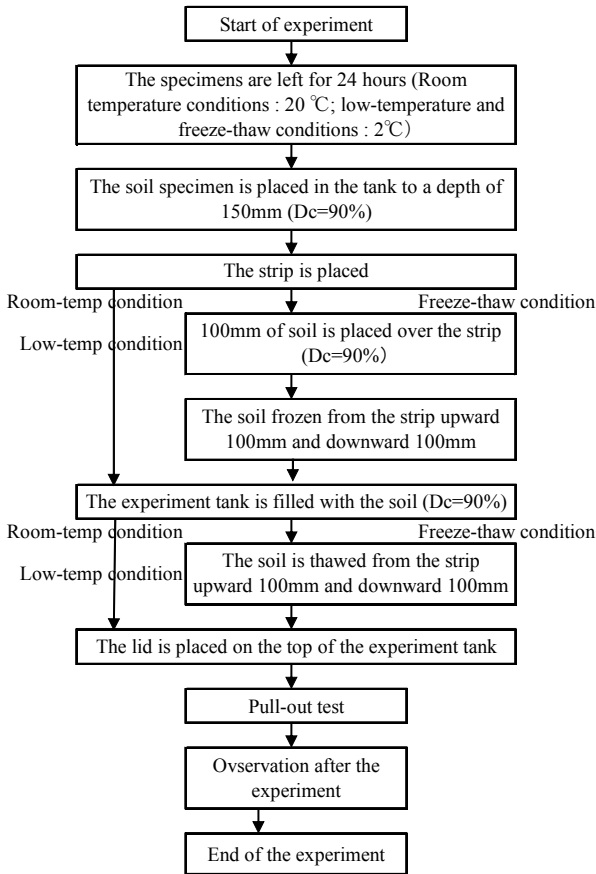


Fig.4 Flow of the experment procedure

temperature and the low-temperature conditions. After the strip was installed, density-adjusted soil material with a degree of compaction of $D_c=90\%$ was put in up to 100mm above the strip. The temperature at the time of embankment preparation was 2°C , which was the same as for the low-temperature condition test.

The 200-mm-thick soil zone consisting of a 100-mm-thick layer above and a 100-mm-thick layer below the strip was frozen by following the procedure specified in the Frost Heave Test (JGS0172) at the freezing speed of $U=1.0 \sim 2.0\text{mm/h}$ to determine the frost heave characteristics. The reason for using a constant freezing rate was to control variations in soil strength that might be caused by differences in freezing rate. Soil temperature was measured by T-shaped thermocouples, which are effective in measuring low temperature because of their high accuracy and low electric resistance, and recorded by ultra-small temperature data loggers installed in the freeze-thaw zone.

The soil zone from 100mm above to 100mm below the strip was measured to determine whether the freezing speed of $U=1.0 \sim 2.0\text{mm/h}$ was achieved. It was confirmed that the freezing speed was within the desired range for each test case (Fig. 5).

After confirming that the temperature of the soil 100mm below the strip was lower than 0°C , the tank was filled with additional soil and the density was adjusted to attain a degree of compaction of $D_c=90\%$.

The temperature inside the container was set as 25°C and the 100-mm-thick layer above the strip and the 100-mm-thick layer below the strip were thawed. After the temperature of the soil at 100mm below from the strip was confirmed to be exceeding 0°C , the same procedure as that done for the room temperature and low temperature tests was taken before the lid was closed.



Fig.5 Freezing condition above to 100mm on the strip

1.5 Experimental cases

Table 2 shows the conditions for each experiment case. For sandy soil under the freeze-thaw condition, the number of days elapsed after thawing was used as a parameter. The thawing period in this experiment was defined as the number of days elapsed from when the reading of the T-shaped thermocouple installed 100mm below the strip exceeded 0°C (i.e., when the reading rose to 0.1°C). For the room temperature and low-temperature conditions, the pullout tests were done after placing the lid on the tank and applying a prescribed overburden stress.

Table.2 Experiment conditions

Case	Embankment material	Compaction	Thermal condition	Overburden stress (kPa)
1	Sandy soil	$\rho_{dmax90\%}(W_n)$	Room-temp	60
2				140
3			Low-temp	60
4				140
5			Freeze-thaw	60
6				140
7				60
8				140
9				60
10				140
11	Volcanic ash soil		Room-temp	60
12				140
13			Low-temp	60
14				140
15			Freeze-thaw (1 day after thawing)	60
16				140

For the freeze-thaw conditions, the pull-out test was done ± 6 hours after 1, 3 and 14 days of thawing.

The overburden stress was applied in two patterns using vertical stress of $\sigma_v=60$ and 140kPa on the strip. The vertical stress was confirmed by the earth pressure gauge installed at the same location as that of the strip.

The displacement velocity of the strip was set as $v=1\text{mm/min}$.

2. EXPERIMENT RESULTS AND DISCUSSION

2.1 Interpretation on the pull-out test results

The pulling force per unit area acting on the strip was defined as the pulling resistance τ . Equation (1) below expresses the area of the strip in contact with the soil, which was obtained by considering the reduction in area corresponding to the increase in the length of strip pulled out ΔL . As expressed in Equation (2), the maximum pulling resistance τ_{max} was determined by dividing A , which was obtained by Equation (1), by the maximum pulling force T_{max} obtained in the pullout test.

$$A = \left(\frac{L_0 - \Delta L}{1000} \right) \times \frac{B}{1000} \times 2 \quad (1)$$

$$\tau_{max} = \frac{T_{max}}{A} \quad (2)$$

where, A : surface area that is determined from the length of strip pulled out (m^2), L_0 : length of the strip laid (mm), ΔL : length of strip pulled out (mm) B : width of the strip (mm), τ_{max} :

maximum pulling resistance (kN/m^2), T_{max} : maximum pulling force (kN)

2.2 Behavior of soil materials in the pull-out test

2.2.1 Examination focusing on the differences between the thermal conditions

The curves in Figs. 6 a) and b) show the relationship between the pull-out force T and the length of the strip pulled out for each soil material.

In Fig. 6 b), the curves are for overburden stress σ_v of 60kPa (Cases 11, 13, and 15) and overburden stress σ_v of 140kPa (Cases 12, 14, and 16). The curves all have a similar, gently convex shape. No clear peaks in pulling force T_{max} are observed.

Fig. 6 a) shows the curves for the two values of overburden σ_v , the group of Cases 1, 3 and 5, and the group of Case 2, 4 and 6. The shapes of the relationship curves are similar to those in Fig. 6 b). T_{max} of Case 5 is about 40% to 50% lower than those of Cases 1 and 3, and that of Case 6 is also 40% to 50% lower than those of Cases 2 and 4.

The above examination reveals that, for the volcanic ash soil, T_{max} differs from the other temperature conditions only in the freeze-thaw condition with overburden stress $\sigma_v=60\text{kPa}$.

For the sandy soil, however, it was found that the values of T_{max} for the freeze-thaw condition were much lower than those for the room temperature and the low-temperature conditions.

Fig. 7 a) and b) show the curves for σ_v versus τ_{max} for each soil material obtained from the pull-out test.

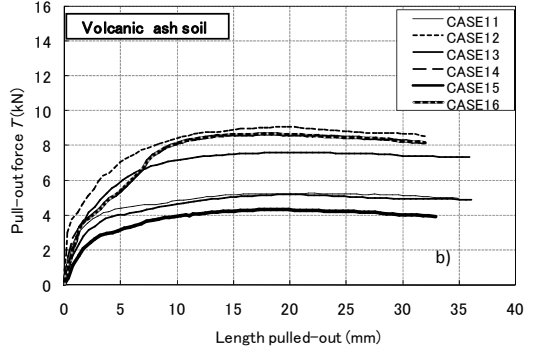
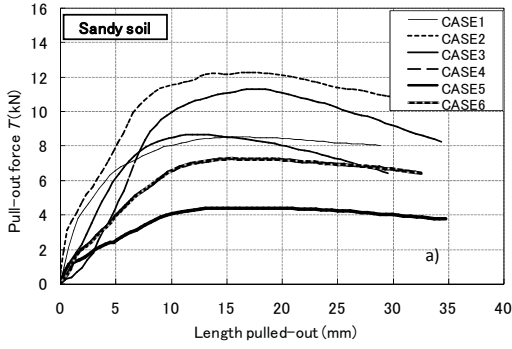


Fig.6 Relationship between pulling force and length of strip pulled-out

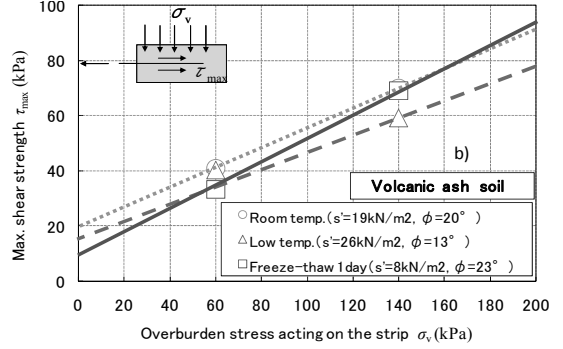
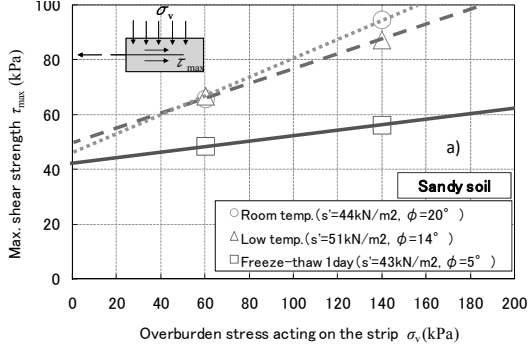


Fig.7 Relationship between overburden stress acting on the strip and maximum shear strength

Previous studies showed that the Mohr-Coulomb yield criterion ($\tau_{\max} = s' + \sigma_v \tan \phi$) holds between σ_v , which is generated between the strip and the ground, and τ_{\max} . In the above equation, s' is the adherence and ϕ is the friction angle between the strip and the ground.

From Fig.7 a), it is found that the relationship between σ_v and τ_{\max} tends to be similar to those for the room temperature and low-temperature conditions, even though there are differences in the values of s' and ϕ .

However, in the freeze-thaw condition, τ_{\max} is very low, regardless of the magnitude of σ_v . In Fig. 7 b), the curves of σ_v versus τ_{\max} tend to be similar for the room temperature and the low-temperature conditions, even though there are differences in the magnitude of s' and ϕ .

For the freeze-thaw condition, it is found that τ_{\max} becomes smaller than those for the other two conditions with decreases in σ_v .

2.2.2 Examination of sandy soil according to temperature conditions

Fig. 8 shows the result of the pull-out test, i.e., the relationship between T and the length of the strip pulled out, for Cases 5 to 10. The shapes of the curves for Cases 5, 7 and 9, in which the overburden σ_v is 60kPa and those for Cases 6, 8 and 10, in which the overburden σ_v is 140kPa are of similar convex shapes. However, the decrease in T_{\max} of Cases 5 and 6 (1 day after thawing), were greater than those for Case 7 (3 days after thawing) and Case 9 (14 days after thawing) with overburden of 60kPa and for Case 8 (3 days after thawing) and Case 10 (14 days after thawing) with overburden of 140kPa.

Fig. 9 shows the results of the pull-out test according to thermal conditions expressed as the relationship between σ_v and τ_{\max} .

τ_{\max} for the freeze-thaw condition (1 day after thawing) is about 30% lower than those for the room temperature and low-temperature conditions regardless of the value of σ_v .

However, the curves for the freeze-thaw condition (3 days and 14 days after thawing) show that τ_{\max} at $\sigma_v = 140\text{kPa}$ for the freeze-thaw condition (14 days after thawing) is only slightly lower than those for the room temperature and the low-temperature

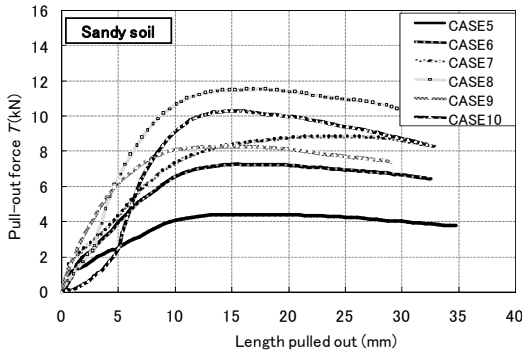


Fig 8. Relationship between pulling force and length pulled out(Sandy soil)

conditions. Based on the above examination, it was found that τ_{\max} recovers with time after the third day after thawing.

In the pull-out test using sandy soil, the maximum shear strength τ_{\max} in the freeze-thaw condition at 1 day after thawing is much lower than those in other cases. The decrease in ϕ is particularly remarkable. The low value of ϕ is attributed to the thawing of pore water between the soil particles, which disturbed the arrangement of the particles.

It is thought that the interlocking effect was temporarily reduced because of the disturbance. It was also found that τ_{\max} recovered with time to the value equivalent to those for the room temperature and low-temperature conditions.

2.2.3 Physical characteristics volcanic ash soil

Many types of volcanic ash soil in Hokkaido exhibit clear fracture characteristics under compaction, consolidation and shear forces, because of the influence of freeze-thaw action. Therefore, use of this type of material in construction has been regarded as problematic. To understand the influence of various temperature conditions on the physical characteristics of soil, physical tests were done after the pullout test.

Fig. 10 shows the particle size distribution curves for Cases 11, 13, and 15. The zone from 100mm above the strip to 100mm below the strip was vertically divided into three layers, and the specimens were collected from each of the three layers. From the particle size distribution curve, no considerable difference among the temperature conditions was

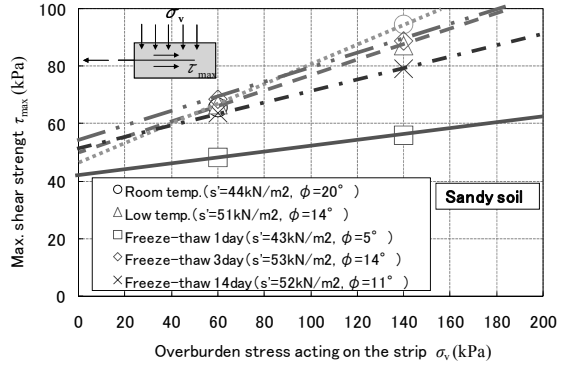


Fig 9. Relationship between σ_v and τ_{\max} (Sandy soil)

found. Table 3 shows the natural water content w_n of the samples collected from the three layers as in the above. The values of w_n for Case 11 and 13 do not differ considerably by the location of sampling; however, for Case 15, w_n for the top layer of the zone is greater than w_n for the bottom layer. This is because the water moved toward the upper part of the soil-filled tank where the cold air was applied.

Fig. 11 shows the soil surface where the strip was placed after the pullout test for Case 15 (volcanic ash soil, 1 day after thawing in the freeze-thaw condition). A trace of strip placement is seen. There is no water visible on

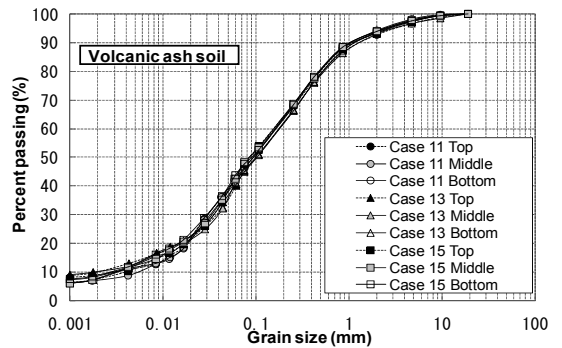


Fig 10. Particle size distribution curve for the freeze-thaw zone

Table 3. Natural water content after the experiment

Material	Thermal condition	Location of the specimen	Natural water content (w_n) (%)
Volcanic ash soil	Case 11	Top	55.15
		Middle	54.21
		Bottom	55.01
	Case 13	Top	54.28
		Middle	55.20
		Bottom	54.79
	Case 15	Top	53.49
		Middle	52.96
		Bottom	50.71

the surface.

The volcanic ash soil used for this study, which has $w_n=50.4\%$ and $\rho_s=2.498\text{g/cm}^3$, is thought to be close to the soil categorized as [Vs₂] in previous studies. It was reported that the shearing resistance of the compacted soil of this category is good in the range of normal loading.

Based on the above knowledge and on Figs. 10, 11, and Table 3, the following were found. In the experiment for this study, material that had similar properties to those of [Vs₂] was frozen and thawed around the strip. When soil with water content of w_n is compacted to a density of $D_c=90\%$, then the movement of water may occur, but the fracture of soil particles does not occur. It was suggested that under the above conditions, an interlocking effect similar to that of compacted soil (embankment) under room temperature and low-temperature conditions can be expected from the compacted soil constructed under the freeze-thaw condition.



Fig 11. The soil surface where the strip was placed, after the pull-out test

3. CONCLUSION

In this report, the results of a strip pull-out test using sandy soil and volcanic ash soil whose frost-heave characteristics differ from each other were examined to understand the effect of temperature conditions on the strip's pull-out resistance characteristics. The results of the examinations are as follows.

- (1) τ_{\max} of sandy soil 1 day after the freeze-thaw process was much lower than those of the room temperature and low-temperature conditions regardless of the magnitude of σ_v . However, it was found that τ_{\max} of the same soil after the 3 day of thawing recovered to a level similar to those of the

soil processed under the room temperature and the low-temperature conditions.

- (2) For the volcanic ash soil, the relationship between σ_v and τ_{\max} had a similar trend under each of three temperature conditions. However, it was confirmed that τ_{\max} of the volcanic ash soil 1 day after thawing (the freeze-thaw condition) decreased more than the τ_{\max} of the volcanic ash soil prepared under the room temperature and the low-temperature conditions with decreases in σ_v .
- (3) Volcanic ash soil from Hokkaido in Japan was frozen and thawed around a strip. When the soil with water content of w_n was compacted to a density of $D_c=90\%$, movement of water occurred, but fracture of soil particles did not occur. This suggests that volcanic ash soil from Hokkaido that experiences freeze-thaw around the strip can be expected to have an interlocking effect similar to that of the same type of soil prepared under the room temperature and the low-temperature conditions.

4. REFERENCES

- Yukihiro, K. 2010. Reliability of Reinforced Earth Retaining Walls in Cold Regions, *Monthly Kiso-ko Magazine*, Feb. 2010, pp. 42-45. (Japanese).
- Hijiri, H. Satoshi, N. Hirochika, H. & Shinichi, K. 2012. Field Survey on Reinforced Earth Retaining Walls Constructed in Hokkaido, *Technical Report of the Hokkaido Branch, Japanese Geographical Society*, No. 52, pp. 49-54 (Japanese).
- Public Works Research Center (PWRC) 2003. Design and Construction Manual of Reinforced Earth (Terre-Armée), 3rd revision (Japanese).
- Geotechnical Society Criteria (JGS0942). 2009. Pull-out Test of Geo-synthetics in Soil.
- Geotechnical Society Criteria (JGS0172). 2009. Test Method for Frost Susceptibility of Soils.
- The Hokkaido Branch, Japanese Geographical Society 2010. Facts on Volcanic Ash Soil for Field Engineers – Characteristics, Design, Construction, and Cases of Damage, pp. 60-61. (Japanese).
- Koichi, I. Mitsuhiko, K. Atsuko, S. Kazuo, S. & Shin'ichiro, K. 2001. Proposal for Method of Engineering Classification of Coarse Volcanic Ash Soils in Hokkaido, *Soils and Foundations*, Vol. 62, No. 8, pp. 16-19. (Japanese)

Methods of Research on Frost Heave of Soil and Foundation - Freezing Soil Bulk Interaction in Terms of Seasonal Deep Frost Penetration including Areas of Pressure Migration

O.Z. Khalimov

Siberian Federal University, Abakan Russia

ABSTRACT: Based on long-term research on soil frost heave conducted in laboratory and in situ including both experimental and expert investigation sites the influence of groundwater level on frost heave-induced deformations has been identified. Nature of change of moisture during frost penetration has been studied, parameters of changes of water accumulation coefficient for the main types of soil in Minusinsk cavity have been obtained. Options of anti-heave activities during construction for driven and end-bearing piles have been proposed.

1. INTRODUCTION

Systematization of long-term research results began in 2008 in the Chair of “Soils and Foundations”, St. Petersburg State Transport University with V.M. Ulitsky being a consultant.

There are the following steps of studying frost heave in Minusinsk cavity:

1976–1985 rr. – Theoretical survey. Performing the first experiments and observations in situ. Laboratory investigations in a thermal chamber, hods, a stationary pavilion with a soil pan. Construction of experimental facilities – buildings of heated and unheated warehouses for medical equipment in the village of Askiz, civil defense warehouses in the station of Orositelnaya, a heated warehouse (18x54) of a design and construction company of a district water household in the station of Podsinee.

1985–1990 – Observations of experimental facilities, processing of results.

1990–2008 – Observations of experimental facilities, expert investigations of soils under the studied buildings.

2008– 2012 – New series of laboratory research on cryogenic textures contacting with various soils. Systematization and analysis of results of laboratory, field and expert investigations.

Frost heave of soils is the most hazardous when an object is under construction or is reconstructed without a heating regime. In this period a freezing area, in particular in buildings with basements, spreads to a larger depth compared to a planned benchmark. If a freezing area exceeds the groundwater level one can mention pressure migration which can lead to

considerable redistribution of moisture during frost penetration.

Nowadays there is a large range of thermal insulating materials which prevent freezing in case of effective thermal protection of subsoil. However it is difficult for a thermal insulating material to remain in a construction site especially in terms of constant movement of machines, vehicles and materials. Nevertheless, thermal protection allowed to preserve a 2-floor building with a basement in the center of Abakan (27, Vyatkina street) and to avoid its demolition. At the same time soil froze from the basement of the groundwater level and frost heave occurred. Moisture of fine-grained sand underlying bases of strip foundation to the width of cushions of reinforced concrete - 1.6 m – increased from 16 % to 40–45 %. When a decision was to be made there was a question whether to dismantle the ground floor or to start construction of the first floor. Although there were through cracks of up to 5 mm opening in walls as well as frost-shattered cracks in frozen soil which cut it between adjacent foundation cushions all basement area was filled with 300-mm layer of claydite gravel. In spring the building was completed, in summer after complete soil thawing claydite gravel was taken from the basement to attic floor.

Thermal insulating material filling provided even thawing of soil from the bottom and a frozen soil layer on the top eliminated the danger of heave of oversaturated thawed lower soil. Soil heave from foundation bases of unconstructed facilities in Khakasia in the thawing period has been described [1]. However it is advisory to make thermal insulation before frost

penetration to avoid migration of water accumulation.

To conclude discussion on thermal protection anti-heave solutions one should mention reconstruction of individual houses built in 1960–70s. Most of them were constructed on shallow foundations with foundation depth of 30–40 cm. To reduce frost heave strains – a house constantly moves in relation to a chimney: in winter it goes up, in summer – down, residents made a mound of earth. Nowadays there is thermal insulation of plinth and paving which prevents freezing and frost heave under the foundation base. However the most efficient method is not thermal insulation of plinth and paving which employs energy of a house and

prevents soil freezing under the foundation base but replacement of a heaving soil by a thermal insulating material which would also exclude heat escape under the building area [2].

2. RESEARCH METHODS

The first laboratory tests for studying frost heave compared with field data resulted in necessity to conduct experiments in hods to reproduce conditions of natural soil cooling in a temperature regime and atmospheric pressure alternating in time. It was found out that in case of negative temperatures fluctuations from –1 to –5°C there is more intensive migration and soil frost heave.

Стационарный павильон с грунтовым лотком

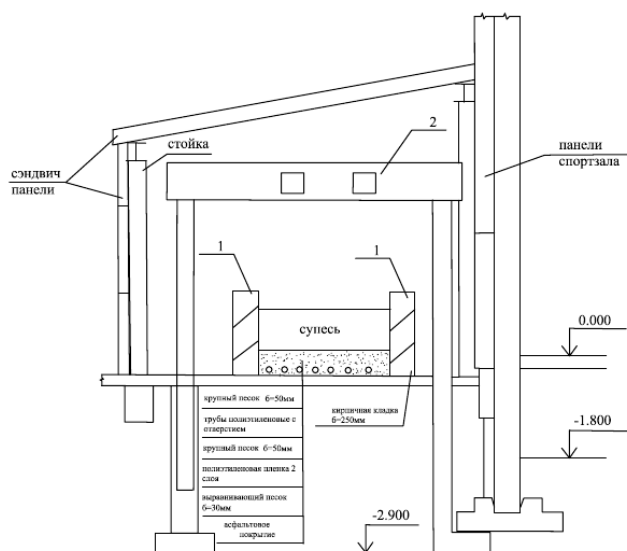
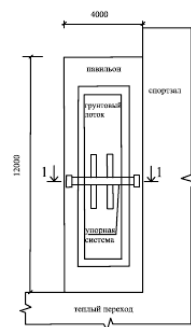


Схема павильона с грунтовым лотком



1 - стены грунтового лотка из кирпича;
2 - упорная система из двух двутавров N60, заполненных бетоном

Figure 1. Setup of the soil pan pavilion.

Стационарный павильон с грунтовым лотком – stationary soil pan pavilion

Схема павильона с грунтовым лотком - scheme of the soil pan pavilion

Сэндвич-панели- sandwich panels

Стойка – post

Панели спортзала – gym panels

Суньсь – clayey sand

Крупный песок – coarse grained sand 6-50 mm

Кирпичная кладка – brickwork 6-250 mm

Трубы полиэтиленовые с отверстием – polyethylene tubes with holes

Полиэтиленовая пленка 2 слоя – two layers of polyfilm

Выравнивающий песок – leveling sand 6-30 mm

Асфальтовое покрытие – asphalt

Павильон – pavilion

Спортзал – gym

Грунтовый лоток – soil pan

Упорная система – thrust system

Теплый переход – heated pass

Стены грунтового лотка из кирпича – brick walls of the soil pan

Упорная система из двух двутавров N60, заполненных бетоном - thrust system of two T-bars filled with concrete

The need to study cryogenic processes in natural freezing environment led to construction a stationary pavilion with a soil pan in the courtyard of Khakassia Technical Institute – 27, Schetinkina str. Methods of research in the pavilion are based on natural freezing of soil in the pan when the pavilion is opened at negative temperatures and artificial thawing of soil when the pavilion is closed and electrical heaters are switched on. Groundwater modeling was made by running water in plastic tubes with holes fed from a 0.5 m³ tank which was filled with water after each cycle. Soil for the pan was taken from

the third field site (4th district of Abakan), where water content distribution from 21% to 74% was recorded (fig. 1). The same pan was used to develop a technology on punching holes, making foundations and studying their behavior during freezing-thawing.

Observations of soil strains in field sites could lead to loss of results due to poor infrastructure. The most valuable field results referred to results of research on changes of moisture after freezing. It was layer by layer sampling from each geological element to define soil water content before and after freezing.

3. RESULTS OF RESEARCH ON CRYOGENIC TEXTURES

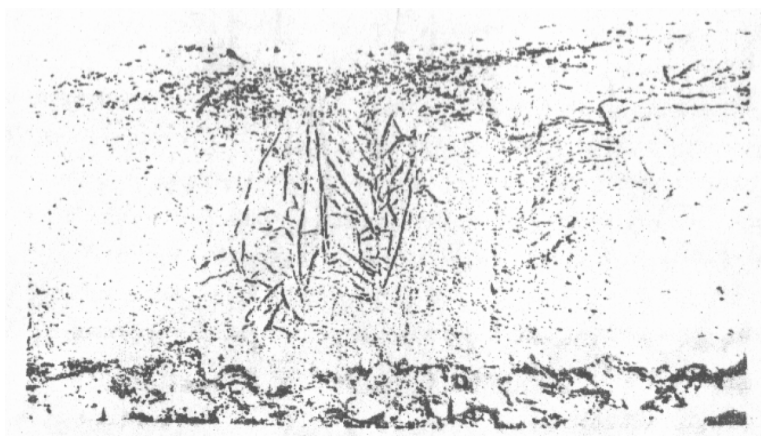
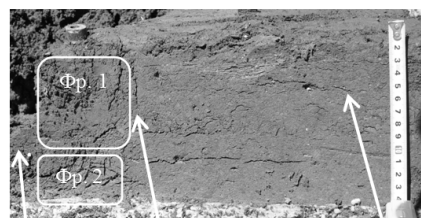


Figure 2. A cryogenic texture in a layer contact area obtained in 1980s.

Due to the fact that the stationary soil pan pavilion was dismantled after the building construction investigation of cryogenic structures continued in spring periods when night temperatures are down to –10°C, and day temperatures reach +10°C. Major interest was attached to interaction of improved and unimproved clayey sand in layer contact areas. During the research vertical and non-horizontal-oriented ice lens formation was recorded (fig. 2). That time the phenomenon was explained as follows: “In the contact area of improved and unimproved soils there is interaction of shrinkage deformations of improved soil and volumetric expansion of unimproved soil. This interaction effect is increased by higher speed of cooling of improved soil and quicker volumetric expansion of the surrounding bulk.



Обработанный слой Граница на контакте слоев Необработанный слой

Figure 3. Cryogenic texture, 2012.



Fragment 1 to figure 3
Improved soil
Unimproved soil
Layer contact boundary



Fragment 2 to figure 3

Therefore, deformation of a cryogenic texture with vertical and tilted ice lenses is explained by interaction of shrinkage and volumetric deformations of improved and unimproved soils as well as corresponding fractures of the contact area where pressured water flows (as there is some release in fractures). Since ice in formed vertical and tilted lenses is not characterized by long-term strength it is easy to imagine that the described weakened contact area later develops and becomes a zone of active movement of various soils [3]". Only recently one has managed to conduct more detailed investigation on causes of forming such lenses and to find explanation of considerable reduction of heave strains for piles with anti-heaving coating (fig. 3). The factor of accelerated cooling of improved soil and horizontal migration of water from unim-

proved soil to the improved one plays the main role.

4. SOIL PROPERTIES CHANGE DURING FROST PENETRATION

The issues of foundation engineering are the most difficult. It is known that a depth of foundation depends on a depth of frost penetration. If the groundwater level is 2–3 m and freezing depth sometimes exceeds 3 m foundation depth is always smaller than the freezing depth, i.e. a foundation base is located in frozen soil. There is a question on regulated freezing depth calculated with account of thermal impact and freezing depth calculated without account of thermal impact (for non-heated buildings or buildings under construction).

In terms of power efficiency one cannot reduce foundation depth counting on heat release from a building, therefore, a foundation should be put at the regulatory freezing depth or a smaller one, however one should rely on properties of soil after a freezing-thawing process. Construction Code 2.02.01.83* admits foundation construction in a seasonally frozen soil but there is a need to comply with requirements of heave deformation and additional settlements occurring after thawing. However vast majority of design and construction companies in Eastern Siberia, in particular in Krasnoyarsky krai and Republic of Khakasia do not risk to construct foundations at the depth smaller than the calculated freezing depth. The coefficient of thermal influence is taken 0.7–0.8. The prospective development is associated with coefficient of thermal influence to be equal to 1 (the calculated freezing depth is equal to the regulatory one).

In order to save energy it is advisory to exclude heat release into the ground. At the same time it is not expedient to deepen under a foundation base where frost penetration can occur. It is difficult to predict how soil properties will change during frost penetration. There is a table below which shows results of expert investigations of soils deformed by frost heave under buildings and structures.

Table 1 Results of expert investigations of soils deformed by frost heave under buildings and structures

Location/floors	Construction scheme	Soil	Groundwater level, m, from designed/ from basement floor	Stress/ soil parameters
Fyrkaly, Khakasia/ 2 floors	Longitudinal bearing walls; strip foundations	Clayey sand	5/4.2	0.2/ up to 5 mm
Askiz, residential house, Khakasia/ 1 floor	Longitudinal bearing walls; strip foundations	Clayey sand	1.7/	0/ up to 8 mm
District hospital Shira/ 2 floors	Longitudinal bearing walls; strip foundations	Clayey sand	5/4.0	0.20/ up to 8 mm
State Technical College -59, Abakan/ 2 floors, basement	frame; foundation posts 0.85x0.85	Gravel with silty-clayey filling	3.5/1.0	0.55/ partly collapsed
Supply depot, 18, Itygina str., Abakan / 1 floor	Walls	Clayey sand	3.5/3.0	0.20/ up to 3 mm
Kindergarten, Zeleny/ 2 floors	Walls	Clayey sand	4.5/1.5	0.20/ more than 10 mm
27, Vyatkina str. Abakan / 2 floors, basement	Walls	Silty sand	4.5/2.5	0.10/ more than 10 mm
Vilner House, Minusinsk/ 3 floors, basement	Walls	Silty sand	4.5/1.5	0.20/ up to 5 mm
Heated parking, Shira, Lineynaya str./ 1 floor	Frame	Sandy clay $I_L=0.5-0.6$	5.5/5.5	0.22/ up to 5 mm in concrete floors

The most serious deformations occurred in the kindergarten, the settlement of Zeleny, Vilner's house in Minusinsk and State Technical College -59 in the city of Abakan which partly collapsed. Analysis of stresses under the base showed that, for example, under State Technical College -59 stresses reached 0.55 MPa. However, the building was standing unconstructed for 3 years, only a part without concrete floors in the basement collapsed (fig. 4). In a part of the building with concrete floors they rose due to soil bulk thrusting along the slipping surface but saved the basement from the heave (fig. 5).

Silty sand was located under Vilner's house foundation base, the ground water level comprised 4.5 m. After the building had been set for reconstruction and heating had been cut frost penetration began from the basement. After the first winter an outhouse containing a three-floor staircase collapsed, a court looking façade was deformed since it served a location where water flows from adjacent areas went to. A western and a central facades were less damaged. Only 2 hair-shape cracks were recorded. It can be explained by the fact there were many transversal walls for the staircase which reduced the load applied to thawing soil. Works on foundation underpinning included installation of a monolith

reinforced concrete disc of floor above the basement which prevented successive development of cracks in the building. Cracks continued to develop only in a partition along the

middle and longitudinal axes where a two-floor part of the building had been originally located, then the third floor was added [6].

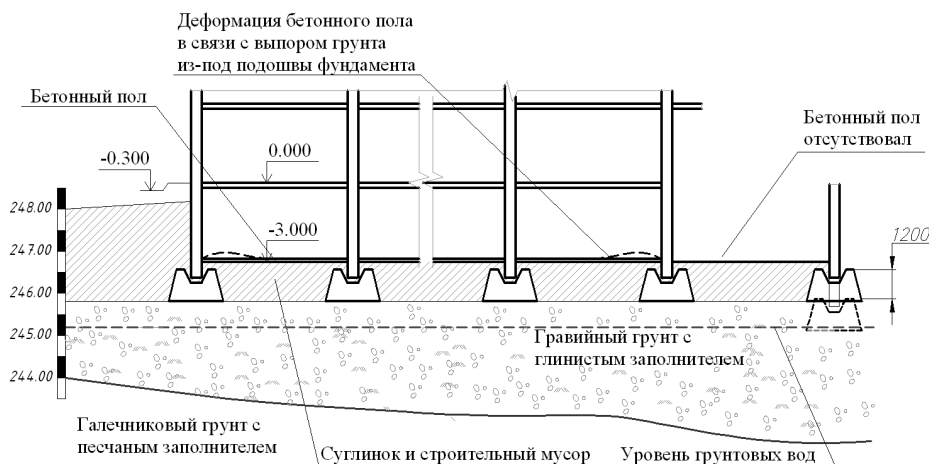


Figure 4. A fragment of the cross-section of State Technical College -59 building including soil profile.

Бетонный пол – concrete floor

Деформация бетонного пола в связи с выпором грунта из-за подошвы фундамента – concrete floor deformation due to soil heave from the foundation base

Бетонный пол отсутствовал – no concrete floor

Гравийный грунт с глинистым заполнителем – gravel with clayey filling

Галечный грунт с песчаным заполнителем – pebble with sandy filling

Суглинок и строительный мусор – sandy clay and construction debris

Уровень грунтовых вод – ground water level



Figure 5. The collapsed eastern part of the workshops of State Technical College -59 in Abakan (1982).

Moisture redistribution analysis in the object [6] on the basis of a designed rotten house in 2, Katernaya str. allowed to enlarge data given in [1] concerning the coefficient of water accumulation as one of the most important parameters of freezing soils. The results of moisture redistribution are given in fig. 6.

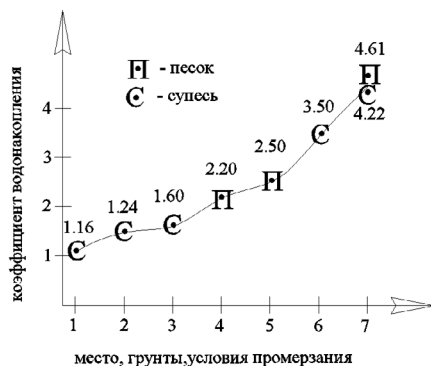


Figure 6. A plot of moisture redistribution (coefficient of water accumulation) at frost penetration in different conditions.

Песок – sand

Супесь – clayey sand

Коэффициент водонакопления – coefficient of water accumulation

Место, грунты, условия промерзания - location, soils, conditions of frost penetration

1) In the freezer with a constant negative temperature;

- 2) *In a soil hod in the open air;*
- 3) *In the stationary soil pan during natural freezing and artificial thawing in the period of negative temperatures;*
- 4) *Under the foundation base in Vilner's house, Minusinsk;*
- 5) *Under the foundation base in 27, Vyatkina str. in Abakan during freezing from the basement.*
- 6) *In a field site during freezing below the groundwater level;*
- 7) *A site of geo-engineering investigations for a residential house, 2, Katernaya str. in Abakan; clayey sand lies at 0.4–0.8 m from the ground surface, silty sand - at the depth of 0.8–1.8 m underlain by gravel, the groundwater level is 3 m.*

Recent results obtained in 2, Katernaya str. have been questioned by the author and his assistants. According to supporters of film migration [3] the presence of a draining material above the groundwater level should have broken a migration flow. However the received values of moisture after frost penetration in March 2013 and their comparison with moisture values before freezing made the author visit the site in June, 2013 to specify data. By July silty sand moisture became stable again - 7.6% - the same as characterized thawed soil in October, 2012. In March wet sand moisture comprised 35%, the coefficient of water accumulation reached the value of 4.61. Meanwhile moisture of clayey sand increased from 18% to 76%, the coefficient of water accumulation was 4.22.

5. CONSTRUCTION AND MONITORING OF EXPERIMENTAL FACILITIES

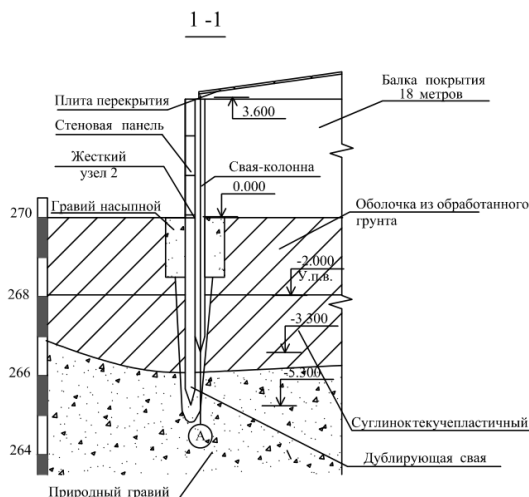
Laboratory investigation in a thermal chamber, hods and the stationary pavilion with the soil pan as well as in situ investigations in 6 sites with different groundwater levels provided sufficient data on nature of frost heave in Minusinsk cavity, allowed to construct experimental facilities on end-bearing piles and to ensure reliable anti-heave stabilization of the constructed structures.

In order to make anti-heave envelope from improved soil a technology of a bearing structure installation has been updated and author certificate for invention № 1101498 has been approved. According to the technology for making anti-heave envelope below the

groundwater level the following operations have been proposed: to drill a 1-m-diameter borehole by a hole driller down to the groundwater level; to put a calculated amount of potash fertilizer on the bottom, to fill the borehole with gravel-sand mixture and to install an end-bearing pile. Salt poured before the groundwater level is needed for a construction period in case of possible lack of loading of the end-bearing pile and lack of thermal influence.

Two end-bearing piles did not show the calculated failure, the actual failure comprised 76 mm, thus, it was necessary to reach the designed benchmark by an idle blow with lifting a hammer part to the middle of a distance of drop. To provide bearing capacity of these end-bearing piles without the designed failure doubling piles were driven (fig. 7).

Figure 7. Construction of warehouses for medical



- equipment in the settlement of Askiz.
- плита перекрытия – floor slab
 - балка покрытия 18 м – floor beam of 18 m
 - стенная панель – wall panel
 - жесткий узел – rigid joint
 - свая-колонна – end-bearing pile
 - оболочка из обработанного грунта – envelope of improved soil
 - гравий насыпной – filled gravel
 - гравий природный – natural gravel
 - суглинок текучеplastичный – liquid-plastic clayey sand
 - дублирующая свая – doubling pile

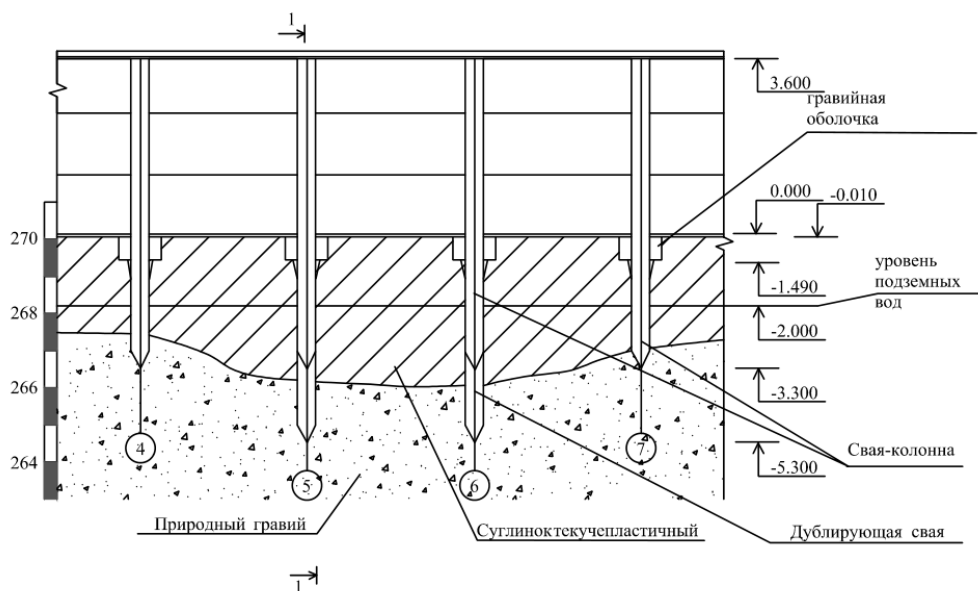


Figure 8. Driving of doubling piles to the lens of soft soils in axes “A”, “5–6”.

свая-колонна – end-bearing pile
 гравийная оболочка – envelope of gravel
 уровень подземных вод – groundwater level
 гравий насыпной – filled gravel
 гравий природный – natural gravel
 суглинок текучеplastичный – liquid-plastic clayey sand
 дублирующая свая – doubling pile

The first negative situation in the warehouse of medical equipment in the settlement of Askiz was caused by the fact that builders failed to implement the design solu-

tion: they did not make an anti-heave gap structure under the wall panel (fig. 9).

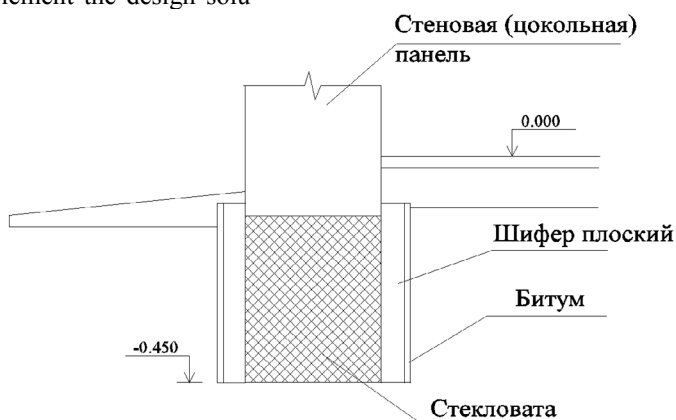


Figure 9. A designed structure of anti-heave gap.

Стеновая цокольная панель – wall base panel
 Шифер плоский – flat slate
 Битум – bitumen
 Стекловата – glass wool

Making a paving concrete was filled under the base panel instead of putting glass wool.

As a result wall panels rose together with paving and moved in relation to end-bearing piles. During a freezing cycle window glasses crackled and activated the emergency alarm.

After fixing this mistake imperfection of the geotechnical solution on anti-heave envelope near frame end-bearing piles started to manifest itself. In 5 years after starting exploitation of the structure frame end-bearing piles of the unheated warehouse suffered from inadmissible tilt.

Thus, heaving soil was removed from the side of paving and replaced by pebble stone with sandy filling down to its boundary with the groundwater level. However in 7 years the tilt of frame end-bearing piles reached the same value (more than 200 mm) as in the first 5 years of utilization.

The decision was made to dismantle wall panel replacing insulation of the northern butt end of the unheated warehouse by light metal molding sheets. Strains of frame end-bearing piles stopped.

In the northern butt end of the heated warehouse frame end-bearing piles tilted from the vertical by 230 mm due to data untightness and low temperature in the garage located at the last axes of the structure. It was explained by horizontal load caused by eccentric moment from applying efforts of the butt end wall panels to the end-bearing piles. In 2007 wall panels were demolished, end-bearing piles were excavated down to the depth of 2 m, aligned; gravel-sand envelope was filled and wall panels were installed.

6. CONCLUSION

Investigations in the stationary pavilion with the soil pan were the most effective sorting out of the set of research on frost heave; they were used as large-size models to test structures and technologies of making anti-heave envelopes to stabilize foundations. Studying interaction of 200-mm-diameter and 600-mm-high foundations and heaving soil bulk allowed to go to experimental industrial facilities which have been monitored for 30 years; the monitoring showed positive solutions and

negative moments of their putting into construction practice.

The results of moisture redistribution in clayey sand and silty sand underlain by gravel with medium-grained sand filling which excludes capillary rise provide confirmation that the migration process passes in a form of vaporous moisture.

7. REFERENCES

1. Khalimov O.Z. Development of a System of Geotechnical Analysis for Heaving Soils. Urban Development and Geotechnical Engineering / Proceedings of the International Conference. St. Petersburg, June, 16-19, 2008.
2. Selivanov V.M., Khalimov O.Z., Portnyagin D.G. Evolution of Thermal Protection of Basements of Buildings. Modern Transformative Economic and Social-Political Processes: Proceedings of IV International Research and Practical Conference (May, 23-25, 2013): Editorial house of Khakasia Technical Institute – Affiliate of Siberian Federal University, 2013-320 p.
3. Khalimov O.Z. The Method of Physical-Chemical Anti-Heave Stabilization of Soils during Construction in case of High Ground Water Level. Synopsis of PhD Thesis. M. 1989.
4. Karlov V.D. Soils and Foundations on Seasonally Freezing Heaving Soils. St. Petersburg, 2007 – 362 p.
5. Krivissky A.M., Korsuunsky M.B., Rossovsky P.D., Gayvoronsky V.N. Research on Water-Thermal Regime of Highway Subgrades in Regions of Excessive Saturation / Proceedings of USSR Road Research Institute, issue 37, Balashikha, Moscow region, 1970.
6. Khalimov O.Z., Talapove G.G., Ermolaeva L.N. Vilner's House: Engineering Investigations, Geotechnical Monitoring. Abakan, Editorial house of Khakasia Technical Institute – Affiliate of Siberian Federal University, 2012.

Oblique pullout capacity of a single drilled pile in sandy grains cemented by methane hydrates: DEM analyses

Fang LIU, Mingjing JIANG

Department of Geotechnical Engineering, Tongji University, Shanghai 200092, China

State Key Laboratory of Disaster Reduction in Civil Engineering, Tongji University, Shanghai 200092, China

Key Laboratory of Geotechnical and Underground Engineering (Tongji University), Ministry of Education, Shanghai 200092, China

ABSTRACT: This study investigates the oblique capacity of a drilled pile embedded in a marine ground containing methane hydrates using the distinct element method. Results indicate that the presence of methane hydrates significantly enhances the uplift and lateral capacity of the pile. The peak shaft resistance of the pile decreases with the decrease of the inclination angle of pile displacement due to de-bonding, while the residual shaft resistance increases as a result of increasing lateral earth pressure mobilized at large pile displacement. The uplift component of the oblique forces has detrimental effect on the lateral capacity of the pile. The oblique capacity of the pile can be empirically correlated to the inclination angle of the displacement of the pile head.

1. INTRODUCTION

Methane hydrate (MH) is burnable ice-like solid formed under low temperature and high pressure, and recognized as new energy resource receiving global interest. MHs bring new challenges to geotechnical engineers due to peculiar mechanical behavior and susceptibility to dissociation because of environmental change.

Due to growing development in continental margins, offshore infrastructures have been constructed using pile foundations to resist oblique pullout loads due to wind and wave actions. These piles likely penetrate existing methane hydrate bearing sediments (MHBS) or are surrounded by newly created MHBS, provided that MHs are found along most continental shelf and slope regions (Maslin et al. 2010). Though the behavior of piles in MHBS under pure uplift or lateral loads has been investigated by authors (Liu et al. 2014), the engineering performance of piles in MHBS under combined uplift and lateral loads is still poorly understood.

Pile-soil interaction has been extensively studied using the finite element method, which is rigorous only if a reasonable constitutive relation of soils is used. Although several constitutive models of MHBS have been proposed (e.g., Miyazaki et al. 2012; Uchida et al. 2012), none of them has received universal acceptance. Alternatively, the distinct element method (DEM) is promising for analyzing the mechanical behavior of MHBS from macro-

scopic and microscopic viewpoints by using relatively simple contact laws. By means of DEM, pore-filling MHs have been modeled as particles occupying voids of a soil skeleton (e.g., Brugada et al. 2010; Jung et al. 2012), while MHs nucleating at interparticle contacts have been also modeled using a bond contact mode of MHBS (Jiang et al. 2014).

This paper aims to investigate oblique uplift capacity of a single drilled pile embedded in MH-cemented soils by implementing the latest bond contact model of MHBS (Jiang et al. 2014) into a two-dimensional (2D) DEM.

2. DEM SIMULATION

2.1. DEM method

DEM is a particular implementation of a broader class of methods known as discrete-element methods. It was firstly applied to soils by Cundall and Strack (1979). Thorough descriptions of the method can be found in literature (e.g., Cundall 1988; Hart et al. 1988).

In DEM analyses, soils are regarded as an assembly of particles interacting by contact and non-contact forces. The calculations performed in the DEM alternate between the application of Newton's second law to the particles and a contact model at the contacts. Newton's second law is used to determine the translational and rotational motion of each particle arising from the contact forces, applied forces and body forces acting upon it, while the contact model is

used to update the contact forces arising from relative motion at each contact.

The contact model of the conventional DEM is only suitable for un-cemented granular materials, since adhesive forces and moments can not be transmitted at the contacts. In view of this limit, efforts have been made to invoke cohesion arising from chemical bonds in order to extend DEM to cemented geomaterials (e.g., Potyondy & Cundall 2004; Jiang et al. 2007; Obermayr et al. 2013; Jiang et al. 2014).

2.2. Problem description

Figure 1 illustrates a hypothetical marine ground with a single drilled pile under plane-strain conditions. This model is configured to match the conditions of a site in South China Sea, where MHs have been truly detected. The truncated seabed is 60 m wide and 24 m deep, at a depth of 800 m below the sea level (i.e., pore water pressure of 8 MPa). It is assumed that the temperature remains constant as 5°C throughout the entire calculation domain, provided that, in South China Sea, the water temperature is about 5.6°C at water depth of 800 m with the averaged geothermal gradient equal to 37.6 °C/km (Wang et al. 2006). Two situations were considered in this study: (1) the clean ground without MHs (clean ground for short), and (2) the ground cemented by MHs with the hydrate saturation degree S_H equal to 25% (MH ground for short). Note that S_H is defined as the ratio of the volume occupied by MHs to the total volume of voids.

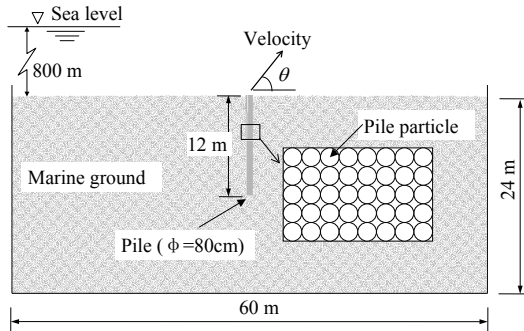


Figure 1. Dimensions of the problem in prototype.

The DEM model was scaled down to 1/20 in size of the prototype to largely reduce the computational cost. Accordingly, the gravity acceleration used in the simulations was scaled up in such way that the scaled model provided the same gravity-induced stress field as the prototype. Considering that water was not

physically modeled in the simulations, the gravity acceleration was justified to account for the reduction of effective stresses due to submergence. Hence, the gravity acceleration was set as 12.31 g here.

2.3. Bond contact model of MHBS

The contact model proposed by Jiang et al. (2014) was used to simulate the mechanical behavior of soil particles cemented by MHs. This model is only recapped here for completeness, and details have been given by Jiang et al. (2014).

In this model, two adjacent sandy grains are idealized as two disks with radii R_1 and R_2 cemented by MH, which forms a symmetric bond in between with a finite width (B) and the minimum thickness (t_0). The bond can resist normal force (F_n), shear force (F_s), and moment (M), which can be computed as follows:

$$F_n = K_n (u_n + t_0); F_s = \sum K_s \Delta u_s; M = K_r \theta \quad (1)$$

where u_n , Δu_s , and θ is the overlap, the relative tangential displacement increment, and the relative rotation angle of particles, respectively; and K_n , K_s and K_r are normal, tangential, and rolling stiffnesses, respectively. The parameters associated with contact stiffnesses can be computed from the bond thickness and Young's modulus of pure MHs, which correlates the temperature and pressure.

Once any component of contact forces exceeds a certain threshold, the bond will break in an irreversible manner and the bond contact model will reduce to a rolling resistance model (Jiang et al. 2005) that characterizes the interparticle rolling resistance by introducing a dimensionless shape parameter δ_r . The thresholds (i.e., bond resistances) can be determined based on a bond failure criterion which was derived from a series of micro mechanical tests (Jiang et al. 2012). This failure criterion depends on the bond width, the tensile strength ($q_{t,max}$) and the compressive strength ($q_{c,max}$) of pure MHs, which correlate the temperature and pressure. Note that the geometry features of each bond (i.e., the bond width and thickness) is determined from a pre-defined S_H for a given packing conditions of soil particles.

Table 1 summarizes the parameters of the model used for MHBS particles with diameters ranging from 6 mm to 9 mm. MH bonds are present between two adjacent particles as long as their separation is less than 5% of the average

particle diameter d_{50} . The width of a MH bond is characterized by a shape parameter δ defined as the ratio of the width to the common radius $R_0=R_1R_2/(R_1+R_2)$, where R_1 and R_2 are the radii of the two adjacent particles. For simplification, δ is identical throughout the entire model, and is computed from $S_H = 25\%$. The parameters of the bonded particles were computed according to the temperature-pressure conditions (i.e., 5°C and 8 MPa) using the approaches presented by Jiang et al. (2014). The parameters of unbonded particles were calibrated by comparing DEM simulation of biaxial compression tests with experimental observation from triaxial compression tests on a clean sand sample (Masui et al. 2005). The stress-strain response of a MHBS sample using the parameters listed in Table 1 was examined from DEM simulation of a series of biaxial compression tests in comparison to triaxial test conducted by Masui et al. (2005).

Figure 2 shows results of one of the simulations under confining pressure of 1 MPa. Different from the clean sample, the MHBS sample exhibits higher stiffness, and more remarkable strain softening and volumetric dilation. Nevertheless, the two stress-strain curves coincide at large axial strains as a result of progressive bond breakage, because the residual strength is mainly controlled by the void ratio regardless of the presence of MHs. DEM simulations under different confining pressures (not shown in this paper) infer that the cohesion and the peak internal friction angle of MHBS are approximately 50 kPa and 30°.

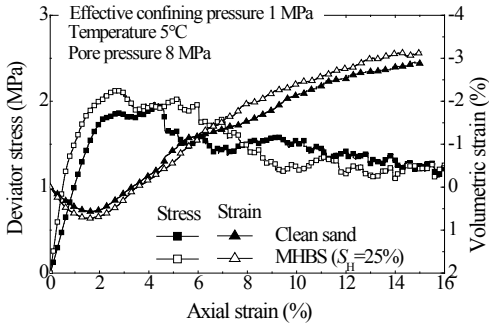


Figure 2. DEM results of biaxial compression tests.

2.4. Contact model for pile particle

The close-up in Figure 1 shows the detail of the pile, which is formed by regularly arranging 960 identical disks with diameter of 5 mm in the loosest packing. The particle density was chosen in such way that the pile was compara-

ble to a concrete pile. The contact behavior of pile particles was modeled by the parallel bond contact model proposed by Potyondy & Cundall (2004) with parameters summarized in Table 2. Extremely large values were assigned to the strength parameters of the parallel bonds in order to avoid failure in pile itself. The interparticle friction coefficient of pile particles was set to be 5 to eliminate unwanted particle slippage. The parameters associated with particle stiffness and parallel bond stiffness were selected in such way that the pile resembled a pile made of C30 concrete with the Young's modulus of 30 GPa.

Table 1. Parameters of soil particles

Parameter	value
Particle size	6 mm ~9 mm
Initial planar void ratio	0.21
Particle density	2.6 g/cm ³
Local damping coefficient	0.7
Viscous damping coefficient	0.0
<i>Bonded particles</i>	
Tensile strength of MH $q_{t,max}$	4.73 MPa
Compressive strength of MH $q_{c,max}$	8.57 MPa
Young's modulus of MH	290 MPa
Minimum bond thickness t_0	5% d_{50}
Shape parameter δ (for $S_H = 25\%$)	0.568
<i>Un-bonded particles</i>	
Particle normal stiffness	6×10^8 N/m
Particle tangential stiffness	4×10^8 N/m
Interparticle friction coefficient	0.75
Shape parameter δ_r	0.8

Table 2. Parameters of pile particles

Parameter	value
Particle number	960
Particle diameter	5 mm
Initial planar void ratio	0.27
Particle density	3.0 g/cm ³
Interparticle frictional coefficient	5
Parallel bond tensile strength	1.0×10^{100} Pa
Parallel bond shear strength	1.0×10^{100} Pa
Particle normal stiffness	6.0×10^8 N/m
Particle tangential stiffness	2.5×10^8 N/m
Parallel bond normal stiffness	5.94×10^{12} Pa/m
Parallel bond tangential stiffness	2.48×10^{12} Pa/m
Parallel bond radius ratio r	1

2.5. Simulation procedure

The simulation was conducted in three steps. First, a homogenous ground consisting of 64,000 particles was generated using the multi-layer with the under-compaction method (Jiang et al. 2003). The ground was consolidated under the gravity acceleration of 12.31 g until the

force equilibrium was reached. In the case of the clean ground, the ground generation was terminated. In the MH ground case, hydrate bonds were activated where the inter-particle distance was less than 5% of the average particle diameter. Second, soil particles were removed and replaced by pile particles where the pile was intended. This pile can be regarded as a non-displacement pile (e.g., drilled shaft), since it was virtually installed in the space left by soils previously removed without disturbing the surrounding soils or changing the stress state at any point of the surrounding soils. Third, external loads upon the pile head were simulated by imposing a uniform velocity to the particles located at the upper 10-mm segment of the pile. Meanwhile, the particle movement and contact forces were monitored over time. As shown in Figure 1, the velocity inclines at an angle of θ to horizontal (loading angle for short). Four loading scenarios were investigated in the simulations, i.e., $\theta = 0^\circ$ (pure lateral load), 45° (oblique load), 60° (oblique load), and 90° (pure uplift load). The magnitude of velocity was selected in such way that quasi-static conditions were satisfied.

3. RESULTS

3.1. Force – displacement diagram

Figure 3 presents the net uplift load (i.e., shaft resistance) against the vertical displacement (d_y) normalized by the pile diameter D at different loading directions. Note that shaft resistance ($P_{\theta,y}$) was computed by summing the vertical components of contact forces between pile and soil particles. In contrast to the ‘hardening-like’ response of vertically uplifted pile in the clean ground, the force – displacement diagram obtained from the MH ground under the same loading conditions exhibits ‘softening-like’ behavior. The shaft resistance rapidly increases until a peak value of 177.3 kN at the displacement equal to 2.5% D , and then sharply drops to a relatively steady value around 66 kN. In addition, the pile exhibits much stiffer response in the MH ground than that in the clean ground. Enhanced stiffness and abrupt drops (i.e., brittle failure) in the shaft resistance were also reported for piles embedded in grouted soils (Ho et al. 2002). Softening-like response is also noted from the pile in MH ground subjected to oblique loads at loading angles of 45° and 60° .

The shaft resistance rapidly reaches the peak at the vertical displacement less than 3% D regardless of the loading angle, and then drops to a relatively steady value. The peak shaft resistance decreases with the decrease of the loading angle, because the increased lateral component of forces cause de-bonding of MH cementation and therefore reduce the shaft resistance at small displacement of the pile. On the contrary, the residual shaft resistance increases with the decrease of the loading angle, because the increased lateral earth pressure against the pile mobilizes the shaft resistance at large displacement of the pile.

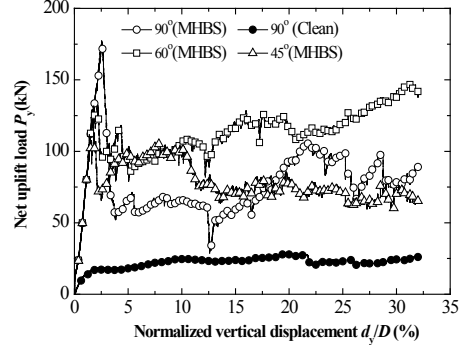


Figure 3. Net uplift load against vertical displacement at different loading angles.

Figure 4 presents the lateral loads ($P_{\theta,x}$) against the horizontal displacement (d_x) of the pile normalized by the pile diameter. Note that $P_{\theta,x}$ was computed by summing the horizontal components of contact forces between pile and soil particles. For the laterally loaded pile in the clean ground, the lateral load increases with pile displacement and approaches to an inclined asymptote. This was commonly observed in many model pile tests (Lee et al. 2011). In contrast to the smooth curve of the clean ground, the lateral load for the laterally loaded pile in the MH ground drops at the pile displacement equal to 2.5% D , and then gradually recovers up to a higher peak of 350 kN at the pile displacement equal to 25% D . Apparently, the presence of MHs significantly increases the lateral capacity of the same pile, since the curve obtained from the MH ground is far above that obtained from the clean ground. As also shown in Figure 4, less lateral load is mobilized on the pile subjected to an oblique load with bigger loading angles, indicating that the uplift component of an oblique force has detrimental effect on the lateral capacity of the pile.

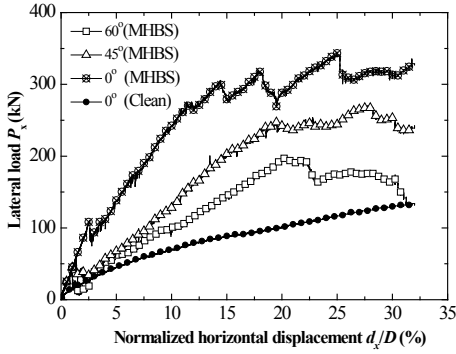


Figure 4. Lateral load against horizontal displacement at different loading angles.

3.2. Oblique capacity

Figure 5 presents the applied oblique load (P_θ) against the resultant displacement of the pile (d) in order to facilitate a possible comparison between different inclined loads. Curves obtained under different loading angles intersect. Nevertheless, the oblique load increases with the decrease of the loading angle when the resultant displacement is larger than 5% D . For the sake of simplicity, the oblique load capacity of the pile is defined in terms of serviceability, i.e., $P_{\theta,p}$, $P_{\theta,10}$, and $P_{\theta,15}$, which are oblique capacity corresponding to the first peak, and displacements equal to 10% D and 15% D .

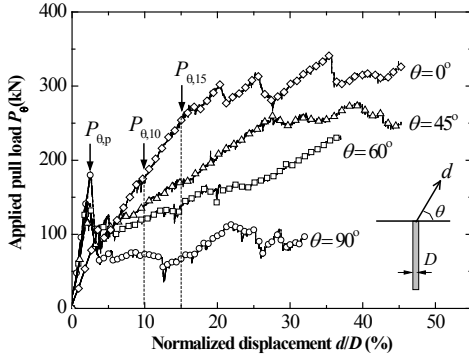


Figure 5. Oblique load vs. resultant displacement

Figure 6 presents the oblique load capacities of different definitions normalized by the uplift load capacity of the pile subjected to a pure uplift load (i.e., $\theta = 90^\circ$) defined in the same manner. The ratio corresponding to the peak capacity decreases with the decrease of the loading angle, while the ratios corresponding to the capacities at service limits increase.

Several semi-empirical relationships were proposed based on model tests to link the

oblique capacity to the lateral and uplift capacity of piles. The method given by Chattopadhyay and Pise (1986) is extended here to predict the oblique load capacity:

$$\frac{P_\theta}{P_U} = \sin^2 \theta \cdot \exp \left[\frac{1-\alpha}{1+\alpha} \cdot \left(1 - \frac{\theta}{90} \right) \right] + \alpha \cos \theta \cdot \exp \left[\frac{1-\alpha}{1+\alpha} \cdot \frac{\theta}{90} \right] \quad (2)$$

where $\alpha = P_L/P_U$ is the ratio of the lateral capacity to the uplift capacity. Note that θ is the inclination of the pile head displacement to horizontal, while it is defined in the original formula (Chattopadhyay and Pise 1986) as the inclination angle of the applied load to horizontal. As shown in Figure 6, Eq. (2) fits the data well particularly for oblique capacities defined in terms of service limits. For comparison, the method proposed by Meyerhof and Sastry (1985) is also superimposed in the same figure, which provides better prediction for $P_{\theta,p}$ while worse for $P_{\theta,10}$ and $P_{\theta,15}$ than Eq. (2).

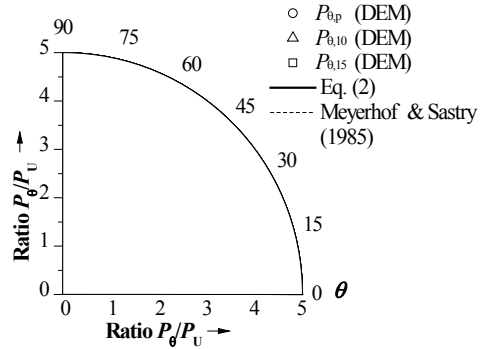


Figure 6. Oblique capacity of the pile in MH ground at different loading directions

4. CONCLUSIONS

This study investigates the response of a drilled pile subjected to oblique forces and in a marine ground with MHs by means of DEM analyses. The major conclusions are as follows:

(1) The presence of MHs significantly enhances the uplift and lateral capacities of the pile, of which the oblique capacity correlates the loading angle.

(2) The peak shaft resistance of the pile decreases with decreasing loading angle due to debonding, while the residual shaft resistance increases because of increasing lateral earth pressure mobilized at large displacement.

(3) The uplift component of an oblique force has adverse effect on lateral capacity of the pile.

ACKNOWLEDGEMENTS

This study was supported National Natural Science Foundation of China (51025932, 51239010), the Fundamental Research Funds for the Central Universities, and Guangxi Key Laboratory of Geomechanics and Geotechnical Engineering (12-KF-02).

REFERENCES

- Brugada J, Cheng YP, Soga K, Santamarina JC. 2010. Discrete element modelling of geomechanical behaviour of methane hydrate soils with pore-filling hydrate distribution, *Granul. Matter.* Vol. 12, No. 5, pp. 517-525.
- Chattopadhyay BC, Pise PJ. 1986. Ultimate resistance of vertical piles to oblique pulling loads. The Proceedings of 1st East Asian Conference on Structural Engineering and Construction, Bangkok, pp. 1632-1641.
- Cundall PA, Strack ODL. 1979. A discrete numerical model for granular assemblies, *Géotechnique.* Vol. 29, No. 1, pp. 47-65.
- Cundall PA. 1988. Formulation of a three-dimensional distinct element model—part I. A scheme to detect and represent contacts in a system composed of many polyhedral blocks, *Int. J. Rock Mech. Min. Sci. Geomech. Abstr.* Vol. 25, No. 3, pp. 107-116.
- Hart R, Cundall PA, Lemos J. 1988. Formulation of a three dimensional distinct element model—part II. Mechanical calculations for motion and interaction of a system composed of many polyhedral blocks, *Int. J. Rock Mech. Min. Sci. Geomech. Abstr.* Vol. 25, No. 3, pp. 117-125.
- Ho CE, Lim CH, Tan CG. 2002. Characteristics of bored piles installed through jet grout layer. *Journal of Performance of Constructed Facilities.* Vol. 16, pp. 160-168.
- Jiang MJ, Konrad JM, Leroueil S. 2003. An efficient technique for generating homogeneous specimens for DEM studies. *Comput. Geotech.* Vol. 30, pp. 579-597.
- Jiang MJ, Yu HS, Harris D. 2005. A novel discrete model for granular material incorporating rolling resistance. *Comput. Geotech.* Vol. 32, pp. 340-357.
- Jiang MJ, Yu HS, Leroueil S. 2007. A simple and efficient approach to capturing bonding effect in naturally microstructured sands by discrete element method, *Int. J. Numer. Meth. Eng.* Vol. 69, No. 6, pp. 1158-1193.
- Jiang MJ, Sun YG, Li LQ, Zhu HH. 2012. Contact behavior of idealized granules bonded in two different interparticle distances: An experimental investigation. *Mech. Mater.* Vol. 55, pp. 1-15.
- Jiang MJ, Zhu FY, Liu F, Utili S. 2014. A bond contact model for methane hydrate bearing sediments with inter-particle cementation. *Int. J. Numer. Anal. Met.* (in press).
- Jung J, Santamarina JC, Soga K. 2012. Stress-strain response of hydrate-bearing sands: Numerical study using discrete element method simulations. *J. Geophys. Res. – Sol. Ea.*, Vol. 117. doi: 10.1029/2011JB009040
- Lee J, Kyung D, Hong J, Kim D. 2011. Experimental investigation of lateral loaded piles in sand under multilayered conditions. *Soils and Foundations* Vol. 51, pp. 915-927.
- Liu F, Jiang MJ, Zhu FY. 2014. Discrete element analysis of uplift and lateral capacity of a single pile in methane hydrate bearing sediments. *Int. J. Numer. Anal. Met.* (under review).
- Maslin M, Owen M, Betts R, Day S, Jones TD, Ridgwell A. 2010. Gas hydrates: past and future geohazard? *Phil. Trans. R. Soc. A*, Vol. 368, pp. 2369-2393.
- Masui A, Haneda H, Ogata Y, Aoki K. 2005. Effects of methane hydrate formation on shear strength of synthetic methane hydrate sediments. The 15th International Offshore and Polar Engineering Conference. Seoul, Korea; pp. 364-369.
- Meyerhof GG, Sastry VVRN. 1985. Bearing capacity of rigid piles under eccentric and inclined loads. *Can. Geotech. J.* Vol. 22, pp. 267-276.
- Miyazaki K, Tenma N, Aoki K, Yamaguchi T. 2012. A nonlinear elastic model for triaxial compressive properties of artificial methane-hydrate-bearing sediment samples. *Energies*, Vol. 5, pp. 4057-4075.
- Obermayr M, Dressler K, Vrettos C, Eberhard P. 2013. A bonded-particle model for cemented sand, *Comput. Geotech.* Vol. 49, pp. 299-313.
- Potyondy DO, Cundall PA. 2004. A bonded-particle model for rock, *Int. J. Rock Mech. Min.* Vol. 41, No. 8, pp. 1329-1364.
- Uchida S, Soga K, Yamamoto K. 2012. Critical state soil constitutive model for methane hydrate soil. *J. Geophys. Res. – Sol. Ea.*, Vol. 117. doi: 10.1029/2011JB008661
- Wang S, Yan W, Song H. 2006. Mapping the thickness of the gas hydrate stability zone in the South China Sea. *Terr. Atmos. Ocean Sci.* Vol. 17, No. 4, pp. 815-828.

Modeling of interaction of polymeric sheet reinforcement and back-fill

P.V.S.N Pavan Kumar¹ & M. R. Madhav²

¹ Associate Professor, Dept of Civil Engrg., GNITC, Hyderabad, India

² Professor Emeritus, Dept. of Civil Engrg., Jawaharlal Nehru Technological University, Hyderabad, India

M. Kumar

Professor, Dept. of Civil Engrg., University College of Engineering, Osmania University, Hyderabad, India

ABSTRACT: The continuum modeling of polymeric sheet reinforcement – backfill interaction is presented. Polymeric sheet reinforcement is subjected to axial pull at one end of the reinforcement. The continuum analysis is carried out by FLAC (Fast Lagrangian Analysis of Continua), a software based on the finite difference method. The displacements of reinforcement are quantified for different pullout forces and the variations of displacement and tension along the reinforcement length presented. The effects of axial stiffness of reinforcement, soil – reinforcement interface shear stiffness and length of reinforcement are quantified.

1. INTRODUCTION

Earth reinforcement such as metallic strips, meshes, polymeric geotextiles and geogrids are widely used in soil structures, such as embankments, slopes, retaining wall backfills and foundation soils. Effect of this reinforcement is to mobilize additional shear stress in soils by developing the tensile force in the reinforcement. The quantification of pull-out resistance of reinforcement is of significance in the design and stability analysis of reinforced soil structures.

Laboratory pullout tests and their interpretation is presented by several researchers such as Juran et al. (1988), Farrag et al. (1993), Palmeira and Milligan (1989), Wilson-Fahmy et al. (1994), Palmeira (2004), Alforo and Pathak (2005), Moraci and Gioffre (2006), Moraci and Recalcati (2006), and Sieira et al. (2009). Influence of different types of backfill consisting of granular and clay soils with different particle sizes, shear strength, density and confining pressures is studied.

Abramanto and Whittle (1993), Sobhi and Wu (1996) and Long et al. (1997) proposed mechanical models based on respectively shear-lag analysis, rigid-plastic and non-uniform shear stress distribution at the soil – reinforcement interface to predict pullout capacity of planar polymeric reinforcement. Yuan and Chua (1990), Wilson-Fahmy and Koerener (1993), Yogarajah and Yeo (1994), Sugimoto and Alagiyawanna (2003), Perkins and Edens

(2003), Marques (2005) conducted finite element analysis to model the pullout behaviour of geogrid and demonstrated that the interface properties play a significant role in the FEM simulations of geogrid pullout behavior.

Madhav et al. (1998) presented a mechanical model to demonstrate the pullout response of geosynthetic reinforcement as shown in Fig. 1. A bilinear shear stress displacement response is considered along the reinforcement – soil interface. The equilibrium of pullout forces is considered along with the elongation of reinforcement. The resulting non-linear equation was normalized and expressed in finite difference form and solved by Gauss-Siedel technique. A parametric study was conducted for a range of relative stiffness and interface shear stiffness values. The same problem is analyzed by FLAC in this paper and the results of parametric study compared with those of Madhav et al. (1998).

2. PROBLEM DEFINITION AND ANALYSIS

A typical sheet reinforcement of length, L embedded at a depth, D , below ground level is subjected to an axial pullout force, T , at node B of reinforcement (Fig. 2). A grid of size 60×60 represents backfill of dimensions $6.0 \text{ m} \times 6.0 \text{ m}$. The width and height of each zone is 10 cm . The aspect ratio (ratio of width to height of the elements) equal one reduces the iteration time

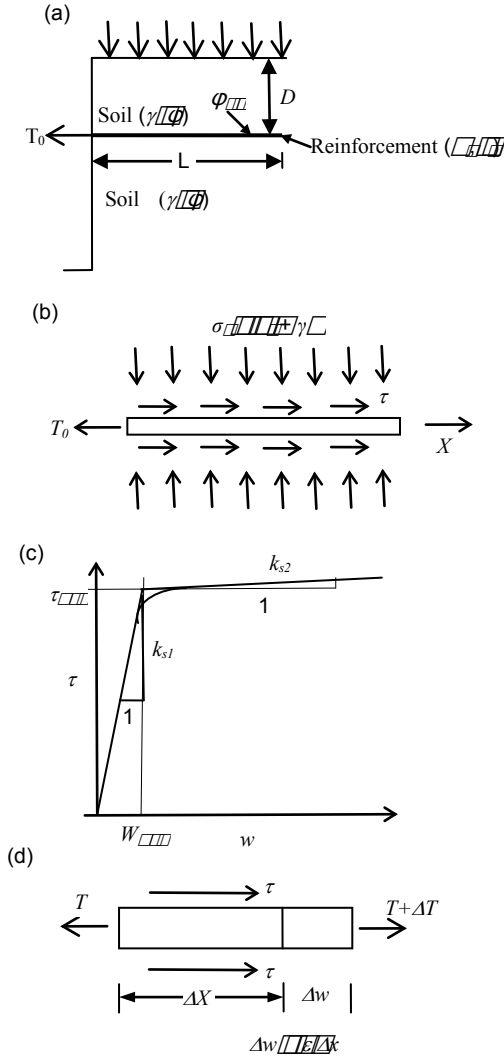


Fig. 1 Schematic of the analysis of extensible geosynthetic reinforcement layer during pull-out: (a) soil-reinforcement system; (b) forces acting on the reinforcement; (c) soil-reinforcement shear stress-displacement curve; (d) forces on a differential reinforcement segment during pull-out. (Madhav et al. 1998)

and ensures stress or strain equilibrium inside the elements. The problem is modeled for different sizes of grid such as 120 x 120, 90 x 90, 60 x 60 and 30 x 30. A grid size of 60 x 60 is found adequate to obtain reliable results not affected by the boundary conditions and at an optimum time required for solving for each set of parameters.

The subgrade beneath the reinforcement is represented as an linear elastic material. The input parameters required are density, defor-

mation modulus and Poisson's ratio of the subgrade. The density of the fill, γ , deformation modulus, E_s and Poisson's ratio, ν taken as 20 kN/m³, 30 MPa and 0.3 respectively are assumed to be the same throughout the analysis. Four different forms of structural elements are available in FLAC - beam, cable, pile and support elements. Both beam and cable elements can be used to model reinforcement. In the present work cable elements are used to represent the sheet reinforcement since they represent the geosynthetic sheet response appropriately than the beam elements. The cable is discretized as one dimensional axial element with interface elements bonded around them. The tensile yield limit of the sheet reinforcement is defined in Fig. 3. Axial cable element can be used as planar sheet reinforcement in the two-dimensional analysis with interface properties between reinforcement and soil described by bonding of in-situ reinforcement such as for soil nails.

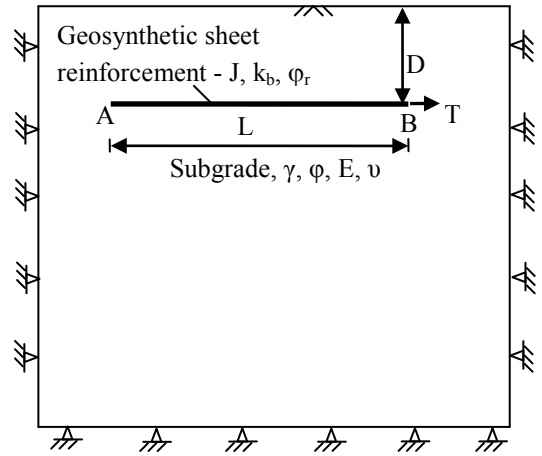


Fig. 2 Problem Definition

The interface shear stress along the geosynthetic sheet depends on the relative displacement between the sheet and the soil interface based on the built in model of Itasca (2006) shown in Fig. 4 (b). The shear stress along the interface

$$\tau = \frac{F_s}{L} = k_b (u_c - u_m) \quad (1)$$

where F_s is the shear force along the reinforcement, L is the length of sheet, k_b is the shear stiffness, u_c and u_m are the axial displacement of sheet and the adjacent soil respectively.

The mobilized shear stress is limited based on the adhesion and the interface friction along the

soil – sheet interface. The maximum interface shear stress from Fig. 4 (a) is

$$\tau_{\max} = \frac{F_s^{\max}}{L} = s_{\text{bond}} + \sigma_c \times \tan(\phi_r) \times \text{perimeter} \quad (2)$$

where s_{bond} is the adhesion, σ_c is the normal stress on the reinforcement, ϕ_r is the interface friction angle. The shear stress - displacement relation in the present continuum model follows the initial slope of shear stress - displacement relation presented by Madhav et al. (1998) (Fig. 1 (c)).

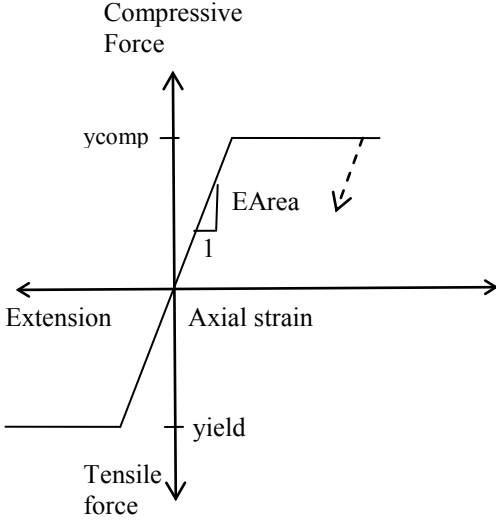


Fig. 3 Material behavior of sheet elements (Itasca, 2006)

The geometric properties of sheet reinforcement such as cross sectional area and perimeter of reinforcement are computed for 2 mm thick sheet reinforcement for unit length perpendicular to the plane.

The left and right boundaries of the model are assumed to be fixed only in the x – direction while the bottom boundary is assumed to be fixed in both x and y directions (Fig. 2). The overburden pressure can be superimposed on the model or input acceleration due to gravity of 10 m/sec² introduces gravity stresses. The model is rebuilt by several iterations and brought to equilibrium under the gravity stresses. In the FLAC model each grid point is surrounded by four material elements and the algebraic sum of the forces contributed by these surrounding elements at any specified grid point is defined as an unbalanced force. The unbal-

anced force should converge to zero when the model reaches the equilibrium state. The other equilibrium criterion is stress ratio defined as maximum unbalanced force to the representative internal force. In the present work the equilibrium of the model is established based on the following criteria - number of iterations are restricted to one hundred thousand, the minimum stress ratio of 0.001 or the maximum unbalanced force of zero Newton. In most of the cases equilibrium state based on minimum stress ratio of 0.001 governs the solution.

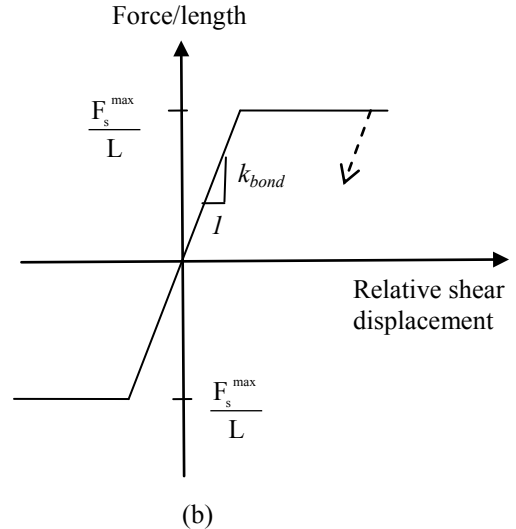
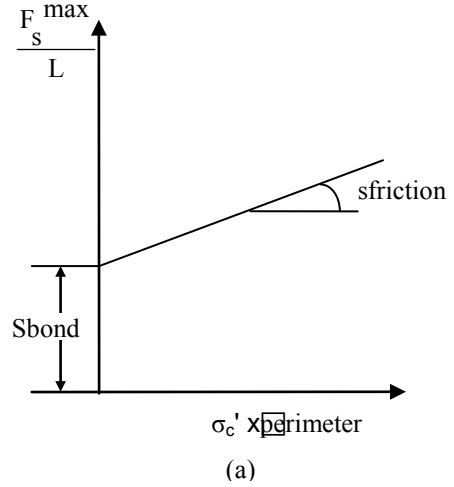


Fig. 4 Interface shear behavior for sheet elements (a) Interface shear strength (b) Shear force versus displacement (Itasca, 2006)

The sheet reinforcement is subjected to axial pullout force, T at node B (Fig. 2) and the

model rebuilt to attain equilibrium. The axial displacement of reinforcement, w , and tension developed at each node, T are recorded from the output of the FLAC.

The node B of sheet reinforcement is subjected to same pullout load and the displacement and tension profiles are obtained. Accurate predictions of deformation and tensile force in the reinforcement are obtained by adopting “large strain” mode of FLAC program.

3. RESULTS & DISCUSSION

The parametric study is carried for the following ranges of parameters: Depth of reinforcement, $D = 1 - 5$ m, length of reinforcement, $L = 3 - 7$ m, shear stiffness of interface, $k_b = 25 - 200$ kN/m³, axial stiffness of reinforcement, $J = 0.1 - 5$ MN/m. Tensile yield strength of sheet reinforcement = 200 kN/m. Interface friction angle, $\phi_r = 30^\circ$.

The tension and displacement profiles for different pullout forces, T_{\max} at node B are presented in Figs. 5 and 6 respectively for an axial stiffness of reinforcement, $J = 1$ MN/m and shear stiffness, $k_b = 100$ kN/m³. The application of axial pullout force or horizontal displacement at node B develops shear stress at the surface of sheet reinforcement. This shear stress decreases towards the free end of reinforcement depending on the displacement of reinforcement at different nodes. The sheet reinforcement subjected to a pullout force, T of order 7 kN/m displaces the node B of reinforcement by 13 mm and the free end of reinforcement by 5 mm. Thus reinforcement slips by 5 mm and elongates by 8 mm. The increase of pullout force, T by about three times to 22 kN/m results in a linear increase of displacement of node B by 40 mm and free end displacement by 16 mm. These results compare closely with the results of mechanical model presented by Madhav et al. (1998). The mechanical model based on discrete approach predicts an increase of displacement at node B and a subsequent decrease of displacement at free end of reinforcement for the same order of pullout force at node B in comparison with continuum model.

The node B of sheet reinforcement with an axial stiffness, $J = 1$ MN/m is subjected to a pullout force, $T_{\max} = 24$ kN/m at node B and the shear stiffness, k_b is varied from 25 kN/m³ to 200 kN/m³. The corresponding tension and

displacement profiles are presented in Figs. 7 and 8 respectively. The tension profiles for different shear stiffnesses, k_b are close to each other and nearly independent of shear stiffness, k_b . The increase of shear stiffness, k_b increases the shear stress acting on the reinforcement for the same amount of displacement compared with that for lower shear stiffness. The axial pullout force, $T_{\max} = 24$ kN/m displaces the end B of sheet reinforcement by 113 mm and free end of reinforcement by 85 mm for shear stiffness, $k_b = 25$ kN/m³ while the node B displaces marginally by 27 mm and the free end of reinforcement by 6 mm for a higher shear stiffness, $k_b = 200$ kN/m³ (Fig. 8). Hence the displacement at node B and the slip of reinforcement decrease drastically with increase of shear stiffness, k_b from 25 kN/m³ to 200 kN/m³ and the elongation of reinforcement decreases marginally from 28 mm to 21 mm.

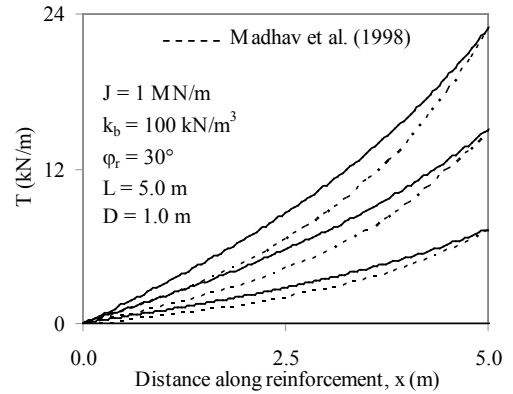


Fig. 5 Tension profiles for different pullout loads

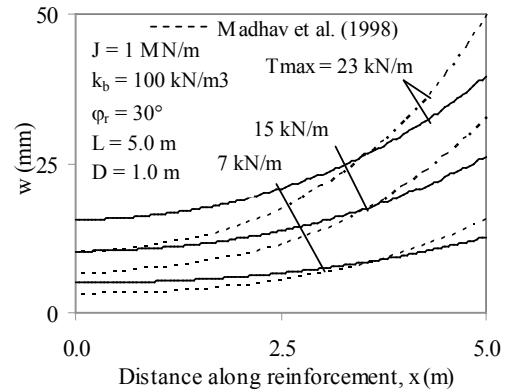


Fig. 6 Displacement profiles for different pullout loads at node B

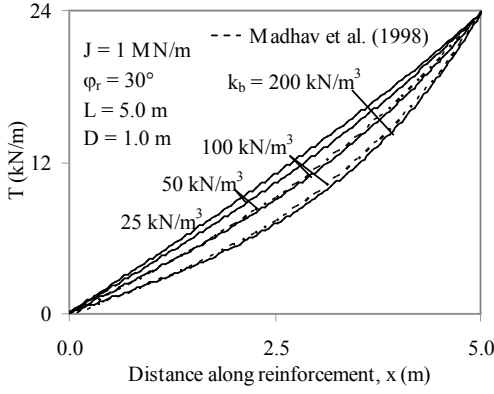


Fig. 7 Effect of interface shear stiffness on tension profiles

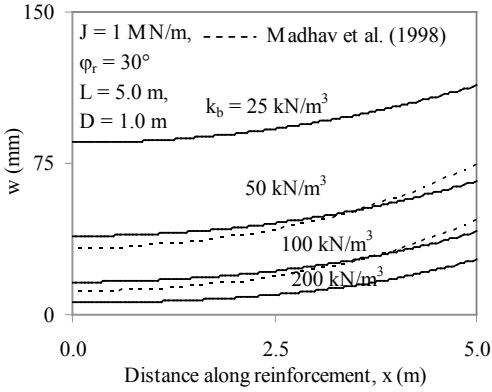


Fig. 8 Effect of interface shear stiffness on displacement profiles

The displacement at node B increases linearly with increase of pullout force, T_{\max} (Fig. 9). The pullout force, T_{\max} increases from 11 kN/m to 44 kN/m with increase of shear stiffness, k_b from 25 kN/m³ to 200 kN/m³ for a displacement of 50 mm at node B of reinforcement. The mechanical model predicts a linear relation between pullout force and displacement. The discrete approach results in slightly larger displacement for the same order of pullout force, T_{\max} for shear stiffness, $k_b = 50$ kN/m³ and 100 kN/m³ presented in Fig. 9.

The influence of axial stiffness of reinforcement, J varying from 0.1 MN/m to 5 MN/m is presented for a shear stiffness, $k_b = 100$ kN/m³. The tension developed in a relatively inextensible reinforcement with an axial stiffness, $J = 5$ MN/m increases linearly along the reinforcement (Fig. 10). The pullout force, $T_{\max} = 23$ kN/m acting at node B decreases rapidly to 8 kN/m at a distance of 1.0 m from

node B for a relatively extensible reinforcement of axial stiffness, $J = 0.1$ MN/m and the tension decreases gradually in the remaining length of reinforcement.

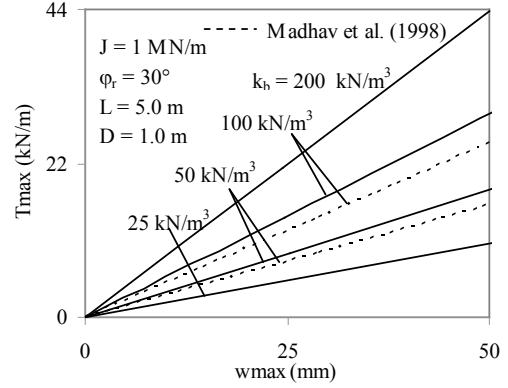


Fig. 9 Variation of maximum tension in reinforcement with horizontal displacement at end B – Effect of shear stiffness

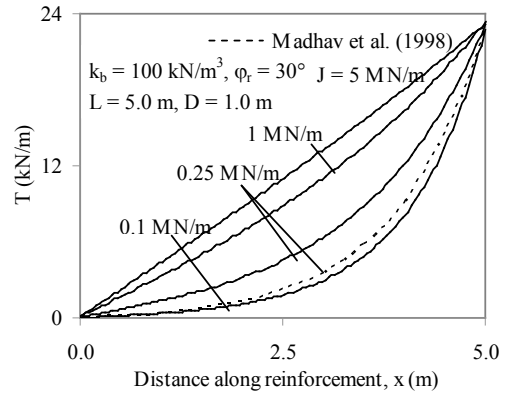


Fig. 10 Effect of axial stiffness of reinforcement on tension profiles

The application of pullout force, $T_{\max} = 23$ kN/m at node B results in a displacement of 114 mm at node B. The displacement decreases drastically to 10 mm at the middle of the reinforcement for a lower stiffness, $J = 0.1$ MN/m (Fig. 11). Displacement decreases gradually to 2 mm at free end of reinforcement. Thus reinforcement elongates by 104 mm in half the length of reinforcement subjected to pullout force and the elongation of other half of the reinforcement is negligible. The behavior of extensible reinforcement changes gradually with increase of axial stiffness of reinforcement, J , from 0.1 MN/m to 5 MN/m. The application of pullout force, $T_{\max} = 23$ kN/m at node B

results in a displacement of 27 mm at node B and the displacement of free end of reinforcement is 21.5 mm for an axial stiffness of reinforcement, J of 5 MN/m. A relatively inextensible reinforcement of stiffness, $J = 5$ MN/m results in a slip of reinforcement by 21.5 mm and elongates by 5.5 mm. The mechanical model predicts an increase of displacement at node B and subsequent decrease of displacement at free end of reinforcement for the same pullout force at node B for a stiffness of reinforcement, $J = 0.25$ MN/m in comparison with continuum model.

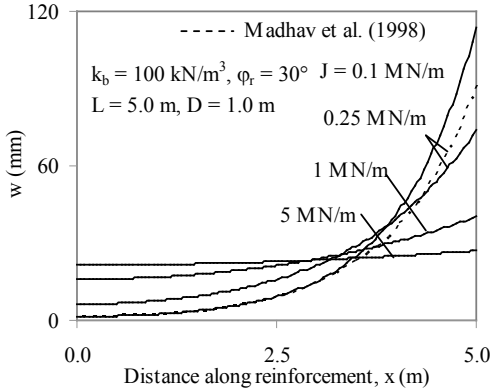


Fig. 11 Effect of axial stiffness of reinforcement on displacement profiles

The displacement of reinforcement increases linearly with increase of pullout force, T_{\max} at node B (Fig. 12). The increase of axial stiffness of reinforcement, J from 0.1 MN/m to 5 MN/m increases the pullout force, T_{\max} from 10 kN/m to 44 kN/m for a displacement of 50 mm at node B. The mechanical model predicts a slightly larger displacement for the pullout force, T_{\max} of same order at node B for a stiffness of reinforcement, $J = 0.25$ MN/m in comparison with that based on the continuum model.

The length reinforcement on either side of failure plane or surface varies with depth below the top of reinforced soil structure. The effect of axial pullout on length of reinforcement, L , for lengths varied from 3.0 m to 7.0 m for a shear stiffness, $k_b = 100$ kN/m³ and axial stiffness, $J = 1$ MN/m is presented in Fig. 13. The tension profile is almost linear for smaller length of reinforcement, $L = 3.0$ m. The increase of length of reinforcement, L to 7.0 m results in a gradual decrease of slope of tension profile towards free end of reinforcement.

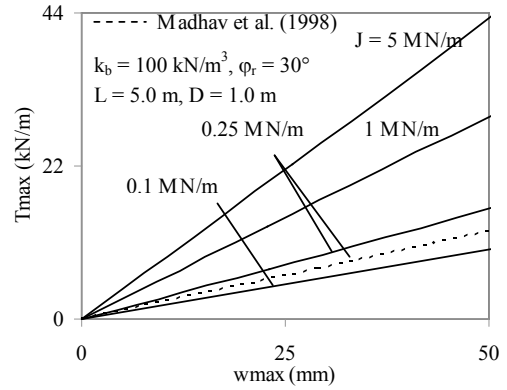


Fig. 12 Variation of maximum tension in reinforcement with horizontal displacement at end B – Effect of axial stiffness of reinforcement

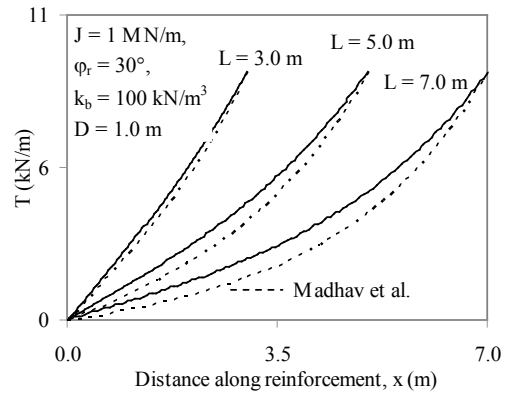
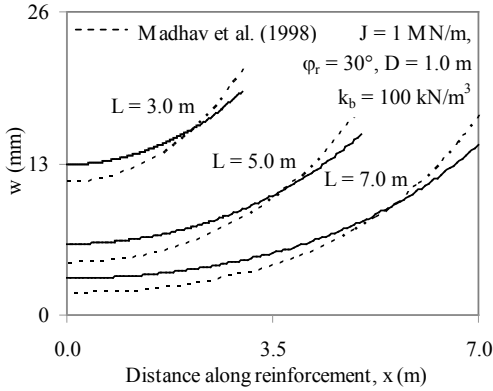


Fig. 13 Effect of length of reinforcement on tension profiles

The application of pullout force, T_{\max} of 9 kN/m at node B results in a displacement of 19 mm at node B and a free end displacement of 13 mm almost similar to rigid body displacement for a shorter length of reinforcement, $L = 3.0$ m (Fig. 14). Reinforcement elongates by 6 mm and slips by 13 mm for a shorter length of reinforcement, $L = 3.0$ m. The pullout force of 9 kN/m at node B on a longer length of reinforcement, $L = 7.0$ m induces a displacement of 15 mm at the node B and the free end of reinforcement of 3 mm. Hence reinforcement elongates by 12 mm and slips marginally by 3 mm for a longer length of reinforcement, $L = 7$ m. The elongation of reinforcement occurs over half of the length of reinforcement subjected to pullout load and the elongation in the other half of the reinforcement is negligible for longer length of reinforcement.

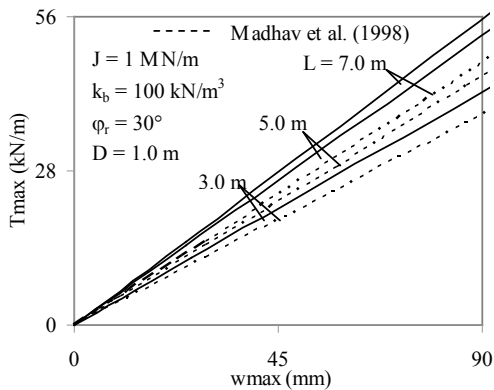
The shorter length of reinforcement results in slip or rigid body displacement while increase of length reinforcement results in elongation of reinforcement for the same pullout load. The displacement and tension profiles presented by mechanical model compare closely with the results of the present model for different lengths



of reinforcement, L ranging from 3.0 m to 7.0 m.

Fig. 14 Effect of length of reinforcement on displacement profiles

The displacement of reinforcement increases linearly with increase of pullout force at node B for different lengths of reinforcement, L ranging from 3.0 m to 7.0 m (Fig. 15). The pullout force, T_{\max} at node B increases marginally by 42 kN/m, 53 kN/m and 56 kN/m for a displacement



of 90 mm at node B for the length of reinforcement, $L = 3.0$ m, 5.0 m and 7.0 m respectively.

Fig. 15 Variation of maximum tension with horizontal displacement at end B – Effect of length of reinforcement

The applied pullout force is less than the maximum pullout resistance of reinforcement and hence the interface friction angle and depth of reinforcement do not have any influence on the response of reinforcement to the pullout force.

4. CONCLUSION

The response of polymeric sheet reinforcement subjected to axial force at its free end is studied using FLAC for a range of interface shear stiffnesses, axial stiffnesses of reinforcement and for different lengths of reinforcement.

- The results of axial pullout of sheet reinforcement based on FLAC compare closely with the results of Madhav et al. (1998). The marginal difference between the two methods is due to the continuum and discrete approaches adopted.
- The displacement of loaded end of reinforcement subjected to an axial pullout force of 24 kN/m increases from 27 mm to 113 mm with decrease of shear stiffness of interface from 200 kN/m³ to 25 kN/m³. The elongation of reinforcement is nearly constant.
- The inextensible reinforcement ($E_r = 5$ MN/m) subjected to an axial pullout force of 23 kN/m mobilizes a uniform shear stress and undergoes a rigid body displacement of about 25 mm.
- Extensible reinforcement ($E_r = 0.1$ MN/m) subjected to an axial pullout of 23 kN/m undergoes larger displacement of 114 mm at loaded end of reinforcement while the displacements of the free end of reinforcement is negligible. The shear stress mobilized at loaded end of reinforcement is large while it is negligible at the free end.
- For the same axial pullout force, the shorter length of reinforcement undergoes rigid body displacement. The loaded end of longer length of reinforcement elongates and the displacement at free end is small compared to that for shorter length of reinforcement.

The present study predicts a linear increase of displacement with pullout force. The pullout force to be applied for a given displacement

increases with increase of shear stiffness, axial stiffness of reinforcement and marginally with length of reinforcement.

5. REFERENCES

- Abramanto, M. and Whittle, A.J. 1993. Shear lag-analysis of a planar soil reinforcement in plane strain compression, *Journal of Engineering Mechanics*, ASCE, Vol. 119, No. 2, 270 – 291.
- Alforo, M. C. and Pathak, Y. P. (2005): Dilatant stresses at the interface of granular fills and geogrid strip reinforcements, *Geosynthetics International*, Vol. 12, No. 5, pp 239 – 252.
- Farrag, K., Acar, Y.B. and Juran, I. 1993. Pull-Out Resistance of Geogrid Reinforcement, *Geotextiles and Geomembranes*, Vol. 11, No. 2, pp. 133-159.
- Flac Version 6.0. 2008. User's guide, 4th Edition, 1.73 – 1.91.
- Juran, I. and Chen, C.L. 1988. Soil-Geotextile Pull-Out Interaction Properties: Testing and Interpretation. *Transportation Research Record* 1188, 37-47.
- Long, P.V., Bergado, D.T. and Balasubramanian, A.S. 1997. Interaction Between Soil and Geotextile Reinforcement, *ASCE Geotechnical Special Publication*, No. 69, pp. 560 – 578.
- Madhav, M.R., Gurung, N. and Iwao, Y. 1998. A Theoretical Model for the Pull-Out Response of Geosynthetic Reinforcement, *Geosynthetics International*, Vol. 5, No. 4, pp. 399-424.
- Marques J.M.M.C. 2005. Finite element modeling of the pull-out test of geosynthetics. VIII International Conference on Computational Plasticity, Barcelona.
- Moraci, N. and Gioffre, D. 2006. A simple method to evaluate the pullout resistance of extruded geogrids embedded in a compacted granular soil, *Geotextiles and Geomembranes*, Vol. 24, No. 2, pp. 116–128.
- Moraci, N. and Recalcati, P. 2006. Factors affecting the pullout behaviour of extruded geogrids embedded in a compacted granular soil, *Geotextiles and Geomembranes*, Vol. 24, No. 4, pp. 220–242.
- Palmeira, E.M. and Milligan, G.W.E. 1989. Scale and other factors affecting the results of pull-out tests of grids buried in sand, *Geotechnique*, Vol. 39, No. 3, pp. 511–524.
- Palmeira E. M. 2004. Bearing force mobilisation in pull-out tests on geogrids. *Geotextiles and Geomembranes*, Vol. 22, No. 28, pp. 481 – 509.
- Perkins S.W. & Edens, M.Q. 2003. Finite element modeling of a geosynthetic pullout test, *Geotechnical and Geological Engineering*, Vol. 21, pp. 357–375
- Sieira, A.C.F., Gerscovich, D.M.S. and Sayao, A.S.F.J. 2009. Displacement and load transfer mechanisms of geogrids under pullout condition, *Geotextiles and Geomembranes*, Vol. 27, No. 4, pp. 241–253.
- Sobhi, S. and Wu, J.T.H. (1996). “Interface Pullout Formula for Extensible Sheet Reinforcement”, *Geosynthetics International*, Vol. 3, No. 5, 565-581.
- Sugimoto, M. and Alagiyawanna, A.M.N. 2003. Pullout behavior of geogrid by test and numerical analysis, *Journal of Geotechnical and Geoenvironmental Engineering*, ASCE, Vol. 129, No. 4, pp. 361–371.
- Wilson-Fahmy, R. F., Koerner, R. M., and Sansone, L. J. 1994. Experimental behavior of polymeric geogrids in pullout, *Journal of Geotechnical Engineering*, Vol. 120, No. 4, pp. 661-676.
- Wilson-Fahmy, R.F. and Koerner, R.M. 1993. Finite element modelling of soil-geogrid interaction with application to the behavior of geogrids in a pullout loading condition, *Geotextiles and Geomembranes*, Vol. 12, No. 5, pp. 479-501.
- Yogaarajah, I., and Yeo, K.C. 1994. Finite element modeling of pull-out tests with load and strain measurements, *Geotextiles and Geomembranes*, Vol. 13, No. 1, pp. 43-54.
- Yuan, Z. and Chua, K.M. 1990. Numerical evaluation of the pullout box method for studying soil-reinforcement interaction”, *Transportation Research Record*, Washington, DC, 1278: 116-124.

Soft grouting for the seismic protection of existing buildings

D. Lombardi, V. Nappa, A. Flora

DICEA, University of Napoli Federico II, ITALY

ABSTRACT: The paper introduces an original approach to face seismic hazard on existing buildings by treating with a soft grout a thin layer of soil at a certain depth. The paper presents a parametric analysis with reference to the case of a typical clayey soil, considering the ideal cases of an horizontal or vertical layer. The information gained from these two extreme cases are essential to understand the true behavior of a real soft caisson, whatever its shape. Surprisingly, the seismic isolation capacity of the vertical layer depends not only on shear stiffness but also on bulk stiffness, and this has to be taken into account in the design of a seismic barrier composed of both vertical and horizontal layers.

Keywords: Seismic Isolation, soil grouting, parametric analyses.

1. INTRODUCTION

The seismic isolation of strategic existing buildings (historical buildings, hospitals, etc.) is still a matter of concern. At the moment, the typical approach for these buildings is the reduction of vulnerability, i.e. the strengthening of the structure out of ground or of its foundations. For buildings having historical or architectonical relevance this is certainly not acceptable, the structure obviously needing to be preserved as it is. In some cases, grouting (jet grouting, low pressure grouting, etc.) of the most superficial soils may be carried out as an alternative or complementary measure (e.g. D'Onofrio et al., 1999). However, even though the stiffening of the uppermost soil by grouting has the positive effect of reducing the seismically induced ground motion, it has little or no effect on the energy transmitted to the structure to be protected, which can still be very high and therefore potentially dangerous. As a matter of fact, a convenient and straightforward procedure is not yet available to seismically isolate relevant existing buildings. A research activity, both theoretical and experimental, is now under course at the University of Napoli Federico II (Italy) on this topic. This paper presents part of this activity, with reference to a

completely new approach which involves soil treatment at depth of a thin layer of soil (Fig. 1) having the aim of artificially changing the shear wave propagation in the upper part of the subsoil.

The grouted layer can be obtained with inclined drilling and injection, multiple local injections or even with guided directional drilling and injection. Whatever the adopted technique, the basic idea is that the grouted layer has to have a very low dynamic impedance $\rho \cdot V_s$ (that is, either a very low density ρ or, more likely, a very low shear waves velocity V_s and shear stiffness G_0). In fact, theoretical indications on one dimensional shear wave propagation suggests that the profile of impedance ratios with depth is the relevant parameter in seismic amplification analysis, and thin layers having a low shear stiffness are needed to sharply reduce the seismic input.

In the following, the effectiveness of the new proposed approach is numerically tested via a parametric analysis, considering different properties of the grouted layer with reference to a simplified scheme.

In particular, the effect of the insertion of a soft layer in the soil will be analyzed considering two ideal conditions (either a single vertical or horizontal layer, Fig. 2). A

combination of the two schemes will then contribute to define the isolating caisson. The goal of these preliminary simplified analyses is to better understand the relevance of the different geometrical, physical and mechanical parameters on the seismic isolating effectiveness.

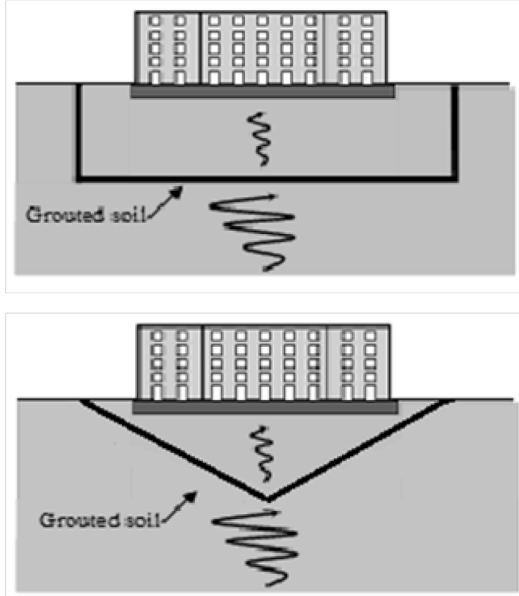


Figure 1. Possible geometrical configurations of the isolating grouted layer

The adoption of new, soft grouts obviously involves a relevant chemical research activity. In principle, the grout to be adopted can either fracture the soil to create a completely artificial layer (solution to be adopted in normally consolidated fine grained soils) or permeate into the soil and create a grouted soil layer (for more permeable soils as for instance sands). Depending on the mechanism and on the grout properties, different dynamic impedances may be obtained. The goal is to reduce the original one as much as possible. Theoretical and experimental research is currently under course, and results will be published in the next future.

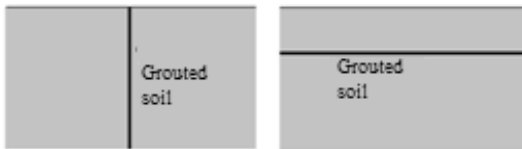


Figure 2. Simplified schemes with a single vertical and horizontal layer of grouted material.

The adoption of soft barriers has been already considered in literature, for instance to reduce the vibratory effects of trains as well as traffic induced vibrations (eg. Chouw 1992, Kellezi 2011). The isolation mechanism which this paper will analyse takes advantage of some experiences reported in literature, like for example the one carried out with a shaking table by Dietz and Woods (2006). A very comprehensive study is reported by Kirtas (2009), who analyzed numerically and experimentally (using a centrifuge) the inclusion of different stiff and soft treatments into a soil with a SDOF (Single Degree of Freedom) at ground level, simulating the case of a structure with shallow foundations.

2. NUMERICAL ANALYSES

2.1. Input motion

The 2D dynamic analyses have been developed using the software FLAC7. Simplified input motions were applied at the bedrock in terms of acceleration by means of the seismic Ricker wavelet model (Ryan, 1994). These simplified seismograms consist of a zero-phase wavelets with a central peak and two smaller side lobes as seen in figure (Fig. 3). This model can be expressed in terms of displacement u as:

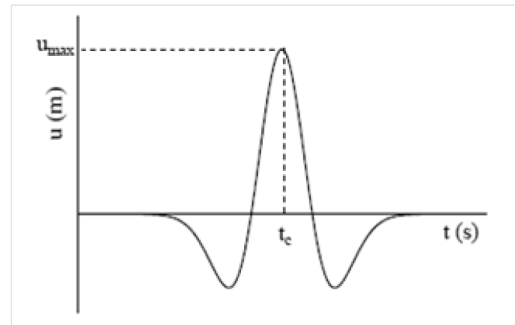


Figure 3. Ricker wavelet in terms of displacement time history $u(t)$.

$$u(t) = u_{\max} \cdot \left[1 - 2 \cdot \pi^2 \cdot f^2 \cdot (t - t_c)^2 \right] \cdot e^{-\pi^2 \cdot f^2 \cdot (t - t_c)^2} \quad (1)$$

where u_{\max} is the maximum value of the displacement and f is the dominant frequency. Obviously, f is inversely proportional to the peak time t_c .

A Ricker wavelet can be uniquely specified assigning the parameters f and u_{\max} .

2.2. Testing program

As previously mentioned, before analyzing more realistic geometrical configurations, simplified schemes with a single vertical or horizontal layer of grouted material have been studied, assuming a thickness of the treated layer of 1 m.

All the analyses consider a linear elastic behaviour for the involved materials, assuming a given value of stiffness and damping ratio D and shear deformations.

The mesh used for these analyses has a width of 120 m in the horizontal direction (x) and a thickness 60 m in the vertical direction (y).

In the scheme with the vertical layer, the vertical layer was placed along the vertical symmetry axis, and the dynamic motion was propagated only on the right side of the soil deposit, to check the isolating effectiveness of the vertical layer.

The geometrical configuration adopted was reported in Fig.4.

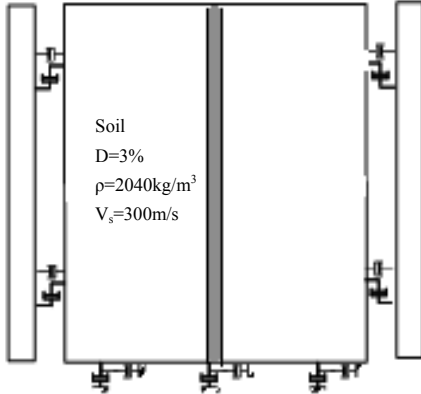


Figure 4. Model adopted for the propagation through vertical layer.

In the scheme with a single horizontal layer, the clay layer has been considered as overlying a bedrock having a thickness of 60 m, for a total height of the mesh of 120 m.

The reference seismic motion has been applied at the base of the bedrock, as described in the next section. In this scheme, the grouted soft layer was placed at a depth $H_g=10$ m.

In Fig.5 the scheme adopted for the analyses is reported.

In all analyses, a homogeneous fine grained subsoil was considered, corresponding to a medium consistency clay. The natural period, of this deposit is therefore $T_s=4H/V_s=0.8$ s, and therefore the natural frequency of the soil deposit is $f_n=1.25$ Hz. Three different dominant frequencies ($f=1, 3, 5$ Hz) were considered, while the peak acceleration (a_{\max}) was kept constant and equal to 0.5 g.

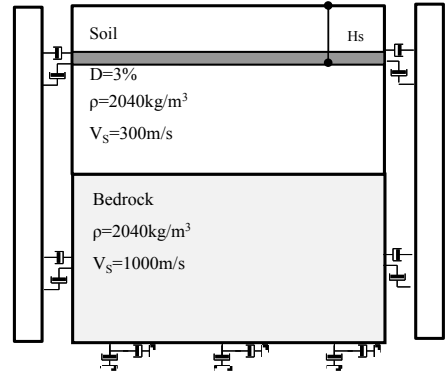


Figure 5. Model adopted for the propagation through horizontal layer.

The properties of the bedrock, of the natural and of the grouted soil are summarized in Tab. 1.

Table 1. Main properties of the materials.

Material	γ [kN/m ³]	ρ [kg/m ³]	V_s [m/s]	D [%]
Natural soil	20	2040	300	3
Bedrock	20	2040	1000	0
Grouted layer	20	1020	10, 20, 50, 100, 200,300	0

For the case of the horizontal layer, only the value $V_{s,g}=20$ m/s was considered for the grouted layer.

Two series of analyses were carried out on two schemes, as summarized in Tab. 2: in the first one, different values of shear wave velocities were considered for the vertical grouted layer, keeping the ratio K/G constant. G was calculated as $G=\rho \cdot V_s^2$, and K had to be changed in each analysis to keep the ratio K/G constant

(actually, this was simply done by imposing a constant value of the Poisson ratio $\nu=0.3$). This first series of analysis had the main goal to check the influence of G of the grouted layer on results.

In the second series of analyses, the value of the volumetric stiffness K of the thick layer has been varied keeping G constant, in order to study its effect on the response of the system.

From a static point of view (i.e. to check the effect of the insertion of a grouted layer on the performance of the building to be protected), it is reasonable to expect that the volumetric stiffness of the horizontal layer has a paramount relevance. However, this paper focuses on the seismic behavior of the grouted barrier. As a consequence, it is more interesting to see what effect (if any) K has on the transmission of waves. From this point of view, being the problem mostly related to the transmission of S waves, it is therefore much more interesting to check the relevance of K on the performance of the vertical grouted layer.

Table 2. Summary of the numerical analyses. All tests were carried out for the three frequencies $f=1, 3, 5$ Hz.

Grouted layer	$V_{s,g}$ [m/s]	G [kPa]	K [kPa]	K/G
vertical	10	102	221	2.17
	50	2550	5525	
	100	10200	22100	
	200	40800	88400	
	300	91800	198900	
	20	408	$K_1=441$ $K_2=884$ $K_3=8733$	1.08 2.17 21.41
horizontal	20	408	$K_1=441$ $K_2=884$ $K_3=8733$	1.08 2.17 21.41

2.3. Results of the analyses for the scheme with a vertical layer

A series of analyses with no treatment has been previously performed for the soil, thus obtaining a reference behavior of the soil deposit. The signals, which are Ricker wavelets transmitted as S_V waves, have been propagated starting from the base of the right side of the model. The left side of the model is thought as the part to be protected from the dynamic input.

The results were evaluated in terms of maximum acceleration at the ground surface.

For the sake of brevity, only the results pertaining to $f=1$ Hz, which is the most critical frequency for the natural deposit, are shown.

Figure 6 demonstrates that the lower is the V_s of the grouted layer, the larger is the reduction of acceleration on the protected (left) side of the mesh. The same results have been obtained for the other Ricker wavelets.

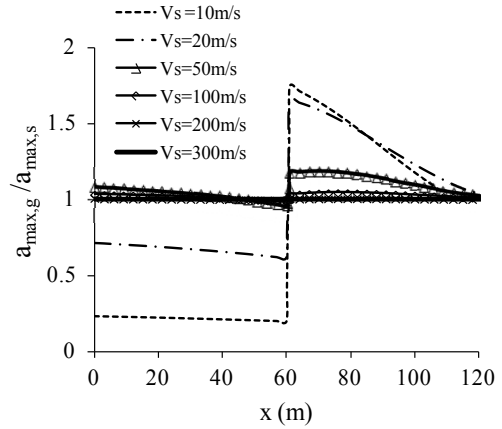


Figure 6. Vertical barrier: results in terms of the ratio between peak ground acceleration with and without treatment at the ground surface under 1 Hz Ricker input motion.

However, the first experimental tests carried out in laboratory have indicated that, even with very soft grouts, the value $V_s=10$ m/s is difficult to obtain. For this reason, a value of shear wave velocity equal to 20 m/s will be considered in the following: such a value, in fact, is still effective in mitigating the dynamic effects, and more realistic.

Therefore, considering a single value of the shear wave velocity for the vertical treated layer, the results for different input frequencies are shown in Fig. 7. At a frequency of 1 Hz, the high values of acceleration are due to the closeness of the fundamental frequency of the signal to the natural frequency of the soil layer without any treatment (assuming $H=60$ m, $f_n=V_s/(4H)=1.25$ Hz).

Then, keeping constant G , the value of volumetric stiffness of the soft layer has been varied, in order to evaluate the influence of this latter in the system response. This variation has

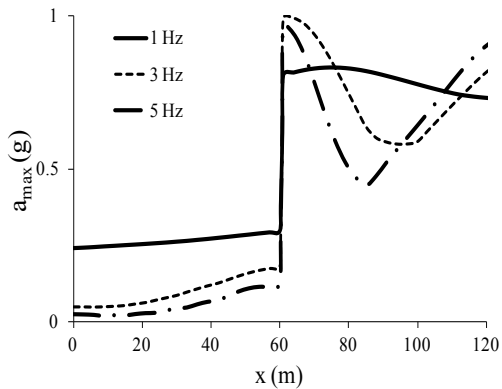


Figure 7. Results in terms of ratio between peak ground acceleration with and without treatment at the ground surface by varying the fundamental frequency of the Ricker wavelet and assuming a shear wave velocity V_s of the thin layer equal to 20m/s .

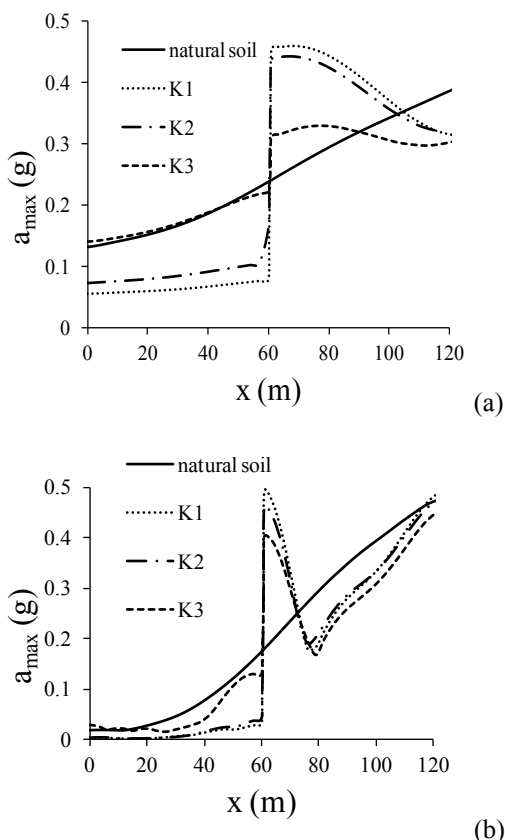


Figure 8. Results in terms of maximum acceleration at ground surface, by varying the volumetric stiffness K for a Ricker wavelet with a fundamental frequency of 1Hz (a) and 5Hz (b)

been assigned imposing values of the Poisson ratio included in a range consistent with the elastic constitutive model ($0 \leq \nu \leq 0.5$).

Surprisingly, looking at the results plotted in Fig. 8, it is clear that the volumetric stiffness of the grouted layer has an influence the wave propagation.

It can be noted that, for the volumetric stiffness $K1$ (the lowest one), the results are almost identical to the ones of the $K2$ scheme, while for volumetric stiffness $K3$ (largest value), the accelerations are close to those of the natural soil.

These numerical evidences point out that it is convenient to have, on the lateral side of a soft caisson (vertical barriers) a grout as soft as possible not only in terms of shear stiffness but also in terms of volumetric stiffness.

The first possible reason for this evidence may be a modal conversion of the waves transmitted through the barrier, with the transformation of energy into compressional waves. However, no modal conversion of the propagated waves was observed on the other side of the isolating barrier.

Then, the only possible explanation of the influence of K of a vertical layer on the transmission of S waves is its effect on the mechanism of deformation of the barrier itself: since vertically propagating S waves induce shear displacements in the vertical grouted barrier, its volumetric stiffness rules the relationship between the displacements of the two sides of the barrier.

For an extremely stiff grouted material (high values of K), it is expected that the two sides display remaining parallel, while for low stiffness a distortion is expected. Fig. 9 sketches the expected mechanism on a single volume element.

2.4. Results of the analyses for the scheme with an horizontal layer

In this section, the effects of the insertion of a horizontal layer of grouted material on the wave propagation are shown.

By assuming a shear velocity equal to 20 m/s, the results of the analyses are plotted in Fig. 10 in terms of peak ground acceleration along the depth.

For each considered seismic input, the peak acceleration sharply decreases above the grouted barrier, keeping reduced values up to

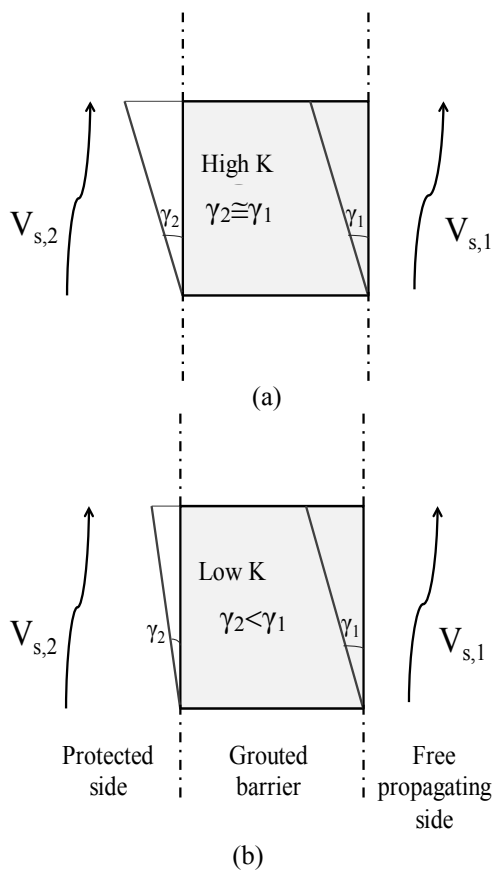


Figure 9. Sketch of the effects of K of the grouted soil on the propagation of V_s through the barrier: for high value of K , $\gamma_1 \approx \gamma_2$ and $V_{s1} \approx V_{s2}$ (a); for low stiffness, $\gamma_1 \neq \gamma_2$ and $V_{s2} < V_{s1}$ (b).

the ground surface. On the contrary, the existence of large reflected waves induces larger acceleration below the barrier. However, these are usually not dangerous, unless underground sensitive structures exist below the grouted layer.

By varying the volumetric stiffness, with the same values of K adopted for the vertical layer, no difference was observed in terms of maximum acceleration along the depth. For this reason, the results of only one value of volumetric stiffness (K_1) are plotted in figure 11.

3. CONCLUSIONS

In this pilot study, the effect of the insertion of a soft grouted layer with a dynamic impedance much smaller than that of the surrounding soil was numerically investigated,

using simplified seismic inputs. It was shown that this treatment is extremely effective in reducing the maximum horizontal accelerations on the ground surface.

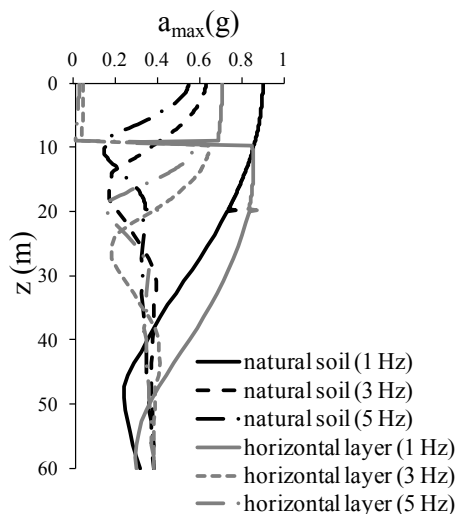


Figure 10. Results in terms of maximum acceleration along the depth with and without treatment with the change of seismic input ($V_s=20$ m/s).

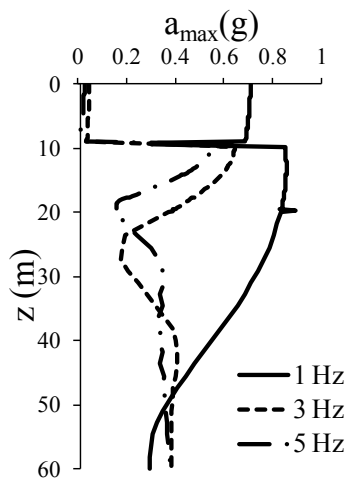


Figure 11. Maximum acceleration along the depth for volumetric stiffness K_1 and under different seismic input

Starting from simplified schemes (vertical and horizontal layers of grouted material), some evidences could be pointed out.

The results were evaluated in terms of maximum accelerations. In particular, for the scheme with a vertical layer, by assuming the same density and different shear wave velocities for the thin layer, the peak ground acceleration strongly decreases passing from $V_g = 300 \text{ m/s}$ to $V_g = 10 \text{ m/s}$. In the parametric analyses, the effect of different values of the volumetric stiffness K of the soft grouted layer has been investigated. In particular, two further values of volumetric stiffness have been considered. Surprisingly, K may have a relevant dynamic effect on the behaviour of vertically placed soft barriers. A high value of volumetric stiffness makes the barrier useless, while a low value of volumetric stiffness is able to sharply reduce the lateral transmission of vertically propagating waves.

By analysing the scheme with an horizontal layer, it was observed that for each seismic input considered, the peak acceleration above the barrier sharply decreases, keeping reduced values up to ground surface. The volumetric stiffness, instead, does not influence the results. Clearly, a high volumetric stiffness may be necessary in the horizontal layer for static reasons.

In conclusions, the proposed innovative approach to the seismic protection of existing buildings seems to be a valid alternative to other more conventional and invasive solutions, such as the structural reinforcement and base isolation, and can result suited for the historical constructions for which integrity has to be preserved.

Since the effectiveness of grouting depends on the dynamic coupling of the input motion with the subsoil and the building response, further analyses considering 2D more realistic geometrical configurations (Fig. 1) need to be carried out to get more conclusive considerations on the feasibility of such interventions.

4. REFERENCES

- Chouw, N. & Schmid, G. 1992. Building isolation using the transmitting behavior of a soil layer. *Proc. 10th World Conference on Earthquake Engineering*, Madrid, 4, 2519-2524.
- D'Onofrio, A., Mancuso, C., Silvestri, F. 1999. Reduction of seismic vulnerability by geomaterial attenuation procedures. *II Int. Symp. On Earthquake Geotechnical Engineering*, Lisboa, 2, 725-730.
- Dietz M.S., Wood D. M. (2006). Shake table testing of a soft caisson for geotechnical seismic retrofit. *Proc. 4th International Conference on Earthquake Geotechnical Engineering*, Thessaloniki (Greece).
- Kellezi, L. 2011. Dynamic behavior of a softer layer overlying hard soil/bedrock and vibration reduction. *GEO-Danish Geotechnical Institute*, Lyngby.
- Kirtas, E. & Pitikalis, K. 2009. Subsoil interventions effect on structural seismic response. Part II: parametric investigation. *Soil Dynamics and Earthquake Engineering*, 13, 3, 328-344.
- Kirtas E., Rovithis E., Pitilakis K. (2009). Subsoil Interventions Effect on Structural Seismic Response. Part I: Validation of Numerical Simulations. *Journal of Earthquake Engineering*, Vol.13(2), pp.155-169.
- Ryan, H. 1994. Ricker, Ormsby, Klauder, Butterworth- A choice of wavelets. CSEG.

Soil Structure Interaction: An analysis of the effect of creep and shrinkage of concrete

Luciana de Moraes Pereira da Rosa
UFF, Brazil

Eliane Maria Lopes Carvalho
UFF, Brazil

Bernadete Ragoni Danziger
UERJ, Brazil

ABSTRACT: The paper presents some results of a joint research of three universities from Rio de Janeiro, Brazil, aiming at the observation of concrete creep and shrinkage effect on soil structure interaction. In this paper an 18 story building resting on shallow and deep foundations was submitted to a site instrumentation to monitor settlements and loads of some columns close to the ground floor during the construction phase. Particular attention is given to the effect of concrete creep and shrinkage in soil structure interaction effects. Due to the extent of the experimental results, only part of the database is presented.

1. INTRODUCTION

The new version of Brazilian Foundation Code states in section 5.5 that: "In structures which foundation settlements can influence the load distribution on columns, the soil structure interaction effect shall be considered in design".

The study of soil structure interaction is a subject of great interest for Brazilian engineers since the beginning of the Brazilian Association of Soil Engineers. Some research papers should be detached: Chamecki (1954), Barata (1986), Gusmão and Gusmão Filho (1994), Danziger et al. (1997), among others.

Several MSc and DSc thesis have studied this subject, many of them forming an extensive database included in the joint research: Costa (2003) and Rosa (2005), from UFF and Gonçalves (2010), from UFRJ, besides those from other Institutions as that from Russo Neto (2005) from USP, São Paulo.

In the present paper some results of the effect of creep and shrinkage of concrete are accounted for in soil structure interaction. Load redistribution and the tendency towards settlement uniformity, as predicted by the Brazilian Code, are relevant aspects in the analysis.

Due to the great extent of the experimental data, in this paper emphasis is given to comparison between predicted and measured settlements. Analyses considering and not considering soil structure interaction, as well as

those also including the creep and shrinkage effects on concrete are presented.

2. ANALYSED CONSTRUCTION

2.1. Case description

It consists of an 18 stories residential building situated in Niterói, a city very close to Rio de Janeiro. The structure is quite conventional, partly supported by shallow foundations, at the central part, with deep foundation close to the neighboring structures, supported by steel I piles, figure 1. The soil profile is predominantly sandy, as illustrated in figure 2, with soil resistance nearly increasing with depth. Two layers of sandy clay layers are also present, showing a hard to stiff consistency. The shallow foundations rest at depths varying from 4,5 to 6,5 depth from the soil surface. The steel piles are embedded into 15 to 21 m depth.

2.2. Construction phases

The construction started at the beginning of 2011 and the site monitoring in July, 2011. Six construction phases have been investigated from November 2011 till June 2012.

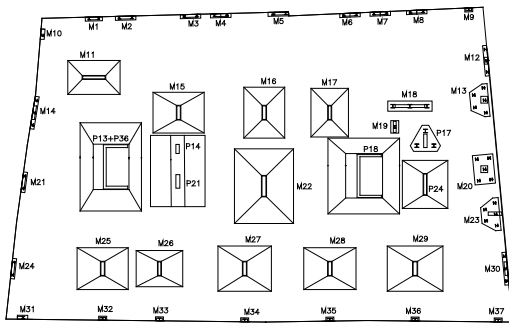


Figure 1. Foundation plant.

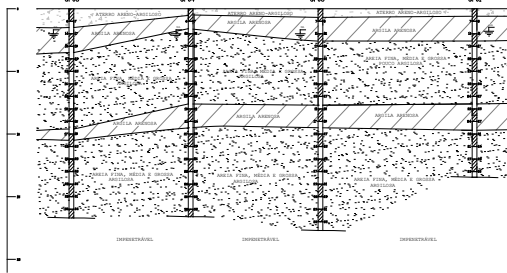


Figure 2. Soil profile.

2.3. Structural modelling

A tridimensional structural model has been developed through a program based on FEM. The updated program version has a concrete creep and shrinkage module, according to CEB-FIP (1993). The beams and columns have been modelled as bar elements and the slabs and walls as plate elements, as shown in figure 3.

Various models have been prepared for the structure analysis. The first model considered the structure resting on fixed support, objecting the comparison to design column loads. The simple design model reached a minor difference in columns load lower than 3%. The remaining models have been prepared with different hypotheses which will be detached in the present paper.

2.4. Site instrumentation

The site instrumentation had the main objective of monitoring the settlement of some main columns with time in different construction phases and also the loads reaching some columns during the various construction phases.

Settlement measurements involve the performance of an optical precise levelling.

Steel rustless pins have been installed on the faces of 11 columns at the basement, 0,3 m above the floor. The measurement settlement procedure consisted basically in levelling the column pins in relation to a fixed external reference ("benchmark"). This last has been installed in order to suffer no influence from the loadings from the proper site or from other sources.

In this specific case, it has not been possible to obtain an external reference of nearly null settlement. The selected option was to consider the reference at an internal column founded on a steel pile, the most isolated one, with a predicted settlement much lower than those from the remaining instrumented columns. As long as the isolated caps with single piles would have measured settlements much lower than the others, the most isolated single pile has been chosen. Figure 4 illustrates the structure at the second construction phase.

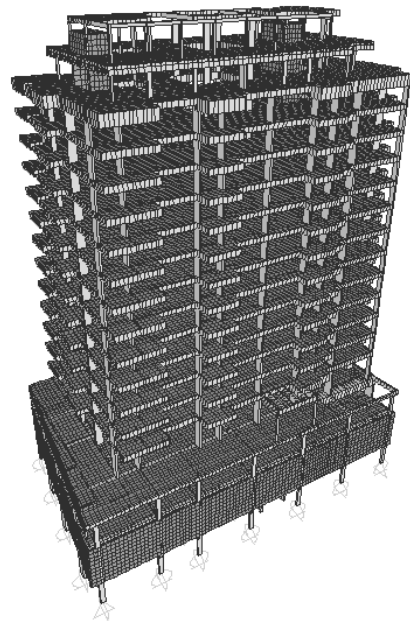


Figure 3. Numerical model of the structure.

For each phase a structural model has been prepared. Table 1 summarizes the construction phases with settlement instrumentation as well as its time from the beginning of the construction. The first monitoring operation occurred with the structure constructed up to the fourth floor.

Figure 5 shows the equal settlement curves mesured for the 6th (last) instrumented phase.

The greatest settlements occurred for the columns founded in spread footings at the central part of the construction whereas the slower ones on the columns founded on deep steel piles.



Figure 4. Construction at the second phase.

Table 1. Construction phases.

Model	Construction Phase	Time (days)
Start	-	0
1 ^a reading (zero)	Structure concreted till the 4 th floor	203
2 ^a reading	Structure concreted till the 5 th floor	217
3 ^a reading	Structure concreted till the 9 th floor, masonry till the 4 th floor	266
4 ^a reading	Structure concreted till the covering ceiling, masonry till the 10 th floor, walls and floors covering up to 2 nd floor	310
5 ^a reading	Structure already finished with masonry up to the 11 th floor and covering up to the 3 rd floor.	336
6 ^a reading	Structure and masonry finished and covering up to the 7 th floor.	413

3. SETTLEMENT PREDICTION

For settlement prediction the method Aoki and Lopes (1975) has been adopted. This method estimates the stresses and settlements in the

interior of the soil mass through a numerical process. In such process the loads that a set of footings and/or piles transmit to the soil mass are decomposed in an equivalent set of point loads with superposed effects calculated at the desired point (selected columns base). In this way settlements for the whole columns of the structure have been estimated from the design loads.

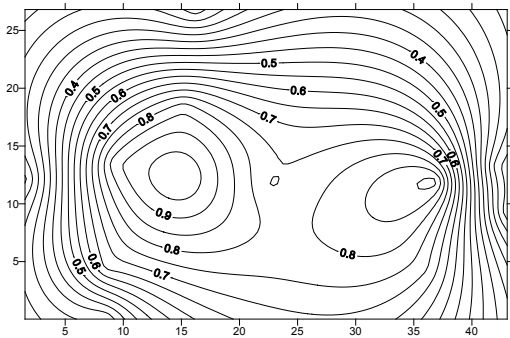


Figure 5. Equal measured settlement curves for the 6th instrumentation phase, values in centimeters.

Figure 5 shows equal settlements curves for the 6th instrumentation phase whereas Figure 6 illustrates the same for the predicted settlements, without due consideration of soil structure interaction.

It should be emphasized that the predicted settlement shown in Figure 6 includes the whole loading whereas the instrumentation curve only contains the settlements due to the load difference generated after the construction the fourth floor. Thus the predicted settlement is greater than the measure one, if no correction is introduced.

4. STRUCTURAL ANALYSIS

4.1. Numerical Models

A single structural model has been established for each construction phase. Thus, it was possible to compare, for each phase, the measured and the predicted settlement. In a first phase of the analysis, the loads have been applied for the model of fixed support, considering the existing loads for each constructive phase. From the foundation loads thus obtained, the settlements for each constructive phase have been calculated using the prediction procedure are embedded into 15 to 21 m depth.

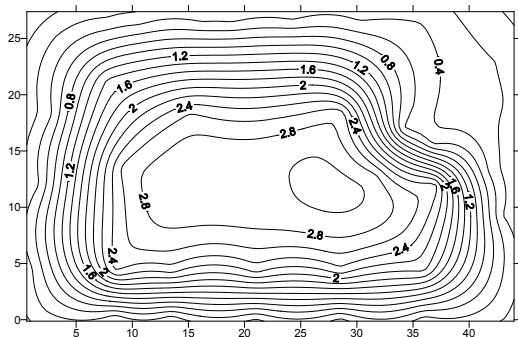


Figure 6. Equal settlement curves (predicted values), in centimeters.

The proposed model to reproduce the soil characteristics was composed of springs. In fact, as the soil consisted of predominantly sandy layers, the simple springs could reproduce the linear behavior of load x settlement curves. The spring stiffness has been estimated by the calculated load obtained by the fixed support model divided by the predicted settlement, in order to reproduce the soil compressibility.

The values of the spring coefficient were considered as the boundary condition in the numerical model. Various iterations have been made for the 1, 3 and 6, spring coefficient of the construction phase up to the convergence of the spring coefficients. The convergence has been attained at the 3rd iteration.

4.2. Analysis Results

4.2.1. Measured and estimated settlements

From the numerical models elaborated for each construction phase, the measured and predicted settlements could have been compared. Figures 7 to 10 present the equal settlement curves for the 6th construction phase, considering the three soil structure iteration analyzed.

It can be observed that the greatest settlements have been estimated with the loads obtained by the analysis with fixed support. The location where the greatest settlement occurs is modified if a soil structure interaction is introduced in the analysis. If a higher refinement is introduced in the interaction analysis, the change in the settlement pattern is less significant (a large number of iteration steps), up to the convergence of the results (figures 8, 9 and 10).

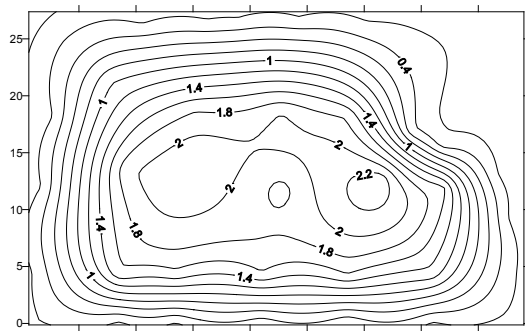


Figure 7. Equal settlement curves for the 6th phase, considering a fixed support analysis (in centimeters).

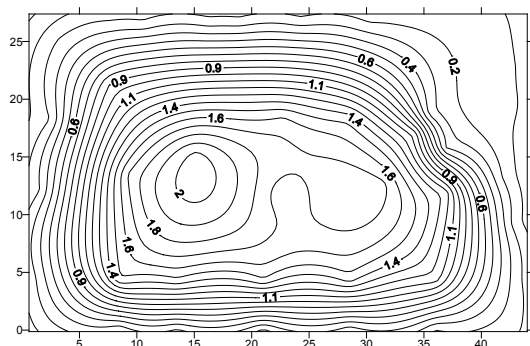


Figure 8. Equal settlement curves for the 6th phase, considering the first iteration calculation (in centimeters).

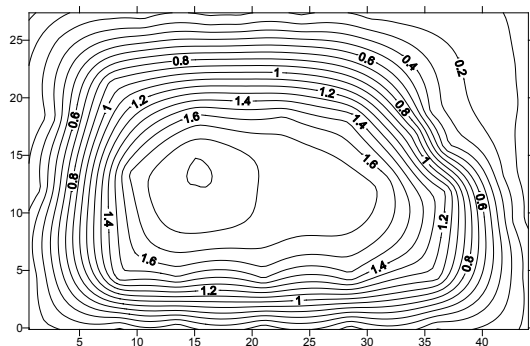


Figure 9. Equal settlement curves for the 6th phase, considering the second iteration calculation (in centimeters).

In fact, it can be observed in the 6th phase that from the fixed support condition to the first analysis with spring supports (from figure 7 to figure 8) 26 out of 43 columns presented loading differences higher than 5%.

In the same 6th phase, if one starts the analysis with the first estimation of spring supports to the second one (from figure 8 to

figure 9) only 3 out of 43 columns presented loading differences higher than 5%. From the second estimation of spring supports to the third (from figure 9 to figure 10) only 2 out of 43 columns presented loading differences higher than 5%.

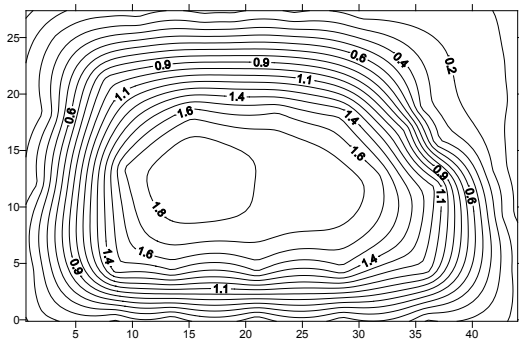


Figure 10. Equal settlement curves for the 6th phase, considering the third iteration calculation (in centimeters).

It can be concluded that the successive iteration analysis are much laborious and do not attain much different values, beyond the first one, when the soil structure analysis is considered. The settlement equalization in a plan view is changed from figure 7 (fixed support) to figure 8 (spring support, first estimation). However, for the remaining calculation, from figure 8 (spring support, first estimation) to figure 9 (spring support, second estimation) and from figure 9 (spring support, second estimation) to figure 10 (spring support, third estimation) no sensible difference has been observed in loading redistribution or settlement equalization.

In the following analysis the equal settlement curves predicted and measured have been compared in order to better infer the compressibility of the soil mass, the capability of the Aoki Lopes (1975) Method to properly estimate the settlement variations and the structural and soil model to reproduce the settlement distribution. For the 6th phase the measured settlements are shown in figure 11 and the predicted settlements in figure 12. As long as the measurements started after the beginning of the construction, the calculated settlement corresponding to the period before instrumentation has been subtracted from the calculated values.

Figures 11 and 12 present a very similar aspect, with greater settlements, of the order of

1 cm, at the central part of the construction, especially for those columns founded on shallow foundations. The columns founded on deep steel piles, mostly situated at the periphery of the site, presented much lower settlement values.

The similarity observed in the settlement values indicates the adequacy of the compressibility of the sandy soil mass, already observed by Conde de Freitas et al. (2012) in distinct case histories. The applied correlation for estimation of the elastic soil moduli from N60, proposed by Conde de Freitas (2012), has been found to be very promising. The similarity in the settlement behavior pattern indicates the adequacy of the numerical model to reproduce the soil x structure interaction.

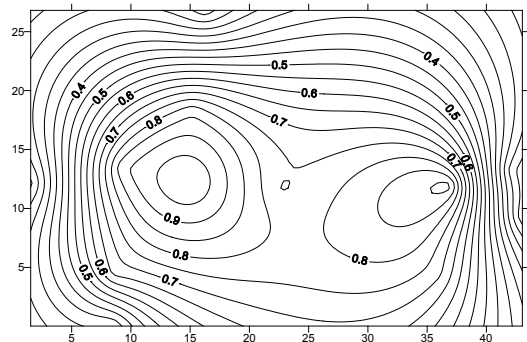


Figure 11. Equal settlement curves for the 6th phase, considering the measured values (in centimeters).

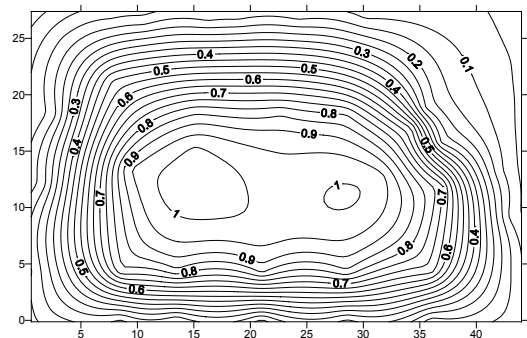


Figure 12. Equal settlement curves for the 6th phase, considering the predicted values (in centimeters).

4.2.2. Analysis considering concrete creep and shrinkage

The previous analysis calibrated the model in relation to the soil compressibility, with values properly selected for the rigidity of the soil springs. For the following analysis the soil

spring as determined after the third iteration has been adopted.

Six conditions have been estimated with time, the same analysis performed by Gonçalves (2010), with a FEM program including creep and shrinkage module, according to CEB-FIP (1993):

- (1) Structure resting on fixed supports;
- (2) Structure resting on elastic supports (like springs) and structural material without creep and shrinkage effects;
- (3) Structure resting on elastic supports (like springs) and structural material with creep effects;
- (4) Structure resting on elastic supports (like springs) and structural material with shrinkage effects;
- (5) Structure resting on elastic supports (like springs) and structural material with creep and shrinkage effects;
- (6) Structure resting on fixed supports and structural material with creep and shrinkage effects;

It should be emphasized that in these analyses the construction phases (1 to 6) have not been all considered, as long as the loadings increase and time intervals between different phases were very small. A phase has been included, previous to the start of the instrumentation, in order to consider the loadings related to the initial construction period (foundation, basement, embedded floor and floor of common use).

Figures 13 to 15 present the normal loads on the columns with time, for each of the six conditions enumerated before.

Figure 13 shows the curves for column M5 (see location in figure 1), in deep foundation. For this column, upper bound loading is related to the structure resting on elastic supports without consideration of creep and shrinkage effects. The lower bound loading is related to the structure resting on elastic supports with the effect of shrinkage alone. The effect of creep resulted in the reduction of the loading for this column, while the soil structure interaction resulted in the increase. The consideration of creep and shrinkage effects resulted in loadings ranging into these two limits: the elastic support and the elastic support with due consideration of creep and shrinkage effects

Figure 14 illustrates the curves for column M19 and figure 15 for column M22. The complete and detailed interpretation for the

loadings for each instrumented column is being analyzed and will be presented afterwards.

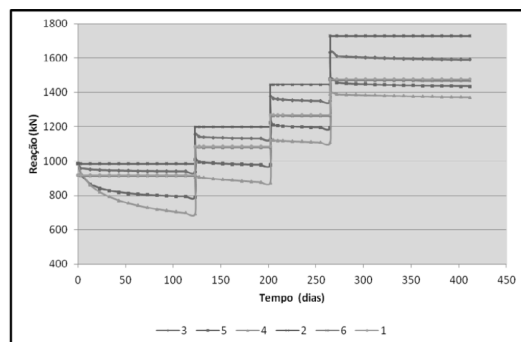


Figure 13. Normal loading with time for column M5, considering the 6 enumerated conditions.

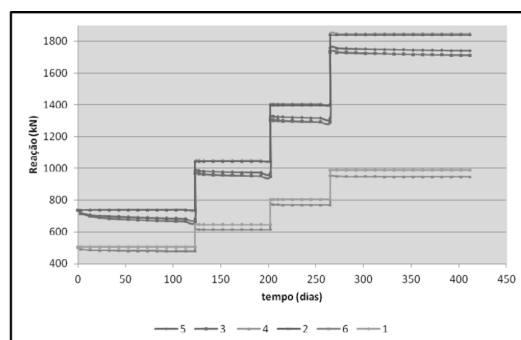


Figure 14. Normal loading with time for column M19, considering the 6 enumerated conditions.

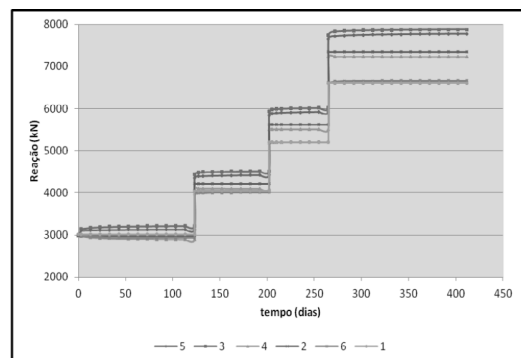


Figure 15. Normal loading with time for column M22, considering the 6 enumerated conditions.

Figure 16 presents the equal settlement curves after the 6th construction phase, considering the soil structure interaction and the effect of concrete creep and shrinkage. The equal settlement curves without consideration of concrete creep and shrinkage are reproduced

another time in figure 17, for ease of comparison, including the whole loading.

In relation to the settlements, the effect of creep and concrete shrinkage have not altered the distribution pattern for the instrumented case, not even its maximum value, as can be observed in figures 16 and 17.

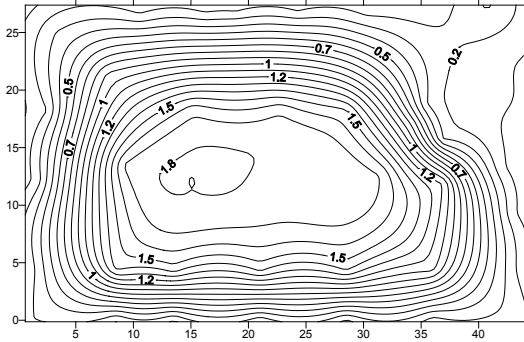


Figure 16. Equal settlement curves predicted for the 6th phase, with soil structure interaction with due consideration of creep and shrinkage of the concrete.

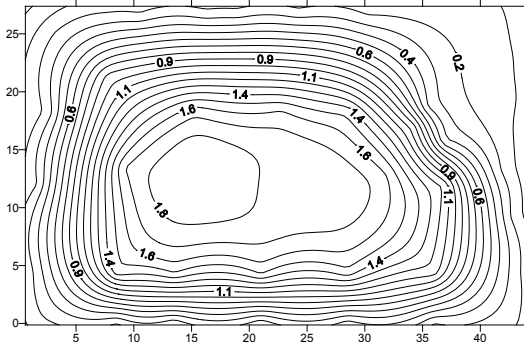
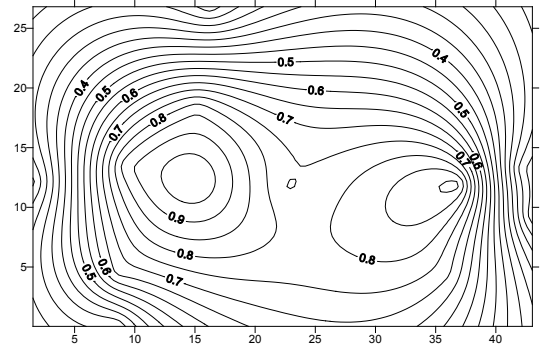


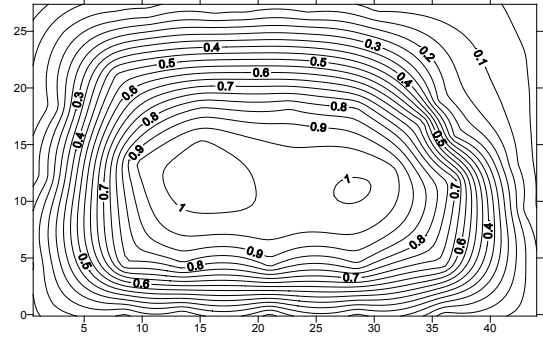
Figure 17. Equal settlement curves predicted for the 6th phase, with soil structure interaction without consideration of creep and shrinkage of the concrete.

It can be concluded that for the case in study the combined effect of creep and shrinkage of the concrete has not contributed to a better equalization of settlement when compared to the really most relevant effect of soil structure interaction.

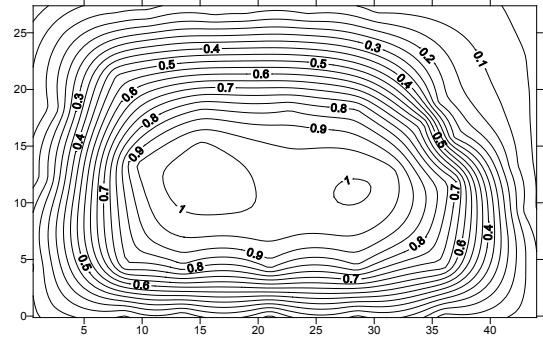
Figure 18 shows the equal settlement curves for the 6th construction phase, reducing for the estimated settlement the part that occurred before the beginning of the instrumentation. Figure 18 includes: (a) the measured settlements, (b) the settlements estimated considering soil structure interaction and (c) the settlements considering also the effects of creep and shrinkage of the concrete.



(a)



(b)



(c)

Figure 18. Equal settlement curves for the 6th construction phase: (a) measured, (b) estimated considering soil structure interaction and (c) estimated considering soil structure interaction and also the effect of creep and shrinkage of the concrete (in centimeter).

It can be observed that there has been a major consistency between the measured settlement curve and that including only the soil structure interaction. When the effect of creep and shrinkage of the concrete is also considered, a change can be observed in the central part of the curve, with a more clear equalization of the settlement.

It can be then concluded that the consideration of creep and shrinkage of the concrete indicates a prediction in the numerical analysis in excess of its real significance when compared to the sole effect of soil structure interaction, according to the instrumentation.

5. CONCLUSION

The article presented an analysis of a construction founded on a shallow foundation, in the central part, and a deep foundation in the periphery. An instrumentation has been performed with settlement and loading monitoring in some columns.

In view of the results the authors consider that for current foundation design, the analysis including soil structure interaction, recommended in the new version of the Brazilian Code, is justifiable for a sole iteration.

The consideration of creep and shrinkage of the concrete in the numerical analysis indicates a prediction in excess of its real significance when compared to the effect of soil structure interaction alone, according to the instrumentation.

6. ACKNOWLEDGEMENT

The authors would like to thanks very much to their colleague Christian Mattos Santana for his valuable help in the beginning of the instrumentation services.

7. REFERENCES

- Aoki, N. e Lopes, F.R. 1975. Estimating stresses and settlements due to deep foundations by the Theory of Elasticity, *Proceedings, 5th Pan American CSMFE*, Buenos Aires, Vol. 1, p. 377-386.
- Associação Brasileira de Normas Técnicas (2010) NBR6122: Projeto e Execução de Fundações, Rio de Janeiro.
- Barata, F. E. 1986. Recalques de edificios sobre fundações diretas em terrenos de compressibilidade rápida e com consideração da rigidez da estrutura. Tese de concurso para professor Titular do Departamento de Construção Civil do Setor de Geomecânica da EEUFRJ, Rio de Janeiro.
- CEB-FIP 1990. Comitê Euro-International du Beton, Model Code, Design Code, Thomas Telford.
- Chamecki, S. 1954. Consideração da Rigidez da Estrutura no Cálculo dos Recalques da Fundação, *Anais do I Congresso Brasileiro de Mecânica dos Solos*, Vol. 1, Porto Alegre, RS, p. 35-80.
- Conde de Freitas, A.; Pacheco, M. e Danziger, B.R. 2012. Estimating Young Module in Sands from the Normalized N60 Blow Count, *Soils and Rocks*, Vol. 35, N.1.
- Danziger, F. A. B.; Barata, F. E.; Santa Maria, P. E. L.; Danziger, B. R. e Crispel, F. A. 1997. Measurement of Settlements and Strains on Buildings from the Beginning of Construction, Vol. II, *Proc., XIV International Conference on Soil Mechanics and Foundation Engineering*, Hamburgo, pp. 787-788.
- Gonçalves, J.C. 2010. A Influência dos Recalques das Fundações no Comportamento de Edificações ao Longo do Tempo, Tese de Doutorado, Engenharia Civil, Universidade Federal do Rio de Janeiro, 301 p.
- Gusmão, A. D.; Gusmão Filho, J. A. 1994. Avaliação da Influência da Interação Solo-Estrutura em Edificações, *X Congresso Brasileiro de Mecânica dos Solos e Engenharia de Fundações*, Rio de Janeiro, RJ.
- Rosa, L.M.P. 2005. Interação Solo-Estrutura – Análise de um Caso de Obra Envolvendo Danos Estruturais, Dissertação de M.Sc., Faculdade de Engenharia Civil, Universidade Federal Fluminense, Niterói, RJ, 117p.
- Russo Neto, L. 2005. Interpretação de Deformação e Recalque na Fase de Montagem de Estrutura de Concreto com Fundações em Estaca Cravada, Tese de Doutorado em Geotecnia, Escola de Engenharia de São Carlos, Universidade de São Paulo, 279 p.

Beneficial and Detrimental Effects of Seismic Soil Structure Interaction (SSI) Analysis of High Rise Buildings

Emad Osman

Prof. Dr. of Geotechnical Engineering, El-Minia University, Egypt

Mohamed Abdelmonem

Assistant Lecturer , El Minya High Institute of Engineering and Technology, Egypt

ABSTRACT: In this research, Soil Structure Interaction is studied for high rise buildings under seismic excitations using the direct method. A high rise building of 13 storeys is selected for this study with different base conditions; fixed base and flexible base. In addition, different soil types are selected in case of flexible base condition to study the effect of subsoil class on the building response. Both beneficial and detrimental effects are demonstrated through the different soil types and input seismic motions. Nonlinear SSI analyses were performed using PLAXIS 2D 2012 suite to achieve precise results. Through the conducted analyses, it appeared that fixed base model can capture the real behaviour of buildings construed in relatively stiff soils however this assumption becomes inadequate for other soil types.

1. INTRODUCTION

It has been known, before, that seismic soil structure interaction has a beneficial effect on structures. Because of considering soil-structure interaction, the structure becomes more flexible and thus, increasing the natural period of the structure compared with the corresponding rigidly supported structure. Moreover, considering the SSI effect increases the effective damping ratio of the system. The smooth idealization of design spectrum suggests smaller seismic response with the increased natural periods and effective damping ratio due to SSI. Therefore, most of structural engineers neglected the effect of soil structure interaction in the seismic analysis of buildings.

This myth about SSI was acceptable for many years till Mylonakis and Gazetas (Mylonakis & Gazetas, 2000a) studied this phenomenon using precise numerical analyses. They have reported that the increase in natural period of structure due to SSI is not always beneficial as suggested by the simplified design spectrums. Soft soil sediments can significantly elongate the period of seismic waves and the increase in the natural period of the structure may lead to the resonance with the long period ground vibration. Additionally, their study showed that ductility demand can significantly increase with the

increase in the natural period of the structure due to SSI effect. The permanent deformation and failure of soil may further aggravate the seismic response of the structure.

2. ADOPTION OF THE DIRECT METHOD FOR SOIL STRUCTURE INTERACTION ANALYSIS

Many methods are available nowadays to solve the problem of soil structure interaction. In this paper, the direct method is selected to carry out the soil structure interaction analyses. This technique has a good level of precision in which the soil and structure are modelled together in a single step accounting for both inertial and kinematic interaction. Inertial interaction develops in structure due to own vibrations give rise to base shear and base moment, which in turn cause displacements of the foundation relative to free field. Kinematic interaction develops due to presence of stiff foundation elements on or in soil cause foundation motion to deviate from free field motions. As illustrated in Figure 1, the earthquake ground motions are specified at the base and the resulting response of the interacting system computed from the following equation of motion (Kramer, 1994).

$$[M]\{\ddot{u}\} + [C]\{\dot{u}\} + [K]\{u\} = [M]\{m\}\ddot{u}_g \quad (1)$$

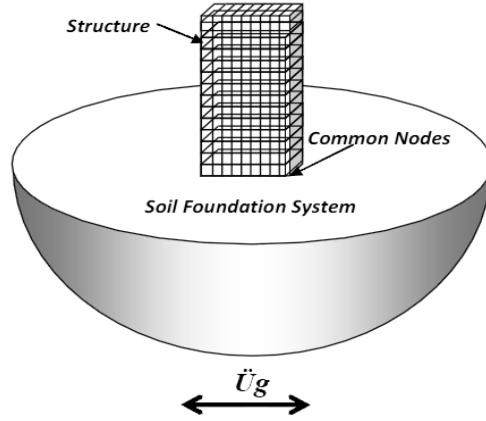


Figure 1. Modelling the entire problem and determining the response to free-field motion in a single step

3. GEOTECHNICAL AND STRUCTURAL CHARACTERISTICS OF THE SOIL-STRUCTURE MODELS

3.1 Geotechnical characteristics of the selected soil mediums

Three soil mediums are considered to represent soil types B, C and D according to the Egyptian Code of Practice (ECP-201, 2008). These utilized soils in this study are Gravel, Dense Sand and Loose Sand with shear wave velocities 600 m/sec, 280 m/sec and 170 m/sec respectively. These soils are modelled by the Hardening Soil model with small strain stiffness (HS-small) which is available in the PLAXIS 2D suite. This soil model can take into account nonlinear soil behaviour during cyclic loadings such as machine vibrations or earthquakes. Additionally this soil model counts the soil hysteretic damping in addition to stress and strain dependency of stiffness so that the dynamic shear modulus is a variable value and depends on the strain level. As a result the dynamic shear modulus is decreased with soil shear strain increments according to nonlinear S-shaped stiffness reduction curve as shown in Figure 2 (Atkinson & Sallfors (1991)).

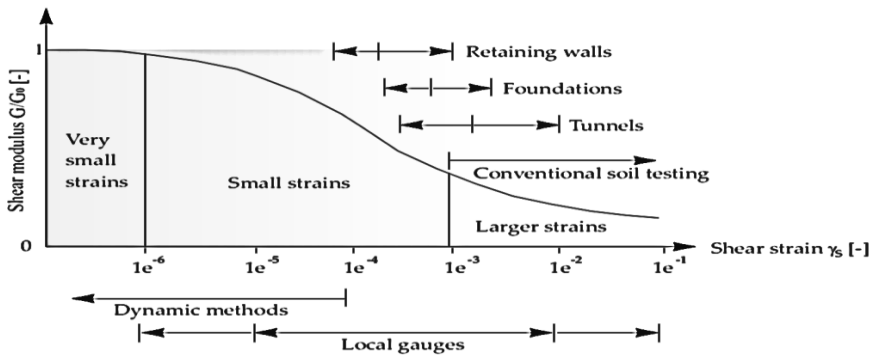


Figure 2. Characteristic stiffness-strain behaviour of soil with typical strain ranges for laboratory tests and structures (Atkinson & Sallfors (1991))

In Table 1, the selected soil models parameters are presented according to different correlations proposed by different Soil Mechanics handbooks (Robert, 1995), Egyptian Code of Practice for Foundation and Soil Mechanics (ECP-202, 2007) and the PLAXIS 2D manual (PLAXIS BV., 2012).

Table 1. Summarized HS-small input parameters of the utilized soils

Soil Classification	Soil B	Soil C	Soil D
Soil Type	Gravel	Dense Sand	Loose Sand
γ kN/m ³	20	18	15
V_S m/s	600	280	170
V_P m/s	1106	461	295
ν	0.26	0.29	0.333
C kN/m ²	0	0	0
ϕ^0	39.6	38	30
ψ^0	9.6	8	0
E_{oed}^{ref} kN/m ²	200000	39000	8000
E_{50}^{ref} kN/m ²	200000	39000	8000
E_{ur}^{ref} kN/m ²	600000	117000	32000
ν_{ur}	0.25	0.25	0.25
G_0^{ref} kN/m ²	735000	140000	45000

The soil stiffness parameters of the HS-small soil model which presented in Triaxial stiffness, Oedometric stiffness, Un-loading/Reloading stiffness and Small-Strain stiffness are shown in Figure 3.

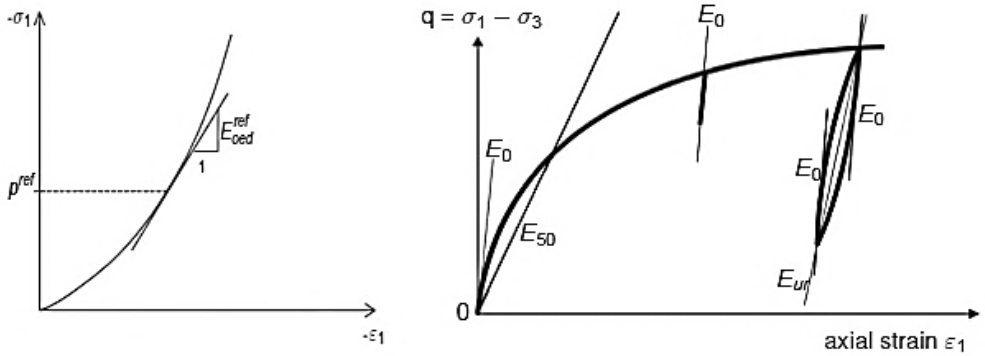


Figure 3. Definition of E_{oed}^{ref} in oedometer test results and stiffness parameters E_{50}^{ref} , E_{ur}^{ref} and E_0^{ref} in the triaxial test (PLAXIS 2012 Manual)

The damping in the HS-Small model is generated due to the model nonlinear behaviour which leads to hysteretic damping in the soil and the generated damping ratio depends on the applied load amplitude and corresponding strain amplitudes which is increased nonlinearly with high strain levels (Brinkgreve, Kappert & Bonnier, 2007). Furthermore the HS-Small takes into account the soil plasticity and hardening behaviour which may generate plastic strains that affect the damping ratio.

3.2 Structural characteristics of the selected building

A typical high rise building with 13 storeys is selected for this study which represents the common type of high rise buildings in Egypt. The building is a moment resisting reinforced concrete frame which is resting on a raft foundation. The analysis and design procedures were conducted according

to the specifications mentioned on The Egyptian Codes of Practice for Calculating Loads and Forces in Structural Elements (ECP-201, 2008) and ECP for Design of Reinforced Concrete Elements (ECP-203, 2007). The summarised dimensional properties of the building are demonstrated in Table 2.

Table 2. Geometrical characteristics of the selected buildings

Reference Name	Number of Storeys	Number of Bays	Storey Height (m)	Bay Width (m)	Total Height (m)
B13	13	3	4	7	52

3.3 Seismic motions characteristics

In this research study, different seismic motions were taken into consideration to investigate the seismic response of the selected high rise buildings constructed on different soil types. These motions are twelve ground motions chosen from different earthquakes having different magnitudes, brought from the Pacific Earthquake Engineering Research Centre (PEER), besides two artificial seismic waves were extracted from the MIDAS GTS software tutorial manual. Brief description of these motions is provided in Table 3 and 4.

Table 3. The selected input ground motions characteristics

NGA Sequence Numbers	Source	Event	Year	M_w
30_C05DWN	PEER	Parkfield	1966	6.19
33_TMB205	PEER	Parkfield	1966	6.19
57_ORR021	PEER	San Fernando	1971	6.61
139_DAY-LN	PEER	Tabas, Iran	1978	7.35
161_H-AEP045	PEER	Imperial Valley-06	1979	6.53
587_A-MAT083	PEER	New Zealand-02	1987	6.6
1107_KAK090	PEER	Kobe, Japan	1995	6.9
1148_ARC000	PEER	Kocaeli, Turkey	1999	7.51
1193_CHY024-E	PEER	Chi-Chi, Taiwan	1999	7.62
1612_1058-E	PEER	Duzce, Turkey	1999	7.14
1619_MDR000	PEER	Duzce, Turkey	1999	7.14
225a	USGS	Upland	1990	5.4

Table 4. The selected Artificial Seismic waves characteristics

Wave Name	Source	Peak Ground Acceleration (PGA)	Arias Intensity (AI)	Specific Energy Density (SED)
Art. Wave 1	MIDAS	0.15g	0.626 m/sec	484.28 cm ² /sec
Art. Wave 2	MIDAS	0.15g	0.302 m/sec	283.69 cm ² /sec

3.4 The Soil-Structure Interaction model configurations

The soil-structure model comprises plate elements to model structural elements, two dimensional plane strain grid elements to model soil medium (15-Node soil element), fixed Boundaries to model the bed rock, viscous boundaries to avoid reflective waves produced by soil lateral boundaries, and interface elements to simulate frictional contact and probable slip due to seismic excitation. The PLAXIS 2D software was used to investigate the buildings response in both fixed and flexible base conditions to address the SSI effects on the structure response. Figure 4 shows the soil structure interaction model configuration in PLAXIS 2D Suite.

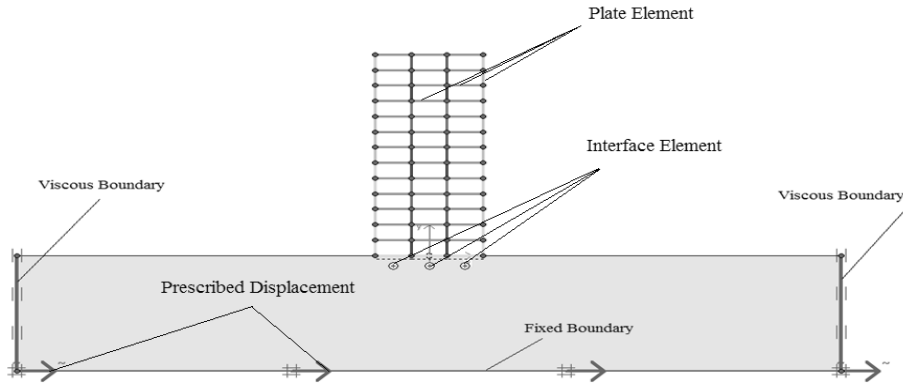


Figure 4. The soil-structure system of building B13 in Plaxis 2D

4. RESULTS AND DISCUSSION

According to the Egyptian code of practice (EGP-201 2008), Soil B can be used to represent the very dense sand and gravel mixtures or soft to stiff rocks. Additionally, Soil B also has a large shear wave velocity value and much higher stiffness values. So that in this section a comparison between the fixed base model and the Soil B SSI model is presented to measure the studied buildings response in both cases to check if the fixed base model can be replaced with the Soil B SSI model or not.

The Imperial Valley 1979 earthquake is selected for this comparison in order to measure the effect of using Soil B SSI to represent the fixed base model. Figures 5 and 6 show the variation of the maximum building tip displacement and the building base shear in case of fixed base model and Soil B SSI model.

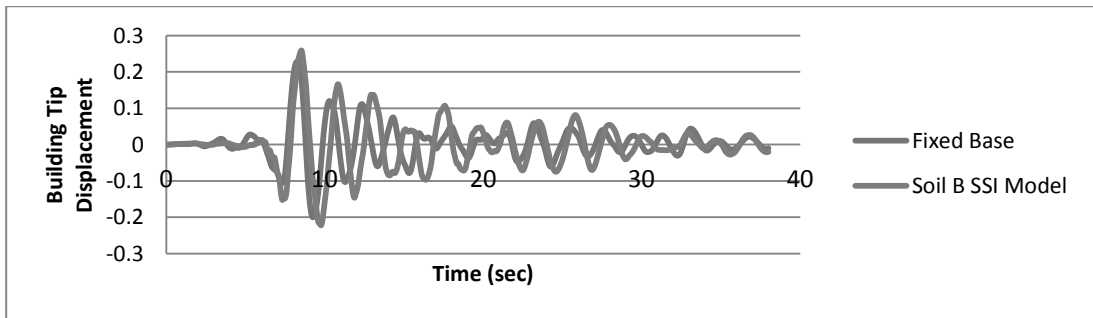


Figure 5. The B13 building tip displacement time history in different base conditions (Fixed vs. Soil B SSI model) under Imperial Valley 1979 earthquake

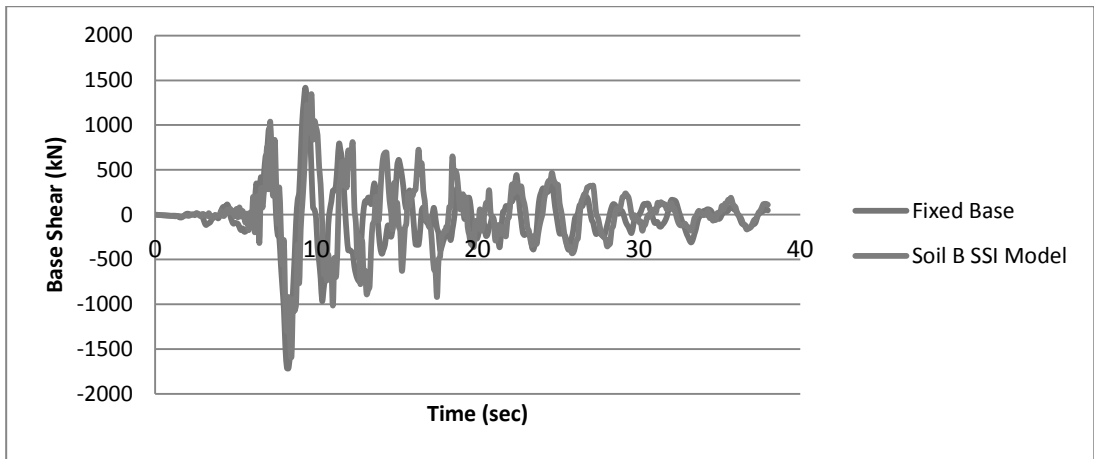


Figure 6. The B13 building base shear time history in different base conditions (Fixed vs. Soil B SSI model) under Imperial Valley 1979 earthquake

Through the previous figure, Small variations were recorded between the fixed base model and the flexible base model in case of Soil B. So that, Soil B SSI model is considered to represent the fixed base behaviour. In addition, Soil B SSI model is considered to be the reference model in our comparisons.

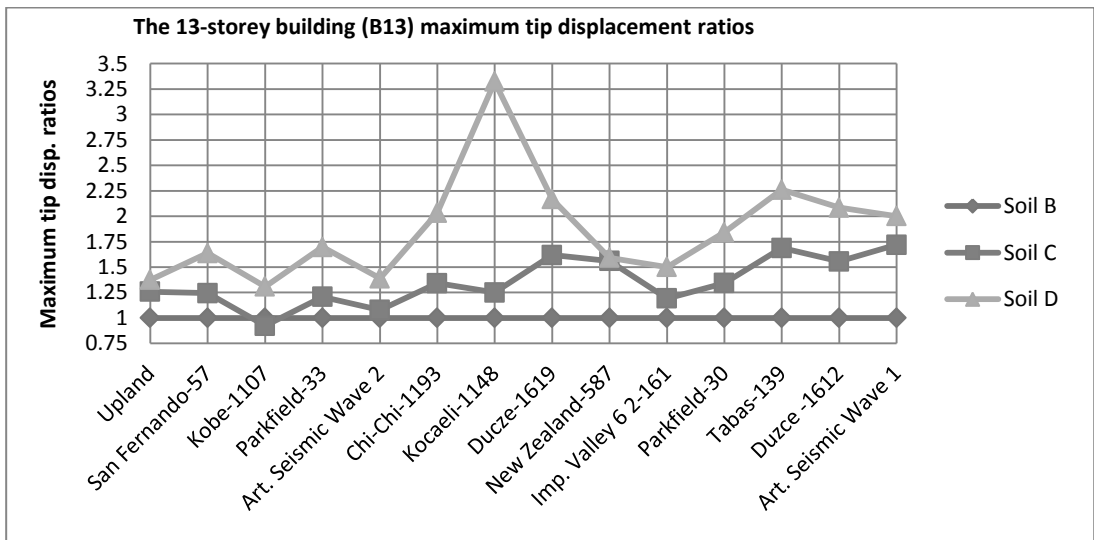


Figure 7. Maximum tip displacement ratios of building B13 under different seismic motions referenced to Soil B SSI model

The Soil Structure Interaction detrimental effect is very clear in Figure 7. The maximum building tip displacement values are magnified with all earthquakes for buildings rested on Soil C or Soil D. Also in Figure 8, the total building drift is increased with the weak soil (Loose Sand) which is appeared from the 1st storey till the last one. For Soil C SSI model, the building total drift is almost the same as the Soil B SSI model up to the 7th storey then it starts to deviate dramatically to be magnified by at least 1.5 times.

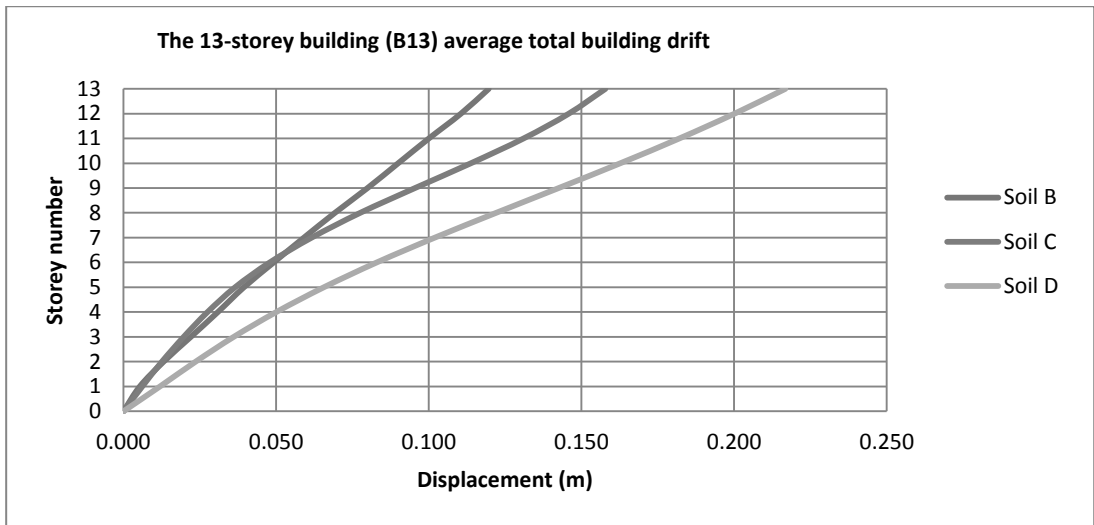


Figure 8. Average total building drift of building B13 for different soil types

Moreover, Figure 9 shows the average inter-storey drift ratios of Building B13 for different site conditions. Inter-storey drift ratios have double values for buildings rested on Soil D in comparison with the Soil B SSI model especially for the intermediate storeys (8th, 9th and 10th storeys). With buildings rested on Soil C the inter-storey drift ratios are being very critical starting from 7th storey to reach its maximum ratio of 1.85 % at storey number 10. It is noticeable that the total building drift curve and inter storey drift ratios of high rise buildings rested on Soil C are almost the same as those rested on Soil B till the 7th storey. However, dramatic increase arises from the 7th storey to the top of the building.

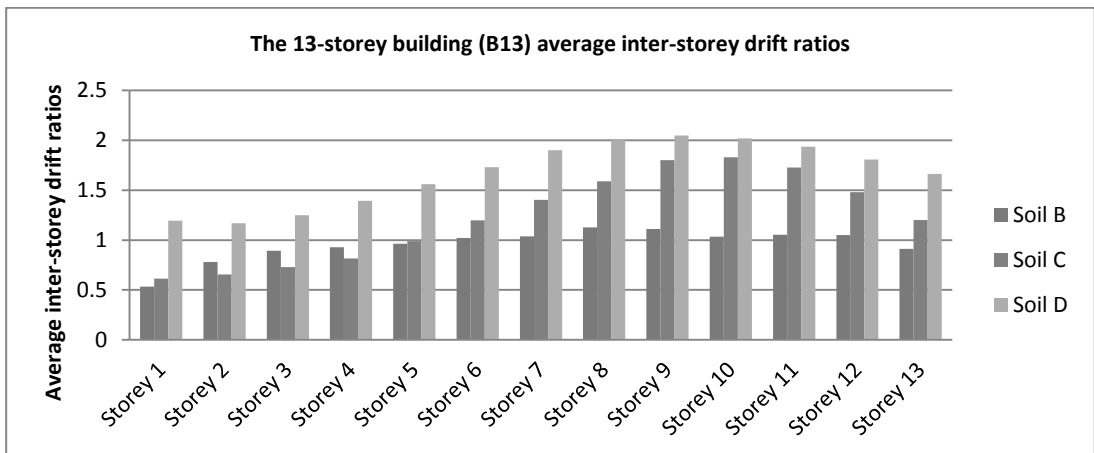


Figure 9: Average inter-storey drift of building B13 for different soil types referenced to Soil B SSI model

According to Figures 10 and 11, soil structure interaction analysis could estimate the base shear and moment of high rise buildings accurately in comparison with the fixed base model. The base flexibility affects the building both base shear and moment positively since they are decreased with buildings rested on medium and weak soils compared with the Soil B SSI model or fixed base model. That happened because of period elongation and higher damping values which they are generated from the

base flexibility conditions (SSI). This effect is typically known by the beneficial side of the SSI analyses.

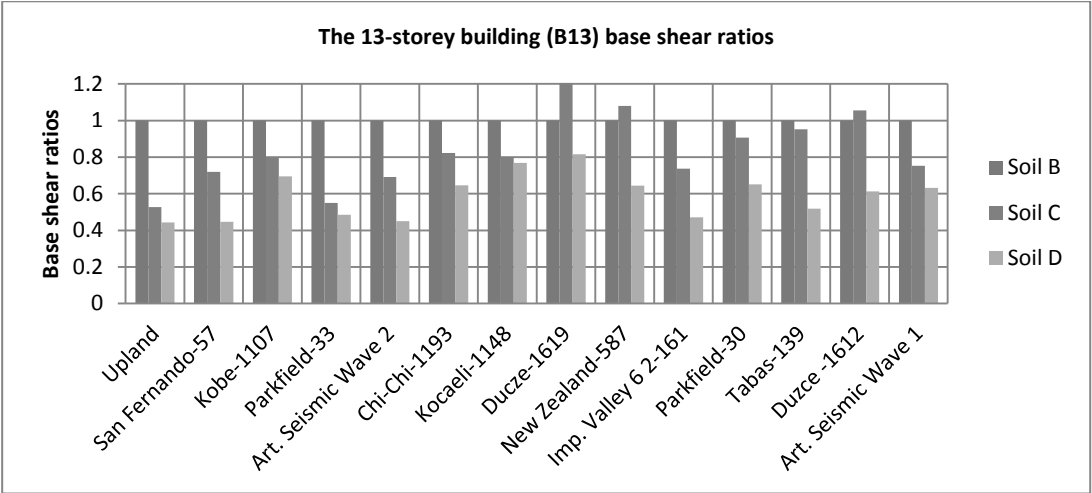


Figure 10. Base shear ratios of the building B13 for different soil types under the selected seismic motions referenced to Soil B SSI model

It is very noticeable that Soil D SSI model has a small base shear and moment ratios in comparison with Soil B and Soil C SSI models. These ratios vary from 40 % to 80 %. For Soil C SSI model, the base shear and moment reduction ratios were found to be from 50 % to 80 %, however these ratios were increased to be a little larger than the Soil B SSI model with Duzce-1619 and New Zealand-587 ground motions. These slight increments do not affect the average reduction ratios.

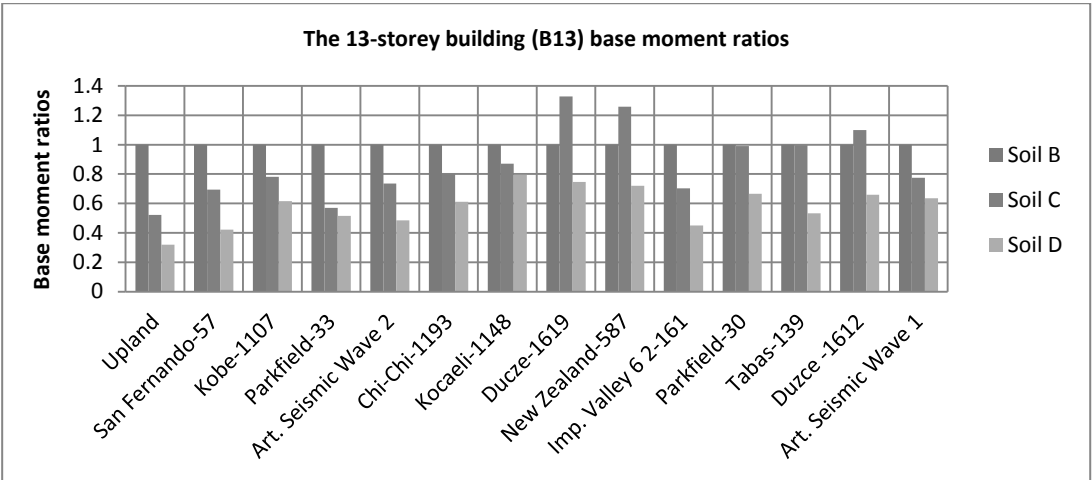


Figure 11. Base moment ratios of the building B13 for different soil types under the selected seismic motions referenced to Soil B SSI model

Finally, it is confirmed that the building base shear and moments are reduced with medium and weak soils in comparison with stiff soils or the fixed base model which is widely known by beneficial effect.

5. CONCLUSIONS

The Nonlinear soil structure interaction analyses were carried out using the PLAXIS 2D 2012 Suite. The analysis accounts for soil nonlinearity, stress and strain dependency of stiffness and hysteretic damping. Three different soil types as well as fourteen different seismic motions are considered to identify the SSI effects on high rise building response. According to the previous results both base shear and moment of the buildings modelled with Soil C and Soil D are always less than the base shear of the Building rested on Soil B or when modelled as fixed-base. This behaviour is considered as a beneficial effect however, it is also a sign of a detrimental effect since it is always accompanied by increasing in maximum building tip displacement, total building drift besides magnification in inter-storey drift ratios. Additionally, it is not necessary to carryout SSI analysis for buildings rested on Soil type B although it is a must for those rested on either medium or weak soils. These detrimental effects can turn the building from its life safe to near collapse or total collapse which affects the whole performance level of high rise buildings.

6. REFERENCES

- Atkinson J. H., Sallfors G. 1991. Experimental determination of soil properties. *Proc. 10th ECSMFE*, 3, 915–956.
- Brinkgreve et al. 2007. Hysteretic damping in a small-strain stiffness model. *Numerical Models in Geomechanics*, NUMOG X, 737–742.
- ECP-201 Committee (2008). Egyptian Codes of Practice for Calculating Loads and Forces in Structural Elements
- ECP-202 Committee (2007). Egyptian Code of Practice for Foundation and Soil Mechanics
- ECP-203 Committee (2007). Egyptian Code of Practice for Design of Reinforced Concrete Elements
- Kramer S. L. 1996 Geotechnical Earthquake Engineering. *Prentice Hall, Inc.*, Upper Saddle River, New Jersey
- Mylonakis, G., & Gazetas, G. 2000a. Seismic soil structure interaction: Beneficial or Detrimental?. *Journal of Earthquake Engineering*, Vol. 4(3), pp. 277-301.
- Plaxis BV 2012. Plaxis version 2012 material models manual, the Netherlands
- Benz T. 2006. Small-Strain Stiffness of Soils and its Numerical Consequences, Ph.D. Thesis, *Universität Stuttgart*
- Robert W. B. 1995. Practical Foundation Engineering Handbook, Second Edition, *McGraw-Hill Book Company*, New York

Comparative analysis of piled foundation design of a highrise building in Bangkok subsoils

N. Phienwej & K. Amornfa
Asian Institute of Technology, Thailand

W. Cheang
Plaxis AsiaPac, Singapore

ABSTRACT: A comparative analysis of a deep foundation of a highrise building in Bangkok subsoil shows that adoption of the piled raft design concept could result in a significant cost saving of the foundation work. When the raft was placed in the first stiff clay layer, the load share by piles was reduced to 77% from 100% generally considered in the traditional practice. The required number of piles could be significantly reduced without scarifying stability of the foundation and settlement requirement for the building. The 3D FEM analysis yielded a more realistic settlement condition of raft and load distribution of piles than the conventional plate on spring analysis owing to its direct and complete consideration of soil structure interaction.

1. INTRODUCTION

Bangkok City has witnessed a rapid increase in number of tall buildings for the past two decades. Because the city is situated in a deltaic plain underlain by a series of thick subsoil layers, the buildings need to be founded on piles. Traditionally, tall buildings in Bangkok require basements for car park spaces which are stipulated by law. Thus, the building foundations are commonly placed at depths of 10-20 m below the ground surface; and often a large number of piles at close spacing are utilized to carry large building loads. Traditionally, the foundation design follows the “piled foundation” concept in which all loads are solely carried by piles. In the past this design concept was justified when considering the effect of land subsidence caused by deep well pumping for ground water supply (Phienwej et al. 2006). However, at present the phenomenon of land subsidence in inner city areas has essentially ceased, thus it is advisable to include the load carrying capacity of the stiff soil underneath raft foundation in sharing building load.

Nowadays, the “piled raft foundation” design concept has been increasingly advocated and adopted in design of tall buildings in many parts of the world (Randolph 1994; Yamashita et al. 1994; Kachzenbach et al. 2000; Poulos 2001; Tan et al. 2006) because it has a potential cost-saving and a better control of differential settlement of the building. With the advance in

numerical computation methodology and tools, the analysis of a piled raft foundation, that was once a complex undertaking and could not be simply adopted in design practice, becomes readily available.

2. CASE BUILDING FOR ANALYSIS

In order to explore application of the piled raft foundation design concept for high-rise buildings in Bangkok, a comparative study is made on a case study. The case is a completed high-rise building situated on the west bank of the Chao Phraya River in the prime business zone in Central Bangkok (Fig. 1). The building has 51 floors built in a small land area. Thus, the foundation was single raft on piles. The building and subsoil are shown in Fig. 2. The second sand layer where the pile tips are placed exists from depths of 54m to 69m.

The actual design of the foundation followed the common design practice in Bangkok. Piles were designed to take all building loads. The number of pile was determined by the conventional combined stress equation. The bending moment and shear force in the raft for structural design were determined using the plate on pile springs analysis. The total superstructure load of 796,890 kN acts on raft foundation and the column load distribution is shown in Fig. 3. A 3.5-m-thick concrete raft was supported by 110 1.8-m-diameter bored piles and 18 barrette piles (1.5m x 3m in size). Due to the high load, the

piles were crowded at spacing of 2.5D. In addition, the raft size needed to extend beyond the building footprint to accommodate the large number of piles. For factor of safety of 2.50 the ultimate capacity of the pile and barrette were 30,000 kN and 45,000 kN, respectively.



Figure 1. Case building

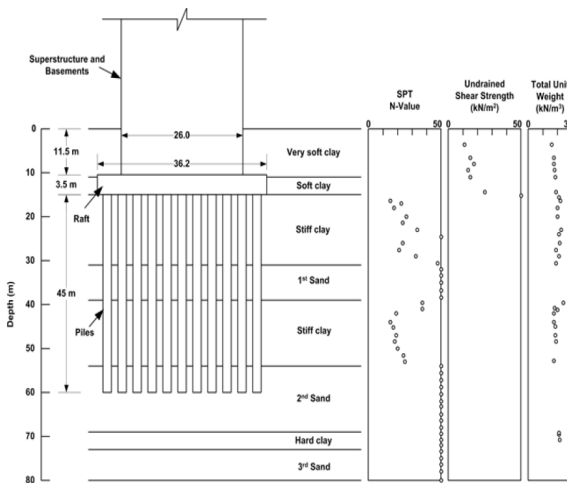


Figure 2. Soil profile and foundation

In the actual construction, the building was built with one floor basement. Thus the raft depth was actually placed in the soft clay layer.

Therefore, the adopted piled foundation concept for the actual design was reasonable. However for the purpose of a comparative study, two additional levels of basement were hypothetically included in analysis to have the raft reach the stiff clay layer at 15m depth. Thus the potential benefit of piled raft foundation design concept could be explored.

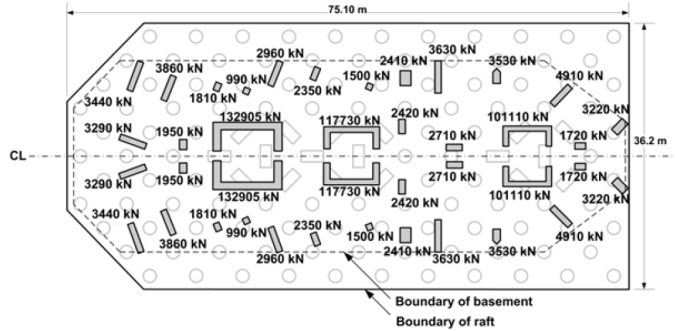


Figure 3. Layout of columns and piles

3. METHODS OF ANALYSIS

Four methods of analysis were considered in the comparative study.

Method 1 (M1): Combined stress analysis (Conventional method): Load distribution on piles was determined using the combined stress equation.

Method 2 (M2): Piled foundation by Plate on pile springs analysis: This method modeled the raft as thin plate elements and piles as a series of vertical springs using a structural finite element program, SAP2000.

Method 4 (M4): Piled raft foundation by Plate on both pile and soil springs analysis: This method was adapted from M2 by adding vertical soil springs at 3.1 m spacing. The stiffness of soil spring was 6.7×10^5 kN/m³.

Method 5 (M5): Piled raft foundation analysis by 3D FEM: The rigorous simulation of foundation was made by PLAXIS 3D Foundation. (Brinkgreve and Broere 2004). Soils and volumetric piles were modelled using 15-node wedge elements, altogether 14,574 elements (Fig. 4). The linear elasto-plastic Mohr-Coulomb soil model of PLAXIS was considered for all soil layers. A static load test result of a 1.65-m diameter bored pile was used to validate the adopted input values of soil properties. The 6-node triangular thin plate elements were used

to model the raft. Soils above the raft depth were idealized as a surcharge.

In this study, all column loads were modeled as point loads and only a half of foundation was modelled owing to the symmetrical shape of the foundation.

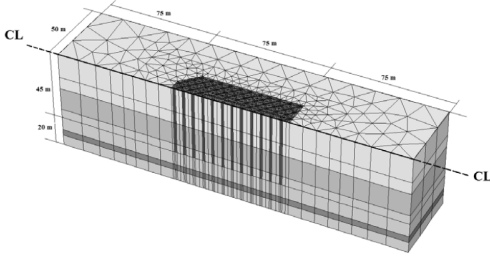


Figure 4. 3D FEM Mesh and elements

4. ANALYSIS RESULTS

4.1 Loads on piles

The comparative results of the analyses are summarized in Table 1. The piled raft foundation analyses by Method M4 and M5 give the load shared by piles of 85%. Load distributions on piles from various methods are shown in Figs 5a-d. The load distribution from M1 analysis is relatively uniform. This is expected because the method was the one used in making pile layout in the actual design. However, it is not the case for other three methods of analysis in which soil structure interaction is considered. The analyses give much higher pile load in areas surrounding the lift cores where the higher proportion of superstructure load is concentrated. Piles along the rim and at corner of the raft carry very small axial loads. In the case of the plate on spring methods (M2 & M4), the contrast in the pile load distribution underneath the raft is very pronounced. The plate on pile springs method (M2) yields the largest contrast among the three methods. In case of 3D FEM (M5), the contrast in pile load distribution is better than those given by the plate on spring methods, but it is still large. In term of factor of safety of individual pile in the raft, the calculated value for the most loaded pile based on the specified capacity is quite high for the conventional method (M1), i.e. F.S is about 4.05, while it is much lower for both the plate on springs methods (M2 & M4), i.e. F.S. = 1.95 and 2.25, respectively. The 3D FEM (M5) gives F.S. of 2.89 for the bored piles and 2.23 for barrette piles. It can be seen that the uniformly distribut-

ed pile load condition underneath the raft given by the conventional combined stress method, which is commonly adopted in the piled foundation design in Bangkok, is un-realistic for this case study.

Even though the stability of the whole pile group under the raft is satisfactory, the designed pile foundation in this case does not seem economical. When considering interaction effect among raft, pile and soil, some of the piles in this designed layout have to bear very high axial loads while others bear very small loads. There is big contrast in factor of safety of individual piles in the group. A better and more rational design would involve rearrangement of the pile layout as well as a change in amount of pile.

Table 1 Results of analyses

	M1	M2	M4	M5
% Load shared by piles	100	100	85	85
% Load shared by raft	0	0	15	15
Max load on Barrette pile, kN	11,042	40,212	35,457	20,214
Max load on Bored pile, kN	7,369	15,524	13,452	10,379
Average load on Barrette pile, kN	10,994	28,666	25,166	12,215
Average load on Bored pile, kN	7,325	4,541	3,898	5,750
Standard deviation (SD) of load on Barrette pile, kN	31	8,421	7,791	4,757
Standard deviation (SD) of load on Bored pile, kN	27	3,558	3,041	2,057
Min FS on Barrette pile	4.08	1.12	1.27	2.23
Min FS on Bored pile	4.07	1.93	2.23	2.89
Max Positive Moment, kN-m	N.A.	36,155	35,684	50,620
Max Negative Moment, kN-m	N.A.	7,753	7,306	6,894
Max Settlement, mm	N.A.	9.1	8.3	37.2
Max Differential Settlement, mm	N.A.	9.4	8.6	34.9

*M1 = Piled foundation by Combined stress analysis

M2 = Piled foundation by Plate on pile springs method

M4 = Piled raft foundation by Plate on pile&soil springs method

M5 = Piled raft foundation by 3D FEM

4.2 Raft Settlement

Settlement profiles of the raft along longitudinal and traverse sections are shown Figs. 6a&b. Figure 7 shows raft settlement in deformed mesh of 3D FEM M5 analysis. The maximum settlement from the plate on springs methods (M2 & M4) are quite low (9.1 and 8.3mm) as compared to M5 method (37.2mm). Whereas the two plate on springs analysis methods (M2&M5) yield almost the same settlement characteristics (profile and magnitude), the 3D FEM analysis yield much larger settlement magnitude and differential settlement. However, if the layout of the pile underneath the raft were rearranged according to the true piled raft design concept, the settlement profile of the raft

could be made more uniform. In that case, the piles would not be placed in the uniformed pattern as they were actually made following the conventional design method.

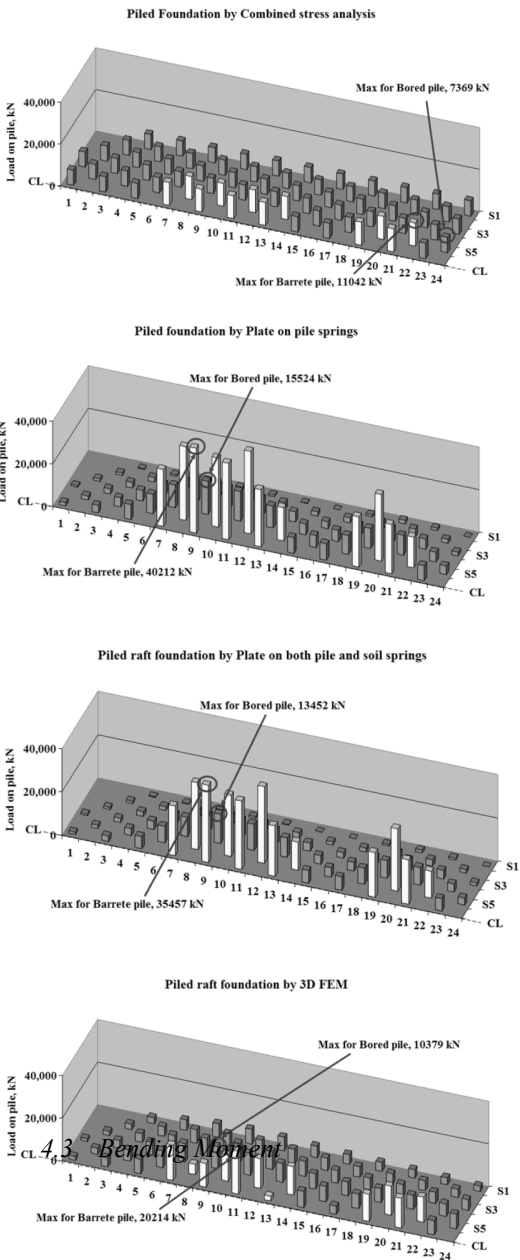


Figure 5. Pile load distributions from different methods of analysis

During the construction of building, settlement was monitored but it was not systematical-ly done. There were no time- or floor progress-

settlement records. It was merely reported at the end that the settlement was in the order of 20-30mm. Nonetheless, it can be seen that the two plate-on-spring analyses (M2 and M4) yielded smaller maximum settlement than the observed value. The rigorous 3-D FEM analysis shows the value that seems to be more reasonable.

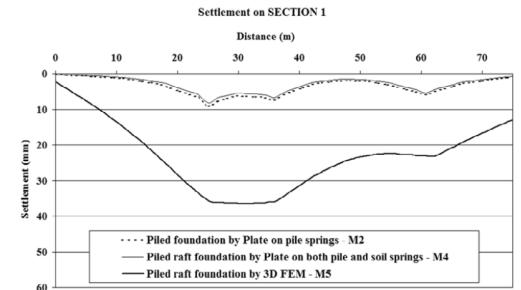


Figure 6a. Settlement profile in longitudinal direction

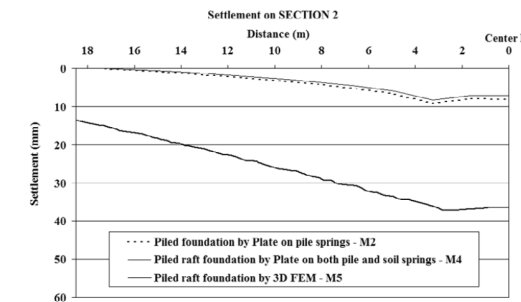


Figure 6b. Settlement profile in traverse direction

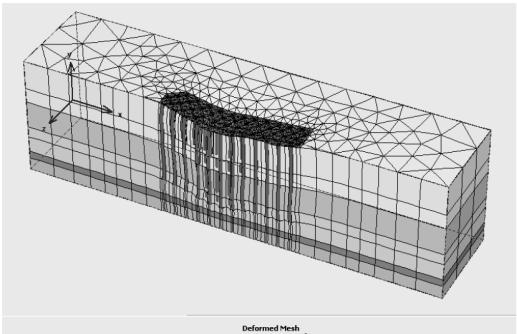


Figure 7. Settlement shown in deformed mesh of 3D FEM analysis

4.3 Bending moment

Bending moments in the raft from the three FEM methods are shown in Fig.8. The maximum positive moment from M5 method is about 1.4 times those given by M2 and M4, while the magnitudes of maximum negative moment from the three methods are not so different. The smaller magnitude of bending moment given by the plate on spring analyses was due to incomplete consideration of interaction effect between piles underneath the raft.

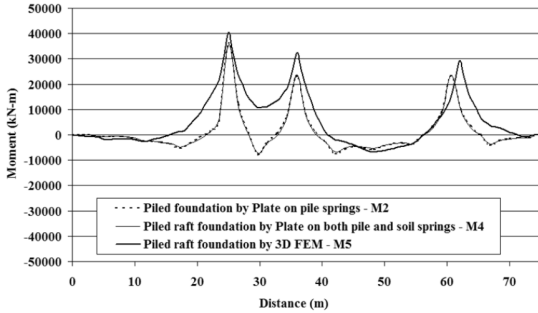


Figure 8. Bending moment in raft along longitudinal axis

5. ADJUSTED DESIGN

The results of piled raft analysis on the actual pile layout of the building indicate that a design improvement could have been made by adjusting pile layout and number. A simple case of adjustment, i.e. reducing number of pile and raft size, was considered in this study and the effect was assessed by aid of the 3D FEM analysis. Number of pile was reduced from 110 piles to 56 piles while number of barrette was not changed (Fig. 9). Along with it, the size of the raft was reduced accordingly.

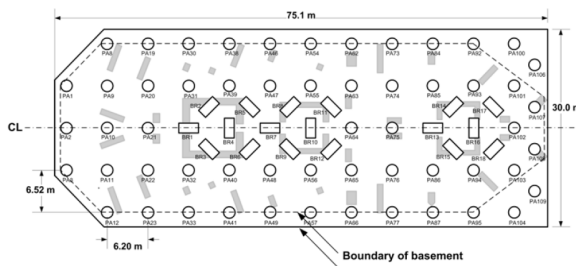


Figure 9. Pile layout in the adjusted design

5.1 Results of the adjustment

The results are compared with those of the initial design as summarized in Table 2. The load distribution on piles for the adjusted design case is shown in Fig. 10. As can be expected, the load shared by piles is reduced to 77%. The minimum safety factor of individual piles decreased from 2.23 and 2.89 to 2.08 and 2.11 for barrette and bored piles, respectively. The maximum settlement only slightly increases from 37.2 to 41.4mm (Fig. 11). The bending moment in the raft was practically unaffected (Fig. 12).

Table 2 Comparison between results of actual and adjusted design of the piled raft

	Actual design	Adjusted design
% Load shared by piles	85	77
% Load shared by raft	15	23
Max load on Barrette pile, kN	20,214	21,658
Max load on Bored pile, kN	10,379	14,205
Average load on Barrette pile, kN	12,215	14,250
Average load on Bored pile, kN	5,750	9,007
Std Dev) of load on Barrette pile, kN	4,757	5,123
Std Dev of load on Bored pile, kN	2,057	3,177
Min FS on Barrette pile	2.23	2.08
Min FS on Bored pile	2.89	2.11
Max Positive Moment, kN-m	50,620	47,675
Max Negative Moment, kN-m	6,894	4,980
Max Settlement, mm	37.2	41.4
Max Differential Settlement, mm	34.9	39.3

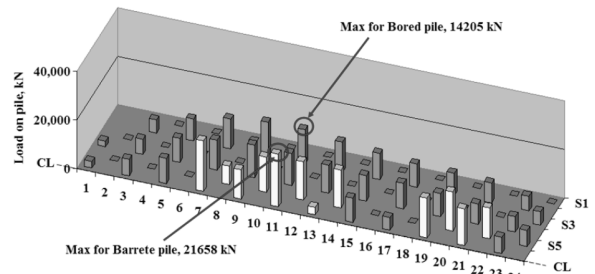


Figure 10 Pile load distribution of Adjusted Design-3D FEM analysis

Basically, it can be seen that by reducing the number of pile and raft size, very little changes can be seen from the raft settlement and bending moment in the raft. Such an effect of the adjustment can be made for purpose of the design improvement with the aid of the 3D

FEM analysis that fully considers soil structure interaction.

5.2 Cost savings

The construction cost of the building (including superstructure, basement and barrette piles excluding raft and bored piles) was 30.25 million US dollars. Cost of the project is significantly reduced by 1.2 million Baht or about 3.5% of the cost of the building. It can be said that by allowing the foundation raft of the building to reach the first Bangkok stiff clay layer, a significant reduction in the number of pile and raft size and thickness can be made without scarifying the safety and stability requirement on the pile capacity, raft settlement and stresses in the raft. In such the condition the stiff clay will share approximately 23% of the vertical superstructure load. The adjustment would result in a significant cost reduction. The adjustment and improvement in the foundation design requires an in-depth soil-structure interaction analysis made possible by the 3D finite element analysis.

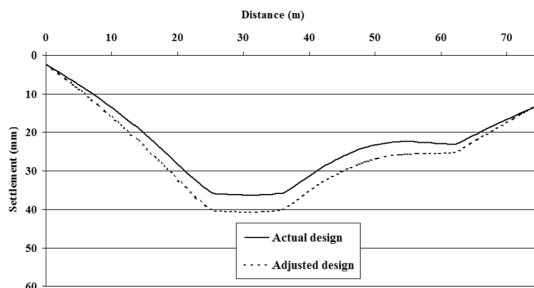


Figure 11. Raft settlement along longitudinal axis of initial and adjusted designs

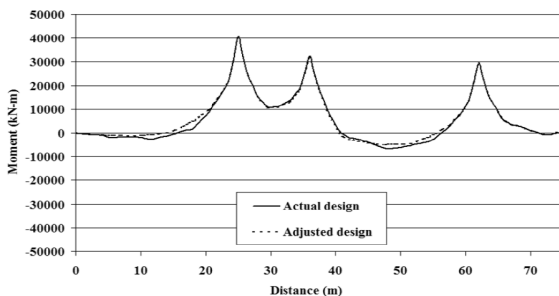


Figure 12. Bending moment in raft along longitudinal axis of initial and adjusted designs

6. CONCLUSIONS

By means of numerical analyses, a comparative study on the design of pile foundation for a highrise building in Bangkok subsoils indicated that the current practice of the design could be improved for valued engineering. If the piled raft designed concept was adopted for the case building, the load share by pile would be only 77% of the total building load when the raft was placed down to the first stiff clay layer. The 3D FEM analysis yielded larger magnitude of raft settlements and consequently larger bending moment than the FEM Plate on spring method of analysis. The latter also gives unrealistic results on load distribution among piles because it can not simulate interaction between piles.

7. REFERENCES

- Amornfa, K. (2012) *Analysis of piled raft foundations with their application to Bangkok subsoil condition*. Doctoral dissertation, Asian Institute of Technology, Bangkok
- Brinkgreve, R.B.J. and Broere, W. (2004). *PLAXIS 3D Foundation manual - version1*. Balkema Publishers, Netherlands.
- Katzenbach, R., Arslan, U. and Moormann, C. (2000). Piled raft foundation in Germany. In H. J.A. (Ed.), *Design applications of raft foundations*. London, Thomas Telford Ltd.
- Phienwej, N., Giao, P.H. and Nutalaya, P. (2006). Land subsidence in Bangkok, Thailand. *Engineering Geology*, 82: 187-201.
- Poulos, H. G. (2001). Piled raft foundations: design and application. *Geotechnique*, 51(No.2): 95-113.
- Randolph, M. F. (1994). Design methods for pile groups and piled raft. *Proc. of the 13th International Conference on Soil Mechanics and Foundation Engineering*, New Delhi:
- Tan, Y.C., Cheah, S.W. and Tahal, M. R. (2006). Methodology for design of piled raft for five-storey buildings on very soft clay. *Foundation analysis and design: innovative methods, Geotech. Spec. Publ. (ASCE)*, 153: 226-233.
- Yamashita, K., Kakurai, M. and Yamada, T. (1994). Investigation of a piled raft foundation on stiff clay. *Proc. of the 13th International Conference on Soil Mechanics and Foundation Engineering*, New Delhi: 543-546.

Foundation System Design for a Tall Structure on Mortar–Column-Improved Ground

Salah Sadek¹ and Samer Hasan²

¹Professor, Department of Civil & Environmental Engineering, American University of Beirut, P.O. Box 11-0236 Riad El-Solh 1107-2020; PH (961) 3850785; email: salah@aub.edu.lb. LGES-ISSMGE Lebanon Chapter

²Ph.D Candidate, Department of Civil & Environmental Engineering, American University of Beirut, P.O. Box 11-0236 Riad El-Solh 1107-2020; PH (961) 3933403, sah25@aub.edu.lb. LGES-ISSMGE Lebanon Chapter

A non-classical alternative was adopted for the foundation system of a thirty-storey building in Beirut, Lebanon. The subsurface strata included a thick layer of highly weathered marls and/marly limestone overlying the karstic limestone base stratum. Ground improvement by rigid inclusions/ mortar columns was proposed, analyzed, designed and successfully executed. 2D & 3D Finite element simulations were conducted to assess the degree of improvement, and then used to perform/finalize the design of the foundation system. The paper discusses the conducted analyses & presents some parametric studies & recommendations.

1. INTRODUCTION & BACKGROUND

The reconstruction of Beirut after the war, has presented geotechnical engineers with increasingly complex challenges, some related to high rise buildings in historic urban environments. Given the great awareness re. value engineering, innovative foundation solutions are being proposed and implemented that target cost effectiveness, practicality, safety and redundancy. This paper addresses the foundation system design of a high rise building in the heart of the heavily urbanized downtown of Beirut. The project consists of three towers of 18, 30 and 32 storeys set on a 7580 m² lot. The towers have several basements requiring 12 -18 m of excavation from the existing grade levels so that the foundation level is at an elevation of – 2m Mean Sea Level (MSL). The footprint for the medium length tower, and the service loads are shown in Figure 1.

Deep foundations were proposed for one of the towers (the tallest), while a ground improvement option using mortar piles was adopted for the other two towers. Noting that the rigid inclusion improvement system has been mostly used for soft deposits (ASIRI 2012 among others), this paper discusses the successful implementation of this technique to a Hard Soil/Soft Rock substratum. The substratum characterization is presented followed by the methodology for ground improvement. Finally the verification analyses are discussed.

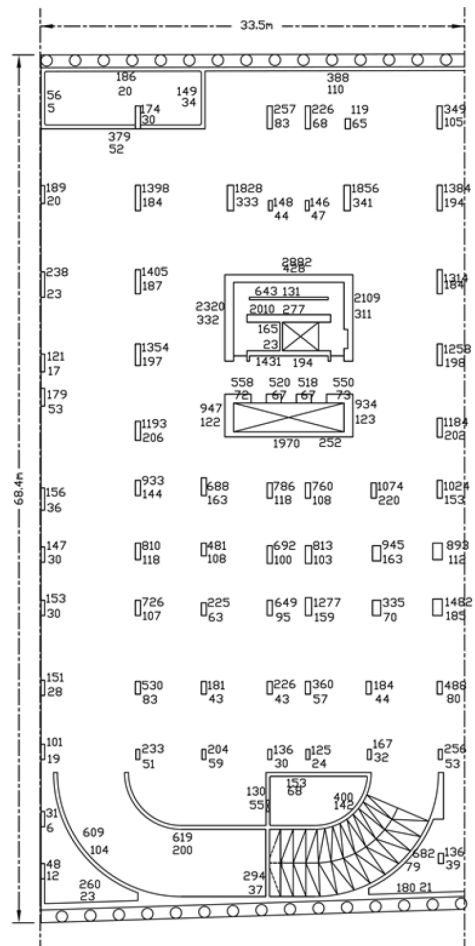


Figure 1: Tower footprint & Loads in tons

2. SUBSTRATUM CHARACTERIZATION

A thorough site investigation campaign was conducted for the site comprising boreholes, laboratory testing and pressuremeter tests. The prevalent strata beneath - 2 m MSL (foundation level) consist of:

- Unit 1: Highly weathered karstic Limestone with cavities, till elevation -22 MSL.
- Unit 2: Dolomitic Limestone of better quality extending well beyond depths of interest.

The unconfined compressive strength results (UCS) and RQD profile (Figures 2 & 3) show the same formation prevailing above and below the foundation level, but with considerable RQD improvement after ~ 20m below the foundation level. The zone above elevation - 22m MSL has been subjected to high levels of weathering and karstification, thus necessitating the delineation of the sub-surface into two units. The UCS plot also shows the variability of the soft rock stratum with an average UCS value ~ 40 MPa.

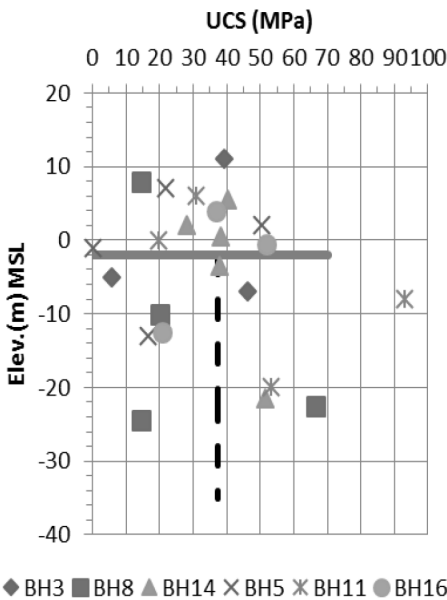


Figure 2. UCS Values

The Menard modulus results showed a large variation from 16 MPa to 387 MPa in Unit 1, reflecting the large degree of weathering and karstification, with higher values below -17.5 m MSL. The characteristic value for Unit 1 was ~ 87 MPa, while a prudent value of ~ 260 MPa was considered for Unit 2.

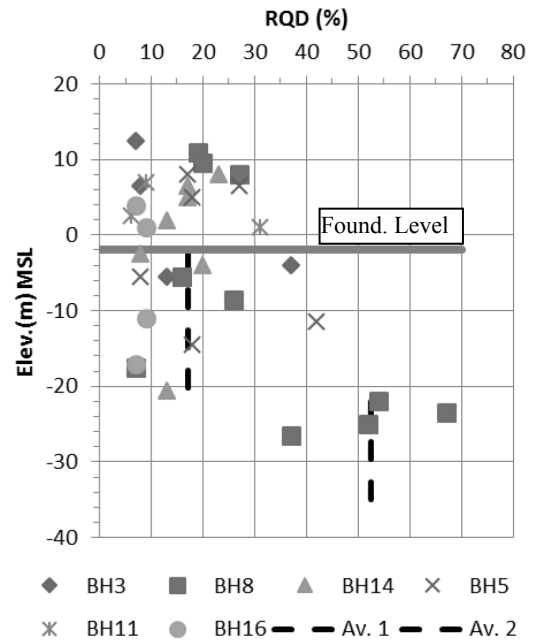


Figure 3. RQD Profile

The adopted mechanical characteristics considering the site investigation results were the following (effective stress parameters):

Table 1. Idealized Units Mechanical Characteristics

Rock Unit	E, MPa	ν	c, kPa	ϕ , deg
Unit 1	150	0.2	40	30
Unit 2	400	0.2	75	30

3. FOUNDATION SYSTEM

3.1. Methodology

The methodology adopted for the foundation system design considered identifying the concerns for every option, and weighing them in reference to cost and practicality. The classical options to consider first were the two extremes: raft foundation on one end, and drilled cast – in – place shafts on the other. The discussion below presents the advantages and concerns of each alternative

3.2. Raft Foundation

The simple raft solution is considered first given that is the most practical and cost effective option. Clearly, the main concern associated with this option is the potential excessive

settlement. Another equally important concern is the karstification, and potential presence of cavities. Thus, a cavity probing campaign needs to be conducted adding to the cost, with little effect in filling the cavities beyond the probe hole due to the nature of the material.

The excessive settlement concern was confirmed by a settlement estimation trial that yielded ~7 cm. Although such a value may be acceptable for certain structures, the structural design team for this project required a maximum total value within 5 cm and strict differential settlement and distortion requirements. Moreover, the presence of large cavities close to the raft elevation would render this option as risky even if settlements were tolerable.

3.3. Piles

The classical foundation piles option would have reduced the settlements at considerable cost. Moreover, it is the authors' opinion that an intermediate option between the two extremes could be sought, especially that the bearing material is not soft/weak and could/should be utilized in resisting part of the applied load.

3.4. Ground Improvement Using Mortar Piles

After identifying the two concerns, a solution that targets them both at a reasonable cost appears viable, especially if this option was also cost effective thus satisfying value engineering requirements. Ground improvement by rigid inclusions has been successfully implemented for soft soil deposits under different names (Controlled Modulus Columns, Vibro-Concrete Columns, deep mixed columns, etc...), resulting in the improvement of the load bearing characteristics of the reinforced ground.

For the current project, adding rigid inclusions would improve the load-bearing characteristics of Unit 1 because of the higher strength and stiffness properties of the inclusions than the surrounding soft rock matrix. Moreover, these inclusions/elements, if executed on a regular grid (on the order of 2m to 3m), will intercept and fill any large cavities that may be present in the first 20m below the foundation level.

The adopted option comprises 20 m long 60 cm diameter mortar piles, and is to be construed as an effective, practical and economical option which could meet the design requirements. It is a relatively easy to execute option with readily available local equipment and skill levels.

Moreover, such an alternative is in line with the growing trend to more sustainable designs by eliminating the reinforcing steel from the mortar pile elements.

It is worth noting that the proposed mortar piles are not directly in contact with the raft, and have a separation layer consisting of a blinding layer with a thickness of ~50 cm. This layer acts as a "softer" transfer cushion and prevents large concentrated stresses from affecting the top of the mortar piles. In addition, this layer facilitates the load transfer process and the subsequent arching instigated by the relative movement around the mortar piles (ASIRI 2012).

In what follows, the methodology and calculations which verify the adequacy of the proposed system are presented.

4. 2D FINITE ELEMENT ANALYSIS

The proposed system requires a three dimensional analysis to capture the prominent interactions between the raft, the separation layer, and the mortar pile elements. Albeit the 3D nature, and knowing that 2D analysis tools are much simpler and more readily available; two simplified approaches are presented herein for the analysis. The advantages and limitations of each approach are discussed, and then compared to a full 3D analysis.

The aim is to provide a raft foundation design that accounts for the serviceability criterion (settlement).

4.1. Unit Cell Idealization - Single Mortar Pile Model

A single mortar pile along with the surrounding in-situ material in its "tributary zone" is considered in axi-symmetric conditions and modeled using a Finite Element Analysis approach (ref. Figure 4 for schematic). The boundaries allow for vertical movement, while no lateral deformation is possible. This model is considered representative for a loaded area in the middle of the raft (away from the edges). This statement is supported by the fact that the mortar pile grid is uniform, and the spacing is relatively close and is comparable to the raft thickness.

This model would be useful for the evaluation of the average resulting settlement after installing the mortar piles, and is expected to result in an upper bound settlement value (as

the model boundary conditions allow for free movement in the vertical direction). An equivalent vertical subgrade modulus could thus be evaluated. However, this model lacks the possibility of determining the differential settlements, and does not account for the flexural rigidity of the raft in affecting the applied pressures.

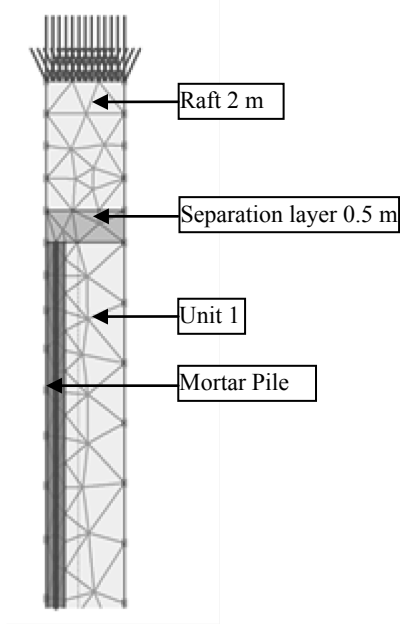


Figure 4. Single Mortar Pile Model

4.2. Idealized Axi-symmetric Model

In this model, a more elaborate idealization of the whole system is conducted, allowing for a better consideration of the spacing and stiffness effects of the mortar piles on the behavior. The model is also an axi-symmetric one, with the piles smeared into concentric “thin cylindrical shells” with suitable “smeared” stiffness values depending on the respective location of each mortar pile row, and the number of mortar piles present on each circle perimeter. The clarification is schematically shown in Figure 5 below.

The limitations of this model are related to the three dimensional load transfer mechanism around the mortar pile elements that cannot be captured by the 2D idealization. This may also lead to an under-estimation of the differential settlement.

It is obvious that to be able to “smear” the mortar pile elements in concentric shells, a

certain grid needs to be present (a polar one being more suitable than a rectangular grid). But, if the mortar pile elements are not laid in a grid, such an approach would not be suitable.

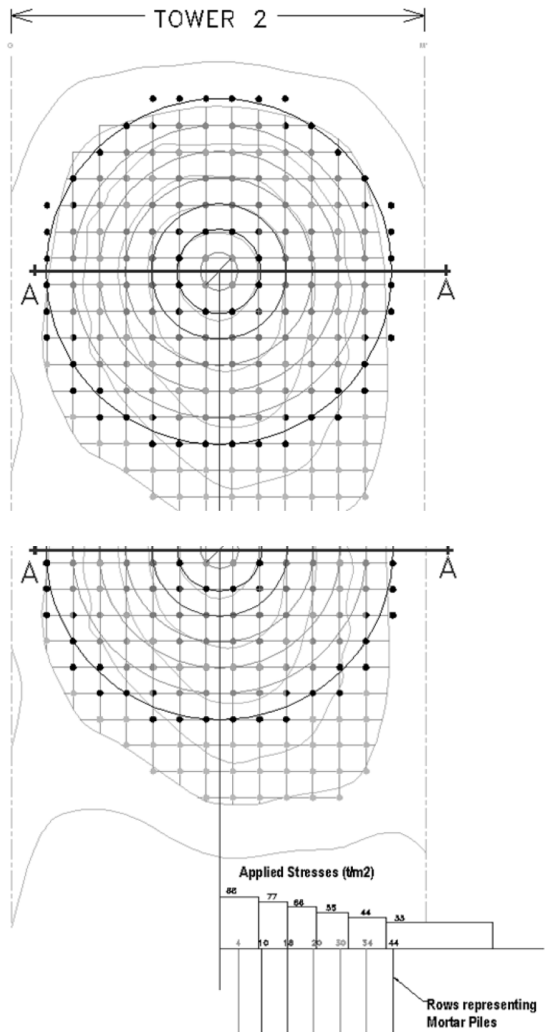


Figure 5. Idealized Axi-Symmetrical Model

In this case, a full 3D analysis is inevitable. It is worth noting that this model also does not consider the raft flexural rigidity in affecting the contact pressures beneath the raft. To overcome this limitation, the bearing pressures were determined from a regular Winkler type analysis using a preliminary subgrade modulus value bearing in mind that the contact pressure distribution is less sensitive to the subgrade modulus value than the settlements. The determined contact

pressures are then used as surcharge loads in this model. The resulting settlement shadings are presented in Figure 6 for a 2.5 m rectangular grid. Clearly, this model has the advantage of estimating the differential settlement, especially that the differential settlement value is crucial for the superstructure.

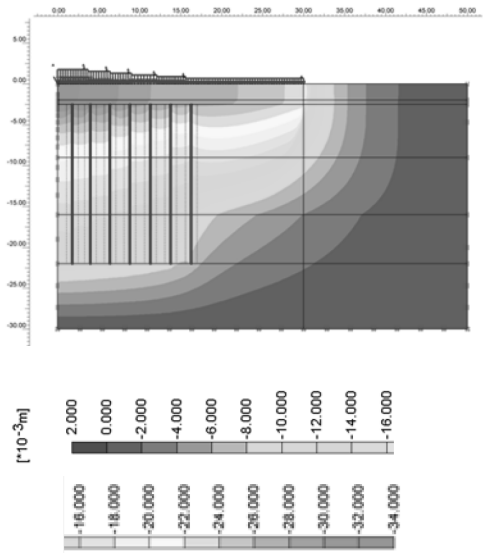


Figure 6. Vertical Settlement Shadings – 2D Axi-Symmetric Model – 2.5 m Spacing

Figure 7 shows the vertical settlements along a section underneath the raft (from the middle till the edge) with and without mortar piles. The results are also compared to those of the unit cell idealization; a remarkable agreement is noticed with the unit cell idealization result being an upper bound value as expected.

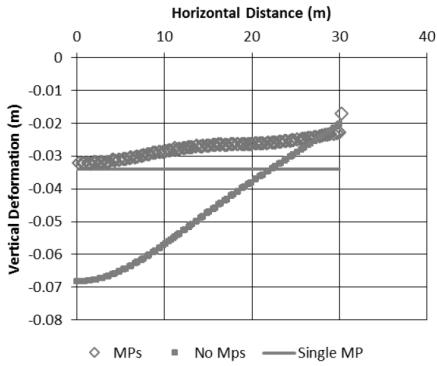


Figure 7. Vertical Settlement – 2D Axi-Symmetric Model – 2.5 m Spacing

5. 3D FINITE ELEMENT ANALYSIS

A full 3D elasto-plastic finite element analysis was conducted for the 2.5 m rectangular grid case.

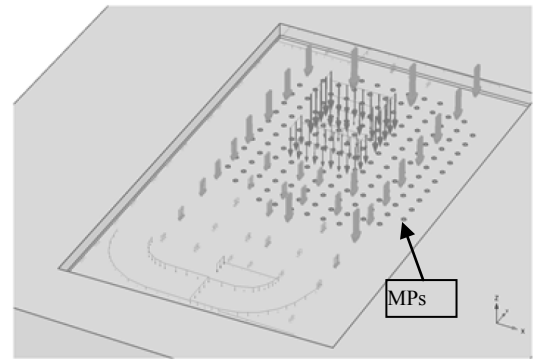


Figure 8. Mortar Pile Layout in 3D Model

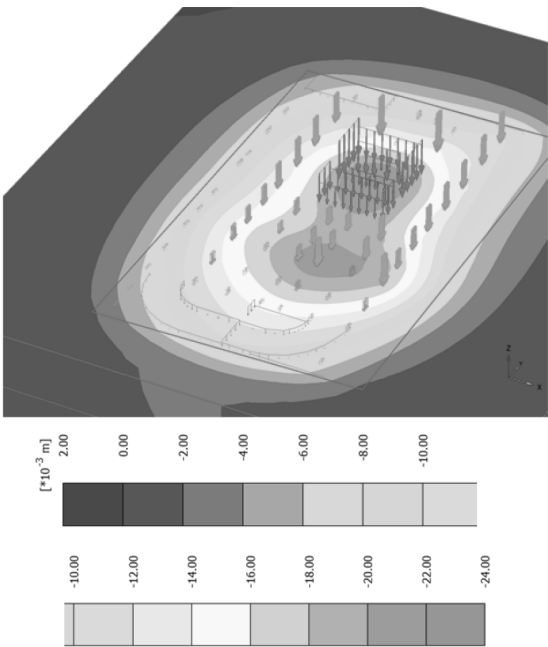


Figure 9. 3D FEM – 2.5 m Grid - Settlements

The maximum settlement resulting in the 3D analysis was very close to that of the 2D case, ~ 2.3 cm. Referring to Section A-A in Figure 5 above, a comparison is conducted between the 2D and 3D analyses and presented in Figure 10. The comparison clearly reveals that the 2D analysis is acceptable and conservative regarding the maximum settlement value, rather the

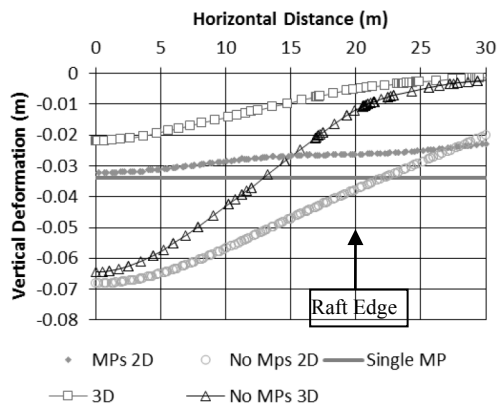


Figure 10. 3D vs 3D FEM Comparison – 2.5 m Rectangular Grid

level of distortion and differential settlements are under-estimated. The 3D analysis resulted in a larger differential settlement, and ~ 3 x the distortion value estimated by the 2D analysis ($\sim 1/1100$ as compared to $\sim 1/3300$ for the 2D case, though still acceptable).

6. PARAMETRIC STUDY

The sensitivity of the settlements and contact stresses is evaluated at Section A-A for two cases for the blinding layer with the same thickness (50 cm). The first is the adopted case with fairly representative parameters, while the other is for a compacted granular bed parameters. The original and reduced properties for the separation layer are:

- $E' = 1000 \text{ MPa}$, $c' = 100 \text{ kPa}$, $\phi' = 30^\circ$
- $E' = 50 \text{ MPa}$, $c' = 25 \text{ kPa}$, $\phi' = 35^\circ$.

Reduction in the mechanical characteristics resulted in increased settlements, and “milder” stress pikes at the mortar pile locations (Figures 11 & 12). It is also noticed that tensile stresses could develop when the separation layer modulus increases. Nevertheless, the increased settlements remained tolerable (within 5 cm) possibly due to the small thickness of the separation layer (50 cm) despite the significant variation in the stiffness. This clearly delimits the role of the separation layer and the advantages of using a “softer cushion” to prevent large stress concentrations, but too low moduli would result in increased settlements originating from the compression of this layer.

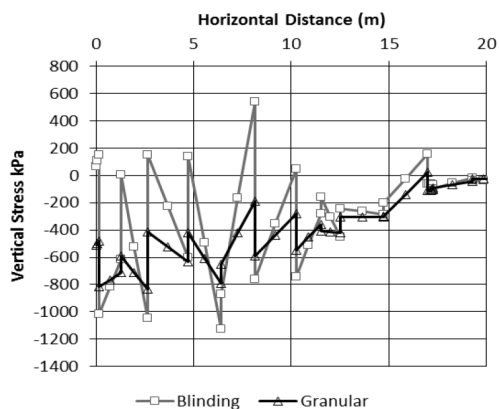


Figure 11. Vertical Stress Distribution along Section A-A – Effect of Separation Layer Parameters

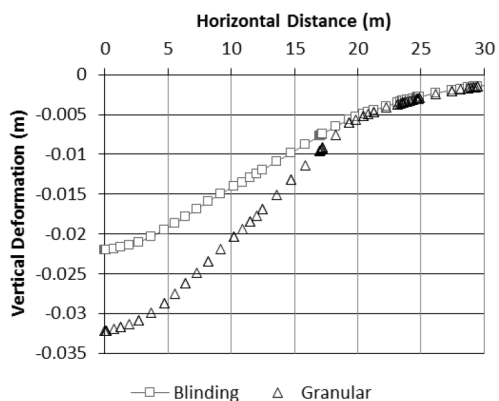


Figure 12. Settlement Distribution along Section A-A – Effect of Separation Layer Parameters

7. MODULUS OF SUBGRADE REACTION

The vertical modulus of subgrade reaction remains a key parameter that is extensively used for the analysis of raft foundations. It is also the main parameter requested by the structural design team. Despite the fact that the 3D FEM tools can determine the different straining actions within the raft, thus allowing for the structural design and dimensioning, the structural design teams still prefer to have the subgrade modulus value so that they can structurally analyze the raft considering the different load combinations already defined for their analysis for the super-structure. This necessitates estimation of the subgrade modulus (either one value underneath the raft, or with a practical zonation). In what follows, a comparison is presented between the full 3D and unit cell averaged

modulus of subgrade reaction values. Due to the uniform grid adopted, a single value is estimated, and compared with that inferred from the unit cell model.

The subgrade modulus value from the 3D FEM case is determined along two lines, one in-between the mortar piles “3D”, and another passing through them “3D @ MP”. The results are plotted in Figure 13. It is noticed that the average subgrade modulus value in-between the mortar piles is lower than that of the unit cell model, while that at the mortar piles is larger, so that the arithmetic average between the “3D” & “3D @ MP” values is reasonably close to that inferred from the unit cell model.

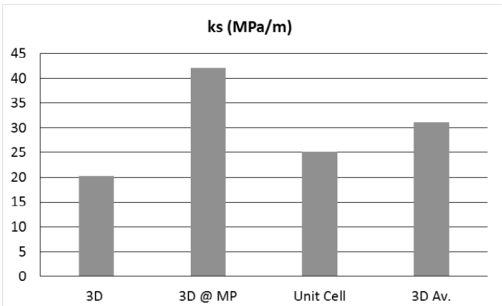


Figure 13. Average Vertical Modulus of Subgrade Reaction – 3D vs Unit Cell Comparison

These results do not apply to the raft edges as other parameters would have effects such as the out-rigger distance for the raft beyond the columns, layout of loading, and presence of the overburden because of the excavation.

8. OPTIMIZED MORTAR PILE LAYOUT

The advent of sophisticated 3D numerical tools allows for a more optimized design and specifically a more refined layout for the mortar piles. It should be noted that the idealized axis-symmetric approach discussed in section 4.2 would not have been possible without the “uniformity” of the grid, be it a rectangular, or a more suitable polar one. In what follows, a “non-uniform” grid is considered in the 3D analysis where the mortar piles target the relatively high settlement zones, and act effectively as settlement reducers (Figure 14).

The resulting settlement shadings are shown in Figure 15 below, with a maximum value of 2.7 cm.

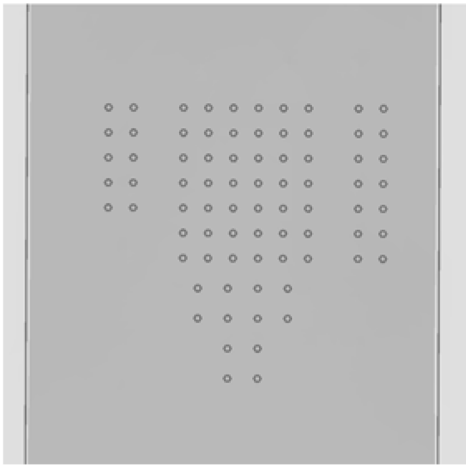


Figure 14. Non-Uniform Layout of the Mortar Piles

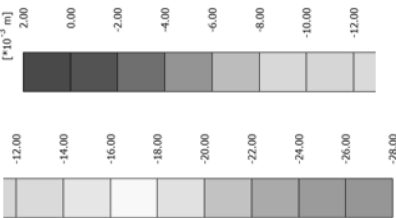
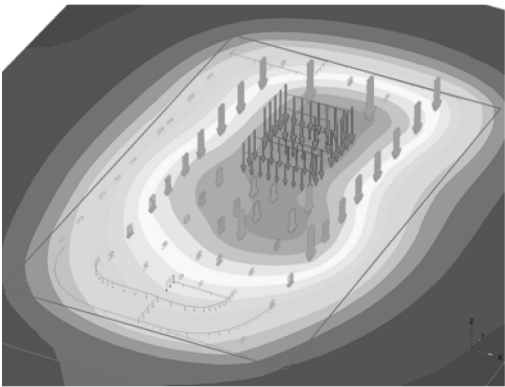


Figure 15. Settlement Shadings for Non-Uniform Layout of the Mortar Piles

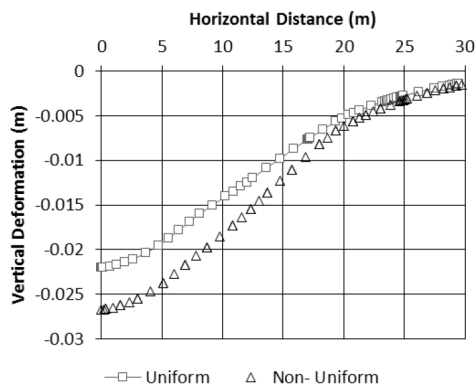


Figure 16. Settlement at Sec. A-A, Uniform vs Non-Uniform Layout of the Mortar Piles

It is noticed from Figure 15 that the differential settlement along the larger dimension were reduced, however, negligible difference was noticed in the transversal direction (Figure 16 along Section A-A). Being a negligible difference, the distortion value is still acceptable, and thus, further refinement is possible using the 3D complete model approach. The savings in terms of mortar column numbers and execution time gained are considerable.

9. CONCLUSION & RECOMMENDATIONS

The use of mortar piles as settlement reducing elements in an application involving a foundation solution for a tower on relatively stiff strata presenting weak/karstified/soft horizons at/ near foundation level is presented. The methodologies available for analyzing/designing such solutions range from the relatively simple to the very complex. These methods are presented in the context of the example case. Their results and limitations are discussed. The benefits of deploying 3D analysis tools were highlighted particularly in reference to accuracy, but more importantly the possibility of adopting non-symmetrical, more targeted layouts for the mortar columns. The equivalent subgrade moduli as would be requested by Structural Engineers were discussed and a critical comparison made between the analysis approaches adopted.

Foundation Engineers have access to tools which should allow them to take bolder and more value conscious solutions into consideration on a case-specific basis.

10. REFERENCES

- Baguelin, F, Jézéquel, J.F, Shields, D.H. 1978. *The Pressuremeter and Foundation Engineering*. Clausthal: Trans Tech Publications.
- Brinkgreve, R, Engin, E, Swolfs, W.M. 2013. *PLAXIS 3D Manual*. Delft: Plaxis BV.
- IREX. 2012. *Recommandations Pour la Conception, la Dimensionnement, l'exécution, et la Contrôle de l'amélioration des Sols de fondation par Inclusions Rigides*. Paris: Press des Ponts

Soil, Foundation, and Superstructure Interactions of Two-Bay by Two-Bay Frames with Isolated Footings on Sand

Hany F. Shehata

Teaching Assistance, El-Shorouk Academy, Cairo, 11511, Egypt, hanyfarouk808@gmail.com

ABSTRACT: In current design practice, some structural engineers disregard the settlement of the supporting ground by representing the foundations as hinged supports, while the other engineers are trying to consider the soil structure interaction using spring support. The stiffness of the spring is calculated by the geotechnical engineer using the allowable bearing pressure of the soil and the corresponding settlement. This way neglects the superstructure rigidity that is not known during the work period of the geotechnical engineers. The main purpose of this paper is to qualify this way of design by qualifying the effect of the superstructure rigidity on the contact stress and the settlement and suggest a new advanced procedure. It is proved that, the superstructure rigidity affects the average contact stress and the settlement, which affects the corresponding differential settlements. These were done because the redistribution of columns loads due to the structural rigidity. This redistribution should affect the spring stiffness and it is not taken into consideration in the recent design practice. Therefore, it is much preferable to follow the suggested design procedure that consider the superstructure rigidity with the underlying soil base in the geotechnical and structural design procedures.

1. INTRODUCTION

Usually, structural and geotechnical engineers are working totally separated from each other. The geotechnical engineers calculate the allowable soil pressure, the settlement, and the corresponding sub-grade reaction modulus disregarding the structure rigidity. Likewise, some of structural engineers are considering the soil interaction using the subgrade modulus that neglects the structure rigidity. He is using this modulus for large and small, concrete and steel buildings. While the other structural engineers are not considering the soil structure interaction and represent the foundations as hinged supports. Although this procedure of neglecting the coupling or interaction between soil and structure tends to simplify the mathematical analysis of the problem, it is, however, an oversimplification of reality. Structural analysis is one of the most important aspects in structural design, since it gives an idea about the performance of the structure under load. The foundation differential settlements influence the load transmitted from one column to another, and hence the redistribution of forces in the superstructure members. The magnitude of the load redistribution is depending on the rigidity of the elements of the superstructure as well as the magnitude of

the differential settlement. Foundation settlements may introduce new conditions of load distribution in the structure, causes distress and cracking of its elements, particularly those in the lower stories, generate appreciable change in footing reactions, and may even lead to stress reversal. An economic solution to a differential settlement problem can be found by suitable simulation of the superstructure during the foundation analyses. The common practice of obtaining foundation loads from structural analysis without allowance for foundation settlement may result in extra cost to avoid settlement cracking that might have been avoided had the effect of soil-structure interaction (SSI) been taken into account in determining the settlements. Rigorous analysis on the soil-foundation-frame interaction gained importance in the late 19th century, particularly after the advance of fast computers and numerical methods. Grasshoff (1957) analyzed a plane frame on a combined footing to bring out the effect of the rigidity of the super-structure and the condition of fixity of columns with the foundation on the bending moment and the contact pressure. King and Chandrasekaran (1974) formulated a finite element procedure and analyzed a plane frame supported on a combined footing in which the frame and the com-

bined footing were discretized into beam bending elements and the soil mass into plane rectangular elements. Sommer (1965) studied the effect of the rigidity of the super-structure in the analysis of the foundation in the homogeneous, isotropic and elastic half-space. He analyzed the structures with different degrees of rigidity including perfectly flexible and perfectly rigid cases. The foundation slab was divided into a number of parts and it was assumed that there was a rigid support at the center of each part. The reaction at these supports was determined from the superstructure loads using the laws of statics. Unit settlement was induced at each of these supports and the reaction forces were found at all these supports. These reaction forces due to unit settlement were then used to find out the reaction forces at the supports. He concluded that the bending moment in the slab increases with an increase in the rigidity of the foundation and decreases with an increase in the rigidity of the superstructure.

1.1. Super-Structure Rigidity Coefficient

The rigidity of structures is between perfectly flexible and perfectly rigid. Potts and Addenbrooke (1997) defined relative bending rigidity ρ^* of a building as:

$$\rho^* = \frac{EI}{E_s H^4} \dots\dots\dots (1)$$

Where H is the half width of the building in the plane of deformation and EI is the bending rigidity of the structure. Potts and Addenbrooke stated that two approaches could be taken to calculate the EI of a structure. The first approach employs the parallel axis theorem to define the structural rigidity about the neutral axis as shown in Equation 2:

$$(EI)_{Stiffstruct} = E \sum_1^n (I_{slab} + A_{slab} h^2) \dots\dots (2)$$

Where n is the number of stories. This can be considered to be an overestimate of the building rigidity as only a rigidly framed structure would approach such mode of deformation. An alternative method was used to obtain the bending rigidity by summing the independent EI values for each slab as shown in Equation 3. This implies that the walls and columns transfer the same deformed shape to each story.

$$(EI)_{Flexstruct} = E \sum_1^n I_{slab} \dots\dots\dots (3)$$

From equations 2 and 3, it is evident that stiff in-fill panels will have a significant effect on the bending rigidity. Currently the bending rigidity calculations are based on these simple assumptions. Researching the real bending rigidity of a variety of buildings will therefore be valuable to predict accurate differential settlement behavior of structures.

It is important to note that most studies of the interaction between a structure and the supporting soil assumed that the building frame is complete before loading commences. In practice, many loadings are applied progressively during construction (Brown and Yu, 1986). Heil (1969) and Goschy (1978) both analyzed progressive loading, but did not attempt to quantify the differences between the effect of progressive loading and the loading of the completed frame. Brown and Yu (1986) analyzed a 3-bay by 3-bay four stories steel framed office building with precast floor and roof slabs on a raft foundation resting on a deep homogeneous linear elastic soil mass. They also analyzed a plane frame representing the mid-span of the structure. Both the plane and space frames analysis showed that the effective rigidity for interaction purposes of a building that is loaded progressively during construction is about half the rigidity of the completed building.

2. MODELING

Analyses were carried out on a space frame (2-bay by 2-bay) foundation-soil system of one-story building by using PLAXIS-3D-2013. The plan of the isolated footings, dimensions, positions of columns, and columns dimensions are shown in Figure (1). It is assumed that, the isolated footings are placed on sand medium with 1-meter embedment depth. The sand properties are as follows: the soil unit weight is 18 kN/m³, modulus of elasticity is 20 MPa, and poisson's ratio is 0.30. The soil was modeled as Mohr-Coulomb soil model with shear parameters Φ of 33° and C of 1.0 kPa. The slab was flat without marginal beams. Slab has different thicknesses; 0.35, 0.5, 0.75, 1.0, 1.5, 2.0 meters. These thicknesses were modeled to represent different structural rigidities coefficients. The properties for all members of the concrete frame were as follows: unit weight of 25.0 kN/m³,

Young's modulus is 2.1×10^7 kPa, and Poisson's ratio is 0.15. Own weight of slab was neglected. Each thickness of the slab was loaded by different distributed loads; 10, 20, 30, 40, 50, and 60 kPa. Different loading levels were to provide the effect of loads increasing on the differential settlement and average contact stresses. Columns dimensions were 0.4×0.4 m² with 7-meter height. All footings have the same thickness of 1-meter. The dimensions of the inner footing were 4×4 -m², and the edge and corner footings were 3×3 -m² and 2×2 -m², respectively.

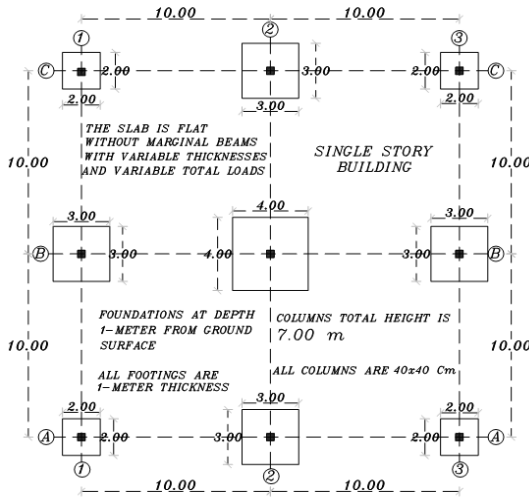


Figure 1. Two-bay by two-bay frame-foundation-soil model

The 1-meter soil depth around the footings was deactivated during the calculation phase. The columns were permitted to rotate at the foundation level. The slab permitted to transfer bending moments to the columns in the two directions. There are no tie beams connecting the foundations, because the long span between footings and to study the structural effects only. Figure (2) displays the generated finite element mesh.

The frame was modeled also using commercial structural finite element program SAFE V12. The same properties, sections, and loads were defined, as shown in Figure (3). Usually for such small buildings, the designers represented the footings as hinged supports to the columns.

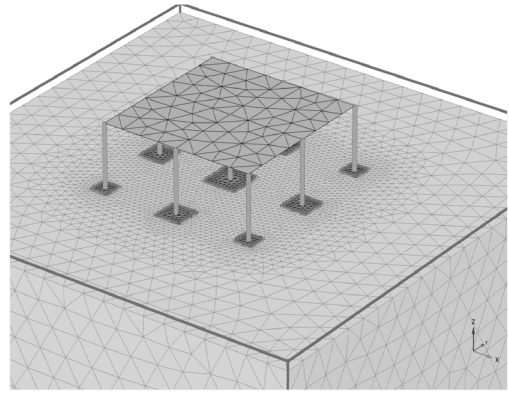


Figure 2. Generated finite element mesh Using PLAXIS 3D

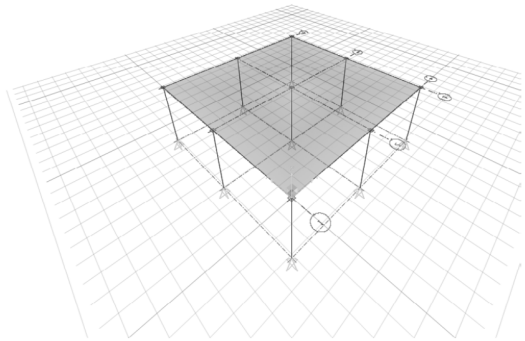


Figure 3. SAFE V12 frame model

3. RESULTS & DISCUSSIONS

There are three objectives for this paper and need to be qualified. First and second objectives are the effect of super-structure rigidity on the average contact stresses and differential settlement, respectively. The final objective is to qualify the differences between the resulted average contact stresses from the geotechnical and the structural finite element programs, by meaning of the differences between the resulted columns loads considering and neglecting the soil structure interaction.

The effect of boundary conditions should be checked by reviewing the resulted settlement and insuring that the affected area is inside the suggested boundaries. Figure (4) is the vertical settlement for the case of 2-meter slab that was loaded by 60 kPa, which requires the boundaries to be most far from the footings; and the results were found satisfactory.

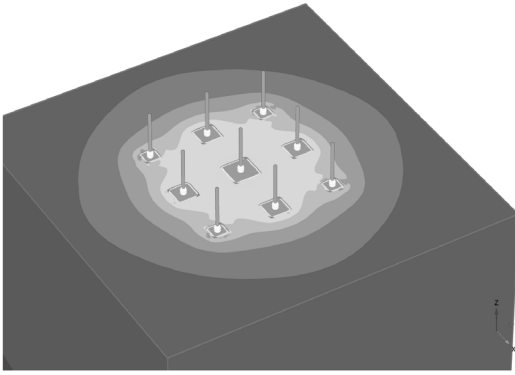


Figure 4. Vertical settlement for 2-m slab loaded by 60 kPa

To qualify the effect of the super-structure rigidity, the relative bending rigidity ρ^* were depicted for each slab thickness from Eq. (1). EI for the structure was calculated using Eq. (3).

The first objective of this paper is to qualify the effect of super-structure rigidity on contact stress. Dimensionless average contact stress (q) under inner, edge, and corner footings were depicted. The dimensionless factor q is the ratio between the average contact stresses under footing to the applied distributed load over the slab. Figure (5) shows the relation between the dimensionless average contact stresses q under inner, edge, and corner footings with the relative bending rigidity of the structure ρ^* for different applied distributed loads over the slab.

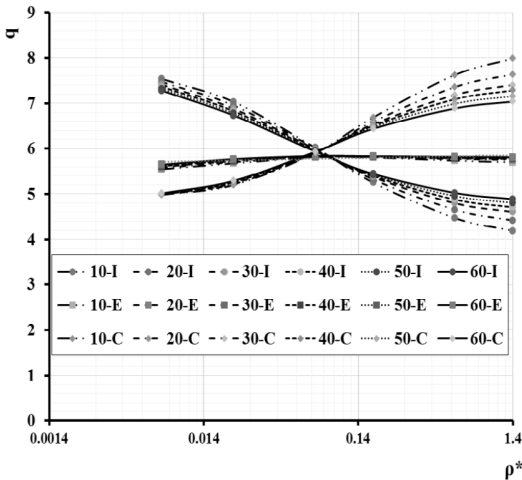


Figure 5. Relation between q under inner I, edge E, and corner C footings with ρ^* for different applied distributed loads

It can be seen that, q under inner footing decreased with the increase of ρ^* , while q under corner footings increased with the same increase of ρ^* . The dimensionless factor q under edge footings was approximately constant. These were because the redistribution of the loads due to the increase of the super-structure rigidity. In addition, unitless average contact stresses under inner and corner footings were affected by the load levels acting on the slab.

The second objective is the effect of super-structure rigidity on the settlement and differential settlement. Dimensional maximum settlements (C_o) under inner, edge, corner footings were depicted using the following Equation:

$$C_o = \frac{S_{max}}{l_{footing}} \times \frac{E_s}{W} \quad \dots\dots\dots (4)$$

Where:

- C_o = dimensionless maximum settlement
- S_{max} = maximum settlement under footing
- $L_{footing}$ = footing length
- E_s = Young's modulus of the soil
- W = distributed loads applied on the slab

The dimensionless maximum settlement C_o was multiplied by E_s , because the settlement is in inverse relationship with E_s . C_o was divided by W , because the settlement is in positive relationship with W . Figure (6) displays the effect of the superstructure rigidity on the dimensionless maximum settlement under inner, edge, and corner footings for different load levels acting on the slab.

It can be seen that, C_o under inner footing decreased with the increase of ρ^* , and C_o under corner footings increased with the increase of ρ^* . C_o under edge footings was not changed. These were the reasons for the variation of contact stresses under inner and corner footings, and the constant contact stress under edge footings with increasing the relative bending rigidity of the structure. The redistribution of the settlements should affect the differential settlement.

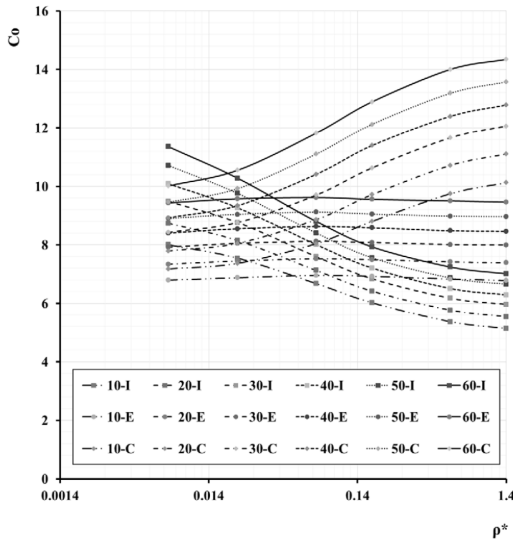


Figure 6. Relation between C_o and ρ^* at different load level

The maximum differential settlement is the difference between the maximum settlements of inner and corner footings, which at the footing center. The dimensionless differential settlement was depicted using the following Equation:

$$\Delta = \frac{D_s}{l_{\text{inclined}}} \times \frac{E_s}{W} \dots\dots\dots (5)$$

Where:

- Δ = dimensionless differential settlement
- D_s = differential settlement between inner and corner footings
- l_{inclined} = inclined length between inner and corner = 14.142-meter
- E_s = Young's modulus of the soil
- W = distributed loads applied on the slab

Figure (7) shows the effect of the structural relative bending rigidity on the dimensionless differential settlement with different load levels acting on the slab.

From the Figure, with the increase of ρ^* , Δ was decreased significantly. The redistribution of loads between the inner and corner footings, due to the increase of the structural rigidity, leads to decrease the differential settlement. In addition, the applied loads on the slab are affecting the resulted differential settlement at low structural rigidity only. At low structure rigidity, the loads cannot perfectly are redistributed. Therefore, with increasing the load level,

the average contact stress under inner footing is increased, which increases the settlement, and the average contact stress under the outer footing decreased, which decreases the settlement. These effects should increase the differential settlement with increasing the loads at low structural rigidity. At high structural rigidity, the loads perfectly are redistributed between inner and corner columns. Therefore, the increase of the settlement under corner footing is more than the increase of the settlement under inner footings.

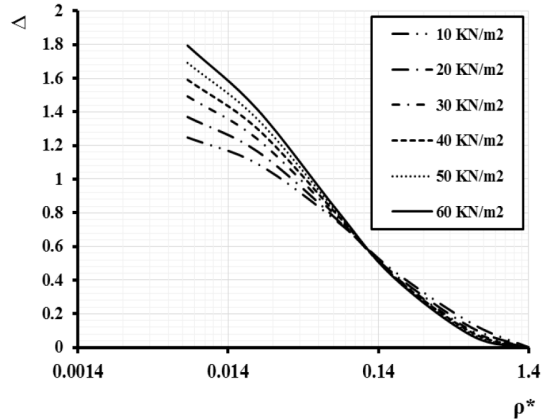


Figure 7. Relation between Δ and ρ^* at different load level

The final purpose of this paper is to qualify the difference between using structural and geotechnical finite element programs in the calculation of columns reactions and the average contact stresses under the footings. Figure (8) shows the relation between dimensionless average contact stress (q) and the structural relative bending rigidity (ρ^*) for the case of 10.0 kPa uniform distributed loads acting on the slab using SAFE-V12 and PLAXIS-3D-V2013 programs, which is neglecting and considering soil structure interaction, respectively.

The increase of structural relative bending rigidity (ρ^*) leads to decrease the dimensionless average contact stress (q) resulted from neglecting and considering the soil structure interaction (SSI). However, neglecting SSI results q under inner footing higher than that resulted by considering SSI, and q under corner footings is lower than that is resulted by considering SSI. In addition, q under edge footings is approximately the same for the both cases. Neglecting SSI leads to increase in the inner column load by 30% of its load that is resulted from neglect-

ing SSI, and leads to decrease the corner columns loads by 50% of its load that is resulted from neglecting SSI.

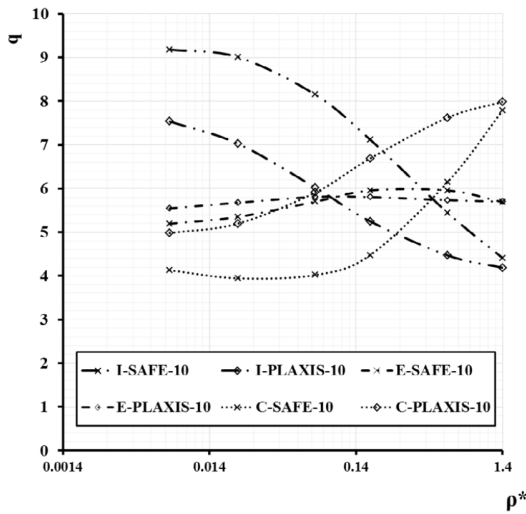


Figure 8. Relation between q and ρ^* at different load level using SAFE and PLAXIS-3D programs

A new advanced design procedure is suggested and could be used for special projects to consider the superstructure rigidity in the geotechnical analysis. The procedure is as follows:

1. The geotechnical engineers should present a preliminary modulus of subgrade using the plate load tests after the modifications.
2. The structural engineers should finish the preliminary design based on the k_s suggested in the geotechnical report.
3. The preliminary structural design should be returned to the geotechnical engineers.
4. A soil structure interaction specialized engineer should model the superstructure with the underlying soil base using an appropriate geotechnical finite element program to recheck the new group of contact stresses and settlements under the foundations, and to find a new group of the average subgrade modulus (k_s).
5. The structural engineers should finalize the superstructure and foundation design based on the new group of k_s .

To qualify this procedure, the average modulus of subgrade reaction (k_s) was depicted from the outputs of PLAXIS 3D under inner, edge, and corner footings. The subgrade modulus was

adopted to define the columns supports in SAFE-V12. Figure (9) shows the relation between ρ^* and q resulted using the two programs for the case of 10.0 kPa uniform distributed loads over the slab; SAFE using k_s with considering of the superstructure rigidity, and PLAXIS-3D.

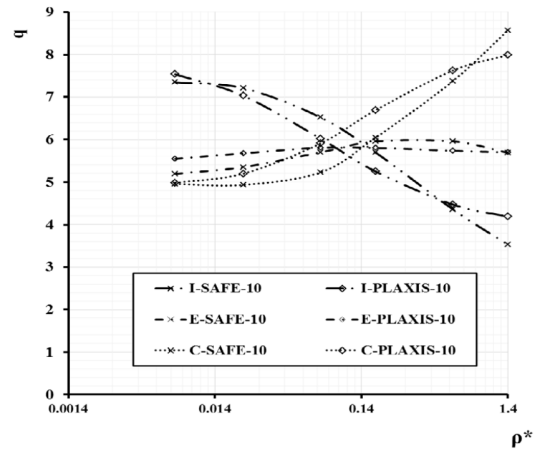


Figure 9. Relation between q and ρ^* at different load level using SAFE and PLAXIS-3D programs

It can be seen that, the resulted q under footings using SAFE considering SSI and PLAXIS are closed to each other. However, there are some differences between the results from the two programs. These differences are the results of using average k_s , but these differences are small and can be neglected.

It can be said that, the suggested new way of design procedure is appropriate and should be used for the heavy superstructures or the special superstructures such as the schools, universities, hospitals, etc.

4. CONCLUSIONS

From the analyses and discussions, the following were concluded:

1. Increasing the superstructure rigidity is decreasing the differential settlement.
2. Increasing the superstructure rigidity is increasing the average contact stresses under corner footings and decreasing the average contact stresses under inner footings in the 2-bay by 2-bay frames.
3. For the 2-bay by 2-bay frames, the edge columns are not affected by the increase of super-structure rigidity.

4. Neglecting the soil structure interaction (SSI) leads to increase in the inner column load by 30% of its load that calculated with neglecting of the SSI, and leads to decrease the corner columns load by 50% of its load that calculated with neglecting of the SSI.
5. The use of structural finite element program considering SSI, by using average ks resulted from the geotechnical report without considering the soil structure interaction is inappropriate.
6. A new advanced design procedure is suggested and could be used for special projects to consider the superstructure rigidity in the geotechnical and the structural analyses.

5. RECOMMENDATIONS

1. Increase the design loads 50% of the corner columns and footings that is calculated by neglecting SSI.
2. Consider SSI in the structural finite element programs, by representing the footings using modulus of subgrade reaction ks resulted from geotechnical finite element program that can simulate the superstructure members.
3. Use a geotechnical finite element program that can represent the superstructure with the foundations and soil to get appropriate straining actions at structural elements.
4. Floor members need additional reinforcement to resist the secondary stresses resulted from the soil structure interaction.
5. If the soil is weak, it is much recommended to design rigid floors with rigid tie beams to resist the estimated differential settlement.

6. ACKNOWLEDGEMENT

Praise and glory are due to Allah whom grants us all our knowledge and success in our life. We would like to express sincere appreciation to the team of EHE Consulting office on their help and encouragement. Furthermore, the researchers are grateful to the Soil Structure Interaction Group in Egypt (SSIE) for their continuous support to the design process.

7. REFERENCES

- Brown, P.T. and Yu Si, K.R. (1986). "Load Sequence and Structure-Foundation-Interaction", *Journal of Structural Engineering*, Vol. 112, No. 3. 481–488.
- Dejong, J. and Morgenstern, N.R. (1971). "The Influence of Structural Rigidity on the Foundation loads of the CN Tower", *Edmonton, Canadian Geotechnical Journal*, Vol. 8, 527–535.
- Hain, S.J. and Lee, I.K. (1974). "Rational Analysis of Raft Foundation", *Journal of the Geotechnic. Engg. Div.*, Vol. 100, No. GT7, 843–860.
- Heil, H. (1969). Studies on the structural rigidity of reinforced concrete building frames on clay. *Proc. 7th Int. Conf. Soil Mech. Found. Engng.*, Vol.2, Mexico City, Mexico, 115-121.
- Hooper, J.A. (1984). "Raft Analysis and Design some Practical Examples", *The Structural Engineering*, Vol. 62A, No. 8, 233–244.
- Hora, M. and Sharm, A. (2007). "Elasto-Plastic Analysis of Building Frame-Soil Interaction System", *Journal of Structural Engineering*, Vol. 34, No. 2 124–139.
- Meyerhof, G.G. (1947). "Settlement Analysis of Building Frames", *The Structural Engineer*, 369–409.
- Potts, D. M. and Addenbrooke, T. I. (1997). A structure's influence on tunneling-induced ground movements. *Proceedings of ICE, Geotechnical Engineering* 125, Issue 2, 109-125.
- Potts, D. M., Standing, J. R. and Addenbrooke, T. I. (1998). Interaction between tunneling and nearby structures. *Proc. Int. Conference on Soil Structure Interaction in Urban Civil Engineering*, Darmstadt, No.4, Vol.1, 113-135.
- Viladkar, M.N., Godbole, P.N. and Noorzaei, J. (1994). "Modelling of Interface for Soil-Structure Interaction Studies", *Computers and Structures*, Vol. 52, No. 4, 765–779.
- King G.J.W. and Chandrashekhara V.S. (1974) "An Assessment of the effects of interaction between a structure and its foundation", *Proc. British Geotech. Soc. Conf on settlement of structures*, Cambridge, p75/70
- Grasshoff, H. Influence on flexural rigidity of superstructure on the distribution of contact pressure and bending moments of an elastic combined footing. *Proc. 4th Int. Conf. Soil Mech. Foundn. Engng.* London, England, Aug. 1957, I. 300-306.
- Goschy, B. (1978): "Soil-Foundation-Structure Interaction." *Journal of the Structural Division*, ASCE, 104 (ST 5), 749-761.
- Sommer H. (1965), A method for calculation settlement, contact pressure, and bending moment in a foundation including the influence of the flexural rigidity of the superstructure, 6th ICSMFE, Montreal, 2: 197.

Design of pile group system for ‘Most Sava – Zeleni’ railway bridge in Zagreb

I. Sokolić & B. Vukadinović

Geotehnički studio d.o.o., Zagreb, Croatia

ABSTRACT: The paper describes the design concept of pile group system for strengthening of ‘Most Sava – Zeleni’ railway bridge. It gives detail description of soil profile, geometry of the system, design methodology and results of static pile load test. The pile group system consists of 24 bored piles, with 1000 mm in diameter and 24.5 m long. Soil profile consists of stiff soils, typical for alluvium of River Sava in the area of Zagreb. The basic design concern was to take into account interaction between the old pier footing, the new pile system and the surrounding soil. The system was designed with Ensoft-GROUP software and it was additionally analyzed by Plaxis 3D software. Static pile load test was performed to validate the performance of vertically loaded pile.

1. INTRODUCTION

The railway bridge ‘Most Sava – Zeleni’ lies on one of the most frequent railway excess of the City of Zagreb, to the main Croatian ports on the Adriatic coast. The bridge was constructed in the year 1939, and it was repaired after the Second World War. The arch steel bridge is 9.6 m wide and it is 306 m long. The maximum span over the river of Sava is 135.5 m long. The piers of the bridge are made of reinforced concrete with the facing of the stone blocks (Figure 1). One of the piers, that has the bearing support for both horizontal and vertical actions, is situated near the riverbank. Due to time degradation effects and demands for higher traffic loads, it was necessary to take the actions for strengthening the pier foundation.

The strengthening system consists of bettered bored piles fully embedded into the pile cap and incorporated into the old pier by reinforced concrete coating. The basic design concern was to take into account interaction between the old pier footing, the new pile system and the surrounding soil. The system was designed with Ensoft-GROUP software that enables the modeling of group of piles connected with the rigid pile cap. The main challenge of the design was to select properly the soil parameters for the ‘*p-y curves*’ and ‘*t-z curves*’, which are used for modeling the soil response to lateral and vertical movement of the pile. It was also important to validate the contribution of the huge old footing to total capacity of the system.

The soil parameters for the model are derived according to recommendations proposed by Reese et. al. (2006). For cohesive soil the parameters were correlated to the undrained shear strength, and for noncohesive soils to the relative density. There is no comparable experience available for proposed methodology of pile group modelling, for the soil profile in the area of City of Zagreb, so it was important to take measures to check the performance of the model and to validate the results.



Figure 1. Railway bridge ‘Most Sava – Zeleni’ during the construction of 1000 mm bored piles.

2. SOIL PROFILE

The soil profile at the site was investigated in two stages. In the first stage, 20 m long bore-hole was performed to define the soil profile for the main design. As the total length of the designed piles was greater than the final investigation depth, it was necessary to perform 30 m long control investigation borehole prior to construction of the piles.

Geotechnical investigation performed include *in-situ* penetration tests (N_{SPT}), standard laboratory tests (seave analysis, Atterberg limits, moisture content, specific weight, uniaxial strength and compressibility modulus) and accessory '*in-situ*' tests (pocket penetrometer, pocket vain test). The characteristic soil profile with corresponding mechanical and physical properties of the soil is shown on Figure 2.

The soil profile consists of four dominant layers and it is characteristic for alluvium of Sava River in the area of City of Zagreb. Surface layer consists of low to medium stiffness humus fill, low plasticity clay and sand, and extends to depths of ~ 3.5 m from the surface level. The second layer consists of alluvial deposits of dense to very dense gravel, partially

mixed with silt, extending down to ~ 11.0 m from the bottom of the footing. The third layer is stiff Pliocene clay to the depth of 22 m. The bottom layer is clayey sand layer with the interlayers of low to intermediate plasticity silts. The gravel contains less than 10% of small particles, the N_{spt} value is in the range 21 to 43 (average $N_{spt}=26$). The relative density is in the range 53 to 85 % (average $ID=68\%$). Plasticity index I_p of the high plasticity clay layer is in the range 16 to 45 (average $I_p = 30$). N_{spt} value is in the range 22 to 30 (average $N_{spt}=27$). Undrained shear strength of the cohesive soil is measured with several tests:

- correlated to the SPT test (Clayton 1995):
 $c_u(SPT) = f(I_p) \times N_{60} = 4.5 \times N_{60}$
- measured in uniaxial compressive strength:
 $c_u(q_u) = q_u/2$
- measured with pocket penetrometer: $c_u(PP)$
- measured with pocket shear vane test: $c_u(PSV)$
- correlated to the Consistency index:
 $c_u(Ic) = 1.7 \times 10^{2Ic}$ [kPa]

The average value correlated to SPT test was used for the design ($c_u = 120$ kPa).

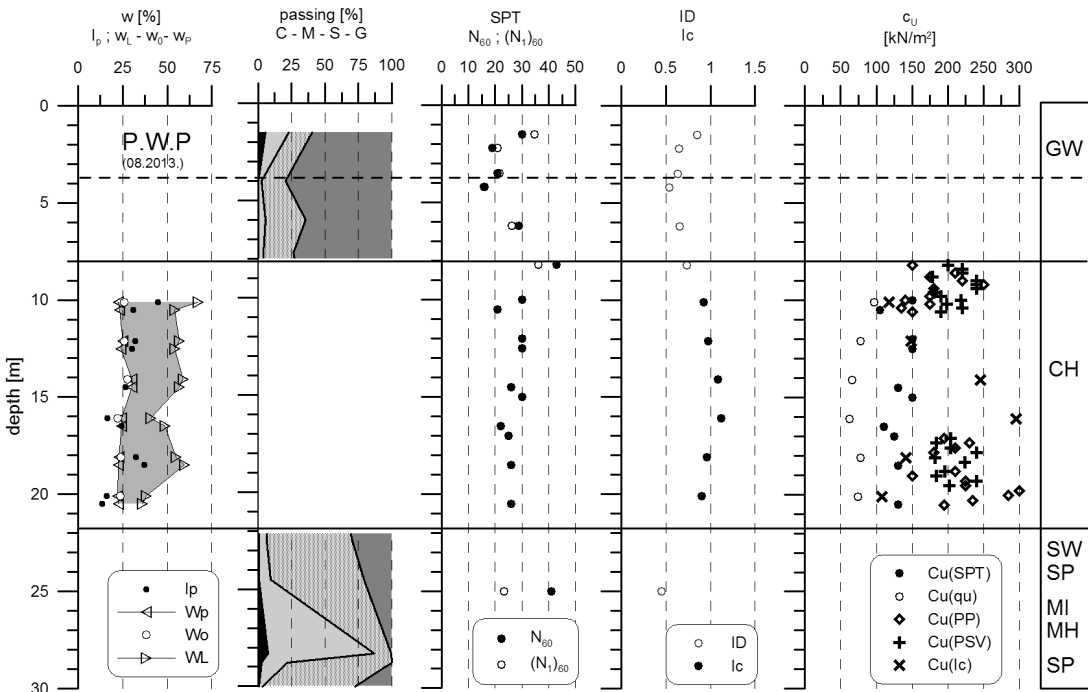


Figure 2. Characteristic soil profile with corresponding mechanical and physical properties of the soil (SPT – standard penetration test; q_u – uniaxial compressive strength; PP - pocket penetrometer; PSV – pocket shear vane; I_c – index of consistency.) . .

3. DESIGN OF PILE GROUP SYSTEM

The strengthening system consists of 24 bored piles, with 1000 mm in diameter and 25 m long. The piles are inclined for 6 degrees from vertical and maximum 55 degrees from the railway axes. The pile head is fully embedded to the pile cap with dimensions Width x Length x Height = 11.0 x 24.0 x 3.3 m (Figure 3).

The basic pile design concept is that the bridge dead load is sustained by the old footing, while the traffic load is transferred to the pile group. Resulting force at the top of the pile group consist of vertical live load V, horizontal live load H and corresponding moment M. For pile bearing capacity calculation it can be assumed that the moment M is completely taken by the vertical forces in the piles which cause the reduction of the axial force at one side of the pile group and amplification on the other side.

On the other hand, for the design of pile internal stability, the effect of pile embedment must be considered. Due to the horizontal movement of the foundation system, the moment reaction appears at the top of the pile, which is critical for reinforcement design. To validate the amount of action sustained, complex static analysis must be performed, including the effect of old footing.

The complete foundation system analysis was carried out using the computer software Ensoft-GROUP 7.0 (Rees et al. 2006). The numerical method used is called '*p-y method*' (Reese & Van Impe, 2011) that consists of Winkler model of the beam on the ground represented by non-linear springs. The shape and the size of the curves that define secant stiffness of the springs are derived from empirical correlations according to the type of the soil, soil parameters and the soil profile. The similar approach called '*t-z method*' is used for modelling pile settlement curve.

The old footing was modeled using circular pile elements as well. The area and the moment of inertia of the cross section were defined equivalent to the square footing, while the diameter was taken 17.0 m, which is the width of the footing in the direction of dominant horizontal movement.

The soil parameters for calculating '*p-y curves*' and pile '*t-z: axial load – settlement curves*' were derived from soil strength parameters and according to recommendations proposed by Rees et al. 2006.

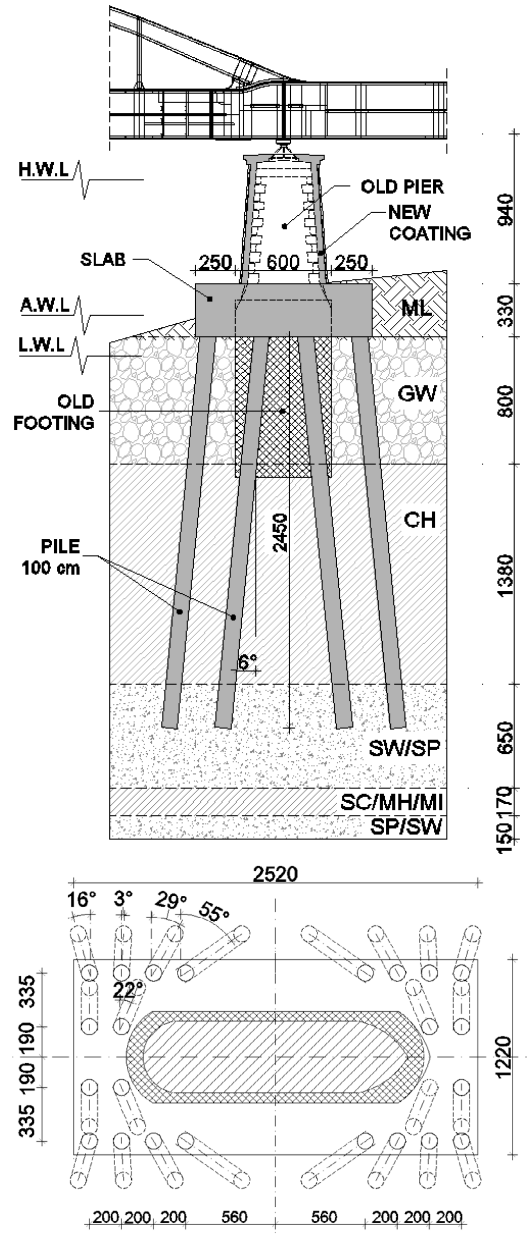


Figure 3. Cross section and top view of the pile group and old pier footing.

COHESIVE SOILS:

Shaft resistance:

$$q_s = \alpha \cdot c_u = 0.55 \cdot c_u \quad (1)$$

Base resistance:

$$q_b = N_c \cdot c_u = 8.8 \cdot c_u \quad (2)$$

Principal strain corresponding to the 50% of the strength of 'p-y curve':

$$\varepsilon_{50} = -0.002 \cdot \ln(c_u [kPa]) + 0.0162 \quad (3)$$

Initial stiffness of 'p-y curve':

$$K_s [kN / m^2] = 1810 \cdot c_u [kPa] \quad (4)$$

COHESIONLESS SOILS:

Shaft resistance:

$$q_s = \beta \cdot \sigma'_v \quad (5)$$

$$0.25 < \beta = 2 - 0.15(y[m])^{0.75} < 1.8$$

Base resistance:

$$q_b = 60 \cdot N_{60} \quad (6)$$

Initial stiffness of 'p-y curve':

$$k [kN / m^3] = 822 \cdot N_{60} \quad (7)$$

The calculation model was analyzed as 2D problem, taking into account the inclination of the piles in the plane parallel to the railway axes. The schematic view of the deformed model is shown on the Figure 4. Detailed description of analysis performed can be found in I. Sokolić et al. 2010. According to the results, almost all the moment action on the pile cap is taken by the vertical reactions in the piles (94 to 110 %) while the rest of the moment is taken by the reaction moment of the piles and the footing. Total amount of the applied load transmitted to the old footing reach maximum 7% of H, 2% of V and only 2% of M action.

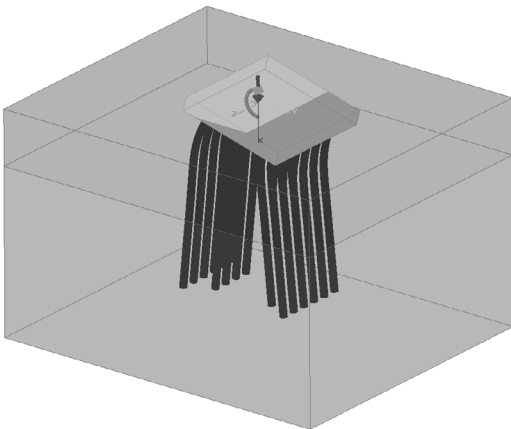


Figure 4. Schematic view of calculation model in Ensoft-GROUP software (two layered soil model according to preliminary investigation results).

Due to complexity of the calculation model used in Ensoft-GROUP software, it was necessary to check the performance of the system with some independent methodology. The basic idea was to model the same structure in numerical program Plaxis, and to use the comparable experience with modelling retaining walls to determine the soil parameters. Full 3D soil-structure interaction model was calculated using the PLAXIS 3D Foundation software (Brinkgrawe & Swolfs, 2007). The old footing was modeled with soil elements using the linear-elastic soil model and corresponding parameters for the concrete. The same parameters were used for foundation slab modeled with the 3.3 m thick floor elements. The piles were modeled with embedded pile elements available in Plaxis 3D software.

The strategy for deriving the parameters for HS soil model was the same as proposed by A. Szavits-Nossan (2008) for numerical modeling of anchored retain structure, for the soil profile typical for the area of Zagreb city. The back analysis of horizontal wall movement, performed on several case histories (A. Szavits-Nossan et al. 2010) show that the reference stiffness of the HS soil model E_{50}^{ref} correlates well with the N_{SPT} values corrected with depth:

$$E_{50}^{ref} = 5x(N_1)_{60} \quad (8)$$

The strength parameter used for the gravel layer is the same as in the GROUP model ($\phi = 35^\circ$), while the undrained strength of the clay layer ($c_u = 120$ kPa) was modeled with effective strength parameters and by performing the undrained type of analysis.

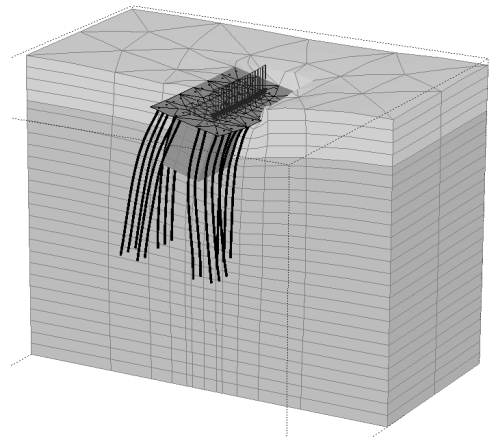


Figure 5. Pile group model with old pier footing in computer software PLAXIS 3D Foundation.

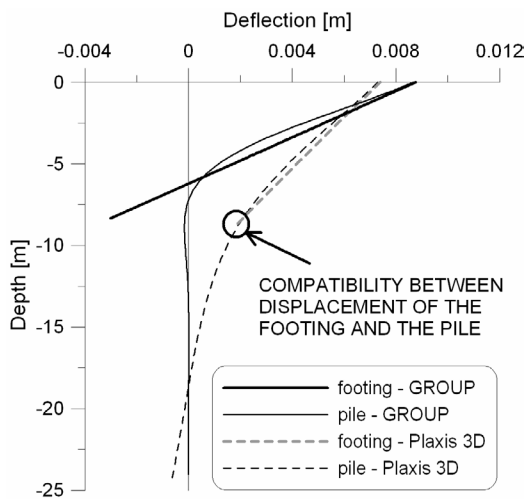


Figure 6. Displacement of the pile and old footing calculated in computer program GROUP 7.0 (full line) and in computer program Plaxis 3D (dashed line)

When comparing the results of numerical models for complex foundation system (Footing + Piles) the benefit of the full 3D modelling is evident (Figure 6). The final displacements and the rotation of the system are reduced. Compatibility between the displacement of the footing and the piles is achieved at the bottom of the footing. The resulting internal moments in the piles is much smaller then calculated by GROUP software. That can be explained by the fact that GROUP software does not account for global movements of the soil that appear around the footing and reduce the final deflection of the piles.

The results of the analysis show that using different modelling approaches and different strategy for deriving the soil parameters, the performance of the single pile in both software is very similar. On the other hand, when modelling the full soil-structure interaction, more realistic and economic results are obtained using the full 3D model (Sokolić et al. 2010).

4. STATIC PILE LOAD TEST

One of the main design concern was to model as real as possible the performance of pile under the vertical loading (load settlement curve). Methodology proposed by Rees et al. 2006. was used for the design. The load-settlement curve, '*t-z curve*', was generated by Ensoft-GROUP software. The shape of the

curve was also checked in Plaxis 3D numerical model (Sokolić et al., 2010).

During the construction of piles one Static load test was performed for quality control, and to validate the calculation model. The test was performed on 600 mm bored pile, and results were extrapolated for the 1000 mm bored piles.

Static pile load test was performed by using eight '*contra weight*' anchors connected by load transformation cap at the top of the testing pile. Anchors type BBR were used, with total length of 22 m, inclined by 30 deg. from vertical with total capacity of 960 kN. Load cell with capacity of 600 tone was used with the travel range of 10 cm. The displacement was measured by four radially displaced linear transducers mounted on the beam that was founded outside the influence area (concrete footings placed app. 4.0 m distance from the center of the pile). The measurements were taken continuously during the load test in the sequence of 20 seconds. The pressure in the load cell was maintained manually during the test. The test setup is shown on Figure 7.

The testing procedure was made according to code ASTM D 1143-81 (Reapproved 1994): Standard Test Method for Piles under Static Axial Compressive Load; and corresponding recommendations: SUGGESTED METHOD of ISSFE: Axial Pile Loading Test – Part 1: Static Loading. Maximum load of 4500 kN was applied in 9 increments of 500 kN. For primary compression, the load was maintained for 1 hour, while for unloading and reloading it was maintained for 10 minutes. The results of testing and the loading procedure are shown on Figure 8.

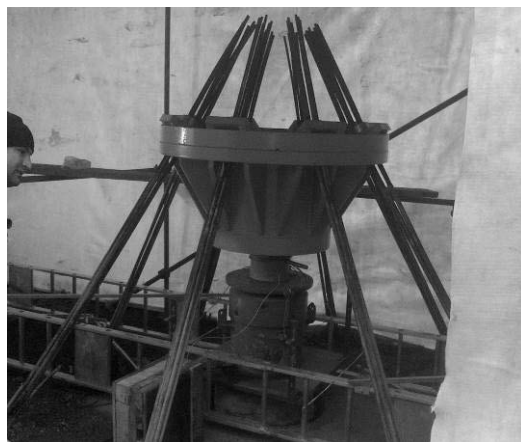


Figure 7. Static pile load test installation for testing 600 mm bored pile to the maximum Load 4500 kPa.

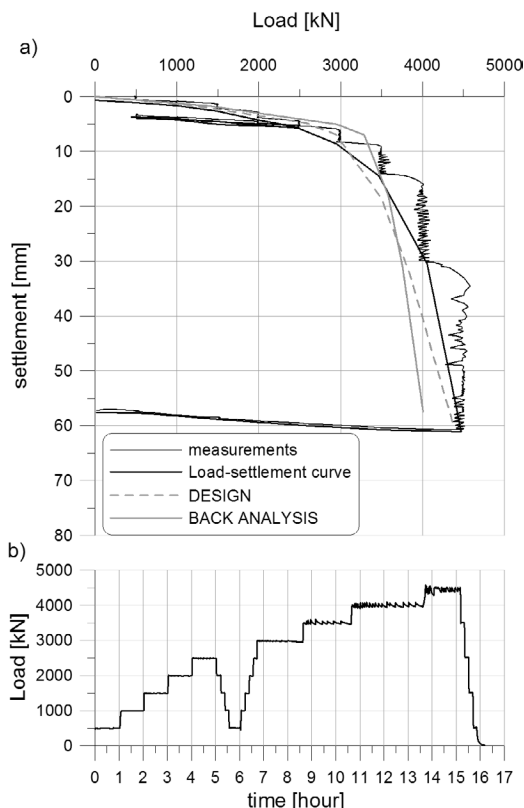


Figure 8. Results of Static Load Test on 600 mm bored pile compared to design load-settlement curve and generated by back calculation.

The results of static load test are compared to design load-settlement curve generated according to methodology described in Paragraph 3 (Figure 8.a). The agreement between the curves is very good both for stiffness and for capacity of the pile. To match the results even better the back calculation of soil parameters was made. Best match of curves was achieved by reducing the shaft capacity of piles by app. 20% and increasing the base capacity by app. 40%. The results give grate confidence to the methodology used for generating load-settlement curve, so it was used for extrapolation of the results to the 1000 mm bored pile.

5. CONCLUSION

Strengthening of bridge foundation by using pile group is very complex geotechnical problem and to provide the quality end economic design, the complex calculation models should be used that account for soil-structure interaction. The computer software Ensoft-GROUP is

very powerful tool for performing such analysis in relatively short time. The software enables modeling complex 3D arrangements of piles in group, connected with rigid cap. Compared to more advanced numerical software Plaxis 3D the results are very similar. Comparing the results of the generated load settlement curve and the measurements of Static Load Test it can be concluded that the methodology proposed by Rees et al (2006) for deriving the parameters of 't-z curves' is very applicable for stiff soils in the area of City of Zagreb. Great advantage of the method is that the parameters of soil are derived for relatively simple investigation methods that are used in common praxis. Comparing the results of calculation performed by GROUP software and Plaxis 3D software for laterally loaded pile group, the same can be concluded for p-y curves'. Additional validation of the methodology should be made by performing Static pile load test under lateral loading.

6. REFERENCES

- Reese, L.C., Wang, S.T. & Vasquez, L. 2006. Analysis of Group of Piles Subjected to Axial and Lateral Loading (Technical Manual). ENSOFT, INC. Austin, Texas.
- Reese, L.C. & Van Impe, W.F. 2001. Single Piles and Pile Groups under Lateral Loading. Leiden, Balkema.
- Brinkgrave, R.B.J. & Swolfs, W.M. 2007. PLAXIS 3D FOUNDATION Reference Manual V.2. PLAXIS bv, AN Delft, Netherlands.
- Shanz, T., Vermeer, P.A., Bonnier, P.G. 1999. The hardening soil model – formulation and verification. *Beyond 2000 in computational geotechnics*.
- Szavits Nossan, A. 2008. Advances and uncertainties in the design of anchored retaining walls using numerical modelling. *Acta Geotechnica Slovenica (1)*: 5-19.
- Szavits-Nossan, A., Sokolić, I. & Plepelić, G. 2009. Design of anchored retaining structures by numerical modelling, *17th International Conference on Soil Mechanics & Geotechnical Engineering, Alexandria, Egypt*. Vol. 3.
- Vukadinović, B. 2010. Željenzički most Sava, Zagreb – projekt održavanja – stup nepomičnog ležaja. *Design Project T.D.:3608-3/10.GS, Geotehnički studio d.o.o. Zagreb. (in Croatian)*
- Sokolić, I., Vukadinović, B., Skazlić, Ž. 2010. Strengthening of old bridge foundation using the pile group system. *Technical Meeting TC207 – Workshop on soil structure interaction and retaining walls, Dubrovnik*, 53-58

Estimation of the Undrained Bearing Capacity of Footings Using Random Finite Element Method: Application in Ankara Clay

Emre Turk & Sami Oguzhan Akbas
Gazi University, Turkey

Oguz Tufenkci
Akademi Geotechnical Ltd., Turkey

ABSTRACT: The Random Finite Element Method, which associates random field theory with deterministic finite elements by considering the mean, standard deviation and correlation length values of the load and resistance parameters, has proven to be an effective tool for solving many geotechnical engineering problems. On this basis, this study involves application of this methodology to the estimation of undrained bearing capacity of footings founded on Ankara Clay. The emphasis is given to the statistical characterization of the geotechnical parameters of Ankara Clay, and estimation of the effects of these parameters on the obtained results.

1. INTRODUCTION

The existence of many sources of uncertainties within the design process are well known by the geotechnical engineers. As an example, the random character of geotechnical properties of the soil has a significant influence on the bearing capacity and settlement based design of footings. Nevertheless, this effect is not usually taken directly into account in practice. Instead, traditional geotechnical design is inclined towards using a lumped factor of safety (FS) to reduce the possibility of adverse system performance. However, the selection of this FS is essentially subjective, as a result, based on how the design models and parameters are selected, the same FS might imply very different levels of risk, which is clearly undesirable.

For geotechnical engineering applications, it is difficult, if not impossible, to maintain a consistent level of adverse performance risk without a theoretical framework that recognizes, quantities and manipulates uncertainties explicitly. It is possible to construct this framework through the random finite element method (RFEM), which considers the distribution of soil parameters over a correlation length based on the random soil model proposed by Fenton and Griffiths (2003). However, it should be stated that, a robust application of RFEM would require the stochastic properties of the soil layers under consideration to be well-defined.

Based on the above points, this study focuses on the specific application of RFEM to the

estimation of undrained bearing capacity of strip footings. For this purpose, a statistically well-defined (Akbas and Kulhawy, 2010) soil, overconsolidated Ankara Clay is considered as the foundation soil. First, a brief overview of the RFEM is given. Then, Phoon and Kulhawy (1999) framework is used to characterize and estimate the variability of the undrained shear strength of Ankara Clay, which has a rather heterogeneous character. The inherent variability is modelled as a random field that is defined by the coefficient of variation (COV) and scale of fluctuation. A first-order second moment probabilistic approach is used to combine various sources of uncertainties consistently, for determining the total variability of the undrained shear strength. Finally, by means of the RFEM algorithm created by Fenton and Griffiths (2003), the effects of uncertainties and the anisotropy in correlation length on the obtained results were discussed.

2. METHODOLOGY

In undrained conditions ($\phi = 0$), the equation for determining the ultimate bearing capacity (q_u) of a rigid footing on the surface of a cohesive soil can be expressed as:

$$q_u = c_u N_c \quad (1)$$

in which c_u = the undrained shear strength of soil, and N_c = bearing capacity factor = 5.14. Thus, the level of adverse performance risk of a

design based on Eq. (1) depends mainly on the selection of the undrained shear strength design value.

On the other hand, it is clear from the above discussions that the undrained shear strength is inherently variable within a soil layer due primarily to the natural geologic processes that produced and continually modify the soil mass in situ. In addition, variability from the measurement and transformation errors enters the determination of undrained shear strength through equipment, procedural-operator, and random testing effects. Finally, in case it is estimated from laboratory indices such as the plasticity index or from in-situ test results such as the SPT N value, a third source of uncertainty, transformation error is introduced.

Thus, the undrained shear strength, c_u , is assumed to be a log-normally distributed random field variable with mean μ_c , standard deviation σ_c , and spatial correlation length θ_{inc} . Note that when isotropy assumption is not valid, different correlation lengths θ_{incx} and θ_{incy} in horizontal and vertical directions, respectively were considered.

A log-normally distributed random field can be derived from a normally distributed random field, $G_{inc}(x)$, having zero mean, unit variance, and spatial correlation length θ_{inc} as follows:

$$c_u(x) = \exp[\mu_{inc} + \sigma_{inc} G_{inc}(x)] \quad (2)$$

in which x = spatial position at which c_u is calculated and μ_{inc} and σ_{inc} = are the mean and standard deviation of the equivalent normal random variable, i.e, the undrained shear strength.

The correlation coefficient between the natural logarithm of undrained shear strength at a point x_1 and a second point x_2 is specified by a correlation function ρ_{inc} :

$$\rho_{inc} = \exp \left[- \sqrt{ \left(\frac{2\tau_2}{\theta_{(inc)x}} \right)^2 + \left(\frac{2\tau_1}{\theta_{(inc)y}} \right)^2 } \right] \quad (3)$$

in which $\tau_1 = y_2 - y_1$ and $\tau_2 = x_2 - x_1$ are the components of the absolute distance between two points in 2-D space, and $\theta_{(inc)x}$ and $\theta_{(inc)y}$ = correlation distances along these two directions (Vessia et al., 2009).

Since $\ln(c_u)$ is normally distributed and a normally distributed random field is simply characterized by its mean and covariance structure, the correlation function given in Equation (3) acts conveniently between values

of $\ln c_u$. Note that the correlation length θ_{inc} can be estimated by evaluating spatial statistics of the log-cohesion data directly (Fenton, 1999). However, such studies are scarce so that little is currently known about the spatial correlation structure of natural soils (Fenton et al., 2008).

3. ESTIMATION OF RANDOM FIELD PARAMETERS FOR ANKARA CLAY

About two-thirds of the Ankara settlement area, with about three million inhabitants, is sitting on Ankara Clay (Tonoz et al., 2003). This clay is composed of sandy, and gravelly levels of variable thicknesses; locally, at shallow depths, there are very thin lime levels, lime nodules, and concretions within clayey levels from lenses with no lateral continuity. Erguler and Ulusay (2003) reported that the thickness of this clayey sequence changes locally, but it exceeds 200 m. Ordemir et al. (1965) described Ankara Clay as an inorganic, preconsolidated clay, with natural water content (w_n) and plastic limit (w_p) ranging between 20 and 35%, and liquid limit (w_L) ranging between 55 and 75%. The shrinkage limit varies between 15 and 20%. Surler (1976) indicated a plasticity index (PI) range of 20 to 40%, which suggests high plasticity. The unit weight ranges between 17.5 and 19.5 kN/m³, and the specific gravity is between 2.60 and 2.70 (Ordemir et al. 1965). Figure 1 illustrates the typical vertical spatial variability for some geotechnical index properties of Ankara Clay, using data from a single borehole.

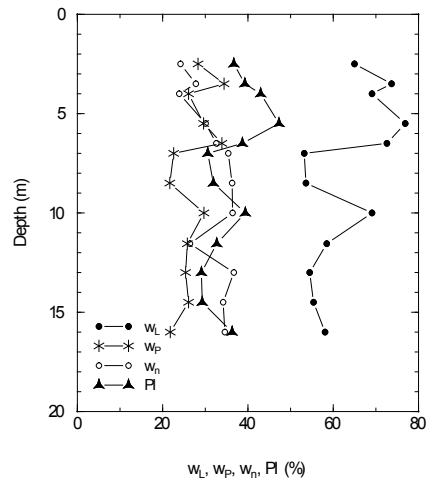


Figure 1. Typical spatial variability with depth for some geotechnical properties of Ankara Clay

Inherent variability results primarily from the natural geologic processes that produced and continually modify the soil mass in situ. This spatial variation, can be decomposed conveniently into a smoothly varying trend function $[t(z)]$ and a fluctuating component $[w(z)]$ as follows (Phoon et al. 1995):

$$\xi(z) = t(z) + w(z) \quad (4)$$

in which ξ = in situ soil property and z = depth. The inherent soil variability can be represented by the fluctuating component, if $w(z)$ is modeled as a homogeneous random field, as suggested by Vanmarcke (1983). To be homogeneous, the mean and variance of $w(z)$ should be constant with depth, and the correlation between $w(z)$ at two different depths should be a function only of their separation distance, rather than their absolute positions (Vanmarcke 1983). A constant mean of w equal to zero can be obtained if the data are detrended. The correlation as a function of separation distance is generally satisfied for data from a homogeneous soil layer (Phoon et al. 1995).

The vertical scale of fluctuation or correlation distance, which is the distance within which the soil property shows strong correlation, also is required to model inherent variability. Vanmarcke (1977) introduced the following approximation to estimate it:

$$\theta \approx 0.8d \quad (5)$$

in which d = average distance between the points where the fluctuating soil property and its trend function have equal values along the soil profile.

The published data that can be used to evaluate the coefficient of variation of inherent variability (COV_w) for c_u is very limited (Akbas and Kulhawy 2010), with the COV_w ranging from 11 to 35%. Note that a comparison of the mean COV_w ranges presented in the literature for fine-grained soils shows that, inherent variability values for Ankara Clay are consistently smaller than the “generic” guidelines. This result shows the possible advantage of developing and using statistics for a specific soil type in probabilistic analyses that lead to reliability-based design.

Akbas and Kulhawy (2010) reports the mean and range for the vertical scale of fluctuation of the undrained shear strength of Ankara Clay as 2.0 m and between 1.0 m and 3.0 m, respectively.

Measurement error enters the determination of soil properties through equipment, procedural-operator, and random testing effects. Note that, by definition, the measurement error (e) is not caused by the inherent soil variability (w), and therefore they are assumed to be uncorrelated. In principle, measurement errors can be estimated by quantifying the variations in repeated measurements of the same property on identical soil samples. For laboratory tests, very few studies of this kind can be found in the literature. Therefore, for Ankara Clay, “generic” values are used herein, which corresponds to a COV range between 5% and 15% for undrained shear strength.

For directly measured laboratory or field test properties, such as the undrained shear strength measured in triaxial tests, the inherent variability and measurement error are the only sources of uncertainty that need to be addressed in the design process. However, many geotechnical properties are estimated from laboratory indices or measurements or from other types of field measurements. This process introduces the third source of uncertainty, transformation error, which occurs where these field or laboratory measurements are transformed into design soil properties using empirical or other correlation models (Kulhawy 1992). These three sources of uncertainty can be combined consistently using the simple second-moment probabilistic approach suggested by Phoon et al. (1995), details of which are given elsewhere (Akbas and Kulhawy 2010).

This probabilistic framework was used to evaluate the total geotechnical variability for the undrained shear strength of Ankara Clay. Input values for the methodology include the previously presented inherent variability and scale of fluctuation, along with the generic measurement errors from the literature. Up-to-date correlation equations developed specifically for Ankara Clay, were used to estimate the transformation uncertainty.

3.1. Direct Laboratory Measurement of Undrained Shear Strength

For direct laboratory measurement of undrained shear strength, no transformation model is required, and therefore the COV of design parameter is given by:

$$COV_{\xi}^2 = COV_w^2 + COV_e^2 \quad (6)$$

in which COV_w and $COV_e = COV$ of inherent variability and measurement error, respectively.

The COV_w and COV_e for the undrained shear strength of Ankara Clay was reported to be between 11 and 35%, and 5 and 15%, respectively. By substituting these values into Eq. 6, the total point COV (COV_ξ) for undrained shear strength can be calculated to be between 12 and 38%.

3.2. Correlation with SPT N Value

Kulhawy and Mayne (1990) noted that a reasonable correlation between the undrained shear strength and the SPT N value can be achieved, provided the correlation is restricted to one type of geology. Sarigol (1988) compiled SPT N data along with the corresponding c_u values for Ankara Clay. These data were used to develop a local correlation, and the probabilistic equation for this correlation in exponential form is:

$$c_u / p_a = 0.17N^{0.58}10^\varepsilon \quad (7)$$

in which, p_a = atmospheric pressure, and ε = transformation uncertainty. After the required second-moment formulations, the corresponding COV is given as:

$$COV_\xi^2 = 0.58^2(COV_w^2 + COV_e^2) + (\ln 10)^2 s_\varepsilon^2 \quad (8)$$

in which s_ε = standard deviation of the transformation uncertainty. The standard deviation of the transformation uncertainty (s_ε) for the data of Sarigol (1988) is 0.33, which is consistent with the significant dispersion around the correlation equation. The COV_w for N is estimated to be between 10 and 46% (Phoon et al. 1995), and the COV_e is between 15 and 45%. Using these data, the total COV of c_u determined from SPT N is between 77 and 85%.

Based on data from 25 clay sites in Japan, Phoon et al. (1995) suggested the spatial average COV for c_u that is estimated from SPT N to be between 38 and 54%, which is significantly lower than the values obtained herein. Therefore, for c_u correlated with SPT N, the use of guidelines developed using data from other geologic settings does not allow the whole range of uncertainties to be taken into consideration in the case of Ankara Clay. This may also lead to unconservative results in reliability-based design.

The difference between the COV values determined for the laboratory measured c_u and c_u estimated from an SPT N value is striking. Intuitively, most geotechnical engineers would have more confidence in the laboratory measured undrained shear strength than that obtained using a local correlation with SPT N, and they would employ a smaller FS for the former case. However, the simple probabilistic framework illustrated above offers an effective tool for the realization of a numerical comparison of expected uncertainties for different levels of information about the subsurface conditions.

4. DESIGN IMPLICATIONS IN RANDOM FINITE ELEMENT METHOD

4.1. Selection of Parameters

The finite element analyses performed herein employs an elastic perfectly plastic stress-strain relationship with Tresca failure criterion. The theoretical basis of the method is described in detail by Smith and Griffiths (1998). The freely available software used in this study is called Mrbear2D. The soil parameters including dilation angle, ψ , elastic modulus, E and Poisson's ratio, ν , are assumed to be deterministic with specific constant values of 0° (i.e., no plastic dilation), 30000 kPa, and 0.49, respectively. Note that the elastic modulus does not affect the bearing capacity. The only random variable is the log-normally distributed undrained shear strength, which has a mean value of 100 kPa.

The finite element mesh consists of $10 \times 25 = 250$ square elements of 0.2 m length and width. The strip footing has a width of 1 m, and thus consists of 5 elements.

Based on the discussions above, the undrained shear strength random variable was characterized by its coefficient of variation (COV) and scale of fluctuation in x (horizontal) and y (vertical) directions. To simulate the level of uncertainty in the undrained shear strength based on its determination method, i.e., direct laboratory testing and correlation with SPT N value, a COV range between 10% and 90% was considered. The selection of this range is based on the analyses presented in the discussions above. Similarly, the correlation length in the vertical and horizontal directions were selected as 2 m and 30 m, respectively.

4.2. The Effect of Parameter Uncertainty and Anisotropy

The effect of the uncertainty in the undrained shear strength parameter was analyzed using a variation of COV between 10% and 90%. The lower values, i.e. a COV between 12% and 38%, correspond to direct determination of undrained shear strength from triaxial tests, and the higher values, i.e., a COV between 77% and 85%, belong to cases where the undrained shear strength is determined from SPT values. Both isotropic, i.e., $\theta_x = \theta_y = 2$ m and anisotropic ($\theta_x = 30$ m; $\theta_y = 2$ m) conditions were analyzed in order to comprehend its affect on the obtained results. The random fields for isotropic and anisotropic cases with COV of $c_u = 10\%$ is given in Figure 2 and Figure 3, respectively.

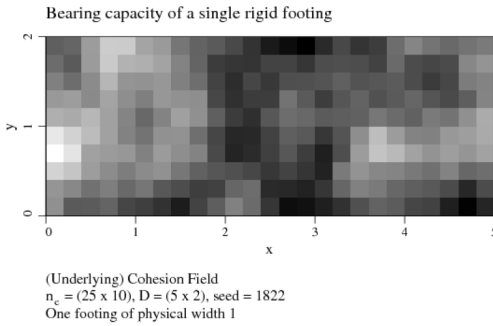


Figure 2. Random field for isotropic case with $COV_{c_u} = 10\%$.

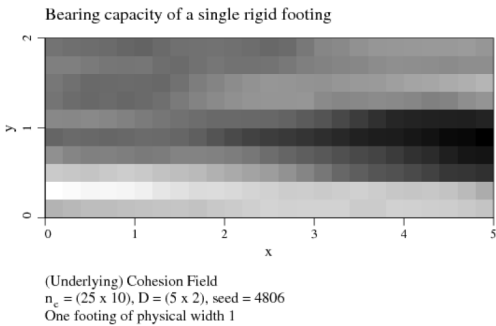


Figure 3. Random field for anisotropic case with $COV_{c_u} = 10\%$.

For the undrained bearing capacity problem considered herein, the theoretical ultimate capacity is calculated as 514 kPa for a mean undrained shear strength value of 100 kPa. Thus, for a typical foundation design which employs a factor of safety of 3, failure is real-

ized when the actual measured bearing capacity is less than $514/3 = 171.3$ kPa. Thus, in random finite element analyses performed in this study, failure is defined in this manner, and the probability of failure, and therefore the reliability index, β , was calculated accordingly.

The variation of reliability index with the coefficient of variation of undrained shear strength is shown in Figure 4, for a design with a factor of safety of 3. Typical results are also tabulated in Table 1 for both $FS = 3$ and $FS = 2$.

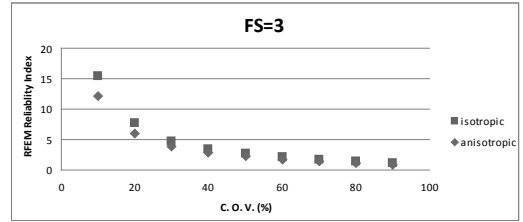


Figure 4. The variation of reliability index with the COV of c_u

Table 1. Reliability Index as a Function of Isotropy/Anisotropy and Factor of Safety

COV of c_u (%)	β (Isotropic)		β (Anisotropic)	
	FS=2	FS=3	FS=2	FS=3
10	9.5	15.4	7.5	12.2
30	2.8	4.8	2.3	3.9
50	1.4	2.7	1.3	2.3
70	0.7	1.7	0.7	1.5
90	0.3	1.1	0.2	0.9

A closer look at the results indicate that, the COV of the undrained shear strength has a very influential effect on the results. The reliability index values significantly decrease with increasing COV, and unacceptable levels of reliability is realized when the COV exceeds about 40% and 20% for designs with $FS = 3$ and $FS = 2$, respectively.

The results also indicate that the consideration of a realistic scale of fluctuation is an important factor in the obtained results. Finite element analyses of isotropic cases almost always resulted in higher reliability index values, compared to those calculated from anisotropic analyses. Note that this difference diminishes with increasing COV of the undrained shear strength.

5. CONCLUSIONS

This paper focused on the statistical characterization of the undrained shear strength of Ankara Clay, and the effects of the obtained parameters on the reliability of undrained bearing capacity calculations. First, a first-order second moment probabilistic approach was used to combine the inherent variability, the measurement error, and when required, the transformation error consistently, for determining the total variability of the undrained shear strength. Then, random finite element method was employed for a robust estimation of the effects of uncertainties on the probability of failure or reliability index of designs. The results indicate that:

- The variability of the undrained shear strength as characterized by the COV is very much dependent on the method by which it was estimated. Undrained shear strength obtained from direct laboratory testing has a much smaller uncertainty compared to that obtained from SPT N values.
- COV of the undrained shear strength has a very important effect on the probability of bearing capacity failure of the resulting design. The calculations performed using typical values of geotechnical parameter variability for Ankara Clay suggests that, it is not possible to reach the target reliability index range for ultimate limit state suggested in the literature, i.e., 3.2 to 3.7, using undrained shear strength values estimated by SPT N values. On the other hand, employing triaxial test results achieves the required safety level for designs with $FS = 3$.
- It is understood that for the current practice, a $FS = 2$ is not capable of reaching the desired reliability in the undrained bearing capacity design of footings, unless the site is unusually homogeneous or well-characterized, i.e., the COV of the c_u is less than about 20%.
- Although the difference becomes negligible for high values of COV of c_u , finite element analyses of isotropic cases almost always resulted in higher reliability index values, compared to those calculated from anisotropic analyses. Thus, the difference in the scale of fluctuation in the horizontal and vertical directions should be taken into account in reliability analyses for foundation design.

6. REFERENCES

- Akbas, S.O. & Kulhawy, F.H. 2010. Characterization and estimation of geotechnical variability in Ankara Clay: a case history. *Geotechnical and Geological Engineering*, Vol. 28, No. 5, pp. 619-631.
- Erguler, Z.A. & Ulusay R. 2003. A simple test and predictive models for assessing swell potential of Ankara (Turkey) clay. *Eng. Geol.*, Vol. 67, No. 3-4, pp. 331-352.
- Fenton, G.A. 1999. Estimation for stochastic soil models. *ASCE J. Geotech. Geoenv. Eng.*, Vol. 125, No. 6, pp. 470-485.
- Fenton, G.A., Griffiths, D.V. & Zhang, X. 2008. Load and resistance factor design of shallow foundations against bearing failure. *Canadian Geotech. J.*, Vol. 45, No. 11, pp. 1556-1571.
- Ordemir, I., Alyanak, I. & Birand A.A. 1965. *Report on Ankara Clay*. Ankara: METU Publications.
- Fenton, G.A. & Griffiths, D.V. 2003. Bearing capacity prediction of spatially random c- ϕ soils. *Canadian Geotechnical Journal*, Vol. 40, No. 1, pp. 54-65.
- Kulhawy, F.H. & Mayne, P.W. 1990. *Manual on estimating soil properties for foundation design*. Report EL-6800. Palo Alto: Electric Power Research Institute.
- Phoon, K.K., Kulhawy, F.H. & Grigoriu, M.D: 1995. *Reliability-based design of foundations for transmission line structures*. Report TR-105000. Palo Alto: Electric Power Research Institute.
- Phoon, K.K. & Kulhawy, F.H. 1999. Evaluation of geotechnical property variability. *Canadian Geotechnical Journal*, Vol. 36, No. 4, pp. 625-639.
- Sarigol, S.I. 1988. A study on correlation of soil parameters for Ankara clay. *M.Sc. Thesis*. Ankara: METU.
- Smith, I.M. & Griffiths D.V. 1998. *Programming the Finite Element Method*. NY: John Wiley & Sons.
- Tonoz, M.C., Gokceoglu, C. & Ulusay, R. 2003. A laboratory-scale experimental investigation on the performance of lime columns in expansive Ankara (Turkey) clay. *Bulletin of Engineering geology & the Environment*, Vol. 62, No. 2, pp. 91-106.
- Vanmarcke, E.H. 1977. Probabilistic modeling of soil properties. *J. Geotech. Eng. Div. ASCE*, Vol. 103, No. GT11, pp. 1227-1246.
- Vanmarcke, E.H. 1983. *Random fields: Analysis and Synthesis*. Cambridge: MIT Press.
- Vessia, G., Cherubini, C., Pieczynska, J. & Pula, W. 2009. Application of random finite element method to bearing capacity design of strip footing. *Journal of GeoEngineering*, Vol. 4, No. 3, pp. 103-112.

Soil-structure interaction analyses for the study of nuclear power plant foundation alternatives under static and seismic loading

Martin Vaníček

GEOSYNTETIKA, s.r.o., Czech Republic

Ivan Vaníček

Czech Technical University in Prague, Faculty of Civil Engineering, Geotechnical Department, Czech Republic

ABSTRACT: Main aim of the study was the evaluation of the possibility to realize construction of nuclear power plant from the foundation point of view for selected locality of the wider character and for existing geological and geotechnical conditions. Paper describes feasibility study, during which both static and seismic loadings were evaluated. Geological and geotechnical conditions are therefore briefly specified. For 2 typical representatives of nuclear blocs of the third generation produced worldwide (one for lower capacity around 1200 MW and second one for roughly 1800 MW) subsoil improvement was proposed in different alternatives. These alternatives were consequently verified using numerical soil-structure interaction modelling.

1. INTRODUCTION

The paper describes some outputs of the feasibility study which was performed by the authors. The main aim of this feasibility study was specification of the geotechnical conditions under which it is possible to realize new nuclear power plant (NPP) for selected geological area with specified geotechnical characteristics and for expected seismic loading.

The basic output of the first stage of the feasibility study was the statement that for the wider selected area the section with a length of 200 m can be found (similarly area 200m × 200m) where the surface and basic subsoil layers are practically parallel and horizontal. Therefore the selected area can be judged as appropriate from the foundation engineering point of view as the potential risk connected with differential settlement is very low.

Geological model specifies 3 basic subsoil layers as the result of most simple interpretation of all data obtained for the selected locality and it's surrounding:

- Top layer with thickness of about 15 m is composed from the fine grained soils, marked as loess or loess loam, in lowest part as alluvial clays;
- Middle layer with thickness of about 13 to 20 m is composed from more permeable, coarser materials as gravel, sandy-gravel, sand. Ground water table was observed there.

- Bottom layer, pre-quaternary is on the top also coarser – gravel, sandy-gravel, sand; however gradually finer up to clay character. Maximum depth in which tertiary clays were recorded was 44 m.

Geotechnical model was specified from the set of realized field and laboratory tests, including geophysical tests. From evaluation it was possible to define for basic layers (and even for more detailed specification of subsoil) characteristic values of geotechnical properties (shear strength, modulus of deformation) needed for calculation model – first of all for numerical modelling.

From the other geotechnical investigation the following outputs are important ones:

- Top loess layer is more compressible however is not sensitive to the structural collapse;
- Layer of sands is not sensitive to the liquefaction during seismic loading;
- Ground water level is relatively stable with minimal observed fluctuations and is not aggressive.

With respect to the nuclear power plant the concentration was focussed on the main object – building of the nuclear reactor and basic specification from the main suppliers of these reactors were collected, firstly from the view of ground plans, depth of foundation, centre of gravity, contact pressure at the foundation bottom or values of acceptable total and differential settlements.

For closer study 2 typical examples of the nuclear reactors were selected, one with so called lower energy output and the second one with higher energy output which also had different ground plans, the first one with circular foundation slab and the second one with rectangular foundation slab.

2. SOIL STRUCTURE INTERACTION FOR STATIC LOADING

Analytical calculation model was used for the basic limit states – ultimate and serviceability limit states. As expected more important is the limit state of serviceability, namely value of the total settlement. Calculated values of the total settlement significantly exceeded acceptable values (usually around 200 mm), even when for the settlement the model using so called principle of structural strength was used, Vaníček I. and Vaníček M. (2008) or Vaníček I. and Vaníček M. (2013). This model is giving generally lower values of settlement than settlement calculation based on the theory of elastic half space. Therefore it was necessary to propose subsoil improvement.

Subsoil improvement was proposed in two different alternatives, specified in the Fig. 1.

Proposals for the subsoil improvement are based on the preference of shallow foundation and the following options were examined:

- Subsoil improvement with the help of sandy-gravel cushion, where part of the less

appropriate soil (loess) is substituted by sandy-gravel;

- Subsoil improvement with the help of piles, which are embedded into gravel layer and are in upper part interconnected by reinforced concrete slab.

Both options have preferred sub-options, when sand-gravel cushion is reinforced by geosynthetic layers. Similarly the piles are also reinforced around outer perimeter by geotextiles or geogrids with very high initial tensile stiffness. The proposal comes from the positive evaluation of the sensitivity of reinforced earth structures during seismic loading when very high initial tensile strength is increasing stiffness for short time seismic loading.

In both cases 0.5 m thick very well compacted gravel layer is proposed between the zone of improvement and foundation slab as this layer has positive impact on the interaction of building of reactor with subsoil for seismic loading.

The thickness of the reinforced cushion is between 4.5 to 6.0 m for different NPP. So it means that still about 2.0 to 3.0 m of fine soil remained in place, which is able to protect ground water in lower gravels from potential contamination from the surface. This fact can play very positive role during the EIA evaluation process.

The length of the piles is about 10 m and they are embedded into gravel layer on the length of about 3 m.

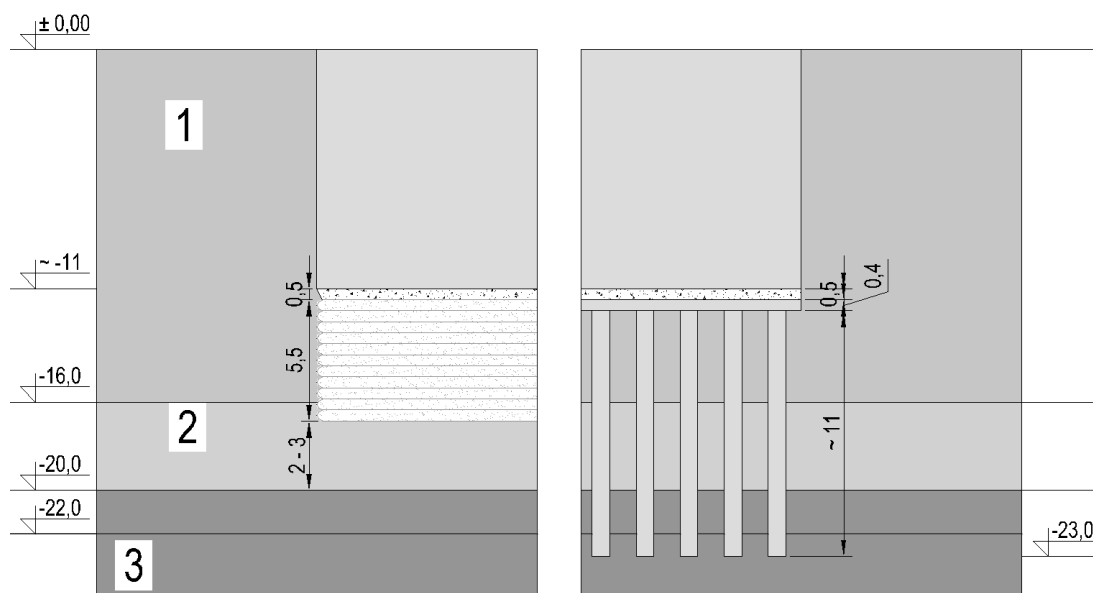


Figure 1. Subsoil improvement options – 1. loesses, 2. alluvial clays, 3. gravels

Subsoil improvement has very positive impact on the limit state of serviceability for both cases of subsoil improvement. Maximum value of foundation slab settlement is now about 160 mm what is now acceptable value.

Software PLAXIS was used for numerical modelling, namely in connection to the soil structure interaction problems. This software based on FEM has the possibility to simulate the real soil behaviour using different constitutive models. During this phase of study the planar solution (2D) was applied for geometrical model with width 2×200 m and depth 100 m. 3 D solution will be applied in the future as it is more sensitive to the arrangement of individual parts of NPP and to the specification of the technology of construction (with respect to the different depth of foundation and different contact pressure for different buildings).

The subdivision of ground respected different layers in subsoil together with ground water table. Finite element spacing was adapted to the boundary conditions with detailed spacing around places of concentration of stresses. With the help of parametric study it was approved that the constitutive model "Hardening soil small strain model" is the closest to the analytical solution for settlement using principle of structural strength. This specified model can define different stiffness of soil; for virgin loading, for repeated loading or for the phase of unloading.

The soil structure interaction for static loading was described in more detail by the authors previously – Vaniček I. and Vaniček M. (2014), with the following main outputs, which are in very good agreement with theoretical assumptions:

- Just before the top of tertiary clays the deformation values are close to zero.
- Total settlement is roughly 160 mm for sandy-gravel cushion even for the cushion thickness of only 4 m.
- Lower total settlement of about 60 mm was calculated for the subsoil improved by piles.
- The contact pressure in the footing base is relatively constant with excesses at the end of slab.
- Small plastic zones are confined and there are no marks of further propagation.

3. ANALYSIS OF SOIL STRUCTURE INTERACTION FOR REACTOR BUILDING DURING THE SEISMIC LOADING

This analysis is the main part of the feasibility study as it should prove that the behaviour of ground and realized structure during the seismic loading is within acceptable limits.

3.1. Evaluation of subsoil from the view of seismic wave spreading

The values of seismic wave spreading were discovered during the ground investigation, namely geophysical investigation. Seismic wave S (secondary/shearing) is generating significant amplitude of the horizontal movement of the earth surface and is evaluated as the main reason of seismic damage. The velocity of the seismic wave spreading S (V_s) is increasing with depth. For upper layer composed from fine grained soil this velocity is increasing from the value of 150 m/s up to 400 m/s. For gravel and sandy soils is increasing up to the 1000 m/s for the base of this layer with another small increase with depth (in the depth of 100 m – for the model base it is roughly 1200 m/s). The velocity of the primary/longitudinal seismic wave P (V_p) were discovered roughly twice higher. For the purposes of the seismic analyses the observed locality was classified into type 2 according to the IAEA, Safety Standard NS-G-3.6, (2006), for which: $1100 \text{ m/s} > V_s > 300 \text{ m/s}$.

3.2. Design seismic level

The observed locality is falling into Seismic Level 2 – SL 2, which corresponds to a level with a probability of 10^{-4} per year of being exceeded, which is characterized by peak acceleration values (PGA) – for the horizontal direction PGA_{hor} and for the vertical direction PGA_{vert} .

Seismic loading with the peak acceleration values of $\text{PGA}_{\text{hor}} = 0,195 \text{ g}$ and $\text{PGA}_{\text{vert}} = 0,101 \text{ g}$ for the model base resp. $\text{PGA}_{\text{hor}} = 0,349 \text{ g}$ a $\text{PGA}_{\text{vert}} = 0,214 \text{ g}$ for the upper layer of gravels was used. This loading respects new directive of IAEA SSG-9 (2010) and also the information obtained on the locality. After that 3 artificially created accelero-graphs with total length of 20 seconds and with step of 0.002 second were specified independently for each

direction, it means 2 for horizontal directions (x and y) and 1 for vertical direction (z).

3.3. Modelling of seismic waves spreading through ground

For specified accelero-graph, see for x direction Fig. 2, its change was modelled from the level of the gravel layer surface (-20 m) to the base of numerical model (-100 m). At the base the accelero-graph was slightly rearranged in such manner that after recalculation to the gravel surface the same maximum value was obtained as initially defined. Software PLAXIS recalculated the given accelero-graph for new boundary conditions at the modelled base – for deformations which are used as input data for the actual numerical modelling – see Fig. 3.

3.4. Results of the soil structure interaction for seismic loading

The modelling with the same software and modelled area was performed step by step, however the outputs are interpreted only for the final phase of seismic loading. From the view of boundary conditions the software is using an adsorption boundary for which the model is using viscose boundary (dashpot).

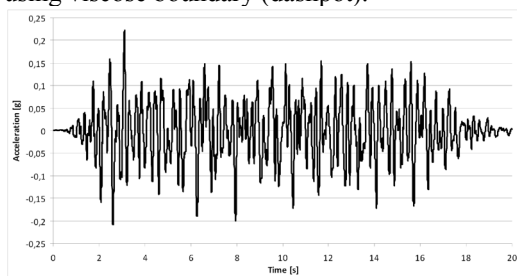


Figure 2. Accelerograms for x direction at the level of -20 m.

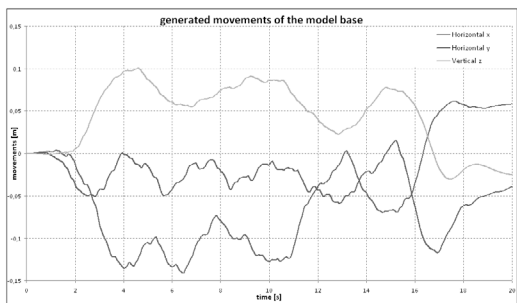


Figure 3. Displacements on the model base generated by the PLAXIS software.

During the first verification phase 2D model was applied which was at the base loaded by accelero-graph from the free field. Numerical modelling was very comprehensive, not only for both representatives of the energy output NPP but also for both cases of ground improvement and for basic combination of accelero-graphs x + z resp. y + z. The results of these analyses are interpreted in the graphical forms as e.g. residual deformation after 20 seconds of the seismic loading, as maximal values of vertical or horizontal deformation during the phase of seismic loading, maximal values of acceleration (in g) during seismic loading, resp. in the form of isolines of the total deformation in individual directions after 20 seconds.

During the second final phase for the actualized accelero-graph defined to the base of the numerical model and recalculated for the new boundary conditions as described earlier, the numerical modelling of the seismic loading started, similarly as during the first phase of verification. The outputs are presented in Figures 4, 5 and 6. However the most illustrative form of the results presentation is the video showing the movement of the reactor building during the phase of the seismic loading.

4. CONCLUSION

From this very comprehensive analysis the following outputs can be emphasized:

- Significance of the simulated seismic loading – the results obtained for both accelero-graphs reflect not only the significance of the maximal acceleration values but also the character of the simulation of the horizontal impulse. From the view of the vertical movement the results for the actualized accelero-graph are less significant, however were emphasized for the residual horizontal deformation, which is around 30 to 60 mm, while for the first accelero-graph was close to zero.
- Significance of the simulated building of reactor – the alternative case for lower energy outputs NPP had higher contact pressure (and also surcharge) for the footing base and so also higher residual vertical settlement reaching up to 60 to 75 mm for the subsoil improved by sand-gravel cushion. However the uplifts of both buildings during seismic loading were very close, for the footing base around 130 to 160 mm.

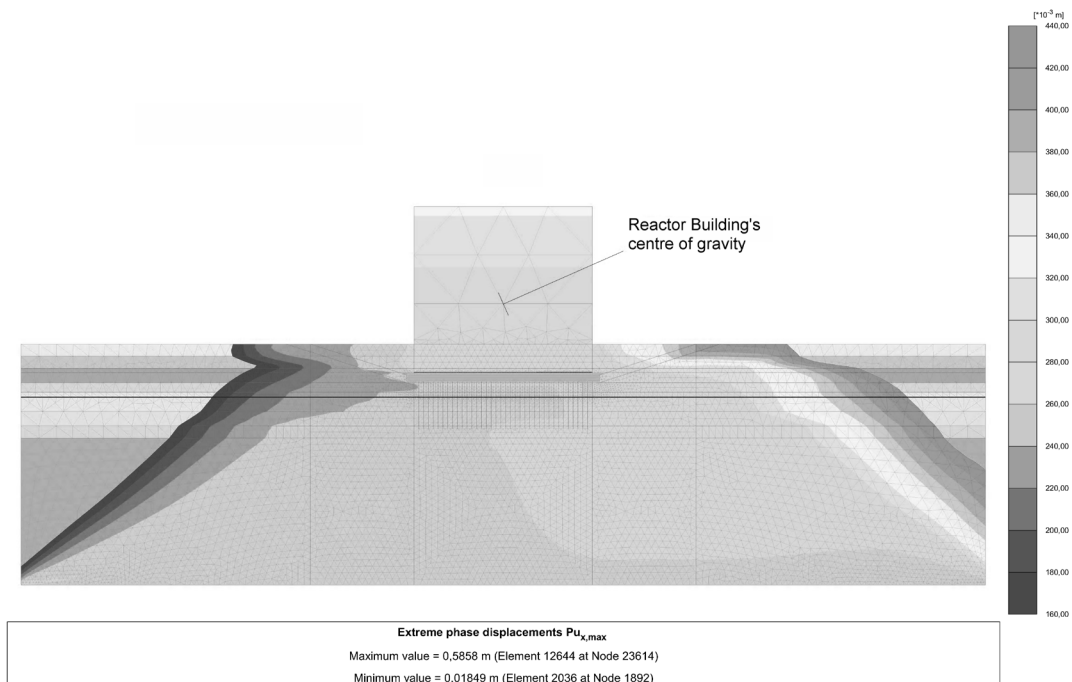


Figure 4. Maximal horizontal deformation during the seismic event - Subsoil improvement by geogrid reinforced sandy-gravel cushion.

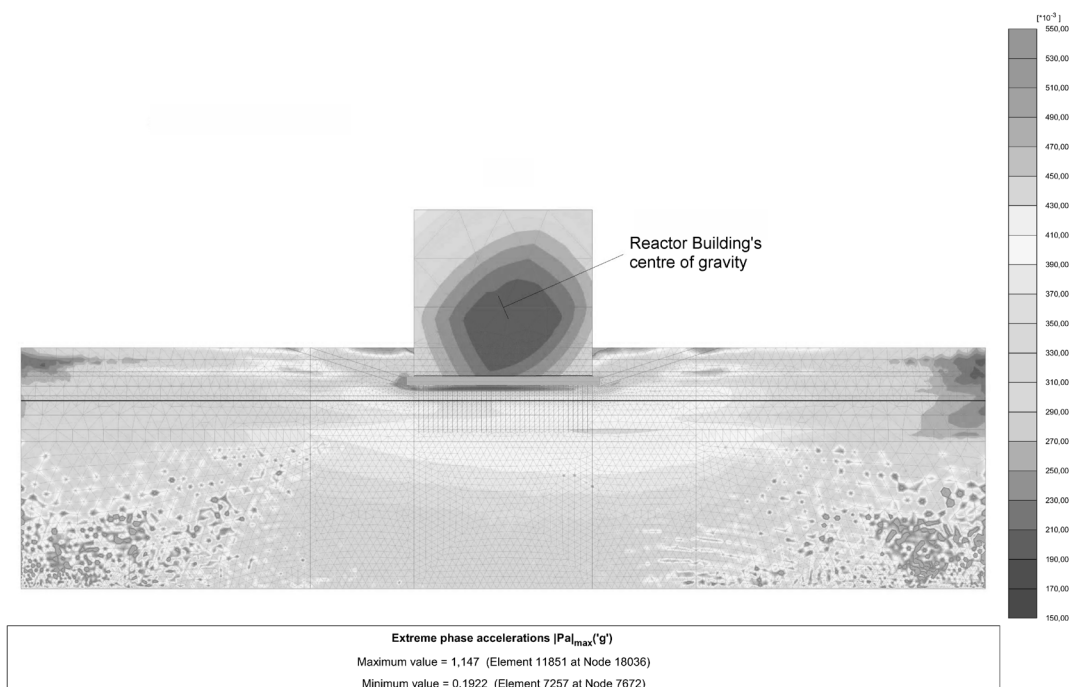


Figure 5. Maximal acceleration [g] during the seismic event - Subsoil improvement by geogrid reinforced sandy-gravel cushion.

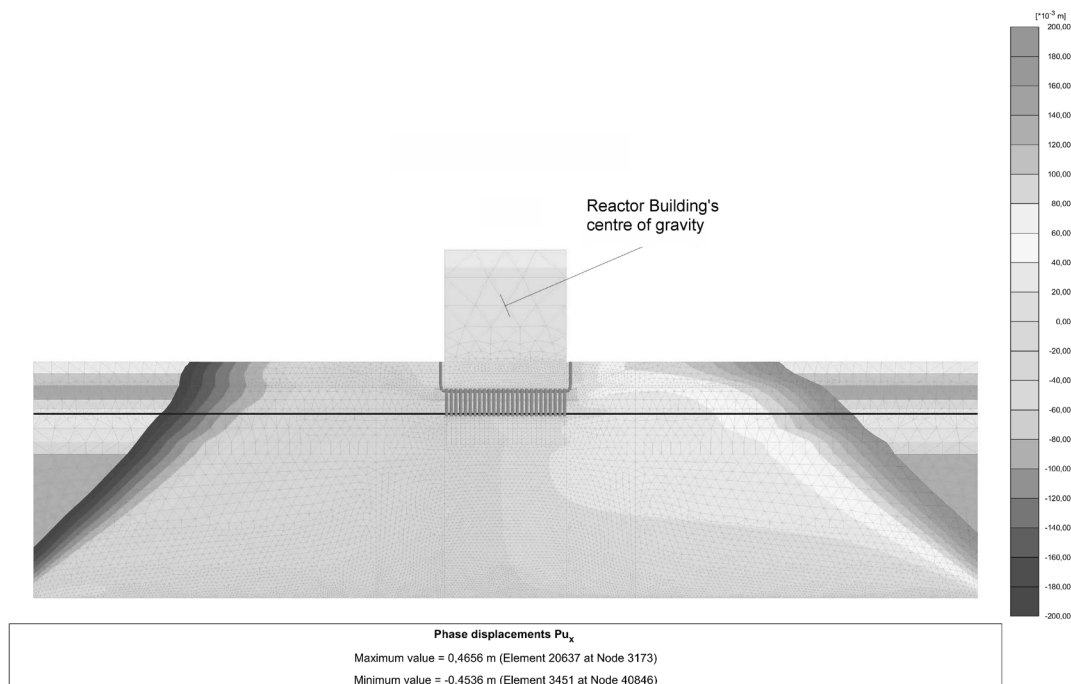


Figure 6. Residual horizontal deformation after the seismic event – Subsoil improvement by piles.

- Significance of the subsoil improvement method – the differences were obtained first of all from the view of residual settlement, when for improvement with piles had lower values, about 40 mm. The differences for the other observed aspects were not so obvious. Probably as the result of the application of the same gravel interlayer (0.5 m thick) between part of improvement and footing base.

The performed analyses approved a safe foundation of the main buildings of the potential NPP in the proposed locality not only for static loading but also for expected seismic loading. Finally this feasibility study also helped to define next steps needed for next phase of project specification.

5. REFERENCES

- IAEA, 2006. *Safety Standard NS-G-3.6, Geotechnical Aspects of Site Evaluation and Foundations for Nuclear Power Plants*. Vienna: International Atomic Energy Agency.
- IAEA, 2010. *Specific Safety Guide No. SSG-9, Seismic Hazards in Site Evaluation for Nuclear Installations*. Vienna: International Atomic Energy Agency.
- Vaniček, I. & Vaniček M. 2008. *Earth Structures in Transport, Water and Environmental Engineering*. Springer, 637 p.
- Vaniček I. & Vaniček M. 2013. Experiences with Limit State Approach for Design of Spread Foundations. *Chapter in book: Geotechnical Design Codes of Practice. Implementation, Application and Development*. P.Arnold, G.A.Fenton, M.A.Kicks, T.Schweckendiek, B.Simpson (ed.). Amsterdam: IOS Press.
- Vaniček, I. & Vaniček, M. 2014. Static Foundation Analysis Study for Nuclear Power Plant. In: *Proc. of the All Russian conference with International Participation: "Deep Foundations and Problems of Underground Space Development"*. Perm.

Analysis of soil-structure interaction by Ménard pressuremeter tests and ground improvement case histories

S. Varaksin

ISSMGE TC211 Chairman, France

B. Hamidi

GFWA, Australia

ABSTRACT: The pressuremeter is one of the leading tools that allow direct measurement of the soil structure interaction. Its almost full scale loading of soils during testing, its applicability to most soil types, and recently, to soft rocks has allowed major progress in the understanding, design and control of soil improvement, where treated soils will have to meet preset criteria. Structures can be designed based on Menard's rules, this with a tested volume allowing the 98 % confidence in predicting the soil structure behavior, which is by far more than current practice. Indeed the approach of Louis Menard directly uses the limit pressure, PLM, as the parameter governing bearing capacity, without relying on failure criteria and hypotheses, and the pressuremeter modulus, EM, is directly related to deviatoric deformation and adopted for volumetric deformations as well. The selected case histories illustrate the essential input of the Menard Pressuremeter in various applications.

1 INTRODUCTION

The first encounter of the first author with the Menard pressuremeter dates back to approximately 40 years ago when, during his military service, he was given the task to perform two borings to the depth of 42 m and to carry out one pressuremeter test every 1.5 m. The tools used were a hand auger, a bentonite hand pump and a tripod with a mechanical winch.

After six months of hard work, he met Louis Menard who laughed about this performance, and then proposed that he join the recently created ground improvement department of Menard's organization.

1 FIRST STEPS IN GROUND IMPROVEMENT

The construction of the Mandelieu la Napoule development in the French Riviera in 1969 was one of the first opportunities for understanding dynamic compaction. There, Louis Menard proposed to the developer to compact the 110,000 m² reclaimed site using Menard's recently invented dynamic compaction technique, and to build his five story buildings using shallow footings rather than implementing the classical and costly piled foundations that had to additionally sustain the negative skin friction created by the fill weight. With Menard's method, the ground would have indeed become so dense that the required bearing would have become available without the risk of excessive total and differential settlements.

The first English publication of Menard and Broise (1975) proposed a relation between the behaviour of saturated fill under heavy impact and pore water pressure (see Figure 1). At that time, the concept of effective stress was only well understood

in academia and still not used in the industry's common practice. However, Menard was able to implement this concept into his work and the grid definition and rest period between dynamic compaction works in phases were born.

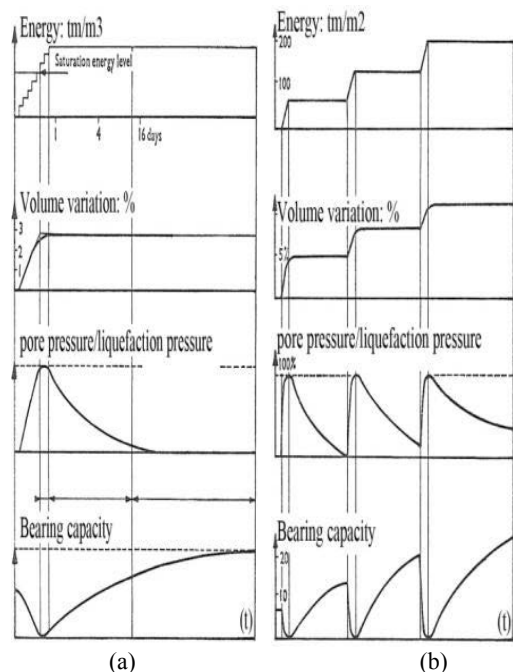


Figure 1. (a) changes in the soil after consolidation phase, (b) Variation to a soil subjected to a series of dynamic consolidation passes (Menard, 1975)

2 PRESSUREMETER AND SELF BEARING IN FILLS

Although theoretical soil mechanics is well advanced in normally and over consolidated soils, little data and theory is available for recent granular fills that are undergoing deformation under self weight with passage of time. It appears that the pressuremeter is indeed the only testing tool that can quantify the phenomenon of self bearing or creep. Menard (1975) proposed, as a rule of thumb, that the pressuremeter limit pressure, P_l , has to be equal to or greater than 6 bars (600kPa) to reach self-bearing in sands of less than 10 m thickness. As a first approximation, he also proposed to estimate the one-year creep of any soil by:

$$w_{year1} = \frac{h}{1000} \frac{1 - \alpha P_l / 2}{\alpha P_l / 2} \quad (1)$$

Where w is settlement in cm, h is fill thickness in cm and α is the structure coefficient variable according to the nature of the soil and the ratio of Menard modulus, E_M , to P_l . The unit for P_l in Equation 1 is bars.

Al Quo'a New Township was a new development in the deserts of UAE that was to be constructed on levelled dune sands. While some areas of this 3.8 million m² site was on competent ground, approximately 1.13 million m² of the project was located on loose fill with thicknesses similar to Figure 2, and sometimes up to 28 m thick (Hamidi et al., 2010). The project's developer had first-hand experience of creep, excessive total and differential settlements and building cracking in the first phase of the development, and was seeking a means to ensure that the same problems would not be repeated.



Figure 2. Leveling desert dunes with backfills up to 28 m thick (Hamidi et al., 2010)

It is the authors' experience that the most suitable acceptance criteria for ground improvement projects should be the same as the design criteria (Hamidi et al., 2011). In order to address the bearing, total, differential and creep settlement requirements, the

project's acceptance criteria were defined as summarised in Table 1 and Table 2.

Table 1. Acceptance criteria for villa areas

	Safe bearing	Self-bearing
Level where parameters prevail	-0.75 to -5.50 m RL	From -5.50 m RL
P_l	750 kPa	600 kPa
E_M	4.8 MPa	4 MPa

Table 2. Acceptance criteria for non-villa areas

	Safe bearing	Self-bearing
Level where parameters prevail	From ± 0.00 m RL	From ± 0.00 m RL
P_l	600 kPa	600 kPa
E_M	4 MPa	4 MPa

Dynamic compaction was implemented in the project using pounders weighing up to 25 tons to treat more than 90% of the loose fill. The excessive treatment depth of the remaining 10% of the project required the implementation of heavier pounders; hence the MARS (Menard Accelerated Release System) that is shown in Figure 3 was developed to drop a 35 ton pounder in cable-less free fall. This release system was able to self-attach itself to the pounder at the end of each drop cycle.



Figure 3. MARS pounder release system (Hamidi et al., 2010)

In addition to the 50 pressuremeter tests that were carried out before dynamic compaction, to confirm the thickness of loose fill over this vast site, an affordable and innovative method of quick probing was used in this project. Rather than performing thousands of conventional tests, such as CPT, that would have required a long execution time and would have resulted in considerable costs, a vertical drain installation rig was mobilised and the mandrel tip pressure was recorded. Although this testing method

cannot be used to estimate bearing capacity and settlements, it was never-the-less an affordable and useful tool for determining the loose fill thickness. At the end of works 200 pressuremeter tests, such as shown in Figure 4, were performed to confirm that acceptance had been achieved. A comparison of pre and post dynamic compaction limit pressures is given in Figure 5.

Varaksin et al. (2005) used the pressuremeter test results to estimate the fill's creep using Equation 1 for a period of one year and then extended it to a period of 50 and 70 years by a decreasing logarithmic law. The settlement, w , for any year, n , and for a total of t years for reaching self-bearing status will be:

$$w = w_{year1} \frac{\ln \frac{t+1}{n}}{t+1} \quad (2)$$

Varaksin et al. (2005) also used Menard's empirical idea of limit pressure doubling for every 3% of strain to estimate the amount of dynamic compaction induced subsidence to reach self-bearing. Hamidi et al. (2010) formulated this concept:

$$\varepsilon = \frac{\log \left(\frac{(P_l)_j}{(P_l)_i} \right)}{\log 2} a \quad (3)$$

ε = strain

$(P_l)_i$ = limit pressure before soil improvement

$(P_l)_j$ = limit pressure after soil improvement

a = percentage of strain induced for doubling of the P_l (3%)

Ground improvement induced subsidence, s , can then be estimated based on the increase in P_l values:

$$s = \sum_{k=1,m} h_k \varepsilon_k = \frac{a}{\log 2} \sum_{k=1,m} h_k \log \left(\frac{(P_l)_j}{(P_l)_i} \right)_k \quad (4)$$

m = number of pressuremeter tests in the borehole within the improvement zone (i.e. the depth where P_l has increased), and h_k is the testing interval length.

This concept was further extended to estimate the increase in P_l (Hamidi et al., 2010a) and E_M (Hamidi et al., 2011a) in depth using dynamic compaction subsidence.

3 PRESSUREMETER AND DEEP RECLAMATIONS

As shown in Figure 6, Tsing Yi Oil Terminal in Hong Kong includes 39 steel tanks, 20 m high and up to 46 m in diameter. This 8 hectare facility has been built on a 40 m deep dredged reclamation formed predominantly of hydraulically placed sand fill (Hendy and Muir, 1997).



Figure 4. Pressuremeter testing

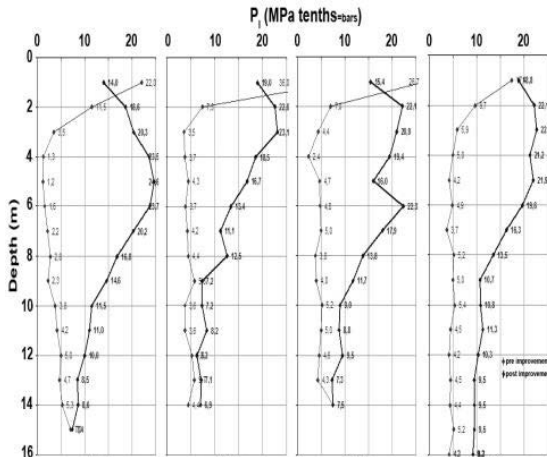


Figure 5. Comparison of typical pre and post dynamic compaction limit pressures in Al Quo'a (Varaksin et al., 2005)



Figure 6. Tsing Yi Oil Terminal

The soft clay and the base sand were dredged up to 40 m depth, a stone dyke was built to contain the fill and ground improvement by vibro compaction and surcharging until total stabilisation of the fill was planned. The project specification allowed the surcharge to be removed only if no settlement was recorded during a one month period. This was a

potential risk for the project that was already bound by a tight schedule.

The settlement criteria specified by the tank fabricators limited total long term settlement at the tanks' shells to 150 mm and the long term differential settlement around the shell perimeters and across the diameters to 1:360 and 1:80, respectively. Settlement limits related to the design life of 50 year design life of the tanks, including hydrotest under a full tank loading.

Thus, an alternative construction method using dynamic consolidation was proposed by the contractor. In the new scheme the fill mass was improved by dropping pounders weighing up to 40 from as high as 40 m. The prints were backfilled with rock and further compacted with the same equipment to create a stiffened raft.

Pressuremeter tests were performed in the rock columns and the sand fill and settlements were predicted using finite element analysis based on a medium of varying stiffness with depth over a rigid base. The D-60 rules (Menard, 1975) were also used and tank settlements of 4 to 7 cm were predicted. Hydrotest settlement data showed comparable results with the analytical estimates. The most critical tank was No. 1311 which was located on a fill with a variable thickness of 20 m from one side to the other side and a maximum fill thickness of 40 m. Hendy and Muir (1997) report the settlement of this 46 m diameter tank during the hydrotest to have been from 55 to 77 mm. The pressuremeter showed to be the ideal tool for measuring the required parameters in the rock columns and the compacted sand fill.

4 PRESSUREMETER FOR PRE-TEST, DESIGN AND SIMPLIFIED CRITERIA

The 5.6 million m² King Abdulla University of Science and Technology (KAUST) is located in Rabigh on the coast of the Red Sea and near the city of Jeddah in Saudi Arabia. KAUST, originally anticipated to have buildings with at most two to three storeys. The project was fast track and master planning, architectural and structural design and construction all had to be completed in less than three years. Thus there was great need for flexibility, coordination and overlapping of tasks (Hamidi et al., 2010b).

The preliminary geotechnical investigation that was carried out rather sparingly indicated that the ground was very heterogeneous loose or soft soils with rapid variations of ground conditions within short distances of even 10 m. This investigation and further testing during the works indicated that more than 2,600,000 m² of the construction area was to be built on soil consisting of up to 9 m of loose silty sand or soft sandy silt that is locally called sabkah. A schematic cross section of the site is shown in Figure 7).

As the investigation was not able to clearly define the soil profiles and consequently the ground improvement method to be applied, a dynamic reconnaissance phase was adopted by dropping a 20 ton pounder from 20 m and visual observation.

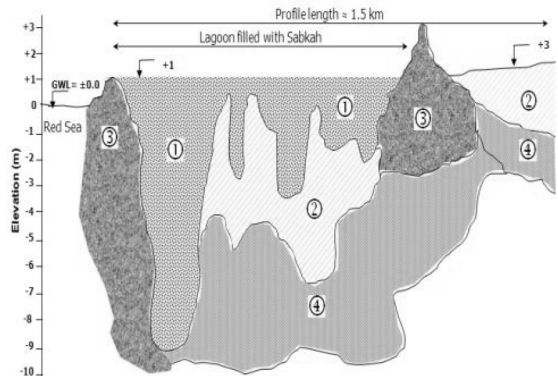


Figure 7. Schematic cross section of the KAUST ground conditions (Hamidi et al., 2010b)

Pressuremeter tests provided the parameters for the design of footings on sand or silt. As the buildings and thus footing locations were not defined at that phase, a 2 m thick sand platform was allowed on top of the silt to ensure the distribution of loads to dynamic replacement columns by arching.

The design and construct ground improvement proposal that met the project manager's technical requirements, schedule and budget was based on the below design criteria:

- Footing location: Any place within the treatment area
- Maximum footing load: 1,500 kN
- Allowable bearing capacity: 200 kPa
- Maximum total settlement: 25 mm
- Maximum differential settlement between two adjacent footings: 1/500
- Liquefaction mitigation for an earthquake with peak ground acceleration equal to 0.07g
- Level: 0.8 m below final ground level, but in any case at least 2 m above sabkah level

A pilot test was realised with pressuremeter testing and SPT (with grain size) to define boundaries of application of the dynamic compaction and dynamic replacement techniques as a function of grain size, limit pressure and applied energy (see Figure 8). Furthermore, a spread sheet based on D60 rules (Menard, 1975) was prepared for the quick estimation of the bearing capacity and settlement by the site engineer.

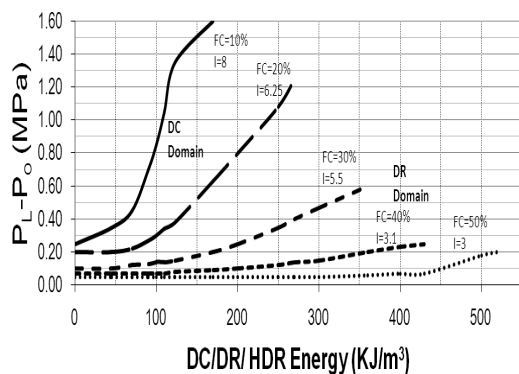


Figure 8. The relationship between net limit pressure, fines content and improvement energy (Hamidi et al., 2010b)

Of course, the boundary of application was a limit pressure of equal to or greater than 760 kPa for dynamic compaction zones and 180 kPa in between the granular columns of the dynamic compaction zones to provide sufficient lateral constraint to the columns.

Ground improvement on site was carried out by using a combination of dynamic compaction and dynamic replacement. Major changes to loads of some buildings later introduced the need to utilise dynamic surcharging as well. Dynamic compaction pounders used in this project weighed up to 21 tons.

Dynamic replacement was used in areas where the maximum depth of sabkah was 5 m. High energy dynamic replacement was used when the sabkah layer's depth was more than 5 m. In such a case, in addition to the engineered fill required for reaching final ground level, a 3 m surcharge was placed over the area for 3 weeks.

After completion of ground treatment in some areas, it became known that the revised master plan incorporated 20 six storey buildings. Hence, dynamic surcharging was also used to consolidate the deep sabkah layers. In this technique a combination of preloading and vibration is used to re-introduce pore pressure in the soil-water system and consequently to accelerate settlement rates. In addition to the engineered fill required for reaching final ground level a 3 m high surcharge was placed and dynamic compaction was performed on it.

Differences in ground behaviour due to pounder impact enabled the site supervisors to assess the rapidly varying ground conditions and to apply the appropriate ground improvement technique as needed. It was observed that while the first dynamic compaction pounder impact penetrated the ground by about 0.25 m, the dynamic replacement pounder penetration was substantially more and in the range of about 1 m. Also, performing dynamic compaction frequently resulted in the seepage of groundwater to the surface, but this phenomenon was rarely encountered in dynamic replacement areas. Ground rest periods in between dynamic compaction phases were 1 to 3 days, but considerably longer and from 7

to 21 days when dynamic replacement had to be performed. Also, ground heave due to pounding was not observed in dynamic compaction areas but was observable in dynamic replacement zones.

A total of 800 pressuremeter tests were performed to insure the quality.

5 NEW VERSATILE TECHNIQUES FOR DIFFICULT SOILS

The development of a new container terminal in Southeast Asia was the opportunity to make a compromise between pressuremeter and Mohr Coulomb approaches.

According to the original design the soft marine clay at the seabed was to be dredged down to the depth of 30 m below sea level where the shear strength of the stiff clay exceeded 250 kPa. The excavated key was to be then backfilled with sand and compacted using vibro compaction under 3 m of additional overburden sand fill. Next, the surcharge had to be removed, a rubble mound was to be placed over the sand key, and as shown in Figure 9, finally caissons were to be sunk onto the mound.

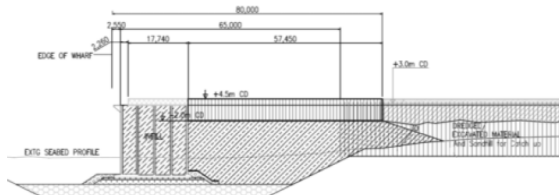


Figure 9. Cross section of container terminal based on original foundation concept

While the clay at dredge level was initially very stiff, dredging works and cutting into the clay softened the upper 1 to 1.5 m of the exposed clay surface and post dredging CPT tests performed before the removal of the overburden sand fill indicated that the clay's shear strength had dropped to about one third of its original value; i.e. to approximately 80 kPa (Hamidi et al., 2010c). Further testing at later stages by the pressuremeter test suggested that the shear strength had even further reduced at some points to as low as 16 kPa.

Dynamic replacement was used as an alternative method to treat the softened clay layer. In the proposed dynamic replacement methodology it was assumed that a 1.8 m thick granite rock fill layer would be placed over the soft clay layer. The blanket material was chosen in such a way that 30% of the stone diameters were from 150 to 200 mm and the remaining 70% were from 200 to 300 mm. The rock columns were designed to be 2 m in diameter, in a 4.5 m grid and with a replacement ratio of 15%.

A pounder weighing 38.5 tons was specifically designed and fabricated for the project. This pounder was grater shaped to allow the passage of water through the pounder with the least resistance. It was

also with dual side functionality; i.e. it was 1.7 m by 1.7 m on one side and used for driving rock dynamically into the clay and 2.3 m by 2.3 m on the side to dynamically compact the rock blanket. Figure 10 shows this marine pounder.

The self-bored slotted tube or *Staf* technique (Arsonnet et al., 2005) was utilised from a jack up barge, to perform the pressuremeter tests down to a depth of more than 30 m. The technique consists of sealing a casing to the sea floor and driving a BX size slotted casing with advanced drilling and by utilising an eccentric bit. The slotted casing is advanced to the required depth, the bit is removed and the pressuremeter probe is inserted to depth. After the test, the slotted casing is jacked up one meter and the next test is performed. Figure 11 shows the Staf drag bit that can either have blades or buttons.

Since the stability analysis was performed using the classical the Mohr Coulomb failure criteria, the friction angle and cohesion were necessary for the stability analysis.

Shear strength, c , can be estimated from the pressuremeter test by (Menard, 1970):

$$c = \frac{P_l^*}{5.5} \quad (5)$$

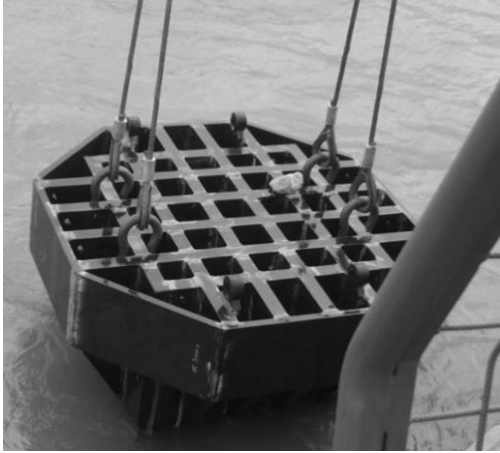


Figure 10. Specially designed multi-purpose marine pounder (Chu et al., 2009)

P_l^* = net limit pressure and can be calculated from

$$P_l^* = P_l - P_o \quad (6)$$

P_o = at rest horizontal earth pressure at the test level at the time of the test.

The internal friction angle, ϕ , for sands can be estimated in sands from the pressuremeter test by (Menard, 1970):

$$P_l^* = 2.5 \times 2^{\frac{\phi-24}{4}} \quad (7)$$



Figure 11. Staf drag bit

Equation 7 is not applicable to rock; hence a method was devised by Yee and Varaksin to develop an equation for rock. For this purpose, a test pit was dug out and backfilled with rock in a loose state. The internal friction angle was determined with failure loading and the limit pressure was measured. A point was set in the diagram of Figure 12, and from this point a curve was drawn parallel to Menard's limit pressure-friction angle curve to develop the proposed formula of Equation 8.

$$P_l^* = 4 \times 2^{\frac{\phi-40}{7}} \quad (8)$$

Pressuremeter tests were carried out at 29 different locations that also included cyclic tests. As reported by Yee and Varaksin (2012) the ratios of reload to Menard modulus was in the range of 3.5 to 4.2 which agrees with the suggested value of 4 for compacted gravel and rock (Menard, 1975). Based on Equation 8, the internal friction angle of the rock after compaction was interpreted to be from 47 to 49°, with an average value of 48.5°, which satisfied the design requirement of 45°.

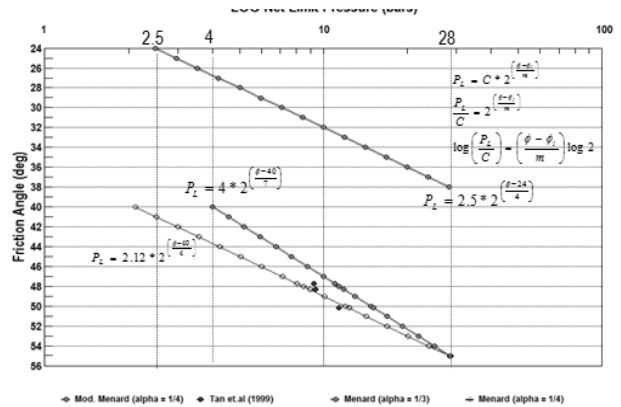


Figure 12. Developing a method for estimating rock friction angle from the limit pressure

6 CONCLUSION

The pressuremeter has not only been a tool for the design and quality control of ground improvement works, which is mostly adapted to non-cohesive soils and the only method for fills.

In the authors' opinion, the pressuremeter is the most versatile field test and proven method of analysis that can satisfy not only the geotechnical engineers' requirements, but also that of the constructors.

Specifying ground improvement acceptance criteria based on design criteria; i.e. bearing capacity, settlement, etc. is a much more realistic and smarter approach than stipulating testing values. In addition specifying calculation methods such as what has been proposed by Menard (1975) makes interpretation of data very clear, without leaving technical and contractual loose ends in a project.

7 REFERENCES

- Arsonnet, G., Baud, J.P., and Gambin, M.P. 2005. Pressuremeter Tests Inside a Self-Bored Slotted Tube (STAF). *International Symposium 50 Years of Pressuremeters (ISP5- Pressio 2005)*. Paris, pp. 31-45.
- Chu, J., Varaksin, S., Klotz, U. & Mengé, P. 2009. State of the Art Report: Construction Processes. *17th International Conference on Soil Mechanics & Geotechnical Engineering: TC17 meeting ground improvement*, Alexandria, Egypt, 7 October 2009, 130.
- Hamidi, B., Nikraz, H., and Varaksin, S. 2010. Soil Improvement of a Very Thick and Large Fill by Dynamic Compaction. *3rd International Conference on Problematic Soils (PSI0)*, Adelaide, pp. 129-138.
- Hamidi, B., Varaksin, S., and Nikraz, H. 2010a. Predicting Soil Parameters by Modelling Dynamic Compaction Induced Subsidence. *6th Australasian Congress on Applied Mechanics (ACAM6)*. Engineers Australia, Perth, Australia, p. Paper 1150.
- Hamidi, B., Varaksin, S., and Nikraz, H. 2010b. Implementation of Optimized Ground improvement techniques for a Giga Project. *GeoShanghai 2010 Conference, ASCE Geotechnical Special Publication No 207: Ground Improvement and Geosynthetics*, Shanghai, pp. 87-92.
- Hamidi, B., Yee, K., Varaksin, S., Nikraz, H., and Wong, L.T. 2010c. Ground Improvement in Deep Waters Using Dynamic Replacement. *20th International Offshore and Polar Engineering Conference*. Beijing. 20-26 June, pp. 848-853.
- Hamidi, B., Nikraz, H., and Varaksin, S. 2011. Ground Improvement Acceptance Criteria. *14th Asian Regional Conference on Soil Mechanics and Geotechnical Engineering Hong Kong*, Paper No. 404.
- Hamidi, B., Varaksin, S., and Nikraz, H. 2011a. Predicting Menard Modulus using Dynamic Compaction Induced Subsidence. *International Conference on Advances in Geotechnical Engineering (ICAGE)*. Edited by M. Shahin and H. Nikraz. Perth. 7-11 November, pp. 221-226.
- Hendy, M.S., and Muir, I.C. 1997. Experience of Dynamic Replacement on a 40 m Deep Reclamation in Hong Kong. *Third International Conference on Ground Improvement Geosystems: Ground Improvement Geosystems - Densification and Reinforcement*. Edited by M.C.R. Davies and F. Schlosser. London. 3-5 June 1997. Thomas Telford, pp. 76-80.
- Menard, L. 1970. Détermination de la Poussée Exercée par un Sol sur une Paroi de Soutènement. *Publication D/38/70*.
- Menard, L. 1975. The Menard Pressuremeter: Interpretation and Application of Pressuremeter Test Results to Foundation Design, D.60.AN. *Sols Soils*, 26: 5-43.
- Menard, L., and Broise, Y. 1975. Theoretical and Practical Aspects of Dynamic Compaction. *Geotechnique*, 25(1): 3-18.
- Varaksin, S., Hamidi, B., and D'Hiver, E. 2005. Pressuremeter Techniques to Determine Self Bearing Level and Surface Strain for Granular Fills after Dynamic Compaction. *International Symposium 50 Years of Pressuremeters (ISP5- Pressio 2005)*, Paris, pp. 687-.
- Yee, K., and Varaksin, S. 2012. Ground Reinforcement in Deep Water. *International Conference on Ground Improvement and Ground Control - Transport Infrastructure Development and Natural Hazards Mitigation (ICGI2012)*. Wollongong, Australia. 30 October - 2 November, Vol.2, pp. 575-585.
- Varaksin, S., Hamidi, B. 2013. Pressuremeter for design and acceptance of challenging ground improvement works. *Proceedings of the 18th International Conference on Soil Mechanics and Geotechnical Engineering, Paris 2013 (Parallel session ISP6)*

Monitoring based analysis of interaction between an integral bridge and GSY-reinforced embankment

Nikolay Vyaltsev

TenCate Geosynthetics Russia, Russia

ABSTRACT: A research project to monitor and analyze the joint less bridge S33.24 was carried out in the years 2009-2011. The research work was divided in two parts: (a) The instrumentation with several different permanent monitoring systems and monitoring of the joint less three-span bridge named 'Marktwasser', on the S33 highway, and (b) the implementation and evaluation of proof loading, measurement and assessment of the traffic flow and the evaluation of temperature effects on the abutments and the approach-slab. The paper presents mainly the monitoring results and analysis on the interaction between bridge structure and GSY-reinforced embankment.

1. INTRODUCTION OF THE RESEARCH PROJECT

1.1 The bridge structure

The joint less bridge S33.24 is a foreshore bridge leading to a recently erected Danube crossing which is part of a highway connection to and from Vienna. The S 33.24 is a three-span continuous plate structure with span lengths of 19,50 m, 28,05 m and 19,50 m orthogonal to the abutment as shown in Fig. 1. The top view shows a crossing angle of 74° between center line of the deck slab and abutment-axis. Further design aspects of this non-prestressed construction are monolithical connections between bridge deck, pillars and abutments as well as haunches going from a constant construction height of 1,00 m to 1,60 m in the vicinity of the pillars to account for the high restraint moment.

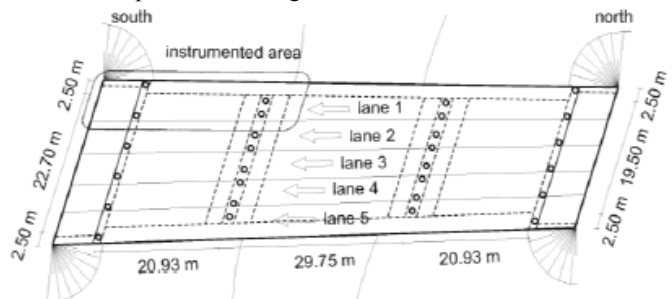


The entire structure is founded on four lines of drilling piles with length of 12,00 m and 19,50 m respectively.

1.2 The monitoring systems

Abutment free bridge structures depend not only on dead loads and traffic loads but especially on constraint loads resulting from temperature differences, earth pressure and creep/shrinkage processes. An integrative monitoring concept had to be developed covering the superstructure, its interaction with the reinforced earth embankment behind the abutment and the dilatation area above the approach slabs. In total 5 different sensor systems consisting of strain gages, temperature sensors and extensometers were permanently installed.

Figure 1. (a) Bottom view of the bridge, (b) ground plan with driving lanes and instrumented area



Due to the different nature of the relevant load cases the instrumentation of the deck slab had to ensure that both a constant and linear strain distribution across and cross section could be detected. Similarly a proper placement of the temperature sensors constant temperature and temperature gradient were to be measured. Based on those requirements the contractor designed the monitoring system opted for a fiber optic sensor (FOS) system consisting of 12 strain and eight temperature sensors which were placed in the southern span's deck slab. For redundancy as well as installation reasons two independent FOS strands were placed in the top and the bottom reinforcement layer of the slab. All temperature and strain sensors are equally distributed between upper and lower reinforcement layers. The location of the temperature sensors allows capturing differences in the environmental conditions due to solar radiation, wind and the development of cold air pockets below the deck. Strain sensors provide information from dead load, creep shrinkage and temperature gradient.

The absolute and relative deformations of the bridge and the backfill were detected by extensometers. The strain field above the approach slab was instrumented by 10 fiber optic sensors plus 20 electric strain gages as illustrated in Fig. 2.

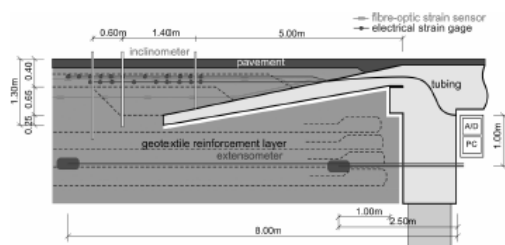


Figure 2. Overview of the permanently installed monitoring systems in the southern backfill area above the approach slab and in the reinforced backfill

1.3 The mechanical model

During design of the monitoring system a 3D finite element model was set up in SOFISTIK in order to optimize the sensor location with respect to the expected structural respond and allow for a meaningful data interpretation. The abutments, columns and deck slab were discretized using shell elements. The four rows of

drilling piles were modeled by means of beam elements. Geometry and material properties were taken out of the initial statics and available drawings. In the initial model all piles are placed on stiff vertical springs. Horizontally neither the abutment nor the deck slab is supported.

2. MONITORING AND ANALYSES OF TEMPERATURE LOADING

2.1 Target of the campaign

Integral bridges are highly statically indeterminate structures. As such, the design of new and the reliability of existing objects is significantly influenced by the development of constraint forces due to the time dependent processes creep and shrinkage as well as temperature effects. They determine both the bearing capacity and the serviceability of critical structure members such as the approach slab between abutment and earth embankment. During the first two years after the construction, temperature in the concrete deck, air temperature, abutment movement and the strain distribution in the bridge deck slab have been monitored. This data allows (a) a comparison with design guidelines and codes with respect to constant temperature loads and temperature gradient, (b) an assessment of the resulting constraint forces with regard to the bearing capacity, and (c) an investigation of the soil-structure interaction with emphasis on the earth pressure development and the adequacy of the chosen approach slab solution.

2.2 Methodology

Due to the distinct daily and seasonal temperature variations, the data analysis is performed separately for 2009 and 2010 utilizing the concept of extreme value statistics. The resulting distribution of weekly and monthly extreme values allows a direct comparison with the temperature load models according to EN 1991-1-5 considering the difference in observation time and the annuality of the design event. This data serves for the inverse determination of constraint forces in the concrete deck slab as well the boundary conditions (e.g. degree of constraint), which is an indicator for the soil-structure-interaction. In particular, the seasonal

soil and abutment movement are captured and analyzed with respect to the code specification (comparison of predicted versus measured deformations). The effects of structural expansion on the strain field development in the area above the approach slab can be investigated based on the derived monthly extreme values of the monitored data. Finally, the strain demand on the pavement can be assessed utilizing extrapolation techniques.

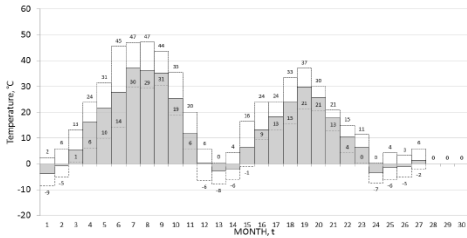


Figure 3. Monthly extreme values of measured and verified concrete temperatures (exemplary for one sensor)

Conclusions

With regard to the temperature load model defined in EN 1991-1-5 and based on the two year monitoring period the following conclusion can be drawn:

- The observed range of constant temperature load in the bridge deck amount to $\Delta T_N \sim 40$ K, which is within the expected range of $\Delta T_N \sim 60$ K according to the specifications in EN 1991-1-5 for the 50 year design event.
- The application of the asphalt pavement has no significant influence on the temperature nor the temperature gradient. Solely an accelerated increase in temperature as compared to ambient conditions can be noticed. After application, a slightly dampened daily temperature development is apparent, for the top reinforcement layer only.

Based on the two-year monitoring period the subsequently summarized statements can formulated with regard to the development of temperature related constraint forces in the bridge deck:

- Thermal strains of approximately $\pm 0,004$ % within the top and the bottom reinforced layer are roughly one order of magnitude smaller than the identified mechanical strains of 0,015% to 0,06% due to dead load and traffic.
- The thermal strains correspond to internal forces of roughly -60 kNm to $+20$ kNm and in consequence amount to only 3 % of the bearing capacity.

With respect to the temperature dependency of the soil-structure interaction the following conclusions can be made:

- Average temperature in the bridge deck and abutment movement are highly correlated. A linear transfer function can be fitted with a coefficient of determination of $R^2 = 93,5$ % for 2010 and $R^2 = 95,0$ % for 2011, respectively see Fig. 4.
- Based on this transfer function, an effective degree of constraint of $\alpha_c = 59,2$ % for the 2010 monitoring period and $\alpha_c = 57,0$ % for 2011 can be deduced. No significant changes in the boundary conditions of the soil stiffness are encountered.

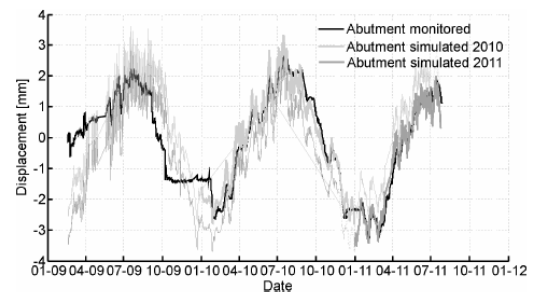


Figure 4. Observed abutment movements (black) versus linear prediction for the 2010 (green) and 2011 (magenta) monitoring period.

3. MONITORING AND ANALYSES ABUTMENT - SOIL AND APPROACH SLAB - SOIL INTERACTION

3.1 Target of the campaign

One of the main advantages of an integral or joint less bridge structure is the removal of the traditionally very maintenance intensive expansion joints between soil embankment and concrete structure. This is associated with an assumed reduction in maintenance costs over the life time at the cost of earth pressure related constraint forces in the concrete deck and seasonal extreme strains in the asphalt pavement in the transition area. Within this research project significant attention is paid on (a) the assessment of the annual earth pressure development, (b) the analysis of the adequacy of the approach slab solution, and (c) evaluation of the strain demand on the pavement.

3.2 Methodology

The investigation of the soil-structure interaction, both in terms of earth pressure development and functionality of the approach slab solution, is based on the recorded soil and abutment movements as well as the strain field development measured by 10 fiber optic and 20 electrical strain gages. The derived extreme value distributions are compared with the code requirements for the different design conditions and/or respective distributions of material resistance on a probabilistic level. This allows the determination of reliability levels in terms of a probability of exceedance. In particular, the existence of earth pressure after closure of the constructive gap, of the active earth pressure or even the increased active earth pressure are investigated. With regard to the transition area, the development of the strain field in time is assessed. The extrapolation to the level of the asphalt pavement finally allows an assessment of the probability of cracking.

3.3 Conclusions

Based on the available monitoring data for the time period between February 2009 and December 2010 the following conclusions with regard to the earth pressure development can be drawn:

- The 15 mm thick constructive gap (elastic sheet) between abutment wall and reinforced soil body is closed with a probability of 23% ($\beta < 0,7$), thus leading to the development of earth pressure, see Fig. 5.
- The active earth pressure is reached with a probability of $p > 1,7\%$ ($\beta < 2,1$).
- The increased active earth pressure has to be accounted for with a probability of $p > 0,00012\%$ ($\beta < 4,9$).

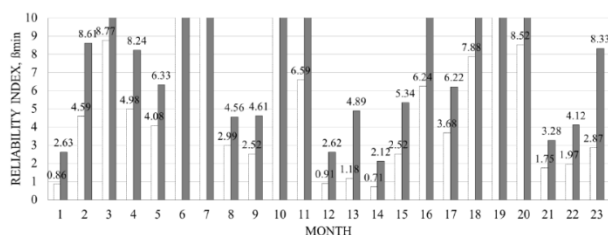


Figure 5. Reliability level with regard to (a) closure of the gap, and (b) the development of the active earth pressure during the monitoring period between February 2009 and December 2010

With regard to the functionality of the approach slab solution it can be concluded that:

- The derived strain fields correspond to the expectations based on the initial design concept and numerical simulations. In particular, areas of high concentration are, as expected, located close the tip of the approach slab and decrease in an inclination band up to the surface.
- Investigations of correlation between average temperature in the concrete deck, abutment movement and strain field in the soil body show predominate linear relationship. However, significant redistribution of strains occur which correspond to the times of maximum expansion and maximum contraction.

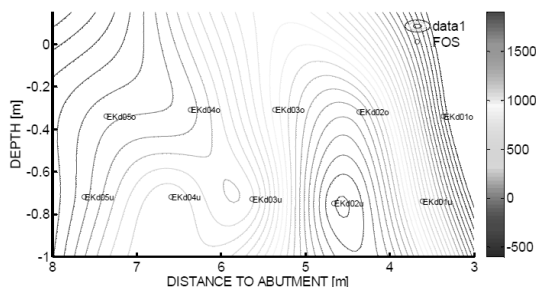


Figure 6. Interpolated and extrapolated strain field based on the monthly mean values derived from the daily recorded maxima for January 2010.

The likelihood of cracking in the pavement can be assessed as follows:

- Although the extrapolated strain at the level of the pavement are significantly smaller to the observed total maxima, they still exceed the admissible level of the simplified analysis – neglected friction between soil and pavement, neglected fiber reinforcement and assumed short term temperature change of $\Delta T = 30^{\circ}\text{C}$ for the determination of the allowable strain.
- Further research with regard to the temperature dependent strain capacity of the reinforced asphalt pavement – bond between fibers and asphalt, temperature and temperature rate dependent asphalt properties – will allow a more detailed analysis and future optimization.

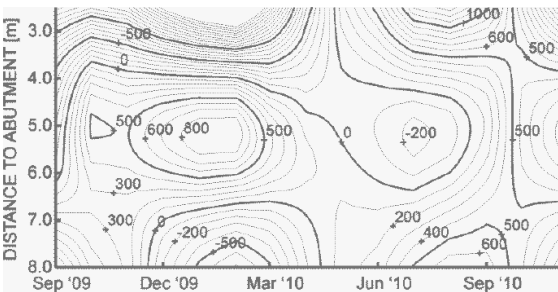


Figure 7. Extrapolated strains [$\mu\text{m}/\text{m}$] at the level of the asphalt pavement as function of time and distance to the abutment wall for the time period between September 2009 and October 2010.

4. ACKNOWLEDGEMENT

The research program on the object S33.24 ‘Marktwasser’ was initiated and financed by the Austrian Transport Safety Fond (VSF) integrated in the Federal Department of Transport, Innovation and Technology and the Austrian Highway and Expressway Financing Incorporate Company (ASFINAG).

The monitoring and analysis work was done by RED Bernard GmbH Research and Development in cooperation with the Department of Structural Engineering and Natural Hazards from the University of Natural Resources and Life Science in Vienna.

REFERENCES

Strauß, A., Wendner, R., Bergmeister, K. & Reiterer, M. 2010. Monitoringbasierte Analyse von Integralen Brücken am Beispiel der Marktwasserbrücke. Schriftenreihe des Departments für Bautechnik und Naturgefahren, Vienna, Austria

Strauß, A., Wendner, R., Bergmeister, K. & Frangopol, D. M. 2010. Monitoring based analysis of a concrete frame bridge „Marktwasser bridge“. Third International fib Congress, Washington, DC, USA

Strauß, A. & Reiterer, M. 2011. Monitoringbasierte Analyse von Integralen Brücke S33.24 Forschungsjahr 2 Endbericht. www.bmvit.gv.at

Piled embankments in soft estuary clay - Experience from design and field measurements for redevelopment of harbour areas in Northern Germany

Lars Vollmert

BBG Bauberatung Geokunststoffe GmbH & Co. KG, Germany

Juri Schlee

NAUE GmbH & Co. KG, Espelkamp

ABSTRACT: Piled embankments to be used under poor subsoil conditions have become popular due to the advantage of high robustness, low settlements and low influences on existing buildings and infrastructural measures and, last but not least, acceptable costs. After several years (or decades) of using this complex geotechnical construction with interaction of soil improvement measures (piles or columns), spanning and supporting reinforcement, arching embankment soil and influence of cyclic/dynamic loading a safe design procedure is already established by the German EBGE. Field measurements and monitoring results are used to improve the understanding of full scale constructions and practical validation of design procedures, giving further input to understanding and therefore optimization.

1. INTRODUCTION

1.1. Development of geosynthetic reinforced piled embankments

Publishing EBGE in the second version dated 2010, defined design rules have been introduced the first time in Germany for piled embankments in combination with geosynthetic reinforcement, spanning the pile caps. The beginning of the construction method starts in the mid of the 1990s. Detailed information on the first experience can be found at ROGNER & STELTER (2002) for road constructions and for railway applications at GARTUNG et al. (1996) and VOGEL (2006). Main idea of the construction is the use of geosynthetics, spanning the pile caps, for improved load transfer of live and dead loads.

The geosynthetic works as a membrane, spanning the pile caps, as well as reinforcement to reduce the risk and deformations of punching effects. The models currently used do not differentiate these effects. Models, differentiating these effects and used in the past therefore have been discussed contrary due to the fact that results with a high variation of strength of the geosynthetics have been gained. CORREIA & BRANDL (2001) focused that systems with a multi-layered reinforcement layout might react with a higher ductility and robustness than single-layered systems. This tendency can also be found within the systematic research by HEITZ (2006), where the “sum of installed

stiffness” given by the stress-strain-characteristic of the reinforcement has been found to be the main factor for increasing robustness. Fig. 1 shows the static principle of the membrane function. Fig. 2 gives the model for a punching reinforcement, which has not been found to give reliable results without combining it with the membrane function, and where no reliable design model has been developed for.

The vertical loads are redistributed and concentrated on the stiff pile caps due to arching effects within the fill. The relation of stress redistribution within the fill is given using empirical relations (BS8006-1, 2010) or shell respectively arching models (KEMPFERT et al. 1997, ZAESKE 2001). Some models allow for the differentiation of dead- and live loads, Fig. 3. Current research is going to focus on concentric arches (VAN EEKELEN 2014). Cyclic loads have been found to be of main importance for the arching effect. Stress redistribution within the fill due to cyclic loads again is positively influenced by the reinforcement, Fig. 4. Fig. 4 shows exemplarily the interaction of membrane-function and reinforcement of shear-zones, developing at the edge of the pile caps. A simple model using ultimate limit state mechanisms has been published by KEMPFERT et al. (1997). This model separates the effects of arching, membrane and bearing capacity of the subsoil, while later developments take care of the deformations of bedding

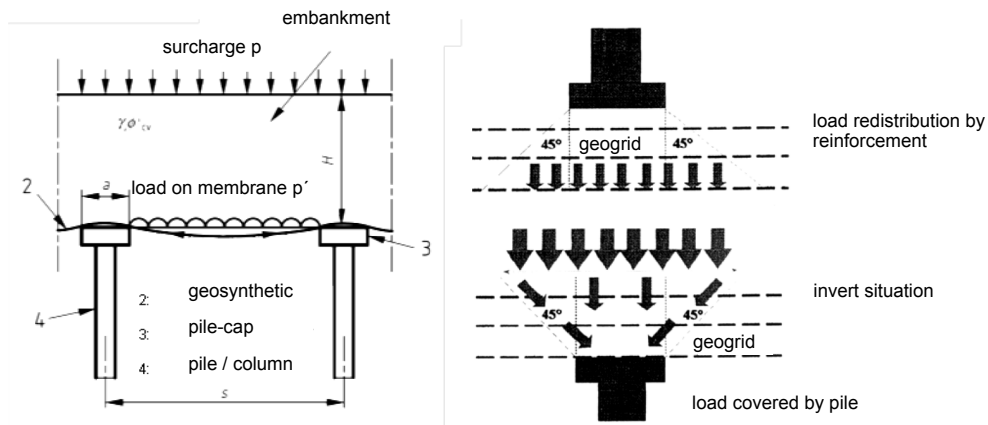


Figure 1. Principle of a membrane, spanning columns or piles (left)

Figure 2. Model of a reinforced zone on piles by BELL et al. (1994), based on findings of GUIDO, KNUEPPEL & SWEENY (1987) for punching effects, reduced by lateral reinforcement (right)

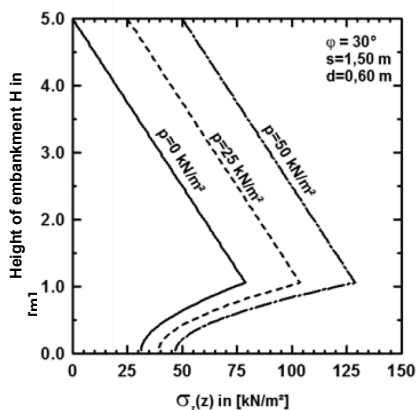


Figure 3. Calculation of vertical stress for a dam with a height of 5m, using the model of ZAESKE (2001), given by GEDUHN & VOLLMERT (2005)

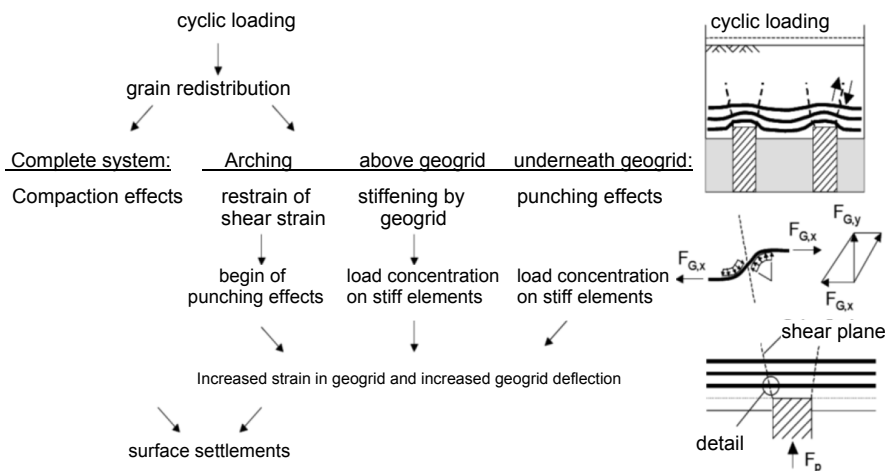


Figure 4. Combined interaction of membrane/punching reinforcement within a geogrid-reinforced embankment at cyclic loading, according to HEITZ (2006)

modulus and stress-strain characteristic of the reinforcement used.

The construction method has been implemented within the wide range of construction methods used for special geotechnical works and can be seen as standard. A majority of projects shows also the economic efficiency of this construction method. The economic savings can be expected in the range of 10 to 20 % against conventional solutions, and shortening the construction period. The options combining the reinforcements and piling systems are nearly without limits.

As piling elements driven piles, piles from wood, steel, pre-cased reinforced concrete or ductile cased metal piles can be used as well as soil improvement techniques as gravel columns, treated or non-treated, CMC-columns, mixed-in-place columns etc. Nevertheless, the load transfer on the piles has to be ensured by e.g. pile caps or widening of columns in the top-area to a typical diameter of approx. 0.6m ... 0.9m.

1.2. Overview of the calculation methods

The first calculation method was developed by KEMPFERT et al. (1997). In this method, the bedding of the subgrade was considered through its bearing capacity. In this method, a uniformly distributed load was taken into consideration as shown in Fig. 5 (Load approach 3).

Following the mentioned Kempfert calculation method, ZAESKE (2001) developed a design method based on the publication of EMDE (1995) where the subsoil bedding could be considered via catenary differential equations for the geosynthetics between the piles. With

this method, it is possible to consider not only the deformation below the geosynthetics but also the pile settlements. This method allows all three load approaches as illustrated in Fig. 5. ZAESKE (2001) has mainly analyzed the load approach 3 and developed an analytical solution method for this one. He also modified the design into a simplified graphical form, which is the basis for the EBGeo (2010) calculation method, where the load figure is assumed as “Load Approach 2” and the piles will be considered as rigid elements in comparison to the soft bedding behavior of the subsoil. In other words, after fulfilling the mentioned bedding requirement, the deformation of piles will be ignored and the design will be focused on the deformation behavior of the geogrids between the piles, which enables a design method on the safe side. This simplified graphical calculation method can be used according to EBGeo after fulfilling a bedding requirement that the bedding modulus of the piles has to be 75 times greater than the subsoil bedding modulus.

After ZAESKE (2001), GEDUHN & VOLLMERT (2005) developed and simplified the Zaeske method (ZAESKE 2001) into a new form, called “Zaeske, simplified”, where the piles are considered as rigid elements analogous to EBGeo calculation method. In addition, the “Zaeske, simplified” calculation method enables to consider all three load approaches (see Fig. 5), which were already described by ZAESKE (2001) and are commented on by VAN EEKELLEN (2011). A brief comparison of the mentioned calculation methods is summarized and illustrated in Table 1.

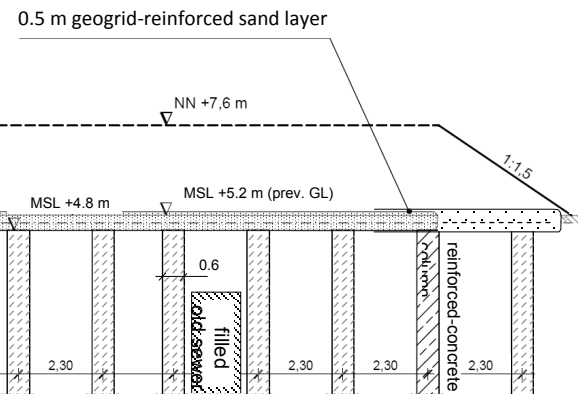
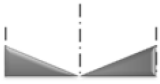





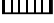



Figure 5. Cross section – piled sand layer, Hamburg HafenCity

Table 1. Load approaches and comparison of the calculation methods

	Method	Pile stiffness	Load function	Calculation
 <p>Load Approach 1</p>	Kempfert (1997)	not considered (rigid)		from free hanging catenary
 <p>Load Approach 2 <small>EBGEO 2010</small></p>	Zaeske (2001)	considered		from DGL for bedded system
 <p>Load Approach 3</p>	Zaeske, simplified (2005)	not considered (rigid)	 	from DGL for bedded system
	EBGEO (2010)	not considered (rigid)		from DGL for bedded system

HEITZ (2006) extended the calculation method of ZAESKE (2001) in terms of cyclic loading. Based on the results of the performed model tests, the soil arching effect of the geogrids tends to be reduced due to cyclic loading. This reduction can be considered by a calculation method which was developed in the mentioned publication of HEITZ (2006).

The effect of the chosen calculation method (Table 1) has a big influence on the design results. The research of VAN EEKELEN et al. (2012a,b) indicates that the shape of a deformed geosynthetic reinforcement between the piles does not follow a power law function lower than the third order in any of the performed tests. The inverse triangular load distribution (load approach 1) also gives a third order power law function, which demonstrates the most similarity (among the other load approaches) to the real deformation form of the geosynthetic reinforcement according to the test results. For the same geometry considered in the publication of VAN EEKELEN (2012b), the same total load with the inverse triangular load distribution (load approach 1) results in a tensile force in the geosynthetics that is 75% of the tensile forces calculated by a triangular load distribution (load approach 2), which shows the big importance of the load distribution choice on the design. To put in a nutshell, load approach 1 leads to a minimum stress on the geosynthetics and a maximum stress on the piles and the load approach 2 shows exactly the opposite tendency, whereas load approach 3 ends up somewhere in the middle. These mentioned tendencies were also confirmed by the parameter study of VOLLMERT et al. (2012).

2. WORKED EXAMPLE: HAFEN CITY HAMBURG (WEIHRAUCH ET AL. 2013)

At the HafenCity in Hamburg, previously part of the harbour area, the current inner-city area south of the historic warehouse district is being extended by some 40 % to a total of 157 hectares. 5,500 dwellings for 12,000 residents are to be constructed, along with office space for 40,000 employees.

In the course of these infrastructure projects, the trafficked areas – with the exception of the quay and embankment promenades – are being raised from the current MSL + 5 m to MSL +7.5 m to + 8.0 m, to make them safe for flood events. The soil conditions around today's Honkongstrasse (formerly Magdeburger Strasse) are typical for the HafenCity Hamburg. Fill material of low bearing capacity overlies soft organic layers of clay and peat which in turn overlie firm sands. Raising the level of the road embankment by approximately 3.0 m would have resulted in long-term settlements of between 300 and 400 mm, and significant differential settlements would have been expected.

The system is characterised by vertical columns (lime-cement treated gravel, unreinforced) and an overlying sand layer horizontally reinforced with geogrids. The placement grid of the supporting elements should be designed to transfer the geogrid loads in an orthogonal manner. For Hongkongstrasse, this resulted in a rectangular grid with a spacing of 2.3 m normal to the embankment axis and 2.5 m in the axial direction, the diameter of the elements was 0.6 m. Reinforced concrete columns with

continuous steel reinforcement were used at the edge of the structure to cope with a bending moment (e.g. should any excavation be required at a later date) as a result of lateral pressure. The geogrid-reinforcement is installed 150 mm above the columns in order to guarantee adequate safety against shear during the construction phase, and in case of large settlements. The design required a short-term tensile strength of 400 kN/m.

To avoid the risk of subsequent construction activity of investors endangering or destroying sections which have already been built, an area of 1.0 m of the traffic section must be able to be removed. Fill which intrudes into investor areas must also be removable. In order to prevent any damage to the embankment support system, the geogrid-reinforced fill layer was built with sufficient overlap. The outer section can thus be removed in the course of normal earthworks.

The geogrid-reinforced layer was designed according to a verification concept which has already been used and proven itself several times at HafenCity Hamburg. The limit bearing capacity was first verified in accordance with a suggestion from KEMPFERT et al. (1997). A conservative value for subgrade reaction was used. This verification procedure does not enable any deformations to be inferred. However, verification of serviceability and of deformation limitation is compulsory for all construction projects in the HafenCity Hamburg. A complementary design procedure was therefore adopted, using a method developed and extended from EBGeo, which at the time of planning was only available in its 2004 draft stage. This extended design method was verified for similar subsoil and loading conditions (VOLLMERT et al. 2006). The anticipated further settlements at the level of the reinforcement were estimated at less than 50 mm after termination of construction. Comparisons with the current EBGeo (2010), available in its final form now that construction is complete, show that the design and verification of the system is sufficiently robust to cater even for the special case "Loss of Subgrade Reaction" in Load Case 3.

Extensive monitoring using horizontal inclinometer, strain gauges and stress transducers has been worked out in this project, reported by WEIHRAUCH et al. (2013) and SCHÄFER et al. (2014). The measurement results figure out the ductility of the system and robustness against subsoil influences gained by an excavation for the new Greenpeace building, right to the construction.

tion for the new Greenpeace building, right to the construction.

3. WORKED EXAMPLE: SCHLEUSE NEUER HAFEN, BREMERHAVEN (VOLLMERT ET AL. 2006)

An essential part of the project New Harbour in Bremerhaven, Germany, in the years 2003 to 2005 was the new development of a sluice as connection between the New Harbour and the Weser River.

For the crossover of a road across the outer head of the sluice fillings with thicknesses of up to 5 m were required in the ramp area. Due to deep clay layers with a low bearing capacity different measures for the reduction of the expected large settlements were required. Amongst others, due to the earlier installed sheet piles a dam filling on cement stabilised columns was planned. Above the columns a geogrid reinforced load distribution platform was installed to support the bearing arch and to transfer the dam loads into the pile group. The sequence of strata is particularly affected by highly compressible, holocene organic soft layers in depths of up to approx. -5 m below sea level or in a total thickness of between 15 m and 20 m. The sea silt is characterised by a predominant weak consistency, a medium oedometric modulus of $E_s = 1.5 \text{ MN/m}^2$ and an undrained shear strength of $c_u \geq 15 \text{ kN/m}^2$.

On an approx. 0.3 m thick sand layer a double-layered biaxial geogrid reinforcement together with an intermediate 0.3 m thick sand layer is installed, followed by the embankment fill. The geogrids with a biaxial short term strength of 80 kN/m (Secugrid 80/80/Q6) are characterised by a very high stiffness of $J_{2\%} \geq 2000 \text{ kN/m}$.

To prove the serviceability of the load distribution platform a comprehensive instrumentation of the geogrids with strain gauges is carried out. The instrumentation has been complemented by vertical pressure gauges above the cement stabilised piles and between the piles as well as by settlement measurements. To register the arch effects earth pressure cells have additionally been installed in the middle of the field and on one pile cap. The earth pressure cells in the middle of the field are thereby graded in the altitude in such a way that reductions of vertical stress due to arching effects can be comprehended, Fig. 6. The strains occurring within the reinforcement are

registered by strain gauges (DMS). The instrumentation could already be prepared in-house and thus in-situ be installed together with the geogrids in only a few hours.

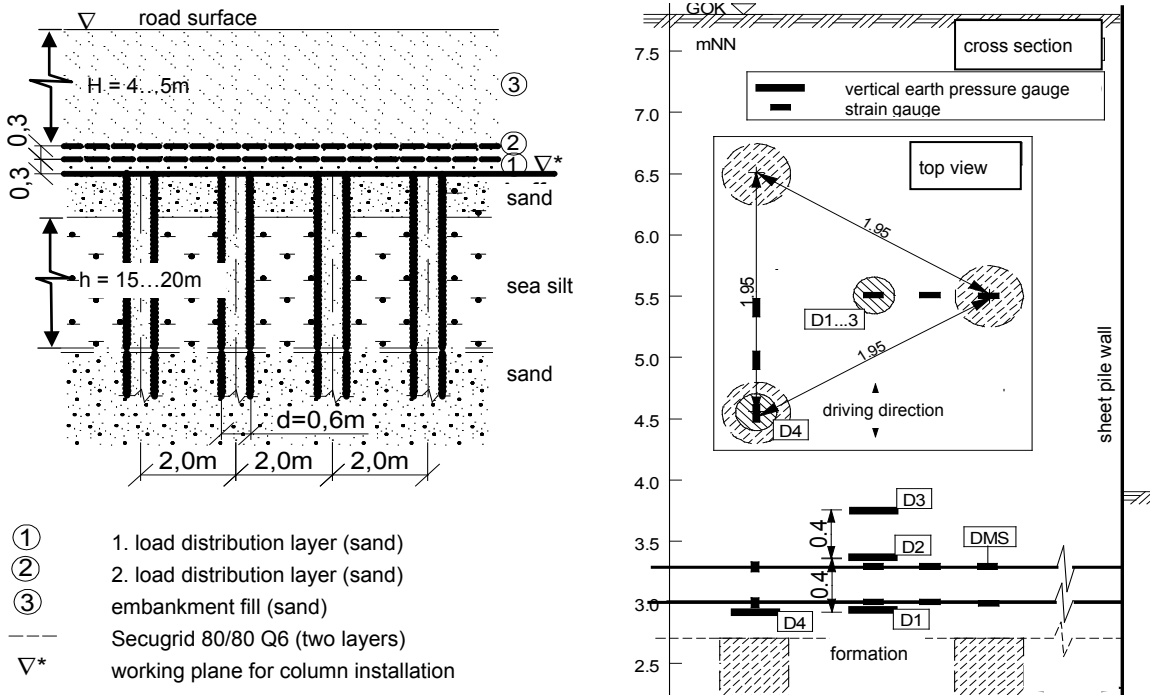


Figure 6. Schematic drawing of cross section and layout of monitoring devices

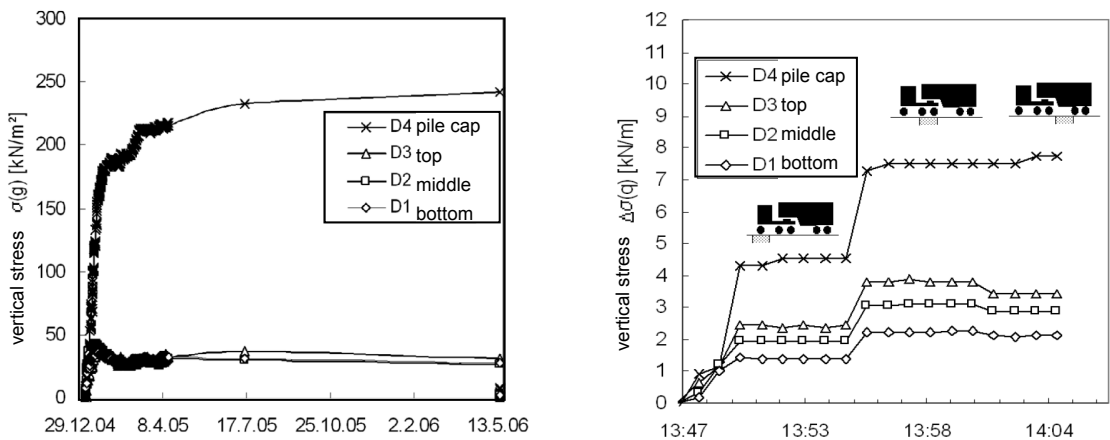


Figure 7. Results of vertical stress transducers illustrating the load concentration on top of the piles from dead load (left) and life load (right)

4. CONCLUDING REMARKS

Piled embankments with lateral geosynthetic reinforcement as soil improvement techniques were widely used in the last 20 years and certain progress in understanding of the structures could be made. Exemplarily, two sites in the area of HafenCity Hamburg and Schleuse Neuer Hafen, Bremerhaven are presented here. The prime objective of the soil improvement is, in all cases, the reduction of subsequent settlements in order to guarantee the serviceability of the trafficked areas under operating conditions. Depending on the construction process of the columns, this method can be used even close to existing structures. Under the conditions applying at the HafenCity, the pile-supported, geogrid-reinforced method is usually somewhat cheaper to construct than an expanded-clay fill layer.

A realistic estimation of bedding modulus and the choice of the decisive load approach play the key role to make safe and still economic designs for geosynthetic reinforced load transfer platforms. Among the available design methods, the calculations following the current EBGeo code without any correction but considering the pile-soil-geosynthetics-interaction with the help of a finite element analysis leads to satisfactory results. One restriction of EBGeo method is that it solely considers the most unfavourable load approach of a triangle, compare Table 1. In contrary to this, the simplified Zaeske method (GEDUHN & VOLLMERT 2005), on which EBGeo is based, enables all three load approaches known in the literature. The simplified Zaeske method supported with FEM to estimate the subsoil bedding, combined with bedding correction and load approach 1 (inverse triangle) leads to very plausible results with respect to in-situ measurements, which leads to economic and still safe designs for daily practice. For future purposes, modifications and verification of model improvements as given by VAN EEKELEN et al. (2014) will give further enhancement of the understanding of reinforced piled embankments.

5. ACKNOWLEDGEMENTS

The author would like to acknowledge the support and fruitful discussions during the monitoring projects Bremerhaven and Hamburg HafenCity of *Steinfeld & Partner*, Hamburg, *Institut für Markscheidewesen und Geotechnik*,

TU Clausthal, Clausthal-Zellerfeld, *Institut für Geotechnik*, *TU Hannover*, Hannover, and *NAUE*, Espelkamp, as well as Suzanne van Eekelen and colleagues for their contribution to further understanding of the structure.

6. REFERENCES

- BELL, A. L., JENNER, C., MADISON, J. D. & VIGNOLES, J. (1994): Embankment Support Using Geogrids with Vibro Concrete Columns. Fifth International Conference on Geotextiles, Geomembranes and related Products. September 1994, Singapore.
- BS 8006-1 (2010): Code of practice for strengthened/reinforced soils and other fills. BSI Standard Publication, 2010.
- CORREIA, A.G. & BRANDL, H. (2001): Geotechnics for Roads, Rail Tracks and Earth Structures. Outcome of ETC 11 of ISSMGE. Balkema Publishers; Lisse, Abingdon, Exton, Tokyo.
- Deutsche Gesellschaft für Geotechnik e. V., Arbeitskreis 5.2. 2010. Empfehlungen und die Berechnung für den Entwurf und die Berechnung von Erdkörpern mit Bewehrungseinlagen aus Geokunststoffen (EBGeo). Berlin: Wilhelm Ernst & Sohn.
- EMDE, O. (1995): Der unterspannte schubsteife Balken – ein mechanisches Modell für geotextilbewehrte Tragschichten. Bericht-Nr.15. Wuppertal: Bergische Universität Gesamthochschule Wuppertal, Grundbau, Bodenmechanik und Unterirdisches Bauen.
- GARTUNG, E., ALEXIEW, D., KIRSCHNER, R. & VERSPOHL, J. (1996): Geogrid-Reinforced Railroad Embankment on Piles – Monitoring. Proceedings of 1st European Geosynthetics Conference, Maastricht 1996, p. 251 – 260.
- GEDUHN, M. & VOLLMERT, L. (2005): Verformungsabhängige Spannungszustände bei horizontalen Geokunststoffbewehrungen über Pfahlelementen in der Dammbasis. Bautechnik Nr. 82(9), P.657-662.
- GUIDO, KNUEPPEL & SWEENEY (1987): Plate loading test on geogrid reinforced earth slabs. Geosynthetics Conference, New Orleans.
- HEITZ, C. 2006. Bodengewölbe unter ruhender und nichtruhender Belastung bei Berücksichtigung von Bewehrungslagen aus Geogittern. Dissertation, Schriftenreihe Geotechnik Universität Kassel, Heft 19, 2006.
- KEMPFERT, H.G., STADEL, M. & ZAESKE, D. (1997): „Berechnung von geokunststoffbewehrten Tragschichten über Pfahlelementen“, Bautechnik, Nr. 74(12), S. 818-825, 1997.

- ROGNER, J. & STELTER, J. (2002): Bauverfahren beim Straßenbau auf wenig tragfähigem Untergrund – Aufgeständerte Gründungspolster. Berichte der Bundesanstalt für Straßenwesen, Heft S 26, Bergisch-Gladbach.
- SCHÄFER, D., VOLLMERT, L. & ACHMUS, M. (2014): Mehrjährige Beobachtung einer Baugrundverbesserungsmaßnahme. Messen in der Geotechnik, TU Braunschweig, 2014
- VAN EEKELEN, S.J.M., BEZUIJEN, A., L.ODDER, H.J., VAN TOL, A.F. (2012a,b): Model experiments on piled embankments. Geotextiles and Geomembranes 32. a: Part I, 69-81, b: Part II: 82-94. Elsevier.
- VAN EEKELEN, S. J. M., BEZUIJEN, A. & TOL, A.F.. (2014): Validation of the Concentric Arches model with inverse triangular load distribution, to be published in Geotextiles and Geomembranes.
- VOGEL, W. (2006): Erfahrungen über den Einsatz geogitterbewehrter Bodenkörper auf Säulen für Eisenbahnfahrwege bei Neubau- und Ausbaumaßnahmen der DB. Symposium Geotechnik – Verkehrswegebau und Tiefgründungen, 26. September 2005. in: Schriftenreihe Geotechnik, Universität Kassel, Heft 18, September 2005.
- VOLLMERT, L., DOYGUN, O. (2011): Geosynthetic Reinforced Load Transfer Platforms for Infrastructural Projects and Wind Energy Plants, Lectures on 18. Darmstädter Geotechnik-Kolloquium on 17.03.2011, Heft Nr. 88. Darmstadt: Mitteilungen des Institutes und der Versuchsanstalt für Geotechnik der Technischen Universität Darmstadt.
- VOLLMERT, L., KAHL, M., GIEGERICH, G. & MEYER, N. (2006): Schleuse Neuer Hafen, Bremerhaven – In-situ Verifizierung eines erweiterten Berechnungsverfahrens für geogitterbewehrte Gründungspolster über vertikalen Traggliedern. Beitrag zur Baugrundtagung. Bremen: DGGT.
- VOLLMERT, L., KÖRLIN, R., HEROLD, A. (2012): Comparison of design methods for geosynthetics spanning over columns. Valencia: EUROGEO.
- WEIHRAUCH, S., OEHRLEIN, S. & VOLLMERT, L. (2013): Subgrade improvement measures for the main rescue roads in the urban redevelopment area HafenCity Hamburg. Proceedings of the 18th International Conference on Soil Mechanics and Geotechnical Engineering, Paris.
- ZAESKE, D. (2001): „Zur Wirkungsweise von unbewehrten und bewehrten mineralischen Trag-schichten über pfahlartigen Gründungselementen“, Dissertation, Schriftenreihe Geotechnik Universität Kassel, Heft 10, 2001.

Vibration of dynamically loaded foundations partially embedded in an elastic stratum

Youpele Orukalama Beredugo

Principal Consultant, Project Engineering Associates, Port Harcourt, Nigeria.

Abstract

The general equations of the response of partially embedded dynamically loaded foundation are presented. The application of these solutions to the vibration of a dynamically loaded foundation partially embedded in an elastic stratum are then presented and discussed. It was shown that an elastic stratum increases the effects of embedment.

1. Introduction

In order to obtain solutions in closed forms in the solution of a dynamically loaded foundation, partially embedded in an elastic half space, a number of basic mathematical models have been proposed such as finite dynamic model for infinite media based on the finite element Method, Boundary element Method (BEM) and Impedance function Method. These methods require considerable computer capacity and are often tedious. The analytical model of a rigid cylindrical body partially embedded in an elastic half space developed by Novak and his associates provides a promising method of solution. The presentation here is based on the original work done by Beredugo (1971).

2. Equations of Motion

The equations of motion are similar to those for surface foundation except that the side reactions due to the embedment are included. Thus

$$\text{Vertical vibration : } m\ddot{w} + R_z(t) + N_z(t) = P(t) \quad (1)$$

$$\text{Horizontal reaction: } m\ddot{u} + R_x(t) + N_x(t) = Q(t) \quad (2)$$

$$\text{Rocking Motion: } I_\psi \ddot{\psi} + R_\psi(t) + N_\psi(t) = T_\psi(t) \quad (3)$$

$$\text{Torsional vibration: } I_\zeta \ddot{\zeta} + R_\zeta(t) + N_\zeta(t) = T_\zeta(t) \quad (4)$$

Where

m = mass of the foundation (plus any machinery mounted on it)

I_ψ, I_ζ = mass moments of inertia of foundation (plus any machinery mounted on it) about a horizontal axis or vertical axis respectively passing through the centroid of the machine and the foundation

$P(t), Q(t)$ = Vertical and horizontal excitation forces

$T_\psi(t), T_\zeta(t)$ = Rocking and Torsional Excitation Torques

$w(t), u(t)$ = Vertical and horizontal displacements of centre of gravity of machine and foundation.

$\psi(t), \zeta(t)$ = Angular rocking and torsional displacements

$R_z(t), R_x(t)$ = Dynamic vertical and horizontal reactions at interface between the foundation and the elastic half space

$R_\psi(t), R_\zeta(t)$ = Reactive moments at the base of the foundation from the elastic half space underlying it.

$N_z(t), N_x(t), N_\psi(t), N_\zeta(t)$ = Dynamic vertical, horizontal, rocking and torsional reactions along the embedded surface of the foundation.

The following assumptions are made:

(a) The foundation is a rigid cylindrical body partially embedded in an elastic half space

(b) There is perfect bond between the foundation and the elastic half space

(c) The exciting forces and torques are harmonic.

(d) Only steady state vibrations occur.

(e) The base reactions for an embedded foundation are the same as those of a surface foundation

The elastic half space reactions $R_z(t), R_x(t), R_\psi(t), R_\zeta(t)$ are functions of Reissner's elastic half space functions.

The side reactions $N_z(t), N_x(t), N_\psi(t)$ and $N_\zeta(t)$ are complex functions of the embedment ratio $\delta = \frac{l}{r_o}$, the

dimensionless frequency a_0 , Poisson's ratio ν , the shear modulus G_s of the elastic medium surrounding the embedded portion of the foundation and the relevant displacements $w(t), u(t), \psi(t)$ or $\zeta(t)$ and are given by

$$R_z(t) = Gr_0(C_{w1} + iC_{w2})w(t) \quad (5)$$

$$N_z(t) = r_0 G_s \delta (S_{w1} + iS_{w2})w(t) \quad (6)$$

$$R_x(t) = Gr_0(C_{u1} + iC_{u2})u(t) \quad (7)$$

$$N_x(t) = r_0 G_s \delta (S_{u1} + iS_{u2})u(t) \quad (8)$$

$$R_\psi(t) = Gr_0^3(C_{\psi1} + iC_{\psi2})\psi(t) \quad (9)$$

$$N_\psi(t) = r_0^3 G_s \{\delta(S_{\psi1} + iS_{\psi2}) + \frac{\delta^3}{2}(S_{u1} + iS_{u2})\}\psi(t) \quad (10)$$

$$R_\zeta(t) = Gr_0^3(C_{\zeta1} + iC_{\zeta2})\zeta(t) \quad (11)$$

$$N_\zeta(t) = r_0^3 G_s \{\delta(S_{\zeta1} + iS_{\zeta2})\}\zeta(t) \quad (12)$$

where

$$C_{w1} = \left(\frac{-f_{w1}}{f_{w1}^2 + f_{w2}^2} \right); C_{w2} = \left(\frac{f_{w2}}{f_{w1}^2 + f_{w2}^2} \right) \quad (13)$$

$$C_{u1} = \left(\frac{-f_{u1}}{f_{u1}^2 + f_{u2}^2} \right); C_{u2} = \left(\frac{f_{u2}}{f_{u1}^2 + f_{u2}^2} \right) \quad (14)$$

$$C_{\psi1} = \left(\frac{-f_{\psi1}}{f_{\psi1}^2 + f_{\psi2}^2} \right); C_{\psi2} = \left(\frac{f_{\psi2}}{f_{\psi1}^2 + f_{\psi2}^2} \right) \quad (15)$$

$$C_{\zeta 1} = \left(\frac{-f_{\zeta 1}}{f_{\zeta 1}^2 + f_{\zeta 2}^2} \right); C_{\zeta 1} = \left(\frac{f_{\zeta 2}}{f_{\zeta 1}^2 + f_{\zeta 2}^2} \right) \quad (16)$$

In which G is the shear modulus of elasticity of the elastic half space, G_s is the shear modulus of the medium in which the foundation is embedded, f_{ij} ($i=w, u, \psi, \zeta$; $j=1, 2$) are Reissner's displacement functions which depend on Poisson's ratio ν and a dimensionless frequency defined by

$$a_0 = \omega r_0 \sqrt{\frac{\rho}{G}} \quad (17)$$

ρ is the mass density of the elastic half space and r_0 is the radius of the cylindrical foundation while ω is the circular excitation frequency.

The functions $S_{w1}, S_{w2}, S_{u1}, S_{u2}, S_{\psi 1}, S_{\psi 2},$

$S_{\zeta 1}$ and $S_{\zeta 2}$ are complex functions of Hankel functions, Bessel functions and Poisson's ratio.

By considering the displacement of infinitesimally thin horizontal layers, independent of each other, Baranov(1967) derived expressions for $S_{w1}, S_{w2}, S_{u1}, S_{u2}, S_{\psi 1}$ and $S_{\psi 2}$, Beredugo (1971) derived approximate equations for these functions in terms of a_0 and are given in Tables 6 to 8. They have also been plotted in Fig. 1. $S_{\zeta 1}$ and $S_{\zeta 2}$ were derived by Novak and Sachs (1973)

If equations (5) to (12) are substituted into equations (1) to (4) we get

$$m\ddot{w} + Gr_0 \{ (C_{w1} + iC_{w2}) + \frac{G_s}{G} \delta (S_{w1} + iS_{w2}) \} w(t) = P(t) \quad (18)$$

$$m\ddot{u} + Gr_0 \{ (C_{u1} + iC_{u2}) + \frac{G_s}{G} \delta (S_{u1} + iS_{u2}) \} u(t) = Q(t) \quad (19)$$

$$I_\psi \ddot{\psi} + Gr_0^3 \{ (C_{\psi 1} + iC_{\psi 2}) + \frac{G_s}{G} [\delta (S_{\psi 1} + iS_{\psi 2}) + \frac{\delta^3}{2} (S_{u1} + iS_{u2})] \} \psi(t) = T_\psi(t) \quad (20)$$

$$I_\zeta \ddot{\zeta} + Gr_0^3 \{ (C_{\zeta 1} + iC_{\zeta 2}) + \frac{G_s}{G} [\delta (S_{\zeta 1} + iS_{\zeta 2})] \} \zeta(t) = T_\zeta(t) \quad (21)$$

These equations are formally equal to the equations for the single degree of freedom system for a foundation attached to the surface of an elastic half space.

3. Solution of equations

With complex excitations

$$P(t) = P_0 \exp(i\omega t) = P_0 (\cos(\omega t) - i \sin(\omega t)) \quad (22)$$

$$Q(t) = Q_0 \exp(i\omega t) = Q_0 (\cos(\omega t) - i \sin(\omega t)) \quad (23)$$

$$T_\psi(t) = T_{\psi 0} \exp(i\omega t) = T_{\psi 0} (\cos(\omega t) - i \sin(\omega t)) \quad (24)$$

$$T_\zeta(t) = T_{\zeta 0} \exp(i\omega t) = T_{\zeta 0} (\cos(\omega t) - i \sin(\omega t)) \quad (25)$$

in which $P_0, Q_0, T_{\psi 0}, T_{\zeta 0}$ are real excitation amplitudes.

The particular solution describing the steady state vibrations are

$$w(t) = w_c \exp(i\omega t) \quad (26)$$

$$u(t) = u_c \exp(i\omega t) \quad (27)$$

$$\psi(t) = \psi_c \exp(i\omega t) \quad (28)$$

$$\zeta(t) = \zeta_c \exp(i\omega t) \quad (29)$$

Where w_c, u_c, ψ_c and ζ_c are complex displacement amplitudes.

Substitution of equations (26) to (29) into equations (18) to (21) gives

$$(k_{ze} - m\omega^2)w_c + i\omega c_{ze}w_c = P_0 \quad (30)$$

$$(k_{xe} - m\omega^2)u_c + i\omega c_{xe}u_c = Q_0 \quad (31)$$

$$(k_{\psi e} - I_\psi \omega^2) + i\omega c_{\psi e}\psi_c = T_{\psi 0} \quad (32)$$

$$(k_{\zeta e} - I_\zeta \omega^2) + i\omega c_{\zeta e}\zeta_c = T_{\zeta 0} \quad (33)$$

In which

$$k_{ze} = Gr_0 \left(C_{w1} + \frac{G_s}{G} \delta S_{w1} \right) \quad (34)$$

$$k_{xe} = Gr_0 \left(C_{u1} + \frac{G_s}{G} \delta S_{u1} \right) \quad (35)$$

$$k_{\psi e} = Gr_0^3 \left(C_{\psi 1} + \frac{G_s}{G} \{ \delta S_{\psi 1} + \frac{\delta^2}{3} S_{u1} \} \right) \quad (36)$$

$$k_{\zeta e} = Gr_0^3 \left(C_{\zeta 1} + \frac{G_s}{G} \delta S_{\zeta 1} \right) \quad (37)$$

$$c_{ze} = \frac{Gr_0}{\omega} \left(C_{w2} + \frac{G_s}{G} \delta S_{w2} \right) \quad (38A)$$

$$= r_0^2 \sqrt{\rho G} \left(\bar{C}_{w2} + \bar{S}_{w2} \delta \sqrt{\frac{\rho_s G_s}{\rho G}} \right) \quad (38B)$$

$$c_{xe} = \frac{Gr_0}{\omega} \left(C_{u2} + \frac{G_s}{G} \delta S_{u2} \right) \quad (39A)$$

$$= r_0^2 \sqrt{\rho G} \left(\bar{C}_{u2} + \bar{S}_{u2} \delta \sqrt{\frac{\rho_s G_s}{\rho G}} \right) \quad (39B)$$

$$c_{\psi e} = \frac{Gr_0^3}{\omega} \left(C_{\psi 2} + \frac{G_s}{G} \left[\delta S_{\psi 2} + \frac{\delta^3}{3} S_{u2} \right] \right) \quad (40A)$$

$$= r_0^4 \sqrt{\rho G} \left(\bar{C}_{\psi 2} + \frac{G_s}{G} \delta \left[\bar{S}_{\psi 2} + \frac{\delta^2}{3} \bar{S}_{u2} \right] \right) \quad (40B)$$

$$c_{\zeta} = \frac{Gr_0^3}{\omega} \left(C_{\zeta 2} + \frac{G_s}{G} \delta S_{\zeta 2} \right) \quad (41A)$$

$$= r_0^4 \sqrt{\rho G} \left(\bar{C}_{\zeta 2} + \bar{S}_{\zeta 2} \delta \sqrt{\frac{\rho_s G_s}{\rho G}} \right) \quad (41B)$$

where ρ_s is the mass density of the medium in which the foundation is embedded and

$$\bar{C}_{w1}, \bar{C}_{w2}, \bar{C}_{u1}, \bar{C}_{u2}, \bar{C}_{\psi 1}, \bar{C}_{\psi 2}, \bar{C}_{\zeta 1}, \bar{C}_{\zeta 2}$$

$$\bar{S}_{w1}, \bar{S}_{w2}, \bar{S}_{u1}, \bar{S}_{u2}, \bar{S}_{\psi 1}, \bar{S}_{\psi 2}, \bar{S}_{\zeta 1} \text{ and } \bar{S}_{\zeta 2}$$

are frequency independent parameters while k_{ze} , k_{xe} , $k_{\psi e}$, $k_{\zeta e}$, c_{ze} , c_{xe} , $c_{\psi e}$ and $c_{\zeta e}$ are equivalent stiffness constants and damping constants e ,

It is seen that the equations of motion are exactly the same as those for surface foundations with the inclusion of the aide reactions. Adopting the same approach, solutions similar to those for surface foundations are obtained, Beredugo (1971). The only problem that remains to be resolved is the determination of the equivalent damping constants and equivalent stiffness constants.

Substituting equations (34) to (41B) into equations (26) to (29), and simplifying, Beredugo (1971) showed that the real displacement amplitudes are

$$w_0 = \frac{P_0}{\sqrt{(k_{ze} - m\omega^2)^2 - (\omega c_{ze})^2}} \quad (42)$$

$$u_0 = \frac{Q_0}{\sqrt{(k_{xe} - m\omega^2)^2 - (\omega c_{xe})^2}} \quad (44)$$

$$\psi_0 = \frac{T_{\psi 0}}{\sqrt{(k_{\psi e} - I_{\psi}\omega^2)^2 - (\omega c_{\psi e})^2}} \quad (45)$$

$$\zeta_0 = \frac{T_{\zeta 0}}{\sqrt{(k_{\zeta e} - I_{\zeta}\omega^2)^2 - (\omega c_{\zeta e})^2}} \quad (46)$$

The undamped natural frequencies are

$$\omega_{0z} = \sqrt{\frac{Gr_0}{m} \left(C_{w1} + \frac{G_s}{G} \delta S_{w1} \right)} \quad (47)$$

$$\omega_{0x} = \sqrt{\frac{Gr_0}{m} \left(C_{u1} + \frac{G_s}{G} \delta S_{u1} \right)} \quad (48)$$

$$\omega_{0\psi} = \sqrt{\frac{Gr_0^3}{I_{\psi}} \left(C_{\psi 1} + \frac{G_s}{G} \left\{ \delta S_{\psi 1} + \frac{\delta^3}{3} S_{u1} \right\} \right)} \quad (49)$$

$$\omega_{0\zeta} = \sqrt{\frac{Gr_0^3}{I_{\zeta}} \left(C_{\zeta 1} + \frac{G_s}{G} \delta S_{\zeta 1} \right)} \quad (50)$$

It is noted here that the stiffness parameters are frequency dependent and appear on both sides of the equations and hence an iteration process has to be used in the solution. Approximate frequency independent stiffness parameters

are available and these can be substituted in the right hand side of the equation to obtain the first approximate undamped natural frequency, which is then substituted in the next equation to obtain a better approximation of the undamped natural frequency. By continuing this process, an undamped natural frequency can be obtained to any required degree of accuracy.

In many practical problems, the excitation forces $P(t)$ and $Q(t)$, and the excitation moments $T_{\psi}(t)$ and $T_{\zeta}(t)$ are caused by unbalanced masses m_e rotating at an eccentric radius e and are given by

$$P_0 = m_e e \omega^2; Q_0 = m_e e \omega^2; \quad (51)$$

$$T_{\psi 0} = m_e e z_b \omega^2; T_{\zeta 0} = m_e e r_e \omega^2 \quad (52)$$

Where

z_b = height of centroid of foundation (plus machinery if any) above ground level

r_e = distance of rotating mass from axis of rotation of foundation

e = eccentricity of rotating mass m_e

The real displacement amplitudes now become

$$w_0 = \frac{m_e e \omega^2}{\sqrt{(k_{ze} - m\omega^2)^2 - (\omega c_{ze})^2}} \quad (53)$$

$$u_0 = \frac{m_e e \omega^2}{\sqrt{(k_{xe} - m\omega^2)^2 - (\omega c_{xe})^2}} \quad (54)$$

$$\psi_0 = \frac{m_e e z_b \omega^2}{\sqrt{(k_{\psi e} - m\omega^2)^2 - (\omega c_{\psi e})^2}} \quad (55)$$

$$\zeta_0 = \frac{m_e e r_e \omega^2}{\sqrt{(k_{\zeta e} - m\omega^2)^2 - (\omega c_{\zeta e})^2}} \quad (56)$$

In many practical problems, it is often advantageous to introduce dimensionless displacement amplitudes

For constant amplitude forces, the relevant equations are

$$A_z = \frac{Gr_0}{P_0} w_0 \quad (58)$$

$$A_x = \frac{Gr_0}{Q_0} u_0 \quad (59)$$

$$A_{\psi} = \frac{Gr_0^2}{T_{\psi 0}} \psi_0 \quad (60)$$

$$A_{\zeta} = \frac{Gr_0^2}{T_{\zeta 0}} \zeta_0 \quad (61)$$

And for frequency dependent forces the equations are

$$A_z = \frac{m}{m_e e} w_0 \quad (62)$$

$$A_x = \frac{m}{m_e e} u_0 \quad (63)$$

$$A_{\psi} = \frac{I_{\psi}}{m_e e z_b} \psi_0 \quad (64)$$

$$A_{\zeta} = \frac{I_{\zeta}}{m_e r_e} \zeta_0 \quad (65)$$

The phase angles are

$$\phi_z = -\arctan \left[\frac{c_{ze} \omega}{(k_{ze} - m \omega^2)} \right] \quad (66)$$

$$\phi_x = -\arctan \left[\frac{c_{xe} \omega}{(k_{xe} - m \omega^2)} \right] \quad (67)$$

$$\phi_{\psi} = -\arctan \left[\frac{c_{\psi e} \omega}{(k_{\psi e} - I_{\psi} \omega^2)} \right] \quad (68)$$

$$\phi_{\zeta} = -\arctan \left[\frac{c_{\zeta e} \omega}{(k_{\zeta e} - I_{\zeta} \omega^2)} \right] \quad (69)$$

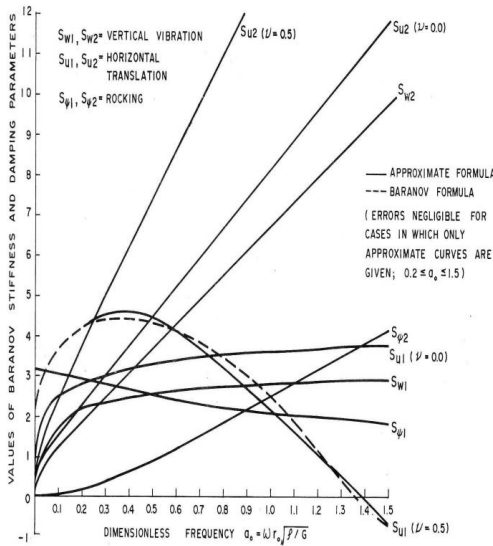


Figure 1: Approximate stiffness and damping parameters for side layer

For zero embedment, the spring and damping constants reduce to those for surface foundations.

3. Effect of an elastic stratum on the vibration of a dynamically loaded partially embedded foundation

The analytical procedure outlined above has a number of advantages over most of the methods currently adopted in the solution of dynamically loaded partially embedded foundations. It allows for the solution of foundations embedded in side fills with different densities. Similarly by substituting the elastic stratum functions in place of Reissner's elastic half space functions, the effect of an elastic stratum on the vibration of a dynamically loaded foundation partially embedded in an elastic stratum can be easily studied. In a 1957 paper, Warburton gave curves of the displacement functions f_{w1} and f_{w2} for an elastic stratum in vertical vibration.

Let

h = thickness of elastic stratum

l = embedment of foundation in elastic stratum

r_0 = the radius of a cylindrical foundation

Then

$\frac{h}{r_0} = \Delta$ is the stratum thickness ratio

$\frac{l}{r_0} = \delta$ is the embedment ratio.

Warburton's (1957) values of f_{w1} and f_{w2} obtained from a curve fitting procedure for $\nu = 0.25$ have been computed by Beredugo (1971) and are given in Table 4

Substituting Warburton's displacement functions for an elastic stratum into equation (62) numerical values of dimensionless displacements (fig. 2) and resonant frequencies (Fig. 3) for vertical vibration of a dynamically loaded foundation partially embedded in an elastic stratum were easily obtained. It is clearly shown

that as the stratum thickness ratio $\frac{h}{r_0} = \Delta$ approaches ∞ ,

i.e. for any given radius r_0 , as h becomes very large the resonant amplitude ratio approaches 1.

In general for any given mass ratio, both the resonant amplitude and the resonant frequency decreased with increasing thickness of the elastic stratum.

It was observed that for any given mass ratio, the resonant amplitude and the resonant amplitude ratios generally increased with decreasing thickness of the elastic stratum. Thus for any given system, the elastic half space gives the minimum response. Embedment in a backfill in elastic stratum reduced the effects of embedment as was the case in the elastic half space. Comparison of the elastic stratum and elastic half space vibrations shows that there is considerable magnification of the amplitudes as the elastic stratum becomes thinner. This may be due to the reflections of the waves on the elastic stratum boundary. For surface foundations, most of the damping occurs as internal hysteresis losses within the stratum. However, with embedded foundations, a considerable part of the elastic wave energy is radiated through the embedded surface and geometric damping becomes important.

For relative embedment ratios δ greater than 0.5, the elastic stratum response approaches that of the elastic half space at the same embedment. Similarly for stratum ratios Δ greater than 5, the elastic stratum response approaches that of the elastic half space.

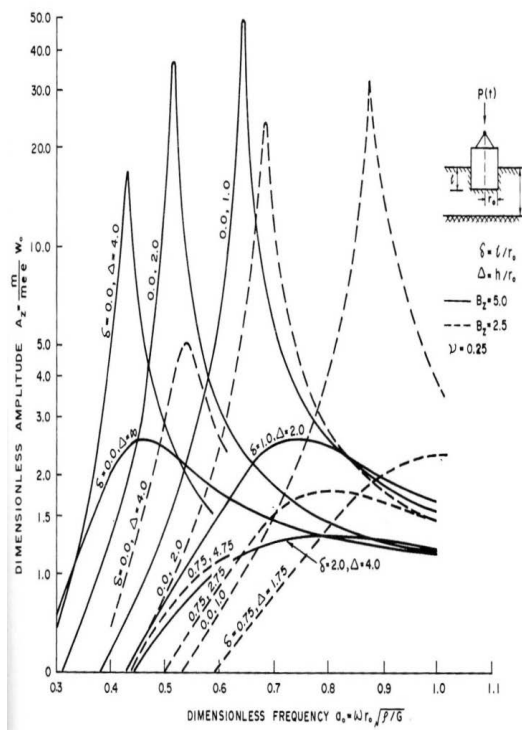


Figure 2 Theoretical response curves for vertical vibration of footing embedded in an elastic stratum (undisturbed soil, various embedments and various thicknesses of elastic stratum, $b_z = 2.5$ and 5.0)

4. Conclusions and Remarks

It has been shown that the mathematical model of a dynamically loaded foundation partially embedded in an elastic half space is very flexible and can easily be adapted to study the effects of back fills of different densities as well as the effect of an elastic stratum. The solutions yield results with minimum effort once the appropriate displacement functions are adopted. There is a paucity of field test results to compare with the theoretical predictions. The few available results indicate a reasonable degree of qualitative correlation. As more field test results become available, they will give us get a better understanding of the effect of an elastic stratum on the vibration of dynamically loaded partially embedded foundations. One major advantage of the approximate analytical method is that once more accurate values of the stiffness and damping parameters become available they can replace the existing values to give more accurate solutions.

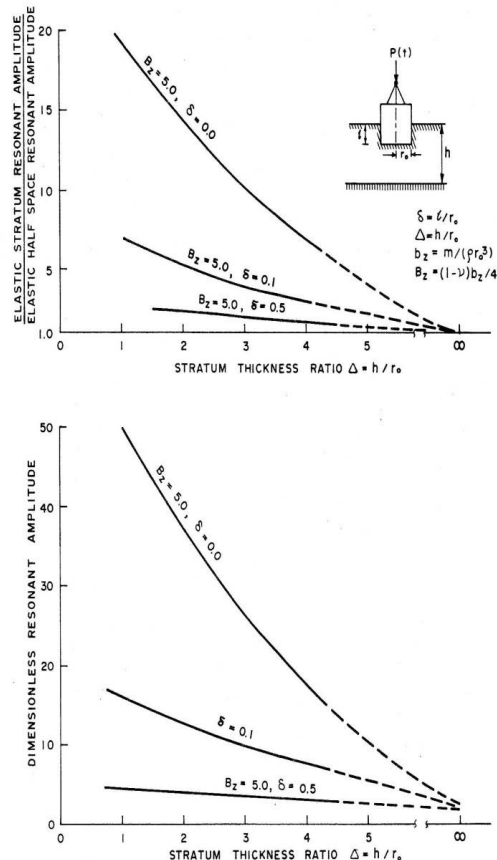


Figure 3 Variation of theoretical resonant amplitude of vertical vibration of footing embedded in an elastic stratum with thickness of stratum (undisturbed soil, various embedments)

Table 1 Reissner's Elastic half space functions (Rigid Base)

ν	Approximate formulas (based on Bycroft (1956))
0.0	$-f_{w1} = 0.251434 - 0.0160204a_0 - 0.141969a_0^2 + 0.0447130a_0^3$
	$f_{w2} = 0.223538a_0 - 0.11985a_0^2 + 0.12077a_0^3 - 0.12444a_0^4 + 0.025808a_0^5$
0.5	$-f_{w1} = 0.125 - 0.01886a_0 - 0.0059818a_0^2 - 0.054409a_0^3 + 0.025808a_0^4$
	$f_{w2} = 0.10659a_0 - 0.0070148a_0^2 - 0.028688a_0^3 + 0.008541a_0^4$

Table 2. Horizontal Translation (from Bycroft 1956) ($0 \leq a_0 \leq 2$)

$$f_{u1} = -\{\pi(\tau^2 + 3)/4 - (0.392\tau^4 + 0.655)a_0^2 + (0.0655\tau^6 + 0.0913)a_0^4 - (0.0055\tau^8 + 0.00701)a_0^6 - (0.0027\tau^{10} + 0.00033)a_0^8 - (0.00001\tau^{12} + 0.00001)a_0^{10}\} \frac{1}{4\pi}$$

$$f_{u2} = -\{(0.667\tau^3 + 1.333)a_0 - (0.177\tau^5 + 0.266)a_0^3 + (0.0203\tau^7 + 0.0271)a_0^5 - (0.0013\tau^9 + 0.0016)a_0^7 + (0.000052\tau^{11} + 0.0006)a_0^9\} \frac{1}{4\pi}$$

Where

$$\tau^2 = 0.0 \text{ for } \nu = 0.5$$

$$\tau^2 = \frac{1}{3} \text{ for } \nu = 0.25$$

$$\tau^2 = \frac{1}{2} \text{ for } \nu = 0.0$$

Table 3 Rotation about horizontal axis (Rocking)

Approximate formulas (based on Bycroft (1956) for $\nu=0.0$)
$-f_{\psi 1} = 0.37681 - 0.2833a_0 + 0.24131a_0^2 - 0.16301a_0^3 + 0.0129923a_0^4$
$f_{\psi 2} = 0.000981a_0 + 0.002839a_0^2 + 0.03986a_0^3 + 0.09333a_0^4 + 0.029022a_0^5 - 0.10425a_0^6 + 0.016429a_0^7 + 0.01127a_0^8$

Table 4. Elastic Stratum Displacement Functions for Vertical Vibrations for a Poisson's ratio of $\nu=0.25$ (Rigid Base Pressure Distribution) from Warburton (1957)

$\Delta = \frac{h}{r_0}$	Approximate formulas	Range of Validity
1.0	$-f_{w1} = 0.0818 - 0.0084797a_0 + 0.0035119a_0^2 + 0.007061a_0^3 +$	$0 \leq a_0 \leq 1.$
	$f_{w2} = 0.0015712a_0^2 + 0.0044574a_0^3$	
2.0	$-f_{w1} = 0.123 + 0.01297a_0 + 0.064407a_0^2 + 0.052779a_0^3$	$0 \leq a_0 \leq 1.25$
	$f_{w2} = -0.0052961a_0^2 + 0.1264a_0^3 - 0.27762a_0^4 + 0.20152a_0^5$	
4.0	$-f_{w1} = 0.152 + 0.0044615a_0 + 0.0035933a_0^2 + 0.51857a_0^3$	$0 \leq a_0 \leq 0.625$
	$f_{w2} = 0.10028a_0^2 - 0.31044a_0^3 - 0.65315a_0^4 + 2.6957a_0^5$	

Table 5 Values of C_{w1} and C_{w2} for Elastic Stratum computed from Warburton's (1957) values of f_{w1} and f_{w2} for $\nu=0.25$

$\Delta = \frac{h}{r_0}$	Approximate formulas	Range of Validity
1.0	$C_{w1} = 12.2249 - 1.2779a_0 - 0.30557a_0^2 - 1.177a_0^3 + 0.41599a_0^4$	$0 \leq a_0 \leq 1.5$
	$C_{w2} = -0.00011042a_0 + 0.23953a_0^2 + 0.56457a_0^3 + 0.022699a_0^4 - 0.34026a_0^5 + 0.10195a_0^6$	
2.0	$C_{w1} = 8.13 + 0.85163a_0 - 3.6643a_0^2 - 8.2893a_0^3 + 11.18a_0^4 - 3.9776a_0^5$	$0 \leq a_0 \leq 1.25$
	$C_{w2} = 0.0040442a_0 - 0.73859a_0^2 + 13.271a_0^3 + 39.608a_0^4 + 49.794a_0^5 + 26.954a_0^6 + 5.069a_0^7$	
4.0	$C_{w1} = 6.5789 + 0.24216a_0 - 0.38892a_0^2 - 29.686a_0^3 + 7.7107a_0^4 + 76.437a_0^5 - 77.419a_0^6$	$0 \leq a_0 \leq 0.625$
	$C_{w2} = 0.028043a_0 + 3.0198a_0^2 + 7.458a_0^3 - 184.15a_0^4 - 655.72a_0^5 - 804.89a_0^6 + 314.21a_0^7$	

Table 6. Side layer rigidity parameters (for Vertical vibration (independent of ν))

$$S_{w1} = 0.215348a_0 + \frac{2.7599a_0}{a_0 + 0.06084}$$

$$\bar{S}_{w1} = 2.70$$

$$S_{w2} = 6.058569a_0 + \frac{0.702158a_0}{a_0 + 0.016157}$$

$$\bar{S}_{w2} = 6.7$$

Table 7 Side Rigidity parameters for Rotation about a Horizontal Axis (Rocking) (Independent of ν)

$$S_{\psi1} = \pi - 0.42151a_0 - 4.20952a_0^2 +$$

$$7.1648a_0^3 + 4.6667a_0^4 + 1.0929a_0^5$$

$$\bar{S}_{\psi1} = 2.5$$

$$S_{\psi2} = 0.0144a_0 + 5.2633a_0^2 -$$

$$4.177a_0^3 + 1.6431a_0^4 - 0.25422a_0^5$$

$$\bar{S}_{\psi2} = 1.8$$

Table 8 Side Rigidity parameters for Horizontal Translation

ν	Approximate Formulas	Rang of Validity
0.0	$S_{u1} = 0.232844a_0 + \frac{3.608825a_0}{a_0 + 0.061585}$	$0.2 \leq a_0 \leq 1.5$
	$\bar{S}_{u1} = 3.6$	
	$S_{u1} = 150.29a_0 - 3629.9a_0^2 - 39477a_0^3 - 19338a_0^4 + 348840a_0^5$	$0 \leq a_0 \leq 0.2$
0.5	$S_{u2} = 7.334118a_0 + \frac{0.865206a_0}{a_0 + 0.008739}$	$0 \leq a_0 \leq 1.5$
	$\bar{S}_{u2} = 8.2$	
	$S_{u1} = -6.591081a_0 + \frac{10.310461a_0}{a_0 + 0.17421}$	$0.2 \leq a_0 \leq 1.5$
0.5	$S_{u1} = 63.184a_0 - 797.39a_0^2 + 5097.7a_0^3 - 11173a_0^4$	$0 \leq a_0 \leq 0.2$
	$S_{u2} = 12.117136a_0 + \frac{1.40432a_0}{a_0 + 0.016158}$	$0 \leq a_0 \leq 1.5$

Table 9 Elastic half space stiffness and damping parameters (Rigid Base Pressure (Approximate formulas derived by Beredugo (1971)

v	Approximate formulas
	Vertical Vibration
0.0	$C_{w1} = 4.00 - 0.83565a_0 + 0.63464a_0^2 - 2.6005a_0^3 + 1.8011a_0^4 - 0.36457$
	$C_{w2} = 3.4384a_0 + 0.57419a_0^2 - 1.1544a_0^3 + 0.74331a_0^4$
0.5	$C_{w1} = 8.0 + 2.1803a_0 - 12.627a_0^2 + 20.733a_0^3 - 16.468a_0^4 + 4.4585a_0^5$
	$C_{w2} = 7.4136a_0 + 2.9857a_0^2 + 4.3245a_0^3 - 1.7825a_0^4$
	Horizontal translation
0.0	$C_{u1} = 4.57143 - 4.65321a_0 + \frac{89.094373a_0}{a_0 + 19.14467}$
	$\bar{C}_{u1} = 4.30$
	$C_{u2} = 2.53068a_0 + \frac{0.134461a_0}{a_0 - 1.923434}$
0.5	$\bar{C}_{u2} = 2.7$
	$C_{u1} = 5.33334 - 1.583648a_0 + \frac{10.385608a_0}{a_0 + 6.552074}$
	$\bar{C}_{u1} = 5.10$
	$C_{u2} = 2.923135a_0 - \frac{0.174072a_0}{a_0 - 1.927455}$
0.0	$\bar{C}_{u2} = 3.15$
	Rocking $((0 \leq a_0 \leq 1.5))$
	$C_{\psi1} = 2.6538 + 0.1962a_0 - 1.7286a_0^2 + 1.4848a_0^3 - 0.48811a_0^4 + 0.034975a_0^5$
0.0	$\bar{C}_{\psi1} = 2.5$
	$C_{\psi2} = 0.0080251a_0 + 0.015826a_0^2 + 0.20351a_0^3 + 1.2021a_0^4 - 1.4478a_0^5 + 0.44907a_0^6$
	$\bar{C}_{\psi2} = 0.43$
	Torsion $(0 \leq a_0 \leq 2.0)$
	$\bar{C}_{\zeta1} = 4.3; \bar{S}_{\zeta1} = 12.4$
	$\bar{C}_{\zeta2} = 0.7; \bar{S}_{\zeta2} = 10.2$

Acknowledgement

The study was supported by a grant-in-aid of research from the National Research Council of Canada and a Commonwealth Scholarship awarded to the author by the Canadian Federal Government.

REFERENCES

- Baranov, V. A. (1967) *On the Calculation of Excited vibrations of an embedded foundation (In Russian)* Voprosy Dynamiki i Prochnosti No. 14, Polytechnical Institute of Riga pp 195-209
- Beredugo, Youpele Orukalama (1971) *Vibrations of Embedded symmetric Footings*. Ph. D Thesis submitted to the University of Western Ontario London in partial fulfilment of the requirement for the degree of Doctor of Philosophy.
- Beredugo, Y. O. and Novak M (1972) *Coupled Horizontal and rocking Vibrations of an embedded footing* Canadian Geotechnical Journal, Vol. 9 No. 4 pp 477-497.
- Bycroft, G. N. (1956) *Forced vibrations of a Rigid Circular Plate on a semi-infinite Elastic Half space and on an elastic stratum*. Philosophical Transactions of the Royal Society, London, Series A, Vol. 248, No. 948 pp 327-368
- Lysmer, J. and Kuhlemeyer, R. I. (1969) *Finite Dynamic Model for Infinite Media*, Journal of Engineering Mechanics Division, Proc. ASCE, Vol. 95, No. EM4 pp 859-877
- Lysmer, J., (1965) *Vertical Motion of Rigid Footings* Dept. of Civil Engineering, University of Michigan. Report to WES Contract Report No. 3-115 under Contract No. DA-22-079-eng-340
- Novak M. and Sachs K. (1973) *Torsional and Coupled Vibrations of embedded footings* Earthquake Engineering and Structural Dynamics, Vol 2 No.1 pp 11-33
- Reissner, E. (1936) *Stationaire, Axialsymmetrische Durch Eine Schüttelnde Mass Erregte Schwingungen Eines Homogenen Elastischen Halbraumes*. Ingenieur-Archiv. Vol. 7 Part 6 pp. 381-396
- Warburton, G. B. (1957) *Forced Vibration of a body upon an elastic stratum* Journal of Applied Mechanics, Trans. ASME, Vol 24 pp 55-58

An efficient method for estimating the dynamic response of base-isolated structure with SSI effect

Zhuang Haiyang^{1,*} & Yu Xu^{2,1} & Zhu Chao¹

¹Institute of Geotechnical Engineering, Nanjing University of Technology, Nanjing, 21009, China

²School of Civil Engineering, Nanjing Institute of Technology, Nanjing, 211167, China

ABSTRACT: To investigate the effect of soil-structure dynamic interaction (SSI effect) on the dynamic response of base-isolated structure, some shaking table tests have been completed before. Based on the test results and the existed studies, an efficient simplified model and corresponding calculation method to estimate the dynamic characteristic of base-isolated structure with SSI effect is developed and verified. Compared with the shaking table test and with the standard specification method suggested in China code without SSI effect, the new developed method can efficiently reflect the influence law and degree of SSI effect on the dynamic responses of base-isolated structure.

1. INTRODUCTION

Base-isolated structure has been widely used to reduce the earthquake damages of many kinds of structures. However, the effect of soil-structure dynamic interaction (SSI effect) is often neglected in these design methods. Existed researches have proved that SSI effect has a significant influence on the dynamic characteristic of isolated structure, which further affects the dynamic responses of isolated structure and the isolation efficiency of isolation layer (Mahmoud 2012, Li 2013). Therefore, SSI effect should be considered in the seismic design of isolated structure efficiently.

At present, the main method used to study this problem is numerical simulation. For example, Constantinou et al. (1988) studied on the dynamic responses of a base-isolated structure looked as a single degree of freedom, and used the fundamental frequency of interaction system to value the effect of SSI on the isolated structure. Additionally, Novak et al. (1989) studied the rotation effect of isolator on the modal characteristics of isolated system by using a multilayer shear structure with fixed dynamic stiffness. The influence of SSI effect was examined by investigating the modal properties, and some important simplifications in the analysis were also suggested. Pender (1987) also analyzed the seismic response of non-isolated structure built on the nonlinear soil foundation by looking the upper structure as a rigid block, and concluded that the nonlinear

soil foundation can be looked as a natural base isolation system. L. E. Pérez Rocha et al. (2013) also investigated the effect of SSI on the seismic responses of a base-isolated structure by using elastic springs and viscous dampers to replace the soil. It proved that SSI effects on the shear force were relatively more important than on the displacement, especially in the superior floors.

In China, Lihua Zou et al. (2004) also proved that the pile-soil interaction has obvious effect on the seismic response of isolated structure by analyzing the seismic response of an isolated structure with pile foundation. Hailing Li et al. (2001) and Wang A-ping et al. (2007) also studied on the effect of SSI on the first-order vibration frequency and the dynamic responses of isolated structure with linear base isolation system, and proved that the seismic design of isolated structure based on the rigid foundation assumption was not always safety. As a whole, most of existed methods are so complicated that they couldn't be used easily by engineer. However, in the past, the simplified method used to estimate the influence of SSI effect on the non-isolated structure have been advanced and used in the Building Seismic Design Code of United States (ATC1978) and BSSC specification (2009). So an efficient simplified method for the seismic design of isolated structure with SSI effect should also be developed for engineer. At the same time, the existed research methods and conclusions are also need to be evaluated and proved by efficient model tests further.

Accordingly, the influence laws of SSI effect on the dynamic characteristic and response of soil-isolated structure interaction system has been studied by four shaking table tests before. In this paper, an efficient simplified method to calculate the dynamic characteristic of isolated structure with SSI effect is developed and verified by tests, which can be used easily in seismic design of isolated structure.

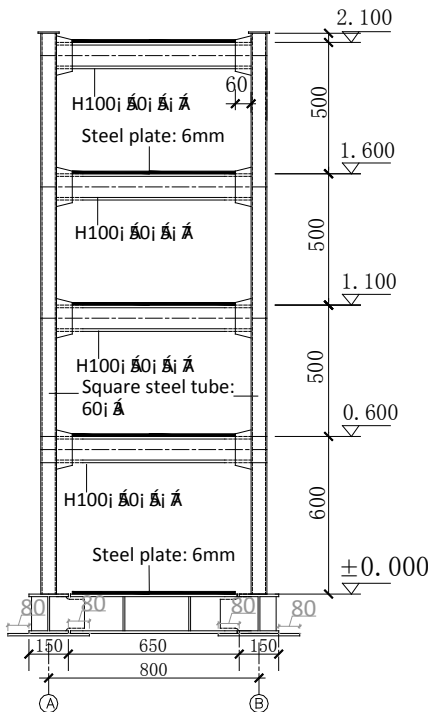
2. SHAKING TABLE TEST

A four-layer steel frame structure is made by square steel tube used to make the columns and H-shaped steel used as the beams. The main sizes of model steel structure are shown in Figure 1(a). The size of model structure's cross section is 0.8m (vibration direction) \times 0.6m (vertical to the vibration direction), which height is 2.1m. Steel plate with thickness 6mm are used as the floor slab. Accordingly, the aspect ratio of model structure in vibration direction is 2.625. The weight of model structure is 0.32t. To consider the similitude ratio of gravity as soon as possible, the

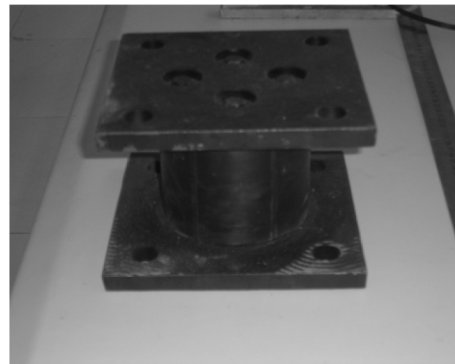
additional weight is added in each floor of model structure with 0.736t. The total weight of the model structure and the additional weight is about 4.0t.

Four lead rubber bearings are used as the isolators in the isolation layer of structure. According to the stress similitude ratio of isolator and the upper weight on them, the model isolators are designed with diameter of transection 100mm and the average compressive stress designed 1.3N/mm^2 , which geometry shape and the physical and mechanical quantities are given in Figure 1(b) and Figure 1 (c).

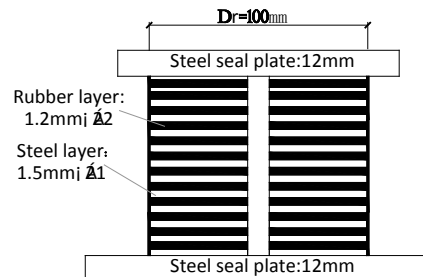
Four shaking table tests are designed to model the dynamic response of a four-floors structure in four different conditions such as the non-isolated structure on rigid foundation (Test I), the base-isolated structure on rigid foundation (Test II), the non-isolated structure on soil foundation (Test III) and the base-isolated structure on soil foundation (Test IV). The tests are explained in Figure 2, and some photos in test are shown in Figure 3.



(a) Size of model structure



(b) Lead rubber bearing



(c) Structure of lead rubber bearing

Fig.1 Model structure and lead rubber bearing designed for test (Unit of size: mm)

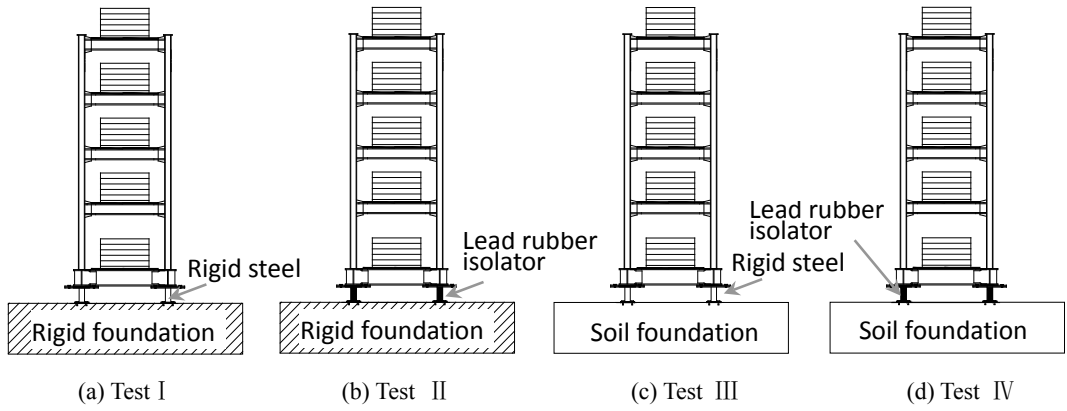
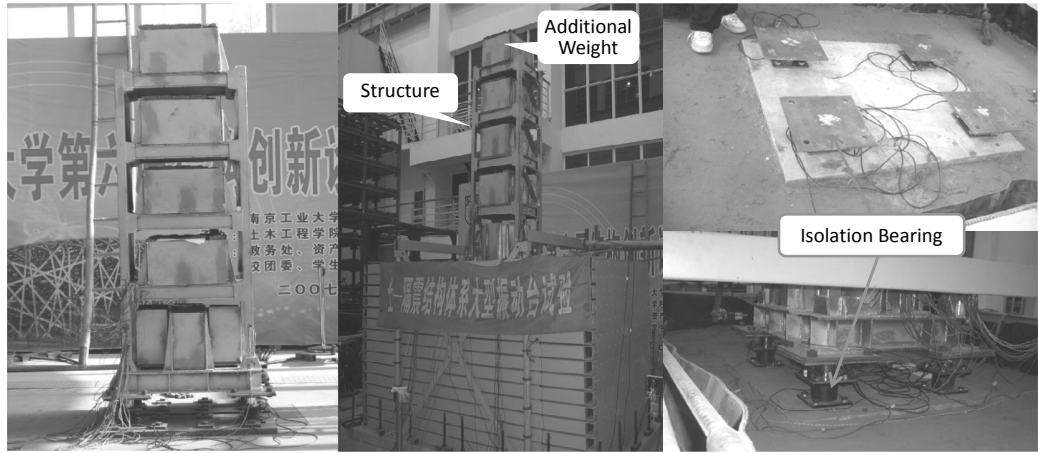


Figure 2. Shaking table tests designed to model four different conditions



(a) Fixed on rigid foundation (b) Fixed on soil foundation (c) Lead rubber isolator

Figure 3. Photos of tests for isolated structure on different foundations

3. EFFICIENT METHOD TO ESTIMATE SSI EFFECT

3.1. Simplified analysis model

In theory, with SSI effect, the inertia force of upper structure will be transited to foundation, which causes additional translation and rotation of foundation. By analyzing on the existed earthquake damages, Sivanovic (2000) also found that the SSI effect is obvious, which causes the swing of foundation. This phenomenon has also been found during the shaking table tests in this paper. Accordingly, an efficient model should be advanced to estimate the influence of SSI effect on the dynamic response of isolated structure. What's more, ac-

cording to the study by Wenguan Liu (2003), the model shown as Figure 4(a) can be simplified to be a more simply model shown as Figure 4(b). In Figure 12, k_0 and c_0 are the horizontal impedances of isolation layer, k_u and c_u are the horizontal impedances of soil foundation, k_θ and c_θ are the rotation impedances of soil foundation, h is the distance from the gravity center of foundation to the whole inertia force's action spot of isolated structure for the first-order vibration mode, u is the horizontal displacement of isolated structure relative to the foundation, u_f and θ are the horizontal displacement and rotation of pile foundation to the lateral soil foundation, respectively, u_g is the horizontal displacement of soil foundation at ground surface.

$$\tilde{T} = T \sqrt{1 + \frac{k}{k_u} \left(1 + \frac{k_u h^2}{k_\theta} \right)} \quad (11)$$

$$\tilde{\xi} = \tilde{\xi}_0 + \frac{0.05}{(\tilde{T}/T)^3} \quad (12)$$

Where, \tilde{T} and $\tilde{\xi}$ are the first-order vibration period and damping factor of interaction system, respectively, $\tilde{\xi}_0$ is the damping factor of foundation which can be decided by the values of \tilde{T}/T , the aspect ratio of structure and the properties of ground motion, T is the first-order vibration period of isolated structure on rigid foundation, which can be calculated by

$$T = 2\pi \sqrt{m/k_0} = 2\pi \sqrt{\sum m_i/k_0} \quad (13)$$

To shallow foundation, k_u and k_θ can be calculated by formula advanced by Bielak (1975). However, to pile foundation, k_u and k_θ should be calculated with the effect of piles (Chen GX et al., 1995), which can be calculated by

$$k_u = \sqrt{(k_u^F)^2 + (k_u^P)^2} \quad (13)$$

$$k_\theta = k_\theta^F + k_\theta^P \quad (14)$$

Where, k_u^F and k_θ^F are the horizontal stiffness and rotational stiffness of foundation without piles, k_u^P and k_θ^P are those of foundation with piles.

By Wenguang Liu (2003), a correction factor can be used to correct the interlayer shear coefficient of isolated structure to consider the rotation of isolation layer

$$\alpha_{im} = \eta_r \alpha_i = \eta_r \frac{V_{ki}}{\sum_{j=1}^n G_j} \quad (15)$$

Where, V_{ki} is the standard value of Interlayer Shear Force (ISF) in i^{th} layer of isolated structure, G_i is the representative value of gravity load of the j^{th} layer, α_i is the interlayer shear coefficient of isolated structure without rotation of isolation layer, η_r is the correction factor used to consider the rotation of isolation layer. It can be calculated by

$$\eta_r = \Psi^{\frac{1}{2} \left(\frac{i}{n} \right)^3} \quad (16)$$

Where, i is the floor number of isolated structure, n is total number of floor and Ψ is the aspect ratio of isolated structure in vibration direction which value is 2.625. For the shaking table test, the parameters used to calculate T and $\tilde{\xi}$ of model isolated structure are given in Table 1.

So far, we can use Equivalent Base Shear Method suggested in ERDC of China to calculate the dynamic response of isolated structure by using Equation (11) and Equation (12) to calculate the first-order vibration period and damping factor of isolated structure.

Table 1. Parameters used to calculate \tilde{T} and $\tilde{\xi}$ of model isolated structure

Physical quantity	Value	Physical quantity	Value
k_u^F (kN/mm)	3.89×10^3	$k = k_0$ (kN/mm)	1.11
k_θ^F (kN.m/rad)	9.1×10^4	C_0 (kN.s/m)	10.93
k_u^P (kN/mm)	1.54×10^5	$\tilde{\xi}_0$ (%)	10.8
k_θ^P (kN.m/rad)	1.46×10^5	T (s)	0.377
m (t)	4	h (m)	1.45

3.2 Verify of the developed method

To verify the effective of the developed simplified method, \tilde{T} and $\tilde{\xi}$ calculated by the

developed method (Method I : with effect of isolation layer's rotation, Method II : without effect of isolation layer's rotation) are compared with those by shaking table test (Method III)

and with those calculated by the method suggested in ERDC of China without SSI effect (Method IV), given in Table 2. As results, \tilde{T} and $\tilde{\xi}$ are all largest by Method III, and which are all smallest by Method IV. However, \tilde{T} and $\tilde{\xi}$ of isolated structure calculated by Method II are very closer to those by shaking table test, especially for the damping factor. It means that the developed method is efficient to estimate the influence of SSI effect on the dynamic characteristic of isolated structure. To rigid foundation, \tilde{T} and $\tilde{\xi}$ calculated by ERDC is very close to the test results.

Based on the acceleration responses at each floor of isolated structure, the displacement responses can be calculated by the integration of acceleration responses. Then, the ISFs of isolated structure can be calculated by the interlayer relative displacements and the interlayer lateral stiffness. The ISFs of isolated

structure by different methods are shown in Figure 5 with EI wave inputted. To other waves, the change laws of ISF are also same to those with EI wave inputted. In Figure 5, zero at the vertical coordinate axis denotes the isolation layer and other numbers denotes the floor number of isolated structure.

By Figure 5, the ISFs by ERDC of China are all smallest compared with other three methods, and the different between them become larger with the PGA of input motions increasing. However, with SSI effect, the ISFs by developed method without corrected by η_r are very closer to the test results, especially for PGA=0.1g and PGA=0.2g. However, the ISFs by η_r are bigger than those by shaking table test, and this effect becomes stronger with the height of structure increasing. It means that the rotation effect of isolation layer is excessively valued by using η_r to correct the ISF. To PGA=0.3g, the ISFs at the upper floor of isolated structure can be corrected by η_r roughly.

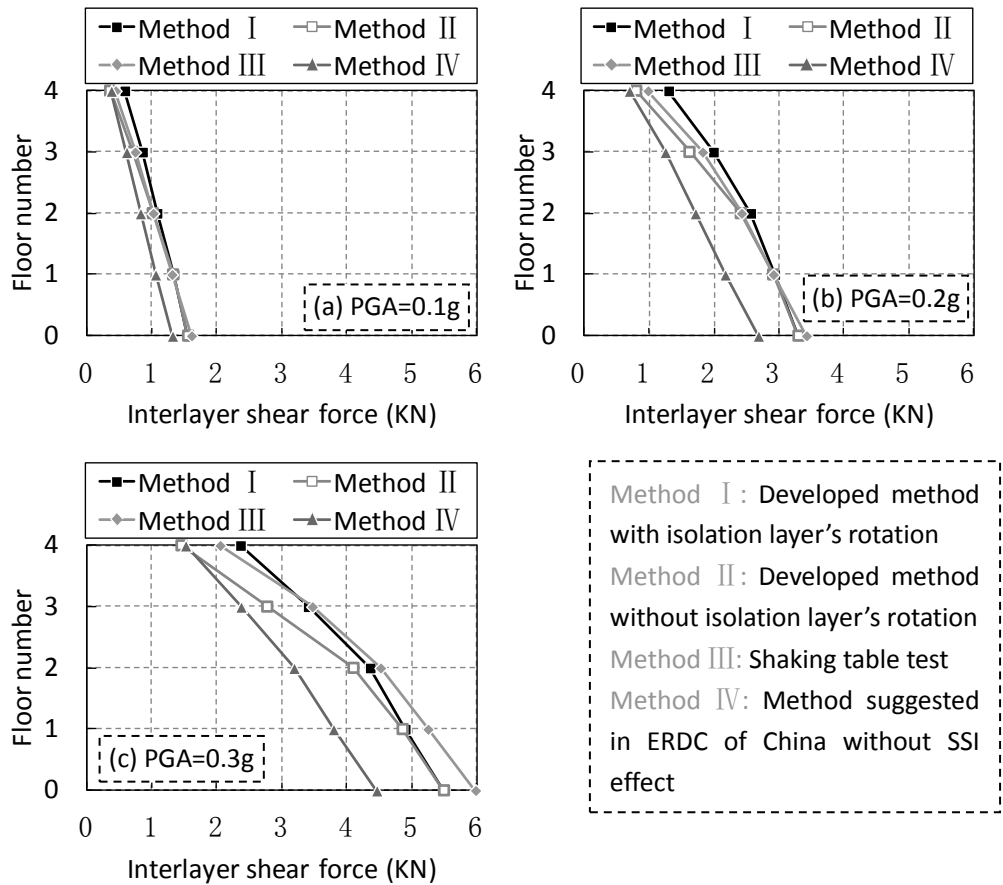


Figure 5. ISFs of base-isolated structure with EI-Centro wave inputted

Table 2. \tilde{T} and $\tilde{\xi}$ of isolated structure by different methods

Dynamic parameters	Soil foundation		Rigid foundation	
	TestIV	New method	Test II	ERDC
\tilde{T} (s)	0.42	0.395	0.38	0.377
$\tilde{\xi}$ (%)	15.40	15.10	8.30	8.20

4. CONCLUSIONS

To study the influence of SSI effect on the dynamic response of isolated structure, based on the test results and existed methods, an efficient simplified method to estimate the dynamic characteristic of isolated structure with SSI effect is developed. The developed simplified method is proved to be efficient to estimate the influence of SSI effect on the dynamic response of isolated structure. It also proves that the method given by Wenguang Liu (2003) to consider the rotation effect of isolation layer on the ISFs of isolated structure couldn't work efficiently, which may excessively value the rotation effect of isolation layer.

5. ACKNOWLEDGEMENTS

This research is funded by Jiangsu Natural Science Foundation of China (JNSF, Grant No. BK2012477). This supports are gratefully acknowledged. All statements, results and conclusions are those of the authors and do not necessarily reflect the views of JNSF. The authors would also like to thank the anonymous reviewers for their comments and suggestions.

6. REFERENCES

Bielak J. 1975. Dynamic Behaviour of Structure with Embedden Foundation. *Earthquake Engineering and Structural Dynamics*, Vol.3, No.3, pp.259-274.

Chen GX, Xie JF, Zhang KX. 1995. Static stiffness and dynamic impedance of pile and pile groups. *World Earthquake Engineering*, Vol.11, No.2, pp.45-50.

Chen YQ, Lv XL, Li PZ, et al. 2003. Simplified method for calculating dynamic characteristics of soil-structure interaction system. *Earthquake Engineering and Engineering Vibration*, Vol.23, No.1, pp.71-77.

Constantinou MC, Kneifati M. 1988. Dynamics of soil-base-isolation structure systems. *Journal of Structural Engineering*, Vol.114, No.1, pp.211-221.

Li HL, Ge XR. 2011. Effect of soil-structure interaction on base-isolated building system. *Journal of China Civil Engineering*, Vol.34, No.4, pp.83-87.

Li CP, Liu WQ, Wang SG, et al. 2013. Shaking table test on high-rise isolated structure on soft soil foundation. *Journal of Building Structures*, Vol.34, No.7, pp.72-78.

Liu WG. 2003. Mechanics properties of rubber bearing and earthquake response analysis of isolated structure. Beijing University of Technology: Beijing.

Novak M, Hendreson P. 1989. Base-isolated building with soil-structure interaction. *Earthquake Engineering and Structural Dynamics*, Vol.18, No.6, pp.751-765.

Pender M J. 1987. Nonlinear cyclic soil-structure interaction. *Pacific Conference on Earthquake Engineering*, New Zealand, pp.83-93.

Rocha L. E. Pérez, J.Avilés López, A. 2013. Tena Colunga, et al. Influence of soil-structure interaction on isolated buildings for SF6 gas-insulated substations. COMPDYN 2013, 4th ECCOMAS Thematic Conference on Computational Methods in Structural Dynamics and Earthquake Engineering, Kos Island, Greece 2013.

Sayed Mahmoud, Per-Erik Austrell, Robert Jankowski. 2012. Non-linear behavior of

- base-isolated building supported on flexible soil under damaging earthquakes. *Key Engineering Materials*, Vol.488-489, pp.142-145.
- Sivanovic S. 2000. Seismic response of an instrumented reinforced concrete building founded on piles. *Proc. 12th World conference of Earthquake Engineering*, Paper No. 2325.
- Wang AP, Yao QF. 2007. Random Earthquake Responses of Base Isolation Structures Considering Soil-Structure Interaction. *Journal of Beijing Jiaotong University*, Vol.31, No.4, pp.40-44.
- Zou LH, Zhao RD, Zhao JC. 2004. Analysis of the response to earthquake of the pile-soil-isolated structure interaction. *Chinese Journal of Geotechnical Engineering*, Vol. 26, No.6, pp.782-786.

Determination of bearing capacity of the precast piles by dynamic cone penetration test (DCPT)

A.Zh. Zhussupbekov, N.T. Alibekova, I.O. Morev and Ye.B. Utepov

Department of Civil Engineering, L.N. Gumilyov Eurasian National University, Astana, Kazakhstan

This paper presents the recommendations of determination of the bearing capacity of driven piles according to dynamic cone penetration test (DCPT). As well as the sufficiently close correlation between the main parameters of dynamic cone penetration test (DCPT) and static cone penetration test (CPT) was identified during the work and presented in this article.

1. INTRODUCTION

Currently, express method of soil testing by dynamic cone penetration test (DCPT) is rarely used as a part of works in geotechnical investigations in case of being in ground massifs gravelly sand and gravel soils.

The geotechnical features of cities, located in floodplains, is the existence of alluvial formations, the upper part of which is represented by loam and sandy loam of various consistencies, under which lie sands in granulometric composition of from small and medium size sand to gravelly soils. These sand formations contain lenses and interlayers of clayey soil, which in the practice of engineering-geological surveys leads to considerable difficulties in test of these soils by cone penetration test (CPT). Under these conditions, when the cone is pushed into the ground, frontal resistance of the cone sensor reaches limit values or insufficiently of down-load force of test machine, whereby the experience stops. However, under the low lay of "clean and high-density" sandy soil, hidden soil, containing lenses and interlayers of clay with a significantly worse strength and deformation characteristics. During the drilling of geotechnical boreholes the sandy soil described above is revealed quite difficult, therefore it is require to make continuous sampling of undisturbed structures that is difficult to perform in sands.

Subsequently, during the driving of test piles, a modern hydraulic piling machines and not rarely diesel hammers easily punch these interlayers of sandy soil, respectively, the depth and bearing capacity of piles, which had previously been accepted by the design institute according to engineering-geological survey appear to be incorrect, therefore, it is appointed to make additional field tests (GOST 5686-94)

of piles of greater length, which can be driven to the maximum depth and can achieve the required rejection.

Application of CPT in coarse sands and gravelly soils leads to unexpected expenses and time of a Customer, as well as accusation the organization performing engineering-geological surveys for giving false geological information.

2. SEARCHING FOR THE DEPENDENCES BETWEEN DCPT RESULTS AND BEARING CAPACITY OF DRIVEN PILES

Due to the fact, that in our practice of engineering-geological surveys, which include dynamic tests of driven piles, frequent the cases when depth of test piles exceed the depth to which CPT tests were conducted, we have attempted to improve this situation. During the performing parallel CPT and DCPT tests, it turned out that the DCPT machine with the average specific energy of penetration (classification of GOST 19912-2001), equipped with a hammer weighing 60 kg, dropped from a height of 80 cm, can significantly penetrate deeper into the coarse sand and even gravelly soils.

DCPT machine is very easy to use, the cost of test is lower than CPT, as well as for fulfillment such experimental works it is not required the highly skilled personnel with special knowledge and skills.

Existing regulations prescribe the DCPT testing regardless of ground conditions of the construction site in accordance with GOST 19912-2001 to estimate the possible depth of piling and the piles' bearing capacity, as well as to define the mechanical and deformation characteristics of investigated soils.

However, to determine the bearing capacity of driven piles in the existing regulations are

given recommendations only for CPT. Currently DCPT is used in clayey soils only for the indirect determination of possible depth of piling and clarify the lithological section (soil strata), in sandy soils, there to evaluate the mechanical and deformation characteristics.

During the detailed study of the sectoral literature (Mariupol,1989) we have found the recommendations to determine the bearing capacity of driven piles according to DCPT results. Mariupol proposes the use for sandy soils the following equations to determine the resistance of the soil under the toe of pile R , MPa, and the lateral surface soil resistivity of pile f , MPa:

$$R = p_d \cdot \left[0.91 - 0.57 \lg \left(\frac{P_d}{p_d^0} \right) \right] \cdot \left(\frac{P_d}{p_d^0} \right)^{0.13} \quad (1)$$

$$f = \frac{P_d}{100} \cdot \left[0.58 - 0.32 \lg \left(\frac{P_d}{p_d^0} \right) \right] \cdot \left(\frac{P_d}{p_d^0} \right)^{0.13} \quad (2)$$

where p_d - dynamic soil resistivity, MPa; $p_d^0 = 1$ MPa.

To determine the resistance of the soil under the toe of pile R , MPa, and the lateral surface soil resistivity of pile f , MPa, in clayey soils it is proposed to use the following equations:

$$R = p_d \cdot \left[0.54 - 0.35 \lg \left(\frac{P_d}{p_d^0} \right) \right] \cdot \left(\frac{P_d}{p_d^0} \right)^{0.17} \quad (3)$$

$$f = \frac{P_d}{100} \cdot \left[2.82 - 2.11 \lg \left(\frac{P_d}{p_d^0} \right) \right] \cdot \left(\frac{P_d}{p_d^0} \right)^{-0.32} \quad (4)$$

where p_d - dynamic soil resistivity, MPa; $p_d^0 = 1$ MPa.

However, during the juxtaposition of the results obtained by aforementioned equations and the dynamic tests of piles, with the results of parallel conducted CPT, the discrepancy of bearing capacities of the piles of all three tests in approximately the same ground conditions is detected. It should be noted that the bearing capacities of the piles, determined by CPT near the test piles with those obtained by dynamic tests are approximately equal.

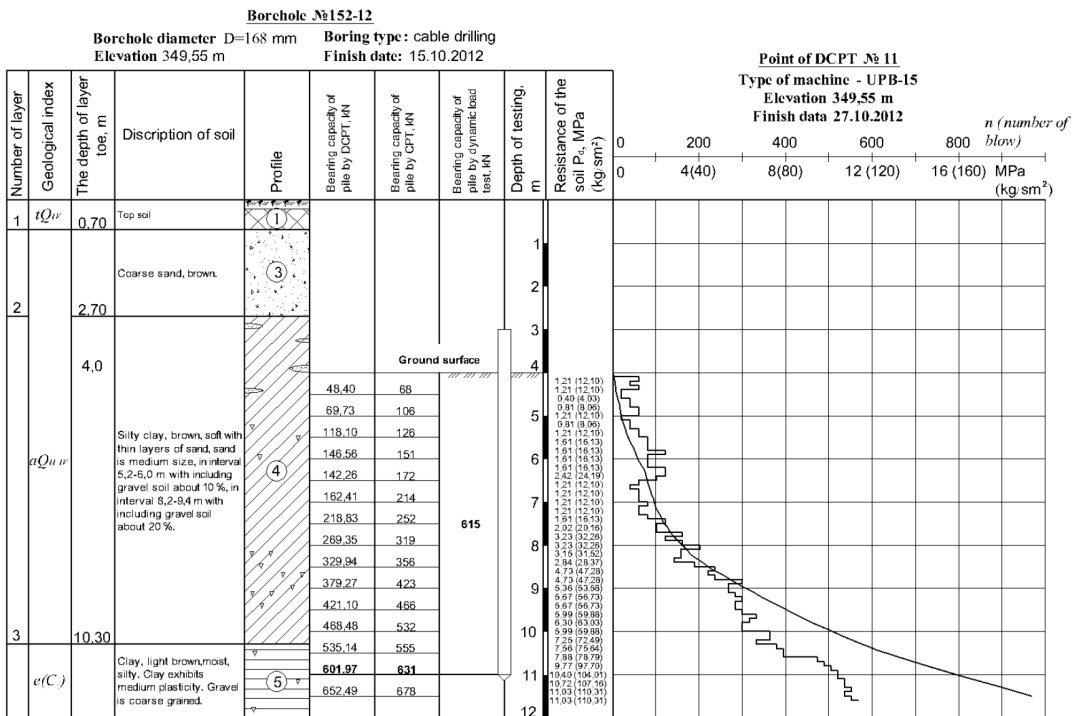


Fig. 1 Comparative analysis of determining the bearing capacity of driven piles in clayey soils by DCPT, CPT and dynamic load test of real pile.

In this situation, it was clear that it is necessary to clarify abovementioned equations, by comparing the values of the bearing capacities of real piles with those of CPT and DCPT.

163 DCPT were performed on 16 construction sites, in the places, assigned for the dynamic tests of the piles according to the pile outlines of the project. CPTs also are carried out at the same places. In other cases, when the depth of DCPT exceeds a depth of CPT for the comparison of bearing capacities of the piles the data of CPT to probing depth was taken and for lower depth the bearing capacity of pile capacity defined by dynamic test has been taken.

The following equations were found according to the results of performed works:

- for the determination of the resistance of the soil under the toe of pile R, MPa, and the lateral surface soil resistivity of pile f , MPa, in sandy soils using the following equations:

$$R = 0.4 \cdot 10^{-5} \cdot p_d^3 - 0.8 \cdot 10^{-3} \cdot p_d^2 + 0.0948 \cdot p_d + 0.0177 \quad (5)$$

$$f = 0.9 \cdot 10^{-8} \cdot p_d^3 - 0.3 \cdot 10^{-5} \cdot p_d^2 + 0.6 \cdot 10^{-3} \cdot p_d + 0.2 \cdot 10^{-3} \quad (6)$$

where p_d - dynamic soil resistivity.

- for the determination of the resistance of the soil under the toe of pile R, MPa, and the lateral surface soil resistivity of pile f , MPa, in clay soils using the following equations:

$$R = 0.2 \cdot 10^{-5} \cdot p_d^3 - 0.5 \cdot 10^{-3} \cdot p_d^2 + 0.0568 \cdot p_d + 0.0056 \quad (7)$$

$$R = 0.0091 \cdot p_d^{0.4456} \quad (8)$$

where p_d - dynamic soil resistivity.

It should be noted that to determine the resistance of the soil under the toe of the pile R, MPa, it is necessary to use an average value p_d , MPa, obtained from the test, in a portion located one diameter d above and four diameters d below the pile toe (where d - diameter or square side, or large rectangular side of a driven pile, m).

As an example for determining the bearing capacity of the piles in clayey soils, we present the lithological column of the borehole with the executed near the CPT and DCPT. Near this borehole the driven test pile was penetrated and was subjected to the dynamic load test for determination it's bearing capacity. The results of experimental works are presented in Fig. 1.

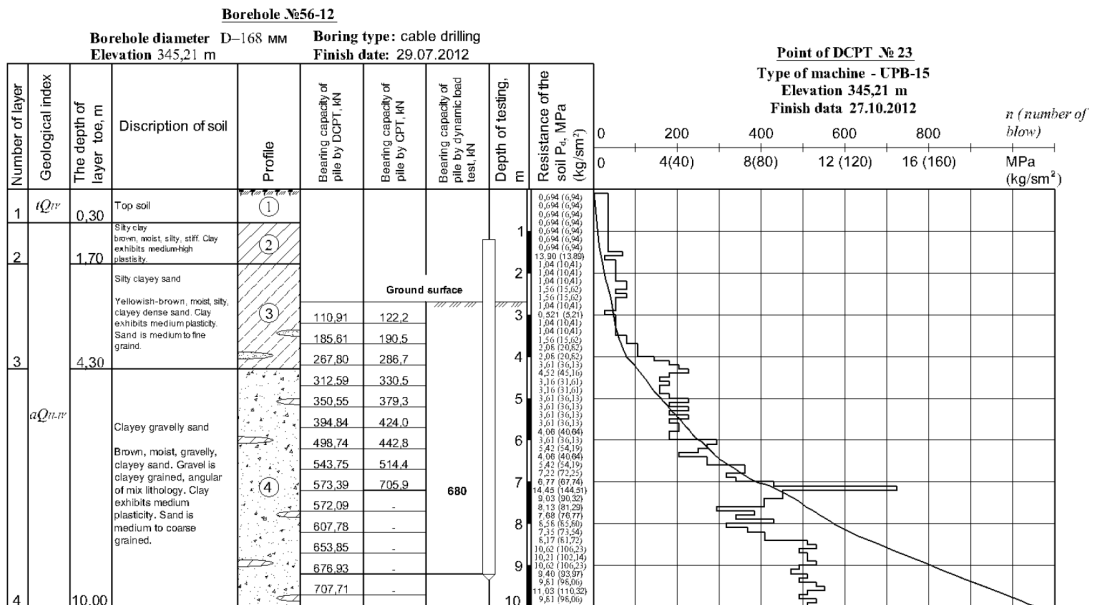


Fig. 2 Comparative analysis of determining the bearing capacity of a driven pile in sand soils by DCPT, CPT and dynamic load test of real pile.

Table 1 Comparative results of CPT, DCPT and dynamic tests of real piles

Soils:		Bearing capacity of driven piles, kN			Relative error ($F_{dz} - F_d$)/ F_d , %
below the toe of the piles	on the lateral surface of the piles	by DCPT, F_{dz}	by CPT, F_{st}	by dynamic tests of the real piles, F_d	
Clay	Clay	602	631	615	- 2
Clay	Sand	710	785	753	- 6
Sand	Sand	701	741	643	+ 9
Sand	Sand				
Note: depth of driving piles up to 4 m		482	634	567	- 15

A characteristic feature of sandy soils is the existence of the relatively clean (free of impurities clay particles) and dense layers of different thicknesses. A representative case is shown in Fig. 2. CPT test was terminated at a depth of 7.2 meters, due to reaching the limit values of frontal resistance of the probe tip. However, during DCPT, the layer described above was traversed. The layer of sandy soil with worse strength and deformation characteristics under abovementioned layer remained hidden; during the CPT. The same fact was confirmed during the dynamic tests of the real piles.

The given above empirical correlations have been repeatedly used on the construction sites, and showed the necessity and feasibility of applying DCPT to assess the bearing capacity and depth of pile foundations. Dynamic tests were conducted by the hydraulic pile driving machines Junttan PM-20 and PM-25 with the hammers HHK-5A and HHK-7A, the results of which were used in real projects of pile foundations.

3. DETERMINATION OF DEPENDENCES BETWEEN THE DCPT AND CPT

During operation on the determination of bearing capacity of the driven piles according to DCPT and comparison with the results of CPT a close enough correlations between the indicators of dynamic soil resistivity p_d (defined by DCPT) and soil resistance below the cone probe q_c and sleeve friction of probe f_s (defined by CPT), depending on the type of soil (sand or clay) has been revealed.

The following relations from a comparison of data in parallel conducted experimental work by DCPT and CPT were found:

- for the determination the resistance of soil under the cone probe q_c , MPa and sleeve friction of probe f_s , MPa, depending on the dynamic soil resistivity p_d , MPa, in sandy soils (Fig. 3 and 4);
- for the determination the resistance of soil under the cone probe q_c , MPa and sleeve friction of probe f_s , MPa, depending on the dynamic soil resistivity p_d , MPa, in clayey soils (Fig. 5 and 6).

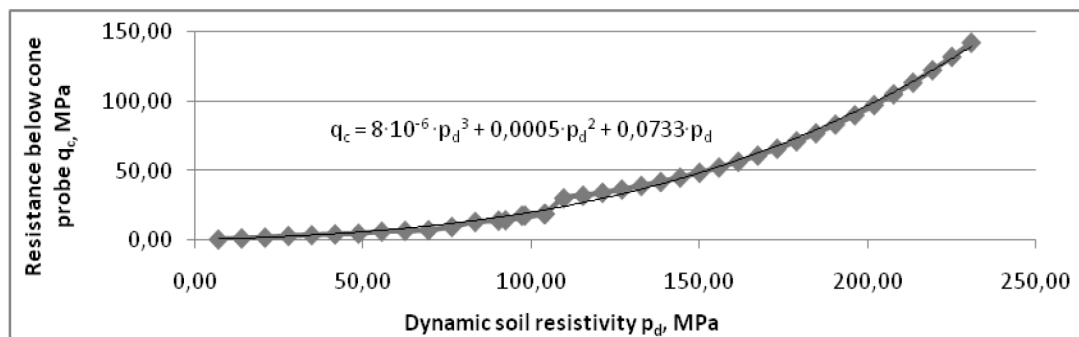


Fig. 3 Diagrams - ratio between dynamic soil resistivity p_d and soil resistance under the cone probe q_c in sandy soils.

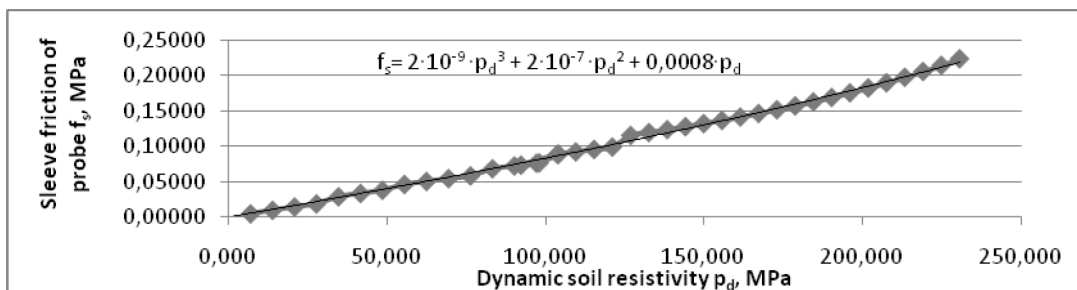


Fig. 4 Diagrams - ratio between dynamic soil resistivity p_d and sleeve friction of probe f_s in sandy soils.

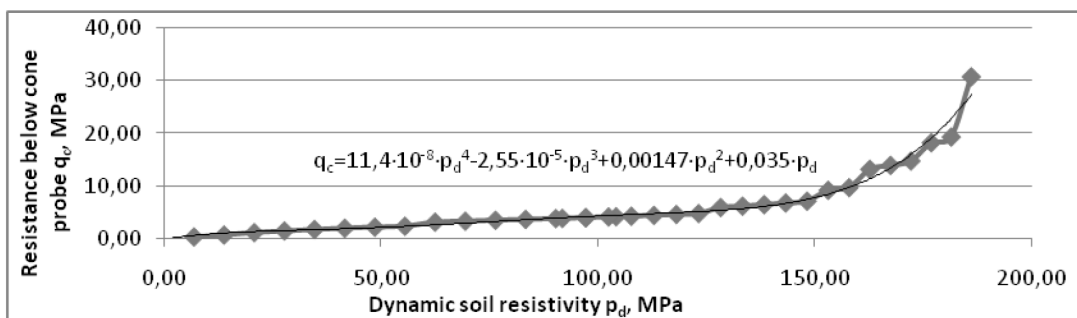


Fig. 5 Diagrams - ratio between dynamic soil resistivity p_d and soil resistance under the cone probe q_c in clayey soils.

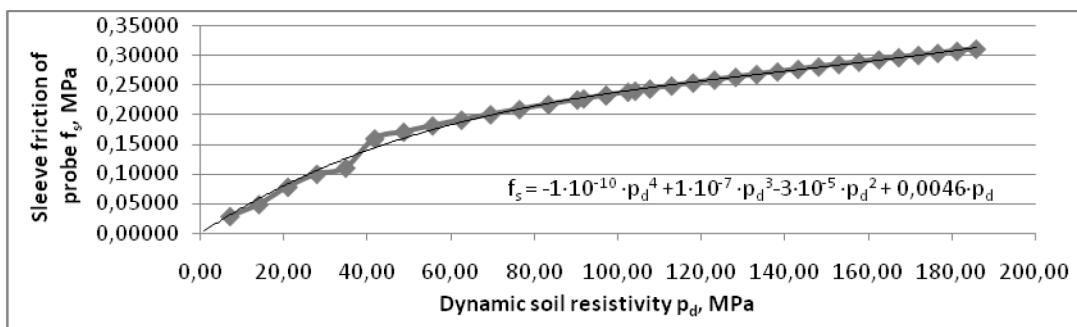


Fig. 6 Diagrams - ratio between dynamic soil resistivity p_d and sleeve friction of probe f_s in clayey soils.

4. CONCLUSIONS

1. According to the results of this work the correlation between dynamic soil resistivity defined by DCPT and bearing capacity of driven piles was found.

2. Bearing capacities of the driven piles, determined by given above equations, has an error not exceed 15%, compared with bearing capacities of the piles determined by dynamic tests of real piles.

3. By comparing the results of experimental work carried out in parallel, the close correlations between measures of DCPT and CPT, presented in this paper were found.

4. The economic feasibility of using DCPT instead of, or in conjunction with CPT, as part of works on geotechnical investigations is proved in practice.

5. REFERENCES

- GOST 19912-2001. *Field test methods by static and dynamic sounding.*
- Mariupol L.G. "Soil analysis for the design and construction of pile foundations". – 1989 year. – 199 p.
- GOST 5686-94. *Soils. Field test methods by piles.*
- MSP 5.01-101-2003. *Design and installation of pile foundations.*

Session 2

UNDERGROUND STRUCTURES AND RETAINING WALLS

Understanding of Soil Responses due to Tunnelling - 3D Numerical Analysis and Case Study of Bendemeer Station (DTL-3), Singapore

Ong, C. W.

Managing Director, ONE SMART Engineering Pte Ltd, Singapore & Malaysia

Thiri Su

PhD Student, National University of Singapore, Singapore

Yong, K. Y.

Professor, National University of Singapore, Singapore

Kulaindran Ariaratnam

Deputy Director, Land Transport Authority, Singapore

ABSTRACT: The increase in demand for underground tunnels in Singapore has added many challenges to tunnelling problems beyond the capability of analytical or empirical methods. The prospect of using 3D numerical analysis in analyzing complex practical applications is becoming more common. The paper presents the application of finite element analysis to assess the soil-structure interactions in real tunneling problems. A benchmarking study was first carried out on a centrifuge test by Ong et al. (2013) using a three-dimensional finite element method for the basic understanding of soil responses to tunneling. FE studies were then extended to a practical application with the field data from a Singapore MRT project, Bendemeer Station, Downtown Line 3 (DTL-3).

1. INTRODUCTION

Even with several years of experience in planning, design and construction of tunnelling and underground works, recent tunnelling projects have posed much more challenges due to limited land space available. Mass Rapid Transit (MRT) lines inevitably passed through greenfield soil conditions as well as underneath or adjacent to the existing structures and foundations. In addition, having highly variable geology, most areas of the tunnel alignment passed through difficult ground conditions like mixed conditions of soft and hard soil and fault lines. The alignment of Singapore MRT Downtown line (DTL) is shown in Figure 1.

Many past researchers predicted the tunnelling induced ground responses well enough by using empirical methods [Peck (1969), New and O'Reilly (1991), Mair et al. (1993)], analytical methods [Loganathan and Poulos (1998)] and many other methods. Recent studies had been extended on the behaviour of soil and pile responses due to tunnelling in Singapore local soils by means of numerical analyses by Pang (2006) and centrifuge test by Ong et al. (2013). In the present study, the back analysis of the centrifuge model tests by Ong et al. (2013) was performed for tunnelling in soft clay by using three-dimensional finite element method (3-D FEM). FEM studies were then

extended to investigate the behavior of tunnelling induced soil movements in Old Alluvium. The predictions of finite element method were then validated by the measured field data from Bendemeer Station project in Downtown Line 3 (DTL-3) MRT construction.

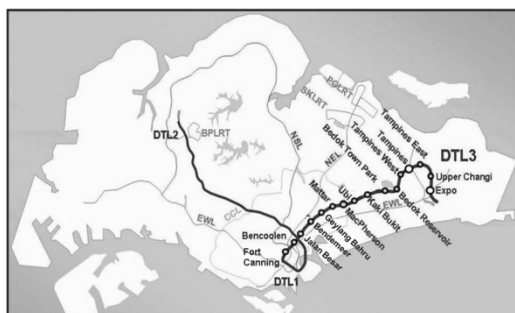


Figure 1. Alignment of MRT Downtown line in Singapore

2. UNDERSTANDING OF SOIL RESPONSES DUE TO TUNNELLING IN SOFT CLAY

A case history, presented by Ong et al. (2013) was back analysed for the study on the effect of tunnelling in soft clay. In this case history, a centrifuge test with 60mm diameter of single tunnel model (i.e, 6m diameter in prototype scale) was carried out under 100g at

National University of Singapore. The tunnel was at 15m depth, and hence, tunnel depth to diameter, H/D ratio of 2.5 was adopted in the centrifuge test. A centrifuge model set-up is shown in Figure 2.

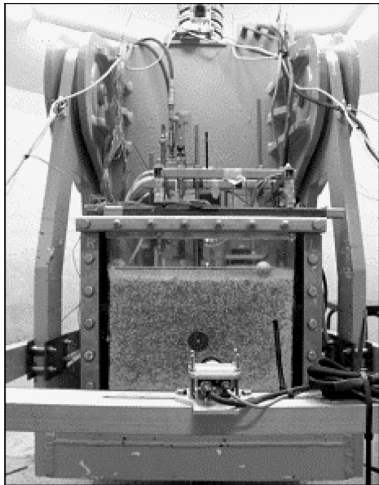


Figure 2. Centrifuge model set-up [Ong et al. (2013)]

2.1. Finite element mesh and boundary conditions

The back analysis for the centrifuge test was carried out using a 3-D finite element GeoFEA software. The size of the model was taken the same as that of the container used in the centrifuge test (i.e. 52.5 m width, 28m depth and 20m length). The finite element mesh of the model is shown in Figure 3.

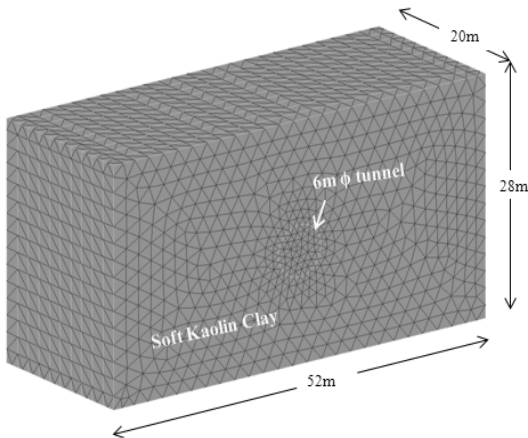


Figure 3. 3-D finite element mesh (Simplified single tunnel for comparison with centrifuge test)

10-noded linear strain tetrahedral solid elements were used in the FE model. The displacement was completely fixed at the bottom bottom. Vertical sides were restrained against transverse movement for the displacement boundary condition. The top surface mesh was assumed as the drainage boundary where $u=0$. The two vertical sides were assumed to be hydrostatic, recharging drainage condition, i.e, $\Delta u=0$ whereas impermeable boundaries were assigned at the bottom plane and tunnel circumferences.

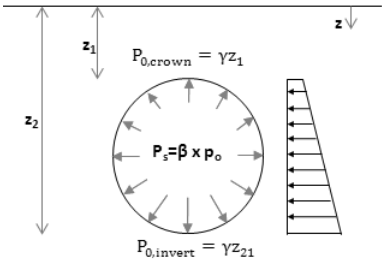


Figure 4. Hydrostatic pressure application

2.2. Soil model and material parameters

The constitutive soil behaviour was modelled using Modified Cam-Clay model. The critical state soil parameters were adopted the same as those used in Goh (2003) and cited by Ong et al. (2007) as presented in Table 1. Permeability of clay was taken as 2×10^{-8} and 6×10^{-8} m/s in x and y directions respectively.

Table 1. Soil Parameters adopted in FE analysis [Goh (2003) and Ong et al.(2007)]

Type of Soil	κ	λ	e_{cs}	M	ν
Kaolin clay	0.053	0.244	3.35	0.9	0.3

2.3. Finite element simulation

In the centrifuge test, due to limitation in the accuracy of equipments in the model, volume loss of 3% that was equivalent to 1mm gap in model scale had been used as minimum value. It was noted that the volume loss experienced in normally consolidated clay range between 1.5% to 4.0% depending on the face pressure applied. Therefore, volume loss of 3% was selected as in FE model for calibration purpose with centrifuge results.

Only single tunnel advancement was performed in FE analysis to simulate the same 2D tunnelling procedure in centrifuge test. Tunnel-

ling process was simulated in the procedures as follow:

Initial step: Initial geostatic stress application.

Step 1 : The soil along the length of 20m (tunnel length in the model) was excavated and the support pressure was applied around the excavated tunnel periphery in the same step.

If the support is equivalent to the initial all round soil pressures, no volume loss is theoretically expected. Any reduction to this value will introduce the volume loss as the end result. Therefore, the support pressure in FE analysis is a predetermined value which produced the target volume loss of 3%.

In this FE analysis study with GeoFEA program, the support pressure was applied in a hydrostatic distribution with the values increasing from tunnel crown to invert level (Figure 4).

2.4. Results and discussion

Surface settlements

Figure 5 shows the transverse settlement troughs of FE and centrifuge test results [Ong et al. (2013)] compared with a typical Gaussian distribution curve by Peck (1969). Maximum soil settlement obtained from Ong's centrifuge test at 3% volume loss (VL) was about 41 mm and from the finite element study at the same volume loss was 37mm. FE analysis was also observed to give the higher far field settlement of about 4mm at the end of the model boundary. This far field settlement contributed as part of the volume loss, which therefore, resulted in the slightly shallower settlement compared to Ong's centrifuge results. Far field settlement is the common problem in FE modelling especially in dealing with simple elastic soil model. This effect can be significantly reduced by simulating hydrostatic pressure application complying with critical state MCC soil model. Apart from this, FE analysis predicted the reasonable results in terms of magnitude as well as profile.

Maximum surface settlement (S_{max}) at different volume losses (VL) are also plotted in Figure 6 and verified with empirical Gaussian distribution and centrifuge test results. The results of FE predictions are found closer to both empirical and experimental approaches. Linear relationships between maximum settlement and volume loss are observed in all methods. However, in FEM, the ratio of S_{max}/V_L is 12.8 while the ratios are 14.6 and 15 in centrifuge and Gaussian curve respectively. In

other words, FEM underestimates the maximum surface settlement results about 17% compared to Gaussian method whereas only 3% by centrifuge test.

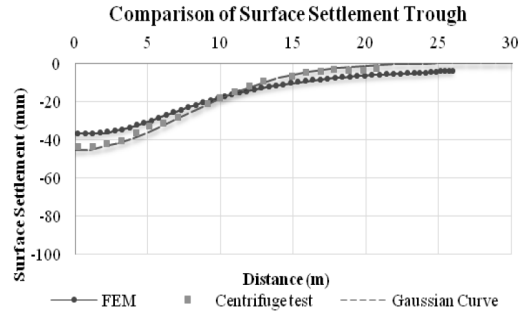


Figure 5. Transverse settlement trough

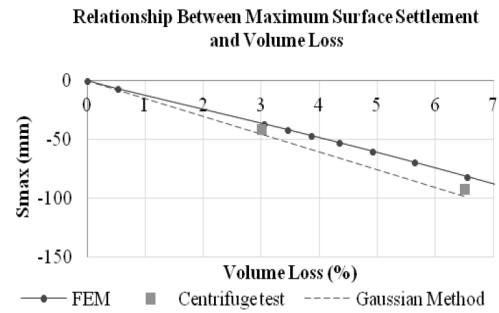


Figure 6. Relationship between maximum surface settlements and volume losses

Subsurface settlements

Figure 7 shows the subsurface settlement profiles with depth, taken at the distance 0m ($x=0m$) and 6m ($x=6m$) away from tunnel center line. The graph confirms that, the settlement increases with depth until above the tunnel crown level. The maximum settlement was 130 mm and found near the tunnel crown. The results at tunnel centre line were not available from centrifuge test, due to the limitation of centrifuge model. The comparison of subsurface settlement at 6m distance showed that the two predicted profiles match very well.

Transverse settlement curves at different depths are plotted in Figure 8 and compared with empirical results from Mair et al. (1993) and quasi-analytical solution by Loganathan and Poulos (1998). In general, all the methods including FE method, centrifuge test, empirical and analytical methods, give the good prediction of tunneling induced settlement troughs in the same trend especially at shallower depth.

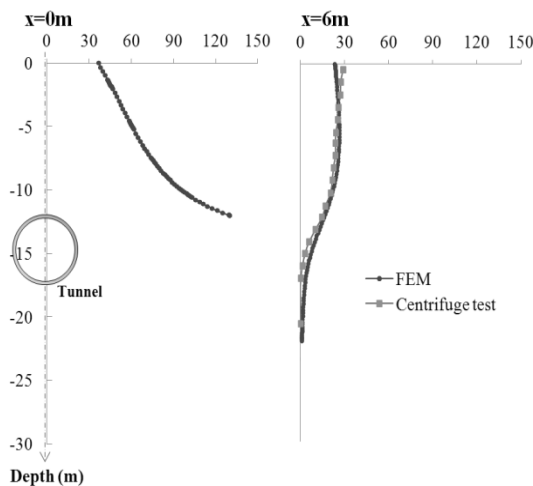


Figure 7. Settlement (mm) versus depth at $x=0m$ and at $x=6m$

The further down the ground level, the more discrepancies are observed among different methods. The differences between the methods are found largest at the tunnel centre line. Among them, FE prediction is closer to empirical method. Maximum difference between the two methods which is found at tunnel centre line is about 20%. However, in centrifuge test, the settlement difference is more than 40% at tunnel centre line. This is likely due to the boundary condition limit in centrifuge test between the beads and the Perspex plate when closer to the model tunnel. Except Loganathan's solution, the confrontations among the methods become insignificant when the distance x is more than a diameter of the tunnel. Unlike the other methods, Loganathan approach gives flatter and wider settlement troughs and the profile do not match well with others. This can be due to the reason, that "The equivalent ground loss values predicted using the new method are in good agreement with reported empirical ground loss values for tunnels in stiff clay by are overestimated for the case of tunnel in soft clay." as stated in Loganathan and Poulos (1998). Nevertheless, the analytical method is still one of the best well-known method which is practically used for greenfield

soil response mainly owing to its simplicity and reliability.

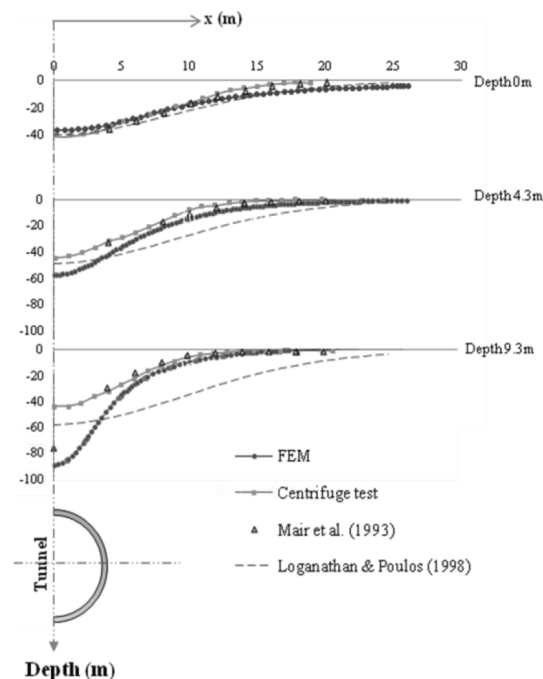


Figure 8. Settlement trough (mm) at depth 0m, 4.3m and 9.3m

Lateral deflection

The soil deflection with depth at various distances of 4m, 6m, 9m, 12m, and 15m from the tunnel vertical centre line are presented in Figure 8. All the methods predict the trend of lateral soil movements which is prominent at tunnel horizontal axis for the distance less than $1D$ (D =diameter of tunnel). When the distance is beyond $1D$, the deflection at the ground surface is more significant than that at the tunnel axis. As can be seen in Figure 9, FEM prediction gives greater lateral soil response than centrifuge test in all cases. FEM provides more similar pattern and trend with experimental results whereas it does not agree well with analytical results by Loganathan and Poulos (1998) in which deflections are more significant in tunnel axis only.

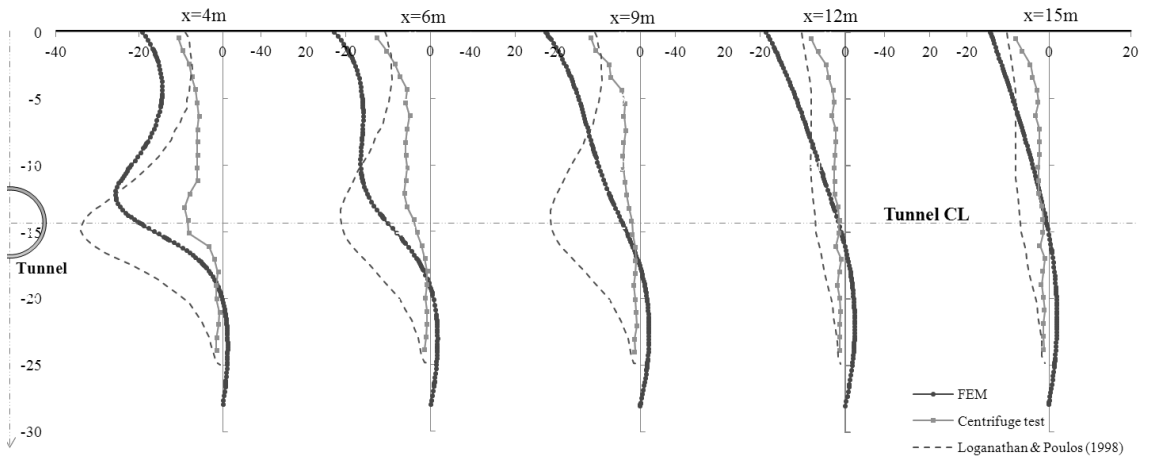


Figure 9. Horizontal soil movement

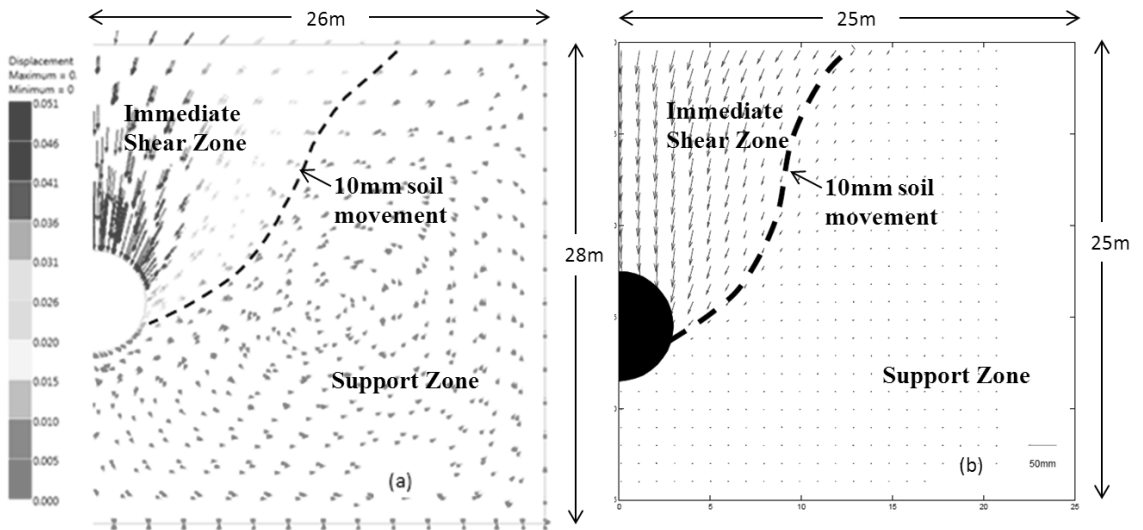


Figure 10. Soil displacement vectors (a) FEM , (b) centrifuge test

Soil displacement vectors

Displacement vectors of FEM and centrifuge test are shown in Figure 10. Tunneling induced disturbance to in-situ soils lead to the changes in effective stresses, and ground movements. Those movements were identified by Ong et al. (2013) as following two zones:

- Immediate Shear Zone which occurs radial stress relieves as a results of the unloading of soil during tunnelling. This zone is defined as the zone of settlement values with more than 10 mm.

- Support Zone which occurs outside of shear zone.

Generally, finite element studies show the similar pattern as reported in centrifuge results by Ong et al. (2013).

However in FE analysis, the soil displacement vectors outside the immediate shear zone flow in reverse pattern (U turn) which is considered unrealistic in real case. This is one of the few limitations of FE models. During excavation, when the soil elements are removed from the mesh, stress relieve occurs and results in the radial soil

flow towards the tunnel. However, since the movements are restrained at the boundaries, reverse soil movements occurred to maintain all the forces in equilibrium state. This kind of effect may be reduced by using large sized FE mesh boundaries. Unlike the centrifuge test, this problem is minimized due to the presence of drained layer at the bottom and the soil flow directly toward the bottom or tunnel periphery. However, the amount of U turn movements are insignificant (<5mm) compared to the movement at immediate shear zone, major occurrence of soil displacements. Except that, the soil displacement pattern in FE results are comparable with centrifuge test results.

3. UNDERSTANDING OF SOIL RESPONSES DUE TO TUNNELLING – CASE STUDY OF BENDEMEER STATION (DTL-3), SINGAPORE

3.1. Background and overview of the project

A 42km long Downtown Line (DTL) is the longest and the fifth stage of underground Mass Rapid Transit (MRT) line in Singapore. The construction of DTL, which is proposed to serve 34 stations, was planned in 3 stages (DTL-1, DTL-2, DTL-3). It will connect the North-Western and Central-Eastern regions to the new downtown of Singapore. The construction of the final stage of Downtown Line, DTL-3, comprises of 16 stations with three interchange stations. A 3-D finite element analysis was carried out for Downtown Line (DTL-3), Bendemeer Station project to investigate the effect of tunnelling in Old Alluvium. The twin tunnels constructed by Earth Pressure Balance machines (EPBM) was passing through from Bendemeer Station

to Jalan Besar Station. At the monitoring array, the tunnels were located at depth of about 32.5m below ground level.

3.2. Geological and Soil Condition

The DTL-3 tunnelling works encountered a high variation in geological condition along its alignment. Bendemeer Station project site also involved the launching of TBM from good OA soil towards the Kallang formation, with the challenging mixed-face soil condition at the transition. The field monitoring section under this study was located in Old Alluvium (O) formation, which was overlain by 2.5m thick Fill and 3m thick Marine Clay (M) layers. The water table from site investigation report ranged between 2 to 2.5m below ground surface. The typical geological profile along the proposed tunnel alignment is shown in Figure 11.

3.3. Ground Instrumentation

Comprehensive instrumentation and monitoring arrays were installed along the tunnel alignment. Figure 12 below illustrates the cross section of proposed monitoring array at the section under this study, which includes:

- series of ground settlement markers across the section for the assessment of transverse surface settlement profile and along the tunnel alignment for the longitudinal surface settlement;
- two magnetic extensometers placed at each side of the two tunnels, for vertical subsoil movements at different depth (tips at 3.5m, 12.5m and 32.5m respectively.)

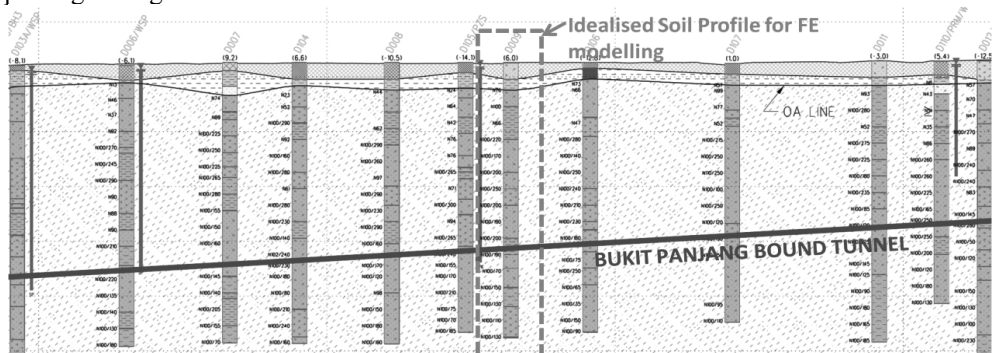


Figure 11. Geological profile along Bendemeer Station tunnel alignment

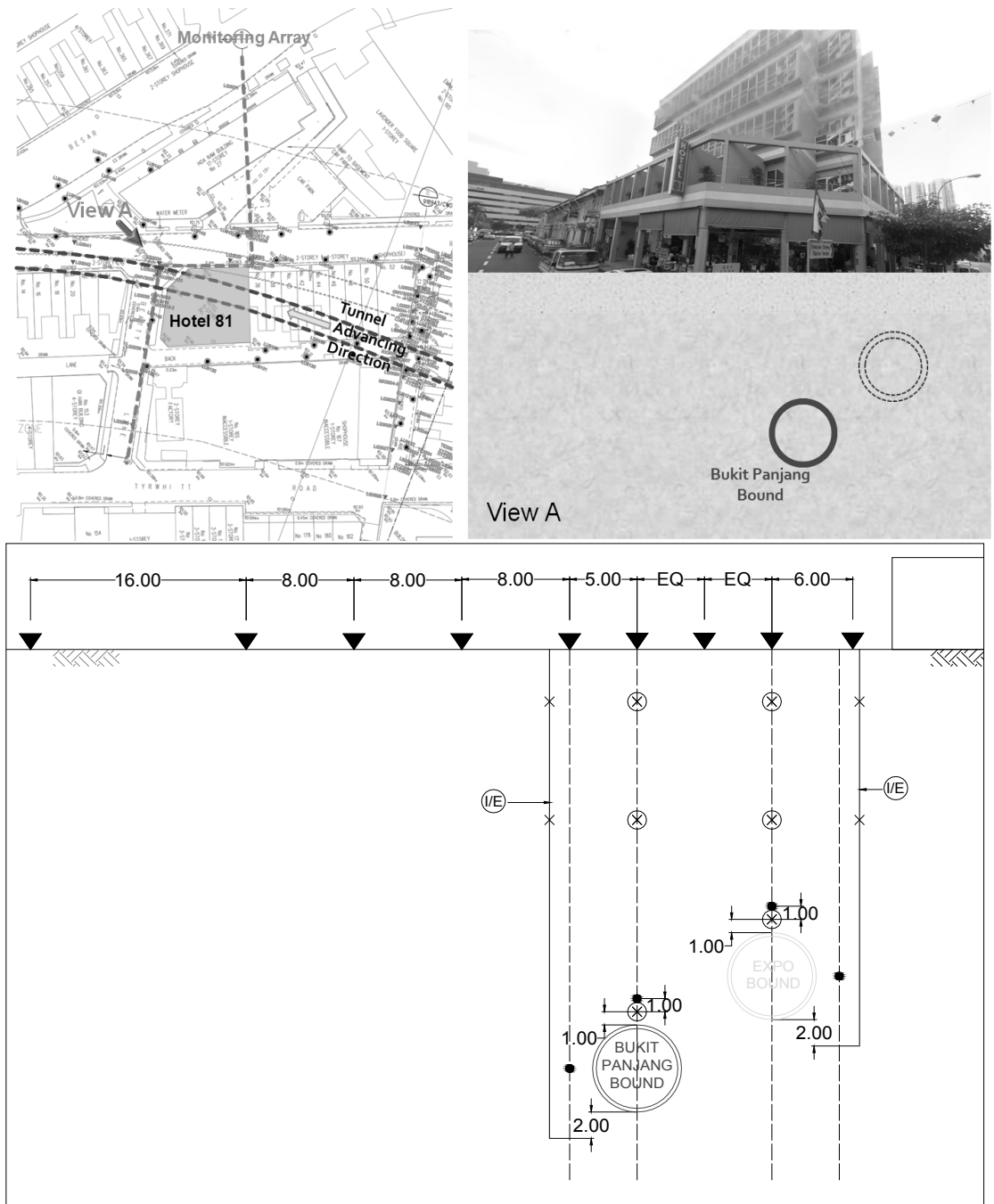


Figure 12. Ground instrumentation layout and section (Bukit Panjang Bound for this study)

3.4. Finite element mesh and boundary conditions

Figure 13 shows the finite element mesh for the simulation of single tunnel advancement. The soil, tunnel liner, overcut, shield and grouting were modelled using a 10-noded

tetrahedral solid elements. By taking into account of the effect of symmetry, only half boundary sizes (105m x 60m x 72.5m) was used. Tunnel excavation was simulated up to 75m out of 105m length.

Displacement boundary conditions were taking the same as the case history of tunnelling in soft clay. For hydraulic boundary condition, the vertical side parallel to the tunnel symmetry axis was assumed to be hydrostatic, recharging drainage condition, i.e, $\Delta u=0$ whereas impermeable boundaries were taken for symmetry plane, bottom plane, tunnel circumferences and remaining vertical sides of the mesh.

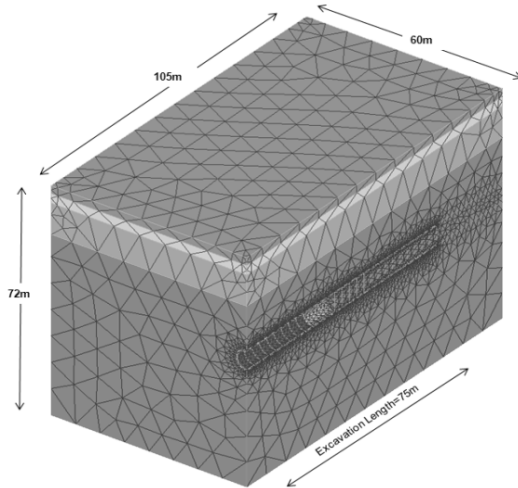


Figure 13. Typical finite element mesh

3.5. Adopted parameters and soil model for the analysis

The design parameters for the soils were obtained from the Geotechnical Interpretative Baseline Report (Arup Singapore Pte Ltd) as summarized in Table 2. Permeability for all soil types except fill layer was taken as 10-8m/s. For fill material, permeability value was 10-6m/s. The structural elements of tunnel were modelled as linear elastic material and the properties adopted were presented in Table 3. Soil constitutive model plays an important role in estimating the correct soil behaviour. Elastic-perfectly-plastic Mohr-Coulomb soil model owing to its simplicity and less input parameters required was adopted as the initial study. However, Mohr-Coulomb model has its own limitations and unable to predict the real soil behaviour under some circumstances, such as in small strain condition, [Addenbrooke (1997), Jardine (1986), Potts (1999)]. Coupled consolidation was carried out in the analysis to simulate the rate of tunnel advancement.

Table 2. Mohr-Coulomb model Soil Parameters

Type of Soil	E', MPa	ν	C', kPa	ϕ , deg
Fill	8	0.3	0	30
Clay	$333c_u$ ($c_u=15+1.5z$) z from +95	0.3	0	22
Old Alluvium (N<100)	125	0.3	10	32
Old Alluvium (N<100)	250	0.3	20	34

Table 3. Tunnel Parameters

Structural Element	E, MPa	ν	k, m/s	γ , kN/m ³
Shield Machine	200,000	0.25	10^{-12}	80
Concrete Lining	28,000	0.2	10^{-12}	24
Overcut	1	0.2	0	0
Grout	2,800	0.2	10^{-12}	24

3.6. Finite Element Simulation

Stage-by-stage excavation process was carried out in finite element analysis. Factors associating with tunnelling works such as the EPBM's advancing rate, face pressure, overcut, grouting, lining installation were considered in finite element the analysis. Figure 14 illustrates the tunnel advancement process adopted in the FE modelling.

Each excavation step was simulated with 3m length elements. Tunnel advance rate adopted was 6m/day (4m/day to 8m/day in most O (A)). The balancing earth pressure when the tunnel face passed though the monitoring array was 325kPa.

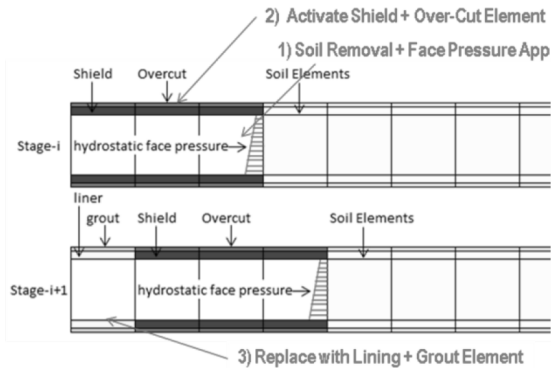


Figure 14. Stage tunnelling process for 3-D FE modelling

3.7. Results and Discussions

The results of 3D numerical modelling were presented in terms of tunnelling induced ground responses and were compared with the measured field data for model validation. 1% Volume loss was adopted as target volume loss which is the upper bound limit as described in LTA Civil Design Criteria (2010) for tunnelling under Old Alluvium. Generally, ground response in Old Alluvium found fairly small.

Transverse Surface Settlements

Figure 15 shows the predicted and measured transverse surface settlement troughs at 5D (where D=diameter of tunnel) distance after the tunnel had passed through the monitoring array.

The measured surface settlement right above the tunnel centre line is 2.5mm, which is equivalent to 0.3% volume loss in Gaussian distribution. As can be seen in the figure, the final settlement trough no longer follows the green field Gaussian curve. The fact that the markers were installed on the road pavement and the stiffening effect of the presence of pile foundations under the existing building can be the contribution factors. If the volume loss is based on the area of settlement trough following the actual field plots divided by the tunnel area, the maximum settlement obtained is 4.8mm. This is fairly comparable with the maximum settlement of 5mm from FE analysis.

Longitudinal Surface Settlements

The development of longitudinal surface settlement profile directly above the tunnel alignment is plotted in Figure 16. The field measured profile follows the same trend as prediction of FE results, except from the somewhat smaller values for those markers located in the zone of existing foundations. In addition, both profiles have the maximum transverse settlement which is about two times longitudinal settlement above the tunnel face. Therefore, both field results and FE predicted results give the similar trend of longitudinal profile which is consistent with behaviour of cumulative probability curve as reported in past literatures such as New and O'Reilly.

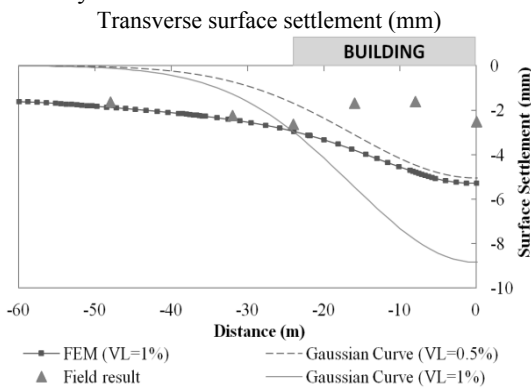


Figure 15. Transverse surface settlement trough

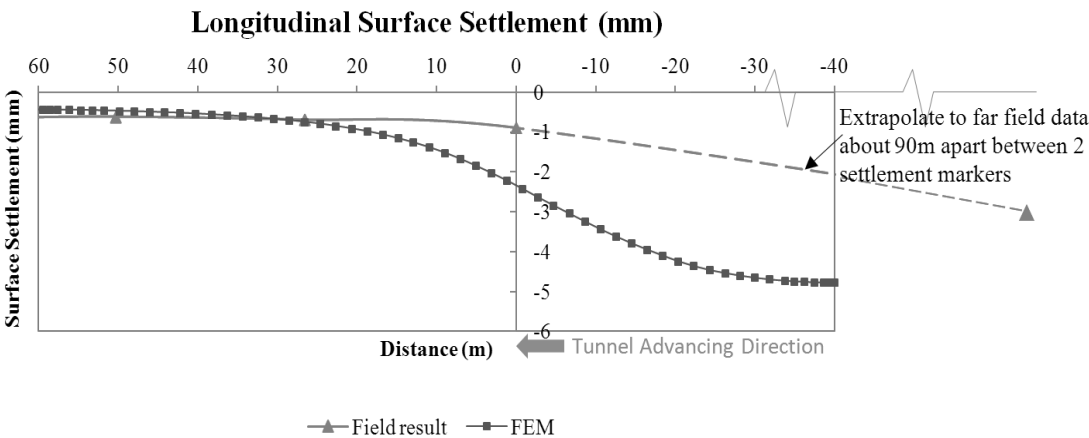


Figure 16. Longitudinal surface settlement trough

Subsurface Settlements

Subsurface soil settlement were extracted at the extensometer locations and compared with the FE predicted profiles in Figure 17 (a). It should be noted that the limited amount of instrument readings (only 3 extensometer tips at 3 different depths) may limit the extent of result interpretation. Nevertheless, a very good agreement of settlement values are observed between FE predicted profile and the field data.

Horizontal Soil Displacements

During tunnelling, lateral soil movement is expected to be prominent at tunnel horizontal axis as reported in various case histories

such as Pang (2006) and Ong et al. (2013). This behaviours are revealed in Figure 17 (b) and (c) where both FEM results and measured data from inclinometer readings are plotted and compared. However, the plot of horizontal displacement in longitudinal direction cannot capture the correct behaviour up to 10m depth. This can be due the fact that longitudinal soil deflection is measured from the inclinometer in B direction. It was found that the readings of inclinometer in B direction are not as accurate as those in A direction where the instrument check sums or errors are very small. Apart from that, it can be concluded that in general, the prediction of FE analysis can provide the satisfactory behaviour of soil responses which are reasonably comparable with the actual field data.

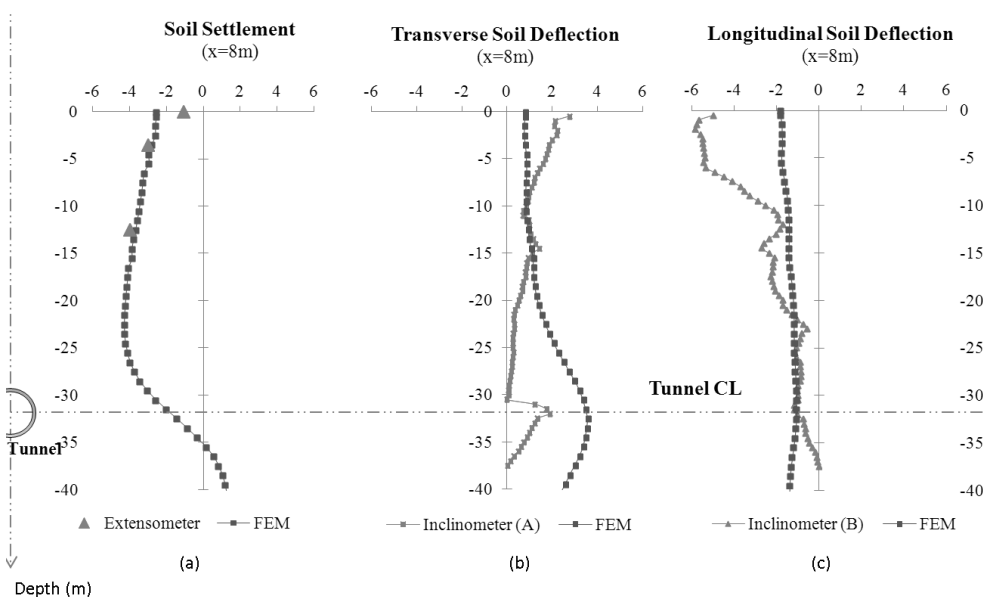


Figure 17. Soil displacement versus depth (a) Soil Settlement (b) Transverse soil deflection (c) Longitudinal soil deflection

3.8. Conclusion

The paper presented an application of 3-D finite element analysis to understand the behavior of soil response to tunnelling problems. FE predictions were verified with centrifuge model test or field measurements from LTA's Contract C933 Bendemeer Station project.

The general findings can be summarised as follows.

(1) FE analyses predict closer to empirical and experimental approaches for both cases in greenfield soil condition. However, the settlement trough no longer follows the green field Guassian curve if there is the contribution of stiffening effect from the presence of pile foundations.

(2) These settlement profiles are in consistent trends at shallower depth in all the methods such as FE method, centrifuge test, empirical and analytical methods. However, discrepancies are observed among the different methods when it is further down the ground level. Among them, FE prediction is closer to empirical method while centrifuge test yield larger differences due to the boundary condition limit. However, the confrontations among the methods become insignificant when the distance x is more than a diameter of the tunnel.

(3) The lateral soil deflections are prominent at tunnel horizontal axis for the distance less than 1D (D =diameter of tunnel). When the distance is beyond 1D, the deflection at the ground surface is more significant than that at the tunnel axis.

(4) The soil displacement vectors in FE results give similar pattern with centrifuge test results except that those vectors outside the immediate shear zone flow occurs in reverse U turn pattern due to the FE boundary constraints.

(5) Ground response in Old Alluvium is found to be fairly small.

The results and findings have shown that with proper understanding of soil behavior and modeling technique, the complex soil structure interactions can be predicted reasonably. These 3-D finite element studies will be extended further in the next paper for the condition of tunnelling in mixed faced soil conditions with hard soil or rock at the lower face of tunnel and soft soil at the upper face.

Acknowledgement

The authors would like to express their sincere gratitude to Bendemeer Station project team, Land Transport Authority (LTA) of Singapore, Trittech Consultants Pte. Ltd. and Trittech Engineering Pte. Ltd. for providing the required tunnel information and field instrumentation data of Bendemeer Station project.

4. REFERENCES

- Addenbrooke, T. I., Potts, D. M. and Puzrin, A. M. 1997. The influence of pre-failure soil stiffness on the numerical analysis of tunnel construction. *Geotechnique*, Vol. 47, No. 3, pp.693-712.
- Geotechnical Interpretative Baseline Report. Arup Singapore Pte. Ltd.
- Goh, T.L. 2003. Stabilisation of an excavation by an embedded improved soil layer. PhD thesis, National University of Singapore.
- Jardine, R. J., Potts, D. M., Fourie, A. B. and Burland, J. B. 1986. Studies of the influence of non-linear stress-strain characteristics in soil-structure interaction. *Geotechnique* 36, No. 3, pp.377-396.
- Lim K. C. 2003. Three-dimensional finite element analysis of earth pressure balance tunnelling. PhD thesis, National University of Singapore.
- Loganathan, N. and Poulos, H. G. 1998. Analytical prediction for tunneling-induced ground movements in clays. *Journal of Geotechnical and Geoenvironmental Engineering*, Vol. 124, No. 9, pp. 846-856.
- LTA. 2010. Civil design criteria for road and rail transit systems, Land Transport Authority, Singapore
- Mair, R. J., Taylor, R. N. and Bracegirdle, A. 1993. Subsurface settlement profiles above tunnels in clay. *Geotechnique*, Vol. 43, No. 2, pp. 315-320.
- New, B. M. and O'Reilly, M. P. 1991. Tunnelling induced ground movements: predicting their magnitude and effects. In Geddes (Ed) *Proc. 4th Int. Conference on ground movements and structures*, Cardiff, invited review paper, Pentech Press, London, pp. 671-697.
- Ong, C. W., Leung, C. F., Yong, K. Y. and Chow, Y. K. 2007. Experimental study of tunnel-soil-pile interaction. *Underground Singapore 2007*, pp. 55-66.
- Ong, C.W., Leung, C. F. & Yong, K.Y. 2013. Understanding Long-Term Effects of Tunnel-Soil Interaction. 18th International Conference in Soil Mechanics and Geotechnical Engineering, Proceedings of the TC207 Workshop on Soil-Structure Interaction and Retaining Walls 4 September 2013, Paris.
- Pang, C.H. 2006. The Effects Of Tunnel Construction On Nearby Pile Foundation PhD thesis, National University of Singapore.
- Pang, C.H., Yong, K.Y., and Chow, Y.K. 2005. Three-dimensional numerical simulation of tunnel advancement on adjacent pile foundation. Proceedings of the 31st ITA-AITES World Tunnel Congress, Underground Space Use: Analysis of the Past and Lessons for the Future, 7-12 May 2005, Istanbul, Turkey.
- Peck, R. B. 1969. Deep excavations and tunneling in soft ground. *Proc. 7th International Conference Soil Mechanics and Foundation Engineering*

ing, Mexico City, State of the Art Volume, pp. 225-290.

Potts, D. M. and Zdravkovic, L. 1999. Finite element analysis in geotechnical engineering: Theory. Vol. 1. Thomas, London.

An investigation into the vertical axial capacities and groundwater cut-off capabilities of secant pile walls

Abid Adekunte

Bachy Soletanche Limited, UK

ABSTRACT: Secant pile walls are increasingly becoming popular groundwater cut-off systems of choice on underground construction sites, as they offer a number of advantages over traditional sheet piling and diaphragm walls. However, some elements of uncertainty surround the design and construction of secant pile walls. Vertical and horizontal installation tolerances are major issues, especially in the case of multi-level basements, as required tolerances are difficult to achieve with deep piles associated with deep basements. In addition, while conventional foundation piles are routinely statically or dynamically load-tested, hard piles in secant pile walls are rarely axially tested and this does not allow for the routine verification of existing design methods and assumptions.

This paper presents the design, construction and testing of the secant pile wall on a 3-4 level basement construction scheme in Central London. Simple empirical correlations for estimating the geometry of secant pile walls for effective groundwater cut-off are derived and validated. An alternative approach for estimating the vertical capacities of secant pile walls is also presented and compared with a common routine method in the industry. The alternative method is shown to be less conservative than the common industry approach, while predictions are also in good agreement with results of a recent series of model tests on perimeter pile groups.

1. INTRODUCTION

The construction of deep basements routinely requires the installation of temporary or permanent excavation support systems, to enable the construction of the sub-structure. Reinforced concrete diaphragm walls and sheet pile walls have been globally adopted for this purpose for many years. However, in recent years, bored pile retaining walls are increasingly becoming more popular, as they offer a number of advantages over diaphragm and sheet pile walls. With bored pile retaining walls, installation process is more straightforward, while production rate is higher and for these reasons, they are often adopted as more economical alternatives to D-walls. Reduced space requirement for machineries is another advantage of bored pile walls over D-walls. When compared with steel sheet piles walls, bored pile walls provide higher stiffness, higher flexural rigidity and higher vertical axial capacity, while durability in the long term is of less concern.

Many publications on case histories of bored pile retaining walls abound in the literature e.g. Adekunte (2013, 2011, 2008 & 2007), Adekunte et al. (2010), Finno & Bryson (2002), Long et al. (2012) and Looby & Long (2007). However, many of these publications have concentrated on wall overall stability, lateral deflection and ground movement under service

loads. Currently, there is a dearth of publications that focus on the design of optimum geometries for pile walls to provide effective groundwater cut-off.

On basement schemes where groundwater cut-off is required in addition to lateral earth retention, secant pile walls are often considered. In the case of multi-level basements, horizontal and verticality tolerances often become major issues to contend with, as it is difficult to achieve required installation tolerances with deep piles associated with multi-storey basements and ultimately, this complexity has a significant influence on the ability of a secant pile wall to provide effective groundwater cut-off.

And nowadays, in addition to soil and water retention, secant pile walls are being commonly required to support vertical compressive and/or tension loading from the superstructure. As piles in secant walls are rarely load-tested, design methods and assumptions are not routinely verified and as a result, there is a degree of uncertainty surrounding common methods of predicting axial capacities of secant pile walls.

This paper focuses on the prediction of vertical axial capacities of secant pile walls, as well as the fundamental principles of design of secant pile walls to provide effective groundwater cut-off. For both subjects, direct references are made to a recently completed multi-level

basement construction project in Central London, United Kingdom.

2. SITE GEOLOGY & GROUND MODEL

The site is located in Vauxhall, Central London. Site stratigraphy comprises of up to 3m thick made ground underlain by a layer of very soft to soft alluvial clay and peat to 9m depth, which in turn overlies a 1m thick layer of medium dense to dense sandy gravel. Firm to stiff to very stiff to hard London clay lies below the sandy gravel stratum at 10m depth and this is underlain by a layer of very dense Thanet Sand at 48m depth. The London clay is an overconsolidated material of high plasticity, with plasticity indices ranging between 35%-45%. As the site was immediately adjacent to the River Thames on the southeastern boundary, groundwater level was subject to tidal fluctuation and standpipe monitoring results show that water level could be as high as 1m below ground level (bgl). Generalised site stratigraphy and associated geotechnical design parameters are presented in table 1.

Coefficient of earth pressure K_0 was generally limited to 1.0 for the overconsolidated materials (after CIRIA Report No. C580, 2003). This was to allow for remoulding and stress relief in the soils; conditions associated with embedded retaining wall installation and excavation. In the temporary condition, effective wall friction angles δ on the active and passive sides were taken to be $0.67\phi'$ and $0.5\phi'$ respectively (where ϕ' is effective angle of shearing resistance). However, in the permanent condition, angle of wall friction was assumed to be zero; this was to allow for the effect of vertical compressive loading on the wall from the superstructure in the long term.

3. PROPOSED DEVELOPMENT & CONSTRUCTION PROCEDURE

The site was adjacent to the River Thames and the Vauxhall Bridge in Central London. The project was a large scale high rise development comprising of two separate structures on the same site; a 28 storey-commercial tower and an 18 storey-residential block of luxury apartments. The development included a 3-4 level basement; a 3 level-basement over the entire footprint of the site and a 4th level of basement

in the centre of the site. Due to the proximity of the site to the Thames River, groundwater level was relatively high and subject to tidal fluctuation. Therefore, in addition to soil retention, groundwater cut-off was also a necessity, to enable basement construction and a hard-firm secant pile wall was considered to be a potentially effective and economical solution for the first 3 levels of basement across the site. The secant pile wall system comprises of interlocking male and female piles. The female piles are only required to provide groundwater cut-off and they do not provide any structural support in respect of wall overall stability. An illustration of the wall geometry is shown in figure 1.

Male piles were made of grade 35 structural concrete and reinforced down to depth required for overall wall lateral stability, while the female piles were made of 10 N/mm² concrete and unreinforced. Both male and female piles were provided with a minimum embedment of 1m in London clay below basement formation level, for groundwater cut-off. Male piles were of 880mm diameter, while female piles were of 900mm diameter. A photo of the secant pile wall is shown in figure 2. However, as the 4th level of basement wholly lies within the London clay stratum, groundwater control was not considered to be a major issue and therefore, a contiguous pile wall was considered to be the most economical and effective solution. Contiguous pile wall comprised of 750mm diameter bored piles spaced at 900mm centre to centre (c/c).

Maintaining a perfect interlock between adjacent male and female piles is often difficult to realize when dealing with multi-level basements, as required horizontal and vertical tolerances are difficult to achieve with many conventional piling rigs, for deep bored piles associated with deep basements. To mitigate this risk, prior to commencement of piling, a guide wall was put in place along the wall alignment, for improved horizontal positional tolerance. In addition, for improved verticality tolerance, male piles were installed with a Cased Secant Piling (CSP) rig, which is a customized version of the traditional Continuous Flight Auger (CFA) drilling rig, equipped with a temporary heavy duty steel casing over the full depth of the pile.

Table 1. Generalised stratigraphy & geotechnical design parameters

Depth (m) bgl	Description	N _{spt}	Angle of Shearing Resistance ϕ' (°)	Young's Modulus E _u or [E'] (kPa)	Cohesion C _u or [C'] (kPa)
0.0 – 9.0	Made Ground & Very Soft to Soft Clay & Peat	1 - 8	25.0	[10000]	[0.0]
9.0 – 10.0	Medium Dense to Dense to Very Dense Sandy Gravel	17 - 41	36.0	[50000]	[0.0]
10.0 – 16.0	Firm to Stiff London Clay	13 – 30	25.0	80000 [65000]	100.0 [5.0]
16.0 – 29.0	Very Stiff London Clay	32 – 44	25.0	120000 [95000]	150.0 [5.0]
29.0 – 48.0	Very Stiff to Hard London Clay & Weak Mudstone Bands	43 – R	25.0	175000 [140000]	220.0 [5.0]
Below 48.0	Very Dense Thanet Sand	R	37.0	[150000]	[0.0]

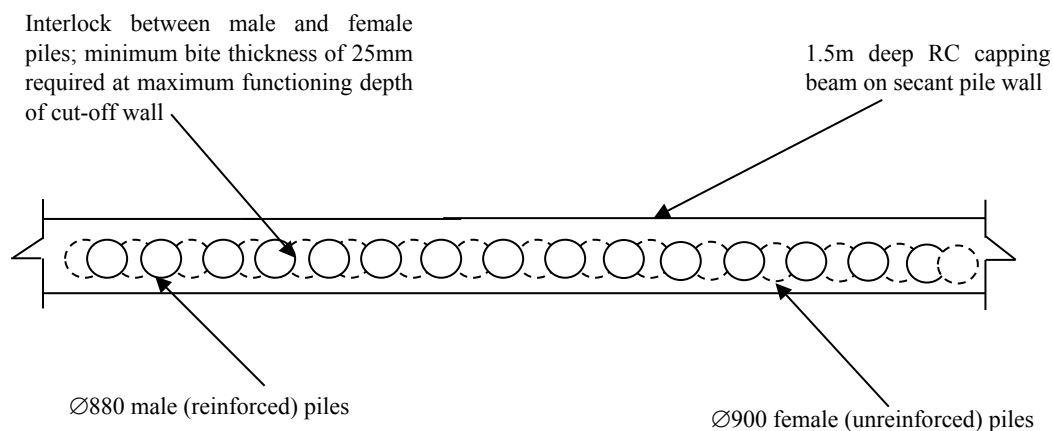


Figure 1 – Layout of hard-firm secant pile wall

The CSP technique improves the achievable vertical tolerance to 1:150, when compared with 1:75 achievable with a conventional uncased CFA bore (after ICE SPERW, 2007). In addition, the customized technique results in better finished wall appearance and reduced overbreak when compared with traditional CFA drilling, while it is also faster and more economical when compared with rotary bored piling.

Economy is another important factor in foundation engineering and construction (especially from a contractor's perspective) and this has to be accounted for in every aspect of wall design and installation. For economical reason, female piles were designed to be installed by traditional CFA drilling; the reduced verticality tolerance was off-set by the commercial benefit

derived from the lower higher rate of the CFA rig, when compared with the CSP rig.

The 4th level of basement at the centre of the site, which had to be constructed beneath the excavation level of the perimeter 3 level-secant pile wall, was supported with a contiguous pile wall. This was installed by a Bachy Soletanche Large Diameter Auger (LDA) rotary boring technique. Above the London clay stratum, the LDA rig advanced the drillhole with the combination of an auger and a thick-walled temporary casing, rotating in opposite directions. The temporary casing was required to provide lateral support to the hole in the unstable made ground and alluvial deposits above the London clay. In the London clay, hole was drilled with the auger only. This rotary boring technique allowed each hole to be partially concreted up to the for-

mation level of the general 3-level basement (approximately 11m bgl), while the rest of the hole was backfilled with carefully selected gravel pees up to ground/piling platform level. This approach allowed for the installation of both the secant and contiguous pile walls from ground/piling platform level, such that excavation for the top 3 levels of basement was done without having to deal with concrete piles projecting from the 4th level contiguous pile wall in the middle of the site; this also resulted in savings in concrete.

Overall, the basement works package involved the use of three different bored piling techniques for improved efficiency and economy. Figure 3 shows wall installation with piling rigs on the site.

4. GROUNDWATER CUT-OFF

Many cases of flooded and/or abandoned secant wall-supported basements have been recorded. Such problems arise because many engineers are unaware of the fundamental principles underlying the accurate estimation of optimum interlock thickness between male and female piles (and ultimately pile spacing) required to ensure an effective groundwater cut-off solution. To provide effective groundwater cut-off with a secant pile wall, many factors would need to be accounted for. These include;

- rig type;
- rig capability;
- installation technique;
- pile size;
- verticality tolerance;
- horizontal positional tolerance;
- depth of sealing stratum;
- minimum required pile embedment in sealing layer.

For effective groundwater cut-off to be guaranteed, all of the above factors must be accounted for. Inability to account for only one of the factors could result in significant consequences. While publications with comprehensive specific information on this subject are very rare, field experience has shown that the minimum required interlock thickness between male and female piles may be expressed by the equation;

$$\beta = \delta + \alpha \quad (1)$$

where β is estimated required bite thickness between male and female piles at piling commencement level in mm. δ is estimated potential gap in mm between male and female piles at pile depth required for cut-off; this is a function of horizontal positional tolerance, verticality tolerance and length of pile L required for cut-off (equivalent to length of female pile). α is minimum allowable bite thickness in mm between male and female piles at cut-off depth. This may be taken as 25mm (after ICE SPERW, 2007).

δ in Equation (1) can be expressed as;

$$\delta = k [(v * L) + h] \quad (2)$$

where v is average verticality tolerance of both male and female piles in mm/m depth of installation, which is dependent on rig type and piling technique. h is horizontal positional tolerance in mm at piling commencement level; this is dependent on availability of guide wall prior to the commencement of piling. A conservative value of 25mm may be assumed (after ICE SPERW, 2007). L is pile length required for cut-off; this is equivalent to depth of female pile toe. k is a constant, which accounts for the potential horizontal and vertical deviation of immediately adjacent male and female piles in opposite directions. Generally, the value of k should be taken to be a minimum of 2. Therefore, Equation (1) may be rewritten as;

$$\beta = k [(v * L) + h] + \alpha \quad (3)$$

The value of β can be used to estimate the required centre to centre spacing of the male piles, provided male and female pile diameters are known. This is illustrated in figure 4. In figure 4, D_m is male pile diameter, D_f is female pile diameter and β is thickness of interlock between overlapping male and female piles. From the figure, male pile centre to centre spacing S can be expressed as;

$$S = \left[\frac{D_m}{2} \right] + \left[\left(\frac{D_f}{2} \right) - \beta \right] + \left[\frac{D_f}{2} \right] + \left[\left(\frac{D_m}{2} \right) - \beta \right] \quad (4)$$



Figure 2 – Hard-firm secant pile wall on the site



Figure 3 – Installation of secant pile wall around the site perimeter

$$\therefore S = D_m + D_f - 2\beta \quad (5)$$

If β is replaced with Equation (3), Equation (5) becomes;

$$\therefore S = D_m + D_f - 2k[(\nu * L) + h] - 2\alpha \quad (6)$$

Adopting a value of 2 for k as suggested above, Equation (6) becomes;

$$S = D_m + D_f - 4[\nu L + h] - 2\alpha \quad (7)$$

$$\therefore S = D_m + D_f - 2[2(\nu L + h) + \alpha] \quad (8)$$

By using the current project as a reference, Equation (3) and Equation (8) can be used to estimate the required bite thickness β at commencement level and associated male pile centre to centre spacing S respectively. On the project, secant pile wall retained height was 11m. Basement formation level was in London clay and a minimum embedment of 1m in London clay (sealing stratum) below basement formation level was required for groundwater cut-off.

Therefore, length of pile L required for groundwater cut-off = $(11 + 1)\text{m} = 12\text{m}$.

Male piles were installed by CSP technique; verticality tolerance = 1:150 (after ICE SPERW, 2007) and this is equivalent to a deviation of 6.67mm per metre depth of installation.

Female piles were installed by CFA technique with heavy duty augers; verticality tolerance = 1:100 (after ICE SPERW, 2007) and this is equivalent to a deviation of 10mm per metre depth of installation.

Therefore, average verticality tolerance ν of both male and female piles = $[(6.67 + 10)/2] \text{ mm/m} \approx 8\text{mm/m}$

While guide wall was installed along wall alignment prior to start of piling works, horizontal positional tolerance h at piling commencement level can be conservatively taken to be 25mm.

Minimum allowable bite thickness α at pile toe can be taken to be 25mm (after ICE SPERW, 2007).

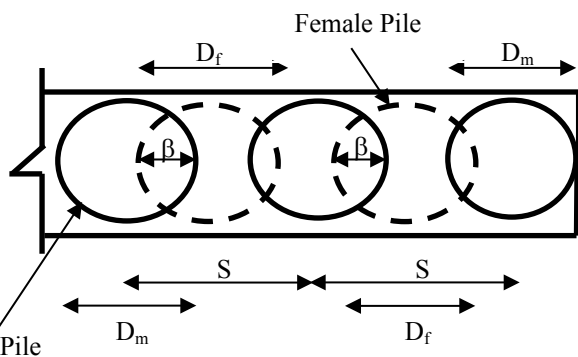


Figure 4 – Secant wall geometry annotation.

Constant k accounting for potential deviation of overlapping piles in opposite directions can be taken to be 2 as suggested above.

By substituting the above values in Equation (3), minimum required bite thickness β between overlapping male and female piles is estimated to be;

$$\beta = 2[(8\text{mm/m} * 12\text{m}) + 25\text{mm}] + 25\text{mm} \cong 270\text{mm}$$

Male pile diameter $D_m = 880\text{mm}$, Female pile diameter $D_f = 900\text{mm}$

Substituting the above values in Equation (8), required male pile centre to centre spacing is estimated to be;

$$S = [880 + 900 - 2[(8 * 12 + 25) + 25]]\text{mm}$$

$$S = 1246\text{mm} \cong 1.25\text{m}$$

Therefore, required centre to centre spacing of male piles is 1.25m c/c, which is approximately equivalent to 1.4D (where D is pile diameter). Installation of the secant pile wall on the site was based on the above figures and the end result was a perfectly dry excavation as can be seen in figure 5 below, despite the wall having to deal with relatively high water level that was subject to tidal fluctuation and more than 10m of cohesionless made ground, very soft to soft alluvial deposits and sandy gravel.



Figure 5 – Perfectly dry excavation was achieved with secant pile wall on the site

5. PREDICTION OF WALL AXIAL CAPACITY

In addition to earth and water retention, the hard piles in the secant wall were required to support vertical compressive column loads from the superstructure. The RC capping beam on the

piles was designed to spread the point loads from the columns over a minimum of 3 No. hard piles, such that the maximum estimated service compressive load on any hard pile was 2450 KN.

As stated in earlier sections, the estimation of axial capacities of pile retaining walls is an area shrouded in uncertainty because unlike traditional bearing piles, hard piles in bored pile walls are rarely tested. It is common practice among designers to routinely approach this problem by estimating the capacity of a singly acting pile in similar ground conditions and thereafter, factoring down the estimated capacity to 50%-60% of estimated figure, to account for pile group efficiency in the wall. This approach is common for walls in clay. However, Rose & Taylor (2010, 2012 & 2013) carried out some experimental work and parallel finite element modelling on the behaviour of pile groups arranged in grids in clay at the City University London. They discovered that piles on the perimeter are subject to higher loads when compared with the internal piles; this they have attributed to increased soil-pile interaction.

Further to this, they carried out a series of tests on piles arranged in single row, to model the behaviour of perimeter pile groups with no internal piles, whilst also considering several variables that influence pile group behaviour; number of piles, pile spacing, length/diameter ratio and soil strength. From their experimental results, Rose & Taylor (2013) discovered that pile group efficiency of perimeter piles could be as high as 100%, while perimeter pile groups with pile centre to centre spacing of less than 2D (where D is pile diameter) tend to exhibit block type failure. Hard piles in secant pile walls are typically spaced at $\leq 1.5D$ centre to centre.

Based on Rose & Taylor's (2010, 2012 & 2013) test results, at design stage, the wall on the current site was considered to act as a continuous deep strip footing below basement formation level, surrounded by a block of soil, with the assumption of a block type failure mechanism in the ultimate state. In addition, the bearing capacity factor N_c in the London clay was reduced by multiplying with a reduction factor f , to account for the existence of non-structural female piles in the wall. The reduction factor f is expressed as;

$$f = \frac{\pi D}{4S} \quad (9)$$

where D is pile diameter and S is pile centre to centre spacing. This approach produces an estimate of the axial capacity of the wall per metre run. Multiplying this value by the centre to centre spacing of the hard piles yields the vertical capacity of an individual hard pile.

Prior to the construction of the RC capping beam on the wall, a number of hard piles in the wall were tested to 1.5 times the safe working load (SWL) in compression. As tests were carried out before excavation for the basement, additional capacities derived by test piles through skin friction in soils above proposed basement formation level were discounted while assessing measured capacities of the test piles. The load-settlement curves for the non-failed load tests were extrapolated beyond the maximum test loads, following the analytical approach of Paikowsky & Tolosko (1999), to determine the ultimate vertical capacities of the piles in compression. Load-settlement curve for one of the test piles is shown in figure 6.

Figure 6 shows a reasonable level of agreement between ultimate capacity predicted with the method outlined above and actual measured capacity, while the common industry approach of factoring down the estimated capacity of an equivalent singly acting pile to 50%-60% to account for pile group efficiency is seen to be quite conservative. In addition, the pile group efficiency of the wall was deduced to be approximately 90%, which is in line with Rose & Taylor's (2010, 2012 & 2013) assertion that pile group efficiency of perimeter piles could be close to unity. The 90% pile group efficiency recorded is also noted to be higher than 50%-60% suggested by some workers (e.g. Broms, 2007 and Sowers et al., 1961) for piles spaced at $< 1.5D$ in clay and which are typically adopted in practice.

6. CONCLUSIONS

The principal factors influencing the groundwater cut-off capabilities of secant pile walls have been identified. These include; rig type, rig capability, installation technique, pile size, verticality tolerance, horizontal positional tolerance, depth of sealing stratum and mini-

um required pile embedment in sealing layer. The dearth of publications with comprehensive specific information on the estimation of optimum interlock thickness and pile spacing for effective groundwater cut-off to acceptable levels of accuracy has also been highlighted. As helpful guides to secant wall designers in the industry, simple empirical equations for estimating optimum bite thickness and pile spacing for groundwater cut-off have been presented and validated by reference to a recently completed multi-level basement project. These equations account for all the factors enumerated above.

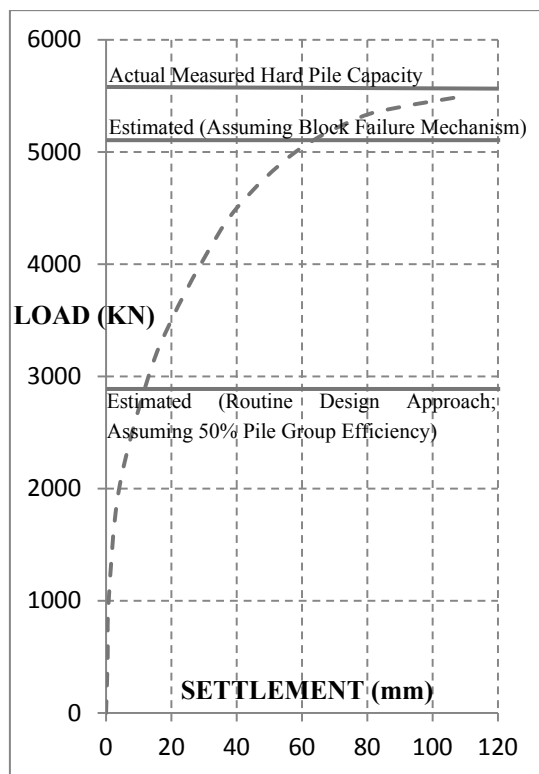


Figure 6. Extrapolated load-settlement curve for a selected hard pile on the site

Estimation of axial capacities of secant pile walls is an area covered in uncertainty as walls are rarely tested, while existing knowledge of pile group efficiency of multi-grid pile groups is not particularly applicable to perimeter pile groups, such as secant pile walls. An alternative approach for estimating the vertical capacities of secant pile walls has been presented. This has

been shown to be considerably less conservative when compared with a common routine design approach, while predictions of the method are shown to be in reasonably good agreement with the results of a recent research-based small scale model tests on perimeter piles.

7. REFERENCES

- Adekunte, A 2013. Alternative deep basement solutions for built-up areas. *Proceedings of the Deep Foundations Institute's 38th Annual Conference on Deep Foundations*, Phoenix Arizona, USA, September 2013.
- Adekunte, A, O'Hara, P and Dennany, A 2010. Novel methods of restraining embedded retaining walls. *Proceedings of the Deep Foundations Institute's 35th Annual Conference on Deep Foundations*, Hollywood Ca., October 2010.
- Adekunte, A 2008. An innovative use of bored tension piles in embedded retaining wall design and construction. *Proceedings of the Deep Foundations Institute's 33rd Annual Conference on Deep Foundations and 11th International Conference on Piling and Deep Foundations*, pp. 167-176, New York, October 2008.
- Adekunte, A 2007. Predicted and observed performance of an anchored retaining wall in granite. *Proceedings of the Institution of Civil Engineers' International Conference on Ground Anchorages and Anchored Structures in Service*, London, November 2007.
- Broms, B.B 2007. Foundation engineering. *Online Text Book*, webforum europe, www.geoforum.com/knowledge/texts/broms/index.asp
- Construction Industry Research and Information Association, 2003. *Report No. C580 – Embedded Retaining Walls – Guidance for Economic Design*, CIRIA, London.
- Finno, R.J and Bryson, L.S 2002. Response of a building adjacent to stiff excavation support system in soft clay. *Journal on the Performance of Constructed Facilities, American Society of Civil Engineers*, volume 16, issue 1, pp. 10-20.
- Institution of Civil Engineers, (2nd ed.) 2007. *ICE specification for piling and embedded retaining walls*. London: Institution of Civil Engineers, the Crown and Thomas Telford Publishing Limited.
- Long, M, Brangan, C, Menkiti C, Looby M and Casey, P 2012. Retaining walls in Dublin boulder clay, Ireland. *Proceedings of the Institution of Civil Engineers, Geotechnical Engineering*, volume 165, issue GE4, pp. 247-266.
- Looby, M and Long, M 2007. Deep excavations in Dublin – recent developments. *Paper First Presented to a Meeting of the Geotechnical Society of Ireland*, Dublin, 11th December 2007.
- Paikowsky, S.G and Tolosko, T.A, 1999. *Extrapolation of pile capacity from non-failed load tests – Report No. FHWA-RD-99-170*. Virginia: US Department of Transportation, Federal Highway Administration.
- Rose, A.V, Taylor, R.N and El Naggar, M.H 2013. Numerical modelling of perimeter pile groups in clay. *Canadian Geotechnical Journal*, volume 50, issue 3, pp. 250-258.
- Rose, A.V 2012. *Behaviour and efficiency of perimeter pile groups*. PhD thesis, School of Engineering and Mathematical Sciences, City University London.
- Sowers, G.I, Wilson, L, Martin, B and Fausold, M 1961. Model tests of friction pile groups in homogenous clay. *Proceedings of the 5th International Conference on Soil Mechanics and Foundation Engineering*, Paris, 1961.
- Taylor, R.N, Rose, A.V and Gorasia, R.J 2013. Pile and pile group capacity; some findings from centrifuge tests. *International Journal of Geo-Engineering*, volume 5, issue 2, pp. 5-15.
- Taylor, R.N and Rose, A.V 2010. Modelling the performance of micropiles at close spacing. *10th International Workshop on Micropiles*, Washington DC, September 2010.

8. ACKNOWLEDGEMENTS

I would like to specially dedicate this paper to my newborn baby; Princess Alicia Omojadesola Adebimpe and her mum Adedoyin. They both make my world so colourful and exciting. The paper is also dedicated to every child in Yewaland, Southwest Nigeria and every member of the Young Yewa Professional Foundation; a non-profit youth-led organization committed to the improvement of the standard of education and the overall standard of living in the community.

The author is grateful to the management of Bachy Soletanche UK, the geotechnical specialist contractors for the study site (Riverwalk House, Vauxhall, Central London) and the main contractor; Sir Robert McAlpines UK. The contributions of Barry Osborn, David Hard, Rob Cunningham, Alistair Mitchel and Dimitrios Leventakis towards the successful completion of the deep basement scheme are acknowledged.

The contribution and support of Tine Gretlund (Bachy Soletanche UK) during the preparation of this paper are also well appreciated.

3D Modelling in Deep Excavations – Case Studies

Önder Akçakal, Turan Durgunoğlu
Zetaş Zemin Teknolojisi AŞ, Turkey
onder.akcakal@zetas.com.tr, durgunoglut@zetas.com.tr

Berkay Koçak, Taşkın Tari
Zetaş Zemin Teknolojisi AŞ Moscow Branch, Russia
berkay.kocak@zetas.com.tr, taskin.tari@zetas.com.tr

ABSTRACT: In 2D modelling computer programs which calculate in plain strain conditions, it is considered that modelled section continues infinitely with the same geometry through the axis perpendicular to the section. However, any variation in soil type, surcharge loads, topography or supporting conditions in this perpendicular axis effects the behaviour of the stress distribution in the soil. Therefore 3D modelling computer programs provide more realistic solution for the sections which contain variety of above mentioned conditions in perpendicular axis. In this paper, calculations in 2D and 3D modelling studies for two different shoring works are presented. Calculated plain strain ratio (PSR) values are compared with previously published studies.

1. INTRODUCTION

Urbanization brings lack of sufficient spaces for basement excavations in growing cities; therefore implication of retention structures for deep excavations is frequently encountered geotechnical engineering subject in big cities. It is clear that dimensioning of the retention structures is important for a reliable and cost effective solution and this brings the necessity of a realistic calculation approach. There are variable computer programs for modelling retention structures and most of these programs are based on two-dimensional modelling. Plain strain condition is the strain representation of two-dimensional models and it is considered that section continues with same geometry infinitely through the axis perpendicular to the section which is calculated. With the advancements of the technology more capable computers are provided which enable three dimensional modelling and new computer programs are released for this purpose.

With three dimensional modelling of infrastructures a more realistic calculation approach can be provided considering the variations of the soil type, surcharge loads, topography and supporting conditions on the axis which is perpendicular to the calculated section. Three dimensional modelling of deep excavations provides significant effects which will be encountered from lateral arching of the retained soil and lateral flexure of the support systems between corners (Lee et al., 1998). A general

background for three dimensional modelling is given below;

In 1975 St. John studied a square shaped unsupported excavation in stiff London Clay. Both 2D plain strain, 2D axisymmetric and 3D models are analyzed. According to the results good agreement was obtained between 2D axisymmetric and 3D models however 2D plain strain analysis significantly overpredicted horizontal movements.

In 1979 Burland et al. also recommended axial symmetry instead of plain strain in square excavations, further if the excavation supported with diaphragm walls large compressive hoop stresses are arisen along diaphragm walls which does not represent a realistic consequence (Lee et al., 1998).

In 1992 Simpson indicated that axisymmetric and plain strain models have negligible differences and attributed this to the shallow depth to a relatively rigid stratum.

In 1993 Wong and Patron pointed the significantly arising corner effects in some several deep excavation projects in Taipei.

Also in 1993 Ou and Chiou reported that 3D calculation is required for a realistic prediction of wall behavior in excavation with short sides.

In 1995 Lee et al. reported that in soft soils corner effect is getting stronger and this showed that 2D models to be much more sensitive to soil parameters than the 3D models.

In 1995 Liu reported that in deep excavations which are strutted densely corner effects

are suppressed above the excavation level but under the excavation level it is again possible to see the corner effect preventing high wall deflection.

Also in 1996 Ou et al. have described “PSR” plain strain ratio as the maximum movement in the center of an excavation wall computed by 3D analyses divided by that computed by plain strain model. Ou et al. originally defined PSR in terms of the ratio of width to length of the wall and distance from the corner.

In 1998 Lee et al. reported a comparison between field data and 2D - 3D analysis. The results of the 3D analysis are mostly in agreement with field data, some differences are also obtained due to the construction delay and over-excavation.

In 2000 Ou et al. published a case study about Taipei National Enterprise Centre Project and it is reported that plain strain condition could be occurred 34.4 m away from the corner, excavation depth was 19.7 m and construction method was top-down.

In 2002 Beadman and Cheng utilized results of four case studies to calibrate an empirical method for calculation of displacements around corners which was developed by Arup Geotechnics in London. Then in 2010 Fuentes and Devriendt developed a new empirical method for calculation of displacements around corners.

In 2007 Finno et al. reported that PSR is affected by the ratio of the length of wall to the excavation depth, the ratio of the plan dimensions of the excavation L/B , L being the side where displacements are computed, the wall system stiffness and factor of safety against basal heave.

In this paper numerical analysis of two deep excavations are summarized and discussed in terms of 2D and 3D modelling.

2. CASE STUDIES

Numerical studies for two different projects with deep excavations are summarized in this section. These excavations are calculated both 2-D plain strain model and 3-D model. Site monitoring data couldn't be submitted within this paper, since monitoring studies are still being performed.

2.1. Water Intake Structure, Samsun

A deep excavation was planned for a water intake structure which was planned to be constructed in an industrial plant site in Samsun, Turkey.

Excavation for the water intake structure is planned to be torch shaped as illustrated in Figure 1. Excavation widths are variable which 23.80 m and 15.70 m. Total length of the excavation is approximately 44.50 m and excavation depths are -11.35 m and -8.30 m respectively.

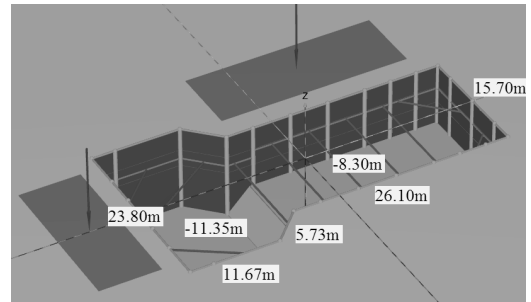


Figure 1. Water Intake Structure Dimensions

Soil profile is considered as given in the table below;

Table 1. Soil Profile for Water Intake Structure

Soil	Depth	γ , kN/m ³	ϕ' , °	c' , kPa	E MN/m ²
Fill	0-3m	17	30°	1	15
Sand	3m-	17.5	34°	1	25

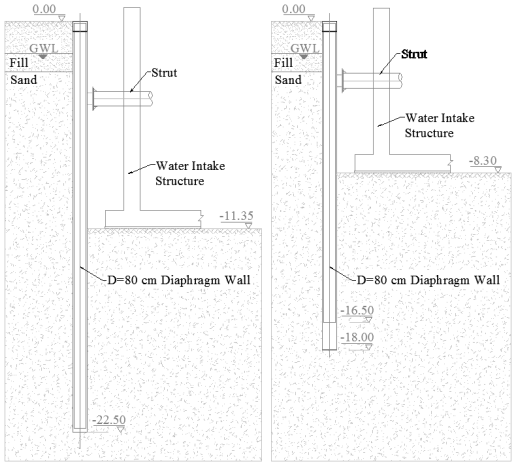
Water level was observed approx. 2.0 m below the ground surface resulting hydrostatic pressures are considered in the calculations behind the shoring wall.

Since no building or heavy structure exist around the excavation only 15 kPa surcharge was considered as an estimated site operational surcharge.

To eliminate the excessive ground water infiltration into the excavation pit diaphragm wall shoring system is planned to be constructed. Diaphragm wall depth will be 22.50 m for the section with 11.35 m excavation depth, and 18 m for the section with 8.30 m excavation depth. In 18 m deep diaphragm wall reinforcement cage is considered to be installed in only first 16.50 m of the diaphragm wall.

Diaphragm wall panels will be supported with steel struts which will be placed at eleva-

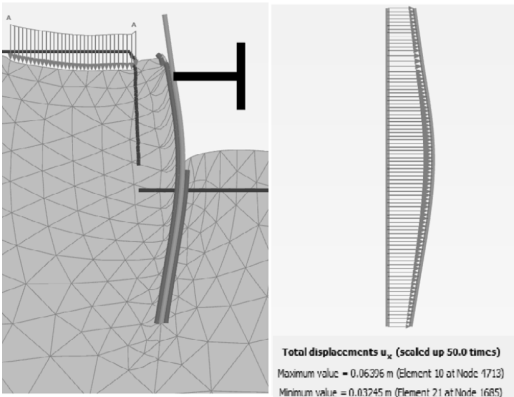
tions of -4.25m and -3.25m for the sections with excavation depths 11.35m and 8.30m respectively. Sections of the shoring wall are given in Figure 2a and 2b;



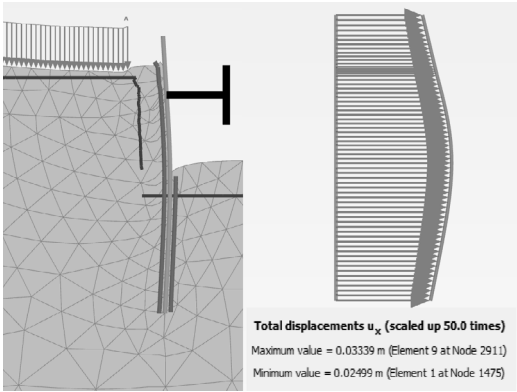
Figures 2a&2b. Diaphragm Wall Shoring Sections

Lateral displacements of the diaphragm walls with 2D plain strain model are calculated as 64mm and 33mm for sections with excavation depths 11.35m and 8.30m respectively. (Figures 3a&3b and Figures 4a&4b)

Surface settlement behind the shoring wall is estimated as 68 mm and 34 mm for the sections with excavation depths 11.35m and 8.30m respectively.



Figures 3a&3b. Diaphragm Wall Lateral Displacement (Exc. Depth is -11.35m)



Figures 4a&4b. Diaphragm Wall Lateral Displacement (Exc. Depth is -8.3m)

Lateral displacements of the diaphragm walls with 3D model are calculated as follows (Figure 5);

For 11.35 m Excavation depth, lateral displacements are 38mm and 30mm for the long and short sides respectively.

For 8.30 m Excavation depth, lateral displacements are 27mm and 18mm for the long and short sides respectively.

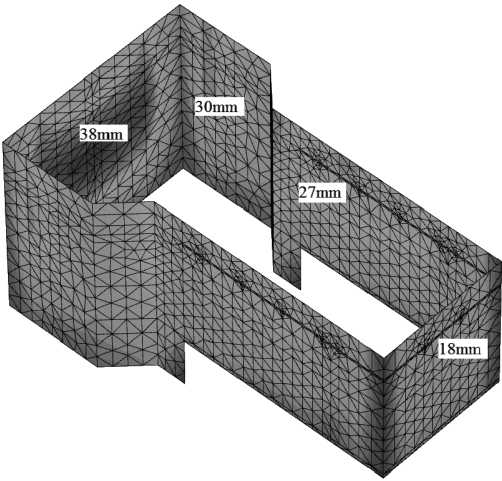


Figure 5. Diaphragm Wall Displacement With 3D Model Calculation

Surface settlements are estimated as follows (Figure 6); For 11.35 m Excavation depth, surface settlements are 34mm and 30mm for the long and short sides respectively.

For 8.30 m Excavation depth, surface settlements are 25mm and 18mm for the long and short sides respectively.

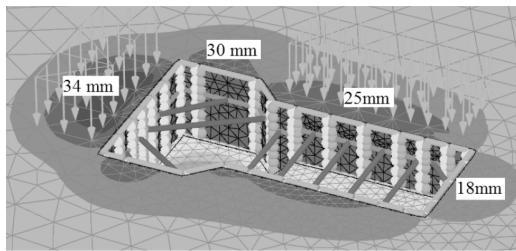


Figure 6. Surface Settlements With 3D Model Calculation

2.2. Hotel Project, Izmir

A hotel structure is planned to be constructed with 3 basement floors in Izmir, Turkey.

Excavation for the hotel basements is planned to be rectangular shaped as illustrated in Figure 7. Excavation plan dimensions are 34m by 22m. Excavation depth is 11.30 m.

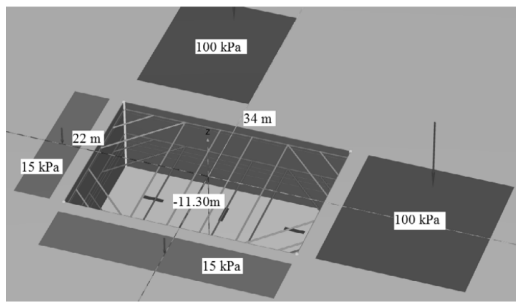


Figure 7. Hotel Basement Excavation Dimensions

Soil profile is considered as given in the table below;

Table 2. Soil Profile for Hotel Project, Izmir

Soil	Depth	γ , kN/m ³	ϕ , °	c , kPa	E , MN/m ²
Fill	0-7m	19	34°	10	25
Sand	7-8m	18	30°	2	5
Clay 1	8-15	17	-	*	10
Clay 2	15-18	17	-	*	25
Gravel	18-19	18	32	5	20
Clay 3	19-21	18	-	*	30
Gravel	21-23	18	32	5	20
Clay 4	23-29	18	-	*	38

* Clay layers modelled with undrained parameters. 30, 50, 60 and 75 kPa c_u values are considered for Clay 1, 2, 3 and 4 layers respectively.

Water level was observed at 1.0 m below the ground surface, resulting hydrostatic pressures are considered in the calculations behind the shoring wall.

There are two neighboring buildings which modelled with 100 kPa surcharge load. 15 kPa surcharge was considered as site operational loads for the other sides.

To eliminate the excessive ground water infiltration into the excavation pit diaphragm wall shoring system is planned to be constructed. Diaphragm wall length will be 20 m for 11.30 m excavation depth.

Diaphragm wall panels will be supported with two rows of steel struts which will be placed under -1.40m and -5.35m below the ground surface. Sections of the shoring wall are given in Figure 2a and 2b;

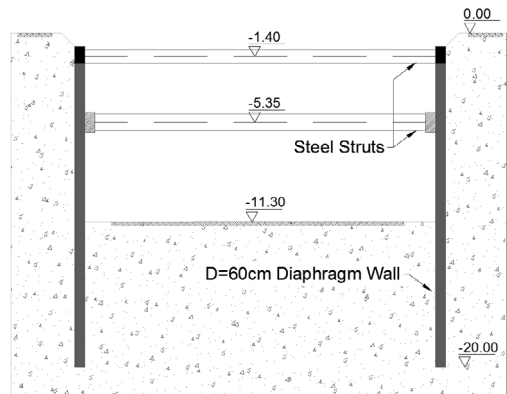


Figure 8. Diaphragm Wall Shoring Section

Also six numbers of barrettes were implemented under the foundation to eliminate the uplift risk. In deep shoring calculations these barrettes are also taken into account.

Lateral displacements of the diaphragm walls with 2D plain strain model are estimated as 147mm and 10mm for sections neighboring building and the street sides respectively (Figure 9).

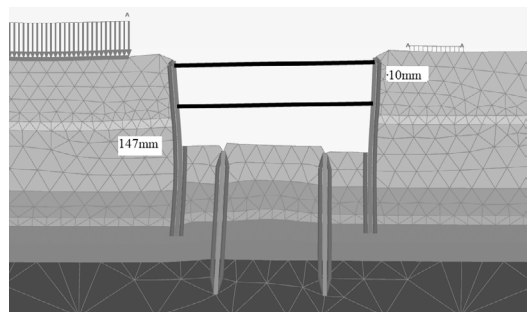


Figure 9. Diaphragm Wall Lateral Displacement

Surface settlement behind the shoring wall is calculated as 102mm and 12 mm for sections

neighboring building and the street sides respectively.

Lateral displacements of the diaphragm walls with 3D model are estimated as follows;

For the sides neighboring the buildings, lateral displacements are 57mm and 54mm for the short and long sides respectively. The lateral displacement of the short side is smaller than the other because the building load effects to only the half of this side.

For the sides neighbouring to the streets, lateral displacements are 33 mm and 37 mm for the short and long sides respectively.

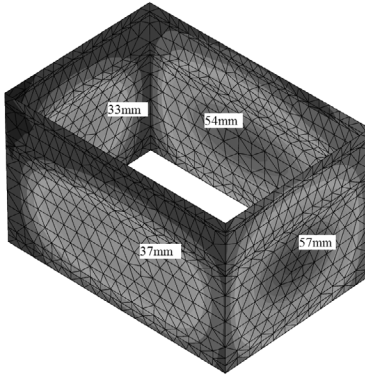


Figure 10. Displacements with 3D Model

Surface settlements are calculated as follows (Figure 11);

For the sides neighbouring the buildings, surface settlements are mm and 31 mm for both long and the short sides.

For the sides neighbouring the streets, surface settlements are 22mm and 16mm for the long and short sides respectively.

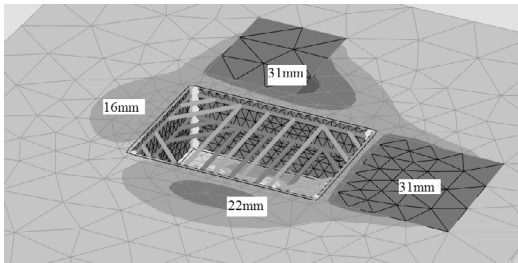


Figure 11. Settlements With 3D Model Calculation

Calculated lateral diaphragm wall displacements and surface settlements in two and three dimensional model analysis and also for both of two cases are summarized in the Table 3.

Table 3. Lateral Displacements and Settlements

Case/Model	Exc. Depth m	Surc. Load kPa	Lateral Disp. mm	Settlements mm
1. / 2D	11.35	15	64	68
1. / 3D	11.35	15	38/30*	34/30*
1. / 2D	8.30	15	33	34
1. / 3D	8.30	15	27/18*	25/18*
2. / 2D	11.30	100	147	102
2. / 3D	11.30	100	54/57*	31/31*
2. / 2D	11.30	15	10	12
2. / 3D	11.30	15	37/33*	22/16*

* First value is for the long, second value is for the short side of the excavation.

3. PLAIN STRAIN RATIO (PSR)

As described in introduction part Finno et al. (2007) reported that plain strain ratio “PSR” is related with the ratios of the length of wall to the excavation depth, the ratio of the plan dimensions of the excavation L/B , L being the side where displacements are computed, the wall system stiffness and factor of safety against basal heave. According to Finno et al. (2007) PSR can be estimated with below formula;

$$PSR = (1 - e^{-kC(L/H_e)}) + 0.05(L/B - 1), \quad (1)$$

“ k ” is system stiffness factor and can be calculated as;

$$k = 1 - 0.0001(S) \quad (2)$$

Where “ S ” is support system stiffness and calculated as; (Clough et al. 1989)

$$S = \frac{EI}{\gamma_w h^4}, \quad (3)$$

Where “ EI ” is bending stiffness of the wall, “ γ_w ” is unit weight of water and “ h ” is average vertical spacing of lateral support elements.

“ C ” is factor that depends of the factor of safety against basal heave.

$$C = 1 - \{0.5(1.8 - FS_{BH})\} \quad (4)$$

L is being the side where movements are computed. B is the secondary length of the wall. H_e is the excavation depth.

PSR values are calculated for the sections both considering plaxis results and the method submitted by Finno et al. (2007) and summarized in the table below;

Table 4. Calculated PSR values

Case	Exc. Depth m	Surc. Load kPa	Lat. Disp. mm-2D	Lat. Disp. mm-3D	PSR, Plaxis Models	PSR, calc. with formula (1)
1	11.35	15	64	38	0.593	0.854
1	8.30	15	33	27	0.818	0.990
2	11.30	100	147	57	0.388	0.748
2	11.30	100	147	54	0.367	0.921

4. CONCLUSIONS

Numerical studies of two different deep excavation projects are summarized above. Two cases which have similar excavation depth but with different dimensions, surcharge loads, soil types and supporting systems have been studied.

Consequences of the calculated displacements and PSR calculations can be listed as;

- In both cases 3D model calculations resulted with less lateral displacements and settlements.

- Lateral displacements and settlements increased with the increase of excavation depth, surcharge loads and the length of the excavation side where displacements are calculated.

- As an exception, in the second case since building load does not affect to the whole of the long wall, smaller displacements are calculated when compared to the short side.

- PSR values which were calculated with Plaxis results are compared with the ones calculated with considering method submitted by Finno et al. (2007). It is seen that PSR values calculated with Plaxis models are below the values calculated with this method.

- In the first case excavation pit is not rectangular and has variable excavation depths. In the second there are heavy surcharge loads which are not a direct parameter of the calculation method submitted by Finno et al. (2007). Also surcharge load is not symmetric and there are barrettes which effects basal heave. All these reasons can be related with the incompatibility of calculated PSR values.

- In both cases since excavation phase will initiate shortly, no monitoring data could be provided for comparison, it is clear that with the results of comprehensive monitoring data in both cases the reasons of the incompatibility of PSR values could be evaluated.

These studies showed that with 3D calculations a more realistic approach could be provided

for estimating displacements in problems that necessitate 3-D modeling.

5. REFERENCES

- Beadman, D., Cheng, A., 2002. *Geoguide* 2002-06. Arup International Document
- Burland, J.B., Simpson, B. & St. John, H.D., 1979. Movements around excavations in London Clay. *Proc. 7th European Conf. Soil Mech. And Found. Eng., Vol.1*, British Geotechnical Society, London U.K. 13-30
- Finno, R.J. & Blackburn, J.T. & Roboski, J.F., 2007. Three-dimensional effects for supported excavations in clay, *J. Geotech. Geoenviron. Eng.*, 133 (1) 30-36
- Fuentes, R., Devriendt, M., 2010. Ground Movements around corners of excavations: Empirical Calculation Method *J. Geotech. Geoenviron. Eng.*, 136 (10) 1414-1424
- Lee, F.H., Yong, K.Y. & Liu, K.X., 1995. Tree-dimensional analysis of excavation in soft clay. *Proc. 11th African Regional Conf. Cairo '95*, Egyptian Geotechnical Society, Cairo, Egypt
- Lee, F.H., Yong, K.Y., Quan, K.C.N. & Chee, K.T. 1998. Effect of corners in strutted excavations: Field monitoring and case histories. *J. Geotech. Geoenviron. Eng.*, 124 (4) 339-349
- Liu, K.X. 1995. Tree-dimensional analysis of excavation in soft clay, MEng thesis, National University of Singapore, Singapore
- Ou, C.Y. & Chiou, D.C., 1993. Three-dimensional finite element analysis of deep excavations. *Proc. 11th Southeast Asian Geotech. Conf.* The Institution of Engineers, Malaysia, Kuala Lumpur, Malaysia, 769-774
- Ou, C.Y., Chiou, D.C. & Wu, T.S., 1996. Tree-dimensional finite element analysis of deep excavations, *J. Geotech. Engrg.* 122(5), 337-345
- Ou, C.Y., Shiau, B.Y. & Wang, I.W., 2000. Three-dimensional deformation behavior of the Taipei National Enterprise Center (TNEC) excavation case history. *Can. Geotech. J.* 37, 438-448
- Simpson, B., 1992. Retaining Structure: displacement and design, *Geotechnique*, London, U.K., 42(7), 541-576
- St. John, H.D. 1975. Field and theoretical studies of the behavior of ground around deep excavations in London Clay. Phd thesis in Cambridge University, Cambridge, U.K.
- Wong, L.W. & Patron, B.C., 1993. Settlements induced by deep excavations in Taipei, *Proc. 11th Southeast Asian Geotech. Conf.* The Institution of Engineers, Malaysia, Kuala Lumpur, Malaysia, 787-791

PSEUDO-STATIC ANALYSIS OF FLEXIBLE RETAINING STRUCTURES INCLUDING SEISMIC THRUST DEPENDENCY ON WALL DEFORMATION

Bruno Becci & Marco Carni

Ce.A.S. s.r.l. Centro di Analisi Strutturale- Milano, Italy

ABSTRACT: The design of flexible retaining structures is very frequently conducted using simplified soil-structure interaction schemes such as the well known non-linear spring method. With this method, several distinguishing aspects of flexible wall behaviour can be usually captured with reasonable accuracy with regards to construction stages and static conditions. Seismic design, however, still represents a challenging aspect. In this paper some common issues of seismic analysis with the spring method are addressed and a proposal to include seismic effects within a pseudo-static framework is presented. Some examples analyzed with the proposed approach are finally discussed.

1. INTRODUCTION

The design of flexible retaining walls is usually based on numerical analyses, aiming at modelling real construction sequence, in particular when several supports are included. One of the most used numerical approaches in this field is the non-linear spring method, a natural extension of the Winkler method traditionally used by practicing engineers in the design of foundation beams and slabs. Even today, in spite of the wide availability of advanced modeling tools, such as 2D and 3D finite element or finite difference codes, the non-linear spring method is very frequently adopted, at least in the early stages of a wall design, because, in authors' opinion, the merits of such simple engineering method still outweigh its intrinsic shortcomings. On the other hand, in seismic design, the non-linear spring approach highlights severe limitations that may, at first glance, discourage its usage. However, once its assumptions and limitations have been clearly addressed, this method may still be helpful in seismic analysis. In this paper, the non-linear spring method as implemented by the authors (Becci & Nova, (1987)) is briefly presented. Then the main assumptions of the pseudo-static methods for seismic design and the so-call performance design approach are reviewed, in the light of its implementation by the non-linear spring approach. A simple modification to the non-linear spring constitutive law is proposed, to automatically include seismic actions on the wall, falling

within selected lower bound thrusts (usually the Mononobe-Okabe (M-O in the following), Mononobe & Matsuo (1929), Okabe (1926)) and an upper bound distribution (to be applied to non yielding walls). Some examples taken from available experimental or numerical benchmarks are reproduced by this approach. The results and limitations of this proposal will be finally discussed.

2. THE NON-LINEAR SPRING METHOD

Within a structural or finite element program, the wall is modeled by an array of elastic or inelastic BEAM elements and just lateral behaviour is considered. The interaction with soil is modelled by special non-linear elements at each face, which may be either one-dimensional simple lateral springs applied at each wall node, or more refined interface elements whose stiffness is calibrated by means of continuum finite element models (Pappin et al. (1985)).

In the constitutive model of such elements, lateral stress σ'_h in each spring is initially set equal to the assumed at rest pressure $K_0 \cdot \sigma'_v$. Hence the wall is initially subjected to self-balanced distribution of pressures, provided same geostatic conditions are prescribed at each side. Subsequent stages are then studied in which an excavation or the insertion of a prop is modelled, as well as any other modification to previous conditions. Based on lateral wall

deformations Δ , soil elements react as shown in Figure 1.

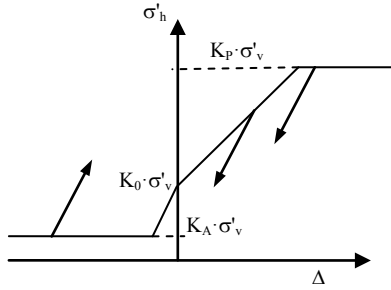


Figure 1. Constitutive law for a non-linear spring (cohesionless soil)

For granular soils, yield limits linearly depend on the effective overburden stress σ'_v via the usual active and passive thrust coefficients K_A and K_P , usually determined according to classical Coulomb equations for K_A and values by Caquot et al. (1973) for K_P , accounting for wall-soil friction δ and dredge line slope.

The spring stiffness depends on the elastic properties of the soil and on the excavation geometry. According to Becci & Nova (1985), at each step, the spring stiffness K is computed by the following equation:

$$K = \frac{E' \cdot t}{L}, \quad (1)$$

where E' is the soil Young modulus, t is the spring spacing and L is a geometrical parameter accounting for actual wall geometry. This value is different between up- (L_M) and down-hill (L_V) side:

$$L_M = \frac{2}{3} H' \cdot \tan\left(\frac{\pi}{4} - \frac{\phi'}{2}\right), \quad (2)$$

$$L_V = \frac{2}{3} (H' - D) \cdot \tan\left(\frac{\pi}{4} + \frac{\phi'}{2}\right)$$

D is the excavation depth, H is the overall wall height and $H' = \min(2D, H)$ (Figure 2).

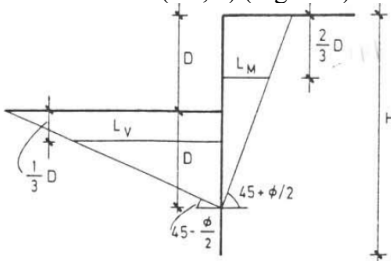


Figure 2. Definition of geometrical scaling factor for non-linear spring stiffness assessment

In essence such geometrical parameters are set equal to the average mobilized soil wedge widths in active conditions (driving side) or passive conditions (resisting side).

The (secant) elastic modulus E' can be determined by means of usual correlations adopted for other geotechnical problems.

For sandy soils, a reasonable estimate can be obtained by the one of the following equations:

$$E' \approx (2 \div 3) \cdot N_{SPT} \text{ (MPa)}, \quad (3a)$$

or

$$E' \approx (0.8 \div 1) \cdot G_0, \quad (3b)$$

where G_0 is the small strain shear modulus.

In Becci & Nova (1987) a simplified cap logic is also included in order to differentiate loading modulus E_{vc} from unloading one E_{UR} . Including such model in a general nonlinear finite element code, several modeling features can be easily considered, such as stage analysis by adding and/or removing parts of the soil as well as ground anchor installation and also the interaction with water. At each analysis stage, balanced conditions are computed by means of Newton-Raphson iterations. The straightforward model definition as well as the simplicity in soil parameters selection makes such kind of procedure a quite attractive option, at least in preliminary design phases, albeit some important design aspects, such as settlements of nearby foundations or global stability checks are not directly available.

3. PSEUDO-STATIC SEISMIC ANALYSIS

Pseudo-static seismic analysis is a widely used method used in the design of retaining walls. Stemming from the pioneering proposal by Mononobe & Okabe, several extensions have been published during last decades, in order to encompass most of the aspects that may arise in the practice. In essence a uniform seismic acceleration with horizontal and vertical components is statically applied to the wall and to the soil mass interacting with the wall. The M-O method and its extensions offer a closed form solution of the total soil thrust on the wall, assuming that the soil mass behind yields during seismic event, thus considering a wall subjected to relevant deformations. Following the approximation proposed by Seed & Whitman (1970), the M-O increment to static

active pressures can be applied as a constant pressure distribution given by

$$\Delta p_{E,M-O} \approx 0.375 \cdot \frac{a}{g} \cdot \gamma \cdot H, \quad (4)$$

where H is the wall height, γ the average back-fill unit weight and a/g the normalized seismic acceleration. Eq. 4 strictly holds for a dry granular fill with a friction angle $\phi=35^\circ$ and a soil-wall angle $\delta=\frac{1}{2}\phi$.

Other methods, including the widely used Wood method (Wood, 1973)) provide the seismic increment of the soil thrust on a wall which is essentially rigidly restrained so as to prohibit remarkable wall deformations. Such increment is represented by a constant pressure distribution given by:

$$\Delta p_{E,Wood} = \frac{a}{g} \cdot \gamma \cdot H, \quad (5)$$

Comparing the formulations above, it can be realized that the seismic thrust increment for rigid walls (Eq. 5) may exceed the M-O increment (Eq. 4) by a factor greater than 2.5. Therefore it is important to select the appropriate approach, in the light of wall behaviour under consideration.

Beyond the method adopted in computing seismic pressures, a most important issue arose even since early '70s: i.e. the selection of an appropriate design acceleration a_c with respect to the prescribed maximum seismic acceleration a_{max} . Thanks to the fundamental works by Richard & Elms (1979), Whitman & Liao (1985) and later works, the concept of design acceleration $a_c < a_{max}$ related to selected wall performance (acceptable deformation) rather than to maximum site intensity was clearly established. Since then, most design standards such as Eurocode comply with this approach. Research efforts have been devoted in extending this method that was originally proposed for gravity walls, to other kinds of retaining structures, such as cantilevered or propped bulkheads. Since the performance design method requires the calculation of a desired ultimate capacity, just rigid-plastic methods, such as the Blum method or similar extensions (e.g. Conti & Viggiani, (2013), Callisto (2014)), are essentially applicable. In other words, reduced design accelerations a_c given by a performance design approach must be applied only if seismic increments are determined by a method like Eq. 4, but not by

Eq. 5 or any other elastic method. In this respect, it is clear that, for many kinds of walls, such as multi-propped bulkheads, the performance (or capacity) seismic analysis with pseudo-static approach requires particular care and further research.

Finally, within the performance design framework:

$$\frac{\Delta p_{E,Wood}}{\Delta p_{E,M-O}} \approx 2.67 \cdot \frac{a_{max}}{a_c}, \quad (6)$$

Therefore active seismic thrusts may drop down to a quite low percentage of elastic thrusts: for example, taking $a_c/a_{max} \approx 0.70$, according to Eq. 6, active thrust is just 26% of elastic thrust.

4. PSEUDO-STATIC SEISMIC ANALYSIS BY THE NON-LINEAR SPRING METHOD

4.1. General

Once the construction process has been completed, seismic conditions are usually modelled according to one the two following alternatives:

- A. the active and passive coefficients are modified to account for seismic effects or;
- B. just passive coefficients are modified whereas, on the driving side, an appropriate distribution of external pressures is applied, whose resultant corresponds with the expected seismic thrust increment: for example Eqs. 4 or 5 may be used, depending on the expected wall behaviour.

Approach A is usually not recommended since it is just applicable to very flexible walls, in which active conditions are reached at the end of excavation process and in general may not sufficiently reproduce expected seismic actions. Approach B, on the contrary, allows the designer to keep under his/her control the seismic actions which, however, do not depend on wall deformations.

4.2. The proposed procedure

As an alternative to such conventional approaches, the following procedure is proposed aiming at automatically include intermediate seismic conditions, based on actual

wall behavior. Consider a soil region in the uphill side on the retaining wall. In a very short time lagging in between seismic wave arrival and the actual wall response, incremental wall deformations may be assumed to be negligible: i.e. the wall may be considered as very rigid, for a while. During such very transient conditions, the seismic thrust increment may be estimated by a rigid approach, such as the Wood method (Eq. 5). Due to such incremental pressure spike, previous equilibrium conditions are violated. Therefore additional deflections must develop, in order to reestablish equilibrium conditions, which are pursued by means of the usual iterative process, exactly as in any static stage.

The proposed algorithm requires the following two modifications to the standard calculation scheme:

1. In the first iteration of the seismic stage, in any uphill soil element only, the effective lateral pressure is increased by the rigid (Wood) pressure increment (Eq. 5): note that such stress increment is assigned with no strain increment, thus it can be revised as an inelastic increment.

2. During further iterations, strain increments are allowed and, at the same time, active and passive limits are updated to the seismic values as discussed later.

Through the iterative process, the initial seismic stress increment may diminish or even vanish at all, but the appropriate seismic yield conditions are ensured, at least.

In figure 3 some particular stress paths for uphill soil elements are outlined, during such automatic seismic procedure stage.

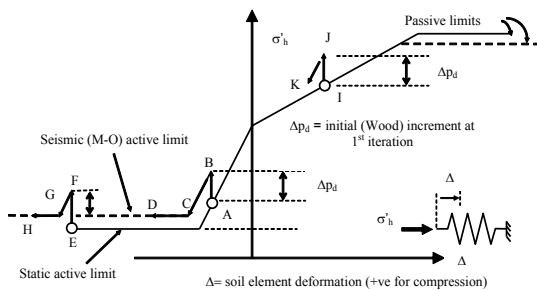


Figure 3. Automatic seismic algorithm in non-linear spring model

A-B-C-D path corresponds with an “elastic” uphill soil region in which the lateral stress was released, in a previous static stage, from at rest conditions, yet not sufficiently to reach active limit state (pt A). Initial rigid seismic stress increment is represented by A-B segment. Further stress evolution toward seismic active conditions is represented by B-C-D path, in which B-C is the “elastic” release part, whereas C-D represents the development of seismic plastic strains.

E-F-G-H path represents an uphill soil region that reached active static conditions (pt. E) prior to earthquake. Initial rigid seismic stress increment (E-F) corresponds with a temporary elastic reloading path. Subsequent elastic strain release is represented by F-G segment, whilst seismic plastic deformation development is associated to segment G-H

I-J-K path: an uphill soil element is represented, which was actually pushed inward rather than being released ($\Delta > 0$, point I): initial rigid seismic stress increment is I-J segment, whereas subsequent unloading is J-K.

Active and passive limit seismic conditions should be computed according to general criteria (for example using M-O equations). K_p should be determined so as to account for wall-soil friction, based on safe formulations (e.g. Lancellotta (2007), Soubra (2000)).

4.3. Discussion

According to this procedure, the computed seismic pressures on the driving side fall between a minimum (active) and a maximum (Wood) distribution. This feature may be considered the most relevant advantage of the procedure because all wall typologies may be analyzed without preliminary (and arbitrary) assumptions on their mechanical behavior. Of course, it also suffers from some limitation, including the following:

- the decrease rate from Wood to active conditions is governed by the same stiffness considered in static calculation;
- the position of the overall active seismic thrust is essentially the same as the static active thrust.

In the light of the performance design method, on authors' opinion, this approach should be used just when the allowed unrecoverable

deformation are very small or even negligible, i.e. when the wall is designed to behave (almost) elastically during seismic conditions.

5. EXAMPLES

5.1. Propped bulkhead - centrifuge model

The propped wall PW2 studied by Conti et al (2012) by means of a centrifuge reduced scale model is considered. Prototype dimensions are summarized in Figure 4.

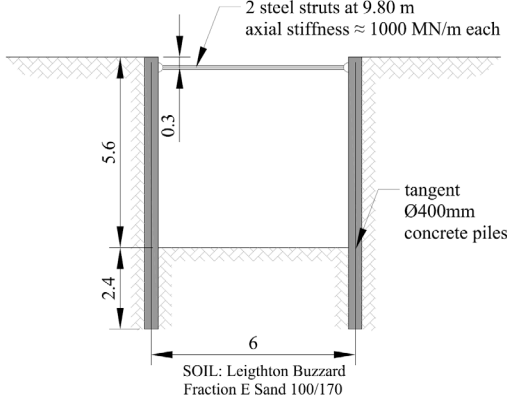


Figure 4. PW2 model (dimensions in [m])

The following soil parameters have been considered:

$$\begin{aligned} D_r &= 42\% & e_0 &= 0.84 \\ \gamma_d &= 14.37 \text{ kN/m}^3 & \phi_{cv} &= 32^\circ \\ E_{vc} \text{ (MPa)} &= 50 \cdot \left(\frac{\sigma'_h}{98 \text{ kPa}} \right)^{0.5} & E_{UR}/E_{vc} &= 2 \\ \phi &= \begin{cases} 38^\circ \text{ uphill side} \\ 35^\circ \text{ downhill side} \end{cases} & \delta/\phi &= 0.30 \end{aligned}$$

In order to account for a likely reduced soil density inside excavation (see discussion below), a reduced friction angle (35°) and reduced elastic moduli (50% of reference values) are assigned to soil elements at the wall toe.

In the experimental study, the model was excited by a set of five contiguous wave motions, modelling five seismic excitations (EQ1 to EQ5), with increasing intensities from 0.21 g up to 0.41 g

Thanks to a set of complex instrumentations, wall displacements, bending moments and strut

forces have been recorded at several model positions.

The following sequence is reproduced:

- stage 0: at rest conditions are established;
- stage 1: a small excavation is performed down to strut position;
- stage 2: the strut is inserted and the excavation is lowered down to final level (results at this stage are compared with static results in Conti et al (2012));
- stage 3: EQ1 seismic conditions are applied.

It should be noted that a reduced value of peak acceleration of the input motion must be usually considered in a pseudo-static analysis, all the more because, in this case, numerical results are compared with the available results at the end of seismic excitation. In this case, a pseudo-static acceleration equal to 0.15 g is considered, representing $\sim 70\%$ of maximum peak EQ1 excitation.

In Figure 5, numerical and experimental results are compared. Bending moments and prop forces are quite well matched by the numerical model, whereas the predicted wall movements are different from the measured ones, in both static and seismic conditions.

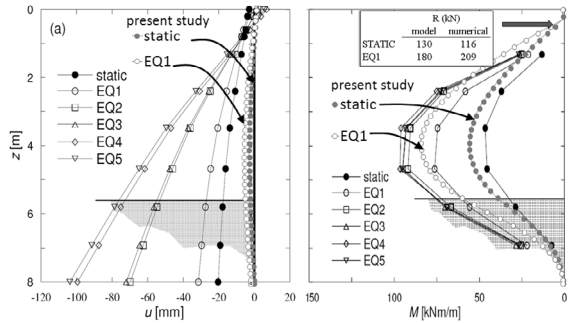


Figure 5. PW2 model results comparison

However, it should be noted that measured deflections in centrifuge tests, in initial static stage, most likely suffer from a insufficient local sand densification, thus displaying some uneven initial tilting not reproduced by our numerical analysis. In this respect, in Conti (2010), such issue is thoroughly addressed.

As for seismic incremental deformations, it should be observed that unrecoverable deformations are accumulated throughout the real seismic event, when applied acceleration exceeds the threshold acceleration a_c related to wall capacity; of course, such contribution

could not be directly reproduced by a pseudo-static analysis, even if much more advanced numerical tools were used. Some a posteriori correction to pseudo-static deformed shape may be possibly added, depending on maximum wall capacity as compared with maximum seismic acceleration, but such topic is beyond the scope of this paper.

Nonetheless, in spite of its simplicity, the non-linear spring algorithm can predict the most important results for design purposes reasonably well. However it must be noted that since in this case active limit conditions are reached along all the wall, seismic results are poorly affected by the amount of Wood pressure applied at first seismic iteration.

5.2. A numerical exercise - seismic analysis of a real wall

A flexible retaining wall benchmark is considered in the following, as a starting point to perform some parametric seismic analyses with the proposed algorithm.

The multi-anchored retaining wall described by Schweiger (2002) is shown, in Figure 6. Such problem, which is selected as a benchmark by some of the most popular numerical modelling tools, such as FLAC (Itasca (2011)) and PLAXIS (Brinkgreve et al. (2010)), is limited to static conditions.

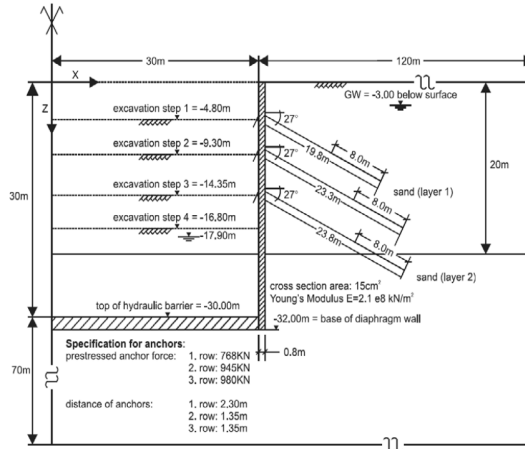


Figure 6. Real wall benchmark (adapted after Schweiger (2002))

A non-linear spring analysis of the constructions stages is performed first, and the obtained results are compared with the reported measures. The following soil properties are assumed (see Schweiger (2002)):

$$E_{vc} \text{ (kPa)} \approx 10000 \cdot \sqrt{z \text{ [m]}} \quad z \leq 20\text{m}$$

$$E_{vc} \text{ (kPa)} \approx 50000 \cdot \sqrt{z \text{ [m]}} \quad z > 20\text{m}$$

$$E_{UR}/E_{vc} = 1.5 \quad \phi = 35^\circ \quad \delta = 0.7\phi$$

Dewatering operations are reproduced by assigning a lower permeability coefficient to the 2 m thick hydraulic plug inside excavation (Fig. 6) and computing the pore pressures by means of a simplified mono-dimensional seepage scheme. Ground anchors are modelled as linear springs whose stiffness is given by the axial stiffness (EA) of the steel stem divided by the deformable length, set equal to the free length plus 50% of the grouted length.

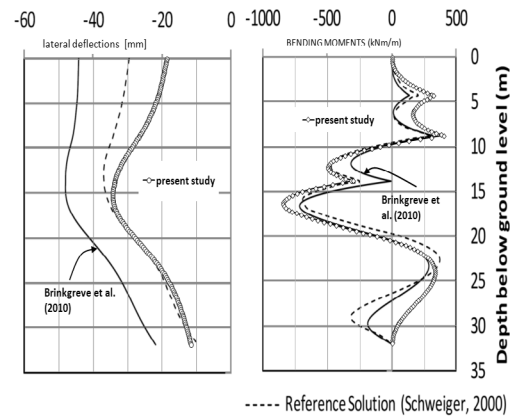


Figure 7. Real wall benchmark (adapted after Brinkgreve et al. (2010))

In figure 7, computed and measured deformed shapes are compared, showing that the numerical model reproduces quite well the observed behaviour, unless in the top part where some reduced anchor stiffness is highlighted by the measures. This effect is likely related to a limited upper anchor length whose foundation is somehow disturbed by wall movements: such aspect cannot be easily reproduced by a non-linear spring method, whereas may be highlighted by a continuum model (Itasca (2011)).

Bending moments are also compared with the values reported in the cited reference. Both absolute values and overall pattern are fairly in agreement, on the safe side. Thus such non-linear spring model can be considered a realistic model of the observed wall behaviour during construction stages, and a valuable starting point for numerical experiments including seismic conditions.

In this respect, seismic experiments outlined in Table 1 are discussed.

Table 1. Numerical experiments on real wall

experiment	a_c/g	Initial Wood p.	Lateral restraints
EXP1	0.15	Yes	Soft
EXP2		No	
EXP3		Yes	Rigid
EXP4		No	

Soft lateral restraints correspond with ground anchors only, whereas rigid restraints are represented by very stiff lateral supports applied at elevations shown in Figure 8, along with ground anchor removal. Bending moments for various assumptions are also shown in Figure 8.

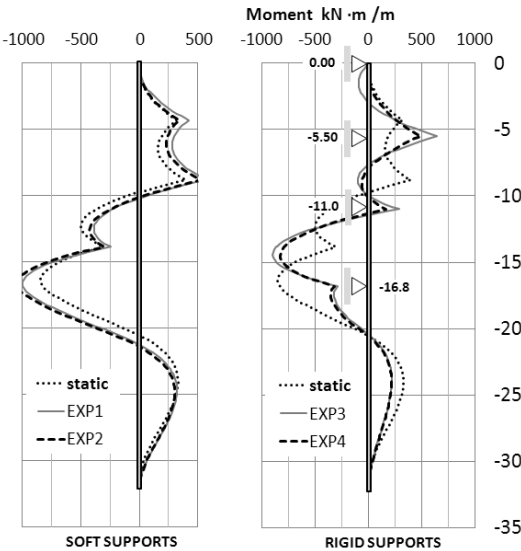


Figure 8. Numerical experiment results

With soft supports, EXP1 and EXP2 results are almost the same since active seismic conditions are easily restored so as to make the initial Wood pressure effect negligible.

With rigid supports, initial Wood pressures (EXP3) significantly increase bending moments and support forces, by ~30% in the upper part and ~9% in the middle part, with respect to an ordinary M-O analysis (EXP4). Support reaction differences are even larger (Table 2).

In practical problems, similar to this example, representing a quite typical configuration for deep excavations in urban areas, the proposed algorithm produces safer predictions with respect to traditional simplified analysis limited to M-O seismic pressures.

Table 2. Rigid support reactions (kN/m)

EL	EXP3	EXP4
0.00	96	6
-5.50	823	520
-11.00	1065	792
-16.80	636	558

On authors' experience on similar examples, this observation can be considered quite general, in agreement with similar findings by other authors (e.g. Psaropoulos et al (2005)).

This statement holds for moderate seismic conditions and for walls designed according to usual criteria, with regards to the most relevant aspects such as the length of ground anchors, which should be normally designed to ensure expected resistance and stiffness in both static and seismic conditions.

6. CONCLUSIONS

A simple algorithm to allow pseudo-static seismic analysis of flexible retaining walls with the non-linear spring method is presented.

As most pseudo-static methods, this approach has a reasonable ability to capture internal forces in soil, as well as in wall and props, but fails in computing physical deformations when relevant plastic deformations are progressively accumulated during seismic events: this circumstance is particularly evident in case of cantilevered or singly propped walls and must be clearly taken into account in final design.

However, on authors' best knowledge, this limitation is also present in any kind of pseudo-static analysis, even using more advanced numerical models.

Based on the examples studied with this approach, the following concluding remarks can be proposed:

- Multi-propped walls with deformable intermediate supports such as ground anchors are normally so flexible to reach active limit state at driving side at the end of excavation as well as during seismic events. In this case both the proposed approach and the classical M-O pressure distribution can be used in practical designs.
- For multi-propped walls with rigid supports, active seismic pressures may be inappropriate,

whereas fully elastic solution such as the one by Wood (1973) may be too conservative. The proposed algorithm can provide a more reasonable estimate of seismic conditions falling between lower and upper bound solutions.

7. ACKNOWLEDGMENT

The authors are grateful to Prof. Giulia Viggiani and Dr. Riccardo Conti of Università Tor Vergata (Roma, Italy) for their kind assistance in providing detailed information on their researches, as well as for their valuable suggestions.

8. REFERENCES

- Becci, B. & Nova, R. 1987. Un metodo di calcolo automatico per il progetto di paratie, *Rivista Italiana di Geotecnica*, 1, 33–47 (in Italian).
- Brinkgreve, R.B.J., Engin E., Engin H.K., 2010. Validation of empirical formulas to derive model parameters for sands. *Proc. Numerical Methods in Geotechnical Engineering NUMGE2010*, Trondheim, Norway, June 2-4, pp. 137–142
- Callisto, L. 2014. Capacity design of embedded retaining structures, *Géotechnique*, Vol. 64, No. 3, pp 204–214.
- Caquot A., Kerisel J., Absi E. 1973. *Tables de butée et de poussée*, Gautiers-Villars, Paris.
- Conti, R. 2010. *Modellazione fisica e numerica del comportamento di opere di sostegno flessibili in condizioni sismiche*. PhD thesis, Università di Roma Tor Vergata, Rome, Italy (in Italian).
- Conti R., Madabhushi G. S. P, Viggiani G. M. B. 2012. On the behaviour of flexible retainingwalls under seismic actions. *Géotechnique*, Vol. 62, No. 12, pp 1081–94.
- Conti, R. & Viggiani, G. 2013. A new limit equilibrium method for the pseudostatic design of embedded cantilevered retaining walls, *Soil Dynamics and Earthquake Engineering*, Vol.50, pp. 143–150.
- Itasca Consulting Group, 2011. Installation of a Triple-Anchored Excavation Wall in Sand, *FLAC version 7.0, Example Applications Manual*, section 17.
- Lancellotta, R. 2007. Lower-bound approach for seismic passive earth resistance, *Géotechnique*, Vol. 57, No. 3, pp. 319–321.
- Mononobe, N., and Matsuo, H. 1929. On the determination of earth pressure during earthquakes. *Proceedings of World Engineering Conference*, Vol 9.
- Okabe, S. 1926. General theory of earth pressure. *Journal, Japanese Society of Civil Engineers*, Vol. 12, No. 1.
- Pappin, J. W., Simpson, B., Felton, P. J., and Raison, C. 1985. Numerical analysis of flexible retaining walls. *Proc., Numerical Methods in Engineering Theory and Applications (NUMETA'85)*, Balkema, Rotterdam, pp 789–802.
- Psarropoulos P.N., Klonaris G., Gazetas G. 2005. Seismic earth pressures on rigid and flexible retaining walls, *Soil Dynamics and Earthquake Engineering*, vol. 25, pp. 795–809
- Richards, R. & Elms, D. 1979. Seismic behaviour of gravity retaining walls, *Journal of geotechnical Engineering Division*, ASCE, Vol. 105, No. GT4, pp. 449–464.
- Schweiger, H. F. 2002. Results from numerical benchmark exercises in geotechnics, *Proc. 5th European Conf. Numerical Methods in Geotechnical Engineering*, Presses Ponts et chaussees, Paris, 2002, pp 305–314.
- Seed, H. B. & Whitman, R. V. 1970. Design of earth retaining structures for dynamic loads. *Proceedings of ASCE Special Conference on Lateral Stresses, Ground Displacement and Earth Retaining Structures*, Ithaca, N.Y., pp. 103–147.
- Soubra, A. H. 2000. Static and seismic passive earth pressure coefficients on rigid retaining structures - *Can. Geotech. Journal*. Vol. 37, pp. 463–478.
- Whitman, R. V. & Liao, S. 1985. Seismic design of retaining walls, *Miscellaneous Paper GL-85-1*, U.S. Army Engineer Waterways Experiment Station, Vicksburg, Mississippi.
- Wood, J. H. 1973. Earthquake Induced Soil Pressures on Structures, Doctoral Dissertation, EERL 73-05, California Institute of Technology, Pasadena, CA.

Soil-structure interaction for sheet pile walls considering ground surface and sub-wall soil conditions

Ö. Bilgin

University of Dayton, Dayton, Ohio, USA

ABSTRACT: The current design practice of sheet pile walls are based on horizontal force and moment equilibrium using active and passive earth pressures. The methods consider soils only in direct contact with the wall to determine the pressures, and do not take into account the effect of existing ground surface profile and conditions below the wall. However, the initial ground and sub-wall soil conditions affect the wall behavior and deformations. The effect of ground conditions and varying sub-wall soil conditions on the behavior of sheet pile walls are presented in this paper.

1. INTRODUCTION

Sheet pile walls, either cantilever or anchored, are commonly used in civil engineering applications. Design of sheet pile walls uses active and passive earth pressures acting on the wall, and is based on the moment and force equilibrium of active earth, passive earth, and water pressures. The wall stability relies on the generation of earth pressures on either side of the wall. While earth pressures depend on wall movements, wall movements depend on the earth pressures, resulting in a close interaction between the sheet pile wall and surrounding soil. These active and passive earth pressures are related to soils in direct contact with the sheet pile walls. Soils below the tip of the wall are not taken into account during force and moment equilibrium considerations in design.

The effect of soils below the wall is partially considered for deep excavations when the basal heave is analyzed. The safety factor used for basal heave takes into account the strength of soils below the excavation level. The depth considered below the bottom of excavation when calculating the safety factor for basal heave depends on the width of the excavation and presence of a firm layer. This safety factor is introduced to ensure that the underlying clay layer does not experience a bearing capacity failure. The soil deformations and basal heave considerations that take soils below the bottom of pile into account are not common in flood-

wall design and when the project does not require deep excavations.

Factor of safety is applied to the passive pressures during the determination of lateral earth pressures (NAVFAC, 1986). The safety factors applied to passive pressures are used to take into account for the uncertainties in soil conditions, the method of stability analysis, the loading conditions, as well as to restraint soil movements to an acceptable level (Potts and Fourie, 1984). Special attention usually is not paid to wall deformations during design.

Depending on the soil conditions below the pile tip, the sheet pile walls can experience significant displacements, based on the size of the project, area and magnitude of the loading, and soil properties. A presence of soft soil layers in soil profile below the wall, although not considered in the structural design, can affect wall displacements. Bilgin (2006) studied the effect of a flooding event on subsurface soil and floodwall deformations. The effect of subsurface soil conditions on floodwall behaviour is also presented by Bilgin (2009).

In addition, conventional methods used in the design of sheet pile walls are based on the limit equilibrium approach and they do not consider processes involved during construction. Varying amounts of cut and fill sections for the walls constructed on a slope cause different loading and unloading of soils around the wall resulting in different wall behaviour. The effect of excavation versus backfill on sheet pile walls, and the cut and fill operations for

varying slope angles and cut to fill ratios on wall behaviour were investigated using numerical methods (Bilgin, 2009 and 2010).

The objective of this study was to analyze and provide an overview of the effects of ground surface and sub-wall soil conditions on the sheet pile wall behaviour. The conditions presented include the presence of soft soil layers below the wall tip and the sloping ground surface where varying amounts of cut and fill is required during the construction. The finite element method was used to perform numerical analyses and to conduct the study.

2. NUMERICAL AND CONSTITUTIVE SOIL MODELS

The finite element analyses were performed by using Plaxis finite element code (Brinkgreve et al., 2006). The finite element modeling comprised two-dimensional plane strain analysis. Soil layers and sheet pile walls were modeled using 6-node triangular elements and 3-node plate elements, respectively. A finer mesh was used around the wall because of the stress concentration.

The Mohr-Coulomb constitutive model, a linearly elastic and perfectly plastic model, was used to model soil behaviour. The Mohr-Coulomb model has been commonly used in the finite element modelling of retaining walls. The yield function, f , is defined by the Mohr-Coulomb criterion using soil stresses (normal stress, σ , and shear stress, τ) and strength parameters (cohesion, c , and friction angle, ϕ) as

$$f = |\tau| - \sigma \tan \phi - c \quad (1)$$

and when the yield function is equal to zero ($f=0$), plastic yielding occurs. The elastic soil behaviour below the yield surface is characterized by Hooke's law to relate the stresses to strains.

An undrained analysis was performed for the cantilever wall (the flooding case) considered. For the sloping ground cases, drained analysis was performed due to cohesionless soils studied.

3. EFFECT OF SOFT SOIL LAYER

The behavior of sheet pile floodwalls when soft soil layer is present below the tip of wall is presented in the following. Parametric study was performed for varying soft soil thicknesses and depths below the wall tip. The finite element method was used to perform the numerical analyses by Plaxis.

3.1. Geometry and material properties

The floodwall height, H , selected for parametric study was 5 m with a depth of wall penetration, D , also equal to 5 m. The baseline case assumed to have medium stiff clays at the site. Then a soft clay layer with varying thickness and depth below the wall tip was introduced for the parametric study cases. Thickness of the soft layer ranged from zero (baseline case) to 25 m, and the depth below the tip of sheet pile to the top of soft layer ranged from 0 to 15 m. There were total of 29 cases analyzed for various combinations of soft layer thickness and depth to soft layer below the wall tip. A schematic of a typical wall section analyzed along with the parameters selected is shown in Figure 1. Soil model parameters used in the analyses for medium stiff and soft clay soils are given in Table 1. Steel sheet pile was modeled using elastic plate elements, with axial and bending stiffnesses of $EA = 2.68 \times 10^7$ kN/m and $EI = 40,000$ kNm²/m, respectively.

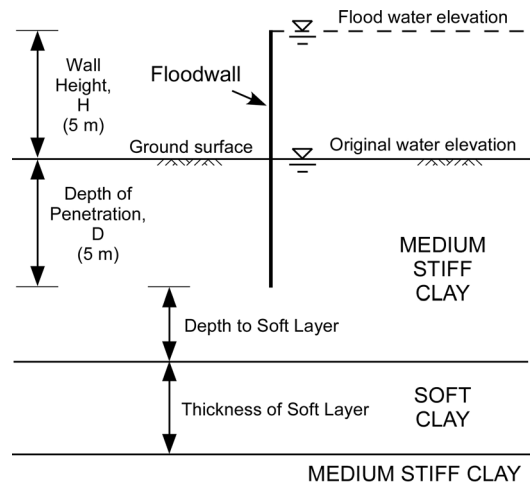


Figure 1. Soil and wall profile used in the analysis.

Table 1. Soil and interface properties

Property	Medium Stiff Clay	Soft Clay
Unit weight, γ (kN/m ³)	19.5	19
Undrained shear strength, s_u (kPa)	50	25
Modulus of elasticity, E_{s0} (kPa)	4,000	2,000
Soil/Wall interface strength ^a , R_{int}	0.6	0.6

^a $R_{int} = \tan\delta/\tan\phi$ (δ =interface and ϕ =soil friction angle)

The analyses conducted and the results are given in details by Bilgin (2009). The overview of the results is provided in the following.

3.2. Wall deformations

The lateral deformed shapes of the wall at maximum flood level of 5 m are given in Figure 2 for three cases: Case A (no soft layer below the wall), Case B (15-m-thick soft layer starting from 5 m below the tip of the wall), and Case C (only soft layer below the tip of the wall). Cases A and C represent two extreme soil conditions possible for the cases studied and therefore the deformed shapes of those two cases define the boundaries for all cases analyzed. The results show that the wall experiences significant translational movement during the flooding event. This is due to a large area loading behind the wall and resulting soil movements during a flooding event (Bilgin, 2006). The deformed wall shapes presented in Figure 2 show that the presence of relatively softer soil layers below the tip of the wall can significantly affect the wall deformations during a flooding event.

3.3. Wall bending moments

Wall bending moments are given in Figure 3 for the three cases: Case A (no soft layer below the wall), Case B (15-m-thick soft layer starting from 5 m below the tip of the wall), and Case C (only soft layer below the tip of the wall). The results show that the bending moments are not affected by the presence of soft soils, because the increase in deformations when the soft soils are present primarily occur as translational wall movements rather than the flexural deformations.

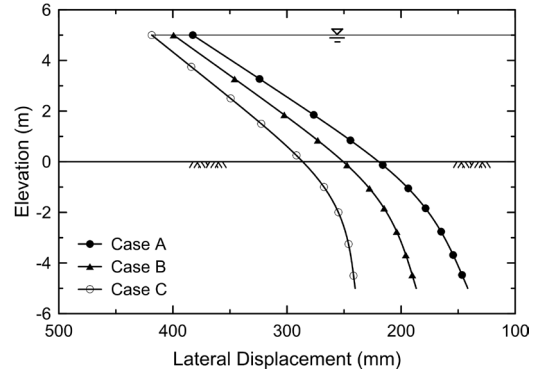


Figure 2. Final wall displacements (Case A: No soft soil layer; Case B: Depth to soft soil is 5 m and soft layer thickness is 15 m; and Case C: All soft soil below wall tip).

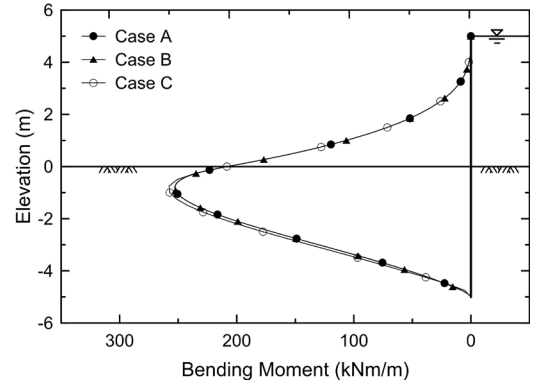


Figure 3. Wall bending moments.

4. EFFECT OF SLOPING GROUND

The anchored sheet pile walls sometimes are needed to be installed on slopes. These situations mostly arise in transportation projects where one highway usually crosses through topographically changing conditions.

Depending on the location of a wall on a slope, the construction may require cut behind the wall, fill in front of the wall, or both some cut behind and some fill in front of the wall (Figure 4). The amount of cut and fill depends on the location of the wall along the slope, e.g. a wall closer to the top of the slope requires more cut than fill while a wall closer to the toe of the slope needs more fill than cut quantities.

Depending on the cut and fill quantities, anchored sheet pile walls at the slopes are expected to behave differently because of the stress paths that are generated in surrounding

soils during cut (unloading) and fill (loading) operations. The conventional design methods commonly used in sheet pile wall design do not consider whether the walls are constructed by cutting, filling, or both. Numerical analyses, on the other hand, allow modelling of the construction processes.

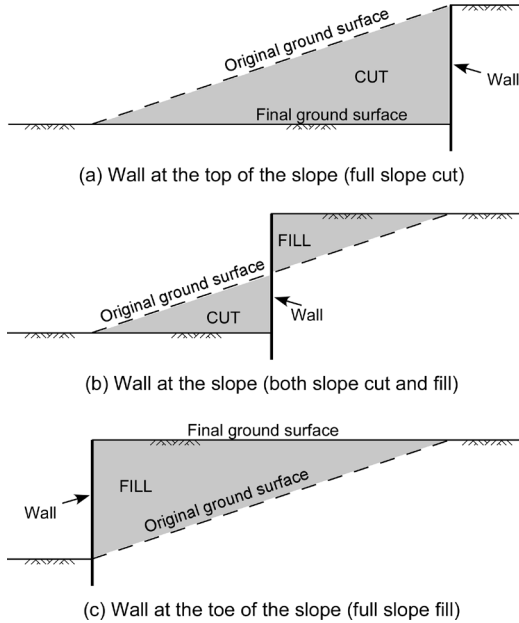


Figure 4. Schematic of cut/fill conditions for a wall on a slope.

4.1. Geometry and material properties

A 12-m-high 3H:1V (horizontal to vertical ratio) slope was selected for the parametric study. The anchor location was fixed at 3 m (25% of wall height) below the top of wall based on a study conducted by (Bilgin, 2009). A schematic of a typical wall and slope section analyzed along with the parameters considered is shown in Figure 5.

The depth of wall penetration, D , used in numerical modelling and analyses was 2.61 m, which was calculated using the free earth support method. The pile section was also selected based on the conventional design calculations. The soils at the site were selected as dry medium dense sand. The soil and wall material properties used in the conventional design calculations and for the finite element analyses are given in Table 2.

Table 2. Soil and wall properties

Property	Value
Soil:	
Unit weight, γ	17 kN/m ³
Friction angle, ϕ	36°
Dilatancy angle, ψ	6°
Modulus of elasticity, E_{50}	35,000 kPa
Poisson's ratio, ν	0.28
Wall:	
Axial stiffness, EA	4.36×10 ⁶ kN/m
Bending stiffness, EI	9.86×10 ⁴ kNm ² /m
Soil/Wall interface strength ^a , R_{int}	0.65

^a $R_{int} = \tan\delta/\tan\phi$ (δ =interface and ϕ =soil friction angle)

The anchor was installed as soon as the anchor location on the wall is available, i.e. at the beginning of construction in fill cases and when excavation reached the anchor level in excavation cases.

The analyses conducted and the results are given in details by Bilgin and Erten (2009). The overview of the results is provided in the following.

4.2. Wall deformations

Horizontal wall deformed shapes, along with their relative locations on the slope, for three cases (100% cut; 50% cut and 50% fill; and 100% fill) are shown in Figure 6.

The results show that the cut to fill ratio has an effect on wall behaviour. The top of wall in cut cases moves towards the excavation, however, wall top deformations decrease as the amount of cut decreases and the fill increases. Eventually, the top of the wall starts moving backwards towards the soil. This is because of the installation of an anchor at the beginning of construction in fill cases compared to the installation when excavation reaches the anchor level in cut cases. In fill cases the wall deformations are restricted at the anchor level from the beginning of construction. In cut cases, however, the wall can move as a cantilever until the excavation reaches the anchor level and the anchor is installed.

4.3. Wall bending moments

The bending moments along the wall height is shown in Figure 7 for varying cut/fill height percentages. The results show that the location of the wall along the slope, which affects the cut

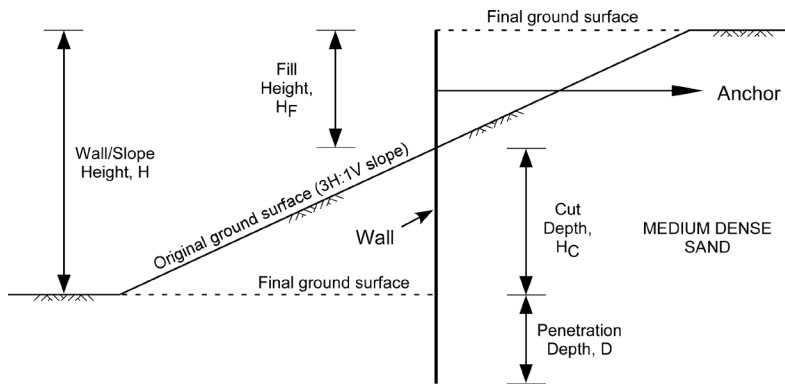


Figure 5. Schematic of conditions analyzed.

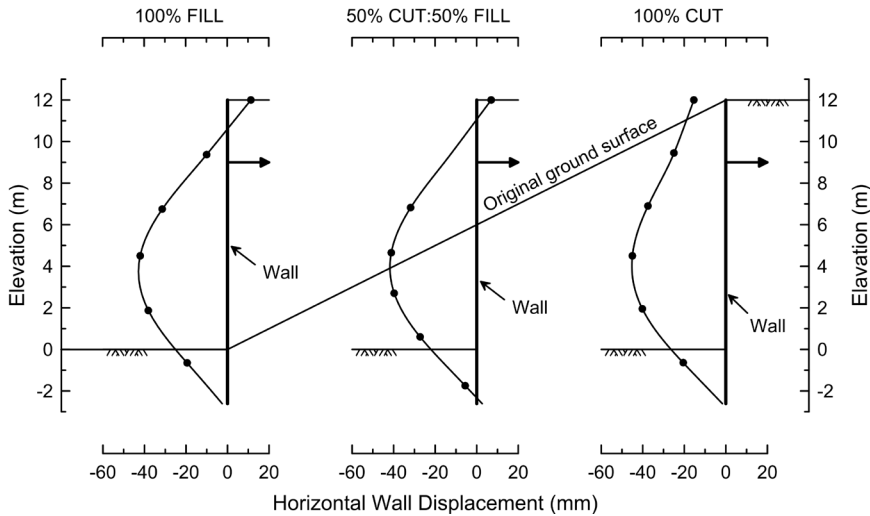


Figure 6. Horizontal wall deformations.

and fill ratios, has an effect on the bending moments. Figure 7 shows that as the amount of cut decreases and fill amount increases, i.e. as the wall location moves from the top of the slope towards the toe of the slope, the maximum moments increase. For the cases studied the increase in bending moment was approximately 14%. In addition, increased fill amounts result in moment reversal close to the tip of the wall. The results also show much higher moments, as much as three times, at the anchor level in cut case compared to fill case (Figure 7).

4.4. Anchor forces

The anchor forces obtained are shown in Figure 8. The figure shows that the location of the wall along the slope, and therefore the cut and fill

ratios, affects the anchor forces significantly. As the cut amount decreases and the fill amount increases, the anchor forces drop. There is approximately 30% difference between only cut and only fill cases. The reason of the decrease in anchor forces is related to the wall deformations. Since the anchor is installed at the beginning of the fill process, the movements are restricted at the anchor level. The stresses developed by the backfill soil cause wall tip to move outwards and rotate the wall about the anchor location. This rotation also causes wall top to move backwards as it was discussed previously and shown in Figure 6.

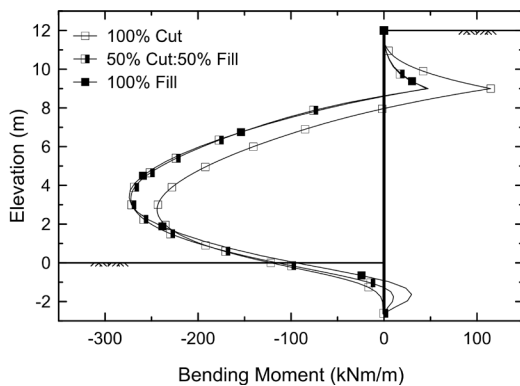


Figure 7. Wall bending moments.

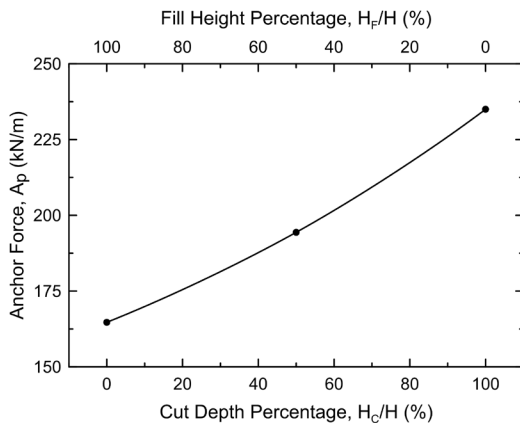


Figure 8. Anchor forces.

5. CONCLUSIONS

The overview of two parametric studies are presented in this paper. The first study investigated the effect of soft soil presence below the wall tip on floodwall (cantilever sheet pile wall) behaviour. The second study investigated the effect of wall location on a sloping ground, and resulting cut and fill conditions/quantities on anchored sheet pile wall behaviour. The results show that both conditions, soft soil presence below the wall tip and sloping ground surface, affect both soil and wall behaviour due to the soil-structure interaction.

The results show that the bending moments are not affected by the presence of soft soils below tip of a cantilever floodwall. However, wall deformations increase significantly, especially within the zone of wall penetration depth.

The results also show that the location of an anchored sheet pile wall along a slope (i.e., the

amount of cut and fill ratios) affects the anchored sheet pile wall behaviour. The increasing cut to fill ratios result in increased wall top horizontal movements towards the excavation, decreased maximum wall bending moments, increased bending moments at the anchor level, and increased anchor forces.

6. REFERENCES

- Bilgin, Ö, 2006. "Size effect analysis of full-scale floodwall tests using numerical methods." *Proceedings, Sixth International Conference on Physical Modeling in Geotechnics*, Kowloon, Hong Kong, 1389-1393.
- Bilgin, Ö, 2009. "Effect of subsurface soil conditions on floodwall behavior." *Contemporary Topics in In-Situ Testing, Analysis, and Reliability of Foundations (GSP 186). Proceedings, International Foundation Congress & Equipment Expo 2009*, Orlando, Florida, 538-545.
- Bilgin, Ö., 2010. "Numerical studies of anchored sheet pile wall behavior constructed in cut and fill conditions." *Journal of Computers and Geotechnics*, Elsevier. Vol. 37, No. 3, 399-407.
- Bilgin, Ö, and Erten, MB, 2009. "Anchored sheet pile walls constructed on sloping ground." *Contemporary Topics in Ground Modification, Problem Soils, and Geo-Support (GSP 187). Proceedings, International Foundation Congress & Equipment Expo 2009*, Orlando, Florida, 145-152.
- Brinkgreve, RBJ. et al. (ed.), 2006. *Plaxis 2D-Version 8 users manual*. Rotterdam: A.A. Balkema.
- Potts, DM and Fourie, AB, 1984. "The behavior of a propped retaining wall: results of a numerical experiment." *Geotechnique*, 34(3), 383-404.
- United States Navy, Naval Facilities Engineering Command (NAVFAC), 1986. *Design Manual, 7.02, Foundations and Earth Structures*. Alexandria, Virginia.

Seismic Soil-Interaction on Earth Retaining Structures. Performance-based seismic design of a Retaining Wall

Carlos Jurado Cabañes (Ph. D., M. Sc. in Civil Engineering)
Full Professor at the Polytechnic University of Madrid,
School of Civil Engineering
e-mail: cjurado@ciccp.es

ABSTRACT: The design of containment walls suffering seismic loads traditionally has been realized with methods based on pseudoanalytic procedures such as Mononobe-Okabe's method, which it has led in certain occasions to insecure designs, that they have produced the ruin of many containment walls suffering the action of an earthquake. A method is proposed in this paper for the design of containment walls in different soils, suffering the action of an earthquake, based on Performance-Based Seismic Design.

INTRODUCTION

The calculation of the static and dynamics pressures of a soil against a wall, as well as the displacements of it, under the action of an earthquake, can be realized by means of analytical pseudostatic, analytical dynamic methods or by means of numerical methods such as: finite differences, finite elements, etc.

For the first methods, different authors (Coulomb^[2], Rankine^[14], Newmark^[9], Richards-Elms^[15], Whitman-Liao^[18], Prakash-Rafnsson-Wu^{[11], [12]}) have developed approximations to the problem, consisting of analytical pseudostatic solutions, presenting in every case different limitations. Other authors (Wood^[19], Scott^[16], Veletsos and Younan^[17]) have obtained analytical dynamic solutions based on the theory of elastic waves.

For the numerical methods different commercial programs have been developed: SASSI^[7], PLAXIS^[1], FLAC/FLAC3D^[5], etc.

The latter programs need normally a high time of preparation of input and an important consumption of computation. On the other hand few of them allow the integration of the dynamic equations in the time domain. Another limitation is the model behaviour of the soil implemented in the program.

The analytical pseudostatic methods on the contrary, need a minor time of computer and have been implemented in the past for the

calculation of walls submitted to static actions with satisfactory results.

For preliminary studies, a computer program has been developed by means of analytical pseudostatic methods for the calculation of pressures and displacements of a gravity retaining wall, in static and dynamic conditions, under the action of one earthquake. The situations of stability are verified to sliding and overturning, warning in case of failure, to increase the dimensions of the wall.

The analysis of a gravity wall submitted to the action of an earthquake by means of the calculation of the possible permanent displacement follows the line of the method of Performance Based Seismic Design.

THE PROGRAM MUROSIS

For the analysis of the behaviour of a wall submitted to seismic actions, it have been developed the program MUROSIS based on pseudoanalytic methods, for the calculation of static and seismic pressures on the back of the wall, as well as the permanent seismic displacement, in case the maximum acceleration of the earthquake overcomes the critical acceleration (Whitman-Liao^[18], 1983).

The program calculates the total force and the moment at the base of the wall. The force in static conditions is calculated by Rankine's method or by Coulomb's method. The seismic force is calculated by Mononobe-Okabe's

$$h = \frac{E_A \cdot \frac{H}{3} + \Delta E_{AE} \cdot \frac{2H}{3}}{P_{AE}}$$

Once calculated K_{AE} , it can be obtained:

$$K_{AEH} = K_{AE} \cdot \cos \delta \quad K_{AEV} = K_{AE} \cdot \sin \delta$$

$$E_{AEH} = \frac{1}{2} \cdot \gamma \cdot K_{AEH} \cdot H^2$$

$$E_{AEV} = \frac{1}{2} \cdot \gamma \cdot K_{AEV} \cdot H^2$$

$$F_e = F_R = \mu \cdot N = (P + E_{AV} \pm E_{AEV}) \cdot \tan \phi_2$$

$$F_d = E_{AH} + \Delta E_{EAH}$$

$$M_e = P \cdot x + E_{AV} \cdot B_1 \pm E_{AEV} \cdot B_1$$

$$M_v = E_{AH} \cdot \frac{H}{3} + \Delta E_{AEH} \cdot \frac{2H}{3}$$

The safety coefficients with the action of earthquake are:

$$FSD = \frac{F_e}{F_d} \geq 1.1 \text{ and } FSV = \frac{M_e}{M_v} \geq 1.1$$

PERFORMANCE-BASED SEISMIC DESIGN OF A WALL

In a containment wall with the action of an earthquake, when the horizontal acceleration is lower than a critical or limit value a_{crit} , the wall does not suffer movement.

But, when the acceleration of the soil equals the critical or limit acceleration, the wall is in situation of imminent sliding. In this instant the total active forces due to the static and seismic pressures equal the stabilizing force due to the friction between the wall and the soil at the base.

Considering only horizontal acceleration and naming P_{AE} the total static and seismic force calculated by Mononobe-Okabe's method and by $(P_{AE})_h$ and $(P_{AE})_v$ the horizontal and vertical components of this, the horizontal and vertical balance of forces on the wall (figure 3.) gives:

$$\begin{aligned} T &= F_h + (P_{AE})_h \\ N &= W + (P_{AE})_v \end{aligned}$$

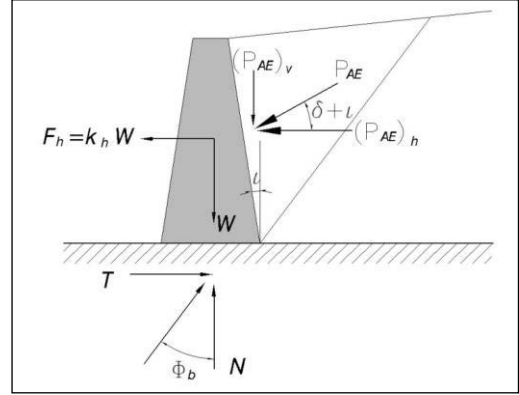


Figure 3. Seismic forces on the wall by MONONOBE-OKABE

Substituting in these equations:

$$T = N \tan \Phi_b$$

$$F_k = a_{crit} \frac{W}{g}$$

$$(P_{AE})_h = P_{AE} \cos(\delta + i)$$

$$(P_{AE})_v = P_{AE} \sin(\delta + i)$$

Where i is the inclination of the back of the wall with the vertical one and δ is the friction angle between soil and wall, obtaining the value of the limit or critic acceleration that it puts in situation of imminent sliding the wall:

$$N \tan \Phi_b = a_{crit} \frac{W}{g} + P_{AE} \cos(\delta + i)$$

$$N = W + P_{AE} \sin(\delta + i)$$

Then:

$$W + P_{AE} \sin(\delta + i) \tan \Phi_b = a_{crit} \frac{W}{g} + P_{AE} \cos(\delta + i)$$

Wherefrom:

$$a_{crit} = \left(\tan \Phi_b - \frac{P_{AE} \cos \delta + i - P_{AE} \sin \delta + i \tan \Phi_b}{W} \right) g$$

Being Φ_b the friction angle between the base of the wall and the underlying soil. In this equation P_{AE} 's value must be obtained with Mononobe-Okabe's method.

The solution of this equation must be solved by iterative form, since before to calculate P_{AE} 's value by Mononobe-Okabe's method is needed

to know the value of \mathbf{a}_{crit} , and it is necessary to proceed by trial and error.

Richards y Elms^[15] (1979) have calculated the permanent displacement of the wall when $\mathbf{a}_{max} > \mathbf{a}_{crit}$ obtaining the value:

$$D_{perm} = 0,087 \frac{V_{max}^2 \cdot a_{max}^3}{a_{crit}^4}$$

Whitman y Liao^[18] (1983) correcting Richards-Elms's simplifications have proposed the following expression for the permanent seismic displacement:

$$d_{perm} = \frac{37V_{max}^2}{a_{max}} \cdot e^{-9,4 \left(\frac{a_{crit}}{a_{max}} \right)}$$

This value must not overcome the admissible limit for the permanent displacement of the wall. If this value is exceeded, it is necessary to increase the dimensions of the wall.

ORDER FOLLOWED BY THE PROGRAM

The order followed by the program (Jurado, C.^[6]) is:

1. First it calculates the weight \mathbf{W} of the wall.
2. A previous value of $\mathbf{a}_h = \mathbf{k}_h \cdot \mathbf{g}$, will be supposed, calculating for the value of $\mathbf{a}_v = \mathbf{k}_v \cdot \mathbf{g}$, the total active force \mathbf{P}_{AE} by Mononobe-Okabe's method.
3. For this value of \mathbf{P}_{AE} it calculates the critical or limit acceleration.

$$a_{crit} = \left(tg\phi_b - \frac{P_{AB} \cos \delta + l - P_{AE} \sin \delta + l \cdot tg\phi_b}{W} \right) g$$

4. If the value of acrit differs of $\mathbf{a}_h = \mathbf{a}_{max}$ less than one prearranged value (0,001), it calculates the permanent displacement by Whitman-Liao's method according with the equation:

$$d_{perm} = \frac{37V_{max}^2}{a_{max}} \cdot e^{-9,4 \left(\frac{a_{crit}}{a_{max}} \right)}$$

5. If the value of acrit differs of $\mathbf{a}_h = \mathbf{a}_{max}$ more than the one prearranged, new intermediate value \mathbf{a}_{max} is used, follow-

ing with the process, until acrit and \mathbf{a}_{max} fulfill this condition.

6. The value of \mathbf{d}_{perm} finally calculated must be less than the prearranged limit value and in contrary the dimensions of the wall must be increased until the mentioned condition is fulfilled.

STUDIED CASES

It has been realized the seismic calculation of 16 cases of walls by means of the program named MUROSIS, using the next two types of walls:

1. Wall with 4,00 m of height
2. Wall with 6,00 m of height

In both cases the static pressures have been calculated by Coulomb's theory. The dynamic pressures have been obtained by Mononobe-Okabe and the permanent seismic possible displacements by Whitman-Liao. All the exits have been verified manually and with the bibliography to check the kindness of the results. In all cases the surface of the embankment is horizontal $\beta = 0^\circ$ and the wall has the back vertical $\alpha = 90^\circ$. The thicknesses of the wall in the base and the on the top has been selected to the specific situations of every case.

The program verifies that the safety coefficients of sliding and overturning in seismic situation fulfill the following conditions:

$$FSD \geq 1.10 \quad FSV \geq 1.50$$

The following situations have been studied for these two types of walls:

- **Wall with 4.00 m / 8.00 m of height**
 1. Without earthquake, without cohesion and without friction soil-wall
 2. Without earthquake, without cohesion and with friction soil-wall
 3. Without earthquake, with cohesion and without friction soil-wall
 4. Without earthquake, with cohesion and with friction soil-wall
 5. Without earthquake, without cohesion and without friction soil-wall
 6. With earthquake, without cohesion and without friction soil-wall
 7. With earthquake, with cohesion and without friction soil-wall
 8. With earthquake, with cohesion and with friction soil-wall

The summary of obtained results in are included in the following tables:

Table 1. Exit of results for wall of height H = 4.00 m.

Wall of 4.00 m

Wall	k_h ($k_v = 1/2k_h$)	$c_1=c_2$ (kPa)	δ (°)	B1 (m)	B2 (m)	k_{crit}	d_{perm} (mm)
1	0	0	0	1.80	1.30	0.120g	0
2	0	0	15	1.60	1.20	0.161g	0
3	0	10	0	1.50	1.20	0.083g	0
4	0	10	15	1.30	1.10	0.126g	0
5	0.10g	0	0	1.85	1.50	0.1497g	0.19
6	0.10g	0	15	1.80	1.50	0.202g	0
7	0.10g	10	0	1.60	1.30	0.1135g	1.84
8	0.10g	10	15	1.50	1.00	0.1435g	0.28

Table 2 Exit of results for wall of height H= 6.00 m.

Wall of 6.00 m

Wall	k_h ($k_v = 1/2k_h$)	$c_1=c_2$ (kPa)	δ (°)	B1 (m)	B2 (m)	k_{crit}	d_{perm} (mm)
1	0	0	0	2.70	2.40	0.1439g	0
2	0	0	15	2.30	2.10	0.1712g	0
3	0	10	0	1.90	1.70	0.050g	0
4	0	10	15	1.80	1.50	0.104g	0
5	0.10g	0	0	2.80	2.50	0.163g	0
6	0.10g	0	15	2.70	2.50	0.212g	0
7	0.10g	10	0	2.20	1.90	0.0985g	4.72
8	0.10g	10	15	2.10	1.90	0.1575g	0

CONCLUSIONS

It has been analyzed 16 cases of walls of 4.00 m and 6.00 m of height for two values of friction angle soil-wall and for two values of the cohesion of landfill, one null and other different to zero.

The analysis of the permanent seismic displacement leads to the conclusion that walls that fulfill to stability in seismic situation can have unacceptable displacements, being advisable the determination of this value in the

seismic design of a wall. This is the line followed nowadays for the "Performance Based Seismic Design".

REFERENCES

- [1] Brinkgreve, R. B. J., 2004. *PLAXIS Reference Manual* Delf.
- [2] Coulomb, C.A., 1776, *Essai sur une application des regles des maximis et minimis a quelques problèmes de statique relatives à l'architecture*. Mémoires de l'Académie Royale près Divers Savants, Vol. 7,
- [3] Fajfar P, Krawinker H., 1977, *Seismic Design Methodologies for the next generation Codes*. Ed. Balkema.
- [4] International Building Code (IBC 2006).
- [5] Itasca Consulting Group. *FLAC3D Manual*. Advance, Three-Dimensional Continuum Modeling for Geotechnical Analysis for Rock, Soil and Structural Support.
- [6] Jurado C., 2012, *Problems of Soil-Structure Interaction on Footings, and Walls of Containment. Influence of Lift-up and Sliding Phenomena*. Ph. D. Thesis. Polytechnic University of Madrid.
- [7] Lysmer, John, Ostadan, Farhang, Tabataaie, Manour, Tajirian, Frederick and Vahdani, Shahrar, 2000, *SASSI 2000- A system for Analysis of Soil-Structure Interaction*.
- [8] Mononobe, N. and Matsuo H., 1929, *On the Determination of Earth Pressures during Earthquakes*. Proceedings 2nd World Engineering Conference, Vol. 9, paper n° 388, pages 177-185.
- [9] Newmark, N.M., 1965, *Effects of earthquakes on dams and embankment*. Geotechnique, v. 15, n2, pages 139-160.
- [10] Prakash, S. and Basvanna, B. M., 1969, *Earth Pressure Distribution Behind Retaining Walls during Earthquakes*. Proceedings Fourth World Conference on Earthquake Engineering, Chile, Vol. 3, pages 133-148.
- [11] Prakash, S. and Rafnsson, E. A., 1995, *On Seismic Design displacements of Rigid Retaining Walls*. Proceedings 3rd International Conference on Recent Advances on Geotechnical Earthquake Engineering and Soil Dynamics, Vol.3, pag. 1183-1192, St. Luis, Missouri.
- [12] Prakash, S. and Wu, Y., 1996, *Displacement of rigid walls during earthquakes*. Eleventh World Conference on Earthquake Engineering.
- [13] Priestley MJN, 2000. *Performance Based Seismic Design*. New Zealand. National Society for Earthquake Engineering.
- [14] Rankine, W., 1857, *On the Stability of loose Earth* Philosophical Transactions of the Royal Society of London, Vol. 147, 1857.
- [15] Richards, R. and Elms, D. G., 1979, *Seismic Behavior of Gravity Retaining Walls*. Journal of

Geotechnical Engineering Division, ASCE, Vol. 105, N° GT4, pag. 449-464.

- [16]Scott, R. F. 1973, *Earthquake-Induced Earth Pressures on Retaining Walls*. Proceedings 5th World Conference on Earthquake Engineering, Rome, Italy, pag. 1611-1620.
- [17]Veletsos, A. S., Younan, A. H. and Bandyopadhyay, 1996, *Dynamic Response of Cantilever Retaining Walls*. Department of Advanced Technology Brookhaven National Laboratory Associated Universities Inc. Upton, New York.
- [18]Whitman, R. V. and Samson Liao, 1983, *Seismic Design of Gravity Retaining Walls*. Report to U. S. Army Engineer Waterways Experiment Station, Vicksburg, Mississippi.
- [19]Wood, John H., 1973, *Earthquake Soil-Induced Soil Pressures on structures*. Ph. D. Thesis, California Institute of Technology, EERL, 73-05, Pasadena, California.

Overview of Shells with Infill used in Geotechnical Engineering Applications

T. Chernova & Ö. Bilgin
University of Dayton, Dayton, Ohio, USA

N. Tsimbelman
Far Eastern Federal University, Vladivostok, Russia

ABSTRACT: This article describes the thin shell structures with infill which are used mainly as retaining structures. Two main types of the construction are examined: thin cylindrical shells with infill and cellular cofferdams. The application and use of these structures for different applications are discussed. The production technologies for the two types along with the sample applications are provided. The paper is proposed a rationale for the choice a theory of calculation for the cylindrical shell depending on the specified dimensions and availability and properties of the filler.

1. INTRODUCTION

Thin shell structures with infill are very rational composite civil engineering structures commonly used in waterfronts and offshore as retaining walls, breakwaters, and berth foundations. They effectively combine the benefits of low-cost infill with shell material which restrains the infill, forming a massive gravity structure. The shell component can be made up from either one large circular piece or from individual sheet piles installed to form the shell, i.e. cellular cofferdam.

The circular shell structures have been used in wide variety of applications by various industries. For instance, in mechanical and energy industry they are used for storage and transport of various liquids, such as fuel (in the form of tank, rocket body, pipeline, and solid-propellant motor). In civil engineering, they are mainly used as massive earth retaining or bearing structure, where infill occupies considerable volume of the whole structures. The infill material can be different types of soil and/or concrete. The shell is made of a more durable material, such as concrete, steel sheet piles, steel sheet, or plastic materials.

A significant increase in the production of materials and goods, such as supply of coal, oil, and natural gas, has been occurring on the global market over the years. This increase results in need of high-capacity ports and other transportation hubs. The widening of Panama Canal project is one of the great examples of the

need in the increased capacity of transportation for larger size vessels now exist. There is also a need for the modernization of existing ports and construction of new berthing facilities. Construction of man-made islands to increase the land area sometimes is the best and only viable solution for the new industrial complexes built. The thin shells with infill, with different modifications, have been utilized in these projects. Area of application of this construction can significantly expand in the future.

Thin shell construction with infill can be applied for the solution of following engineering tasks:

- allowing passage of vessels near the coastal areas and safe approach to the shore, handling operations in ports and others by building berthing, fencing and bank protection structures (Figure 1a);
- providing construction environment for culverts, crossings, bridges foundations, underground structures;
- the vertical planning of an area in industrial, civil and transport construction: design of retaining walls of large and small-piece shell element with infill (Figure 1b);
- forming construction of bridge girders and other shell elements with tubular structures with different infill, such as concrete ("pipe-concrete") and sand ("soil-concrete"); and
- supplying the strength and stability for the structures by improving subsurface.

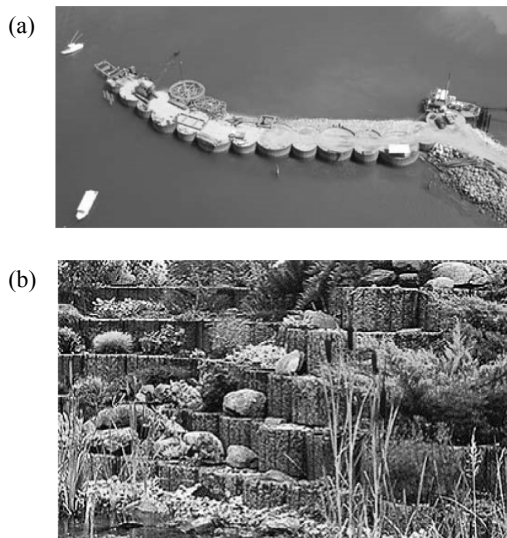


Figure 1. Examples of shells with infill: (a) breakwater in Quepos, Costa Rica¹, (b) retaining wall².

2. ADVANTAGES OF THE STRUCTURES

Composite behavior of a shell with infill provides several advantages. First, it allows distributing the external load using both of these elements. Wall of thin shell has equally distributed over the thickness (membrane) stresses, and the wall thickness of the shell is significantly reduced for perception of stresses. Second, the rational design collaboration and composite behavior action of thin shells with infill results in reduced costs of construction materials for the project. Third, although large parts of the structures' materials can exceed the elastic deformation limits and substantial displacements occur, it is possible for whole structure to continue operating safely.

3. TYPES OF THIN SHELLS WITH INFILL

The most common types of thin shell with infill, which mainly act as a gravity structure, in civil engineering applications are:

- thin monolithic steel cylindrical shells with soil infill; and

- cellular cofferdams with soil infill which are made from steel sheet piles.

While the first type of these structures are widely used in Japan, Russia, and the European Union, the second type is commonly used in the United States of America.

3.1. Thin cylindrical shells

Thin cylindrical shells consist of three main elements: thin shell, infill, and superstructure. The material used for the shell is usually steel, however reinforced concrete and some types of polymeric materials sometimes are also used. Sizing of the structure is based on the diameter, D , to height, H , ratio (D/H), which ranges from 0.7 to 0.8. The shell can be constructed rock, coarse, sandy, and clayey foundation soils (Morflot, 1978).

Thin shells are installed on a prepared stone bed or directly on the ground surface with a 1.5 to 2.5 m deep penetration into the soil. The shell is settled by installing into a prepared trench or driven through scour. The method of immersion depends on the characteristics of the foundation soil. Deepening excludes the possibility of burying ground bulging, inside the shell and its undermining. The infill material of the shell usually includes sands, gravels, cobbles, and/or boulders. Filling of the shell is carried out simultaneously with the filling of the backfill cavities with using vibratory compactors.

The superstructure of thin shell is built from reinforced concrete or prefabricated reinforced elements (Morflot, 1978). It closes any gaps exists between the adjacent shells from the water side.

As an example, thin cylindrical shell structure used in the construction of a pier in Russia (Kozmino Bay in Primorsky Region) is presented in Figure 2. This berth was made by 37 shells, each having 8 m diameter and 8 m height. The thickness of the shell was 16 mm and each shell weighed 28 tons.

¹ From <http://palplanches.arcelormittal.com/projects/display/title/Quepos>

² Information was taken from website <http://www.rcp.com.gh/>

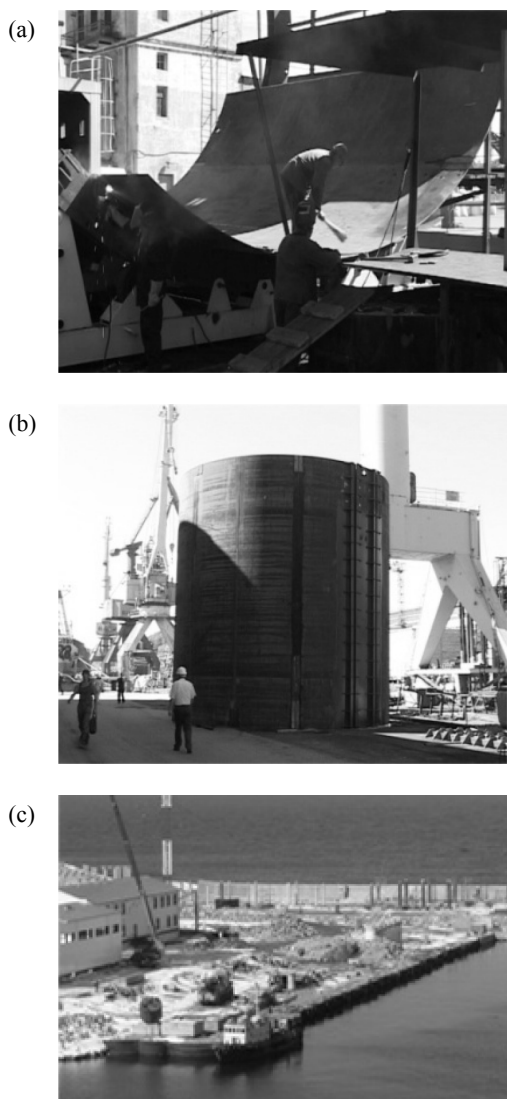


Figure 2. Thin cylindrical shell in Kozmino Bay, Russia: (a) and (b) manufacturing process of steel shell, (c) installation of the shells³.

3.2. Cellular cofferdams

The cellular cofferdams are commonly used in the United States and in several countries in Asia. They are built by using steel sheet piles and driving them next to each other. Cellular cofferdams are used as both temporary and permanent earth and water retaining structures. Temporary ones are mainly used to provide dry conditions inside them to allow construction.

Depending on the layout and design requirements cellular cofferdams are divided into three main groups:

Diaphragm cells: They are arranged by connecting individual straight segments or cylindrical arches (Figure 3). The resulting curve elements have the same radius along the entire length of the projected structure and connected to each other at an angle of 120° . Excavation and filling of shells along the entire length of the berth is done in layers (1.5 m in height) in order to avoid deformation of the sheet piles. Installing shell is closely dependent on already immersed shell because the deviation from the design level of a single shell can lead a deviation of the entire series. This type of cofferdam is commonly used for relatively small sizes (height to width ratio of less than one).

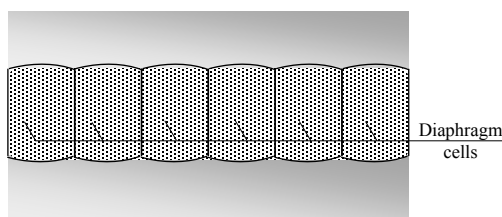


Figure 3. Schematic of diaphragm cells.

Circular cells: They include semicircular or complete circular cells combined by curved sections (Figure 4). These types are arranged by connecting the individual curvilinear segments at an angle of $30-45^\circ$ to form a detached circular cofferdam (Arcelor Mittal, 2009). The process of excavation and filling each shell is independent of the filling operation of adjacent shells. These cofferdams are commonly used for height to width ratios of 1 to 1.5. Circular cell cofferdams are the most common type of due to relative ease of construction which can significantly reduce the construction time resulting in cost savings.

³ From <http://kaskad.vtn.ru/news/964/>

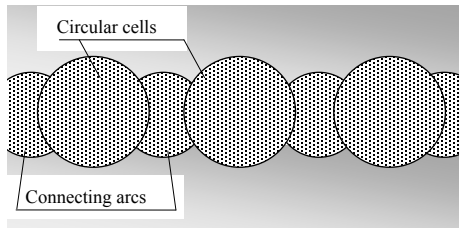


Figure 4. Schematic of circular cells.

Cloverleaf cells: These cofferdams have four curved segments connected to each other at an angle of 120° (Figure 5). Each cloverleaf cell is connected to the next cells by arcs. They are commonly used as corner cells and also their increased base width and large mass is good when the sliding or overturning is a concern. The individual shells can be constructed independently, but the level between the adjacent cells during infilling process should not exceed 1.5 m. This type of cells is relatively difficult to construct and expensive. They also create very large shell widths.

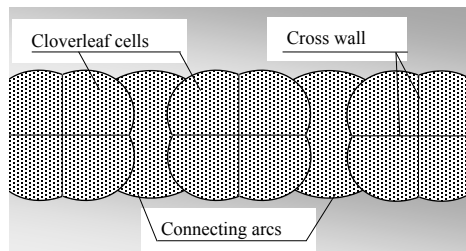


Figure 5. Schematic of cloverleaf cells.

Installation of cellular cofferdam shell consists of several stages:

- installation of bracing frame (Figure 6) to the design level;
- installation of sheet piles forming a circular shell. Depth of pile penetration depends on the properties of foundations soil (Arcelor Mittal, 2010). Each sheet piles has own number for correct dipping into the cofferdam;
- excavation of soil inside the shell to the design depth; and
- filling of the shell in lifts with sands and gravels. The lifts are placed in 1.5 m thick-

nesses and compacted by using vibrating compactors.

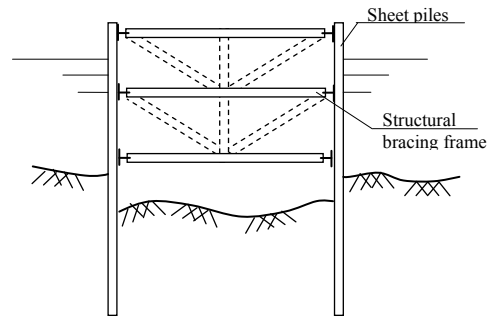


Figure 6. Schematic of circular cell installation.

As an example, cellular cofferdam used in Kentucky Dam Lock Addition project is presented in Figure 7. The project included construction of three 30 m diameter circular sheet pile cells with connecting arc-cells, and a sheet-pile land-side tie-in wall.

There are several factors should be taken into consideration when selecting the type of thin shell with infill (thin cylindrical shell or cellular cofferdam) for a specific project as listed in the following:

- experience of the company and availability of the necessary equipment;
- availability of the construction materials and production facilities;
- costs associated with the project location and necessary infrastructure; and
- optimally adapted to the project construction and operation conditions.

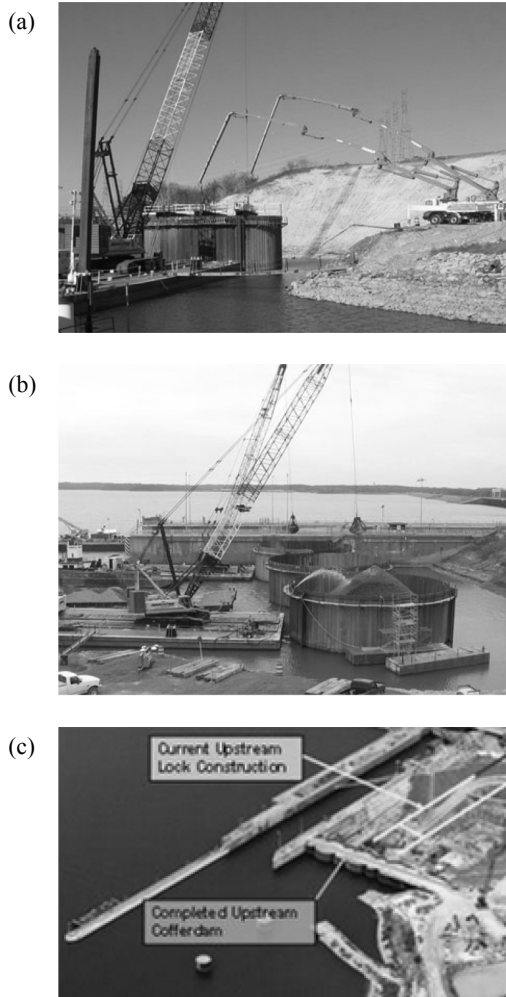


Figure 7. Cellular cofferdam Paducah, Kentucky, U.S.A.: (a) and (b) manufacturing and filling process of circular cellular cofferdam, (c) project overview⁴.

4. DESIGN CONSIDERATIONS

From the engineering design point of view several factors and constraints play a key role in selecting the thin circular shell type for a project. These factors allow choosing the best solution depending on the site conditions and future operating parameters of the structure and they can be listed as:

- subsoil conditions;
- availability of materials and equipment;
- dimensions of the shell construction; and
- construction conditions.

4.1. Subsoil conditions

Thin shells with infill are usually constructed in difficult geotechnical conditions of coastal zones where the upper soil layers are weak and the load are needed to be transferred to solid support layers. One of the important considerations in the design of these structures is the hydraulic analysis of seepage conditions and erosion of the bottom when built in streams or rivers. Thin cylindrical shells are installed usually on a specially prepared solid base which is not always possible because of the complexity of underwater works.

4.2. Availability of materials and equipment

Availability of materials and equipment sometimes is the main determining factor in choosing the type of shell construction. Thin cylindrical shell or its parts are a unique type of construction, which are made at the factory to order and delivered to the construction site by using large-sized land or water transportation. An absence or remoteness of factories increases the costs and duration of the project. In these situations, the cellular cofferdam would be the better solution. The steel sheet piles used in cellular cofferdams are selected from the available sizes determined from the design calculations. The piles are delivered to the construction site in a relatively shorter time, because it is a routine process and does not cause difficulties.

4.3. Dimensions of the shell construction

The thin shells in most cases are made in the form of a cylinder and they are installed next to each other in a straight line or circular arrangement. Each shell connected to the adjacent shells by arc segments which are made with the same or different radius compared to the cylindrical shell radius (Figure 2). Using different set of whole thin shells is quite limited. On the other hand, cellular cofferdams can be arranged in various configurations depending on the need and desired configuration of the future structure (Figures 3, 4, 5, and 7). The technology used in cellular cofferdams allows construction of shells with diameters up to 30 m (Design & Execution Manual, 2009). These size diameters cannot be

⁴ From <http://www.cjmahan.com/static/upstream.php>, <http://www.lrn.usace.army.mil/Missions/CurrentProjects/Construction/KentuckyLockAdditionProject.aspx>

possible with thin cylindrical shells, which are limited to maximum of approximately 20 m diameter (Manual 31.3013-77, 1978).

4.4. Construction conditions

Retaining structures made thin cylindrical shell are more applicable in case when the construction is conducted under water: where the main components of cellular cofferdam (sheet piles) cannot be installed into the deep soil layer (Gurevich, 1969).

5. CALCULATION MODELS

Cellular cofferdams are not rigid gravity structures and therefore it is not possible for them to fail by overturning stability mode. The structures would fail due to the pulling out of individual sheet piles and loosing the infill soil before the cofferdam could reach moment equilibrium for overturning. Cellular cofferdams should be designed for the sliding and bearing capacity failure. In addition, both sliding and overturning stability modes for deep-seated failure should also be checked during the design and the structures should be designed accordingly. The cellular cofferdams also need to be designed considering the internal cell stability conditions, such as pile interlock tension and pulling out of piles to resist overturning.

Fundamentals of the theory of thin cylindrical shells laid in the 1940s (Vlasov, 1962; Zhemochkin, 1951; Timoshenko, 1966), and further developed later in relation to the various areas of activity (Cummings, 1960; Fedorov and Titova, 1952; Kalaev, 1954; Khristoforov, 1964; Ovesen, 1962). Investigations on the theory of shells with an internal elastic array (filler) are well developed in the calculation and design of solid motors (Summerfield, 1963).

Calculation model of the thin shells and cellular cofferdams are based on the same basics of the theory of shells. Usually, the stress-strain state of the infill is modeled as an elastic body which treats the filler as a homogeneous medium, where there is a linear relationship between stress and strain.

Depending on the size, material properties, and loading conditions various computational models can be used for the shells, based on the three main possible types of stress-strain state of the structure: the membrane (Biederman, 1977;

Gurevich, 1969), half-membrane (Vlasov, 1962) and moment state (Tsurpal, 1988).

The behavior of a shell of large diameter with infill is best described by using half-membrane theory, for which there are approximate numerical methods developed (Cummings, 1960; Ovesen, 1962; Vlasov, 1962).

Increasing the wall thickness of the shell diminishes the influence of infill's strengthening the shell, but provides stability by increasing the weight of the shell. As a result, a certain thickness of the shell can be calculated by a simple cantilever beam scheme.

Calculation theory of the cylindrical shells depending on the specified radius of the shell, R , to the wall thickness of the shell, δ , ratio (R/δ) and the availability of infill offers a solution for quick selection. Further, it provides an analysis of appropriateness during the preliminary design stages of a thorough half-membrane theory and simplified moment theory for the closed cylindrical shells with infill depending on their size.

The calculations have been carried out using two approaches, moment theory (it was calculated for cantilever beam rigidly fixed to the base) and half-membrane theory (the finite element method was used for the shell that is rigidly fixed to a base with the account of the effect of soils infill). The maximum stresses in the most loaded areas of the structure have been chosen for the analysis of results.

As a result, the ratio of normal stresses in the compressed zone of the structure (which were calculated by half-membrane theory) to the stresses of the cantilever under the simplified scheme were determined for the test dimension ratios. The equation for the ratio is given as $\Delta = \sigma_1 / \sigma_2$ (where, σ_1 is the stress of the cylindrical shell from half-membrane theory and σ_2 is the stress of the cantilever beams from the "simplified" calculate moment scheme).

In the final stage, the range of the shell size, for which it is acceptable to use the "simplified" calculate moment scheme was defined (Figure 8).

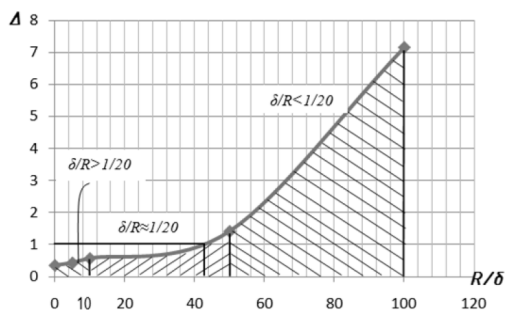


Figure 8. Comparison of shell stresses calculated using two different design schemes depending on the size of the shell.

The summary of the applicability of theories of calculation for varying R/δ intervals obtained are given in the following:

- at a ratio of R/δ ranging from 1 to 10, shell structure can be considered under the simplified beam theory (calculated as cantilever beams annular section) and should take into account the existence of a large stock of the bearing capacity ($\Delta \approx 0.4$ to 0.6);
- at a ratio of R/δ ranging from 10 to 50, the stress-strain state of shell can be determined by beam theory, while for $R/\delta \approx 50$ stresses defined by the beam theory are closer to the stresses resulting from settlement half-membrane theory;
- for $R/\delta > 50$, calculation based on the beam theory cannot be applied; and
- for a range of $R/\delta > 50$, which is the case for the thin cylindrical shells and cellular cofferdams, half-membrane theory of calculation should be applied even for the preliminary calculations.

6. CONCLUSIONS

Shell structures with infill, such as thin cylindrical shells and cellular cofferdams, are widely used in the construction for a solution of different engineering problems. Depending on the operating conditions, the ratio of the main dimensions of construction, and characteristics of the foundation soil, particular type of shells with infill are preferred and corresponding appropriate theory of calculation is used.

In this article the design conditions that would play a role in determining the type of shells have been discussed.

A solution for the selection of theory for preliminary calculations for the shells is provided. This decision depends on the ratio of shell's main dimensions, radius and wall thickness. Comparative calculations were performed. The ranges of the radius to the wall thickness of the shell ratio for different calculation schemes (cantilever beam or for model taking into account the half-membrane stress-strain state) are shown.

Research analysis of the shell structures shows necessity of formation a common calculation method that would create the conditions for a wide range of the shell constructions with infill for civil engineering projects, such as retaining structures, as well as in solving problems in other fields where thin shells with infill are used.

Theory of calculation should be based on an analysis of the joint work and composite action of a shell with infill, should take into account the edge effects, and should preserve performance of the shell structures under static and dynamic loads.

7. REFERENCES

- Arcelor Mittal Commercial RPS 2009. Design & Execution Manual AS 500 Straight Web Steel Sheet Piles. *Luxembourg*. 60 p.
- Arcelor Mittal Commercial RPS 2010. Sheet Piling Handbook, 3rd edition. *Luxembourg*. 60 p.
- Biderman VL. 1977. "Mechanics of thin-walled structures. Static" *M.: "Engineering"*, 488p.
- Cummings, EM 1960. "Cellular Cofferdams and Docks." *American Society of Civil Engineers, Transaction*.
- Fedorov, IV and Titova, VI 1952. "Cellular Structures from Metal Rabbet." *M*.
- Gurevich VB. 1969. "River port waterworks". *M*. 416p.
- Kalaev, AI 1954. "On the Resistance to Sag Fenced Ground Arrays." Report of the VNIIG after B.E. Vedeneev. *M*.
- Khrstoforov, VS, Meleshko, RG, et al 1964. "On the Analysis of Pile-Lane Construction on the Results of Field Tests." *L*.
- Morflot. 1978. "Manual for Calculation of Marine Hydraulic Structures from the Shells of Large Diameter." *Manual 31.3013-77*. 30 p.
- Ovesen, NK 1962. "Cellular Cofferdams, Calculation Methods and Model Tests." Bulletin 14, Danish Geotechnical Institute. *Copenhagen, Denmark*.

- Summerfield M. 1963. "Investigation solid propellant rocket engine." *M.*: IL, 440p.
- Timoshenko SP, S. Voynovskiy-Krieger 1966. "Plates and Shells". *M.* 632p.
- Tsurpal A. 1988. "Resistance of Materials. Laboratory work". Textbook. Manual for schools. *K.*: High School. 245p.
- Vlasov, VZ 1962. Selected Works, Publishing House of Academy of Sci. *USSR*, Vol, I.
- Zhemochkin, BN 1951. "On the Design of Cellular Structures." Investigations on the Theory of Elasticity, *Issue V*.

Investigation on Effects of Tire Crumb Cushion on Seismic Performance of Retaining Wall

Ayşe Edinçliler & Yasin Sait Toksoy

Boğaziçi University, Kandilli Observatory and Earthquake Research Institute, Department of Earthquake Engineering, İstanbul-Turkey

ABSTRACT: The objective of this study is to examine whether the new proposed tire waste cushion material can reduce the load and restricting the permanent displacement of retaining structures during earthquakes by using the compressibility, the ductility and the energy absorbing capacity of the tire wastes. This paper presents a series of numerical studies to investigate the use of compressible tire crumb material to attenuate dynamic loads against rigid retaining wall structures. Three different widths tire crumb cushions retaining a sand backfill were analysed under a real earthquake record. The results are compared with an identical retaining structure without a seismic cushion.

1. INTRODUCTION

Tire wastes (TW) are evaluated in many different engineering applications due to their convenient engineering properties such as thermal insulation, permeability, compressibility, stiffness and also high damping. A further reason to such convenience is their differentiated sizes and shapes. Tire wastes were mainly used in landfill construction and operations, landfill closures, alternative daily covers, leachate collection systems, gas venting systems, septic system drain fields, subgrade fill and embankments, backfill for walls and bridge abutments, subgrade insulation for roads, vibration dampening layers (STMC, 2010). Tire wastes are used in geotechnical applications as lightweight fill, embankment fill, and retaining wall backfill. Recently, a new seismic buffer proposed to use tire wastes as energy absorption material due to its enhanced damping and stiffness properties compared to sand itself.

Scrap tires can be managed as whole, slit, shred, chip, ground, or crumb rubber according to transformation by means of a mechanical size reduction process into a collection of particles, with or without a coating of a partitioning agent to prevent agglomeration during production, transportation, or storage. For most practical purposes, tires and tire products function as homogeneous mixtures, but processing can impact physical characteristics as size and shape are altered and as reinforcing wire and fabric are removed (Edinçliler, 2007). Using tire

wastes in construction requires an awareness of the properties and the limitations associated with their use. Edinçliler et al. (2010) investigated the influence of processing techniques on the mechanical properties of tires wastes. They found that the three factors as normal stress, processing techniques, and the tire waste content significantly affect the mechanical properties of the processed tire wastes. Typical processed tire wastes generally used in civil engineering applications is given in Figure 1 (Edinçliler et al., 2010).

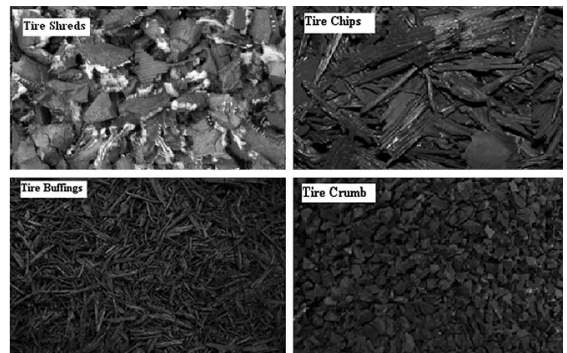


Figure1. Typical shapes of different processed tire wastes (not to scale) (Edinçliler et al., 2010)

Geotechnical structures, such as retaining structure, are key elements of ports and harbors, transportation system lifelines, and other infrastructural facilities. These structures are likely to suffer excessive deformation or damages

resulting from the increased earth pressure during the earthquake. It is necessary to implement a cost effective technique to retrofit such structures, hence enhancing their seismic performance. Inclusion of vertical compressible layers called as cushion can be a solution to increase the stability of the retaining structures in seismic regions. One function of the cushion is to reduce the load against the structure, due to energy absorption capacity of the cushion material. Another function is to curtail permanent displacement of the structure due to inherited flexibilities derived from using such elastic and compressible materials (Hazarika et al., 2008).

The use of vertical compressible layers placed against rigid soil retaining wall structures to reduce lateral static earth pressures has been reported in the literature by different researchers (Partos and Kazaniwsky, 1987; Horvath, 1997; and Karpurapu and Bathurst, 1992). In the literature, two different compressible materials as expanded polystyrene (EPS), which is called geofom and tire wastes (tire chips and tire shreds) to attenuate earthquake-induced dynamic earth pressures against rigid walls were studied.

An innovative cost-effective disaster mitigation technique was developed using tire chips, the emerging geomaterial, which can be utilized as a seismic performance enhancer of geotechnical structures (Hazarika et al., 2008). This research was explained as an attempt towards developing an environmentally friendly earthquake resistant technique that has a reasonably good balance of cost and performance, for improving the seismic performance of waterfront retaining structures. The function of the tire chips cushion is to reduce the load and restricting the permanent displacement of such waterfront retaining structures during earthquakes by exploiting the compressibility, the ductility and the energy absorbing capacity of tire chips.

The concept of reducing static earth forces against rigid wall structures by placing a compressible vertical inclusion between the wall and the backfill has been demonstrated using small-scale laboratory tests. Reduced-scale physical models using shaking table tests have since demonstrated quantitatively that the technique (used a high compressibility sponge material to create the compressible layer Hazarika et al., 2003; Zarnani et al., 2005; Bathurst et al., 2007; Zarnani and Bathurst,

2007). Hazarika et al. (2003). The tests by Zarnani and Bathurst (2007) and Zarnani et al. (2005) have demonstrated that peak lateral loads acting on the compressible model walls during simulated earthquake loading were reduced by as much as 40% of the value measured for the nominally identical structure but with no compressible inclusion (Zarnani and Bathurst, 2008).

Parametric studies using a finite element model (FEM) code to model rigid wall structures with a compressible inclusion have been reported in the literature for the static loading case by Karpurapu and Bathurst (1992). Ravichandran and Huggins (2014) investigated the performance of retaining wall backfilled with shredded tires by applying design earthquake acceleration-time histories using Plaxis Software and compared with that of sand backfill. Results show that the shredded tire backfill significantly reduces the wall tip deflection and maximum shear force and bending moment along the wall.

The protective cushion layer should provide flexibility, and thereby stability to the structures during earthquakes by absorbing the energy. This study aims to use a new potential seismic cushion as tire crumb material in minimizing structural hazard of retaining wall during earthquake loading by making good use of the lightweight, compressible, and ductile characteristics of the material. This paper describes the numerical study to investigate the use of compressible tire crumb (TC) cushion to attenuate dynamic loads against rigid retaining wall structures. The effects of three different widths TC cushions retaining a sand soil were analysed under real earthquake record. The results of numerical simulations are compared to an identical retaining wall without a cushion.

2. NUMERICAL STUDY

The aim of this study is to increase the static and dynamic performance of retaining structures. To do so, a cantilever type of retaining wall with a TC cushion is modelled by a finite element program called Plaxis. Due to the lightweight of the material and high energy absorption properties, the cantilever type retaining wall is expected to perform better both under static and dynamic loads. The protective cushion layer was placed at different widths for a better understanding of the performance effect

on the retaining structure. During the experiments, the width of the protective cushion layer was selected as 0.5m and 2.0m for different cases.

2.1 Materials

The sand used during the study is named as “Silivri Sand” which is locally found around Istanbul region and it is commonly used for highway embankments. According to the USCS system, the sand material is classified as poorly graded sand (SP) with C_u : 2.29 and C_c : 1.1 (Cağatay, 2008)

In this study, a new cushion material as tire crumb is proposed to use as a compressible material behind the retaining wall. Crumb rubber, also referred to as ground rubber, is a wire-free fine rubber particle made by size reduction from scrap tires. Various size reduction techniques can be used to achieve a wide range of particle sizes down to 600 μm or less. Crumb rubber has been successfully used in a number of civil engineering applications. Crumb rubber can be considered as lightweight aggregate source due to its low specific gravity, which distinguishes it from other recycled aggregate sources (Pierce and Blackwell, 2003).

Tire crumb used in this study is a granular material and it is obtained by processing scrap tires. Tire crumb used in this study is purchased from a local company in Istanbul (Figure 2). The tire crumb used in the experiments has an aspect ratio of 1-1.5. The grain size distribution curve of tire crumb is represented in Figure 3.

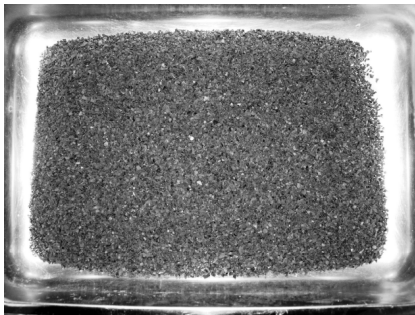


Figure 2. Tire crumbs used in this study.

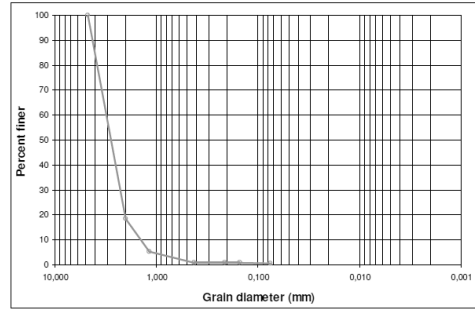


Figure 3 Grain size distribution of tire crumbs.

2.2. Numerical Model

Numerical studies are performed using the finite element modelling software PLAXIS D 2012. PLAXIS is a trusted multi-purpose finite element modelling program which enables to model various types of real geotechnical applications. Since there is no circular element in the models, plane strain model is used for the geometries instead of axisymmetric model. In this study 15-node triangle is selected as recommended in the manual which provides very accurate and detailed stress results for complex problems.

The retaining structure is modelled as a cantilever retaining structure with the dimensions of H:5m and L:3m. The retaining wall is modelled as a plate element. For the dynamic analysis, prescribed displacement is introduced to simulate the desired earthquake motion. And due to prevent unexpected spurious wave reflections at the boundaries of the model, absorbent boundaries are applied to the model. The cantilever retaining wall model is represented in Figure 4.

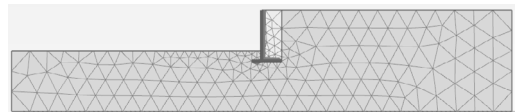


Figure 4. Cantilever retaining wall model

The hardening soil model was selected to define the material used for the model. The hardening soil model is an advanced model in order to simulate the behavior of different kinds of soils. The hardening soil model considers both shear hardening and compression hardening situations that is why it is also named as isotropic hardening.

In this study, Silivri Sand is used as a back-fill material and tire crumbs is used as a protec-

tive cushion. The protective cushion is placed along the right part of the foot (W=2m). The material properties are taken from previous studies with the same kind of sand. Input parameters for Silivri Sand and tire crumbs are represented in Table 1, below.

Table 1. Input parameters of materials for hardening soil model

	Sand	Tire Crumb
γ_{unsat}	16.5kN/m ³	6.5kN/m ³
c'_{ref}	0kN/m ²	14kN/m ²
ϕ	33°	24°
ψ	8°	0°
E_{50}^{ref}	13560kN/m ²	900kN/m ²
E_{oed}^{ref}	13560kN/m ²	900kN/m ²
E_{ur}^{ref}	40680kN/m ²	2700kN/m ²

Dynamic analysis were performed using the real record of the 1940 El Centro earthquake. Input ground motion is represented in Figure 5.

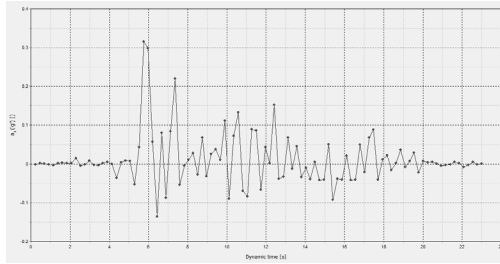


Figure 5. Input ground motion

3. NUMERICAL RESULTS

Table 2 represents shear forces and bending moments acting on the wall for three different cases. It is seen that TC cushion are capable of reducing the lateral forces acting on the wall. When there is no protective cushion layer on the model, the maximum shear force is measured as 55.55kN/m, but due to the material properties of this lightweight fill, the shear force is reduced by 14.6% to 47.43kN/m when only 0.5m layer is applied to the model. The reduction of the shear force is significant when W:2m of cushion layer is considered. This time, the maximum shear force was reduced by 30.8% to 38.44kN/m. Bending moments also decreases when the horizontal loads are reduced. In the no cushion case, the bending moment of the retaining wall model was measured as

101.4kNm/m and in the W:0.5m cushion case, the same value is 92.2kNm/m, which equals to a 9.1% reduction. And, finally when W:2m of TC cushion is placed beside the wall, the maximum bending moment acting on the wall model is 79.50kNm/m. It is understood that this lightweight protective cushion layer reduces the bending moments of the system up to 21.6%.

Table 2. Shear Forces and Bending Moments acting on the Wall

	Shear Force	Bending Moment
No Cushion	55.55kN/m	101.4kNm/m
W:0.5m Cushion	47.43kN/m	92.2kNm/m
W:2.0m Cushion	38.44kN/m	79.50kNm/m

Under static load conditions, the maximum displacement value of the model without cushion is 4.1cm (Figure 6). And under dynamic loading, the same measurement is 57cm but this value occurs at the boundary region. However, the maximum displacement value in the backfill is determined as 35cm (Figure 7). By means of factor of safety (FS), after the earthquake excitations, the FS value of the model decreased from 1.41 to 1.32.

As can be seen in Figure 8, the model with W:2m cushion displaces 2.7 cm under static loads. Similarly, 55 cm of total displacement value under dynamic conditions is concentrated at the boundary level. The displacement in the backfill region is restricted to 30cm (Figure 9). Cushion application can significantly increases the FS values of the systems. FS values before and after earthquake excitations are 1.72 and 1.62, respectively. These values are greater than the minimum required FS value for dynamic analysis, which is 1.2.

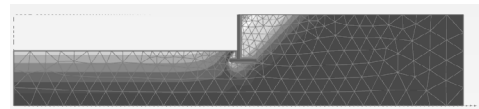


Figure 6. Total Displacement Contours of Model with No Cushion Under Static Loads

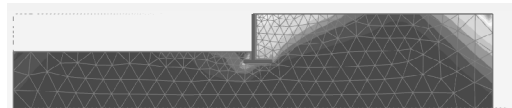


Figure 7. Total Displacement Contours of Model with No Cushion Under Dynamic Loads

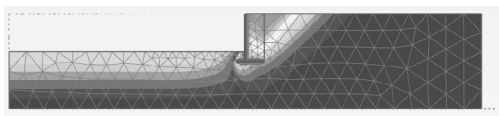


Figure 8. Total Displacement Contours of Model with W:2m Cushion Under Static Loads

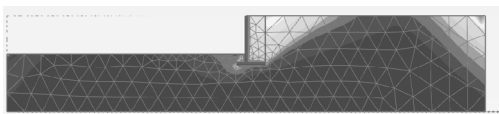


Figure 9. Total Displacement Contours of Model with W:2m Cushion Under Dynamic Loads

4 CONCLUSIONS

In this study, an earthquake resistant technique for a retaining wall is proposed that involves the use of tire crumbs-scrap tire derived material as a cushion between the backfill soil and the structure. The performance of retaining wall with TC cushion is investigated by applying design earthquake acceleration-time histories using PLAXIS software and compared with that of only sand backfill. Results show that the TC Cushion inclusion significantly reduces the maximum shear force and bending moment along the wall. Inclusion of the lightweight tire crumbs as cushion material can reduce the lateral load on retaining walls allowing for a more economical wall design.

5. REFERENCES

- Bathurst, R.J., Zarnani, S., Gaskin, A., 2007. Shaking table testing of geofoam seismic buffers. *Soil Dynamics and Earthquake Engineering*, Vol. 27, No.4, pp.324–332.
- Cagatay, 2008, Investigation of the effect of tire waste inclusions on the shear strength parameters of sand, MSc Thesis, Boğaziçi University (in English).
- Edinçliler, A., Baykal, G., and Saygılı, A., 2010. Influence of different processing techniques on the mechanical properties of used tires in embankment construction, *Waste Management*, Vol. 30, pp.1073–1080.
- Edinçliler, A., 2007. Using waste tire–soil mixtures for embankment construction. In: *International Workshop on Scrap Tire Derived Geomaterials “Opportunities and Challenges”*. Kanto Branch of Japanese Geotechnical Society, pp. 319–328.
- Hazarika, H., Kohama, E., and Sugano, T. (2008). Shaking Table Tests on Waterfront Structures Protected with Tire chips Cushion, *Journal of*

Geotechnical and Environmental Engineering, ASCE, pp.134–11.

Hazarika, H., Okuzono, S., Matsuo, Y., 2003. Seismic stability enhancement of rigid nonyielding structures. In: *Proceedings of the 13th (2003) International Offshore and Polar Engineering Conference*, Honolulu, HI, USA, 25–30 May 2003, pp. 1244–1249.

Horvath JS. 1997. Compressible inclusion function of EPS geofoam. *Geotextiles and Geomembranes*, Vol.15, No.1–3, pp.77–120.

Karpurapu R, Bathurst RJ. 1992, Numerical investigation of controlled yielding of soil-retaining wall structures. *Geotextiles and Geomembranes*, Vol.11, pp.115–31.

Ravichandran and Huggins, (2014), Applicability of Shredded Tire Chips as a Light Weight Retaining Wall Backfill in Seismic Regions Geo-Congress 2014 Technical Papers, pp.3336-3505.

Partos AM, Kazaniwsky PM. 1987. Geoboard reduces lateral earth pressures. In: *Proceedings of Geosynthetics’87*, Industrial Fabrics Association International. New Orleans, LA, USA, pp. 628–39.

Pierce, C.E., Blackwell, M.C., 2003. Potential of scrap tire rubber as lightweight aggregate in flowable fill. *Waste Management*, Vol. 23, pp.197–208.

Scrap Tire Management Council, 2010. Used Tire Facts and Information - What To Do With All These Tires?’, <http://www.epa.state.il.us/land/tires/used-tires-facts-and-information.html>.

Zarnani, S., Bathurst, R.J., 2007. Experimental investigation of EPS geofoam seismic buffers using shaking table tests. *Geosynthetics International*, Vol.14, No.3, pp.165–177.

Zarnani, S., Bathurst, R.J., Gaskin, A., 2005. Experimental investigation of geofoam seismic buffers using a shaking table. In: *Proceedings of the North American Geosynthetics Society (NAGS)/GRI19 Conference*, Las Vegas, NV, USA, pp.11.

Zarnani, S., and Bathurst, R.J., 2008, “Numerical Modelling of EPS Seismic Buffer Shaking Table Tests, *Geotextiles and Geomembranes*, Vol.26, pp. 371– 383.

Shoring-structure interaction in stabilization of excavation adjacent to historic buildings - A Case Study

Hamidreza Elahi

Assistant Professor, Dept. of Civil Engineering, Univ. of Science and Culture, Iran

Mohsen Sabermahani

Assistant Professor, School of Civil Engineering, Iran Univ. of Science and Technology, Iran

Hesam Vahidifard

Senior expert at Samanpey Soil Improvement Services Co, Iran

ABSTRACT: This paper deals with the assumptions and analyses used to stabilize the excavation of holy Alavi courtyard located in Iraq. Numerical modeling of the problem is performed using PLAXIS software. Due to the connection of the main structure to the retaining system which consist of multi strand cable anchored concrete piles, the interaction between the structure inside the excavation and the retaining structure has been taken into account and its amounts has been investigated based on different scenarios for retaining system connection to the structure. Accuracy of the analysis is evaluated through comparing with actual displacements derived from monitoring of the excavation face during construction and useful conclusions are drawn.

1. INTRODUCTION

Stabilization of the excavations proximate to the historic buildings is very sensitive and complex in comparison with similar projects being carried out in ordinary urban conditions. The project described in this paper is related to the holy Alavi courtyard development project in Najaf city being accomplished by constructing the courtyard of Hazrat Fatima in an area about 62000 m² and excavation depth equal to 15.5 m (Fig. 1).

As seen in figure 1, northern and southern faces of excavation, are in close proximity to some hotels and inns separated by a local street. In addition, the excavation is adjacent to Hazrat Ali shrine form the east and its western face is restricted to a street. This paper is primarily focused on stabilization of the eastern face of excavation located adjacent to the historic structure of Hazrat Ali shrine (whose antiquity spans more than 400 years).

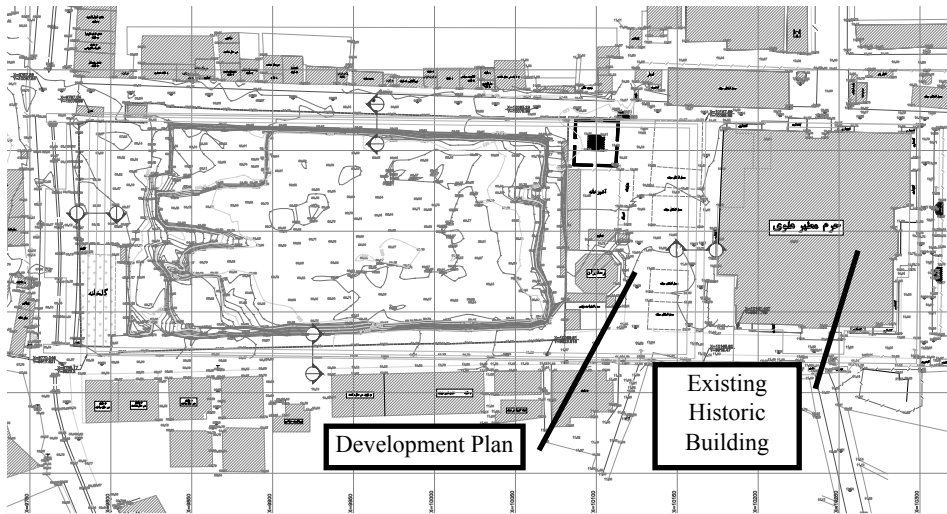
Anchorage and piling is the method selected to stabilize the face of excavation adjacent to the historic structure. In this method, anchor elements provide axial and pre-stressed force in excavation face and vertical pile elements are employed as lateral bearing elements. Additionally, the piles cause integration in the performance of anchors. Horizontal elements known as walers are also used among the piles to provide proper integration of the system.

In this method, after constructions of piles and the first excavation lift, anchors are in-

stalled in the pre-drilled holes and required design load is mobilized along them. The process of excavating and installing the anchors proceeds until the excavation depth reaches to the required level. Some of the details of stabilization plan as well as photos of this method in the current project are shown in Figures 2 and 3, respectively.

Some of the key benefits of this method are as follows:

- Providing a suitable working space inside the excavation without restrictions
- Performing tensile test and ensuring proper performance of all reinforcing and stabilizing elements
- Providing an almost rigid wall by in-situ concrete piles and solving the problems of instability raised by the existence of voids, cavities and spaces to do with the old adjacent structures
- Providing behavioral integration among anchors due to the presence of piles
- Appropriate factor of safety against global and sliding overturn of the excavation face
- To better control deformations of the excavation face adjacent to the buildings sensitive to deformation



KEY PLAN:

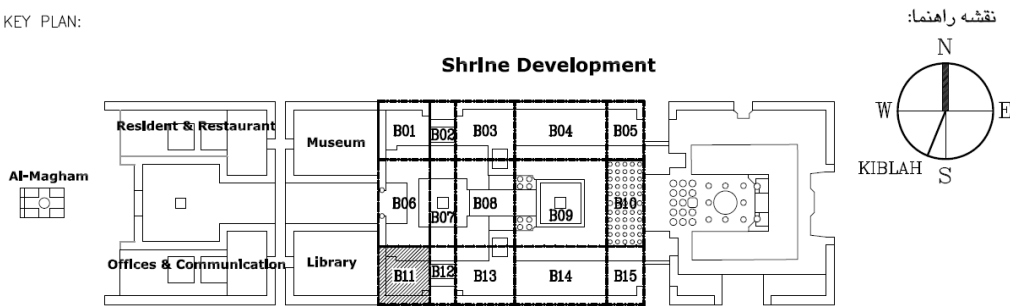


Figure 1. (top) Layout plan of the excavation in project site, (bottom) Layout plan of the blocks in the courtyard of Hazrat Fatima [1]

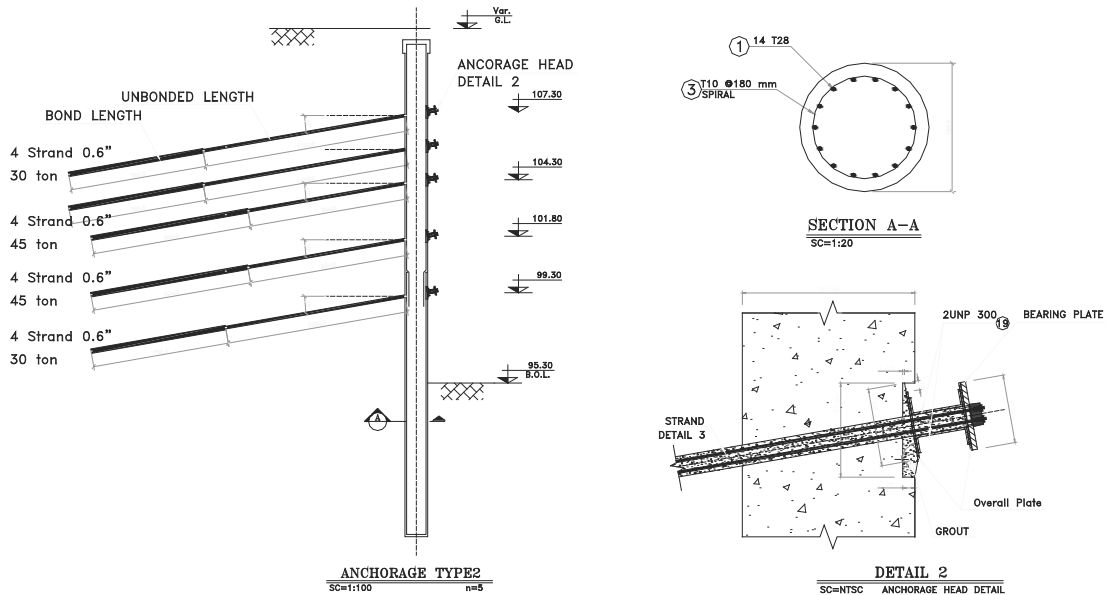


Figure 2. Some details of the stabilization plan [1]

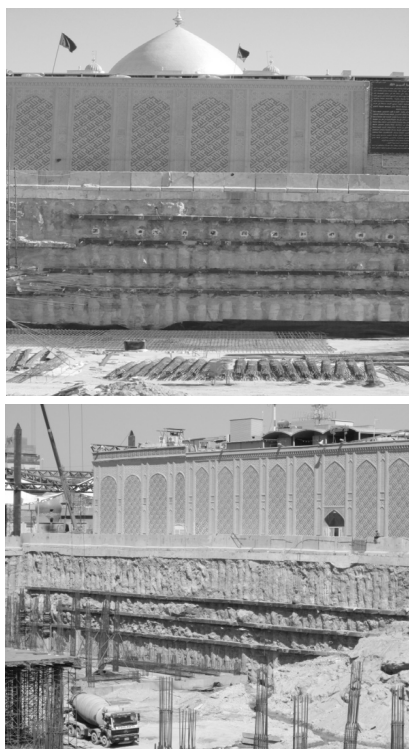


Figure 3. Excavation stabilization using piling and anchorage method

2. GEOTECHNICAL CONDITIONS OF THE PROJECT

Based on the soil mechanics investigation carried out in project site [2], the soil profile consists of five layers as presented in Table 1. Underground water table is reported to be 15m from the ground surface.

Table 1. Geotechnical profile selected for excavation stabilization

Depth (m)	Soil Type	ϕ , (Deg.)	C (kPa)	γ (kN/m ³)
0 to 4	Fill	25	20	18
4 to 8	Sand	30	30	19
8 to 14	Weak Sandstone	20	2000	20
14 to 17	Loose saturated Sand	30	5	19
Below 17	Weak Sandstone	20	2000	20

3. NUMERICAL MODELING

Numerical modeling of the present project has been carried out by PLAXIS software. For this reason, stage construction technique as well as static and pseudo-static methods were utilized. It should be mentioned that in pseudo static analyses, only horizontal seismic coefficient is considered and taken to be one-half of the peak ground acceleration ($K_h=0.5PGA=0.125g$). Figure 4 demonstrates modeling stages of the interaction among soil, retaining structure and main structure. Material properties of the structural components and applied loading are described in Table 2.

Table 2. Parameters applied in numerical modeling

Part	Element	Specification
Pile	plate	Concrete pile Dia.=1.0 m, spacing=1.0 m, $EI=1.03e6$ kNm ² /m, $EA=1.65e7$ kN/m
Anchor	(Bond length) Geogrid	$EA= 8.25e4$ kN/m
	(Unbound Length) Anchor	$EA= 9.45e4$ kN
Structure	plate	Concrete beam and column, $EA= 1.73e6$ kN/m, $EI=4.58e4$ kNm ² /m
Surcharge	Continuous wall	240 kPa
	Uniform load	30 kPa
Pile to structure connection	Rigid connection	Fixed horizontal displacement boundary
	Axial Beam	Flexible connection, $EA= 5.55e4$ kN/m
	No element	Free displacement (No connection)

Some results included horizontal deformation counters for static and pseudo-static cases are presented in Figures 5 and 6.

4. COMPARISON WITH MONITORING RESULTS

Figure 7 shows the monitoring results of one of the piles in block 10 which derived from surveying methods. Comparing Figures 7 and 5, illustrates that results obtained from monitoring

and numerical modeling are in a good agreement. At the top of the piles horizontal displacement obtained about 4 mm from monitoring results while the calculated value is 5.4 mm at the end of excavation time.

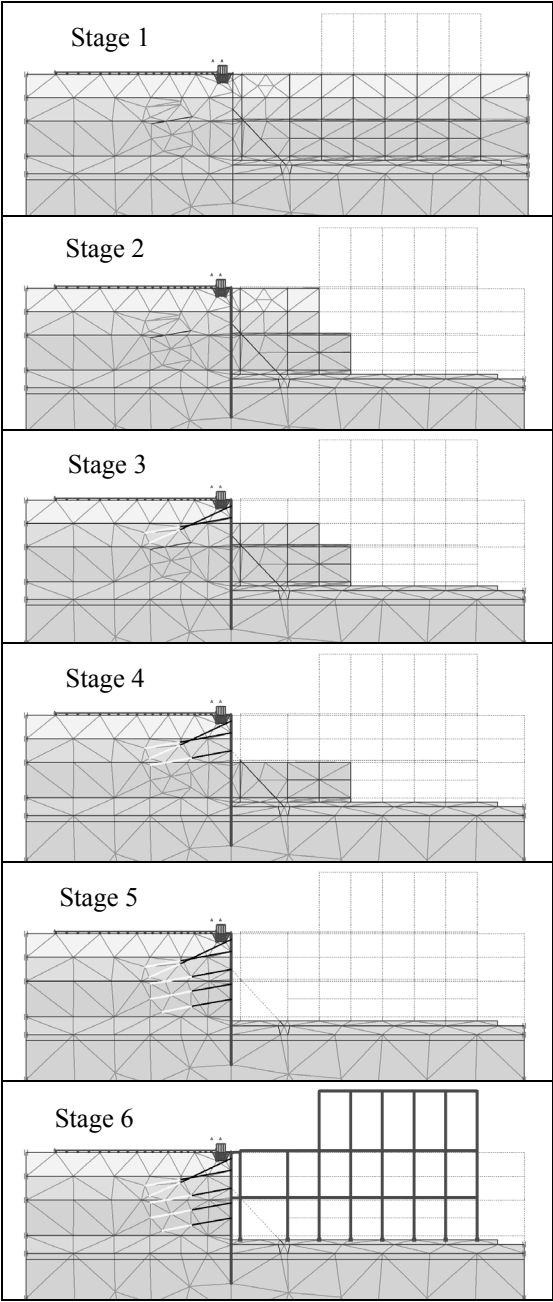


Figure 4. Stages of numerical modeling

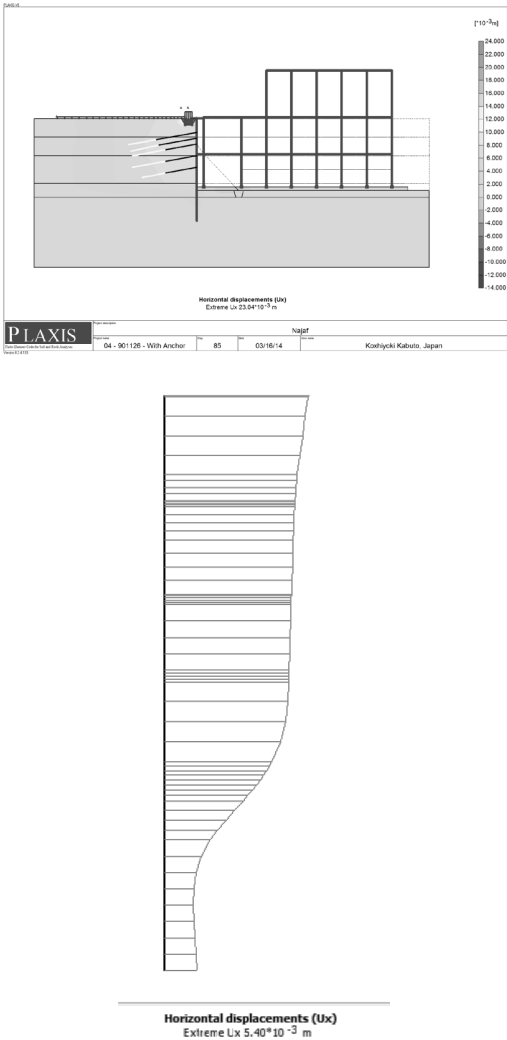


Figure 5. Top) Horizontal displacement of Excavation face adjacent to block 10 (static) – Bot) Pile displacement profile

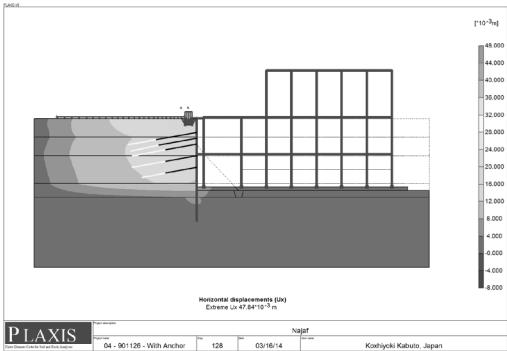


Figure 6. Horizontal displacement of eastern face adjacent to block 10 (Pseudo-static)

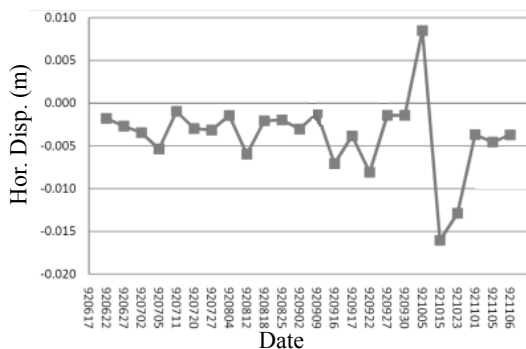


Figure 7. Monitoring results pertinent to one of the piles of block 10

5. SHORING-STRUCTURE INTERACTION

As shown in Table 2, in order to study the interaction of shoring system and structure, three scenarios for connection of concrete piles to the main structure are taken into account (Figure 8).

- Rigid Connection:** A rigid constraint against lateral movement of piles exists.
- Flexible Connection:** Conventional connection of pile to the main structure using appropriate elements to transfer horizontal loads.
- No Connection:** No interaction between the main and retaining structures exists.

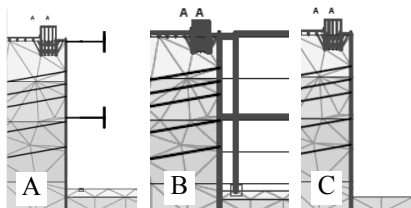


Figure 8. Scenarios considered for Shoring-Structure Interaction analyses

Based on abovementioned scenarios, numerical analyses carried out and profile of shoring pile displacements, shear and moment forces after pseudo-static loading are drawn in figure 9. Also anchors' force and transferred horizontal force to main structure from shoring structure are presented in figure 10 and table 3, respectively.

As seen in above results it is demonstrated that considering the interaction effects between retaining system and main structure in excavation area affect on design of both of them. In the other hand connecting the shoring system to

main structure reduced displacements of piles via transferring applied lateral soil pressure to the main structure. As shown, assumption of rigid behavior of structure results very large amount of transferred force to it. This assumption is not correct and causes the structure elements unnecessarily oversized.

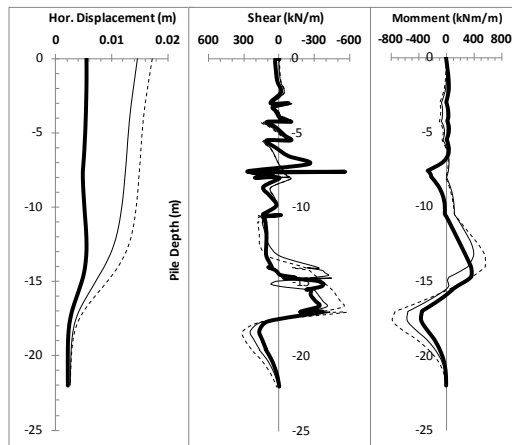


Figure 9. Shoring pile displacements, shear and moment forces after pseudo-static loading for different interaction scenarios

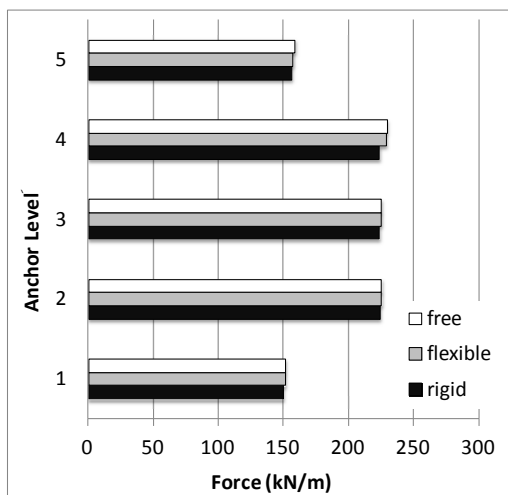


Figure 10. Anchors' forces after pseudo-static loading for different interaction scenarios

Table 3. Transferred horizontal force from shoring structure to main structure after pseudo-static loading for different interaction scenarios

	Rigid	Flexible	Free
Top force (kN/m)	36	7	0
Bottom force (kN/m)	863	23	0

6. CONCLUSION

According to numerical modelling of an excavation stabilization system in adjacent of a historic building in Najaf (Iraq) and considering interaction between shoring and main structure, following conclusions can be presented:

- According to comparison with monitoring results (horizontal displacement after static loading) and good agreement between numerical and monitored results, it seems numerical modeling procedure carried out well.
- Type of interaction assumed between shoring system and main structure located in the excavated area, affects the behavior and also design of both structures (main and retaining)
- If someone assumes the main structure behave rigidly against retaining structure then shoring structure design un-conservatively and the main structure become much overdesigned because of very large transferred lateral soil forces.

7. REFERENCES

- [1] TJCE, Design Report of Fatima Courtyard Excavation Stabilization, 2013.
- [2] Zaminsakht CE, Geotechnical Site Investigation of Fatima Courtyard Development, 2012.

Design and construction of reinforced retaining wall in the railway of Korea

D.S. Kim

Ph.D, Principal researcher, Korea Railroad Research Institute, Cheoldo bangmulgwan-ro, Uiwang, Gyeonggi-do, 437-757, Korea

S.Y. Park

Senior researcher, Hanwha Engineering and Construction, 6 Shinsung-Dong, Yousung-gu, Daejeon, 305-804, Korea

ABSTRACT: Reinforced retaining wall for railways has been designed and constructed near Jupo station in Korea. Its purpose is to reinforce failed railway embankment slope and to increase line capacity. Reinforced retaining wall could make double the line capacity without additional land. This could be realized using short reinforcement (35%H, half level of current specification) and rigid wall. The use of short reinforcement makes it possible to construct in small space and to decrease footing costs. Another advantage is to minimize residual settlement with special procedures to construct wall after backfill. The reinforced retaining wall could be highly applicable, such as concrete slab track ruled by rigorous standards for residual settlement and difficult to maintain while opening to traffic. In this study, we revised overseas GRS to upgrade applicability in Korea focused on cutting down construction cost and period to 25~30% without losing safety.

1. INTRODUCTION

In these days, the use of concrete slab track on soil subgrade is being increased for railway construction in Korea. The concrete slab track requires less maintenance works but high levels of accuracy to construct than the ballasted track do. That's why it's very difficult to repair. So, we should take care from construction stage not to deform after train opening. Mainly, the settlement of the track comes from ground and subgrade. To minimize the settlements directly affecting track alignment and crack on track concrete layer, we should do lots of measures during construction. Consequently, these efforts enhance the serviceability and riding comfort of railway and decrease maintenance works.

Mechanically stabilized retaining walls are frequently adopted in Korea, which has small land and high population to use land efficiently. However, in the field of railway, mechanically stabilized retaining walls are used limitedly due to safe issues. We need some special technology to satisfy both use land efficiently and guarantee the safety of railway. Small use of land to construct railway is directly linked with cost down for railway construction.

This study introduces the revised reinforced subgrade of Reinforced Roadbed for Railroads (RRR) which was firstly developed in Japan

(Tatsuoka et al. 1997), focused on economic viewpoint and construction period.

2. REINFORCED SUBGRADE

Geosynthetic reinforced subgrade(GRS) with rigid wall have advantages to increase safety and high applicability to small space compared with mechanically stabilized retaining walls. On the other hand, it cost more and take time to construct compared with other competitive technology.

2.1. Reinforced roadbed for Railroads

It was firstly developed in Japan (Tatsuoka et al. 1997, 1998), and has been used for railroad construction. It has some useful characteristics different from existing retaining wall and reinforced earth wall. These are as follows.

- 1) It has rigid wall with small footing.
- 2) It has special construction procedures. The backfill soil is constructed in advance and wall firmly connected with reinforcement be next to minimize residual settlement.

- 3) It use short reinforcement. It makes possible to increase line capacity of railways very economically without additional land (Figure 1).

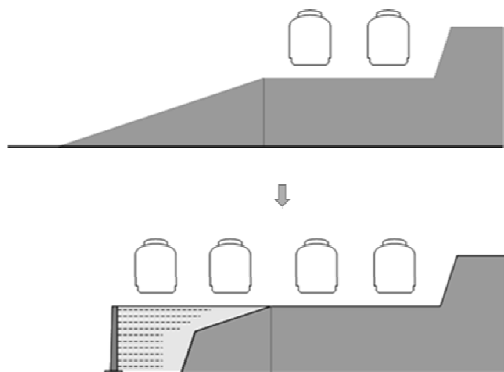


Figure 1. Increase of line capacity of railways without additional land

2.2. Revised reinforced subgrade(RRS)

Even though the RRR has lots of advantages as explained before, they say it's not economical applying it in Korea and need to be modified to easily apply it for railroad construction environment in Korea. Different earthquake environment between two countries is one of important reasons not to use it.

So, we revised reinforced subgrade with rigid wall to cost down and to take less time to construct. Main differences between RRR and RRS are as follows.

- 1) Vertical spacing of geotextile reinforcement from 30cm to 40 cm.
- 2) Connection types between rigid wall and supporting rebar form for the compaction of backfill materials from welding to prefabricated bolt.
- 3) Flexible length and vertical spacing of long reinforcement depending on earthquake environment.

3. FIELD APPLICATIONS

3.1. Design of revised reinforced subgrade

Fig.2 shows the design drawing of testbed at Jupo station. It was constructed at left side of the slope of operating line. It has 40m long, 7m high.

The length of short reinforcement was 0.4H which was shorter than the length of conventional GRS wall (0.7H) in Korea. It makes possible to minimize the cutting work of the slopes and ensure the safety of temporary slope.

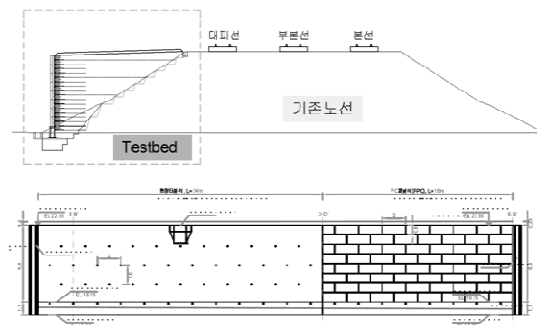


Figure 2. Design drawing of reinforced subgrade

The wall consists of 24m cast-in-place and 16m precast type. GRS parts consist of 17-layers. Top of the GRS parts has 3% down grade for drainage and 10cm mixed gravel layer are installed in order to prevent loss of surface of roadbed. Drainage system is designed that inflow water into the backfill is run to the drainage layers installed at the left end and discharged from the rigid face wall through discharge pipes.

Now, GRS parts were constructed and maintained, while measuring settlement of the backfill soils and ground. In 2014, cast-in-place type face wall and precast type face wall will be constructed. An electric pole with big horizontal load coming from catenary system is designed to install on the cast-in-place type wall without other foundation.

3.2. Construction of revised reinforced subgrade

The footing and backfill soils of RRS testbed was constructed from 10/15/2013 to 11/16/2013 during 28days. Fig. 3 shows the construction procedures which were divided into 3 categories with foundation installation, GRS work, and installation of rigid face wall.

Foundation construction was as follows: 1) clearing and gruffing work of slope; 2) re-

placement of weak subsoil with cement mixed gravels and placing concrete; 3) installation of reinforcement and form for small foundation; 4) concrete placing into the foundation form; 5) leveling work for GRS;

GRS work was as follows: 1) placing of geogrid, reinforcement form and gravel for compaction and drainage; 2) placing of backfill soils and compaction; 3) repetition of 1 to 2 stages till aimed level; 4) measurement of settlement and deformation of RRS.

After converging the settlement of the RRS, the rigid face wall will be constructed during May 2014. Rigid face wall have two types. One is cast-in-place concrete wall type for cost down and the other is precast concrete panel type to decrease construction period.

4. CONCLUSION

It's not easy to directly apply overseas reinforced subgrade to our country without revision because there are differences in construction environment, design loads, and backfill soils.

This study is for the revision of overseas GRS to upgrade applicability in Korea focused on cutting down construction cost and period to 25~30% without losing safety. Until now, total settlement of RRS near Jupō station is less than 2cm and bulging of GRS face wall is negligible.

We hope that, based on those efforts, the RRS could be applicable to construction fields in Korea.

5. REFERENCES

- Tatsuoka, F., Tateyama, M., Uchimura, T., and Koseki, J., 1997. "Geosynthetic-reinforced soil retaining walls as important permanent structures", 1996–1997 Mercer Lecture. *Geosynthetics International* 4 (2), pp.81–136.
- Tatsuoka, F., Koseki, J., Tateyama, M., Munaf, Y., and Horii, N., 1998. "Seismic stability against high seismic loads of geosynthetic-reinforced soil retaining structures", Keynote Lecture. *Proceedings of the 6th International Conference on Geosynthetics*, Vol. 7, pp. 103–142.



(a) Clearing and grubbing works of slope



(b) Replacement of subsoil



(c) Foundation



(d) Placement of geogrid, rebar form



(e) Backfilling



(f) Compaction



(g) Repetitions of (d) ~ (f) steps



(h) Completion of RRS

Figure 3. Procedures of revised reinforced subgrade construction

A bold constructive method for the retaining structures of the excavation of the underground parking Clinics, in Brazil

C. E. M. Maffei

PhD Full Professor University of São Paulo (USP)-Carlos E. M. Maffei Eng. S/C Ltda Brazil

H. H. S. Gonçalves

PhD Professor University of São Paulo (USP) -Brazil

M. C. Guazzelli

MsC Engineering-Carlos E. M. Maffei Eng. S/C Ltda Brazil

ABSTRACT: This work presents a heady constructive method used for the retaining structures of the Underground Parking Clinics. The project of the parking includes 315m long for 15,5m wide and 4 undergrounds which work was concluded in the end of 1998. The retaining structures of the excavation was executed through screw piles of 80cm diameter, with 23m of length, spaced at every 2,50 m. The slabs of structure of the parking had been set up with precast beams of prestressed-concrete and the bottom slab with cast in-place reinforced concrete. The excavation was accomplished in two phases, in the first one the walls worked as cantilever; and the second one, after the installation of the upper slab working as struts, it was made the final excavation.

1. INTRODUCTION

São Paulo, capital of Mercosul, is a dynamic metropolis that doesn't stop of growing and of presenting challenges. Everyday 500 new vehicles enter in circulation to dispute the few spaces that the city offers. In face of this same problem, capitals all over the world found underground solutions showing the way to be followed by the city of São Paulo. Thus, critical areas identified by the City Hall were placed in competition for the construction of underground parkings over the concession regime with resources originating from of the private initiative. It fit to the Consortium Dr. Enéas de Carvalho Aguiar to assist to the area of greatest concentration of hospitals of América Latina. In the parking underground Clinics there were incorporated unpublished constructive techniques in the country, trying to interfere with to the minimum with the people's life that would transit in this area during the construction (Figures 1 and 2).

The great challenge in a work of this type is to have the skill to execute it with the best possible quality and minimum cost. So that this was possible, there were studied several alternatives of support project besides having had an investment in testing and appropriate instrumentation.

The initial project foresaw the execution of screw of 70 centimetres of diameter at each 2,5 meters with 16 meters long. The structure of the parking foresaw the execution of two central

columns, whose foundations would be formed by piles of 1,40m of diameter and 14 to 18 meters long, between axes 18 to 26 and 55 to 66, respectively. Between the other axes concrete tubing piles would make the foundation of the central columns with diameter of the fuste equal to 1,40 meters and diameter of the base of 3,65 meters. The height of the enlargement was of 1,95 meters and the distance between the bottom slab and the beginning of the enlargement should be larger than 1,5 meter. However, to promote the insertion of the columns in the foundation structures it would be necessary the execution of a "chalice", whose constructive process was shown very difficult.

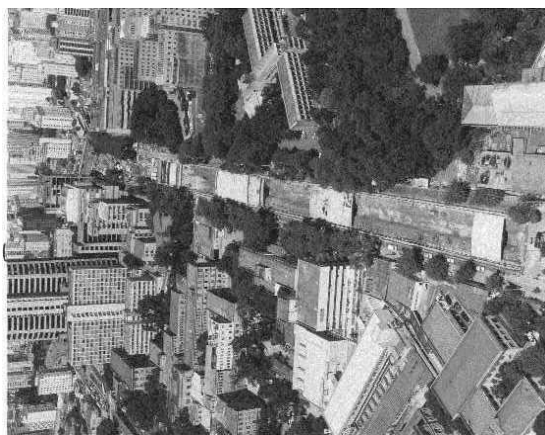


Figure 1- Aerial view of the parking area during the works



Figure 2 – Aerial view of the parking after conclusion

So, it was decided to modify the project, the structure should be executed without intermediary columns and precast beams of prestressed-concrete that won the empty space of 15,5 meters should be used. There were studied new support alternatives, being adopted screw piles of 80 centimetres of diameter, that were used so much as retaining structures of the excavation as well as for foundation of the structure of the parking. The piles were arranged at every 2,5 meters in the two faces of the excavation, and they had the length increased for 23 meters and the steel reinforcement introduced in the piles presented 19 meters. The structure of the parking was conceived with the upper slab and the intermediary levels beam, in precast beams of prestressed-concrete and the bottom slab with cast-in-place reinforced concrete. The bottom slab works as complement of the foundation of the structure, because the piles just have load capacity compatible in relation to temporary phase, that is to say, without being considered the overloads in the floors of the underground.

The work began with the remotion of the interferences and execution of the piles. The placement of the upper precast beams was accomplished with the aid of a portico of 30 tons of capacity. The constructive method was just constituted basically in two excavation phases. The first excavation phase presented 5 meters of depth and the walls worked as cantilever; after the installation of the upper slab that worked as struts, it was executed the final excavation. Due to the excellent characteristics of the soil a fine layer of 2 centimetres of shotcrete among the piles was just applied.

Temporary berms had been foreseen during the phase of final excavation, whose removal would depend on the instrumentation results that were constituted in measures of tension of the steel of the reinforcement of the pile and horizontal displacements of the piles. The obtained results checked the viability of execution of the excavation without the use of the berms.

After the excavation and execution of the bottom slab, the installation of the intermediary levels slabs was proceeded and the piles restrained.

The screw piles are constituted, generally speaking, an economic solution for foundations and as is not common to use them, in Brazil, at that time, as retaining wall due to the constructive difficulty of reinforcing this type of pile, tests were executed previous to the beginning of the work to confirm the executive viability of the piles with 19 meters of reinforcement.

2. GEOLOGICAL-GEOTECHNICAL PROFILE

The geological-geotechnical profile of the area, shown in the figure 3 presents a layer of approximately 1 to 1,5 meters of embankment of silty clay, followed by a layer of 10 to 12 meters of silty clay with brown and red fine sand (porous) that presents index SPT variable among 10 to 20. Below this layer it comes a layer of 6 to 10 meters of silty clay with a lot of variegated fine sand, SPT among 8 to 16, over a layer of silty-clayed sand of varied granulation. The level of the water was found at 17 meters deep, therefore below the final excavation.

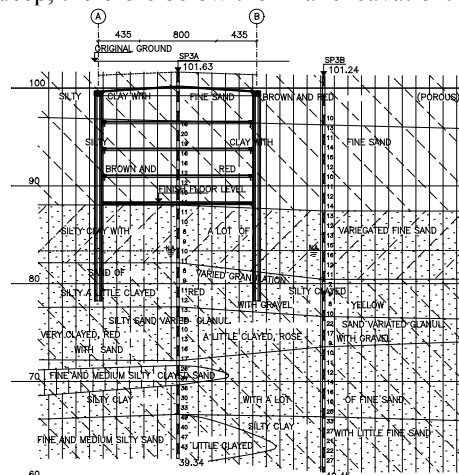


Figure 3 - Geological-geotechnical profile

3. METHODOLOGY OF CALCULATION OF THE RETAINING STRUCTURES

The active pressure was calculated through the method of Rankine and the obtained values were smaller than the minimum values that are considered for clay. Therefore the pressure values were calculated by the diagram of minimum active pressure proposed in the norm "Calculation of the works executed by the method of the trench", of the Company of the Metropolitan of São Paulo.

The underground of the area is very favourable to the excavation, because it is constituted in its first 12 meters of a porous clay with cohesion estimated in 40 kN/m^2 , that would allow vertical cut of 8,40 meters. It is important to remind that the water level was met below the bottom level of excavation. There were adopted for calculation of the pressures the following parameters for the several soils layers.

- Embankment $c=0$ $\phi=25^\circ$ $\gamma=17\text{kN/m}^3$
- Porous silty clay $c=40\text{kN/m}^2$ $\phi=20^\circ$ $\gamma=19\text{kN/m}^3$
- Silty clay with a lot of fine sand $c=20\text{kN/m}^2$ $\phi=27^\circ$ $\gamma=17\text{kN/m}^3$

The diagram of minimum pressure is presented in figure 4.

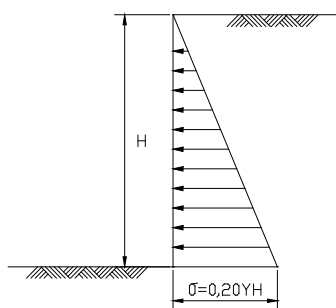


Figure 4 - Diagram of minimum pressure

To determine the efforts and the displacements due to the excavation the evolutive and no-evolutive models were used.

In function of the geological-geotechnical profile, a compartment was accomplished; in which were determined three types of piles:

Type "light"–axes 0 to 17–trench constituted of porous silty clay red, level of water of 3

meters above the end level of the embedded length, or below it.

Type "average"–axes 35 to 53–trench constituted of a homogeneous layer of silty clay very sandy. The level of water was above 3 meters the end level of the embedded length.

Type "heavy"–axes 18 at 34 and 54 to 68 - trench constituted of 3,70 meters of embankment, presenting till the bottom of the excavation a layer of silty clay very sandy and in the area of the embedded length the silty red porous clay. The level of water was met 1 meter above the bottom of the excavation.

The piles were calculated considering the following materials:

- Concrete $f_{ck} = 20 \text{ MPa}$.
- Steel $f_{yk} = 500 \text{ MPa}$.

The main reinforcement was constituted of special bars with 19 meters of length. The raising level was the final level of the support of the beams and the polluted concrete was removed and the surface regularised with grout.

The piles were calculated to present 127 tons of vertical load capacity to permanent load and 18 tons for accidental load.

The maximum displacements of the piles foreseen through the evolutive model were the following ones:

Type "light" – $\delta = 10,81 \text{ mm}$

Type "average" – $\delta = 16,00 \text{ mm}$

Type "heavy" – $\delta = 20,03 \text{ mm}$

To guarantee the good acting of the work and to check the adopted parameters, temporary berms were left during the final phase of excavation and appropriate instrumentation it was done. Before the remotion of these berms the instrumentation results were compared with the one foreseen by the project.

4. CONSTRUCTIVE METHOD

4.1 General Constructive method

The outlines of the constructive method are presented bellow. After the remotion of the interferences the screw piles were executed in the whole contour of the parking and metallic piles were installed with pre-hole in the extremity of the parking where the ramp was located that served as service road during the works and exit of the parking after the conclusion of the work (Figure 5).

In other to turn it possible the excavation till the installation level of the upper slab, with the walls presenting 5 meters of cantilever, it was

used an support understanding part of the piles and wood board among them. This was possible introducing a rib in the fresh concrete through vibration, settling forms for the concreting of a half-moon (Figures 6 and 7).

Among the half-moons, the excavation was executed, being placed in the same time the boards that would be involved with geotextile blanket where there was risk of carriage of material (figure 8).

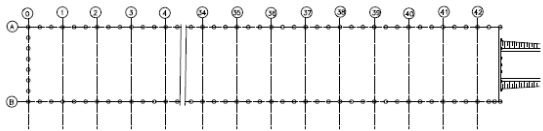


Figure 5 – Service road

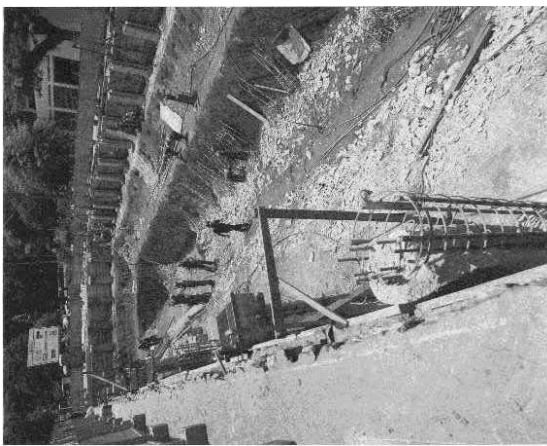


Figure 6 – Detail of the half-moon

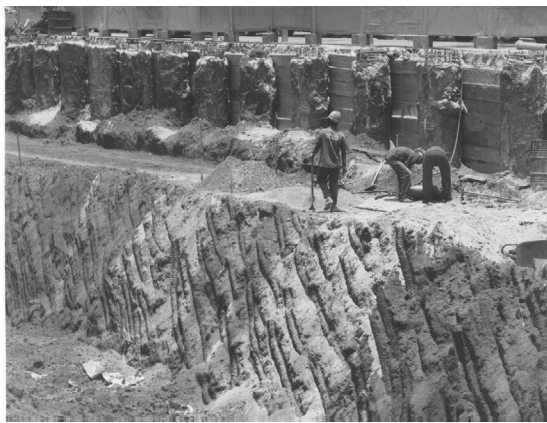


Figure 7 – First phase of excavation – detail of wood boards between the half-moons

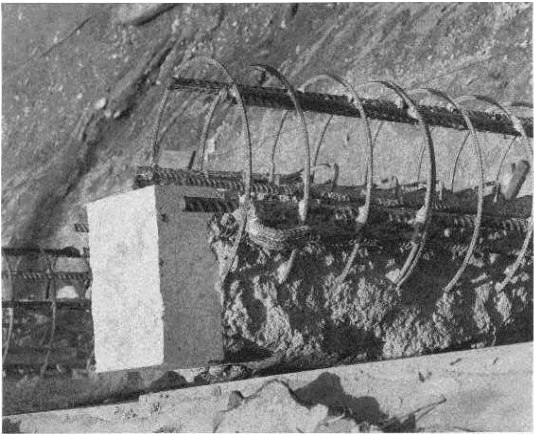


Figure 8 – Detail of the crowning beam

After the concreting of the crowning beam the excavation was made till the level of the upper slab. The crowning beam sustained the portico, weighing 15 tons that transported the precast elements during the whole work, turning the process faster (Figures 9 and 10). After the partial demolition of the remaining reinforcement of the pile, until the razing level, coincident with the installation level of the upper slab, there were then installed the beams and the tie-rods that were executed in the work niches (figure 11a and 11b).

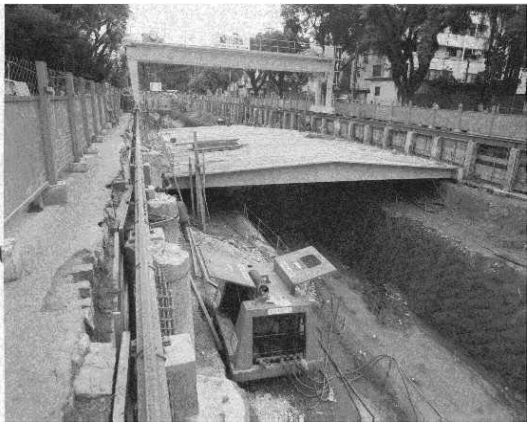


Figure 9 – View of the portico used to transport the precast elements

Subsequently it was executed the upper slab, the compacted embankment and the revamping of the surface



Figure 10 –View of the berms of the first phase of excavation

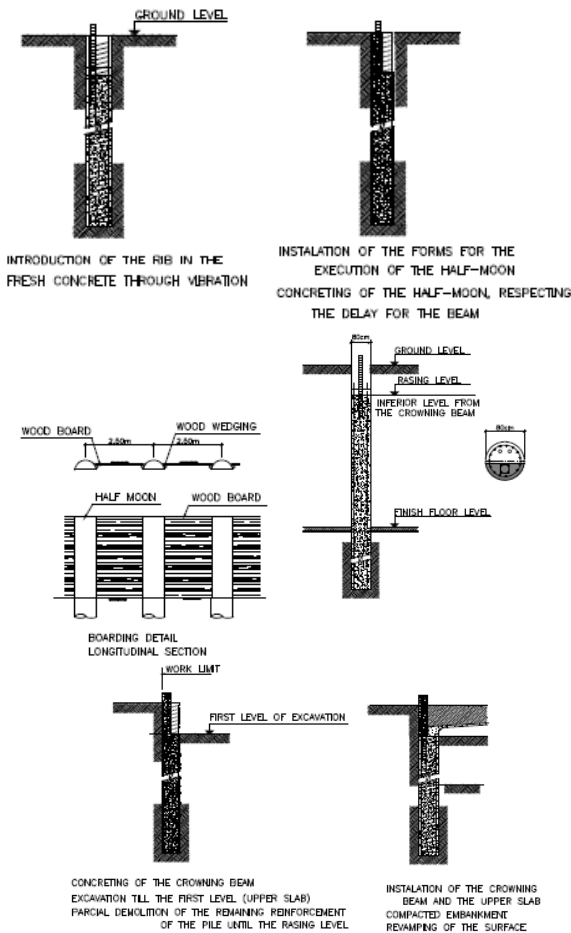


Figure 11a

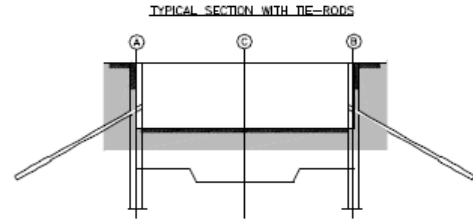
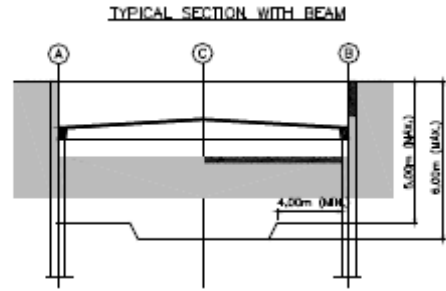


Figure 11b

The excavation was made under the upper slab with 8,6 meters of free empty space, continuing until the final level, berms were maintained with 4 meters of wide and 3 meters high in the whole turn of the parking. The berms were protected with shotcrete or mortar lining (figure 12a and 12b). Among the piles, the excavation was made in arch form and the soil mass protected with 2 centimetres of shotcrete (Figures 13 and 14).

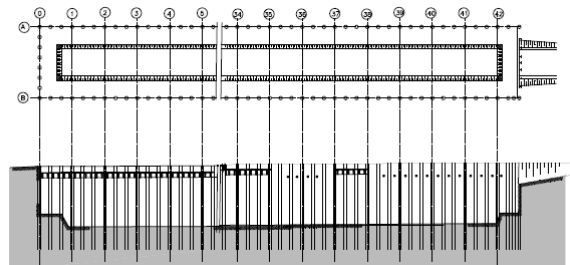


Figure 12a

Next, the beams of the intermediary levels were installed and piles restrained (figure 12c). Subsequently the berms were removed and the bottom slab executed (figure 12d; figures 15,16 and 17).

The remotion of the berms before the installation of the intermediary levels beams was only authorised after the confirmation of the validity of the project hypotheses through

the results of the instrumentation as presented in the item 4.3 (Figures 18 and 19).

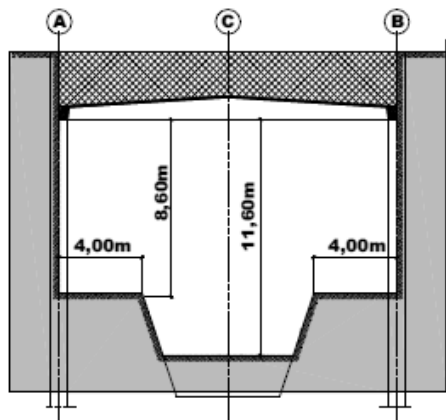


Figure 12b

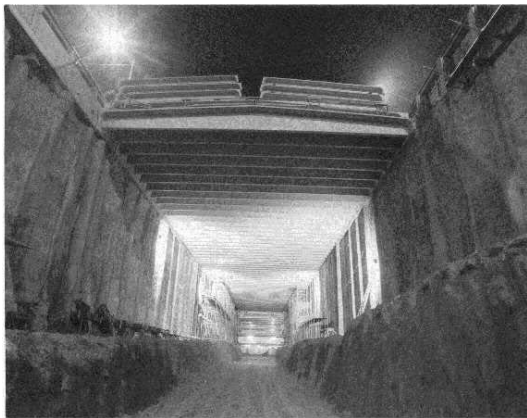


Figure 13 – Internal view of the parking, excavation till the final levels and the lateral berms

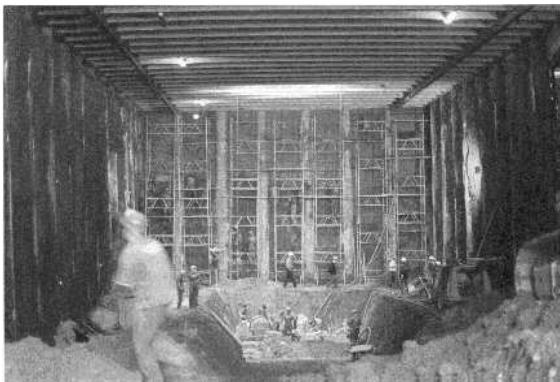


Figure 14 – View of the extremity of the parking, execution of the shotcrete

After the execution of the bottom slab, the inside structure of the parking was completed; it means the walls, the intermediary columns and

the layers over the precast beams. Soon, the upper slab and the embankment were concluded in the areas used as work niche.

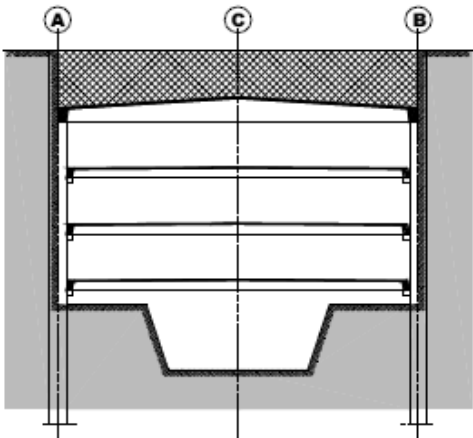


Figure 12c

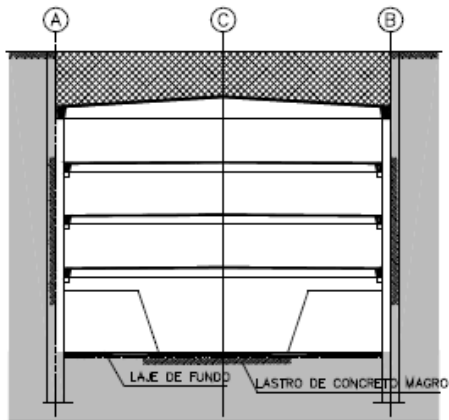


Figure 12d

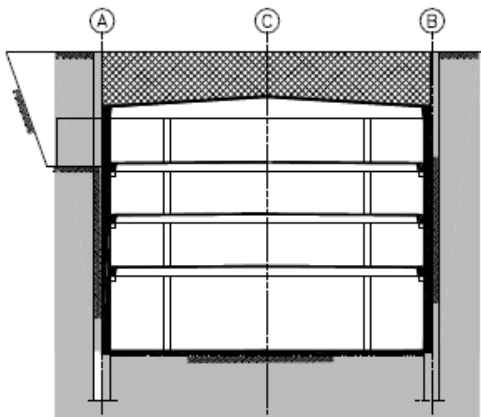


Figure 12e



Figure 15 – Execution of the supports for the intermediary level beams

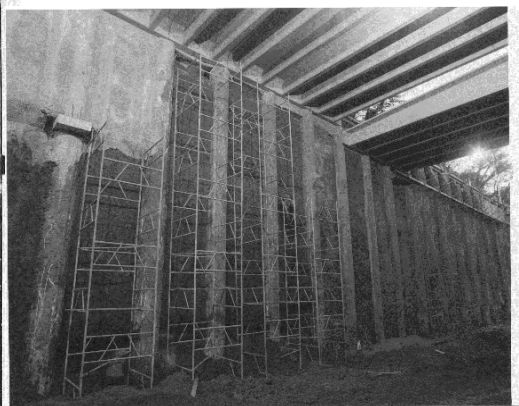


Figure 18 – Overall view of the excavation with the berms removed

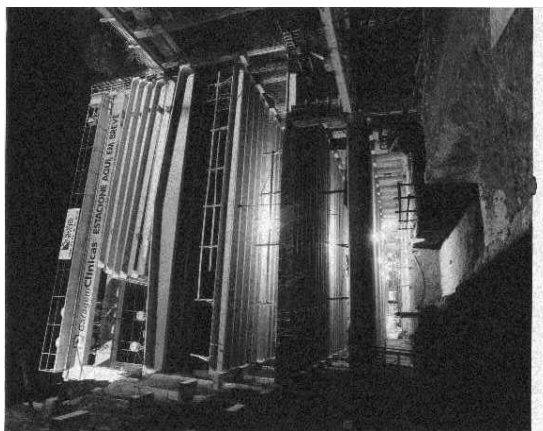


Figure 16 – View of the work in the phase shown in figure 12c.



Figure 19 – Removal of the berms with machines

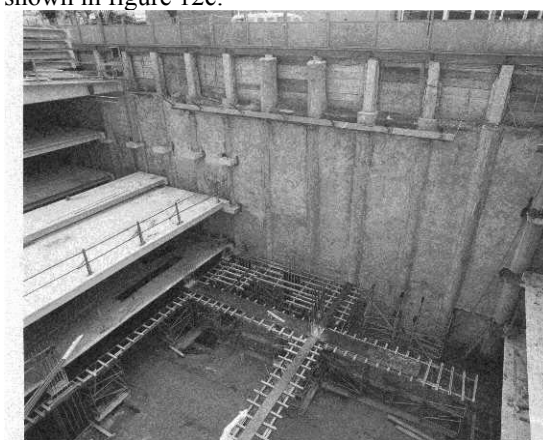


Figure 17 –View of one of the areas used as work niche, piles supported by tie-rods



Figure 20 – Pictures of one of the piles cut in the stall area

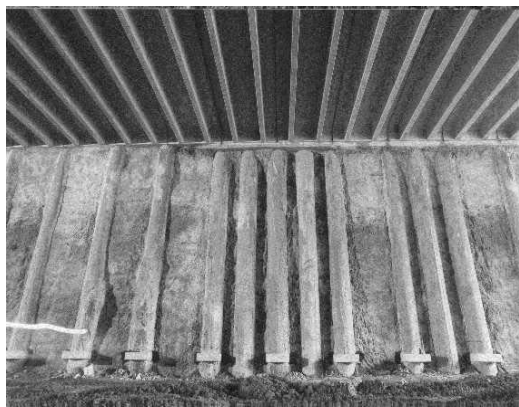


Figure 21 – Detail of the decrease of space between piles in the stall area

In the first underground there was the need to enlarge two small areas of the parking for entrance and exit stalls of the vehicles. The excavations were made in slopes; the piles located in the areas of the stalls were cut (figure 12e). The spacing between the piles was decreased close this area with the purpose of supporting the concentration of loads in these locals (Figures 20 and 21).

4.2 Constructive method of the screw piles

The great challenge for the use of the screw piles, with 19 meters of reinforcement, was the capacity of introducing the reinforcement, since the concrete should have peculiar characteristics to make possible going down 19 meters of the frame. Two tests were accomplished and it was possible to point out some indispensable conditions for the success of the pile execution:

- use of a crane compatible with the height of the frame to guarantee its gone down in the plumb line;
- precise planning for the arrival of the concrete, concreting and immediate introduction of the frame.

The excavation of the piles was mechanised to the point level foreseen, 23 meters below the level of the surface, without aid of bentonite slurry, and then the piles were concreted close to the surface level. The introduction of the main frame of 19 meters long in the fresh concrete was executed through vibration.

4.3 Instrumentation used to determine the behaviour of the excavation and the possibility of the remotion of the berms

It was proposed an instrumentation program, because in function of these results it could not have the need of the use of berms. The

instrumentation was constituted in the installation of inclinometers and anchorage points for the measure of horizontal displacements of the piles and verification of the tensions through extensometric test in the bar of steel closer to the inside face, in the section of maximum calculated bending moment.

The inclinometers were installed in the axes 8, 26 and 39 one-meter far from the longitudinal axes of the piles. The results of the inclinometers were harmed by the proximity of the same ones to a cable of the Electricity Company. The maximum convergence observed in the several axes, among the piles, didn't surpass 5 mm.

The results of the instrumentation supplied for the requested bar a tension of the order of 100 MPa. As the tension of work of the frame is of the order of 300 MPa, it was made a retroanalysis that allowed refining the parameters and through new calculations allowed the feasibility of excavating without berms.

5. CONCLUSIONS

The work presented an unprecedented constructive method used in the retaining structures of the Underground Parking Dr. Enéas de Carvalho Aguiar for that time.

The opening of a trench of 15,50 meters wide, 315 meters of extension and 11,6 meters of free empty space between the level installation of the upper slab and the final level of the excavation, presenting as only retaining structures screw piles at every 2,5 meters restrained by the upper slab, it was accomplished with great success.

The comparison among the foreseen results and the observed one, checked the efficiency of the used support, therefore so much the efforts as the displacements of the retaining structures were smaller than calculated one. This constructive method was shown an economic and fast solution.

Deepening of some Brazilian quays using the technique of reinforced jet-grouting

C. E. M. Maffei

PhD Full Professor University of São Paulo (USP)-Carlos E. M. Maffei Eng. S/C Ltda Brazil

H. H. S. Gonçalves

PhD Professor University of São Paulo (USP) -Brazil

M. C. Guazzelli, MsC Eng & J.P. Ciriades & P.E.M. Maffei & R.A.Simoni & C.Goulart

Carlos E. M. Maffei Eng. S/C Ltda Brazil

ABSTRACT: The expansion of the Brazilian economy in recent years has led to a significant expansion in the import-export activities, drawing in improvement of ports including, necessarily increase of quays depths to allow mooring of larger ships. The first port to have its depth increased using jet grouting technique was the port of Santos. This paper presents the method used in Santos' wharfs and other ones along Brazilian coast.

1. SANTOS PIER

The Port of Santos, the largest in Latin America, was officially opened in 1892, when the Companhia Docas de Santos, delivered world's shipping the first 260 m of quay, in the area now called Valongo. Currently total length of wharfs occupies an extension of more than 12 km the estuary of Santos. The Port has handles around 60 million tonnes per year, with a forecast to quadruple by 2022 this volume and deepening the entrance channel to 17m to receive larger ships.

Since the beginning of this century, the operating companies in the port are modernizing terminals to increase their competitiveness in international trade. Within this framework, it has become urgent to carry out works to increase quay depths of Santos wharfs due to operational advantages larger ships offer.

When the port was first opened starting 20th century, retaining structure consisted of stone-walls allowing mooring of ships with up to 8 m depth. In the mid-twentieth century, concrete sheet piles were performed and the port depth had increased to 11 m depth. Dimensions of concrete pile are 40 cm thick, 50 cm wide and approximately 18.50 m in length, reaching elevation -16.42 m. The space back of sheet piling received an embankment of silty sand. First quay deepened in Santos (COSAN) presented structure of the deck itself resting on three rows of inclined piles and one row of vertical pile of 37.5 cm X 37.5 cm and 25.50 m

in length as shown in Figure 1. Despite all wharfs are danish type deck structures and foundations are not the same.

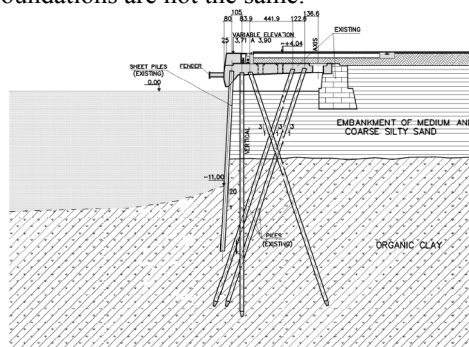


Figure 1- Retaining structure with 11m initial depth

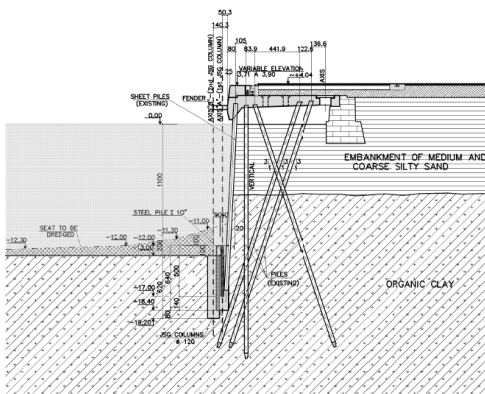
At Cosan wharf increase depth in 1.30 m without any modification in the retaining structure was impossible because excavation of 1.30 m from the sea side would reduce piles embedded length of 5.40m to 4.10 m, so that seaside outward passive thrust available would be insufficient.

Using conventional retaining structure to increase the depth with steel sheet piles would bring operational difficulties during the execution of the work, since the piles have to be placed in series and deck must be widened, interfering with ships mooring.

2. NEW RETAINING METHOD TO INCREASE QUAY DEPTH

It was proposed and successfully implemented a new method that besides being able to be built in parts, does not affect the operation of the terminal, significantly reducing the cost of the work itself.

This method consists in use of secant jet-grouting columns in front of concrete sheeting piles, in order to increase embedded length as is shown in Figure 2. The length of the columns was calculated in order to preserve internal forces of existing sheet piles and not decrease the safety factor. To provide enough resistance to bending, steel piles are introduced in the columns of jet grouting.



steel piles profiles are defined in order to maintain unless same safety coefficients before and after deepening.

Table 1: Undrained shear strength of marine clay

Elevation	Seaside	landside
m	kN/m ²	kN/m ²
-7 to -9	-	30
-9 to -11	-	35
-11 to -13	20	40
-13 to -15	30	40
-15 upward	40	45

For the structure of soil-cement column of jet-grouting was admitted a modulus of deformability of 0.7 GPa and compressive strength of 2.5 MPa at 60 days. As already said, steel piles dipped in jet-grouting columns were used to ensure the ability in resisting bending and shear, providing also integrity of soil-cement columns. Spacing between columns is adopted to ensure interpenetration between adjacent columns, allowing the spacing for the installation of steel piles.

4. IMPLEMENTATION AND CONTROL

For implementation of jet-grouting columns without interfering with the activities of loading and unloading of the port terminal, the extension of the pier was divided into three sections. The jet -grouting services began at one end, and other end sequentially and finally the central passage, taking a shorter period of ships movement .

The topographic location of columns, taken at the board of the pier, guided the installation of steel platforms, which served as a work plan for drilling and grouting. Furthermore, these platforms contain templates to guided the drill in the water and the steel pile during the installation process.

To introduce steel pile listing in jet-grouting column, a crane was used to lift the pile (I 10" with 6 m long) and lead to work platform. Because steel piles would be introduced shortly after the execution of jet -grouting and therefore the resistance of the soil-cement is still very low, steel piles would be suspended within the columns, tied to the dock for any type of supports .

Due to uncertainties regarding the representativeness of extracted samples using rotary drilling, to determine the strength parameters of the jet -grouting columns, it is common to verify this technology through excavation to allow visual inspection of the columns and removal of large blocks for laboratory tests. This procedure was not feasible in this work and the technological control of jet grouting was carried out by performing tests on samples taken from test samples in columns and reflux .

Sampling cores was taken 14 days after the execution of the column throughout the test column. Some specimens were tested with approximately 28 days of age whereas others were put up for possible confirmation tests up to a maximum period of 90 days.

The columns were alternately executed so that adjacent to the newly formed columns were only performed when it obtained the minimum resistance of the soil - cement, ie after about 24 hours.

Against the odds, be able to introduce the metal profiles in the newly implemented columns simply by using their own weight, it was necessary to use a hammer attached to the head of the steel piles.

The interpenetration of the columns of jet-grouting was evidenced throughout the length of the work by means of rotating surveys performed halfway between adjacent columns . With the borehole thus obtained also could be verified through laboratory tests, the unconfined compressive strength and deformability that were being obtained with treatment at different ages of the marine soil module. Table 2 shows the results.

Regarding the treated soil structure both unconfined compression strength and the modulus of deformability obtained met the design requirements (respectively, 2.5MPa and 0.7GPa).

The E50/RCS ratio ranged between 412 and 832 at day 30 (667 is the average). At 60 days, with a larger number of data available, this ratio varied even more: between 463 and 2364, with 1021 as the average value.

Table2. Average values of unconfined compressive strength (RCS) and secant deformation modulus (E50, 50% of rupture stress) obtained in treating jet grouting of marine clay

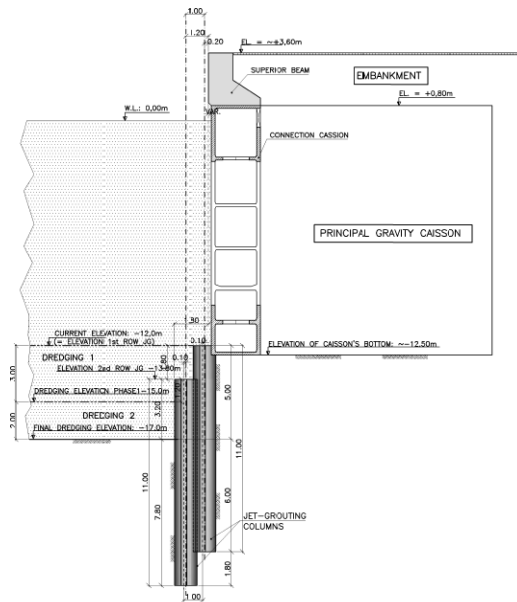


Figure 7 – Execution of the jet-grouting columns in Caju Pier

8. TECON PORT, SALVADOR

Tecon's Quay needed to be deepened 5m, from elevation -12,00 m to elevation -15,00 m. Due to occurrence of weathered rock solution was installing all jet-grouting columns reaching the rock, as shown in figure 8. After jet grouting obtained resistance 50cm holes was driven inside, drilling rock under columns. Then, steel pipes were introduced in holes and grouted, as shown in detail in figure 9.

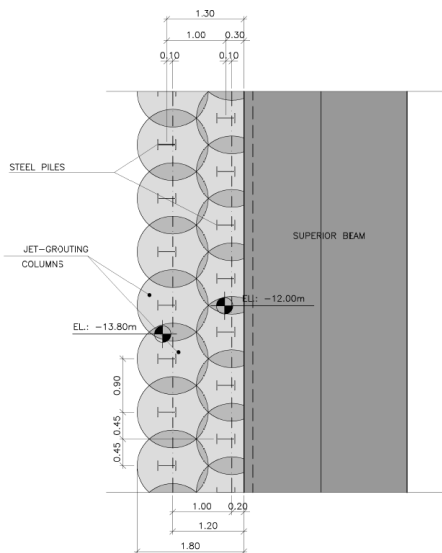


Figure 6 - Detail plan of jet grouting columns.
Caju Pier

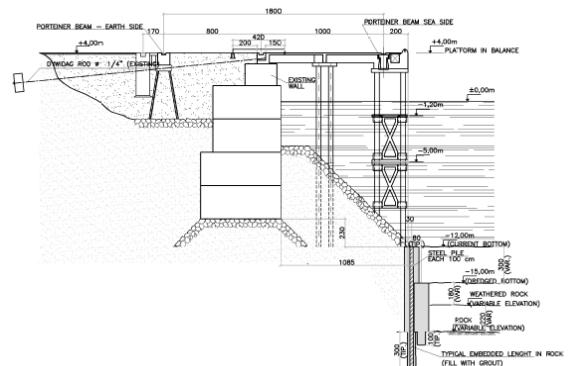


Figure 8 - Typical cross section of Tecon's Quay

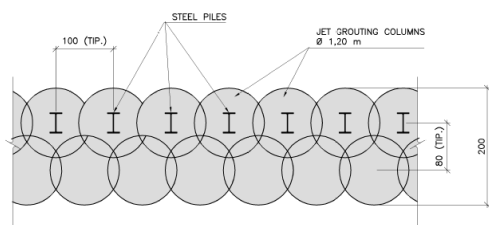


Figure 9 - Detail plan of jet grouting columns.
Tecon's Quay

9. CONCLUSIONS

The use of jet grouting reinforced with steel piles or root piles, to increase quays depths, proved to be technically efficient. The biggest attraction of using this technique is in fact not have been necessary to halt shipping operations while works of the new structure are made.

Comparison of finite element and limit equilibrium methods in analysis of soil nail walls

S. Melentijevic & J.L. Fernández
Grupo Rodio-Kronsa, Madrid, Spain

ABSTRACT: Soil nailing is a world-wide frequently used technique for temporary and permanent slope stabilization applications and excavations with vertical or nearly vertical cuts. A case study is analyzed applying both limit equilibrium (LEM) and finite element method (FEM), including comparison with internationally used codes and standards. In this paper different approaches are used in FEM for simulation of soil nails by different structural type in order to study its influence on results, e.g. (a) only axial stiffness in nails is taken into account or (b) bending and shear stiffness beside the axial stiffness.

1. INTRODUCTION

Soil nailing is a frequently used in situ earth retaining technique for temporary and permanent slope stabilization applications. The passive steel bars, called nails, are introduced in soil as the excavation is in progress. Nails essentially work in tension that is developed under skin friction between bars and soil, although can work partially in bending and shearing. Additionally the facing wall is constructed on site, e.g. shotcrete applied before or after the installation of nails.

Soil nail walls are well suited for vertical or nearly vertical cut slopes, used in highway cuts, in the repair and reconstruction of retaining walls, etc, whenever soil conditions permit it.

There are a lot of international codes and standards that establish general principles for the execution, testing, supervision, monitoring and design of soil nail walls published in last decades: Clouterre (1991), XP P 94-240 (1994), Federal Highway Administration (FHWA, 2003), CIRIA C637 (2005), EN 14490 (2010), BS 8006-2 (2011), etc.

The generally used method for its analysis is the two-dimensional limit equilibrium method (LEM) due to its simplicity. It is important to emphasize that LEM design has its shortcomings due to the lack of deformation predictions, not considering the deformation needed to mobilise resisting forces in the ground and nail and not determining the contribution of each nail to the global stability of the soil nail wall.

On the other hand rigorous numerical techniques, based on either finite element or finite difference methods, permit analysis of a complex soil-structure interaction assessing the performance and stability of soil nail structures and providing the estimation of deformations, although they are not used so often in the every day design practice of soil nail walls.

In this study the comparison of rigorous FEM with the frequently used LEM is presented for a real case study of a soil nail wall, for a vertical cut of nearly 20.00 m height, as a temporary structure, applying commercial programs Plaxis 2D and Talren 4 (Terrasol) for finite element and limit equilibrium analysis respectively.

In the FEM a plane strain problem in a commercial code Plaxis 2D is studied presenting the influence of some parameters on results, e.g. (a) different structural element type for simulating nails, (b) connection of nails to the wall facing, etc.

It is important to emphasize that generally only the axial forces in nails are considered when LEM and FEM are applied, while bending moments and shear forces, generated at the intersection of the slip surface with the nail after large displacements have occurred, are usually ignored in the analysis. Geogrid elements are used in FEM for simulation of nails with the consideration of only axial forces, but if plate elements are introduced in FEM the analysis of both bending moments and shear forces are taken into account. In general the importance of

contribution of bending stiffness is still questionable (Shlosser, 1991; Jewell & Pedley, 1990, 1991, 1992). Bending stiffness contribution comes into play when the reinforced mass is near failure and its major significance is in softer soils (Cheang et al, 2000). According to FHWA (2003) the bending and shear stiffness are conservatively overlooked due to their contribution of not more than 10 % on the overall stability of the wall.

2. CODES AND STANDARDS

As it was stated previously, the standards and codes for the analysis of soil nail walls usually applied are: Clouterre (1991), XP P 94-240 (1994), Federal Highway Administration (FHWA, 2003), CIRIA C637 (2005), EN 14490 (2010), BS 8006-2 (2011), etc.

According to FHWA the conventional design includes the preliminary design using simplified charts and final design. The final design of soil nail walls includes analysis of external failure modes (global stability, sliding stability, bearing capacity), internal failure modes (pull-out failure and nail tensile strength failure) and design of facing and its failure modes (flexure and punching shear failure).

The required factors of safety, applicable when allowable stress design is applied when loads are unfactored, for temporary soil nail walls are given in Table 1.

Table 1. Minimum FS for temporary structures

Failure mode	Minimum recommended FS	
	Resisting component	Static
External stability	Global stability	1.35
	Sliding	1.3
Internal stability	Pull-out resistance	2.0
	Nail bar tensile strength	1.8
Facing strength	Facing flexure	1.35
	Facing punching failure	1.35

One of the most important parameter for the evaluation of soil nail wall performance during its design life is the deformation of the same wall and its influence on the adjacent structures. There are empirical correlations for its estimation, mostly based on Clouterre (1991). According to Clouterre (1991), based on extensive experimental study, the magnitude of horizontal and vertical displacement at the top of the facing is practically equal being in the range of

(0.1-0.4)% H, considering the lower value appropriate for nails constructed in weathered rocks / stiff soils and the higher value for nails in clayey soils. The horizontal surface displacement behind the wall (δ_0) generally ranges from (0.04 - 0.05)% H. These displacements leads to the distortion of the soil nail mass resulting in small bending moments that should be developed near the failure surface. The length over which deformations are dampened (λ) behind the soil nail wall is defined as:

$$\lambda = H \cdot (1 - \tan \eta) \cdot k \quad (1)$$

where k is a coefficient in function of the soil type according to the Table 2, H is the slope height and η is the inclination of the facing regarding the vertical axis.

Table 2. Displacement parameters (Clouterre, 1991)

Parameter	Soil type		
	Weathered rocks Stiff soils	Sandy	Clayey
$\delta h/H \approx \delta v/H$	1/1000	1/500	1/250
k	0.80	1.25	1.50

During construction the allowable horizontal deflections are up to 0.005H according to FHWA (2003). Furthermore a post-construction deformation tend to occur, depending on the ground type, leading to the increase of additional tension in nails (FHWA, 2003).

By defining following four parameters (CIRIA C637, 2005), the comparison between designs of different projects is allowed and evaluation of a global performance of soil nail walls:

$$L_r = L_{\max} / H \quad (2)$$

$$B_r = D \cdot L_r / s_h \quad (3)$$

$$S_r = D^2 / s_h \quad (4)$$

$$P_r = \delta_h / H \quad (5)$$

where L_{\max} – the maximum nail length, L_r – length ration, B_r – bond ratio, s_h – horizontal spacing, D – drill hole diameter, S_r – strength ratio, P_r – performance ratio, δ_h – horizontal displacement.

One of the applications of analysis of performance of soil nailed walls based on case

studies executed in soils of similar nature, using design parameters as defined by CIRIA C637 and presented in Section 2 of the present paper is given in Durgunoglu et al (2007).

3. SOIL NAIL WALL CASE STUDY

The paper is referred to a real case study of a 20.75 m vertical cut excavation in soil, supported using soil nail wall system as a temporary structure (see Figure 1). 12 rows of nail bars separated horizontally 1.70 m were used for this temporary structure (diameters: $\Phi 20$, $\Phi 26$ and $\Phi 32$).

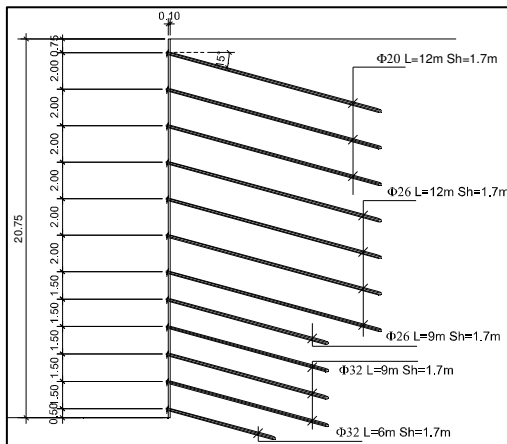


Figure 1. Cross section of the studied soil nail wall.

In Table 3 and 4 the summary of design parameters for a case study soil nail wall according to CIRIA C637 (2005) is given.

Table 3. Design parameters

Parameter	
Excavation height	$H=20.75\text{m}$
Soil nail wall angle	$\beta=90^\circ$
Nail orientation	$i=15^\circ$
Nail drill hole diameter	$D=110\text{mm}$
Horizontal spacing	$Sh=1.7\text{m}$
Vertical spacing (average)	$Sv=1.75\text{m}$
Area per nail (average)	$S=2.98\text{m}^2$
Nail density	$\eta=3.53\text{m}/\text{m}^2$
Length ratio	$Lr=0.506$
Bond ratio	$Br=0.388$
Strength ratio	$Sr=4.07 \cdot 10^{-3}$

According to Clouterre (1991), following values presented in Table 4 for deflections as

defined in Section 2 would be obtained in this real case study for the range of possible soil types.

Table 4. Displacement parameters (Clouterre, 1991)

Parameter	Soil type		
	Weathered rocks Stiff soils	Sandy	Clayey
$\delta h \approx \delta v$ (mm)	20.75	41.5	83
δ_0 (mm)	8.3		10.4
Pr	0.0004		0.0005
λ (m)	16.6	25.9	31.1

4. LEM ANALYSIS

The two-dimensional calculation, i.e. plane cross-sections, by the commercial programme Talren 4 is performed. The analysis includes the global and local failure calculations by the Bishop method after each construction stage, with no stress-strain and/or displacement calculations. The ground is modeled with all soil layers as encountered at the site. The wall facing was not taken into account in the LEM analysis.

The following Figure 2 shows a case study analyzed with the soil introduced with all layers encountered at the site by extensive in situ explorations. The global stability is presented after the final construction stage.

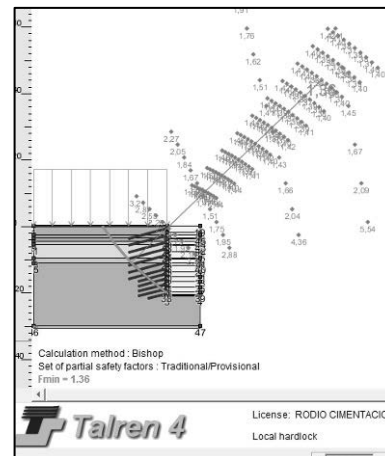


Figure 2. Cross section of the soil nail wall analyzed by Talren 4.

5. FEM ANALYSIS

For further insight into the behavior of soil nail wall, a detailed FEM analysis was performed in

order to compare it with results of LEM analysis and to study the influence of different parameters on results. For that purpose the commercial code Plaxis (version 8.6) was used. The plane strain two-dimensional model is used.

The 15-node triangular elements were used to generate the finite element mesh. The boundary conditions were set at 70.00 m away from the soil nail wall, and 50.00 m below the soil nail wall, which is large enough to avoid boundary effects, i.e. minimize its influence on numerical simulation results. The global coarseness mesh was set to medium type. To ensure the accuracy in the analysis, the mesh is further refined in the vicinity of soil nail wall at 20.00 m laterally and 10.00 m below the soil nail wall.

Figure 2 shows the mesh and geometry used in FEM for the analysis of the soil nail wall in the case of geogrid elements used for modeling of nails. The same mesh type and geometry is used for all different finite element analysis. The general rule in FEM is the finer the mesh the more accurate analysis, although the increase in mesh density results in greater overall calculation time. The influence of mesh density on finite element simulation of soil nail walls is given in Babu & Singh (2009), being max 6% for FS and 26% for displacement analysis, for the range of very coarse and very fine mesh.

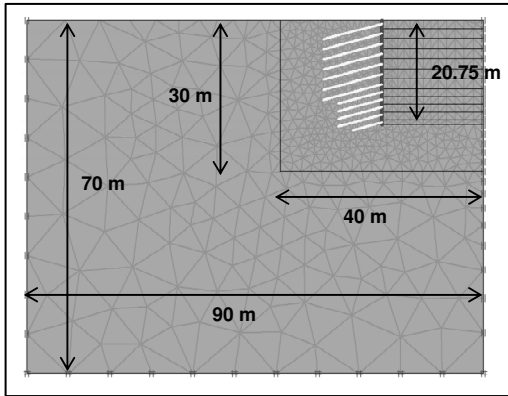


Figure 2. Mesh and geometry of the soil nail wall.

The material model adopted to simulate the soil is the hardening soil model, as the most appropriate to simulate the soil for excavation analysis by FEM. The average geotechnical parameters of the soil profile presented in the LEM are used in the FEM in order to simplify the analysis and to reduce the calculation time.

Soil nails and facings are modeled as elastic materials.

The common practice is to use geogrid elements for simulating soil nails, which considers only the axial stiffness of nails. By that way the bending and shearing resistance of soil nails is conservatively ignored. In this study the use of both geogrid and plate elements is studied, in order to quantify the influence of bending and shear resistance on results.

Moreover the simulation of soil nail walls usually does not take into account wall facing, being by that way on the safe side in the analysis. In this study the influence of the facing element on the global stability is studied. The wall facing is modeled as a plate structural element in order to simulate the rigid nail-facing connection.

The input parameters required for modeling plate elements are bending (EI) and axial (EA) stiffness, while for geogrid modeling only the axial stiffness is required. Considering that soil nails are circular and distributed at certain horizontal distance, it is necessary to determine the equivalent stiffness as rectangular elements per linear meter.

The equivalent modulus of elasticity (E_{eq}) of the soil nail is determined by taking into account both reinforcement bar and grout cover. That value is later used for calculation of bending (E_{eqI}) and axial stiffness (E_{eqA}).

$$E_{eq} = E_n \left(\frac{A_n}{A} \right) + E_g \left(\frac{A_g}{A} \right) \quad (6)$$

where: E_n and E_g are the modulus of elasticity of the nail bar and grout material respectively; A_n and A_g cross section area of the nail bar and grout material; and A is the total cross section of the grouted soil nail ($=0.25\pi D^2$).

The interaction between soil and nail and wall facing plate elements is accounted by interface elements. Bearing in mind that the value of soil reinforcement interaction obtained by pull out tests is larger than unity (Wang et al, 2002), the defaulting set of rigid interface in soil material is used instead of the use of interface elements.

An axial vertical distributed load 20 kN/m² was applied at the soil surface beside the soil nail wall.

The complete soil mass was initially simulated for gravity loading before excavation in order to generate initial stresses. Displacements due to gravity loading were set to zero at the

beginning of the staged construction used for general numerical simulation of the soil nail wall. In each excavation stage, soil cluster representing excavation side is deactivated and the corresponding soil nail and wall facing is activated. Each step of calculation comprised sufficient number of calculation steps in order to reach the steady state condition after excavation.

Table 5 summarizes material properties adopted in numerical simulation using Plaxis. The soil is modelled with its average characteristics along whole depth.

Table 5. Material model parameters

Parameter	
Nails	
Yield strength reinforcement	$f_y=420\text{MPa}$
Elasticity modulus reinforcement	$E_y=200\text{GPa}$
Elasticity modulus grout	$E_g=23\text{GPa}$
Soil	
Unit weight	$\gamma=15\text{kN/m}^3$
Internal friction angle	$\phi=31^\circ$
Cohesion	$c=17.5\text{kPa}$
Poisson's ratio	$\nu=0.2$
Triaxial secant stiffness modulus	$E_{50}^{ref}=10\text{MPa}$
Oedometric tangent stiffness modulus	$E_{oed}^{ref}=10\text{MPa}$
Unloading/reloading stiffness modulus	$E_{ur}^{ref}=40\text{MPa}$
Power of stress dependency	$m=0.5$

6. COMPARISON OF RESULTS

Due to limited extension of the paper, only some of the results are presented.

The external failure mode as a global stability is studied under static conditions in this case. Figure 3 presents results of factor of safety for both LEM and FEM during construction stages. The comparison of simulation of soil nails by use of geogrid and plate structural elements has been studied. The comparison of results obtained by introducing facing element simulating a shotcrete of 10 cm thickness is done. Following abbreviations are further introduced in function of FEM simulation: G - geogrid element, G+F - geogrid element + facing, P - plate element, P+F - plate element + facing.

From the Figure 3 the following can be concluded: (a) values of factor of safety

obtained by modeling soil nails as geogrid elements is lower than when modeling as plate elements both for modeling with and without facing; (b) the results obtained by LEM are close to results of FEM with soil nails simulated as plate elements during all construction stages; (c) the influence of bending resistance of nails on values of factor of safety is concluded especially during the beginning of construction due to much lower safety factors obtained by modeling of nails as geogrid elements; (d) the difference between results obtained for FEM of soil nails as plate and geogrid elements is more pronounced during first construction stages while being very similar for final stages; (e) the contribution of wall facing element on the stability during excavation is more pronounced during first construction stages.

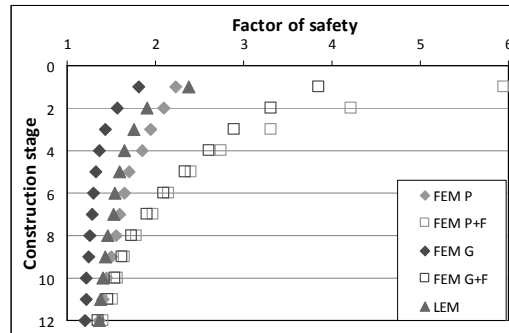


Figure 3. Global factor of safety during different construction stages.

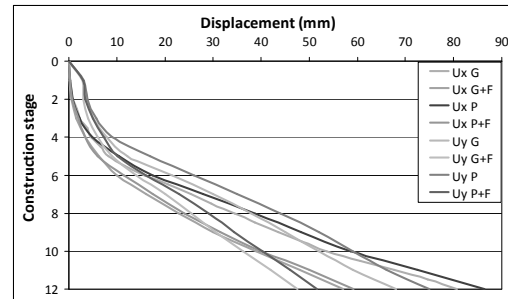


Figure 4. Displacement of the top of the soil nail wall.

Figure 4 shows maximum values of horizontal and vertical displacement at the top of the soil nail wall with construction stages. During first stages the difference is negligible both for horizontal and vertical displacements under all four assumptions (G, G+F, P, P+F).

For later stages there are little difference when modeling soil nails as geogrid or plate elements, as well as modeling geogrid or plate elements with facings. When taking into account the facing by modeling it as a plate element there is a significant reduction in displacements at later stages.

Figure 5 presents the maximum axial force at each soil nail level during construction stages for both cases of modeling of soil nails as geogrid and plate elements, and with and without taking into account the facing element. Figure 6 presents the variation of axial force along some of the soil nails lengths at different levels for both simulation cases of soil nails as geogrid and plate elements. At different soil nail levels the obtained variance ranges up to approximately 15%, considering it insignificant for practical purposes. Very similar axial force distribution along nail length is observed when modeling nails as geogrid and plate elements (see Figure 6).

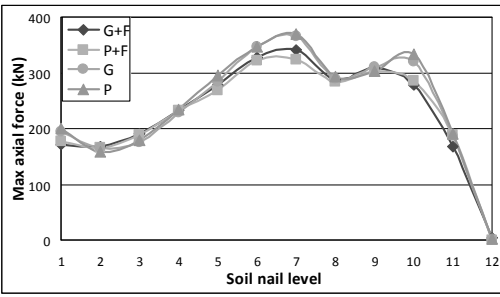


Figure 5. Maximum values of axial forces at different soil nail level.

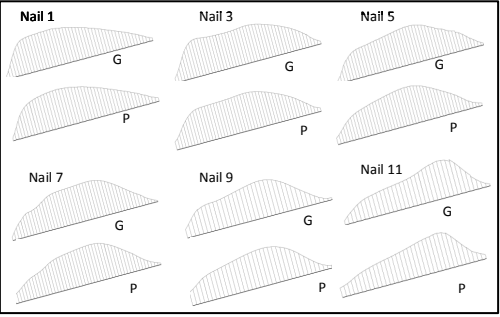


Figure 6. Variation of axial forces along soil nail lengths at different levels for modeling nails by G and P elements.

The difference in axial force distribution when modeling with and without facing element

for nails simulated as plate elements is given in Figure 7. Diagrams are of similar nature, the only difference would be the higher value of axial force at the point of connection with wall facing. The confirmation of the maximum tensile force occurring at $(0.3-0.4)H$ behind the wall facing, and in the lower portion of the wall at $(0.15-0.2)H$, is observed (FHWA, 2003).

Figure 8 shows maximum values of bending moments and shear forces at each soil nail level during construction stages when modeling soil nails as plate elements. There is a difference between correlations when taking into account facing element, due to rigid connection between soil nails and facing, being greater values of mobilized bending and shear forces in case of considering the facing element.

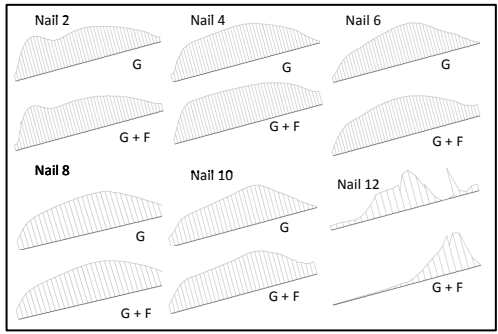


Figure 7. Variation of axial forces along soil nail lengths at different levels for G and G+F.

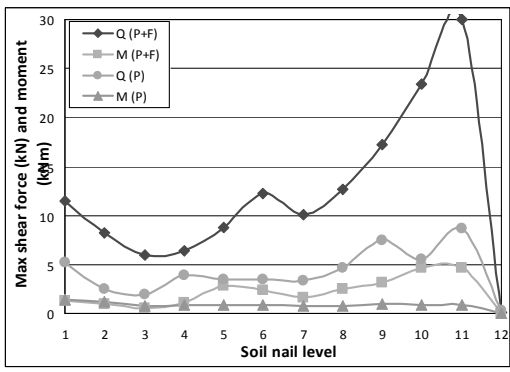


Figure 8. Maximum values of shear forces and bending moments vs. soil nail level.

Figure 9 shows the variation of bending moments and shear forces along the soil nail length at diverse levels, for soil nails modeled as plate elements. The expected concentration of forces near face of the wall is observed.

Figure 10 presents the variation evaluated in percentage between maximum tensile force in the nail when modeled by G or G+F, as well as the difference in maximum tensile and shear forces and bending moments developed when simulation performed as P and P+F elements, at each nail level.

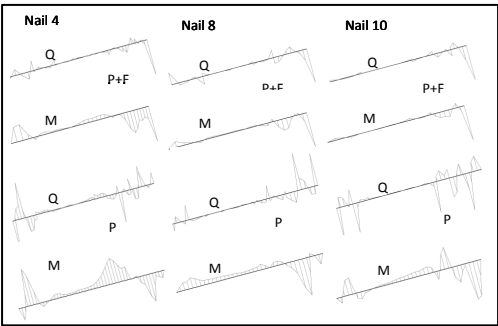


Figure 9. Variation of shear and moment forces along soil nail lengths at different levels for modeling nails as P elements.

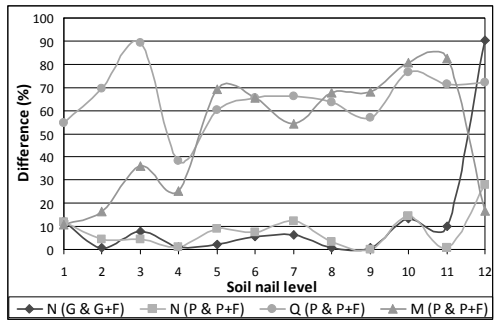


Figure10. Difference in tensile and shear forces and bending moments at each soil nail level for simulation by G, G+F, P and P+F elements.

Figure 11 summarizes the variation of axial and shear forces and bending moments along the facing elements for simulations by G+F and P+F elements.

Figure 12 is an example of obtained deflections behind the soil nail wall mass in the case of nails modeled as geogrid elements by FEM.

The comparison of deformation parameters as described in Section 2 by empirical formulations given in Clouterre (1991) and its values deduced from FEM analysis is presented in Tables 6 and 7. Table 6 shows horizontal and vertical displacements, and its corresponding ratios to the height of soil nail wall. Table 7

presents values of displacements behind the soil nail wall and the length over which the deflections are damped.

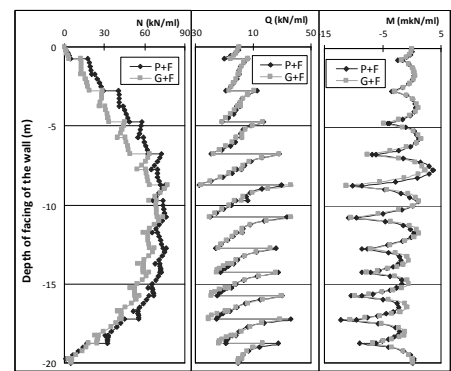


Figure11. Variation of axial forces, shear forces and bending moments in facing elements for simulation by G+F and P+F elements.

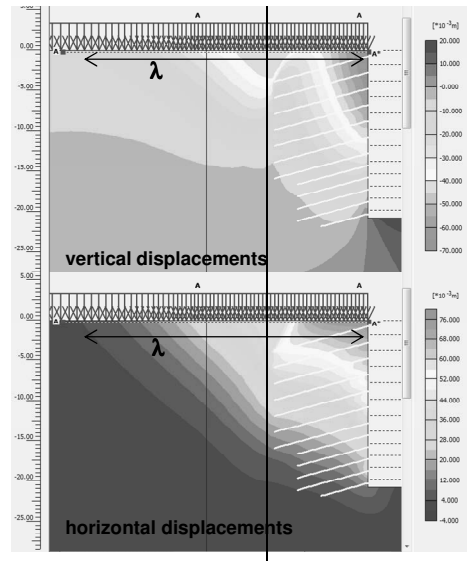


Figure 12. Deflections behind the soil nail wall.

Table 6. Displacements according to FEM and Clouterre (1991)

	δ_h (mm)	δ_v (mm)	δ_h / H	δ_v / H
FEM (G)	80.62	68.07	1/257	1/305
FEM (P)	86.42	75.09	1/364	1/277
FEM (G+F)	57.05	47.57	1/240	1/436
FEM (P+F)	59.23	51.61	1/350	1/402
Clouterre	max 83	max 83	max 1/250	max 1/250

Table 7. Displacements behind the wall nail mass and length over which the displacements are dampened according to FEM and Clouterre (1991)

	δ_0 (mm)	λ (m)
FEM (G)	41.7	35.5
FEM (P)	44.9	35.5
FEM (G+F)	37.1	35.25
FEM (P+F)	36	35.25
Clouterre	max 10.4	max 31.1

7. CONCLUSIONS

The comparison of a case study by FEM and LEM is presented.

The FEM is preferred to LEM in order to obtain a global performance of a soil nail wall and an evaluation of deflections of the soil nail wall.

The comparison of empirical deflection formulations according Clouterre (1991), generally adopted in other international standards, with FEM results is presented. The estimation of displacements by mentioned empiric formulae is sufficient at the preliminary stage of the study.

The plate elements for simulation of soil nails is preferred to geogrid elements in order to account for the bending stiffness and shear resistance of soil nails.

The global stability and deformation considerations indicate a stable system of the case study.

Values of factor of safety obtained by modeling soil nails in FEM as geogrid elements is lower than when modeling as plate elements both for cases with and without facing. The results of FS obtained by LEM are close to results of FEM with soil nails simulated as plate elements.

The influence of bending resistance of nails on values of factor of safety is observed at mayor scale during the beginning of construction of soil nail wall considering significantly lower safety factors obtained by modeling of nails as geogrid elements.

The difference between results obtained by FEM with soil nails modeled as plate and geogrid elements is more pronounced during first construction stages reaching almost similar values at final stages.

The contribution of wall facing on the stability during excavation is more pronounced during first construction stages.

8. REFERENCES

- Babu, G.L. & Singh, V.P. 2007. Stabilization of vertical cut using soil nailing. *Plaxis Bulletin Iss.* 22. pp.6-9.
- Babu, G.L. & Singh, V.P. 2009. Simulation of Soil Nail Structures using Plaxis 2D. *Plaxis Bulletin Iss.* 25. pp.16-21.
- BS 8006-2. 2011. *Code of practice for strengthened/reinforced soils. Part 2: soil nail design.*
- Cheang, W. L., Luo, S. Q., Tan, S.A. & Yong, K.Y. 2000. Lateral bending of soil-nails in excavation. *Int. Conf. Geotech. and Geol. Eng. (GeoEng 2000, Melbourne, Australia).*
- CIRIA C637. 2005. *Soil nailing – best practice guidance.* London.
- Durgunoglu, H.T., Keskin, H.B., Kulac, H.F., Ikiz, S. & Karadayilar, T. 2007. Performance of soil nailed walls based on case studies. *Geotechnical Engineering in Urban Environments.* Proc. 14th European Conf. on Soil Mechanics and Geotech. Eng. Madrid, Spain. Vol 2, pp. 559-564.
- European Standard EN 14490. 2010. *Execution of special geotechnical works: soil nailing.*
- Federal Highway Administration. 2003. *Geotechnical engineering circular No. 7 – soil nail walls.* Report FHWA-AO-IF-OS-017. Washington DC. USA.
- French National Research Project. Recommendations Clouterre. 1991.
- Jewell, R.A. & Pedley, M.J. 1990. Soil nailing design: the role of bending stiffness. *Ground Engineering.* pp. 30-36.
- Jewell, R.A. & Pedley, M.J. 1991. Discussion closure. *Ground Engineering.* pp. 34-39.
- Jewell, R.A. & Pedley, M.J. 1992. Analysis for soil reinforcement with bending stiffness. *Journal of Geotech. Eng. Vol 118. No. 10.* pp. 1505-1528.
- Plaxis. 2012. Plaxis user manual. University of Technology & Plaxis bv. The Netherlands.
- Shlosser, F. 1991. Discussion: The multicriteria theory in soil nailing. *Ground Engineering.* pp. 30-33.
- Wang, Z. & Richwien, W. 2002. A study of soil-reinforcement interface friction. *Journal of Geotech. & Geoenv. Eng. Vol. 128. No.1.* pp. 92-94.
- XP P 94-240. 1998. *Soil reinforcement – nail reinforced in situ retaining and slope structures - Verification of dimensioning.*

Assessment Analysis of Lateral Movement of Gate Shaft Structure on Fractured Rock Mass, Jatigede Dam Area, West Java, Indonesia

Putera Agung M, A; Pramusandi, S; Ardianto, A
Civil Engineering Department, State Polytechnic of Jakarta, Indonesia
E-mail: putera_agung2002@yahoo.com; pramusandis@yahoo.com

Sunaryo, B
Senior Engineer for Jatigede Dam Project, West Java, Indonesia

ABSTRACT: Gate shaft is one of parts the power waterway system of dam structure and as an intake vertical tunnel or well function for hydroelectric power plants in Jatigede area, Sumedang, West Java. Paper concerns some consideration in determining a constitutive model of soil and rock material. Comparison of existing lateral movement and the analysis results identified that Hoek – Brown failure criterion were more suitable than Mohr – Coulomb. Study analysis was carried out using without and with reinforcement system, the risk assessment to a rock shaft during excavation is greater than that to a soil shaft, even though the two averages designed safety factors are the same. For the analysis, it should be considered to use the failure criteria of intermediate material.

INTRODUCTION

Power waterway is a structure for water channel of hydroelectric power plant. Structure consists of several components, then they called as: intake, headrace tunnel, sluice gate control wells or gate shaft; surge shaft; and penstock tunnel. One case study was concerned for a back stability analysis of the gate shaft power waterway in Jatigede dam construction, Sumedang, West Java, Indonesia (Figure 1). Some considerations in determining of critical state parameters are focused in this paper.

Power waterway was designed to discharge 73 m³/sec based on a need of water for irrigation system at the downstream of the Rentang in study area. By using hydraulic analysis, the original vertical tunnel diameter was predicted by D = 4.50 m. Then, the tunnel dimensions were redesigned from the original diameter of D = 4.50 to 5.50 m for of 175 MW for hydroelectric power plant with the discharge (Q) = 123 m³/sec, and D = 4.50 m was applied for 110 MW with discharge of 73 m³/sec (source: Design Report for Jatigede Dam Project, 2011).

Gate shaft was applied to place the emergency and regulator sluice gate for hydroelectric power generation, where it was made from reinforced concrete structures. At the topside of the well was constructed a building for operation room to control the sluice gate. The control room was also completed by some equipment for air compressors and high-pressure tank capacity of 25 bars to operate jet nozzles.

Excavation of the gate shaft was designed with using the temporary reinforcement system. Some stability analyses during excavation works are required to predict stress and strain of soil or rock layers around the gate shafts during excavation. When the soil or rock is not able to resist load or deformation occurred, they were required to use some reinforcement system. Since the study area have some variations of soil and rock layers, the selection of critical state parameter is important to be discussed.

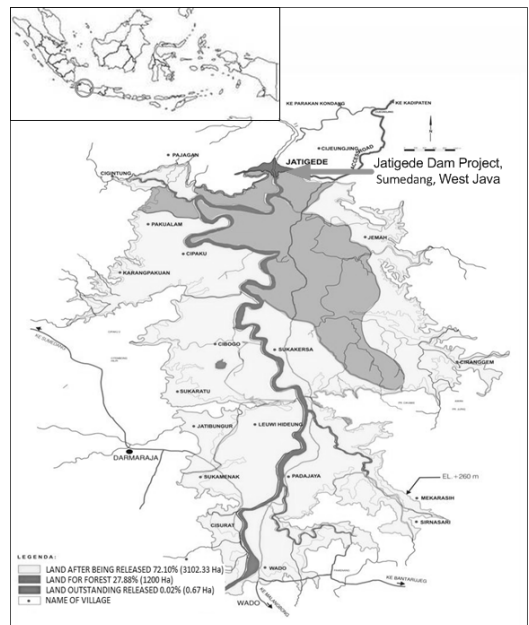


Figure 1. Location of Jatigede Dam project.

2. FAILURE CRITERION OF ROCK

Rock cycle of earth's surface consists of three main groups, namely: (a) Frozen Rock (Igneous-Rock); (b) Sedimentary Rock; and (c) Metamorphic-Rock. Thus, soil material is the result of weathering of the three rocks. Some parameters were obtained by the results of soil and rock investigation in the laboratory works. However, the selection of rock parameter is more discussed for this paper.

Figure 2 shows the diagram of stress – strain relationship for rock material. Theoretically, elastic deformation of rock requires the change of volume; however, plastic deformation usually occurs at the constant volume. Then, based on the data results from laboratory and field test performed for the rock formation at Jatigede area which will be discussed on this paper, mostly the rock layers from study area can be classified into a class of fractured rock masses. Figure 2 also shows an incremental stress – strain relation for elasto – perfectly plastic deformation processes with and without hardening–softening considerations.

A constitutive behavior of fractured rocks masses as equivalent continua covers a non-linear material model. The deformation contributed by fractures is then assumed as plastic deformation of the equivalent continuum and the hardening–softening rules of plasticity are adopted to simulate similar behavior of fractured rocks. The elasto-perfectly plastic deformation are presented briefly in here using Mohr–Coulomb and Hoek–Brown criterion as the yielding functions, since these criteria are used widely in many discrete element method (DEM) models for rock block behavior.

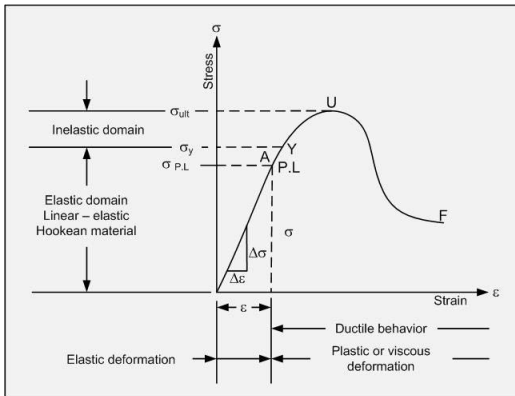


Figure 2. Stress – strain diagram of rock (Moesdarjono, 2009).

Together with the Mohr–Coulomb criteria, the Hoek–Brown criteria can be applied wide applications, especially for fractured hard rocks, for both numerical modeling and rock classification. The two criteria can be transformed from one to another (Hoek and Brown, 1997).

Behavior of collapse for soil is mostly approached by the Mohr – Coulomb method. however, parameters of c' and ϕ' determined by Hoek – Brown criteria also uses the Mohr – Coulomb method following the equation:

$$c' = \frac{\sigma_{ci} [(1+2a)s + (1-a)m_b \sigma'_{3n}] (s + m_b \sigma'_{3n})}{(1+a)(2+a) \sqrt{1 + \frac{(6am_b (s + m_b \sigma'_{3n})^{a-1})}{(1+a)(2+a)}}} \quad (1)$$

$$(\phi') = \sin^{-1} \left[\frac{6am_b (s + m_b \sigma'_{3n})^{a-1}}{2(1+a)(2+a) + 6am_b (s + m_b \sigma'_{3n})^{a-1}} \right]$$

$$\text{where } \sigma'_{3n} = \frac{\sigma'_{3\max}}{\sigma_{ci}}$$

$\sigma'_{3\max}$ is the upper limit of confining stress predicted by relationship between Mohr–Coulomb and Hoek – Brown. Fig. 2 shows the correlation equation of $\sigma'_{3\max}$ Hoek – Brown and Mohr – Coulomb (Hoek, 2002).

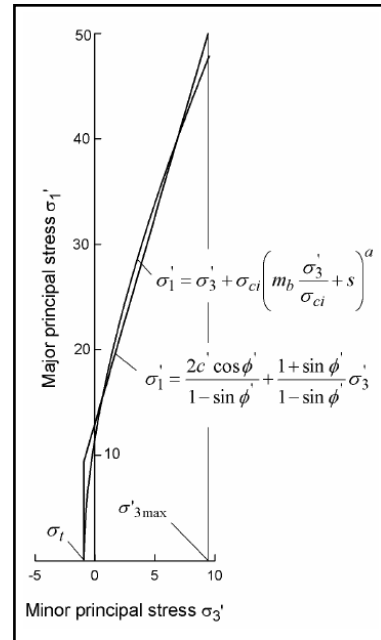


Figure 2. Major and minor relationships based on the principal stresses of the Hoek – Brown and Mohr – Coulomb (Hoek, 2002).

From Figure 2, relationship between upper limit of confining stress ($\sigma'_{3\max}$) and strength of the rock mass (σ'_{cm}) is:

$$\frac{\sigma'_{3\max}}{\sigma'_{cm}} = 0,47 \left(\frac{\sigma'_{cm}}{\gamma H} \right)^{-0,94} \quad (3)$$

$$\text{where } \sigma'_{cm} = \frac{2c' \cos \phi'}{1 - \sin \phi'}$$

From this figure, c' and ϕ' values were found by the interval of $\sigma_1 < \sigma_3 < \sigma_{ci} / 4$ obtained from:

$$\sigma'_{cm} = \sigma_{ci} \frac{(m_b + 4s - a(m_b - 8s))(m_b / 4 + s)^{a-1}}{2(1+a)(2+a)} \quad (4)$$

The equation was applied when rock collapse only occurred around the excavation shaft below the ground surface.

3. PHYSICAL PROPERTIES OF ROCK

Rock formations at Jatigede dam area consist of Pliocene Breccia, claystone from upper Halang Formation, Breccia from lower Halang Formation, and claystone from Cinambo Formation. Rock formations are covered by layers of sand and clay. Bedrock layer of power shaft consists of claystone, volcanic breccia and local tuff breccia or lapilli tuff (Figure 3). Typical of description of rock mass at Jatigede Dam area shows in Table 1 and Figure 4 indicated by the core-box of rock material.

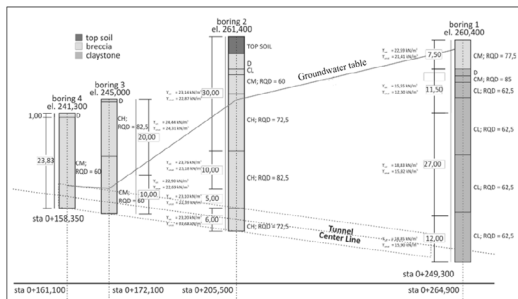


Figure 3. Existing profile of the rock mass

Based on Figure 3, all the rock masses can be classified into the fractured rocks and analyzed with using failure criterion proposed by Hoek and Brown (1980, 1988, 1997) and Hoek (1983, 1994). Table 1 shows typical description of rock mass classes (classification from Central Research Institute of Electric Power Industry (CRIEPI), Japanese National Committee, 1950).

Table 1. Typical of physical properties of rock from field core-box at the site

Depth (m)	Description	Rock class
0.0 – 2.0	No core, reaming concrete.	
0.2 – 3.75	Concrete.	
3.75 – 5.9	Volcanic breccia, slightly weathered, average RQD 60% - 95%. Most core breaks are horizontal, filled by calcite.	CM
5.9 – 6.15	Claystone, dark grey, partly fractured, maximum core length 15 cm.	D
6.15 – 6.8	Claystone, light grey. max core length 50 cm	CL
6.8 – 7.0	Claystone, light grey, fractured/fragments. Partly sheared. Soft rock. Mostly spontaneous cracking on storage.	D
7.0 – 8.0	Claystone - sandstone, light grey. maximum core length 50 cm. RQD 85%.	CM
8.0 – 9.4	Coarse sandstone, light grey. maximum core length 60 cm. RQD 45 - 80%. Medium hard. Mostly spontaneous cracking on storage.	CM
9.4 – 12.0	Fine sandstone, light grey, interbedded sandstone - siltstone. maximum core length 60 cm. RQD 45 - 80%. Soft rock. Some calcite veins about 1 mm. Average RQD : 10% - 95%.	CL
12 – 12.3	Claystone, light grey, broken rock. Soft rock. Mostly spontaneous cracking on storage.	D
12.3 – 29.5	Mostly claystone interbedded with siltstone, light grey, some soft or sheared claystone layer, generally moderately weathered (dark grey color). Slickenside in some part.	CL partly D
29.5 – 31.7	Coarse sandstone interbedded with siltstone, medium hard. Slightly weathered, maximum core length 60 cm.	CM
31.7 – 35.8	Mostly claystone interbedded with siltstone,	CL partly

	light grey, some soft or sheared claystone layer, generally moderately weathered. Slickenside in some part.	D
35.8 – 36.3	Coarse sandstone, medium hard. Slightly weathered (dark grey color), max core length 60 cm.	CM
36.3 – 38.4	Volcanic Breccia, medium hard. Slightly weathered, max core length 60 cm.	CM
38.4 – 39.4	Claystone, light grey, broken rock. Soft rock. Mostly spontaneous cracking on storage.	D
39.4 – 43	Fine sandstone, light grey, interbedded sandstone - siltstone. Maximum core length 60 cm. Partly soft rock of sheared claystone. Some calcite veins about 1 mm. Average RQD : 10% - 95%.	CL partly D

From Table 1, average of RQD (Rock Quality Designation) value of 2 (two) bore hole can be classified as shown as Table 3. According to Deere's classification system (1966) for rock mass with RQD values 40 – 95 % is classified into “*fair to good rock*” level, where the condition is assumed as the form of blocky and seamy rock as part as volcanic breccia (Figure 4). Coefficient permeability (k) of rock mass was measured by the groundwater inflow through at join or discontinuities of rock mass. Figure 4 shows estimation values of coefficient of permeability.

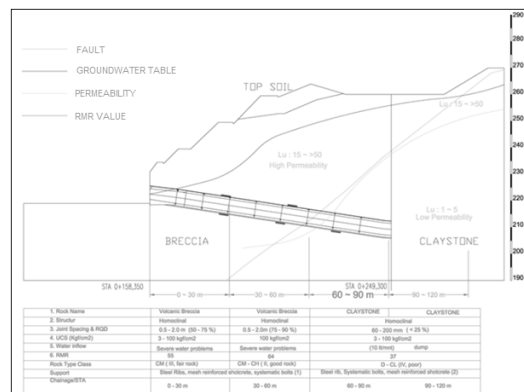


Figure 4. Coefficient permeability of rock

4. STRENGTH PROPERTIES OF ROCK

Deere and Miller (1966) describe the values of strength below of 250 kgf/cm² for rock can be classified as “*very low rock strength*”. Since the characteristic of rock material exists between soil and rock or an intermediate material, so that the failure criterion has to be selected according with the conditions of the existing rock layers.

There are many constitutive models of rock fractures and rock masses for numerical modeling of the physical behavior of fractured rocks. However, it should be noted that it is difficult to determine the constitutive models are suitable to the intermediate material (soil – rock). Based on some references, theoretically one selected approximation should be determined by some observations in reality, based on certain assumptions according to the different theoretical principles and mathematical approaches adopted, and the material behavior observed in laboratory or field observations. Numerical analysis on this paper deals with the method of assessing the rock shaft excavation stability using the failure criteria from Mohr – Coulomb and Hoek – Brown material. Furthermore, the relationship will be applied to determine strength parameter of rock (Figure 5).

5. REINFORCEMENT SYSTEM

Rock reinforcement method is purposed to support two layers of rock mass, such as: *volcanic breccia* and *claystone* layers. Design for reinforcement system is required to minimize some deformations around the tunnel construction. The rock mass reinforcement system designed uses *Q system* (Grimstad & Barton, 1993).

Selection of rock reinforcement system for volcanic breccia and claystone layers is determined by Grimstad & Barton chart (1993) (Fig. 6), where volcanic breccia includes in the category (4) and claystone exists in the category (8), respectively. *Shotcrete* and *concrete collar* will be applied for both layers.

Excavation works will use drilling and blasting methods. Depth of excavation works in one stage is around 1.5 m. For every stage will be installed the temporary construction included shotcrete with 20 cm in thickness, rockbolt with

6.0 m length and lattice arch for the wall side, and also concrete collar with 1.5 m in thickness from the top side of gate shaft. Distance of each rockbolt point is 1.5 m for vertical and 1.0 m in horizontal directions. Input parameter data to the selected improvement system can be considered by Table 4.

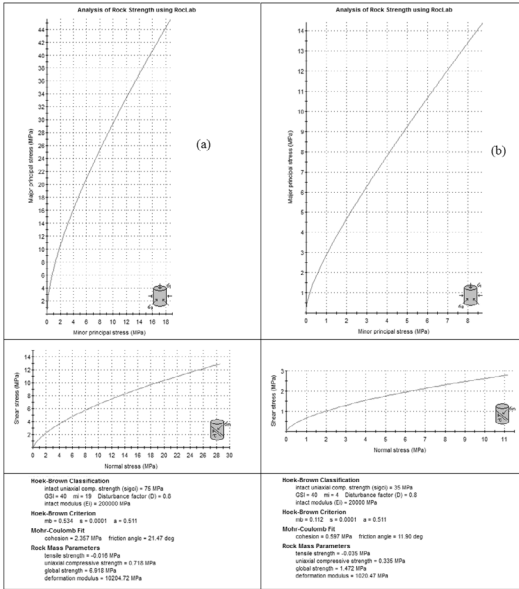


Figure 5. Typical analysis to determine the strength parameter of volcanic breccia (a) and claystone (b) layers based on Hoek – Brown and Mohr – Coulomb using RocLab analysis (Hoek, 2002)

Typical simulation analysis of axisymmetric model (2D and 3D) of gate shaft is shown by Figure 7, at the top layers was volcanic breccia (5 to 7 m) and followed by claystone layers.

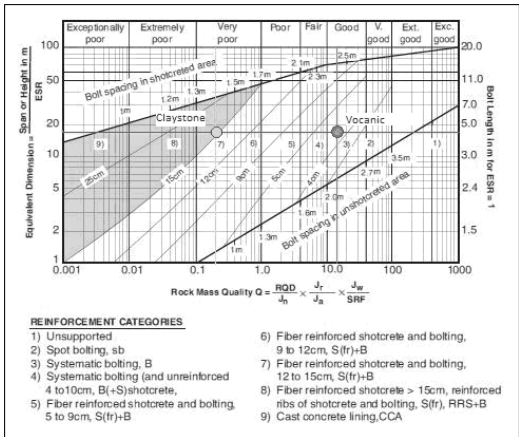


Figure 6. Rock improvement system for volcanic breccia and claystone (Grimstad & Barton, 1993)

Table 4. Parameter of reinforcement system

Parameter	Unit	Value
Rockbolt (as node to node anchor)		
Diameter (d)	m	0.025
Elastic modulus (E)	kPa	2.00E+08
Area (A)	m ²	4.91E-04
EA	kN	9.82E+04
Concrete collar (as a plate)		
Thickness (t)	m	1.5
Elastic modulus (E)	kPa	2.19E+07
Area (A)	m ²	1.5
Inertia moment (I)	m ⁴	2.81E-01
EA	kN	3.29E+07
EI	kNm ²	6.16E+06
Grouting and geogrid		
EA	kN	2.50E+02

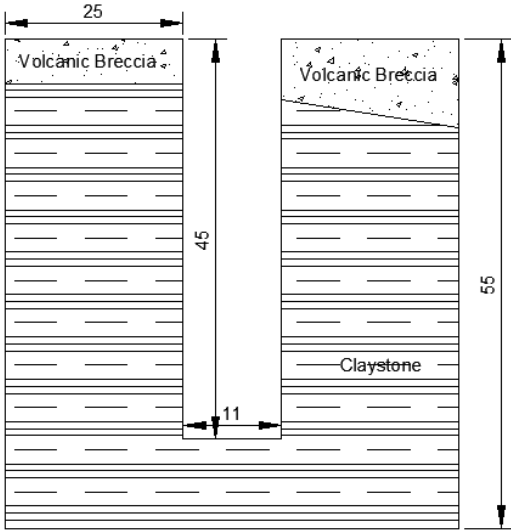


Figure 7. Typical of geometric model of gate shaft

6. SIMULATION ANALYSIS RESULTS

In 2D and 3D models using Finite Element Method (Brinkgreve, 2007), the staged excavation was conducted at every 1.50 m depth; installing of rock mass improvement system; and applying distributed loads at the surface around the gate shaft during excavation process are similar. Distributed loads or (A) were assumed to be 50 kN/m². Figure 9 and 10 shows the all construction process before the assessment analysis, and fluctuation of groundwater table. Fluctuation of groundwater table was due to influenced by every the staged excavation.

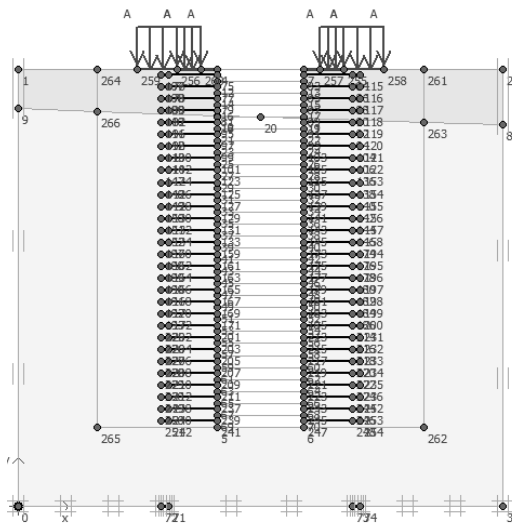


Figure 9. Construction process of gate shaft

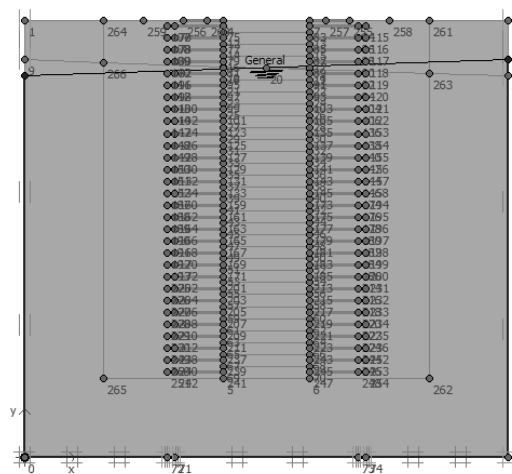


Figure 10. Groundwater level fluctuation

At initial condition for 2D or 3D analysis, overall excavation and installation process of reinforcement system was not performed yet. On the first stage, there was not applying load and rock mass improvement system. However, on the next step, excavation was started to the depth of 1.5 meters and then followed by reinforcement system process installation. Distributed load on each stage of excavation process until to the depth of 45 m was 50 kN/m². Figure 11 shows the initial stress condition where there was not activity of works. Figure 12 illustrates the process of excavation to the maximum depth and reinforcement process installation for each stage after initial condition.

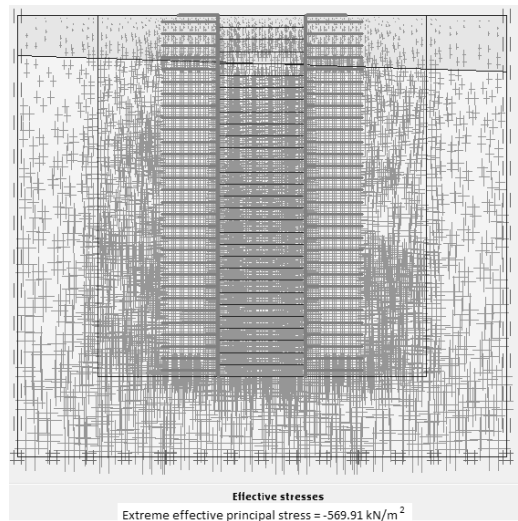
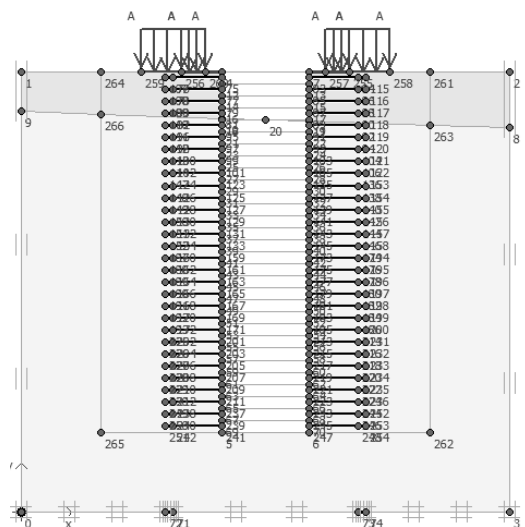


Figure 11. Initial condition of gate shaft before applied of distributed load and no reinforcement



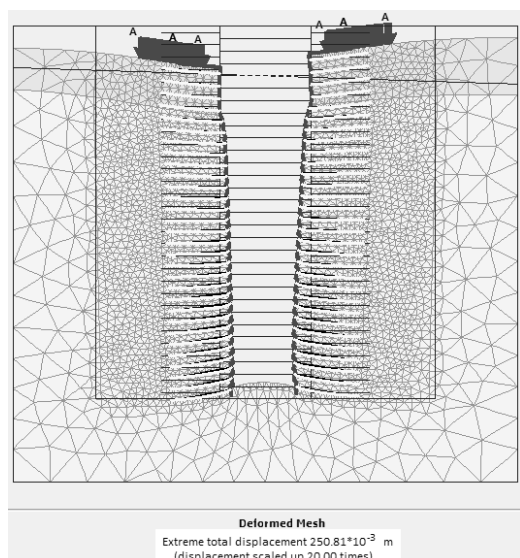


Fig. 13 Typical deformed mesh on 2D gate shaft element with the reinforcement system

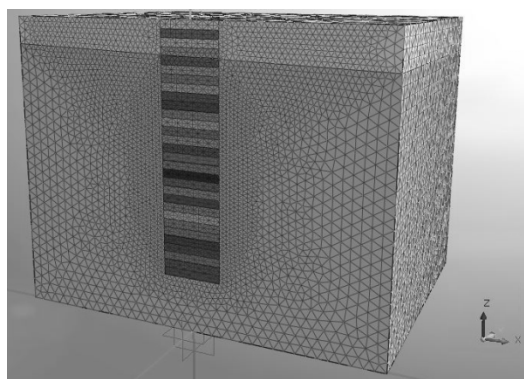


Fig. 14 Typical deformed mesh on 3D gate shaft element with the reinforcement system

7. EVALUATION USING INCLINOMETER

Inclinometer instrumentation was installed on collar concrete wall of the gate shaft. Position inclinometer points around the collar concrete wall (Elevation+ 295.500) was 1 (one) m depth from the top of excavated gate shaft. Number of installed inclinometer devices was 4 (four) points with code number of BH 1, BH 2, BH 3, and BH 4. The depth of installed inclinometer devices were between 44.0 and 56.0 m depth. Coordinates and depths of each inclinometer devices are shown on Figure 15. Measurement of inclinometer was performed for 8 (eight) months continually according to the time interval and sequentially in accordance with the cycle excavation works from initial reading as described by the flowchart in Figure 16.

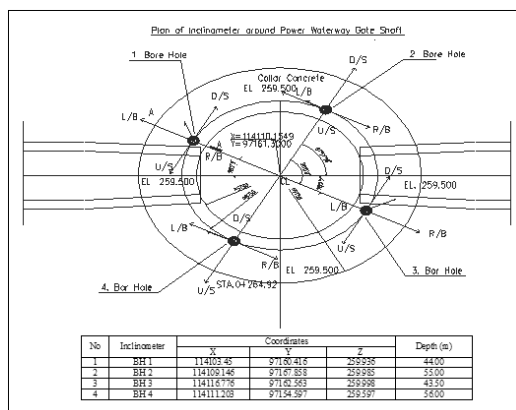


Figure 15. Position of inclinometer points at collar concrete wall of the gate shaft

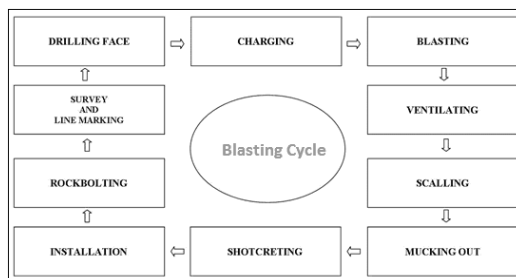


Figure 16. Work excavation cycle of the gate shaft

8. DISCUSSION AND RECOMMENDATION

Based on results of the simulation data, horizontal displacement of gate shaft structure can be reduced significantly by reinforcement system. However, horizontal displacement determined by using 2D, and or 3D analysis was quite different. The difference of analysis results is caused by the difference approach of material constitutive models used in the simulation. Figure 17 shows the comparison between of horizontal displacement using Mohr – Coulomb and Hoek – Brown material, and also the existing maximum lateral movement measured inclinometer system during time observation.

From the Figure 17, the lateral movement predicted by using Mohr – Coulomb material constitutive model is larger than Hoek – Brown. The results from inclinometer device show that the existing lateral movement measured is smaller than assessment results applied by the Hoek – Brown material failure criterion. From observation at the field during the inclinometer measurement, the lateral movements were more caused by the vibration during the excavation process using blasting method. The lateral

movement on volcanic breccia layers initiated by the collapse of material composed of broken rock fragments varying in size. However, the lateral movements on claystone layers were started by the emerged of the fault or crack zones. The fault zone of claystone layers can be subjected to slumping and magnitudes of lateral movement were dominated by claystone layers.

When pore water pressure generated by the consolidation calculation using Mohr-Coulomb model will not be representative of those in – situ excess pore water pressures produced under an undrained loading condition, even though they involved consolidation or seepage condition according to the change of excess pore water pressure and mean effective stress. However, the Elasto-perfectly plastic deformation using Hoek – Brown model is the non-linear computation carried out for loading stage during excavation process with varying applied loads. All steps analysis do not consider time - dependent phenomena such as volumetric consolidation or pore pressure dissipation.

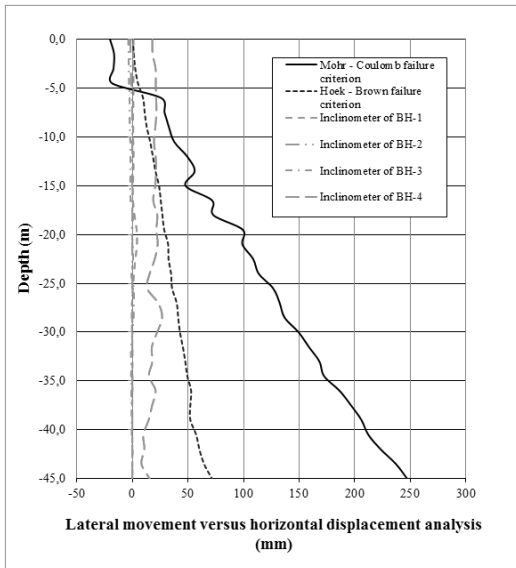


Figure 17. Comparison between of maximum lateral movement and horizontal displacement based on Mohr – Coulomb and Hoek – Brown failure criterion

The layers of claystone stability condition were more influenced by movements than volcanic breccia layers. Small movements of both layers could determine a large fall in the available shear strength and therefore cause a large safety reduction. Some reinforcement

systems (such as: concrete collar, shotcrete, and rockbolt) could reduce the both soil movement vertically and horizontally. From back analysis, safety factor without reinforcement system was existed between 0.98 - 1.03. And then, with using reinforcement systems were generated between 2.32 - 2.97 analyzed by constitutive model from Mohr – Coulomb and Hoek – Brown. However, the risk to a rock shaft during excavation is greater than that to a soil shaft, even though the two average designed safety factors are the same. Consequently, the analysis, it should be considered to use the failure criteria of intermediate material.

REFERENCES

- Brinkgreve, R. B. 2007. *Plaxis*. Delft University of Technology and Plaxis b.v. Holland.
- Central Research Institute of Electric Power Industry (CRIEPI), 1950. *Rock Classification Report*, Japanese National Committee on Large Dam and Standard for Geological Investigation of Dam Foundations.
- Deere, D.U., and Miller, R.P. 1966. *Engineering classification and index properties for intact rock: Air Force Weapons Laboratory Technical Report AFWL-TR-65-116*, 277 p.
- Grimstad E. and Barton N., 1993. *Updating of the Q-system for NMT*. International Symposium on Sprayed Concrete. Fagernes, Proc., pp. 46-66.
- Hoek, E., Carranza-Torres, C. and Corkum, B. 2002. *The Hoek-Brown failure criterion – 2002 Edition*. Proc. 5th North American Rock Mechanics Sym. and 17th. Tunneling Assn of Canada conf. pp. 267-271. Toronto: NARMS-TAC.
- Hoek, E. and Brown, E.T. 1997. *Practical estimates or rock mass strength*. Int. J. Rock Mech. Min.g Sci. & Geomech. Abstr.. 34(8), 1165-1186.
- Hoek, E. 1994. *Strength of rock and rock masses*, ISRM News Journal, 2(2), 4-16.
- Hoek, E. and Brown, E.T. 1988. *The Hoek-Brown failure criterion - a 1988 update*. In Rock engineering for underground excavations, proc. 15th Canadian rock mech. symp., (ed. J.C. Curran), 31-38. Toronto: Dept. Civ. Engineering, University of Toronto.
- Hoek, E. 1983. *Strength of jointed rock masses*, 23rd. Rankine Lecture. Géotechnique 33(3), 187-223.
- Hoek E. and Brown E.T. 1980. *Underground Excavations in Rock*. London: Instn Min.Metall. 527 pages.
- Moesdarjono, S. 2009. *Teknik Pondasi pada Lapisan Batuan*. Surabaya, itspress.

A case study of a Deep Excavation on a Soft Lacustrine Clay of Bogota, Colombia, with emphasis between Predicted and Measured deformations

Lucero Amparo Estevez Rey & Natalia Alexandra Daza Rodríguez
Universidad Santo Tomás, Bogotá, Colombia

ABSTRACT: The paper presents the results of the geotechnical analysis conducted of a deep excavation in the lacustrine soft soil of Bogota city, with emphasis on the differences between the predicted and the measured deformations of the diaphragm walls. The excavation had 11.25m of depth, and following the construction process, seven inclinometers in order to date the spatial displacements induced during the construction of three basements and 40 m deep friction piles under the building infrastructure, including the monitoring of deformations related to base stability. The measurements were extended about 17 months. The project was located in the lacustrine soft soil of Bogota city, which is a very high compressible-plastic clay with void ratios from 3 to 5, compression indexes (Cc) from 1.2 to 2.0 and elastic young modulus under 1000 kPa, with medium to high organic matter contents. It was found that the overall predicted deformation behavior is not consistently with the measured deformations, mainly due to the differences between the real boundary conditions and the model, the localization of the instrumentation and the stiffness properties of the soils.

Keywords: deep excavations, displacements, diaphragm walls, lacustrine soft soil, base stability

1. INTRODUCTION

Through the different field and laboratory tests, the best modeling scenarios can be evaluated, which will allow to do an approach to the theoretical and real behaviors of a flexible element such as screens. It is well known that the boundary conditions and constructive methods have a great influence in a deep slurry concrete wall performance and their induced deformations in excavations on soft clays; these are the main reasons to be especially carefully to how those processes are made and implemented. In this paper, an integrated analysis of the instrumentation and finite element modeling of a three basement excavation is shown, in order to present the development of deformations and other particularities of the case studied. Throughout this work, a benchmark between measured and predicted wall deformations in several stages of an excavation is presented, in order to understand the principal differences and limitations of both sources of information and how this benchmark could make possible a

more robust and rational practice in soft grounds.

2. SOIL CHARACTERISTICS

Given the geotechnical classification established in Decree 523 of 2010 of the Construction Code of Bogota Capital District, the limits of the Seismic Microzonation are identified and the design spectra for the city are adopted, it is defined that the project studied, is located at the lakeside area A, which is mainly formed by deposits of soft clays reaching depths of up to 500m with occasional presence of peat and / or medium to low thick sand. Likewise, a preconsolidated surface layer with variable thickness of ten (10) meters is present.

This information could be reaffirmed and supplemented with specific soil boring conducted in the project area. For this purpose 5 boreholes were executed that reached depths of 50m. Based on the geotechnical data

from laboratory tests, it was possible to make an adjustment of the stratigraphic profile where

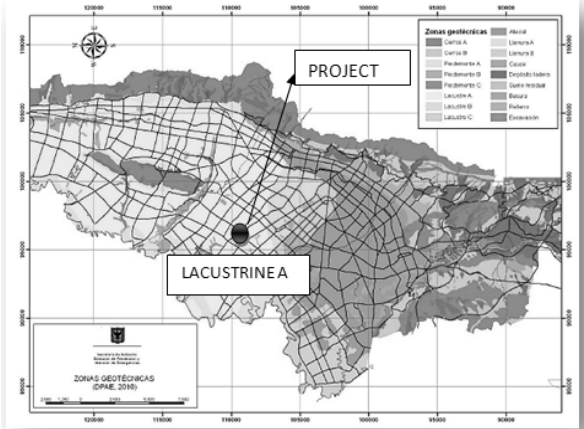


Figure 1. Bogota, D.C. Seismic Microzonation map.

they took into account the UCSC sample classification, unit weights, liquid limit, plastic plasticity index and the number of resulting shock SPT test. As a result, 3 layers made up of organic debris and dark brown silt with presence of roots, with a hard firm consistency (0.0/0.5-1.50) were obtained; greenish gray brown silt clay with roots and presence of oxide and very soft to medium firm consistency (1.5-4.0), and finally olive gray clay in sandy matrix, fine-grained sandy presence.

Other geotechnical properties were determined through the Morh Coulomb model, among which is the Young's module (E) Poisson Ratio (ν), cohesion (C) and angle of friction. For the first, it was necessary to perform a Hold Down correlation of the study conducted in a nearby place to the evaluated and the one determined in the project. Likewise, the similarities to do the calculation of Young's module were established. The other three parameters were interpreted from the resulting Coulomb Failure. Figure 2 Down Hole compared values.

Accordingly, the information used for finite element modeling was associated with the Table 1.

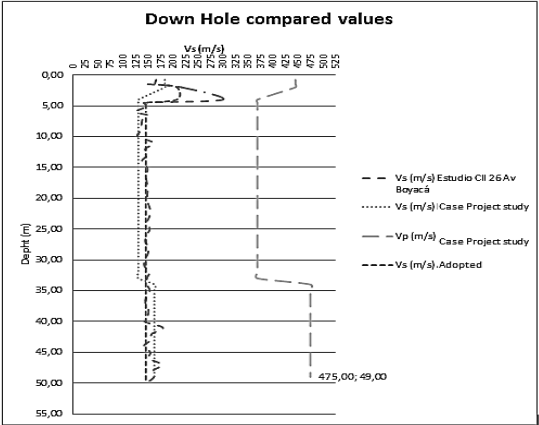


Figure 2. Down Hole compared values

Table 1. Summary Tab of geotechnical properties of the stratigraphic profile. Source: Elaborated by the

Layer	E (kPa)	E (MPa)	C (kPa)	C (MPa)	ϕ (°)	ν
1	113329,14	113,32914	0,00	0,00	26	0,40
2	167172,95	167,17295	0,08	0,00008	22	0,40
3	79454,04	79,45404	1,88	0,00188	19	0,40

author.

3. FINITE ELEMENT MODELING

3.1 Excavation Methodology and Stages

An investigation of the excavation methodology and stages used for the construction of 3 basements and with the excavation memories granted for the site was done in the first instance. From this it was concluded that the deconfinement was performed on 81 stages characterized by the removal of soil through a interlayered sequence based on an octagonal geometry. This allowed the builder to control by sectors the efforts and resulting pressures. However, in order to make a general outline for cuts, it was observed Figure 3.

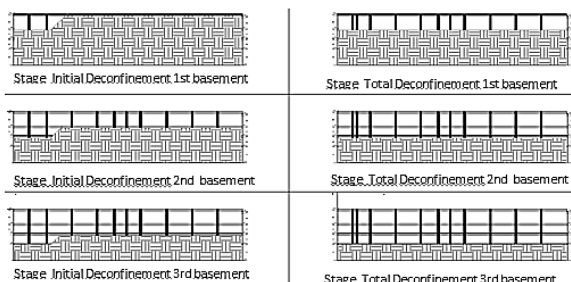


Figure 3. General outlining of the modeling steps from the excavation stages of the project. Source: Elaborated by the author.

3.2 Modelling of excavation stages in Phase2 software

Seeking to give us an idea about the problematic possibly generated in a project of this magnitude, we chose the Phase 2 program which allows you to enter the geotechnical variables of the stratigraphic profile interacting directly with structural elements such as screen walls, piles, structure of the building and the surrounding elements to the project. These were preset taking into account the activity and date of completion.

1st stage: Definition of the land limits and soil characteristics.

2nd stage: Conformation of the screens, the building and final piles (31/01/2011)

3rd stage: Establishment of the pier cap beams (28/02/2011)

4th stage: First moment of the first basement deconfinement in the assessed profile. (31/03/2011)

5th stage: Deconfinement of the first basement in the assessed profile. (28/04/2011)

6th stage: Belt beam. (28/04/2011)

7th stage: First moment of the second basement deconfinement in the assessed profile. (30/06/2011)

8th stage: Deconfinement of the second basement in the assessed profile. (28/07/2011)

9th stage: Belt beam. (31/08/2011)

10th stage: First moment of the third basement deconfinement in the assessed profile. (30/09/2011)

11th stage: Deconfinement of the third basement in the assessed profile. (31/10/2011)

12th stage: Suppression plate. (30/11/2011)

13th stage: Loads on the piles due to the superstructure. (30/12/2011)

3.3. Constitutive Model

The program is developed by a Gaussian methodology, which allows by using algorithms to achieve solutions to a system of linear equations, find matrices and inverses. Thus, it is possible to introduce soil characteristics and structural elements, using as unit of measure Mega Pascal (MP). As described above in Section 2 and with some of the pre-established conditions in the Colombian construction standards, the main characteristics of the boundary conditions and the structure formed at each stage were established. The constitutive model used in this work is the conventional M6hr-Coulomb failure criteria, with elastic parameters E and G. In Table 2 the soil properties used are presented, and in figure 4 the general aspect of the FEM model is show.

3.4. Modeling results.

The advantage of using a program like Phase 2 is that you see the results through a range of colors that represent the screen soil movements and at the same time can be graphically quantified such movements.

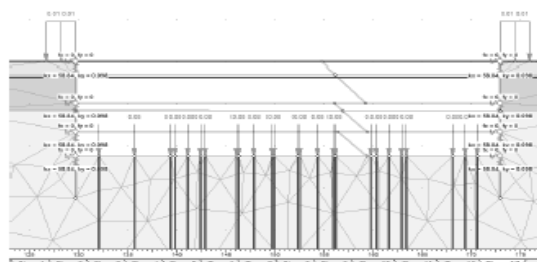


Figure 4. Conformation of the MEF through the Phase 2 program: Source: Elaborated by the author.

3.4.1 Visual result

In the resulting palette is evident that in the conformation stages of the pier cap beam and underpinning beam, no significant changes were generated in the variations of pressures of the floor against the building components, contrary to when the partial and total deconfinements start. The first shows that the soil is backfill and on the opposite side of the excavation, it tries to move to compensate the released efforts. This implies that due to this phenomenon, the screens of that side are likely to be affected by high strains and if applicable, phenomena similar to the mass landslide as the background failure.

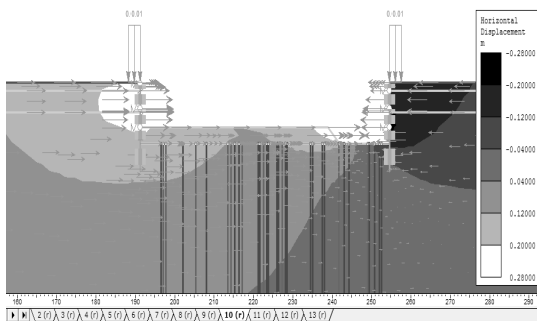


Figure 5. Conformation of the MEF through the Phase 2 program – Partial deconfinement stage 10.

Source: Elaborated by the author.

Clearly when total excavation is generated by level, the displacements that occur in the evaluated two ends can increase proportionally deforming the screens. This also shows that increasing the pushing from the bottom towards the inside of the excavation. A key element is the *suppression floor* as this conforms the first restriction of soil to keep moving towards the interior the excavation. To this the piles help because they work by tension and compression, they prevent said earthenware immerses after being subjected to increases in the pushings. Soil maximum displacements obtained were 0.33m to 0.27m.

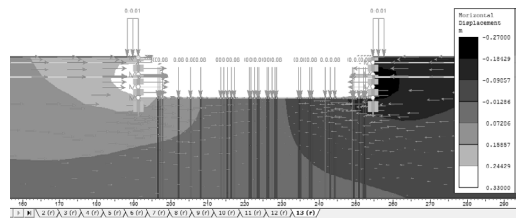


Figure 6. Conformation of MEF through the Phase 2 program, stage of total deconfinement. Source:

Elaborated by the author

3.4.2. Graphic result

Likewise, it is shown that the pier cap beam and the underpinning beam do not affect the increase of deformations of the screen, although they are the point at which it can represent a change of tendency or movement caused by the subsequent deconfinement. These graphics allow a better understanding of the screen as a structural element that acts elastically and it deforms as the internal pressure of the excavation is eliminated.

In the comparative analysis of the screens represented by each inclinometer, it was observed that for instruments 7 and 3 the maximum displacements at the depth of 10.65 m, deep-rooted earthenware section line and point from which for lower altitudes a detriment is presented. Furthermore, inclinometers 1,2,4,5 and 6 allowed to see maximum depth of 5.5m position of the first underpinning.

4. INSTRUMENTATION

The inclinometers and piezometers (brand Slope Indicator reference) were the tools used to carry out the monitoring of the movements of the screens and soil. The first were located inside the screen and the second on the floor in front of the above. Both reached the screen depth (16.15m). This instrumentation was installed before beginning the excavation process, recording movements for 15 to 16 months in total. Every 3 times a week readings were taken

until the end of work. In figure 7 the location of the instruments is show.

4.1. Analysis of the data recorded by instrumentation

Results from the inclinometers correspond to the sum of the incremental displacements starting from the starting date. Because of this, it is possible to determine the minimum and maximum displacements obtained in each of the dates or stages evaluated.

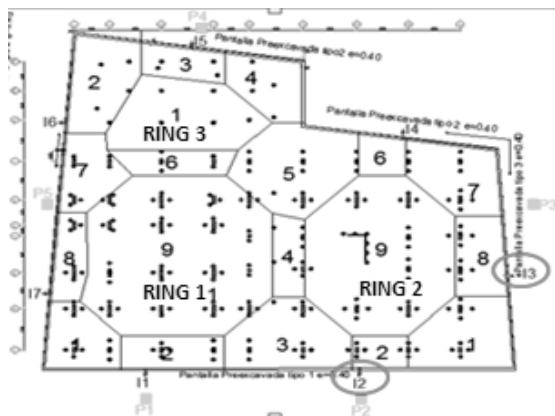


Figure 7. Location plant of the instrumentation of each screen.

The DigiPro program version 1.0, made possible to get bi-dimensional readings (X and Y axis) where X corresponded to the horizontal axis and Y to the vertical. Similarly, the readings show that in a negative sense, it is being generated adisplacement towards the neighbors and positively towards the excavation.

In each of the excavation stages for the 7 inclinometers, measures increases to reach the depth of 11.25m area where the bottom concrete suppression plate is conformed. From there to the culmination of the wall, there are significant reductions in displacement. However, lines that show similar tendency are given according to the stages in which they were developed. For example, for the first dates where the first

structural elements such as slurry wall, piles and piles caps beams are constructed, no significant displacements (20 to 30mm) are presented. From the deconfinement due to excavation to the construction of the bottom suppression plate, it appears that there are more important displacements reaching movements between 50mm to 130mm.

5. COMPARATIVE ANALYSIS BETWEEN THE INCLINOMETRY AND THE MODELING

At this point, it was proposed to give an interpretation between the similarities or major differences between the results of the instrumentation and modeling. This procedure was performed for all inclinometers and modeling for the evaluated date. For practical purposes, and after noting that the movements were negligible at the time of installation of confinement beams the trends were simplified in the analysis. The excavation steps analyzed are shown in Table 2.

Results comparison	
Instrumentation (Date)	Modeling (Stage)
31/03/2011	4
28/04/2011	5
30/06/2011	7
28/07/2011	8
30/09/2011	10
31/10/2011	11

Table 3. Guide to compare the graphic results. Source: Elaborated by the author.

Trends in some comparisons were very similar, although a bit distant in values, while others were completely different in every aspect. An example was that obtained by the inclinometer 3 and 7, the others had total discrepancy. As a representative sample, it was then exposed the results of the inclinometers 2 and 3, in the plan they are located in the left inferior sector ring 2 (Fig. 7 inclinometers highlighted with circles).

Starting from the premise that the dotted lines represent the inclinometry, the lines the results of the modeling, and the positive direction is towards the excavation, you can infer in the Figure 8.

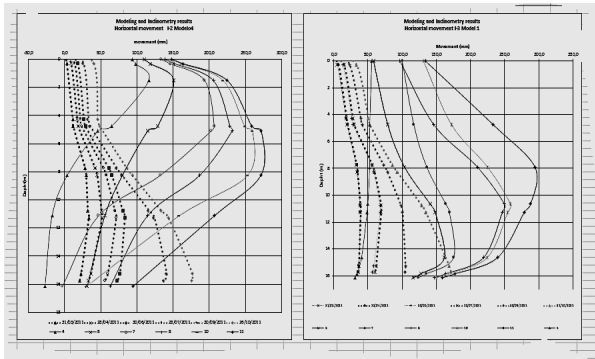


Figure 8: Comparative graphics between modeling and inclinometry for inclinometers 2 and 3.

As can be seen in inclinometer 2 Model 4, the instrumented tendency is always growing as it descends through the screen, reaching maximum displacements the subfloor earthenware sector or final dates to finish off the wall (17.5 cm) while the model indicates maximum deformations at 5m (27.1 cm) and then present detriments from 0.5 cm to 9.4 cm.

Contrary in the inclinometer 3 Model 1, which both instrumentation and model appear to present maximum displacements (17.14 cm and 29.4 cm respectively) between the second and third basement (8 to 11.1 m) case. However, these sectors are where trendlines of modeling decrease the deformation approaching 17cm.

5.2 Results discussion

5.2.1 Instrumentation

To make sure you get the most reliable data to model in finite elements, you must perform an inverse analysis which can optimize the parameters of different constitutive models (Finno, 2009)

The inclinometry location should be strategically designed, since better results would be presented if they are located out of the screens and not embedded as performed in the studied project, This will better represent the elasto-plastic constitutive models of soil behavior. (Rechea, 2006)

Likewise, a length of the greater inclinometry would also provide more complete results since it would not only be performed for the screen and soil measurement until the end of the previous blinding element, but it can be more closely detailed the soil movements under this, allowing to understand if these thrusts can cause a substantive failure.

The errors associated with the measurements can be determined by the accuracy of the instrumentation and the processes carried out to obtain them. (Langousis, 2007).

5.2.2 MEF

A very important and influential in shaping the modeling is the angle of friction parameter (Rodriguez, 1982; Oteo and Rodriguez, 2003), since the tests where this factor was modified, greater displacements having lower angles were presented. Now, assuming that this value can be obtained from the SPT test, it is vital that the equipment and power corrections are made or should be made to not introduce ambiguous values in the model.

A finite element model associates only two-dimensional movements, which incurs the exclusion of understanding of integrated excavation and interaction stages between the other assessed screens or actual contour conditions. (Finno, 2009).

Another important element that should be included in the modeling for the factor that allows the soil-structure interaction (Sanhueza and Oteo, 2007), which in this case correspond to the Ballast module. However, this is defined for homogeneous and granular soils, reason why it was not introduced into the modeling, which possibly affected the results obtained.

Values of the Field tests like Triaxial, show that the values may be lower in the modeling in comparison with the ones done in the field like Down Hole. Due to lack of information of this type, it was only done with the field test and developed correlations between soil type present in the lacustrine A of the Seismic microzonation of Bogotá.

5.2.3 Constitutive model

It is necessary to simulate all aspects that affect the efforts conditions during construction around the excavation to give more accurate predictions (Finno, 2009). That is how you should evaluate not only the phenomena occurring in the same length of the screen but also extend this to a firmer sector or that it covers the security zone of a substantive failure.

There are programs with greater precision with them it is possible to determine the constitutive model for clays, example is the Elasto-plastic model of Hardening soil that considers the soil stiffness in a more accurate manner than the Mohr model. Therefore, they could enter load and unload values owned by tests like the Triaxial or other aspects that are not easy to find (and OteoSanhueza, 2007), such as:

- Load Triaxial Stiffness, through E_{50} secant deformation module.
- Unload Triaxial Stiffness, through the E_{or} unload-reload deformation module.
- Deformation module obtained from the oedometer, E_{oed} .

Furthermore, after the H-S resulting designs of using a triaxial that generates reliable models with about 0.10% difference in the simulations, or lower (Burland, 1989).

5.2.4 Other important aspects

5.2.4.1 How to calculate the substantive failure.

This aspect was vital to understand whether this phenomenon was formed or not in the project. In the calculation of this variable, it was taken into account the variables of Table 3.

When $N_e \geq 4$, the deformation in the excavation and the outline of the same become unmanageable, and the substantive failure can occur.

Table 3. Calculation of security factor against the substantive failure. Elaborated by the author

How to calculate the security factor against the substantive failure on soft soils											
Cu (KN/m ²)	Y (KN/m ³)	H (m)	B (m)	Cub (KN/m ²)	Hc	Cul (KN/m ²)	Hor	q (KN/m ²)	Tezaghi	Bjerrum yEide	Num Estabilidad
14,7	13,11	13	25,51	30	7,2	30	7,2	1,5	0,534	1,379	1,256
										1,256	5,681

Thus, using this parameter has a perspective of what would happen if proper measures are not taken. In the project, thanks to the constructive methodology and screen configuration, they prevented this from happening.

5.2.4.2 Structure-Soil weight.

Through the weight calculation of the entire structure and the excavated soil, it was intended to assess whether the structure was overcompensated or not. The results were inconclusive since the excavated soil outweighed the structure, thus indicates that the structure may rise by the thrust magnitude that has to be supported. However, when the piles have tension and compression, it prevents this phenomenon from occurring.

Table 4. Soil and structure weight. Elaborated by the author

Structure weight(T)	Removed soil, total weight (T)	Highervalue
303,41	511,72	Suelo

6. CONCLUSIONS

To obtain more accurate and closer to reality values, it is important that excavations in soft soils can be modeled with more specific information obtained from more specific tests like the Triaxial, because through this is possible enter values for loading, unloading and deformation. This is preferable to change the

Morh-Coulomb constitutive model to a more specialized such as the hardening elasto-plastic model, or the hardening soil for clays.

The location of the instrumentation must be the product of a deep analysis done within simulations in order to understand the areas that are more prone to deformations and be able to monitor the same in more detail, making preventive action to avoid irreversible damage. It is therefore important that the inclinometry is not embed and allows better representation of the elasto-plastic constitutive models of soil behavior.

For a good modeling, it is necessary to have modules that allow attesting of the soil-structure interaction. To do this, it can be used the ballast module that integrates the structure with the floor through serving as an independent module that each time reaches a higher depth.

To make comparative analysis between the modeling and the real data obtained by the inclinometry, it is necessary to do inverse analysis to adjust or calibrate the assessed values and thus be able to better interpret these results.

7. REFERENCES

- BOWLES, Joseph E. Physical and geotechnical properties of soils. Spanish version translated by Eugenio Retamal and Hugo Cosme. Bogotá: McGraw – HILL Latinoamericana. 1982. CAMBEFORT, Henri. Géotechnique de l'ingénieur reconnaissance des sols. Spanish version translated by juanjosésanz llano. Barcelona: editorial eécnicos asociados. 1975. COLOMBIA. Bogotá mayor's office. Decree 525 of December 16th, 2010. "Por el cual se Adopta la Microzonificación Sísmica de Bogotá D.C" (Adopting the Seismic Microzonation of Bogotá, D.C.). Administrative District Planning Department. Design and execution of excavations in Bogotá district Standard. Final version, non official work document.
- Bogotá:Colombian Geotechnical Society. July of 1996. Spanish version. Geotechnical instrumentation for monitoring field performance /John Dunncliff, with the assistance of Gordon E. Green.Dunncliff, John. Editorial John Wiley & Sons.Colección a Wiley –Interscience publication. Publicado en new york, estadosunidos. 1993.
- LAMBE, William T., *et al.* Soil Mechanics. Spanish version translated by José A. Jiménez, *et al.* México D.F.: Limosa S.A. Grupo Noriega Editores. 1998.
- LARRAÑAGA RUBIO, Sherley C; LOPEZ CLAVIJO, Carlos. Quatitative analysis of some building systems to mitigate risk fault in the execution of large excavations in Bogotá, D.C. Uniagraria Foundation's Teshes. Civil Engineering, 2003. Adapted.Spanish version.
- MOYA BARRIOS, Julio E., *et al.* Excavations in complex situations. Compilation of written course materials excavations in complez situations. Bogotá, Colombian School of Engineering, 1997. Spanosh versión.
- PINEDA JAIMES, Jorge A. Analysis of building systems Up and Down for buildings with largue basements. Article. Spanish version.
- SAAVEDRA, Rodolfo. Slope Indicator, translation of Sistematic planning to create a monitoring program using Geotechnical Instrumentation. February of 2012. SANHUEZA PLAZA, Carola. Criteria and design parameters for Pile Wall File in Madrid. Madrid, 2008. PhD Theses (Civil Constructor). Polytecnic University of Madrid. E.T.S. Roads, Canals and ports Engineering. Engineering and Spot motphology department. Spanish version.

San Pasquale station of the Linea 6 in Napoli: dewatering field tests, measurements and back-analyses

Gianpiero Russo, Silvia Autuori, Marco Valerio Nicotera
University of Napoli Federico II, Italy

ABSTRACT: Since 1839, when the historical railway Napoli – Portici was inaugurated, Napoli has been characterized by a significant system of urban and suburban railways. The idea of a fully integrated urban rail network dates back to the 1950s, but only in 1990s construction began. At present, the system includes 54 km of tracks and 69 stations belonging to 6 lines currently operating; when the City Transport Plan will be completed, 10 lines with 93 km of track and a further 30 km of new light rail linking 114 stations with 21 interchanges are foreseen.

1. INTRODUCTION

With an urban population of 1.2 million people and 5 million in the metropolitan area (CENSIS, 2008), Napoli is the third largest city of Italy. The density of population is nearly 2,000 inhabitants per square kilometer, the highest in Italy and among the highest in Europe. At the end of 90s Napoli has become notorious for its horrendous traffic problems with increasing air pollution, unacceptably long travel times in rush hours and negative effects on the public health and economy (Viggiani et al., 2011).

In 1997 the Municipality of Napoli approved a new City Transportation Plan, that has led to a significant pressure for the construction of new underground train lines, stations and car parks.

Metropolitana di Napoli, or Napoli Underground, is the metro system serving the city, including at present six underground rapid transit railway lines, a commuter rail network and four funicular lines, with planned upgrading and expansion works underway. With nearly 54 km of track and 69 stations currently operating and more due to open as part of the expansion plan, Napoli Underground had a daily ridership of 470,000 in 2005, expected to rise to over 700,000 in 2013. Among the six already operating lines some are experiencing a substantial development with new stretches under construction

One out of these is the Line 6. When com-

pleted according to the current design state Line 6 (Figure 1) will connect the Western borough of Bagnoli to the city centre at Municipio station, with a total length of 8 km and 12 stations. The full line can be broken down into 3 stretches:

- the stretch between Mostra and Mergellina stations, partially connecting the borough of Fuorigrotta to the city centre, is already operating;
- the stretch between Mergellina and Municipio stations is presently being constructed;
- the stretch between Mostra and Porta del Parco stations is under design.

In the following, attention will be focused on the design and the construction problems of San Pasquale station of Line 6, which is currently under construction the main civil works being almost completed.

2. SAN PASQUALE STATION

The Station is intermediate along the new stretch of the line under construction and is located in a crowded area which is a sort of fashion district (Figure 1).

The main body of San Pasquale station has a rectangular shape in plan of 85.50 m × 24.10 m and the maximum excavation depth is approximately 27 m (26 m underground water table) (Figure 2).

The long side of the station is parallel to the longitudinal tunnel axis and the closest build-

ings are all located on the north side keeping approximately a unique alignment which is again parallel to the long side of the station. The main and rather large shaft contains the passenger platforms and eliminates the necessity of excavating platform tunnels underground.

The excavation is supported from T-section diaphragm walls made by reinforced concrete and built using huge hydromill equipped by a 90° rotating head. Each panel of the diaphragm walls were built by intersecting two separate excavations with a rectangular shape in plan. The depth of the panels is about 50 m which allows a substantial embedment in the Neapolitan Yellow Tuff formation (NYT). The first stretch of the panel was excavated under the protection of Cutter Soil Mixing (L'Amante et al, 2012)

The decision was taken to build the station fully top-down, avoiding the complexity of drilling ground anchors at large depth below the groundwater table. The diaphragms have been executed first, leaving soft eyes with fiberglass reinforcement bars to be drilled by TBM. The passage of the TBM was the second main step while the excavation of the station was executed as the final step and required the demolition of the tunnel lining within the station area.

At the design stage geotechnical investigations were carried out in the area occupied by the station which is approximately 2000 m². The site is inserted in an urban area bounded by historical buildings on the north side and by the sea with the interposition of a public garden on the South side. The area is relatively flat with the ground level located between +2 and +2.30 m a.s.l.. The groundwater table lays at +1.30 m a.s.l..

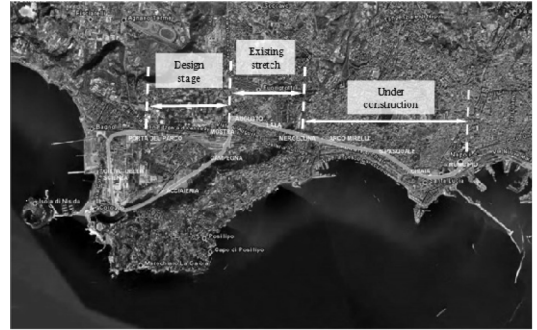


Figure 1. Line 6 of Napoli Underground.

Both in situ and laboratory geotechnical tests were programmed and executed. As usual boreholes with continuous coring and Standard Penetration Tests were initially carried out. In two out of the ten boreholes permeability tests of the Lugeon type were carried out. Samples to be submitted to laboratory tests were retrieved. The laboratory tests were mainly aimed at the determination of the grain size distribution, unit weight and porosity. Further site investigations consisting in CPTs, Dilatometers test and Cross Hole tests were subsequently carried out but being out of the scope of the paper their results are not presented herein. In Table 1 the boreholes with the main information retrieved are summarized.

Figure 3 shows the geological soil profile corresponding to the transverse cross-section located in the middle of the station. It is characterized by the upper marine sand underlying the hand made soil to a depth of 17 m from the ground surface (layer A), followed by a layer of pyroclastic products consisting of silty sands, or

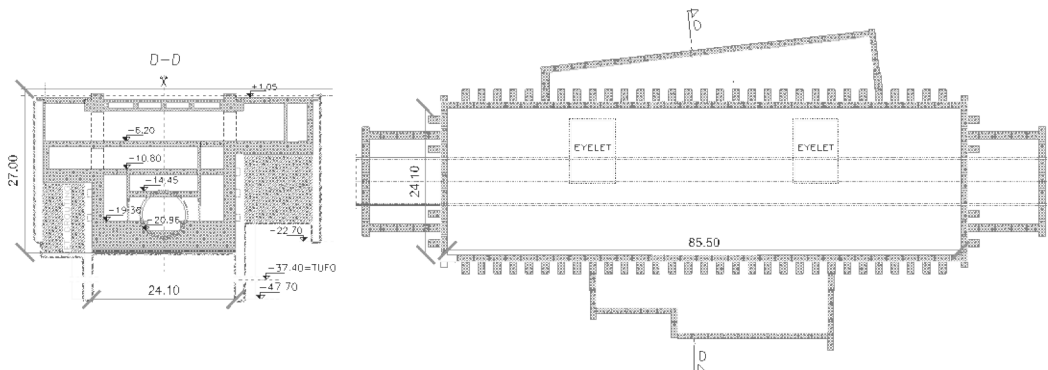


Figure 2. Plan view and transverse vertical section of the San Pasquale Station

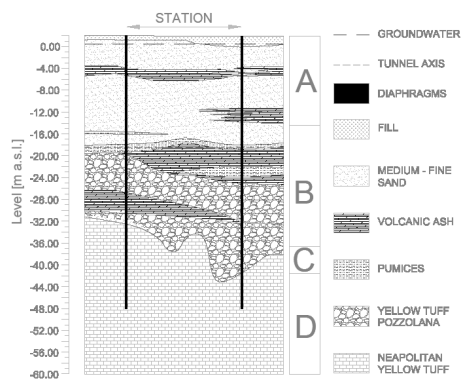


Figure 3. Stratigraphy of San Pasquale site.

ashes and pumices from the depth of 17 m down to a depth of 41 m (layer B). Going deeper a thin layer of yellow tuff pozzolana (layer YTP) separates the layer B from the formation of the NYT (Autuori et al. 2013).

As already mentioned, particular attention was paid on permeability evaluations. One of the important design issues was in fact the groundwater management being the excavation accompanied by a substantial dewatering obtained via pumping the water out from deep wells. For this reason Lugeon tests were carried out at several depths in the NYT layer during the design stage while, during the execution stage, field scale dewatering trial tests allowed the final setup of the pumping apparatus to be defined. The present paper is almost exclusively dedicated to these aspects.

Table 1. Boreholes and information retrieved.

Id	Tuff level (m a.s.l.)	Ground water level (m a.s.l.)	SPT (#)	Lugeon (#)
S1	-31.97	1.3	8	5
S2	-38.94	1.3	9	4
SG1	-38.43	1.3	9	
SG2	-42.23	1.3	9	
SG3	-45.23	1.3	9	
SG4	-35.71	1.3	8	
SG5	-33.97	1.3	8	
SG6	-37.63	1.3		
SG7	-34.21	1.3	8	
SG8	-43.49	1.3	9	
SSP1	-39.87	1.3	0	
SSP2	-47.23	1.3	0	

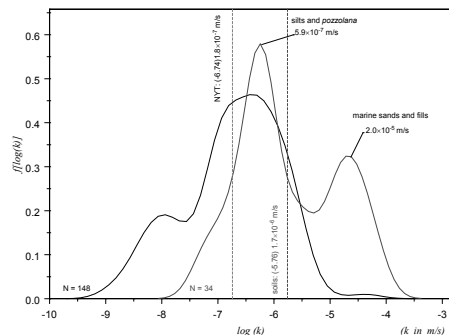


Figure 4. Frequency density plots of permeability values of soils and NYT.

Preliminarily, in the design stage approximated permeability values were assigned to the different materials present in the subsoil. The permeability assigned to the NYT was obtained from 9 Lugeon tests whose results are summarized in Table 2. Furthermore the permeability values used for marine sands (layer A) and pyroclastic silty sand (layer B) were assigned from statistic distribution built with permeability values available in literature.

Figure 4 shows the frequency density plots of the permeability values of k of soils and NYT.

Table 2. Lugeon testing in YT

Borehole	Depth (m)	k (10^{-7} m/s)
S1	34.0-36.0	16.6
	36.2-38.2	1.53
	38.5-40.5	4.38
	40.3-42.5	4.22
	42.5-44.5	5.18
S2	41.5-43.5	8.40
	43.5-45.5	2.03
	45.5-47.5	2.28
	47.5-49.5	3.66

3. DESIGN ISSUES

As already mentioned in the introduction, San Pasquale station is very close to some historical and valuable buildings belonging to the downtown. It is excavated in granular soils sitting above a rather homogenous and not largely altered NYT layer with a rather superfi-

cial groundwater table governed by the nearby sea level.

Of course the design first and the construction later had to cope with several difficulties arising by the above mentioned features. First of all the need to preserve the structure of historical buildings some of these being enriched by valuable frescoes which could results as highly vulnerable to even small displacement.

The method of construction and the stages of execution were revised several times in order to minimize such effects. In the end it was preferred the excavation with top-down technique using the intermediate slabs as temporary supports and the association of deep dewatering wells to depress the ground water table inside the main shaft (Russo et al., 2012).

It is clear that the problem is a very complex one with the settlement induced by subsidence increasing the already critical settlement induced by the deformations of the diaphragm walls. With the main aim of correctly calibrating the pumping stations needed to depress the inner groundwater table and of judging the entity of the external induced subsidence without having to sum the displacement induced by the excavation a preliminary dewatering test was carried out in a trial field. The main steps of the dewatering field tests are first described allowing the presentation of the main experimental results. Subsequently the interpretation carried out via numerical analyses is presented essentially to discuss about permeability values attributed to the different soil layers.

4. DEWATERING TRIAL TEST

A dewatering trial test was designed with the agreement of the construction company whose main aim was simply to establish the minimum configurations of wells and pumps capable of lowering down the groundwater table on the whole station area (see Figure 5 and 6). Preliminary calculations based on the design values adopted for permeability were carried out.

A total of six pilot wells were installed in the station area included within the existing diaphragm walls. Four pilot wells were installed in the western part of the station area. Diameters and locations had to be discussed and agree also with the Board of archaeological remains still involved in surveying activities which usually stop when the excavation proceed below the sea

level .The wells were 600 mm in diameter and were deep enough to get into the NYT deep layer. The main features of the pumping wells are summarised in Table 3.

Moreover internal and external piezometers were installed in couples on the same vertical at two different depths. The internal piezometers were located respectively at -37.8 m a.s.l. and -40.8 m a.s.l.. The external ones were respectively located at -12.80 m a.s.l. and -27.80 m a.s.l. below the ground surface.

The trial field started on 18/05/2010 and finished on 10/07/2010. Preliminary tests were carried out on the single wells P1 and P2 separately. These initial tests were of the maintained step type setting various outflows and waiting the time needed for stationary conditions to be reached. The large dewatering of the whole station was carried out later since 26/05/2010 to 05/07/2010, for a total duration of 40 days. Initially only wells P1 and P2 were activated while at a given time also P3 and P4 were additionally activated reducing the amount of water pumped out by the first two wells. The well P3 had some troubles and it was rapidly switched off relying upon the remaining three wells P1, P2 and P4 which were however capable of lowering the groundwater table in the whole station area (Mormone et al., 2013).

Table 3. Well's features

	P1	P2	P3	P4
ground level (m a.s.l)	0.17	0.07	1.04	0.96
depth (m)	39.97	39.87	38.84	43.76
well screen (m a.s.l.)	-27.8 -37.8	-27.8 -37.8	-25.8 -35.8	-27.8 -37.8
diameter (mm)	600	600	600	600
pump power (kW)	7.5	7.5	11	11

5. TEST RESULTS

San Pasquale station was subjected to a careful monitoring since the beginning of the construction. The main civil works are now completed but the present paper deals essentially with the interpretation of the dewatering trial field test carried out before the main excavation took place. The full result of the case history are still under examination and will be published

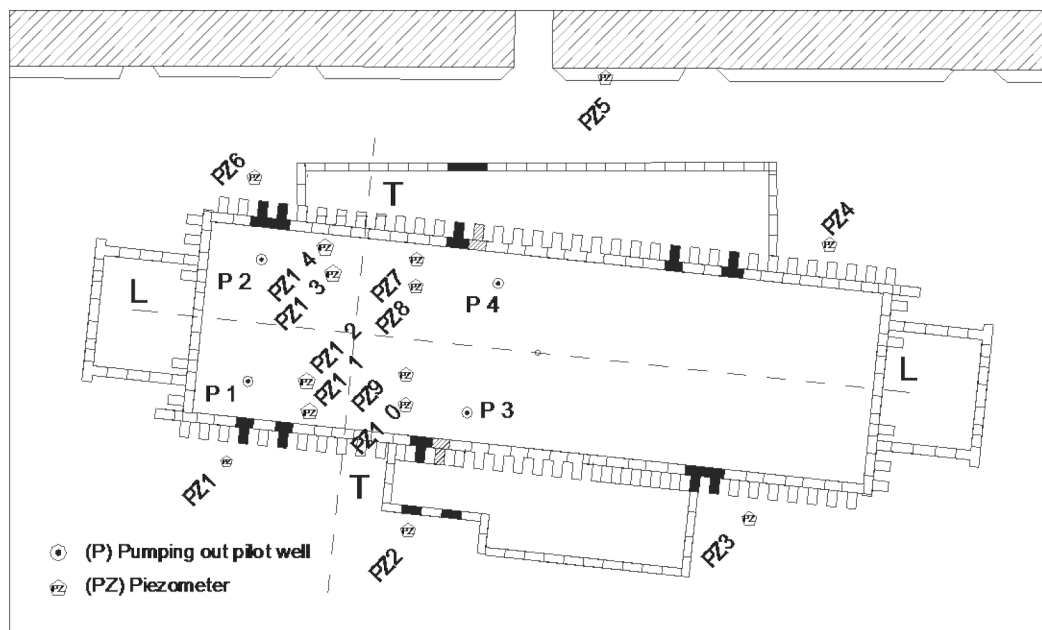


Figure 5. Plan view of station shaft with layout of monitoring system for the dewatering trial test.

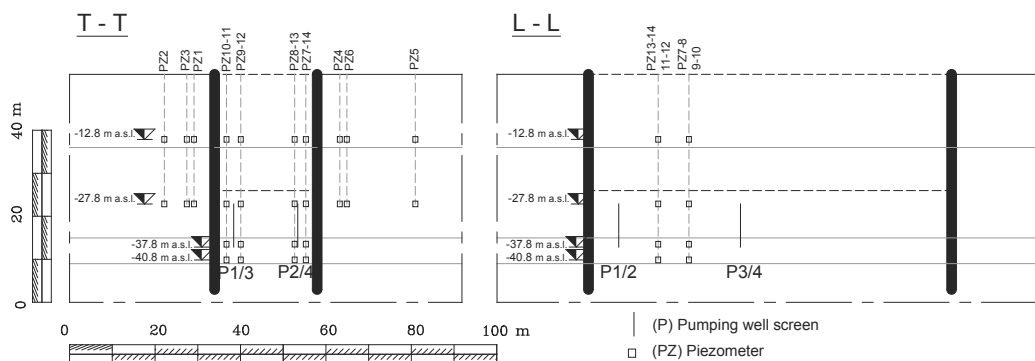


Figure 6. Cross and longitudinal section of station shaft with layout of monitoring system for the dewatering trial test.

elsewhere. This work focuses only on the interpretation of few measurements for sake of simplicity and for obvious space reasons.

Figure 7 shows the pumping rates and the measured groundwater hydraulic heads during the dewatering trial test. Two different phases can be clearly distinguished. During the first phase only two wells (P1 and P2) were activated. A flow rate of about 10 l/s was imposed at each well.

The second phase started when the other two wells (P3 and P4) were activated. After a few days pumping from the P3 well was stopped for problems at the electric pump. Therefore the

rest of the test was conducted using the wells P1, P2, and P4, with a flow rate measured at the end of the test approximately equal to 22 l/s.

The average flow rate pumped during the whole test was 21 l/s as it can be seen by the full line in the Figure 7. In the same figure the actual outflow at each well and globally imposed is of course represented at each time during the whole test. At the end of the test the total volume pumped in 40 days was 72425 m³, 30657 m³ coming from well P1, 27661 m³ from the well P2, 1010 m³ from the well P3 and 13097 m³ from well P4.

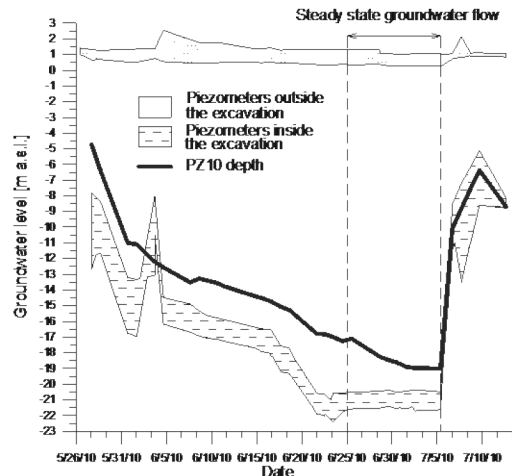
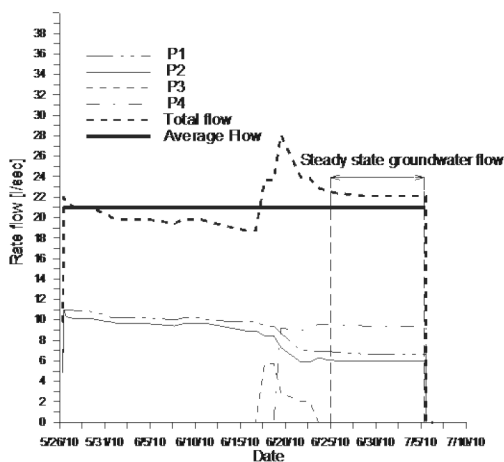


Figure 7. Pumping rates and measured groundwater hydraulic heads during the dewatering trial test

The elevations of the groundwater table inside and outside the shaft are shown in Figure 7. The diagram reported in Figure 7 was simplified and only the two envelopes coming out from the internal and the external piezometers readings were represented as two different shaded areas. It can be inferred that the huge lowering of the groundwater table inside the excavation shaft was practically not causing any significant effect outside the excavation. The only internal device showing some difference, PZ10, was left out of the envelope for the group of internal piezometers because no reasonable cause of the difference could be detected.

It is worth noticing that the hydraulic head registered by the two piezometers composing each external couple disposed along the same vertical are practically identical. It follows that the monitoring system did not detect any significant hydraulic head gradient in the vertical direction across the soil layers outside the station shaft; however it is very likely that the differences in the groundwater head between the inside of the station shaft and the

surrounding area were mainly dissipated inside the NYT layer.

As a matter of fact the loose sandy deposits located above the tuff in the external areas appears acting simply as a high capacity reservoir providing water without any significant downwards flow. The average hydraulic gradient appreciated with several couples of external piezometers is practically null and exactly $i=-0.008$ (negative is for downwards flow). On the other hand the internal piezometers allow to detect upwards flow with an average hydraulic gradient equal to $+0.16$.

6. BACK ANALYSIS

The analysis and interpretation of the problem is highly complex due to three dimensionality, soil heterogeneity, filtration problems.

The main purpose of this study is to obtain the best interpretative model that allows to capture the induced effects inside and outside the station due to the excavation and the process of pumping.

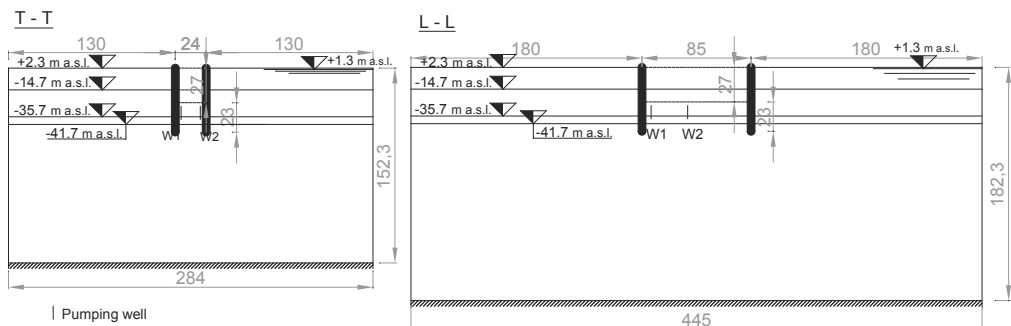


Figure 8. Geometry of the fem models

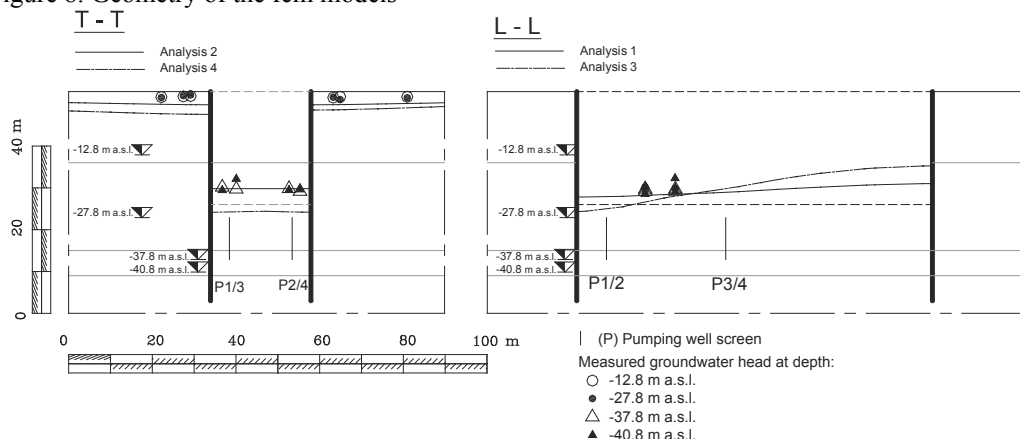


Figure 9 Transversal and longitudinal section of the shaft of San Pasquale Station: comparison between analyses and measurements

The permeability values of the soil layers were back-calculated by means of two bi-dimensional finite element models. However it was indispensable to adopt a conventional criterion of equivalence to reduce a three-dimensional problem to a simpler 2D one. First of all it was necessary to estimate an equivalent pumping rate to be assigned to the indefinitely long “bi-dimensional” wells considered in the 2D model. Two fem models were implemented referring respectively to the longitudinal and to the transversal cross section of the station shaft. Figure 8 shows the two alternative cross sections adopted for the 2D parametric analyses. The geometry of the box meshed and used for the fem calculations is such to minimize the edge effects. The simplified stratigraphic sequence is the same for all calculations and consists of 4 layers: the layers labelled with capital letters A, B, C and D correspond to those already identified in the simplified stratigraphy

of figure 3. The models permitted to simulate the filtration process that takes place in the station during the “stationary condition” of the dewatering test. A trial and error procedure was adopted to estimate the soil water permeability. Among many different simulations only a few best cases have been selected and summarised in Table 3. The results are plotted in the diagrams of figure 9 where also the comparison with the measured values is found.

Several attempts were carried out corresponding to different hypotheses. First of all the values of permeabilities available from site and laboratory investigations were immediately checked as being too low. The equivalence on the pumping rate obtained in such a case was considered as completely out of place and thus ignored. The trial and error procedure started investigating higher values of permeability compared to those obtained by laboratory tests and Lugeon tests. It can be seen from the plot

Table 3 Cases analysed and selected for the representation of figure 9.

Analysis (#)	Section	pumping rate (m ² d ⁻¹)		permeability k (10 ⁻⁶ m/s)					
		W1	W2	A	B	C		D	
						x	y	x	y
1	L	50	25	800	400	7.0	70	7.0	70
2	T	30	30	800	400	7.0	70	7.0	70
3	L	50	25	700	60	30	30	30	30
4	T	30	30	700	60	30	30	30	30

of figure 9 that the best agreement between the results and the analyses is found with both longitudinal and transversal sections respectively in the case 1 and 2. In these two cases for the NYT formation a significant anisotropy was also presumed according to the widely diffused knowledge that vertical fissures are present in the deposit due to the rapid cooling process subsequent its deposition. The letter y in the table 3 represents of course the vertical direction. After several attempts the best case among the several isotropic ones were individuated in the case labelled 3 and 4. As it is shown in the figure 9, in this case keeping the same pumping rate of the case 1 and 2, the lowering of the groundwater head is rather overestimated. In conclusion none out of these two further cases is as satisfactory as the cases 1 and 2.

7. CONCLUSIONS

Huge excavations are going on in the city of Napoli to build a new line of the underground network. Some of these excavations present among the other difficulties the management of significant dewatering processes in area which are closely surrounded by important buildings. As briefly shown in the present paper dewatering tests are important in order to check in the execution stage the possibility of obtaining the wished results in the excavation area without producing external effects on the groundwater table. These last would of course be accompanied by subsidence problems on the existing buildings which must be carefully prevented. The back-analyses of the executed tests allowed also to deepen the knowledge of the permeability of the geological formations involved at the field scale.

8. ACKNOWLEDGEMENTS

This work was possible thanks to the monitoring data obtained within a partnership agreement among DICEA of Federico II, AnsaldoSTS Spa and Metropolitana di Napoli spa.

9. REFERENCES

- Autuori S., Russo G., Nicotera M. V. (2013), Studio preliminare degli effetti indotti dallo scavo della stazione San Pasquale, Incontro Annuale Ricercatori di Geotecnica, Perugia, ISBN 9788890642135
- L'Amante D., Flora A., Russo G., Viggiani C. (2012). Displacements induced by the installation of diaphragm panels. *Acta Geotechnica*, 7:203-218.
- Mormone L., Falconio G., Mandolini A. (2013). Groundwater management during excavation of S. Pasquale station in Naples. *Geotechnical Engineering for the preservation of monuments and historic sites*, ISBN 978-138-00055-1
- Russo G., Viggiani C., Viggiani G.M.B., 2012. Geotechnical design and construction issues for Lines 1 and 6 of the Naples Underground. *Geomechanics and Tunnelling* 5, No. 3. Berlin.
- CENSIS, 2008. *42° Rapporto sulla situazione sociale del Paese*. Roma. Franco Angeli.

Frost Protection for Geotextile-reinforced Soil Walls in Service

Atsuko Sato & Takahiro Yamanashi
Civil Engineering Research Institute for Cold Region, Hokkaido, Japan

Teruyuki Suzuki
Kitami Institute of Technology, Japan

Naoki Tatta & Kouichi Yoshida
Maedakosen Co.,Ltd., Japan

ABSTRACT: Cases have been reported of deformed geotextile-reinforced soil walls in cold regions. The deformation is likely to be caused by frost heave in the backfill soil of reinforced soil walls. To prevent the deformation caused by frost heave, the Hokkaido Regional Development Bureau of the Ministry of Land, Infrastructure, Transport and Tourism has established specific construction techniques. However, no preventive measures have been specified for geotextile-reinforced soil walls already in service. Toward proposing countermeasures to frost-heave deformation, full-scale tests were conducted. The results demonstrated that application of insulating materials to the outer surface of geotextile-reinforced soil walls helps to control frost-heave deformation.

1. INTRODUCTION

Geotextile-reinforced soil walls have been increasingly used in road embankments in recent years. However, cases of deformation in geotextile-reinforced soil walls in winter have been reported in cold regions. The deformation is typically caused by frost heave to the soil on the back side of the walls.

Based on the findings of past studies, the use of materials insusceptible to frost heave is required in constructing embankments in which materials susceptible to frost heave and geotextile-reinforced soil walls are used. Specifically, materials insusceptible to frost heave should be applied to the portions of the walls that tend to freeze in winter.

However, partial replacement of materials used in existent geotextile-reinforced soil walls is not easy. In view of this, this study focuses on the application of insulating materials to the outer surface of geotextile-reinforced soil walls as a way of controlling deformation due to frost heave.

To determine the effectiveness of insulating materials in deformation control, full-size geotextile-reinforced soil walls were used for tests on wall freezing and frost heave. The test results are summarized below.

2. FACTORS INVOLVED IN DEFORMATION DUE TO FROST HEAVE IN GEOTEXTILE-REINFORCED SOIL WALLS

When ground containing fine-grained soil susceptible to frost heave freezes, water passing through the ground from the unfrozen soil feeds the formation of ice lenses near the frozen surface. On the back side of the geotextile-reinforced soil walls, where the soil is susceptible to frost heave, ice lenses form in layers parallel to the wall surface (Figure 1). As a result, the wall surface deforms by being

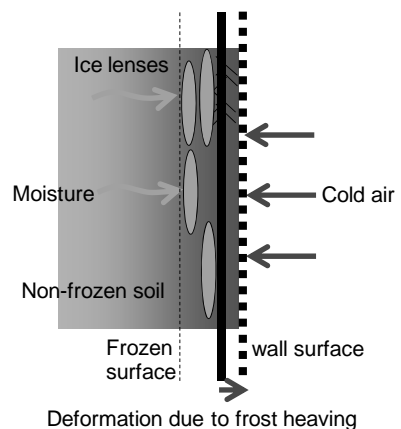


Fig. 1 Principle of freeze-drying

pushed outward. Once deformed, the wall surface does not return to its original state even when the temperature rises, which leads to cumulative deformation. When the cumulative deformation reaches a certain level, the wall surface materials protrude outward due to frost heave and the wall collapses (Photo 1).

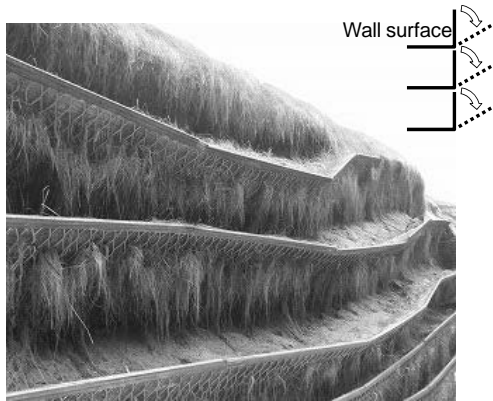


Photo 1 Example of deformation in geotextile-reinforced soil walls

3. TESTING METHODS

The factors influencing frost heave are soil quality, air temperature and water drainage; thus, soil replacement, maintaining temperatures above the freezing point and insuring proper drainage are the keys to preventing frost heave. Because it is very difficult to improve drainage and replace soil in existing geotextile-reinforced soil walls, full-scale model walls were constructed for conducting tests focusing on temperature.

3.1. Specifications of the full-scale model walls

The model walls were built in the City of Tomakomai, Hokkaido Prefecture, with the soil materials shown in Table 1 for the purpose of

measuring the deformation due to frost heave in winter. The embankment material was volcanic ash soil whose maximum dry density is not measurable. Cone indexes set according to soil-trafficability testswere3000kN/m² or greater. This volcanic ash soil is a good material for the construction of embankments, in that compaction is relatively easy. But this soil is not totally insusceptible to frost heave, and frost heaving may occur.

The model walls were built in an earth tank 5 m square and 2 m deep. The bottom of the earth tank was covered with gravel 30cm thick for drainage. Above the gravel, three tiers of embankments were built. Each tier was 2.4m wide, 60cm high and 3.0m deep. Two sets of model walls were built in the earth tank, with each set separated by 10cm-thick Styrofoam. A total of five sets of model walls were used for testing: Cases 1, 2, 3, 4 and 5.

The five cases are outlined in Table 2, and side views of thefive models are shown in Figure

Table 1 Basic physical property values of fill material

Physical property		Volcanic ash
Soil particle density ρ_s (g/cm ³)		2.470
Natural water content w_n (%)		46.98
Grain size	2 mm or larger (%)	22.8
	75 μ m to 2 mm (%)	51.4
	Less than 75 μ m(%)	25.8
Consistency limit		N.P.
Classification symbol of soil material		SVG
Frost heaving	Velocity of frost heaving (mm/hr)	0.27
	Percentage of frost heave (%)	18.1
	Degree of frost heaving	Medium level
Permeability coefficient k (cm/sec)		2.34×10^{-5}
Maximum dry density ρ_{dmax} (g/cm ³)		Not determined
Cone index q_c (kN/m ²)		3000 or larger

Table 2 Outline of test cases

CASE	Control measure	Specific measure		Vegetation
1	None	None		Existing
2	Replacement	Replacement with gravels (0.8 m from wall surface)		Existing
3	Insulation	Constructed geotextile-reinforced earth wall	Gourd-shaped body 40 mm + unwoven cloth 1 mm	None
4	Insulation		Unwoven cloth 10 mm x 3 sheets	None
5	Insulation		Unwoven cloth 10 mm x 2 sheets + material for vegetation base 30 mm	None

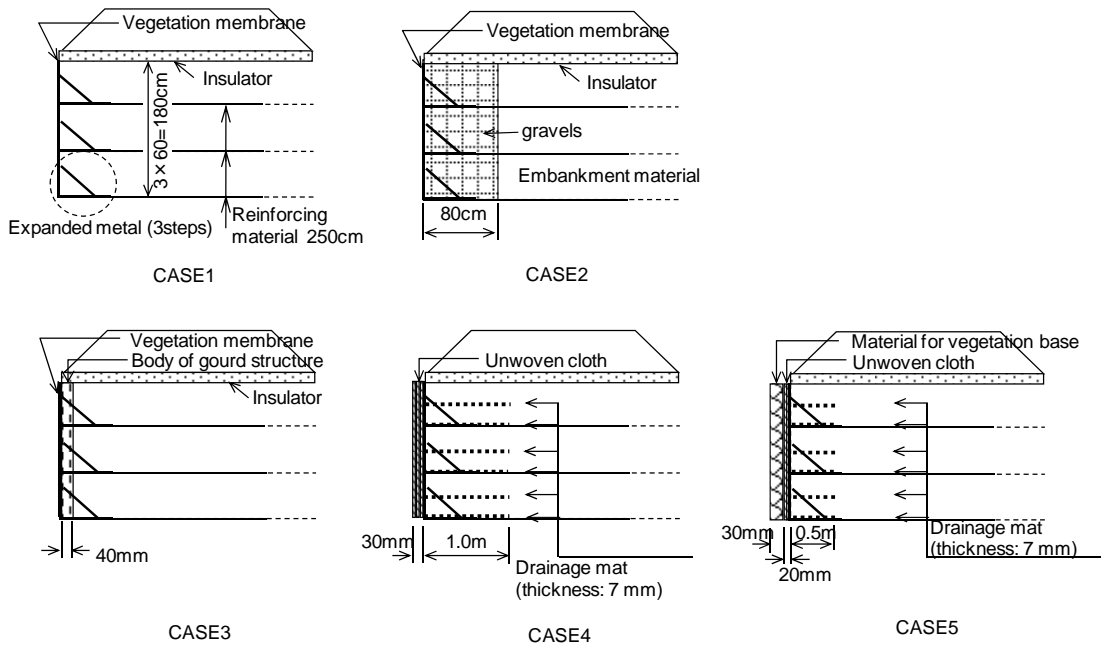


Figure 2 Profiles in respective test cases

2.

These models were built in 2008. Case 1 represents standard geotextile-reinforced soil walls. In Case 2, soil replacement was performed to control frost heave when the model walls were built. The thickness of soil replacement is 80cm, according to specifications set by the Hokkaido Regional Development Bureau for Tomakomai. The embankment material to the depth of 80cm from the wall surface was replaced with soil insusceptible to frost heave (Table 3).

The replacement soil was gravelly soil whose natural moisture content was nearly the same as the optimum moisture content, and this gravelly soil contained almost no fine-grain fraction. For

the purpose of examining temperature-related measures, materials that provide insulation and can be planted on were applied to the outer surface of the reinforced soil walls in Cases 3, 4 and 5. These materials, however, were not planted, in order to avoid the additional insulation that would be provided by growing plants. In these five cases, the wall surface was built of expanded metal, and an insulating material was applied to the wall surface in 2009.

In Case 3, reinforced soil walls were built without applying expanded metal in 2008. Because the wall surface partly collapsed afterward, a thermal insulating material with a mesh structure was applied to the back of the expanded metal when the collapsed wall was repaired in 2009.

The insulating material used in Case 4 consisted of 3 layers of 10mm-thick nonwoven textile. In Case 5, a 30mm-thick vegetation base material was affixed to the surface of 2 layers of 10mm-thick nonwoven textile.

In actual geotextile-reinforced soil walls in service, water fed from the back side of the walls seems to promote frost heave. In the earth tanks used for testing, however, water was not supplied from the rear face of the model walls. Thus, simulated conditions were prepared by fully immersing the model walls in water for

Table 3. Properties of non-frost-heaving material

Soil particle density ρ_s (g/cm ³)		2.739
Natural water content w_n (%)		11.01
Grain size	2 mm or larger (%)	38.8
	75 μ m to 2 mm (%)	52.3
	Less than 75 μ m (%)	8.9
Consistency limit		N.P.
Classification symbol of soil material		SG-Gs
Maximum dry density ρ_{dmax} (g/cm ³)		2.050
Optimum water content w_{opt} (%)		10.5
Cone index q_c (kN/m ²)		3000 or larger

Table 4. Measurement items and methods

Measurement item	Points of measurement	Measurement instrument	Interval of measurement
Temperature	At the boundary between the first and second stages from the bottom and in the air 10 cm outside the wall surface.	Thermoelectric thermometer	One hour
Earth temperature	At the boundary between the first and second stages from the bottom, near the top surface of thermometer reinforcing material at the second stage and at points 10, 30, 50, 70, 90 and 140 cm from the wall surface.	Strain gauge	One hour
Strain of geotextile	At the boundary between the first and second stages from the bottom, top and bottom surfaces of reinforcing material at the second stage and at points 10, 30, 50, 70, 90 and 140 cm from the wall surface.	Thermoelectric thermometer	One hour
Horizontal displacement of wall surface material	Top and bottom of the first and second stages from the top of geotextile-reinforced earth wall.	Scale	One week in freezing period and two weeks in thawing period

about 2 weeks before the temperature fell into the sub-zero range. Then the water level was lowered to the height of 10 cm above the gravel layer, so that the water would be supplied to the geotextile-reinforced soil walls.

In all cases, both the wall surface and the top side of the walls were exposed to cold air. To protect the top side from cold air, the top side was first covered with 10cm-thick EPS insulating material and then with the same 50cm-thick volcanic ash used for the embankment work. Thus, the wall surface alone was exposed to cold air.

The model walls were built vertically, facing north.

3.2. Measurement items

Table 4 shows the measurement items (e.g. temperature and displacement) and methods, and Figure 3 shows the locations of measurement instruments installed in the model walls. Measurements were taken of the strain in the geotextile in the second tier of the reinforced soil walls and of the temperature nearby. The distance between a leveling line that was set vertically along the earth tank surface and the wall surface was measured to determine the horizontal displacement of the wall surface material.

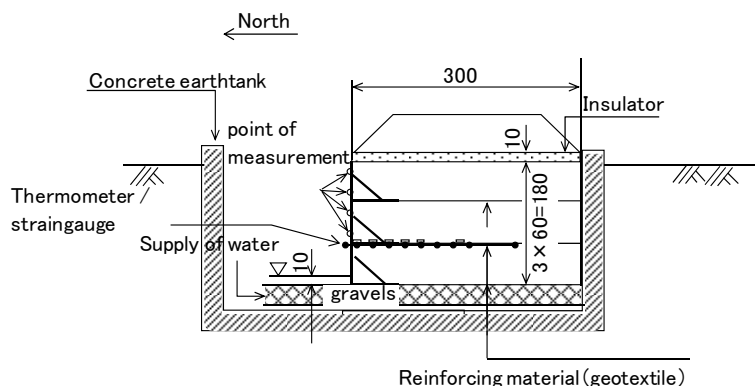


Figure 3 Locations of measurement instructions installed in the model wall

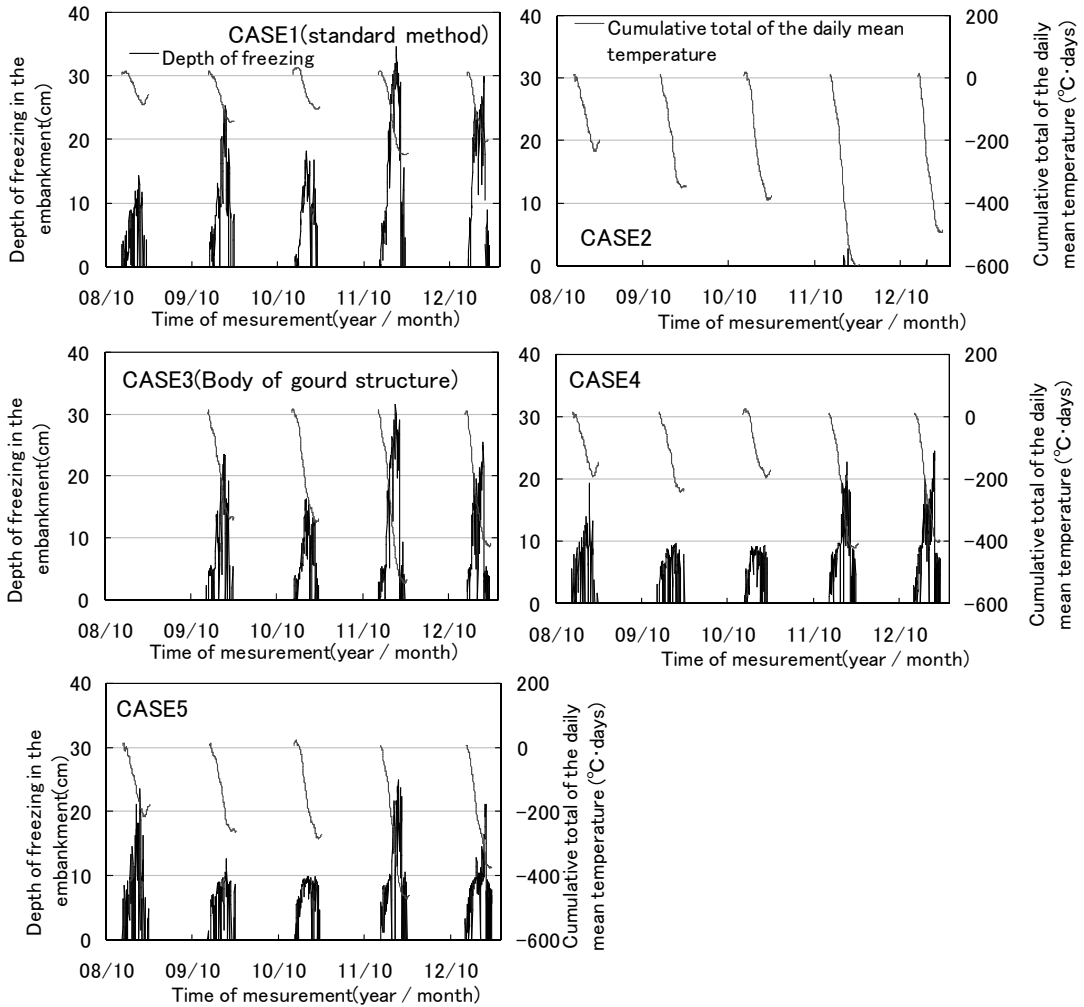


Figure4 Depth of freezing in the fill of model wall

4. TEST RESULTS

4.1. Depth of frost penetration in the embankment on the back side of the model walls

Figure 4 shows the frost penetration depths in the embankments on the back side of the model walls. Figure 5 shows the maximum annual frost penetration depth in the volcanic ash embankment in each case. In Case 2, in which soil was replaced with gravelly soil, there was almost no freezing anywhere in the embankment. In Case 3 in which an insulating material having a mesh structure was applied to the back of the expanded metal, it was not possible to measure the frost penetration depth accurately in 2008 because the reinforced soil walls had partially

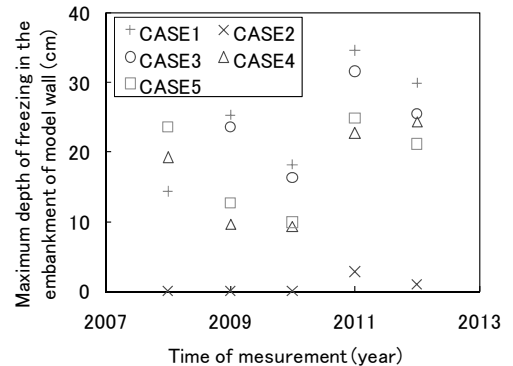


Figure 5 Maximum annual frost penetration depth in the volcanic ash embankment in each case

collapsed. In and after 2009, the frost penetration depth was smaller than for standard geotextile-reinforced soil walls (i.e., Case 1). But the insulating materials used in Case 3 were proven to be only marginally effective because the difference from Case 1 in frost penetration depth was only about 4cm. In Cases 4 and 5, a 7mm-thick drainage mat was placed in standard geotextile-reinforced soil walls to control frost heave. In 2008, the frost penetration depths in these two cases were much greater than the frost penetration depth in Case 1. In and after 2009, when an insulating material was applied to the reinforced soil walls, the frost penetration depths were smaller than in Case 1. Over the four years after the application of insulating materials, frost penetration depths in Cases 3, 4 and 5 were smaller in comparison with Case 1; thus, it can be concluded that the insulating materials used are effective in preventing frost heave for at least 4 years after application. The effectiveness of the insulating materials will be monitored over a long period.

4.2. Horizontal displacement of the wall surface material

Figure 6 shows the horizontal displacement of the wall surface material in each case. When the walls began to freeze, the wall surface material began to be displaced outward. When the embankment material completely thawed, the wall surface material was displaced slightly inward. Outward displacement took place again in the following freezing season. The process of outward and inward displacement was repeated annually over the course of five years, resulting in cumulative residual displacement outward. In Case 1, the model walls were displaced outward by 8 cm over the course of the five years after

construction. The data on maximum frost penetration depths in the embankments shown in Figure 4 suggest that the wall surface material is displaced on a larger scale for greater frost penetration depths.

The maximum annual displacements are shown in Figure 7. In Case 3, expanded metal as a wall surface material and insulating materials were applied in 2009. Except for Case 2, the largest value of the maximum annual horizontal displacement was observed in the first freezing season after the construction of the walls. Through the testing period, the value of the maximum annual horizontal displacement varied depending on the frost penetration depth. In Case 3, displacement was not effectively controlled. Except for Case 4 in 2012, application of insulating materials helped to control displacement. Changes in displacement will be monitored.

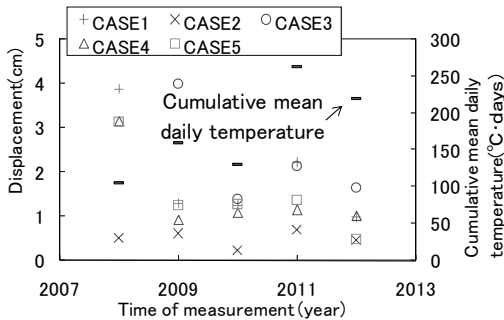


Figure 7 The maximum annual displacements

4.3. Strain in the reinforcing material

Strain in the reinforcing material (i.e., geotextile) in Case 1 is shown in Figure 8. Except at the measurement point 140cm from

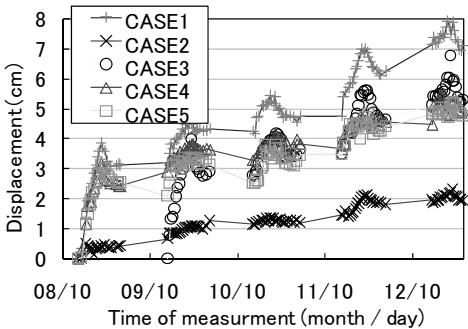


Figure 6 Horizontal displacement of the wall surface material in each case

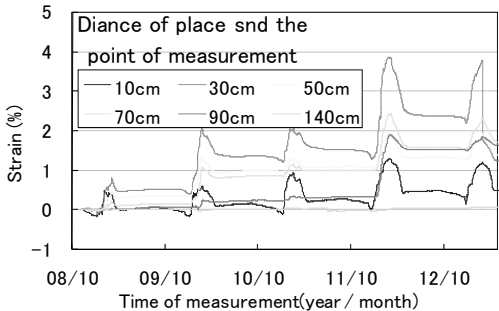


Figure 8 Strain of reinforcing material on case 1

the reinforced soil wall surface, the strain increased in the freezing season and slightly decreased in the thawing season, but the strain never decreased to 0. Strain in the following freezing season added to the residual strain. In Case 1, the greatest amount of strain was measured at a point 30cm from the reinforced soil wall surface, and the second- and the third-greatest amounts of strain were measured at points 50cm and 70cm, respectively. At the measurement point 90cm from the reinforced soil wall surface, the strain remained almost constant for the 3 years after the construction of the walls, but relatively large strain occurred in the 4th year. At the measurement point only 10cm from the wall surface, the strain decreased to 0 before the beginning of the freezing season every year.

A similar tendency was confirmed in the other cases, although the strain varied and the distance from the wall for the greatest strain was mutually different for each case. In Case 1, the strain at the point 30cm from the wall surface was the greatest (3.9%). The greatest strain in the other cases occurred at various distances from the wall surface.

Figure 9 shows the time-dependent change in the strain at the point where the greatest strain was measured in each Case. The largest strain was measured in Case 1 (i.e., standard geotextile-reinforced soil walls) and the second-largest strain was measured in Case 3 (i.e., geotextile-reinforced soil walls with an insulating material of mesh structure). The strain was relatively small in Case 2, in which soil was replaced with gravelly soil, and in Cases 4 & 5 in which nonwoven textile was used for insulation.

It is concluded that the application of insulating materials to the outer surface of the

geotextile-reinforced soil wall is as effective as soil replacement with gravelly soil in embankments, because the strain is roughly the same for these two methods.

5. SUMMARY

This study focused on methods for controlling deformation due to frost heave in geotextile-reinforced soil walls in service in cold regions such as Hokkaido. Specifically, materials that provide insulation and are suitable to be planted on were attached to the outer surface of reinforced soil walls, and the effectiveness of these materials in controlling deformation due to frost heave were examined. Although the effectiveness was found to vary with the insulating material used, it was determined that the application of an insulating material to the outer surface of a reinforced soil wall helps to control deformation caused by frost heave. Insulating material can be easily applied to a wall surface. Geotextile-reinforced soil walls are designed to be planted on, and plants can grow on the attached insulating material. Over time, growing plants provide additional insulation^{8) 9)}, thereby suppressing deformation further.

6. REFERENCES

- Hokkaido Regional Development Bureau, *Road Design Guidelines*
http://www.hkd.mlit.go.jp/zigyoka/z_doro/download/pdf/01/1-7-1.pdf
- Japan Road Association, 2009, *Road Earthwork Guideline*
- Ono Takashi, 2012, Effects of Vegetation in the Frost Heave Control, Collection of Lectures, *the 47th Workshop of The Japanese Geotechnical Society*, 7
- Sato Atsuko, Nishimoto Satoshi, Suzuki Teruyuki, and Nakamura Dai, 2010, Insulating Effect of Vegetation on Slopes, *the 65th Annual Meeting*, 9
- Sato Atsuko, Nishimoto Satoshi, and Tatta Naoki, 2012, Elucidation of and Measures against the Factors Involved in the Deformation of Geotextile-reinforced Soil Walls Due to Frost Heaving, *the 55th Hokkaido Development Technology Conference, Hokkaido Regional Development Bureau, Ministry of Land, Infrastructure, Transport and Tourism*
- The Japanese Geotechnical Society, 1994, *Soil Freezing - Its Mechanism and Actual Conditions*
- The Japanese Geotechnical Society, 2009, *Frost Heave Test Methods for Determining the Amount of*

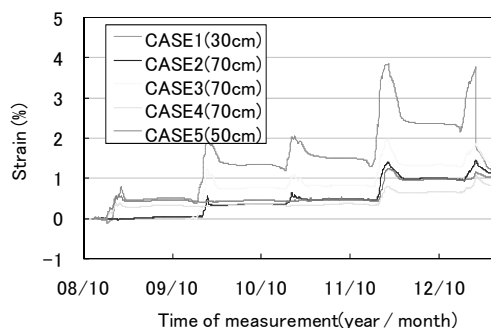


Figure 9 Change in maximum Strain in respective cases

Frost Heave; Frost Heave Test Methods for Determining Susceptibility to Frost Heaving; *New Standards Established by The Japanese Geotechnical Society and the Guide to the New Standards*, p. 247

Yoshida Koichi, Shinmura Junichi, and Suzuki Teruyuki, 2009, Report on the Deformation of Geotextile-reinforced Soil Wall Surface in Cold Regions, *the 44th Workshop of The Japanese Geotechnical Society*, pp. 809-810

Evaluation of pile behaviour on sloping clayey soil in supporting a diaphragm wall for building excavation

Sivapriya S.V

Associate Professor, SSN College of Engineering, India

Gandhi S.R

Professor, Indian Institute of Technology Madras, India

ABSTRACT:

In the present paper, an attempt is made to monitor the behaviour of steel pipe pile on clayey slope while excavating for a basement of a building. The basement excavation is supported by RCC diaphragm wall, which gets the lateral support from temporary steel pipe piles to enable top-down construction in the peripheral area, which are connected to the diaphragm wall with basement floor slabs. The horizontal displacement of the piles is measured based on inclinometer tubes embedded in the diaphragm wall. A detailed finite element analysis has been carried out using PLAXIS 3D model and the theoretical results are compared with the field observations.

1. INTRODUCTION

In deep basement excavation or other underground structures, use of diaphragm wall as a permanent retaining wall is widely adopted. This paper presents a case study of three basement deep excavation where the peripheral area is constructed by top-down method and the central area is constructed by bottom-up method. The diaphragm wall and pile behavior for the adequacy has been checked using soil-structure-interaction analysis.

Field monitoring to study the interaction was carried by Wong and Poh (1999). The behaviour of pile during excavation was studied by Muthukumaran et al. (2004 a and b). Ong et al. (2009) did 50 g centrifuge test to study the behaviour of pile groups behind a retaining wall in soft clay. It was observed that the formation of soil arching and “separation” of soil which occurred between the front piles of a pile group when the soil moved due to excavation. The front pile in the group shadows the rear pile due to the excavation-induced soil movement. Stuedlein et al. (2010) studied the performance of mechanically stabilised wall. The structural flexibility of the wall is estimated as maximum angular distortion of approximately 1/25.

The previous literature study deals with the behaviour of the retaining wall due to excavation, but the behaviour of pile in the slope that is formed during excavation is not much focused. Hence, an attempt is made to focus the behaviour of the retaining wall as well the pile. The

retaining wall deflection is obtained through field monitoring and simulated the same in finite element analysis to observe the behaviour of piles.

2. GEOTECHNICAL AND STRUCTURAL DATA

A typical borehole data is given in Figure 1. The presence of water table was observed at -2.70 m from the natural ground level. From ground to level to -3.8 m loose to medium dense sand with silty clay is found and from -3.8 m to -9 m medium stiff clay is observed. Below this layer till -17m is marine clay layer followed by hard shale with sand stone.

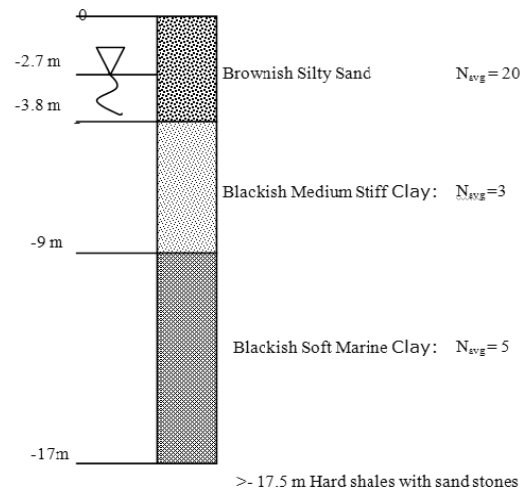


Figure 1. Typical Bore- Log Data

A multi-storied G + 12 commercial building with three basements is used for this study. Due to the presence of high water table and weak soil at a shallow depth, open excavation for foundation was technically not possible. Hence, retaining structure comprising of 0.8 m thick diaphragm wall which serves as permanent wall of the basement was opted to overcome the instability problem during excavation. The diaphragm wall along with two rows of sacrificial pile is installed along the periphery of the construction area in order to support the wall and to avoid any strut or anchors. The remaining central area was constructed with open excavation using the bottom-up method with an open excavation.

Diaphragm wall of 800 mm thickness and length varying from 17 to 23 m is constructed initially throughout the perimeter of the construction area. Sacrificial piles of 860 mm diameter were then driven in the specified location adjacent to the wall. The displacement in the diaphragm wall panel was measured at selected location using inclinometer.

It is assumed that the displacement in the diaphragm wall is equal to that of sacrificial pile, because of the rigidity of the floor slabs. The typical reading for one panel was taken and analysed. Figure 2 shows excavation beneath the floor slab.

2.1. Construction of Basement

The first step was to level the ground to the required level. Then sacrificial and permanent piles were installed at required locations. For the construction excavation was carried out upto the first basement level. Over the diaphragm wall panels an *in-situ* beam is constructed connecting all the wall panels. MS brackets are welded around the sacrificial piles to support the floor slab. The soil was compacted, over which M10 PCC of 150 mm thickness was laid.

The floor slab of 200 mm thick in the first basement was cast and once the slab concreting was finished and cured the excavation of the basement below slab was done by mechanical means. Subsequently the entire slab is cast and the sacrificial piles supported the lateral loads through the basement slab.

The first basement was cast only for a limited width of 12 m covering the two sacrificial piles and a construction joint was left to extend the slab further later. The central portion without floor slab was excavated to the next

basement floor level of - 5.5 m as an open excavation.

The excavation then progressed under the slab already cast with support from sacrificial pile as shown in Figure 2. In addition to the vertical weight of the floor slab, the sacrificial pile is also subjected to lateral load due to the deformation of the diaphragm wall towards the excavation. The behaviour of the piles and the wall is analyzed using the FEM and the deflection of the diaphragm wall obtained is compared with the actual deflection measured using an inclinometer. The input parameters of soil have been varied till the theoretical deflection matches with the measured deflection. At this stage, the shear in pile on slope and corresponding deformations are noted.

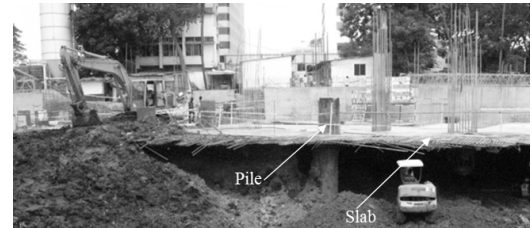


Figure 2. During excavation

3. GEOTECHNICAL AND STRUCTURAL DATA

A three-dimensional model is generated with 17 m deep; 6 m wide and 0.8 m thick diaphragm wall as shown in Figure 3 (a and b). The soil model accommodate slab and pile along with the diaphragm wall; their corresponding dimensions are given in Table 1. The soil is extended to 10 m in other side of the excavation. The temporary steel piles are placed at a centre-to-centre distance of 3.5m.

Table 1. Structural Material Details

Element	Dimension	Material Type	Element Model
Diaphragm wall	17m long, 6m wide and 0.8m thick	M35	Plate
Slab for Basement I	9m long, 6m wide and 0.2m thick	M25	Plate
Slab for Basement II	9m long, 6m wide and 0.28m thick	M25	Plate
Sacrificial Pile	Outer diameter 0.86m with 8mm thick	Hollow Steel Pipe	Embedded Pile

The soil was modelled as Mohr-Coulomb, diaphragm wall and the slab as plate material and sacrificial pile as embedded pile element. The elements has in-built interface element, which is generated automatically when it is modelled. At the same time, the soil property is worked back to real conditions and it is given in the Table 2. Discretization of the soil element is a 10-node tetrahedral soil element and 3-node line element for beam with medium mesh with element dimension of 0.075m. General fixity condition is opted as $U_x=U_y=U_z=0$.

Table 2. Soil properties

Layer Number	Layer Depth, m	c_{us} , kPa	Φ , °	E, kPa
I	0 – 3.8	5	27	1250
II	3.8 – 9	80	0	20000
III	9 – 17	20	0	5000

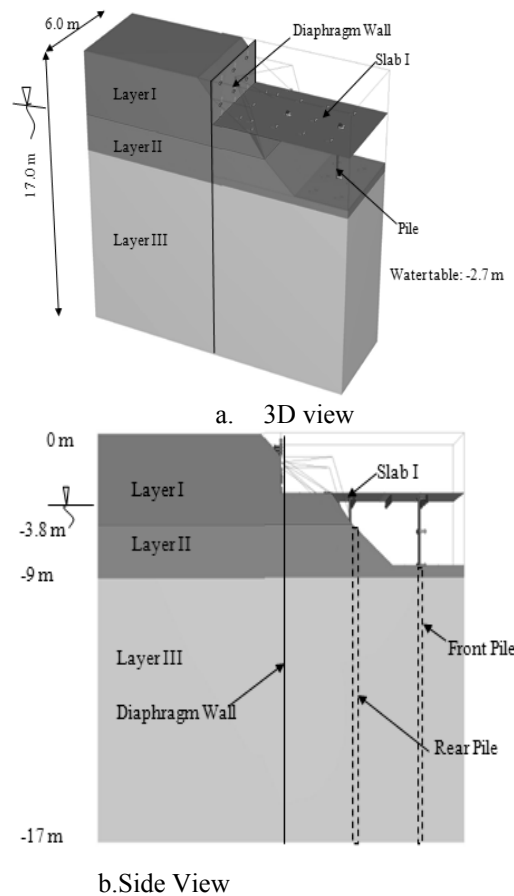


Figure 3. Model generated

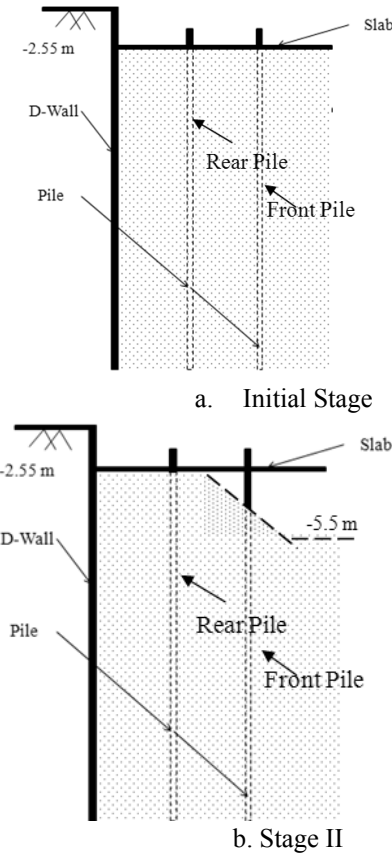
4. ANALYSES

In this, analysis was done for different stage of excavation with an inclination of 45° with PLAXIS 3D of 8124 nodes. Each stage of reading was recorded after the analysis and it was deducted from the initial reading. Figure 4 (a - d)shows initial stage, Stage II, IV and V

The analysis is done stage by stage as given below,

- Initial stage- excavation till -2.55 m
- Excavation carried till -2.55m with an inclination of 45° from one end of the slab – Stage I
- Excavation with a inclination of 45° from the stage I excavation – Stage II
- Excavation with a inclination of 45° from the stage II excavation – Stage III
- Excavation with a inclination of 45° from the stage III excavation – Stage IV
- Excavation till -5.5 m – Stage V

The calculation was done in two stages: 1. Initial phase (*k0- procedure*) and 2. Plastic analysis. The numerical analysis was done for one typical panel and compared with panel number 49 which was monitored with an inclinometer.



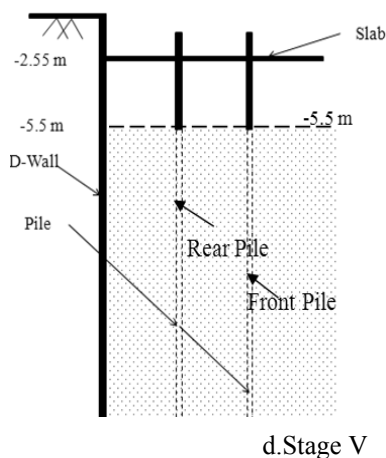
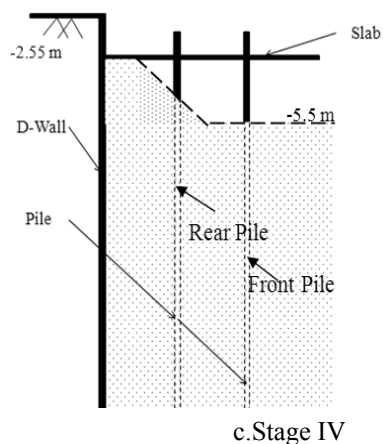


Figure 4. Different Stages of Excavation

5. RESULTS AND DISCUSSION

In order to arrive at appropriate parameters for the field condition, the excavation in different stages was analysed using PLAXIS – 3D. The parameters related to soil property were varied till the deflected shape of the diaphragm wall is found to match with the inclinometer in Figure 5.

Using the above soil parameters, the excavation stages at different stages were analysed with piles placed at different position from the crest of the slope.

For each stage of excavations from the PLAXIS analyses, the shear load at the pile top transmitted from the diaphragm wall through the basement slab and the corresponding displacement have been obtained as shown in Figure 6. This figure shows the behaviour of the pile supporting the slab under different shear load and for different slope condition. The

results also shows that for a given shear load, the front pile deflect more compared to the rear pile.

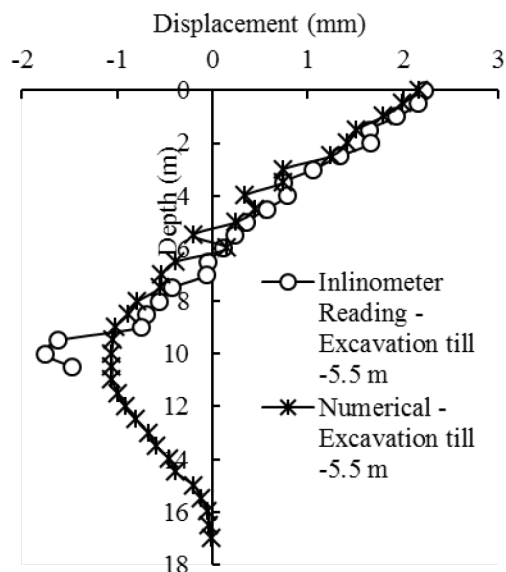


Figure 5. Comparison of measured and observed displacement reading

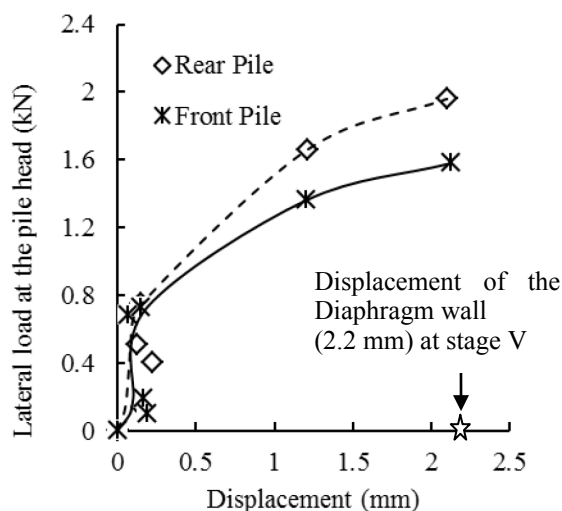


Figure 6. Load shared by the piles due to excavation

The bending moment in the rear pile is more due to slope effect. This is mainly due to the fixity and the reduction in the resistance in the rear pile. The bending moment of the pile was within the safe limit. The bending moment of the front and rear piles is shown in Figure 7.

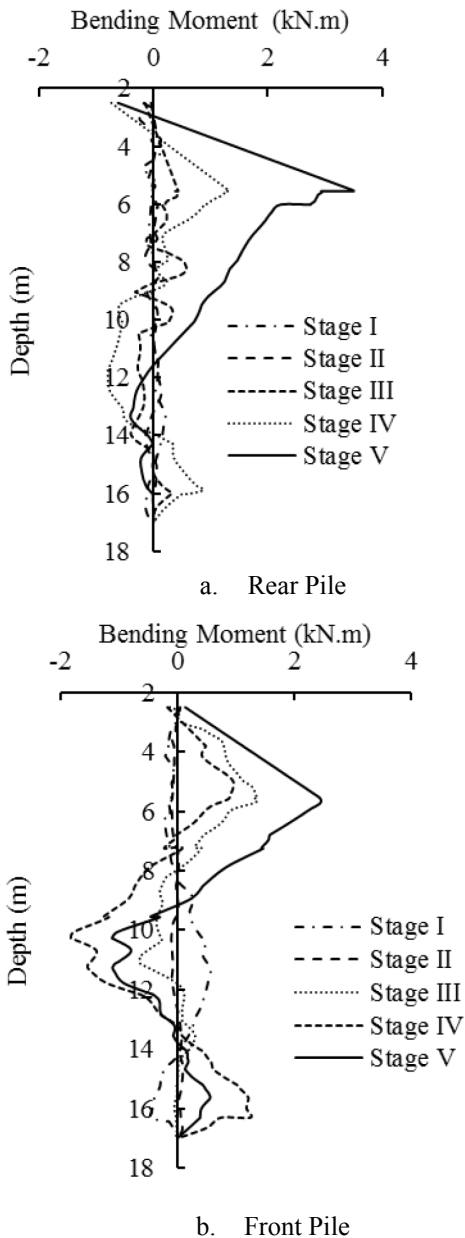


Figure 7. Bending moment in pile due to excavation

6. CONCLUSION

The case study helps us to understand the behaviour of pile in a sloping ground. The displacement in front pile is higher than the rear pile. There is a reduction in displacement which is due to the presence of the slab, which behaved like a strut and it provided high fixity to

the pile head. The soil-structure-interaction analysis using 3D PLAXIS was very useful to check the adequacy of the temporary piles which provided vertical support to the basement slab and the lateral support to the diaphragm wall during the excavation.

7. REFERENCES

- Wong, I.H. and Poh, T.Y. 1999. Comparison of retaining walls for basement construction in stiff clays. *Tunnelling and Underground Space Technology*, Vol. 14, No.4, pp. 461-468.
- Muthukkumaran, K., Sundaravadivelu, R. and Gandhi, S.R. 2004 a Monitoring of lateral deflection in a berthing structure during dredging- A case study. *5th International Conference on Case histories in geotechnical engineering*, paper No.5.35
- Muthukkumaran, K., Sundaravadivelu, R. and Gandhi, S.R. 2004 b Effect of slopping ground on single pile load deflection behaviour under lateral soil movement. *13th World conference on earthquake engineering*, Canada, 1-6.
- Ong, D. E. L., Leung, C. F. and Chow, Y. K. (2009) Behavior of Pile Groups Subject to Excavation-Induced Soil Movement in Very Soft Clay. *Journal of Geotechnical and Geoenvironmental Engineering*, ASCE, Vol. 135, No. 10, pp.1462-1474.
- Stuedlein, A.W., Bailey, M., Lindquist, D., Sankey, J. and Neely, W.J. 2010. Design and performance of a 46 m high MSE wall. *Journal of Geotechnical and Geoenvironmental Engineering*, ASCE, Vol. 136 , No.6, pp 786 – 796.

Effect of Base Soil Stiffness on the Earth Pressure of Cantilever Retaining Walls

Hany F. Shehata* and Tamer M. Sorour[‡]

[‡] Assistant Professor, Ain Shams University, Cairo, 11511, Egypt,
tamer.sorour@eng.asu.edu.eg

* Teaching Assistance, El-Shorouk Academy, Cairo, 11511, Egypt,
hanyfarouk808@gmail.com

ABSTRACT: This paper presents the effect of the base soil stiffness for sandy soils, under a retaining wall on the resulted earth pressure and the wall deformation. The most common method that is widely used in the calculation of the lateral earth pressure on the retaining wall is Rankine Theory. This method didn't take the effect of the base soil stiffness on the value of the earth pressure into consideration. Earth pressure also depends on the value of the wall displacement, which in turns; depends on the wall rigidity. In this study, a set of 2D finite element models were prepared to simulate the effect of retaining wall's rigidity, different base soil stiffness and the embedded width of the footing inside the backfill on the lateral earth pressure distribution and the maximum bending moment acting on the wall. It is found that the soil base and the wall rigidity are significantly affecting the movement of the wall. The different FE models showed that the wall's base is rotated and displaced horizontally and vertically due to the backfill weight and the base soil stiffness. Also, the wall rigidity and the rotation of the wall base are affecting the maximum deflection the wall. Due to this movement, the resulted earth pressure is affected by the base soil rigidity and the wall rigidity. In general, Rankine theory is still has a good agreement with the results and has a satisfactory safety factor in most cases.

1. INTRODUCTION

In Terzaghi's 1934 classic experiments with a large-scale model retaining wall, it was found that only a small amount of movement, 0.25% of the wall height, was required to achieve the active condition and that a larger amount of movement, 1% of the wall height, was required to achieve the passive condition. Morgenstern and Eisenstein 1970 compared Rankine's theory, which assumes no wall friction, to several approaches that do account for wall friction and found that for the active condition, the other theories were all within about 10% of each other. To determine earth pressure, Coyle et al. 1974 installed EPCs behind a 4.9 m 16 ft high cantilever retaining wall resting on H piles. Translation was measured relative to a fixed point using an engineer's steel tape, and displacement of the stem from vertical was recorded using a plumb bob suspended from the top of the wall as a vertical reference line. The earth pressure compared well with the theoretical active pressure for the top 2.1 m 7 ft of the wall, but it was between the active and at-rest values for the bottom of the wall. Coyle and Bartoskewitz 1976 also presented the results

from instrumenting a 3 m 10 ft high, 3.7 m 12 ft wide precast panel retaining wall founded on drilled piers. The results regarding lateral earth pressure were very similar to the results of Coyle et al. 1974 in that the earth pressure reduced to active levels at the top of the wall, but not at the bottom. Most wall movement during backfilling was in the form of translation, but some rotation and translation away from the backfill occurred for a few months after backfilling had ended. Several researchers have performed finite element analyses of concrete retaining walls, including gravity walls Clough and Duncan 1971; Kulhawy 1974 and cantilever walls Horvath 1991; Goh 1993. Clough and Duncan 1971 examined the behavior of a wall founded on sand using increments of loading to simulate the placement of backfill Goodman and Brown 1963; Clough and Woodward 1967. Goh 1993 modeled backfilling in a similar manner and found that a cantilever wall rotated into the backfill and translated forward from its original position. Differential settlements between the toe and heel of the footing caused rigid body rotation into the backfill. The stem tilted forward due to elastic deflection, and the base of the wall

translated forward. The stem displaced sufficiently for the top part of the lateral pressure distribution to be approximately active. For the bottom third of the wall stem, in particular, the lateral pressures were between active and at-rest values.

2. RESEARCH OBJECTIVES

The research has two objectives. The first objective is to qualify the effect of the base soil stiffness and wall rigidity on the resulted earth pressure, horizontal wall movement (Δx), and the maximum bending moment (M_{max}). The second one is to compare the results of the FEM with those are resulted using the Rankine's theory.

3. RESEARCH MODELS

To reach the paper objectives, a total of 43 (forty three) FEM were analyzed using PLAXIS 2D-AE.

Six sandy soils with different properties are adopted to represent the soil media using the hardening soil model. The backfill used in all models is sand and is represented using the hardening soil model. Different properties and parameters for the soil base and backfill are illustrated in Table (1).

Five wall thicknesses (t), which are used to simulate different wall rigidities, are analyzed using the previously indicated soil properties. The used wall thicknesses are 0.2, 0.4, 0.6, 0.8, and 1.0-meter.

Four embedded base widths (X) inside the backfill are simulated for the different soil bases. The values of (X) are 0, 1.1, 1.8, and 2.8-meter. The total footing width (B) and its thickness are constant for all models and equal to 3.50 and 0.60 meter, respectively.

The wall height (H) is constant in the analyses and is equal to 4.00-meter. The construction stages are simulated in PLAXIS, but the total displacement and the total lateral earth pressure produced from the backfill soil are presented in this paper. The passive soil opposite to the wall is not considered, while the passive soil opposite to the footing is considered with the same parameters of the backfill, as shown in Figure (1).

The excavation slope angle is taken less than the angle of internal friction of the base soil (ϕ_{base}). The horizontal boundary condition is taken equal to double the wall height for the

excavation side, while the other side boundary is taken more than the safe excavation slope width. The vertical boundary is taken more than triple the footing width.

Table 1. Soil Parameters for Hardening Soil Model

Para-meters	BASE SOIL						BACK FILL
	A	B	C	D	E	Z	
ϕ°	24	26	30	34	38	38	34
C kPa	1	1	1	1	1	1	1
E MPa	1	2	5	10	20	100	20
E_{eod} MPa	1	2	5	10	20	100	20
E_{ur} MPa	2.5	5	12.5	25	50	250	50
m	0.5	0.5	0.5	0.5	0.5	0.5	0.5
γ kN/m ³	1.5	1.6	1.7	1.8	1.8	1.8	1.8

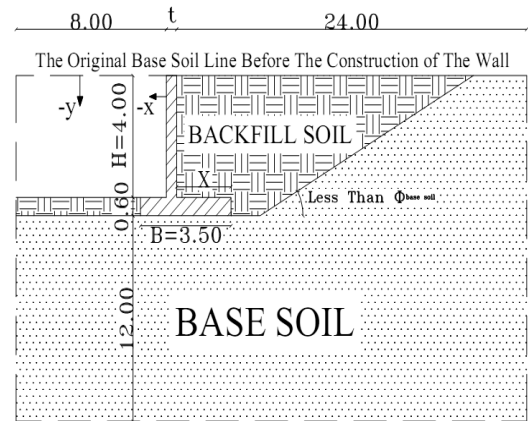


Figure 1. FE model discretization

4. ANALYSES AND DISCUSSIONS

To study the first objective of this research, eleven (11) Figures are conducted; from Figure (2) to Figure (12). Figure (2) represents the effect of the different soil stiffness on the horizontal displacement distribution along the wall height using a thickness (t) of 0.2-meter. For small soil stiffness (weak soil A), the wall base is displaced horizontally and rotated towards the backfill due to the differential settlement resulted from the backfill weight, as shown in Figure (3). The wall stem is tilted away from the backfill due to the elastic wall deflection. For firmer soil, the rotation of the

base is decrease due to the reduction in the resulted differential settlement. In addition, the horizontal displacement is decreased due to the increase of the soil stiffness.

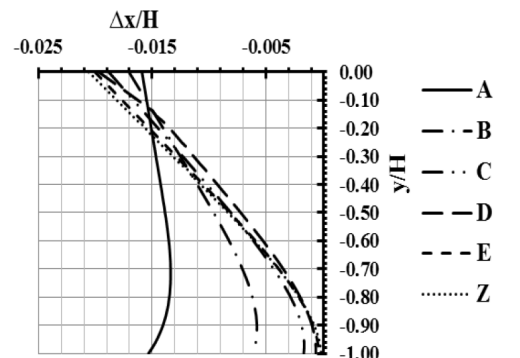


Figure 2. Horizontal movement (Δx) distribution along the wall height (for $t=0.20$ m and $X/B=0.71$)

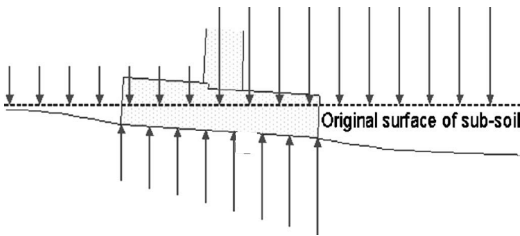


Figure 3. Qualitative response from weight of the backfill

With increasing the wall rigidity by taking ($t= 0.4$ -meter), the distribution of the horizontal movement along the wall height is presented in Figure (4).

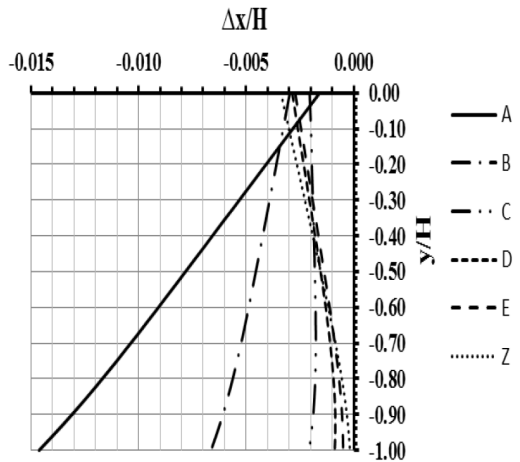


Figure 4. Horizontal movement (Δx) distribution along the wall height (for $t=0.40$ m and $X/B=0.71$)

The results showed a significant decrease in the elastic wall deflection for different soil stiffness, which results in a reduction of the stem movement.

The effect of the soil stiffness on the lateral earth pressure for ($t= 0.20$ -meter) is presented in Figure (5). The results showed a significant deviation from Rankine’s distribution. The FEM results are in good agreement with the behavior of the test results by Goh_1993_ that was presented in the introduction. The top part of the lateral pressure distribution to be approximately active. For the bottom third of the wall stem, in particular, the lateral pressures were more than active values.

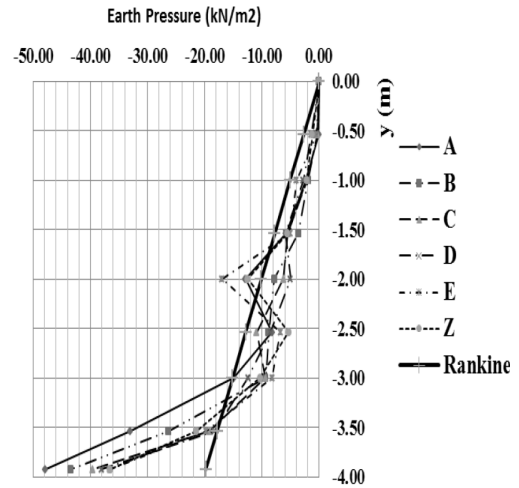


Figure 5. Lateral earth pressure distribution along the wall height (for $t= 0.20$ m and $X/B= 0.71$)

The values of the lateral earth pressure coefficient (K) are calculated from the previous lateral pressure and are presented in Figure (6).

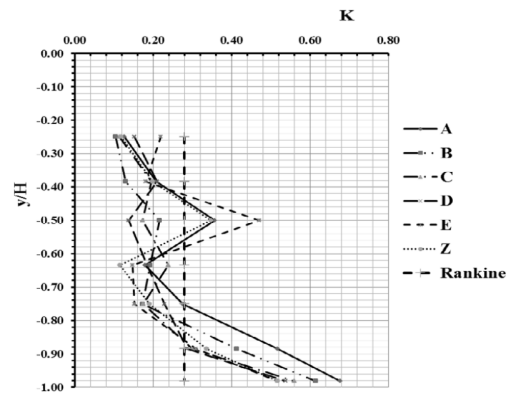


Figure 6. Distribution of earth pressure coefficient (K) along the wall height (for $t= 0.20$ m and $X/B=0.71$)

The values of K resulted from the FEM are varied along the wall height, which contradicts Rankine's theory, in which the value of K is constant.

In the case of more rigid wall ($t = 0.40$ -meter), the earth pressure is behaved in the same manner, with more deviation from the Rankine's distribution, which refers to the effect of wall rigidity on the wall deflection as shown in Figures (7 and 8).

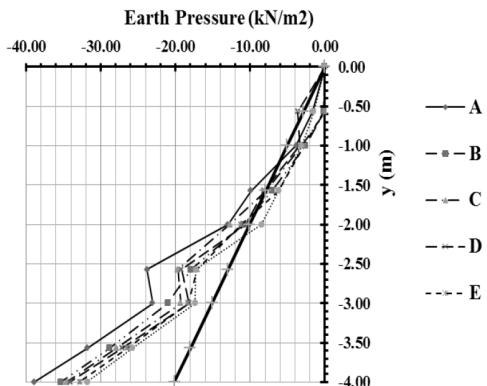


Figure 7. Lateral earth pressure distribution along the wall height (for $t = 0.40$ m and $X/B = 0.71$)

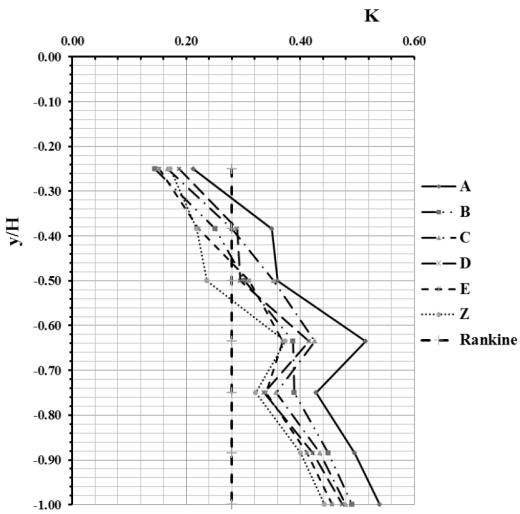


Figure 8. Distribution of earth pressure coefficient (K) along the wall height (for $t = 0.40$ m and $X/B = 0.71$)

Comparisons between the average values of K from the FEM with the constant value of Rankine's theory for different soil stiffness ratios ($E_{base}/E_{backfill}$) and different wall thickness ratios (t/H), are presented in Figures (9, 10) for $X/B = 0.71$. The results showed that Rankine's theory gives high values of K in most the cases except for the cases of rigid walls. Increasing of the wall thickness is increasing the total rigidity and is increasing the resistance to the elastic deformation of the wall, which increases the resulted lateral earth pressure.

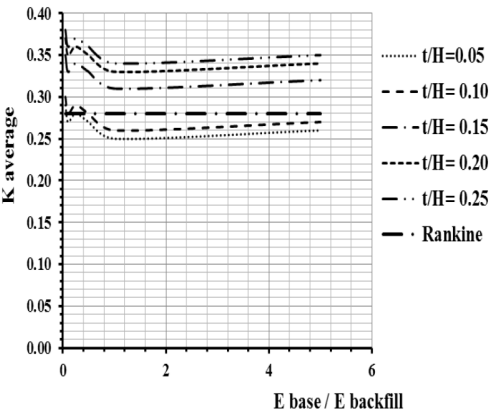


Figure 9. Values of K_{av} vs. soil stiffness ratio for different t/H and $X/B = 0.71$

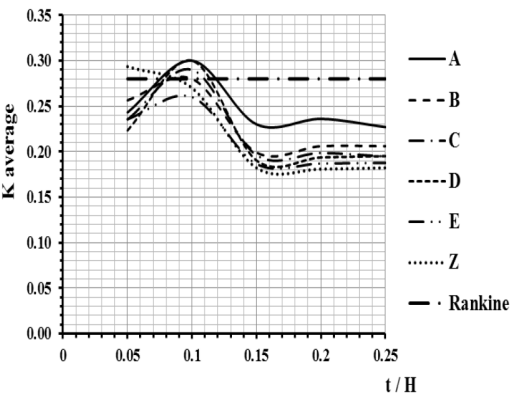


Figure 10. Values of K_{av} vs. wall thickness ratio (t/H) for different soil stiffness and $X/B = 0.71$

An extended analyses are performed to show the effect of the embedded widths of the base inside the backfill (X) on the average values of K for different soil stiffness ratios ($E_{base}/E_{backfill}$) and different wall thickness ratios (t/H), and the results are presented in Figures (11, 12) for $t/H = 0.1$.

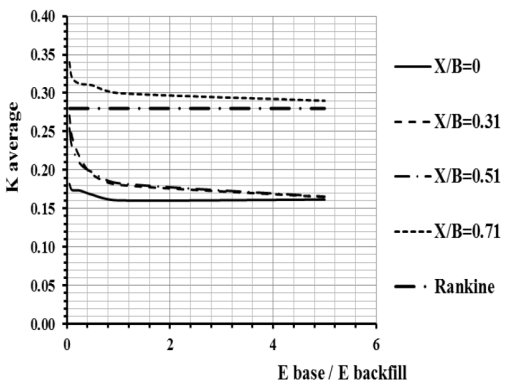


Figure 11. Values of K_{av} vs. soil stiffness ratio for different X/B and $t/H = 0.1$

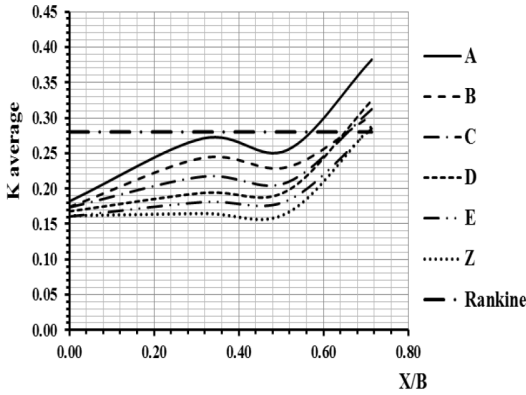


Figure 12. Values of K_{av} vs. X/B for different soil stiffness and $t/H = 0.1$

The results showed that by increasing (X/B) , the values of K_{av} are increased; this refers to the significant increment in the differential settlement and base rotation towards the backfill due to the backfilling weight. For the case of $(X/B = 0)$, the backfilling weight has a slight effect on K_{av} . The effect is increased with the increase of (X) .

Now, the second objective of this research is studied with the following four Figures. The values of K are calculated with respect to the maximum bending moment that is resulted from the FEM and compared with Rankine's coefficient. Figure (13) present the relation between K vs. soil stiffness ratios for different thickness to height ratios for $(X/B=0.71)$

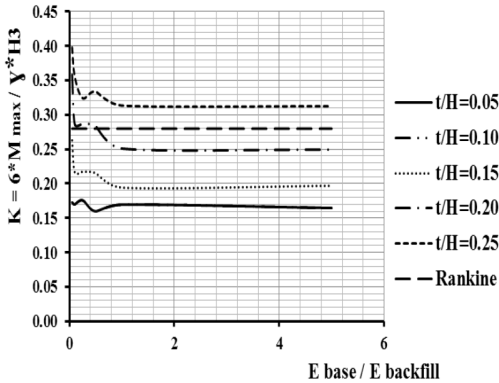


Figure 13. The values of K vs. soil stiffness ratio for different t/H and $X/B = 0.71$

In addition, Figure (14) presents the relation between K and thickness to height ratios (t/H) for different stiffness ratios with $(X/B = 0.71)$. The result showed that the maximum value of bending moment that is resulted from Rankine's theory is greater than those are resulted from the similar cases of FEM, except for the cases of higher rigid walls. These results are in good agreement with the previous presented results in this research.

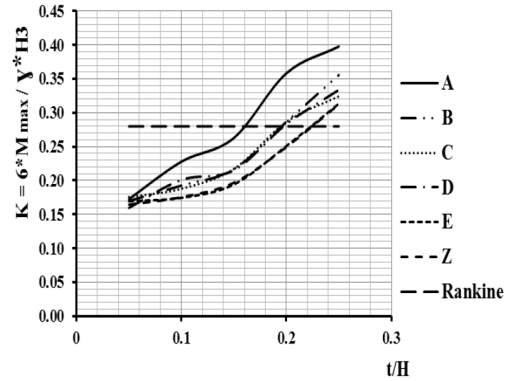


Figure 14. The values of K vs. thickness ratio for different soil stiffness and $X/B = 0.71$

Figures (15, 16) present the values of K with different (X/B) ratios and $(E_{base}/E_{backfill})$ for $t/H = 0.1$.

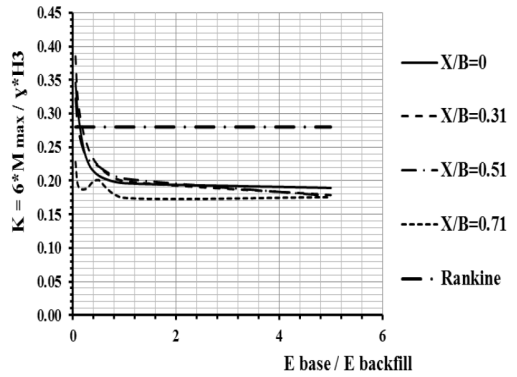


Figure 15. The values of K vs. soil stiffness ratio for different X/B and $t/H = 0.1$.

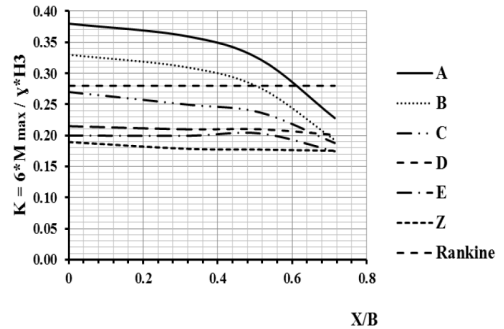


Figure 16. The values of K vs. X/B for different soil stiffness and $t/H = 0.1$.

The increase of the embedded foundation width in the backfill (X) is decreasing the maximum bending moment resulting on the wall. In the other hand, it increases the maximum bending moment that is acting on the embedded footing width, but this effect is not studied in this research.

5. CONCLUSIONS

This research has studied the effect of the wall rigidity, footing embedded width inside the backfill, and the soil base stiffness on the resulting earth pressure distribution and the maximum bending moment acting on the wall. The research has proved that:

- a. The loose or soft base soils affect the lateral earth pressure distribution on the wall in a different behavior than the active pressure that is calculated using Rankine's theory.
- b. Increasing the wall thickness more than about 0.10 of the wall height; the lateral earth pressure is increased significantly up to the at-rest pressure or more.
- c. Increasing the wall rigidity is also producing an increase in the lateral pressure.
- d. The increase of the embedded width inside the backfill decreases the resulted bending moment on the wall, but it increases the bending moment acting on the footing and increases the footing rotation.
- e. In most cases, the Rankine's coefficient is having a sufficient safety factor for the cantilever retaining walls, except for the cases of rigid walls.

6. ACKNOWLEDGEMENTS

Praise and glory are due to Allah whom grants us all our knowledge and success in our life. We would like to express sincere appreciation to the team of EHE Consulting office and INFINITY Consulting Office on their help and encouragement. Furthermore, the researchers are grateful to the Soil Structure Interaction Group in Egypt (SSIE) for their continuous support to the design process.

7. REFERENCES

- Aggour, M. S., and Brown, C. B. _1974_. "The prediction of earth pressure on retaining walls due to compaction." *Geotechnique*, 24_4_, 489–502.
- Bentler, J. G., Labuz, J. F., and Schultz, A. E. _2005_. "Earth pressure behind a retaining wall." Rep. 2005-14, Minnesota Dept. of Transportation, Saint Paul, Minn.
- Clough, G. W., and Duncan, J. M. _1971_. "Finite-element analysis of retaining wall behavior." *J. Soil Mech. Found. Div.*, 97_12_, 1657–1673.
- Clough, R. W., and Woodward, R. J. _1967_. "Analysis of embankment stresses and deformations." *J. Soil Mech. Found. Div.*, 93_4_, 529–549.
- Coyle, H. M., and Bartoskewitz, R. E. _1976_. "Earth pressure on precast panel retaining wall." *J. Geotech. Eng. Div., Am. Soc. Civ. Eng.*, 102_5_, 441–456.
- Coyle, H. H., Bartoskewitz, R. E., Milberger, L. J., and Butler, H. D. _1974_. "Field measurements of lateral earth pressures on a cantilever retaining wall." *Transportation Research Record*. 517, Transportation Research Board, Washington, D.C., 16–29.
- Das, B. M. _2000_. *Fundamentals of geotechnical engineering*, Brooks/Cole, Pacific Grove, Calif.
- Goh, A. T. C. _1993_. "Behavior of cantilever retaining walls." *J. Geotech. Eng.*, 119_11_, 1751–1770.
- Goodman, L. E., and Brown, C. B. _1963_. "Dead load stresses and the instability of slopes." *J. Soil Mech. Found. Div.*, 89_3_, 103–134.
- Horvath, J. S. _1991_. "Effect of footing shape on behavior of cantilever retaining wall." *J. Geotech. Eng.*, 117_6_, 953–978.
- Kulhawy, F. H. _1974_. "Analysis of a high gravity retaining wall." *Proc., ASCE Conf. on Analysis and Design in Geotechnical Engineering*, Univ. of Texas, Austin, Tex., 159–172.
- Labuz, J. F., and Theroux, B. A. _2005_. "Laboratory calibration of earth pressure cells." *Geotech. Test. J.*, 28_2_, 188–196.
- MacGregor, J. G. _1997_. *Reinforced concrete: Mechanics and design*, 3rd Ed., Prentice-Hall, Upper Saddle River, N.J., 337–340.
- Minnesota Department of Transportation _MnDOT_. _2000_. *Standard specifications for construction*, Minnesota Dept. of Transportation, Saint Paul, Minn., 717–720.
- Morgenstern, N. R., and Eisenstein, Z. _1970_. "Methods of estimating lateral loads and deformations." *Proc. ASCE Specialty Conf. on Lateral Stresses in the Ground and Design of Earth Retaining Structures*, Cornell Univ., Ithaca, N.Y., 51–102.
- Terzaghi, K. _1934_. "Large retaining-wall tests—I." *Eng. News-Rec.*, 112, 136–140.
- Theroux, B. A., Labuz, J. F., and Dai, S.-T. _2001_. "Field installation of earth pressure cells." *Transportation Research Record*. 1772, Transportation Research Board, Washington, D.C., 12–19.

Numerical Analysis 3D of a Deep Circular Excavation in the City of Rio de Janeiro

Jose Carlos Solis Tito & Celso Romanel

Departamento de Engenharia Civil, Pontifícia Universidade Católica do Rio de Janeiro, Brasil.

ABSTRACT: At present, due to the need for engineering works of large scale, we have the challenge of solving problems related to deep excavations, where instability problems often occur. In this paper is presented the analysis and validation of the excavation of the service well PS – 39, of the executive project of collectors for treatment of sanitary sewage, located in the city of Rio de Janeiro. This well was constructed using a contention system of a wall of secant column, ring structure type of “shotcrete” covering the columns, and a slab of “jet grouting” anchored with passive tiebacks. The soil parameters of the different layers that compose the geotechnical profile, necessary for numerical modeling, were determined based on the geotechnical information available of the field instrumentation, laboratory data and specific literature review, considering the Mohr-Coulomb constitutive model. The results and interpretation, of the stresses and displacements during the excavation process, were determined using the PLAXIS 3D (2012) program. These results were validated with the measurements determined by instrumentation; then the numerical model will predict rationally the behavior of the set soil-structure during the excavation process. This allows to solve similar problems in advance, allowing proper planning.

1. INTRODUCTION

The different types of large-scale works that are built today require deeper excavations. In this type of excavation, failures often occur due to resistance problems or excessive deformations, presenting stability problems at different stages of the excavation, or in some cases, complete collapse. This has generated a growing interest in the evaluation of design methods, construction and control of excavations, and the different containment structures. This interest is also set in the numerical analysis of these problems, because from these models can be obtained important conclusions that will contribute to a better design of the work according to appropriate control systems.

The general objective of the research is to validate the 3D numerical analysis of the excavation of a circular well, based on the data from the field instrumentation available, through the application of the numerical method of finite elements using the PLAXIS 2D and 3D program.

2. METHODOLOGY

The project of excavation of the service well PS-39, of the executive project of the collectors for sanitary sewage treatment, is located in the Boas Vindas Avenue, in the District of Caju, in the city of Rio de Janeiro. Its location corresponds to the coordinates N = 7469236000, E = 682000000. The dimensions of the well are 16 m of deep and 8.60 m of inside diameter.

The geotechnical information consisted of 5 perforations of recognition SPT, identified as SP-30, SP-58, SP-59, SP-60A and SP-61, conforming the cross sections AA and BB, allowing to determine two geotechnical profiles for modeling the terrain, as shown in Fig. 1. From the SPT tests results, by determined correlations, were determined the index, physical and mechanical properties of the soil.

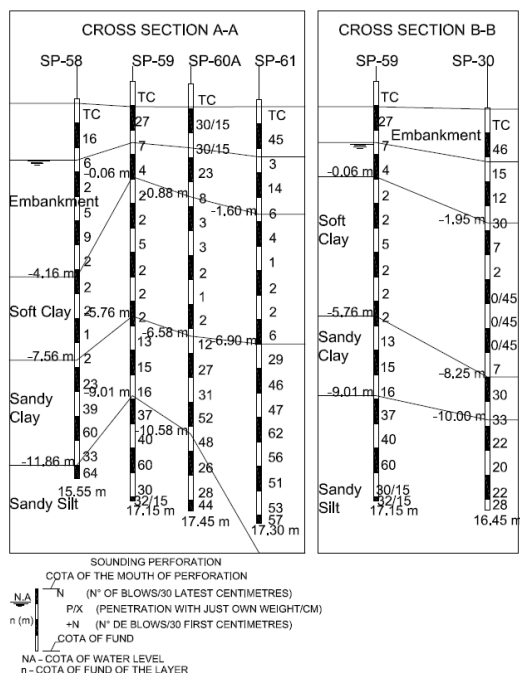


Figure 1. Geotechnical profiles from geotechnical sections. The Section AA is formed by the soundings SP -58 , SP -59 , SP -60A , SP -61 , and Section BB is formed by the soundings SP -59 and SP -30.

According to the geotechnical profile of the ground for the analysis of the excavation, determined according to the perforation SP-59, presented in Fig. 2, the soil presents a layer of embankment with an average thickness of 2.9 m, followed by a layer of very soft clay, with an average thickness of 5.70 m. The next layer consists of a sandy clay, with an average thickness of 3.20 m. The last layer consists of a compact sandy silt (residual soil), with an average thickness of 21 m.

The structure of primary containment consists of the secant columns, which have a diameter of 0.80 m, and are superimposed 0.20 m, in alternate columns were positioned 12 reinforcing bars ($\phi = 25$ mm), these columns were performed with the technique of "wet - mixing" around the perimeter of the well to a depth of 19 m, which was modeled with a solid element with linear elastic behavior. The second containment structure is formed by a ring of shotcrete with 0.20 m of thickness, and built as the excavation progressed, this structure was modeled by plate elements with elastic behavior. The third structural element was a base plate with thickness of 3 m, made with 67

columns of "jet -grouting" with nominal diameter of 1.20 m and 32 columns with nominal diameter of 1.50 m, this plate was anchored with 25 passive tiebacks in the foundation ground. The jet-grouting plate was modeled with a solid element, and passives tie-backs with a combination of embedded piles and spring connections.

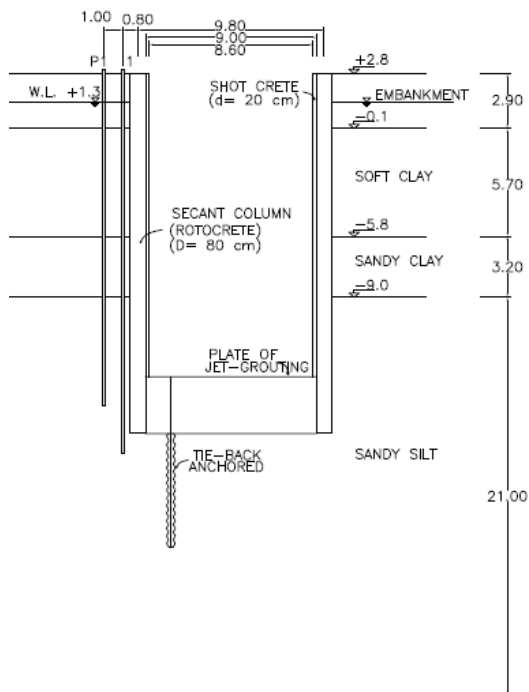


Figure 2. Geotechnical profile for the excavation of the well PS -39.

For analysis of the results is available the registers of measurements for the last stage of excavation, of the horizontal displacements registered with the inclinometer I-01. Also is available the registers of piezometric heads, determined during the period of excavation (consisting of 18 stages of excavation), registered with the piezometer P-03, at an average depth of 13.50 m, corresponding to the layer of silt.

The parameters used for modeling, according to the model of Mohr Coulmb were determined based on the results of field and laboratory test, data from field instrumentation, research results with similar soils in different areas of the city of Rio de Janeiro, and specific literature review. These parameters allow to validate the model with measurements from field instrumen-

tation. The parameters used in the modeling are presented in the Table 1(a) and Table 1(b).

Table 1(a). Parameters of the soil layers that form the geotechnical profile

Material		Embankment	Soft clay
Model		Mohr Coulomb	Mohr Coulomb
Behavior		Drained	Undrained
Parameter	Unit		
γ_{unsat}	kN/m ³	19	13.3
γ_{sat}	kN/m ³	20	13.3
e_0	-	0.5	3.9
k_x	m/s	10 ⁻⁵	10 ⁻⁶
k_v	m/s	10 ⁻⁵	10 ⁻⁶
k_z	m/s	10 ⁻⁵	10 ⁻⁶
c_k	-	10 ¹⁵	10 ¹⁵
K_{0x}	-	0.43	0.59
K_{0y}	-	0.43	0.59
Model parameters			
E'	kN/m ²	6000	1800
ν'	-	0.3	0.3
c'	kN/m ²	2	3.3
c_u			
ϕ'	°	35	24
ψ	°	0	0
Interface			
R_{inter}	-	1	1

Table 1(b). Parameters of the soil layers that form the geotechnical profile

Material		Sandy clay	Sandy silt
Model		Mohr Coulomb	Mohr Coulomb
Behavior		Undrained	Drained
Parameter	Unit		
γ_{unsat}	kN/m ³	15	17
γ_{sat}	kN/m ³	15	17
e_0	-	2.8	0.9
k_x	m/s	7×10 ⁻⁶	10 ⁻⁵
k_v	m/s	7×10 ⁻⁶	10 ⁻⁵
k_z	m/s	7×10 ⁻⁶	10 ⁻⁵
c_k	-	10 ¹⁵	10 ¹⁵
K_{0x}	-	0.58	0.38
K_{0y}	-	0.58	0.38
Model parameters			
E'	kN/m ²	3000	5×10 ⁴
ν'	-	0.25	0.3
c'	kN/m ²		10
c_u		25	
ϕ'	°		38
ψ	°	0	0
Interface			
R_{inter}	-	1	1

3. DISCUSSION OF RESULTS

According to the Fig. 3 for the first stage of excavation, the maximum displacements occur at the surface of excavation (E1), with a value of 0.01364 m. In the middle stage of excavation (E9) this displacement is 0.03185 m in surface excavation. At the end of the excavation (E18), the largest displacements are shown in the middle part of the retaining wall, located in the region of the clay layers, its value is 0.02379 m.

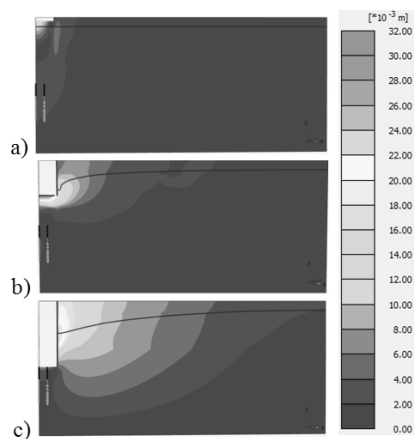


Figure 3. Displacement in the steps of excavation a) (E1) 0.9 m, b) (E9) 8.6 m, c) (E18) 16 m.

In the Fig. 4 is shown the horizontal distribution effective stress acting on the surfaces of the containment walls, determined for the initial conditions (E0), the first stage of excavation (E1), the intermediate stage of excavation (E9) and the last stage of excavation (E18). In this diagram, the negative effective pressures correspond to those exerted over the surface of active pressures (excavated side) and the positive over the surface of passive pressures (supported side). As the excavation proceeds, horizontal effective stress on the passive side is increased to its maximum value, acting directly on the plate of jet grouting.

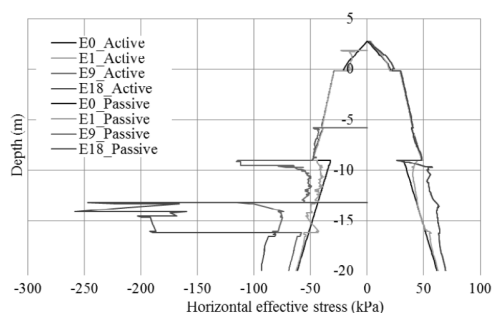


Figure 4. Evolution of the horizontal effective stress on the active side and the passive side, during the excavation process.

To model the effect of the water flow is considered the flow at a steady state, because the mechanical analysis was established as a resistance analyze, excluding the effect of consolidation due to the short term of execution of the excavation, lasting almost a month.

In the Fig. 5 is presented the pore pressure distribution in steady state, on the surfaces of the containment wall of secant columns, determined during the initial stress state (E0), at a depth of excavation of 0.90 m (E1), at the depth of excavation of 8.60 m (E9) and 16 m (E18). The negative pressures correspond to those exerted over the surface of active pressures (excavated side) and the positive over the surface of passive pressures (supported side). In the first stage of excavation (E1), the levels and distribution of pore pressure are identical because the excavation did not reach the water table. In the intermediate stage of excavation (E9) the pore pressure decreases to a height of 0.11 m, due to the drawdown corresponding to this level of excavation. In the last stage of excavation (E18) can be observed the effect of the stiffness of the structural element formed by the plate of "jet grouting", in the elevation of -13.2 to -16.2 m.

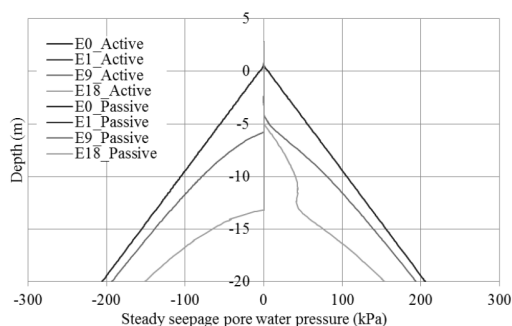


Figure 5. Evolution of the pore pressure on the active side and the passive side.

In the Fig. 6 (1a), 6 (2a), 6 (3a), according to the distribution of total head, can be observed that at the end of the excavation, the drainage is established primarily through the layer of residual soil drained.

The excess pore pressure generated during the excavation process, considering steady state flow conditions are shown in Fig. 6 (1b), 6 (2b), 6 (3c). At the end of the excavation, the most significant changes are verified on the passive side, due to drawdown of the water level, corresponding to a pressure decrease, concentrated in the undrained layers. At the end of the excavation, in the excavated side, the effect of excess pore pressure is practically zero, because the level of excavation reached the drained layer, but this had effect in the previous excavation stages.

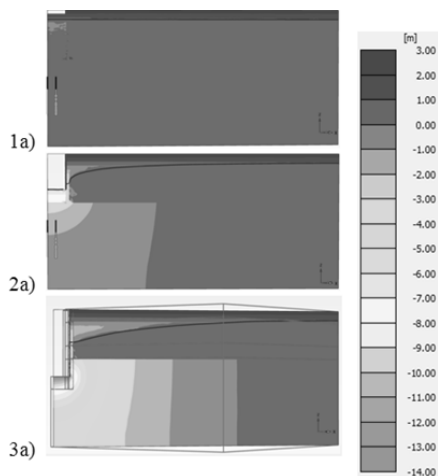


Figure 6 (a). Total heads in the condition of steady state flow, for the stages of excavation (E1) at the level 1, (E9) at the level 2, (E18), at the level 3.

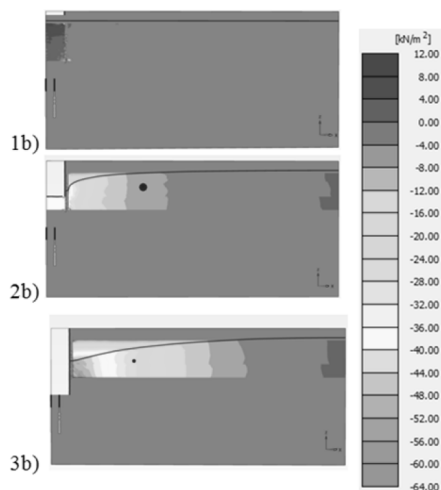


Figure 6 (b). Excess pore pressure in the condition of steady state flow, for the stages of excavation (E1) at the level 1, (E9) at the level 2, (E18) at the level 3.

In the Fig. 7, is presented the profile of horizontal displacements of the control line (corresponding to the location of the inclinometer I-01). According to the diagram, the distribution of horizontal displacements with 3D modeling is similar to axis-symmetric 2D model. The modeling results show a pronounced curvature in the interface between the layers of soft clay and sandy clay with a convexity oriented toward the interior of the excavation. The displacements registered with 2D model show a marked discontinuity in the change of layer. At the end of the excavation,

the maximum horizontal displacement in the control line was presented at elevation -5.5 m, with a value of 0.0143 m, which corresponds to the position of the interface soft clay and sandy clay.

The minimum horizontal displacement had a value of 0.000953 m corresponding to the elevation of 2.10 m, in the control line. In this region, next to the plate of jet-grouting, the displacements were lower, by the effect of confinement offered by this structure.

On the surface, the soil displacement is lower, accompanying the movement of the wall. The effect of the flow in steady state has a minimum influence in the horizontal displacements. The effect of modeling the water flow in steady state in the 3D modeling was concentrated in the layers of clay, producing a minimal influence in the displacements. It produced a contribution to the maximum horizontal displacement of 0.00096 m.

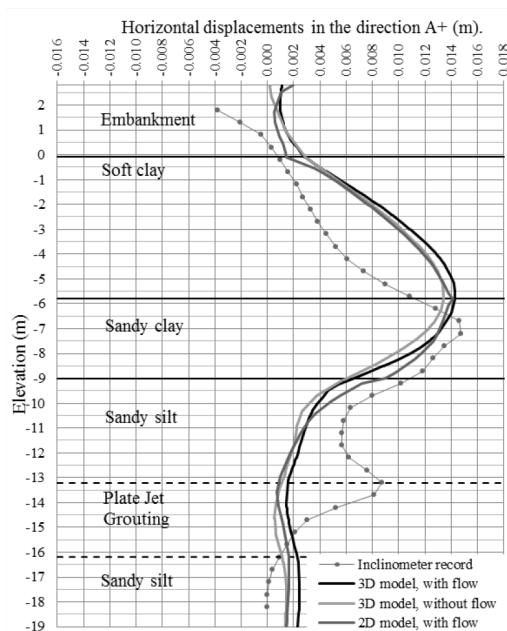


Figure 7. Profile of horizontal displacements, in the radial direction, toward to the center of the excavation.

In Fig. 8 are presented the piezometer heads registered during the 18 stages of the well excavation. The piezometer level present a fall of about 6 m, when the excavation reached the layer of very soft clay (whose base is at an elevation of -0.10 m). Also can be observed the validation of the 2D and 3D models with the

piezometer heads recorded. The maximum difference between the determined head and the piezometric head was presented at the excavation stage 12 (corresponding to the date 14/10/1999). In the 2D model was 1.438 m and in the 3D model was 1.481 m. This drawdown was due to the flow that occurred in the drainage holes that were dropped off at the coating of shotcrete. This shows that the overlapping secant columns were not waterproof ring.

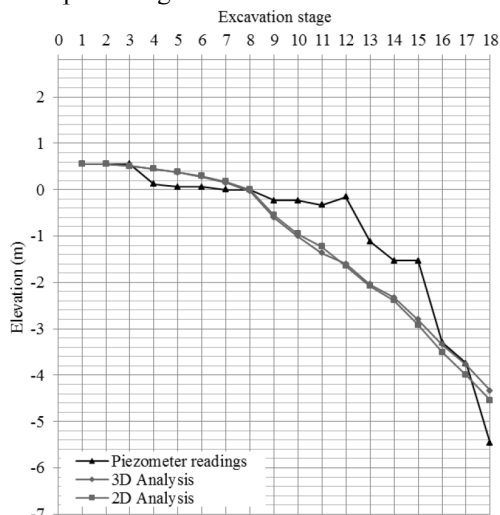


Figure 8. Drawdown of the water level, in the piezometer P 03, along the process of excavation.

4. CONCLUSIONS

After collecting the index, physical and mechanical properties of the different soil types that form the stratigraphic profile of the well PS-39, according to the results of field and laboratory test, field instrumentation data, results of research conducted with similar soils in different areas of the city of Rio de Janeiro and specific literature review, were obtained the values used in the 3D numerical analysis.

Once established the values of the soil parameter, of the four layers corresponding to the stratigraphic profile of the well PS-39, required by the model Mohr Coulomb and using the PLAXIS 3D program, the maximum displacements were determined in the control line. In the last stage of excavation, the maximum horizontal displacement has a value of 0.0143 m at elevation -5.5 m, representing a ratio of the horizontal displacement/ wall height of 0.000918. And according to the inclinometer readings, the maximum horizontal displacement

at the elevation of -7.2 m, has a value of 0.0147 m. The difference between the displacements determined with the program and field measurements is 0.000403 m, representing a percentage of deviation of 2.74 % relating to the horizontal displacement registered in the inclinometer.

Concerning to the earth pressures acting on the secant columns, of the active horizontal pressure side. For the elevation of - 13.2m (corresponding to the bottom of the excavation) the horizontal effective stress is 246.87 kN/m², for the elevation of -16.2 m (corresponding to the base of the secant column) the stress is 189.21 kN/m². For the passive horizontal pressure side, the horizontal effective stress for the elevation of 2.80 m (corresponding to the top of the secant column) is 1.439 kN/m², and for the elevation of -16.2 m (corresponding to the base of the secant column) is 64.296 kN/m².

According to the 3D numerical analysis of the excavation, considering steady state flow, the effect of excess pore pressures in the wall of secant columns is greater in the soil content side, in the clay layer. This is due to the undrained behavior of these soils, the discharge process and the drawdown of the water table, generating positive pore pressures (excess pore pressure of suction) on the boundary of the excavation, increasing the effective stress. In the establishment of the boundary conditions for the analysis, the inside of the well acts as a drainage system, generating a progressive drawdown of the water level, as the excavation progresses; contributing to the horizontal displacement, at the last stage of the excavation, in the interface of the layers of soft clay and sandy silt, in an amount of 0.00088 m.

The finite element method has many advantages due to its generality and ease of determination of clusters of complex calculation in analysis of two and three dimensions, constituting a tool to make a lot of analysis, preventing the occurrence of failures. This tool allows to determine an approximate representation of reality by modeling, using numerical analysis. Also allowing the drafting and designing of quality projects, obtaining results with adequate speed to the requirements and possibly offering better cost, therefore constitutes a competitive tool.

5. REFERENCES

- Almeida, M. S. S., Futai, M. M. and Lacerda, W. A. 2008. Laboratory Behaviour of Rio de Janeiro Soft Clays - Part 1: Index and Compression Properties. *Soils & rocks*, Vol. 31, pp. 69-75.
- Barrios, J. E. M. et al. 1997. *NOTAS. Excavaciones en condiciones complejas*. Bogotá: Editorial Escuela Colombiana de Ingeniería.
- Brinkgreve R. B. J., Engin E. and Swolfs W. M. 2012. *PLAXIS 3D. Material Models Manual 2012*. Holanda: Plaxis bv.
- Christian, J. T. and Wong, I. H. 1973. Errors in simulating excavation in elastic media by finite elements, Soils and Foundations. *The Japanese Geotechnical Society*, Vol. 13, No. 1, pp. 1-10.
- Cintra, J. C. A., Aoki, N. 2010. *Fundações por estacas, projeto geotécnico*. São Paulo: Oficina de Textos.
- Craig, R. F. 2004. *Mecânica dos Solos, Sétima Edição*. Rio de Janeiro: LTC – Livros Técnicos e Científicos Editora Ltda.
- Duncan, J. M., and Clough, G. W. 1971. Finite Element Analyses of Port Allen Lock, *Journal of the Soil Mechanics and Foundation Division, ASCE, SM8*, pp.1053-1068.
- Formigheri, L. E. 2003. *Comportamento de um Aterro Sobre Argila Mole da Baixada Fluminense*, Master's Dissertation - Departamento de Engenharia Civil, Universidade Católica do Rio de Janeiro, Rio de Janeiro.
- Massad, F. 2005. *Escavações a céu aberto em solos tropicais Região Centro-Sul do Brasil*. São Paulo: Oficina de textos.
- More, J. Z. P. 2003. *Análise Numérica do Comportamento de Cortinas Atirantadas em Solos*, Master's Dissertation - Departamento de Engenharia Civil, Universidade Católica do Rio de Janeiro, Rio de Janeiro.
- Morgenstern, N. R. and Eisenstein, Z. 1970. Methods of Estimating Lateral Loads and Deformations, *Conference Proceeding Paper ASCE Specialty Conference on Lateral Stresses in the Ground and Design of Earth-Retaining Structures*, pp.51-102.
- Palmer, J. H. L.V. and Kenney, T. C. 1972. Analytical Study of a Braced Excavation in Weak Clay, *Canadian Geotechnical Journal*, Vol. 9 (2), pp. 145-164.
- Pereira, C. D. D. 2008. *Aplicação de Jet-grouting em escavações profundas em solos moles*, Master's Dissertation - Departamento de Engenharia Civil, Universidade do Porto, Portugal.
- Potts, D. M. 2003. Numerical analysis: a virtual dream or practical reality?. *Géotechnique* 53, No. 6, pp. 535–573.
- Rodríguez, A. R. and Mejía, H. C. 1984. *Instrumentación de campo, Apuntes del libro: La Ingeniería de Suelos en las Vías Terrestres Carreteras, Ferrocarriles y Aeropistas Vol. 2*. México: División de Educación Continua, Facultad de Ingeniería UNAM.
- Sandroni S. S. 2000. Os casos de escavações na região da cidade de Rio de Janeiro, *SEPE* 4, Vol. 2.
- Schnaid, F. and Odebrecht E. 2012. *Ensaio de campo, e aplicações à Engenharia de Fundações. 2a ed.* São Paulo: Oficina de Textos.
- Whitlow, R. 1994. *Fundamentos de Mecânica de Suelos*. México: Compañía Editorial Continental S.A. de C.V.
- Zdravkovic, L., Potts, D. M. and John ST H. D. 2005. Modeling of a 3D excavation in finite element analysis, *Géotechnique*, Vol. 55, Issue 7, pp 497–513.

Finite element analysis of the soil type effect on buried pipelines under strike-slip faulting

Abbas Soroush¹ & Mehdi Hashemzadeh²

¹ Associate Professor, Department of Civil & Environmental Engineering, Amirkabir University of Technology (Tehran Polytechnic), Tehran, Iran; email: Soroush@aut.ac.ir.

² Former MSc. Student, Department of Civil & Environmental Engineering, Amirkabir University of Technology (Tehran Polytechnic), Tehran, Iran; email: Mehdi1368@aut.ac.ir.

ABSTRACT: One of the phenomena which damages buried pipelines is fault movement. In this study, the finite element program ABAQUS has been employed to simulate pipelines behavior under strike-slip fault movement. For pipeline and soil modeling, shell and solid elements are employed, respectively. Also, the soil-pipe interaction is considered by defining the tangential and normal components. Comparatively softer surrounding cohesive soils and looser non-cohesive soils lead to axial strain and ovality factor reduction, and onset of local buckling occurs in large fault displacements. Also, pipeline damages in non-cohesive soils are less than cohesive soils; due to low thickness and more flexibility of HDPE pipes, they are less vulnerable against faults.

1. INTRODUCTION

Buried pipelines are vulnerable to earthquake hazards, including permanent ground deformations (PGD) such as faulting, liquefaction and landslide or deformations due to seismic waves' propagation. Because of large axial and bending strains which lead to pipelines' tensile failure or buckling, permanent ground deformations are serious threats.

The behavior of buried pipelines was studied by Newmark and Hall [1] for the first time. Kennedy et al. [2] developed an analytical methodology considering soil-pipe interactions, and modelled the pipe as a flexible cable. Wang and Yeh [3] improved this methodology considering pipeline bending stiffness. Takada et al. [4] proposed a new methodology for calculating the critical strain for a pipeline subjected to faulting, using a relation between pipeline longitudinal and cross-sectional deformations. They modelled pipelines near and far from the fault as a shell-mode and beam-mode, respectively. Karamitros et al. [5] presented an analytical methodology using a combination of beam-on-elastic-foundation and the elastic beam theory, and computed axial force, bending moment and maximum strain in a pipeline. Also, they compared the above analytical results with a 3D finite element model using nonlinear springs for the soil behaviour.

Vazouras et al. [6] investigated the response of a steel buried pipeline subjected to strike-slip faulting, using a 3D finite element model. They

evaluated effects of pipe material, fault width and soil type on the pipeline response. Xie et al. [7] examined the behaviour of a polyethylene buried pipeline subjected to normal faulting. They used finite element program ABAQUS modelling (2D and 3D) of buried pipeline subjected to faulting, and evaluated a number of numerical and analytical methods with the aid of centrifuge testing results.

This paper examines responses of high-density polyethylene (HDPE) and steel pipelines, buried in different soil types, to strike-slip faulting by means of numerical analyses. First, some performance criteria for buried pipelines are introduced and then results of the analyses are presented and discussed.

2. PERFORMANCE CRITERIA FOR BURIED PIPELINES

2.1. Local buckling

As compressive strains increase in a pipe, local buckling may happen (Fig. 1). For calculating the critical strain in which local buckling starts, Gresnigt (1986) introduced (Eq. 1) [8]; this equation has been included in the new edition of the Canadian Oil and Gas Pipeline Systems Standard [9]:

$$\varepsilon_{cr} = 0.5\left(\frac{t}{D}\right) - 0.0025 + 3000\left(\frac{\sigma_h}{E}\right)^2, \quad (1)$$

Where,

t = pipe thickness

D = pipe diameter

p = pipe internal pressure

σ_y = yield stress of pipe material

E = Young's Modulus of pipe material

σ_h = hoop stress, which is defined as:

$$\sigma_h = \begin{cases} \frac{pD}{2t} & \text{if } \frac{pD}{2t\sigma_y} \leq 0.4 \\ 0.4\sigma_y & \text{if } \frac{pD}{2t\sigma_y} > 0.4 \end{cases}, \quad (2)$$

With increasing of fault-induced displacements, compressive strains in the pipe develop. The value of displacement, at which local buckling in the pipe starts, is called "critical displacement" (d_{cr}).

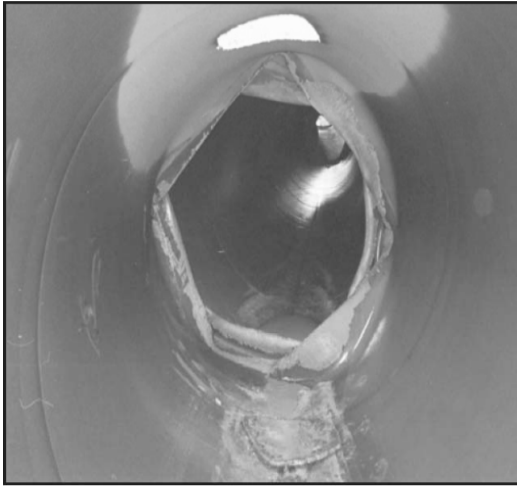


Figure 1. Internal view of pipeline with local buckling.

2.2. Maximum tensile strain

Tensile capacities of pipelines depend mainly on their welds tensile strength. The critical tensile strain for HDPE pipes equals 20% according to the Indian Guidelines for Seismic Design of Buried Pipelines [10], and for steel pipes are 4.5% and 3% according to Canadian and American Pipeline Standards [9,11], respectively.

2.3. Pipeline cross-section distortion

When in a cross-section of a pipeline local buckling occurs, concavity of the pipe in that cross-section will change. As local buckling occurs, intense strain variations are induced that are dramatically intense in thinner pipes. Consequently, comparing longitudinal strains after onset of local buckling are not always valid. In this case, Ovalization Factor ($O.F.$) is used for the pipeline performance evaluation. This factor demonstrates pipeline distortion and it is calculated according to (Eq. 3). The distortion limit is reached when the value of $O.F.$ equals 0.15 [8].

$$O.F. = \frac{D_{max} - D_{min}}{D_{max} + D_{min}}, \quad (3)$$

Where, D_{max} and D_{min} are major and minor diameters of the pipe after distortion, respectively (Fig. 2).

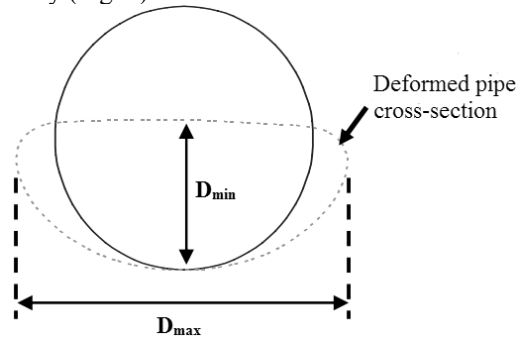


Figure 2. Distortion of pipe cross-section after faulting.

3. NUMERICAL MODELING

Numerical modeling has been conducted using ABAQUS (6.11.3 Version) for steel and HDPE pipes subjected to strike-slip faulting. For a full 3-D analysis of a pipeline, a finite element model has been developed that includes shell elements for the pipe and solid block elements for the soil. Specifically, the pipeline has been modeled using 4-noded, doubly curved, reduced-integration shell elements (S4R) and the soil has been modeled using 8-noded, reduced-integration solid elements (C3D8R).

The soil-pipe interaction has been considered by defining tangential and normal components. The tangential component has been defined with the aid of penalty model in ABAQUS which is based on Coulomb's law of

friction; friction coefficients for the steel and HDPE pipes have been considered 0.4 and 0.5, respectively. The normal component has been defined by the hard contact method in which soil-pipe separation may occur. Further assumptions of the modeling are as follows:

- The angle between the pipe axis and the strike-slip fault plane (β) is 90° .
- The surrounding soil has dimensions of $6m \times 4m \times 40m$ in directions of x , y , z , respectively.
- Diameter and thickness (D, t) of the steel and polyethylene pipes are (0.6m, 0.008m) and (0.4m, 0.024m), respectively.
- Pipe's burial depth (H) is 1.5m; (minimum burial depth should be 2 times of pipe diameter according to the pipeline design practice standards [11]).
- Pipe internal pressure (p) and fault width (w) are 0 and 0.3m, respectively.
- A large-strain Von Mises plasticity model with isotropic hardening has been employed for the pipe material. This has been achieved by introducing axial stress variations versus plastic strain to the analysis.
- The mechanical behavior of soil material is defined by the non-associated elastic-perfectly plastic Mohr-Coulomb constitutive model.

The fault movement parameters are defined in Fig. 3. The soil body comprises two parts: Foot Wall (FW) and Hanging Wall (HW). In strike-slip faulting, these two parts can move along the fault trace, oppositely. According to the relative motion concept, it is assumed that FW is fixed and only HW moves.

The analysis has been conducted in two steps, gravity loading is applied first and, subsequently, the fault movement is imposed. In the first step, the vertical boundary nodes of the two parts and pipeline remain fixed in horizontal direction (x). In the second step, a uniform displacement (d) in x direction is exerted to the external nodes of the HW and pipeline in order to model the fault movement. Deformation of pipeline-soil system after faulting is shown in Fig. 4.

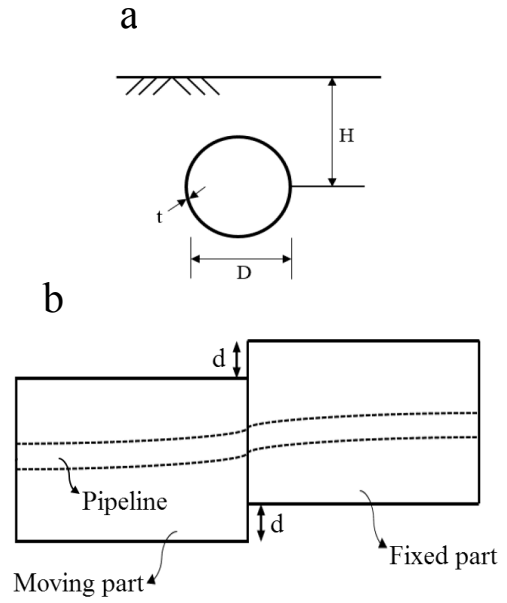


Figure 3. Definition of fault movement parameters (a) Cross-section (b) Plan.

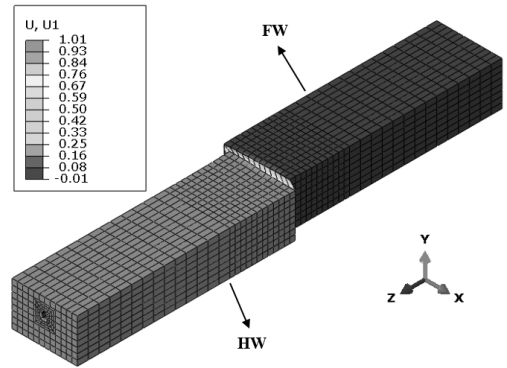


Figure 4. Deformation of pipeline-soil system after fault displacement (d).

The FE mesh was selected based on a number of sensitivity studies. The size of the shell elements for pipe in the longitudinal direction near the fault was chosen 0.1m and for the pipe parts far from the fault, a coarser mesh (0.7m) was adopted.

In order to model the HDPE and steel pipes cylinder circumference, 32 and 40 shell elements were required, respectively. Also, surrounding soil elements in the vicinity of the fault are finer (0.3 m) as compared to the soil elements (1 m) far from the fault.

Soils and pipes parameters are shown in Tables 1 to 3. Figs. 5 and 6 show stress-strain behavior of the steel and HDPE, respectively.

Table 1. Parameters of non-cohesive soils used in numerical analysis

Parameter	Sand I	Sand II	Sand III
E (MPa)	8	25	50
ν	0.3	0.3	0.3
ϕ (°)	30	35	40
ψ (°)	0	5	10
c (kPa)	6	6	6

Table 2. Parameters of cohesive soils used in numerical analysis

Parameter	Clay I	Clay II	Clay III	Clay IV
E (MPa)	25	50	75	100
ν	0.499	0.499	0.499	0.499
ϕ (°)	0	0	0	0
ψ (°)	0	0	0	0
c (kPa)	50	100	150	200

Table 3. Pipe parameters used in numerical analysis

Parameter	Steel	HDPE
ρ (kg/m ³)	7850	950
E (GPa)	210.7	0.8
ν	0.3	0.4

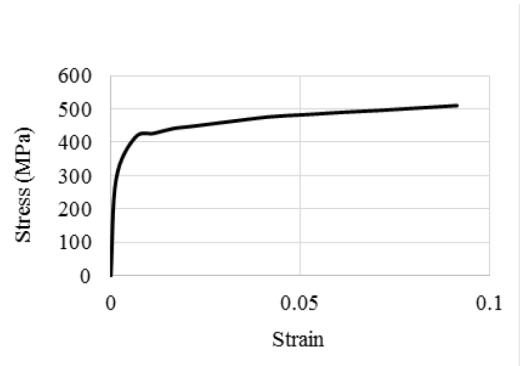


Figure 5. Steel pipe stress-strain behavior.

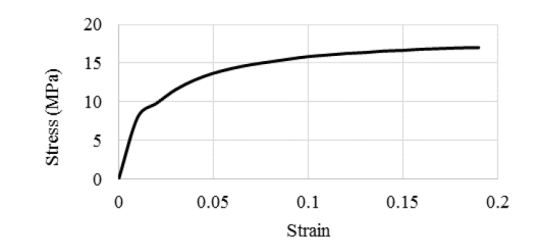


Figure 6. HDPE pipe stress-strain behavior.

4. ANALYSES RESULTS

4.1. Non-cohesive soils

Figures 7 and 8 show respectively variations of axial strain along the steel and HDPE pipes for the three type of sands (loose, medium dense and dense). Also Figures 9 and 10 illustrate Ovalization Factor respectively for the pipes for a range of d/D values. The results indicate that axial strain along the pipes increases as the soil becomes denser (Fig.7); this effect is, however, less pronounced for the HDPE pipe (Fig. 8). Another result is that location of the maximum axial strain for the HDPE pipe is comparatively closer to the fault location.

As shown, The values of axial compressive strain at which local buckling starts (ϵ_{cr}) for the steel and HDPE pipes are 0.0042 and 0.0275, respectively (from (Eq. 1)), so as indicated in Figs. 7 and 8 for the steel pipe local buckling has been occurred in all of the three non-cohesive soils but in HDPE pipe this happened only in dense sand conditions. Therefore, HDPE pipes exhibit comparatively better behavior in terms of local buckling.

In addition both steel and HDPE pipes have great difference with critical tensile strain values recommended in guidelines [9, 10, 11]. Moreover, in denser non-cohesive soil conditions, the locations of local buckling and maximum tensile strain are closer to the fault (Fig. 7).

According to Figs. 9 and 10, as the soil becomes denser, Ovality Factor increases and cross-section is increasingly distorted. Consequently, looser soil conditions result in a larger deformation capacity of the pipeline.

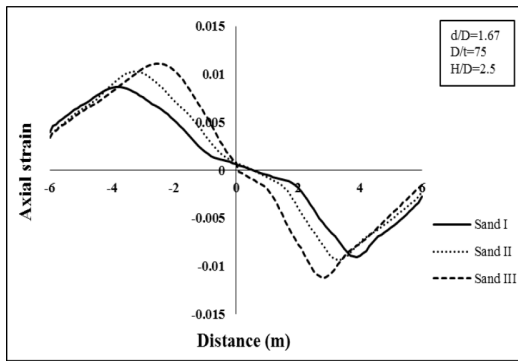


Figure 7. Variation of axial strain along steel pipe buried in three different sands.

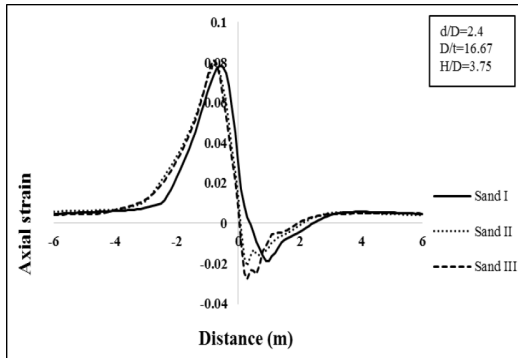


Figure 8. Variation of axial strain along HDPE pipe buried in three different sands.

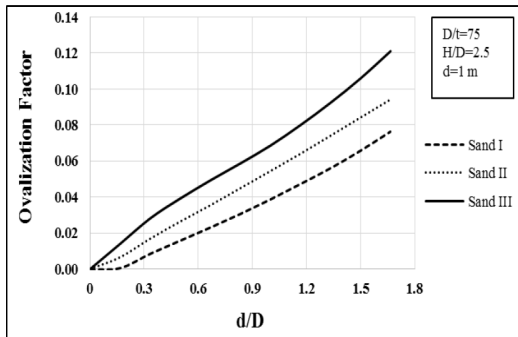


Figure 9. Evolution of steel pipes Ovalization Factor versus normalized fault displacement (d/D) in three different sands.

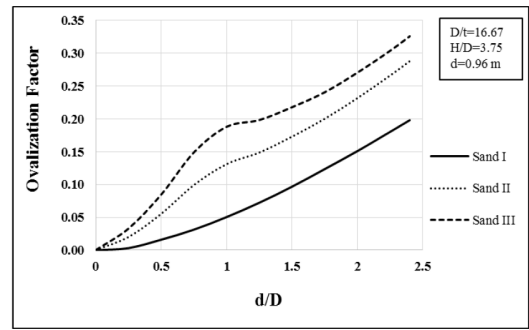


Figure 10. Evolution of HDPE pipes Ovalization Factor versus normalized fault displacement (d/D) in three different sands.

4.2. Cohesive soils

Figures 11 and 12 show variations of axial strain along the steel and HDPE pipes, respectively, for the four types of clays (soft, medium, stiff and very stiff). Also Figures 13 and 14 illustrate Ovalization Factors respectively for the pipes for a range of d/D values.

Fig. 11 demonstrates that as the soil becomes stiffer, both extensional and compression axial strains along the steel pipe increase and they occur in sections closer to the fault application point.

Fig. 12 shows that as the soil becomes stiffer, tensile strains in the HDPE pipe increase and the location of their maximum get closer to the fault; these effects, however, are less pronounced for compressive strains. As mentioned in Section 2.3, after onset of local buckling, compressive strains decrease suddenly; in this case, Ovalization Factor should be used for investigating the pipeline behavior.

Figs. 13 and 14 show that as the soil becomes stiffer, Ovalization Factor increases. This effect is less pronounced for lower d/D values (say $d/D < 0.6$).

Figs. 15 and 16 show deformed shapes of HDPE pipe and its cross-section distortion for the four cohesive soils. Fig. 17 shows deformed shape of the steel and HDPE pipes after fault movement for a similar set of data. It is seen that beam buckling of the HDPE pipe is comparatively more pronounced due to its higher flexibility.

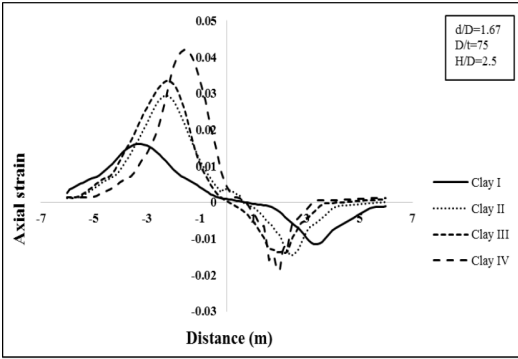


Figure 11. Variation of axial strain along steel pipe buried in four different clays.

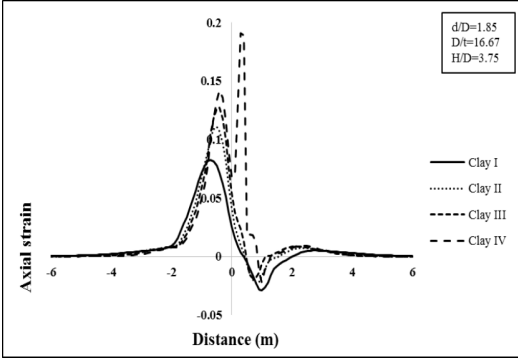


Figure 12. Variation of axial strain along HDPE pipe buried in four different clays.

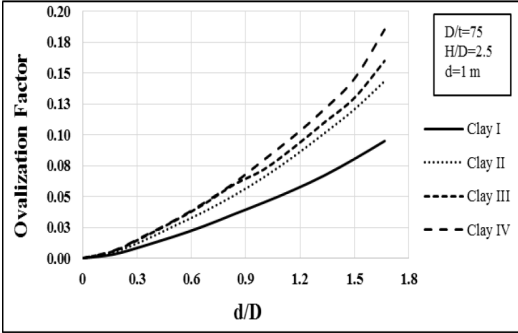


Figure 13. Evolution of steel pipes Ovalization Factor versus normalized fault displacement (d/D) in four different clays.

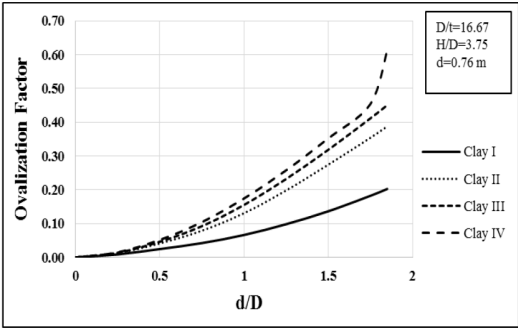


Figure 14. Evolution of HDPE pipes Ovalization Factor versus normalized fault displacement (d/D) in four different clays.

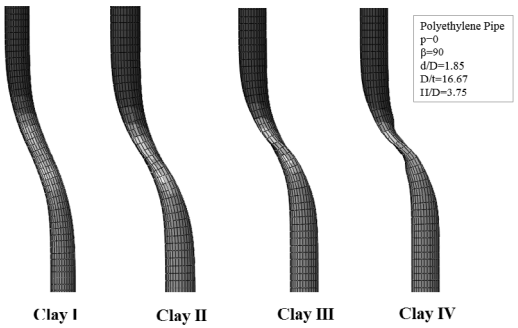


Figure 15. Deformed shape of HDPE pipe in four different cohesive soils.

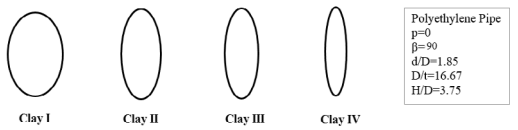


Figure 16. Cross-section distortion of HDPE pipe in four different cohesive soils.



Figure 17. Deformed shape of a steel and HDPE pipes [Clay II, $\beta = 90^\circ$, $p = 0$, $d = 1\text{ m}$, $D = 0.6\text{ m}$, $H = 1.5\text{ m}$].

5. CONCLUSIONS

- In non-cohesive soils, denser surrounding soils result in higher local buckling of pipes; also the buckling peak is closer to the fault as the soil becomes denser. Moreover for denser soils, Ovalization Factor increases.
- In cohesive soils, stiffer surrounding soils result in higher local buckling of pipes; the buckling peak is closer to the fault as the soil becomes stiffer. Moreover, for stiffer clays, Ovalization Factor increases.
- As far as pipes' behaviors in response to strike slip faulting are concerned, surrounding non-cohesive soils are more favorable.
- HDPE pipes are comparatively less vulnerable to damages due to strike slip faulting.

6. REFERENCES

1. Newmark, N.M. and Hall, W.J. 1975. Pipeline design to resist large fault displacement. *Proc. of the US National Conf. on Earthquake Engineering*, University of Michigan, Ann Arbor, pp. 416-425.
2. Kennedy, R.P., Chow, A.W. and Williamson, R.A. 1977. Fault movement effects on buried oil pipeline. *Journal of Transportation Engineering*, ASCE, Vol. 103, pp. 617-633.
3. Wang, L.R.L. and Yeh, Y. 1985. Refined seismic analysis and design of buried pipeline for fault movement. *Earthquake Engineering and Structural Dynamics*, Vol. 13, pp. 75-96.
4. Takada, S., Hassani, N. and Fukuda K. 2001. A new proposal for simplified design of buried steel pipes crossing active faults. *Earthquake Engineering and Structural Dynamics*, Vol. 30, pp. 1243-1257.
5. Karamitros, D.K., Bouckovalas, G.D. and Koutretzis, G.P. 2007. Stress analysis of buried steel pipelines at strike-slip fault crossings. *Soil Dynamics and Earthquake Engineering*, Vol. 27, pp. 200-211.
6. Vazouras, P., Karamanos, S.A. and Dakoulas, P. 2012. Mechanical behavior of buried steel pipes crossing active strike-slip faults. *Soil Dynamics and Earthquake Engineering*, Vol. 41, pp. 164-180.
7. Xie, X., Symans, M.D., O'Rourke, M.G., Abdoun, T.H., O'Rourke, T.D., Palmer, M.C. and Stewart, H.E. 2013. Numerical modeling of buried HDPE pipelines subjected to normal faulting: a case study. *Earthquake Spectra*, Vol. 29, pp. 609-632.
8. Gresnigt, A.M. 1986. Plastic design of buried steel pipes in settlement areas. *HERON*, Vol. 31 (4), pp. 1-113.
9. Canadian Standard Association. 2007. *CSA-Z662*, Mississauga, Ontario, Canada.
10. Indian Institute of Technology Kanpur. 2007. *IITK-GSDMA guidelines for seismic design of buried pipelines*. Kanpur, November.
11. Mohitpour, M., Golshan, H. and Murray, A. 2007. *Pipeline Design and Construction: A Practical Approach*. 3rd edition, *ASME Press*, New York, USA.

Performance of soil-cement column retaining wall used with top-down construction method for basement construction in Bangkok subsoil

Pornpot TANSENG & Vichit NAMWISET

Suranaree university of technology, Nakhonratchasima, Thailand

ABSTRACT: The performance of soil-cement column (SCC) retaining wall system with top-down construction method was observed and present in this paper. From the observation data, the 3D finite element model is used for back calculation to obtain appropriate stiffness parameter for ground movement prediction during SCC installation stage and during excavation stage. The suitable stiffness parameter for prediction of ground movement for soft clay is $50 S_u$ and $500 S_u$ at the SCC installation stage and at excavation stage respectively. The influence of stiffness on lateral force is also reported.

1. INTRODUCTION

Due to very congested area of Bangkok, the need of underground space is rapidly increase as the city growth is quite fast in recent year. The underground construction in soft Bangkok clay is quite challenges task for geotechnical engineer. In the past, the most commonly used retaining structure for underground excavation is temporary steel sheet pile with temporary bracings. The stiffness of steel sheet pile is relatively low compare to cast-in-place contiguous pile wall or diaphragm wall. Therefore, the deflection of sheet pile wall is larger than reinforced concrete wall. The extraction of temporary sheet pile also the source of ground movement. This problem can be solved by using cast-in-place retaining wall, but cost of cast-in-place wall is higher than sheet pile wall especially for medium deep excavation (6-8m depth). For medium deep excavation in soft Bangkok clay, the alternative retaining wall is soil-cement column (SCC) wall. This type of wall was used in a deep excavation project since 1991 (Tay, 1991). Some year later, SCC wall were used for 3m to 5m deep excavation in several projects but there are no publish results on behavior of the wall. But Samanrattanasatien (2002), Wisuttiapat (2005), and Rojkansadarn (2008) report on some case study of SCC wall failure. Some failure cases are ultimate limit state and some failure cases are serviceability limit state. From report on failure cases, some of the retaining wall designers are fear to use

SCC for retaining wall. Last four years, the authors has been ask to design retaining wall for basement excavation. In some cases, i.e. very wide excavation area, the SCC wall is more appropriate than other type of retaining wall as it does not need any temporary bracings and less disturbance noise from construction activities. The behavior of the SCC wall is not well understood and no successful performance reported. Therefore, the intensive analysis by using finite element has been done to study behavior of the SCC wall. Finally, the SCC wall without any temporary support was design constructed successfully and the performance of the SCC walls are reported (Tanseng, 2011 & Tanseng, 2012). In this paper, the authors present the design, construction, and observed performance of a hybrid construction technique i.e. soil-cement column wall supported with permanent basement slab construct from top-to-bottom. The behavior and performance on SCC installation stage and on excavation stage including the back analysis by using observed behaviors are also presented in the following sections.

2. PROJECT DETAILS AND SUBSOIL CONDITION

This project is a condominium project with two underground car park in Sukumvit road, Bangkok. To construct underground car park, the excavation depth of 7.9m must be made on very soft clay layer. At the preliminary design

stage, the SCC wall with no temporary bracing was proposed. The SCC wall must be design as gravity wall so it can resist earth pressure without any horizontal support. The gravity wall must be thick enough to resist overturning, sliding, bearing failure. However, at the detail design stage, the space for thick gravity wall is found to be insufficient. The design has to be changed from SCC gravity wall to SCC wall with lateral support. The owner’s representative does not want to use temporary bracing as it spend extra time for installation and removal. Finally, the design team decide to use permanent basement as lateral support and construct basement from top to bottom which is known as “top-down” construction technique. The combination between SCC wall and top-down construction has not been used before, therefore, the geotechnical design parameters (especially soil stiffness) are adopt from the observed performance of SCC gravity wall. Figure 1 is the layout of SCC wall and foundation pile layout. Two sides of the project are close to public road and another two side close to two-storey and eight storey reinforced concrete building. The concrete block fence with short pile foundation is on the boundary line. The figure also indicate location of temporary strut and inclinometers.

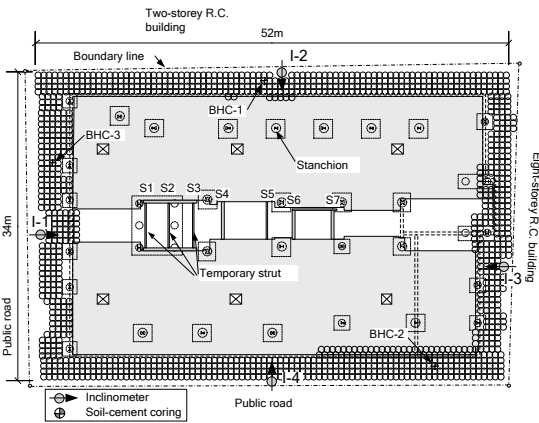


Figure 1 SCC wall and foundation pile layout.

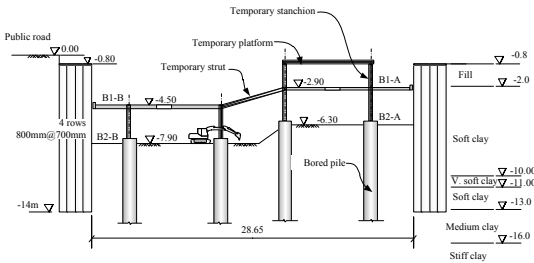


Figure 2 Cross section of the project.

Figure 2 is the cross section of the site. The maximum excavation level is -7.9m close to public road. On the opposite side, the excavation level is -6.3m. There are two basement, B1 and B2. The basement slab level is not equal, B1-A slab is at level -2.90m and B1-B slab is at level -4.50m. The excavation for B2 is unequal, for B1-A side the excavation level is -6.3 while the excavation level for B1-B side is -7.9m. As the construction is top-down method, the basement B1-A and B1-B which are the support to SCC wall must be constructed before foundation construction. Therefore, the slab must be supported with temporary stanchions which are pre-installed and embedded into bored pile foundation.

Figure 3 is the subsoil profile from site investigation. Subsoil consists of 2m thick fill soil overlying 11m thick very soft to softy clay. Below this layer is 3m medium stiff clay. The soil below medium stiff clay is very stiff clay.

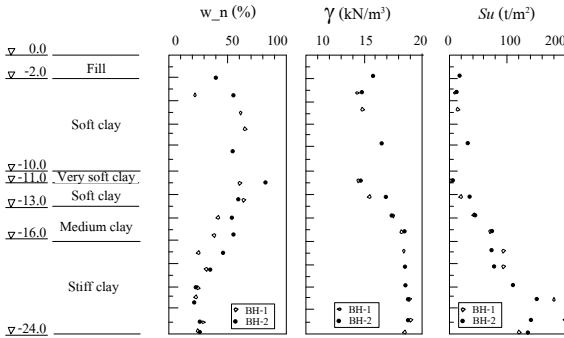


Figure 3 Subsoil profile.

3. DESIGN AND CONSTRUCTION OF SCC WALL

3.1. SCC wall Design

The SCC wall used for this site consists of four rows of 800mm diameter SCC with 100mm overlapping. The arrangement is square pattern which does not have any different from triangular pattern. The tip of SCC is embedded 1m into medium stiff clay layer. The tip is not embedded in stiff clay layer because the experience of construction shows that the stiff clay has low natural water content and high shear strength make difficulty of pulverizing and mixing.

At the design stage, 2D finite element program PLAXIS was used to model the excavation to investigate behavior of the SCC wall. In the model, plane strain condition is assumed. The soil and SCC are modelled with 15-node triangular elements. The interface elements with 50 percent strength reduction are used at overlap between SCC which is not homogeneous. The foundation pile is assume to be plate with average stiffness per 1 meter. The basement slabs are modelled with plate elements. The soil is assume to be undrained as the excavation period is about two months so the excess pore water pressure in low permeability clay is slightly dissipated. Mohr-Coulomb model is used with total stress parameters. For stiffness parameters, Young's modulus value of $250 S_u$ is used with Poisson's ratio of 0.495. The total strength parameters are obtained from subsoil investigation data in Figure 3.

Figure 4 is the displacement contour plot from FEM results. The results shows the maximum ground movement at the deeper side is 95mm and at the opposite side is 55mm. The shear stress in the soil and SCC are lower than shear strength of soil and design shear strength of SCC (30 kPa).

In the model, the temporary strut has to be installed between basement B1-A and B1-B due to discontinuity of the slab. The anchor element is used. The strut force from FEM is 226 kN/m at construction stage where the soil is still in undrained condition.

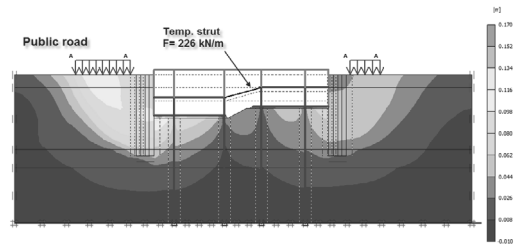


Figure 4 Displacement contour from FEM 2D analysis at design stage.

3.2. SCC wall installation

The SCCs are installed by using low pressure mechanical mixing method as shown in Figure 5. Cement content is 250 kilogram per cubic meter of soil. Water cement ratio is 1.1. From author's experience, the ground movement due to SCC installation is very critical for using of SCC wall in urban area. For some project in soft Bangkok clay, the ground movement of 150mm was observed at 6-10m depth. This amount of movement push the building with long foundation 20mm sideways. For short pile foundation, the movement cause severe cracks on plastered wall and the door frame was distorted so the door could not be close. The movement come from soil displacement by cement grout and mixing tool movement. There are several technique proposed to solve this problem. Some technique are not suitable for practice as they need special equipment or tools which make construction more difficult. For this project, the method used to reduce ground movement due to SCC installation is pre-mixing of 3 to 4m top soil with water to increase water content hence reduce shear strength of the soil. This softening part allow flowing of displaced soil by cement grout to ground surface not to the side of mixing hole. For this project, the SCC wall installation can be made at 200mm away from neighbor concrete wall (Figure 6) without any damages or cracks. After the completion of installation, the coring was made for SCC sample. The average unconfined compressive strength of SCC

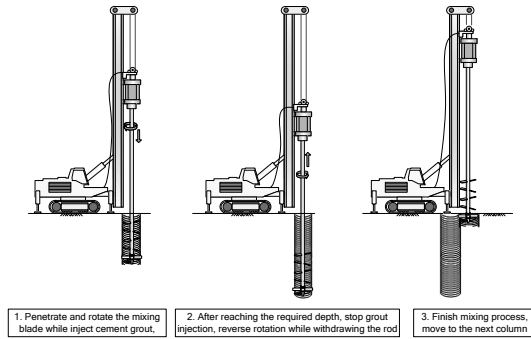


Figure 5 SCC wall installation method



Figure 6 Installation of SCC 200mm close to neighbor fence.

4. INSTRUMENTATION PROGRAM

Inclinometers were installed on four side of the excavation boundary to monitor lateral ground movement due to SCC installation and during excavation as shown in Figure 1. To measure force in temporary struts installed between B1-A and B1-B, electrical strain gauges are attached to the neutral axis of the strut to avoid bending stress component. The dummy strain gauge is used to eliminate temperature effect. As the strut is supported with wale which is similar to pin support; therefore, the bending moment transfer to strut is minimum.

The monitoring was taken at every major change in stage of construction as shown in Table 1. The starting day of monitoring is at completion of SCC installation. Force in struts are read after the struts are installed.

Table 1 Observation schedule.

Day	Activity
100	Excavate to level -3.2m and construct basement B1-A
120	Excavate to level -4.8m and construct basement B1-B
127	Excavate to level -6.3m at middle area of the site
155	Excavate to level -6.3m under basement B1-A
178	Excavate to level -7.9m under basement B1-B

5. OBSERVATIONAL RESULTS

As there are inclinometers and strain gauges installed in the site, the observation are presented in two parts first, the ground movement and second force in strut.

5.1. Ground movements

There are two stages of ground movement during construction, first stage is ground movement due to SCC installation and second stage of ground movement due to excavation for basement. Figure 7 is the horizontal displacement at SCC installation stage. The maximum ground movement on A-direction which perpendicular to wall alignment is -110mm at 9m depth. On B-direction, the maximum movement is -70mm. The negative sign means the ground move outward the excavation area. This movement caused by displacing of ground by 1.78 cubic meter of cement grout and mixing action of the mixing tool.

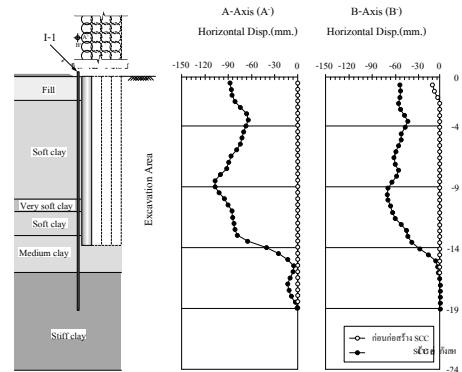


Figure 7 Ground movement at SCC installation stage.

Figure 8 is the second stage ground movements which come from the excavation of soil for basement construction. The initial reading (zero reading) are set to the day when SCC installation is completed. For I-4 side at final

excavation stage, the wall movement show very small curvature which means that the wall is tilt like a block. The movement at the top is 58mm and the movement at the bottom is 15mm. This means that the wall movement is the combination of slightly overturn and sliding.

For inclinometer I-2, the amount of wall movement is less than I-4 as the depth of excavation is shallower. The maximum ground movement is 40mm. Most of the movements occur when the excavation level reach -3.2m before construct B1-A. After B1-A is constructed, the incremental movement due to further excavation is very small. This because the wall is supported at relatively shallow depth, so the cantilever type of movement is restraint. In addition, the excavation level between two sides are unequal. The earth pressure at I-4 side is greater than earth pressure at I-2 side; therefore, the greater force on wall at I-2 transfer through basement and push the wall I-4 in the opposite direction.

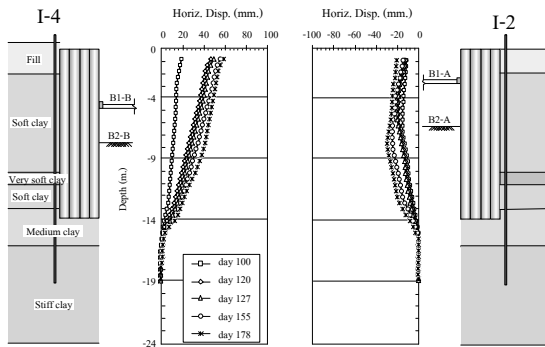


Figure 8 Observed ground movement at excavation of the soil for basement construction.

5.2. Force in strut corresponding to wall movement

Observed force in struts are shown in Figure 9. The strut forces are plotted with corresponding excavated ground elevation and maximum ground movement from inclinometers. It can be seen that when the excavation is made at I-2 side to level -3.2m the maximum ground movement is 25mm. Then follow by the excavation to level -4.8m at I-4 side. After excavation, the wall movement increase to 48mm. When the excavation reach -6.3m at I-2 side, the maximum wall movement is not increase. However, the excavation at I-4 side to level -

7.9m cause slightly increase in ground movement.

The force in temporary strut measured with strain gauge shows that the strut force increase with the excavation depth. The maximum strut force of all seven struts is 450 kN per strut which is lower than the prediction with FEM (FEM prediction is 678 kN). The observed maximum strut force is lower than the predicted one because of the contact between bracing and basement slab is not close. There are 5 to 10mm gap left between basement slab and temporary bracing; therefore, when the wall move to close the gap earth pressure reduce and also strut force. The gap is not modelled in FEM, so the strut force from FEM is higher than the observed one.

The strut S3 is removed first for widening working area. The load on S2 and S4 are expected to be increase as the load on S3 will redistributed to adjacent strut. However, the strut load on S2 and S4 are not increase significantly. The reason of no load increasing may come from the resistance of 150mm plain concrete slab which cast against SCC wall before strut S3 is removed.

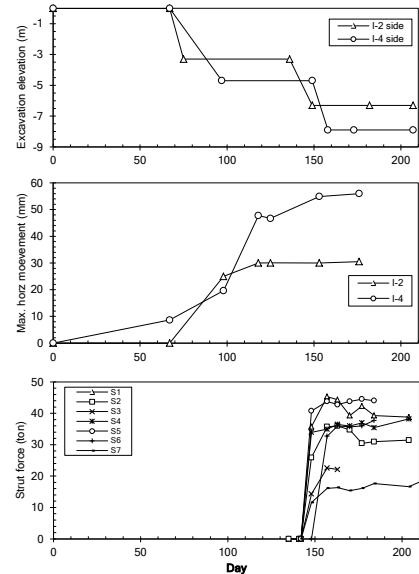


Figure 9 Measured strut force and maximum horizontal movement versus time.

6. BACK ANALYSIS FOR STIFFNESS PARAMETERS

After the excavation is completed, the observed displacements are compared with dis-

placement from FEM at the design stage. The calculated ground movement is 1.64 time larger than the observed one. The important factor is the stiffness parameters used in FEM at design stage which is lower than it has to be. Therefore, in this research, the back analyzes by using observed ground movement are performed. In the back analysis, 3D finite element program PLAXIS 3D Tunnel is used. The model parameter are similar to the one used in the design stage. The work start with selection of suitable Young's modulus. The approximation of shear strain in soil due to excavation is done by assuming that the distortion angle of the ground from the vertical axis is the approximate shear strain. By assuming this, the shear strain profile can be plotted as shown in Figure 10 and Figure 11 for SCC installation stage and excavation stage respectively. The average approximate shear strain at SCC installation stage is 1 percent where at the excavation stage is 0.3 percent which is quite small strain. These average approximate shear strain is used to determine shear modulus from results of self-boring pressure test on soft Bangkok clay reported by Teparaksa (1999) as shown in Figure 12. The estimated shear modulus, G for SCC installation case is $50S_u$ and estimated shear modulus or excavation case is $125S_u$. From the estimated shear modulus, the Young's modulus can be calculated, the calculated Young's modulus in term of E_u/S_u is 150 and 375 for SCC installation stage and excavation stage respectively.

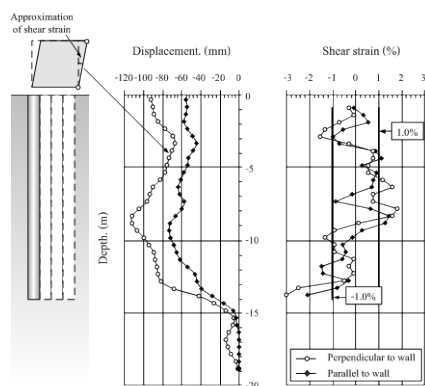


Figure 10 Shear strain profile: SCC installation stage.

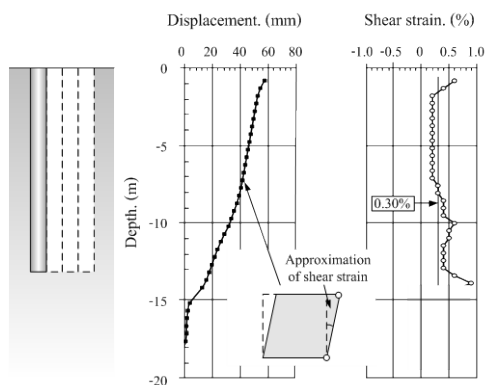


Figure 11 Shear strain profile: excavation for basement stage.

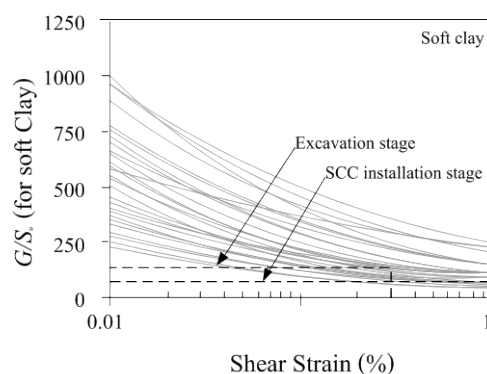


Figure 12 Relationship between shear modulus and shear strain from self-boring pressuremeter test (Teparaksa, 1999).

In back analysis procedure, $E_u/s_u=250$, 500, and 750 was tried as input parameters for soft clay to FEM. The ground movements from each trial are compared with observed ground movement and choose the best fit one for suitable stiffness parameters. Figure 13 is the back analysis results from FEM compared with observed data. From the figure, Young's modulus parameter E_u/s_u of 500 gives the best fit to observation movement. The value is higher than estimation one from self-boring pressuremeter data this may be the result of soil-structure interaction in FEM.

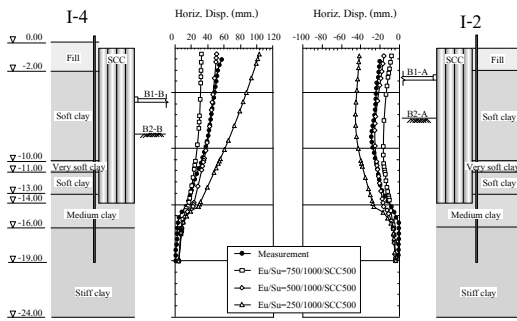


Figure 13 Back analysis results: excavation stage.

As the SCC wall tip is not embedded into stiff clay layer; therefore, the stiffness of stiff clay may not play any role. However, the back analyses are also done to verify that the stiffness of the clay is insensitive to the movements. The E_u/s_u of stiff clay at 750, 1000, and 1500 were tried as input stiffness. Figure 14 shows that the calculated ground movement is insensitive to the stiffness of stiff clay. This proved that the excavation does not have any influence on stiff clay layer.

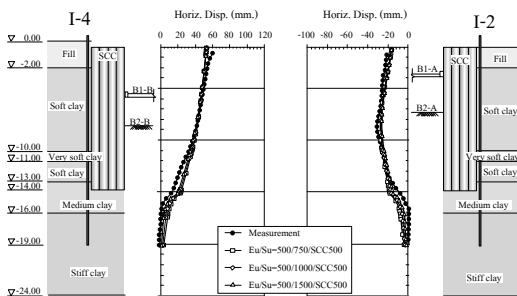


Figure 14 Comparison of FEM and observed results by using $E_u/s_u = 500$ for soft clay and vary E_u/s_u of stiff clay at 750, 1000, and 1500.

In case of ground movement during SCC construction, the approximate shear strain is about 1 percent. In this case the stiffness of the soil is lower than the stiffness used for excavation analysis because larger shear strain occur in the soil. The back analysis is done by applying volumetric strain to soil element where the SCC is located. The amount of applied volumetric strains are calculated from SCC installation record as shown in Figure 15. The soft clay stiffness parameter E_u/s_u of 50, 100, and 150 are used for input parameter for FEM. The soil condition is assumed to be undrained due to

short period of construction. The shear strength of soil-cement slurry is assume to be 5 kPa.

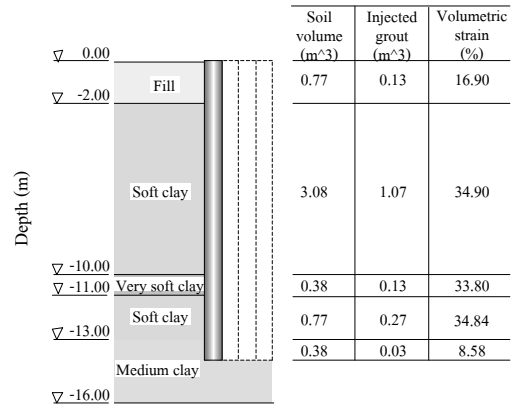


Figure 15 Approximation of volumetric strain for back analysis: SCC installation stage.

Figure 16 is the back analysis results. From the results, the stiffness parameter E_u/s_u of 50 give the best fit of ground movement between FEM and observation for A-direction. For B-direction, the ground movement form FEM is lower than the observed one. This may be because of the stress independence stiffness of Mohr-Coulomb model. The stiffness for shearing path which occur along B-direction is higher than it should be. However, the ground movement in A-direction is more important than in B-direction; therefore, the E_u/s_u of 50 is suitable for practical purpose.

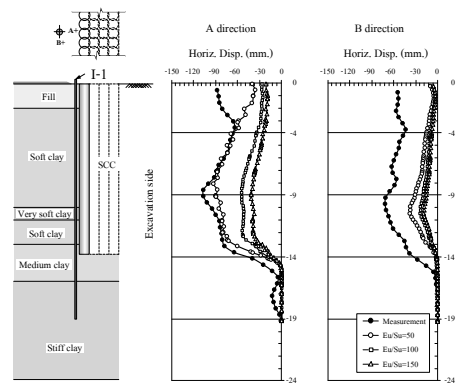


Figure 16 Back analysis result: SCC installation stage.

This research also study influence of soil-stiffness on force in strut. In the study, the E_u/S_u of 250, 500, and 750 are used. Figure 17 is the plot between strut force from FEM and observed strut force. It can be seen that the calculated strut forces reduces as the Young's modulus increase. This study try to obtain the suitable stiffness parameter for movement prediction; therefore, for the proposed $E_u/S_u = 500$ of soft clay, it is on the conservative side as the strut force from FEM are larger than the observed one.

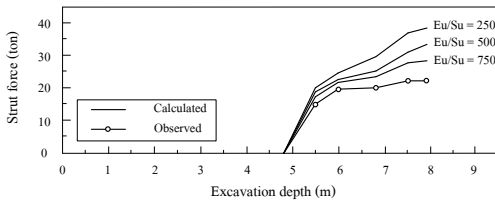


Figure 17 Comparison between strut forces obtained from observation and FEM at various excavation depth.

7. COCLUSION

The conclusions of this research are:

1. The Young's modulus value of $250 S_u$ used in FEM analysis give larger horizontal movement than the observed one.
2. The back analyzed Young's modulus by using observed ground movement is $500 S_u$ for soft clay under excavation stage. For stiff clay, the Young's modulus value used in FEM is insensitive as there are no effect on the calculated ground movement.
3. For SCC installation stage, the back analyzed Young's modulus of $50 S_u$ give good match with the observation value. The smaller Young's modulus value than the one used in excavation stage is due to higher shear strain occur in the ground.
4. For strut force, the strut force reduce as the Young's modulus increase. The Young's modulus value of $750 S_u$ give fair comparison to observation one. However, the Young's modulus of $750 S_u$ is conservative for practical purpose.

8. ACKNOWLEDGEMENT

The authors express their appreciation to to Siamese Asset Co., Ltd. and Standpile Co., Ltd. for their supporting on data collection for this research. We would like to thank to Associate Professor Wanchai Teparksa for his kindly help on PLAXIS 3D Tunnel program's using.

9. REFERENCES

- Namwiset, W., (2014). Behavior of soil cement column wall used for deep excavation with top-down system in Bangkok soft clay. Master thesis, Suranaree university of technology, Nakhon-ratchasima, Thailand
- Rojkansadarn, S. & Mairaing, W. (2008). Soil properties effect on construction of soil-cement column in drainage system Suvarnabhumi international airport project. Proc. of the 13th national convention on civil engineering, Thailand.
- Samanrattanasatien, P. (2002). The behavior of cement column wall during construction. Master thesis, King Mongkut's university of technology, Thailand.
- Tanseng P. (2012) Soil-cement column wall with wall-strut to minimize ground movement for a road tunnel construction in Bangkok subsoils, World Tunnel Congress (WTC2012), Bangkok, Thailand
- Tanseng, P. (2012). Soil cement column wall with top-down construction method for a deep excavation project. Seminar on foundation engineering 2012, Bangkok.
- Tanseng, P. (2011). Soil-Cement Wall without Bracing for Mat Foundation Construction in Bangkok Sub-Soils. ATC18 Mega Foundations 5th Workshop. Hong Kong.
- Tay, S. H. (1991), Jet grouting al alternative to sheet pile method for basement excavation. Seminar on foundation and underground construction, Bangkok, Thailand.
- Teparaksa, W. (1999). Analysis of lateral wall movement for deep excavation in Bangkok subsoils. Proceedings of the civil and environmental engineering conference. Bangkok, Thailand, pp. II-67 – II-76
- Wisuttiapat N. (2005). Movement behavior of deep cement mixing column for retaining structure. Master thesis. Chulalongkorn university, Thailand.

Session 3

SITE INVESTIGATION AS SOURCE OF INPUT PARAMETERS FOR SOIL-STRUCTURE INTERACTION

Standard Penetration Test and Its Discrepancies in Bangladesh Perspective: A Comparative Study Between Automatic Trip Hammer And Donut Hammer.

Mohammad Abu Sadeque & Partha Saha
Housing and Building Research Institute, Bangladesh

A. R. M. Farid Uddin
Housing and Building Research Institute, Bangladesh

ABSTRACT: The Standard Penetration Test (SPT) is one of the most popular field tests in sub-soil investigation techniques since a long ago. It is admired due to its simplicity and ease of operation. In spite of its a lot of advantages, geotechnical engineers had to face different types of discrepancies among SPT (N) values even if the soil parameters are reasonably similar. These dissimilarities are generally considered to be the major consequence of test assembly and the hammer energy transferred during Standard Penetration Test. This paper has been prepared as an initiative to reveal the discrepancies between Standard Penetration Test Procedures in Bangladesh perspectives.

1. INTRODUCTION

Standard Penetration Test was first standardized by Harry Mohr around 1927. Since then the method has been improved and standardized as ASTM 1586 during 1958 with periodic revisions to date. Till now Standard Penetration Test (SPT) is the widely used and most economical means of sub-surface investigation. The concept of using split spoon sampler was first developed by Charles R. Gow and lately adopted by Karl Terzaghi and Arthur Casagrande. Again Karl Terzaghi was the pioneer to develop the concept of using "standard" blow counts to estimate soil properties, which seems to be ludicrous until 1947 when Karl Terzaghi himself along with Harry Mohr developed correlations allowable bearing pressure and SPT blow counts in sandy soil.

Different types of discrepancies have regularly been observed even after the ASTM standardization of SPT values. N values from adjacent boreholes obtained by using various types of equipments or similar equipments from different manufacturers have been found inconsistent. Gibbs and Holtz (1957) described the overburden pressure and length of drill rod as the principal causes of this non-reproducibility. Without these, N values can be influenced by numerous factors permitted by ASTM. Some of these factors include wrapped or worn driving shoe, pushing a rock, cross-

section of drill rod, type of anvil, blow rate, technique of the operator, alignment of the hammer, use of liners or bore hole fluid, bore hole diameter and last but not least the hammer type.

Among all the factors, driving energy is the most important and remained opaque until de Mello (1971) presented a comprehensive literature survey focusing the driving energy (Schmertmann, 1975). According to Kovacs and Salomen (1982) the actual driving energy transferred to the sampler may vary from 30 to 80 percent of the theoretical input energy whereas Riggs et al. (1983) found it to a range of 70 to 100 percent. These types of discrepancies have been depicted as the effect of using different hammer type and anvil system, cross-section and material of drill rod and most of all the workmanship especially incase of rope-pulley operated Standard Penetration Test procedure.

2. CONVENTIONAL N-VALUE CORRECTIONS:

Standard Penetration Test was basically developed as a simple and reliable means of predicting engineering properties of soil for example; relative density, angle of internal friction, cohesion, modulus of elasticity etc. Inappropriate corrections of field SPT values may anticipate the soil properties erroneously. The traditional recommended corrections for Standard Penetration Resistance (N) value are;

i) Correction for overburden pressure, ii) Correction for energy ratio, iii) Correction for borehole diameter, iv) Correction for rod length and finally v) Correction for samplers with or without liners.

3. DISCREPANCIES OF “N” VALUES AND BANGLADESH PERSPECTIVE

Due to the availability of human resource, the common practice in Bangladesh is to use completely manually operated Standard Penetration Test procedure and rope-pulley operated donut hammer. Donut hammer is comprised of a hammer itself of weight 63.5 kilogram, a guide rod, anvil or drive head and a rope-pulley mechanism to lift or drop the hammer manually. Use of safety hammer is rare all around the country.

In Standard Penetration Test, the hammer is raised up to 30 inch by a rope wrapped around a rotating pulley and released it again to dissociate the hammer in such a way so that the hammer fall on the anvil attached at top of the drill stem. Main problem associated with this procedure is the efficiency of energy transferred to the anvil and subsequently to the sampler. First of all the rope-pulley mechanism itself is not entirely frictionless and may absorb a few amount of energy. Sometimes the rope is not completely dissociated during the test. It requires skilled workmanship to minimize these losses. The most important problem encountered during SPT is to maintain the height of free fall exactly to 30 inch in field condition. Another source of losing energy may be the damping effect of the material of the system itself, which is inherent and inevitable as well.

All the uncertainties are very difficult to take into consideration accordingly during the performance of field test. Therefore the obtained result may be inconsistent with workmanship and as well as the material quality of the equipments. Besides, a trend of using automatic trip hammer is growing now a day to resolve the uncertainties of donut hammer. Though it is considered to be a good sign but the matter of concern is that the N values obtained from donut hammer and automatic trip hammer can not be treated equally due to the difference in their energy transfer efficiency. It is to be mentioned here that the efficiency of automatic trip hammer may be typically up to 90 percent (Youd et al. 2008). So a correlation

need to be established between the SPT values obtained from Automatic Trip Hammer and Donut Hammer prior to a wide range of usage of these two hammer types.

4. COMPARISON OF AUTO TRIP HAMMER & DONUT HAMMER:

A lot of efforts have been made world wide to resolve the uncertainties of Standard Penetration Test and one of the major consequences is the development of automatic trip hammer. In this types of hammer drop height could be properly maintained by mechanical means and similarly the losses due to rope-pulley friction can also be avoided here. The author has anticipated here a tentative approach of performing side by side boring to correlate the SPT values of manually (rope-pulley) operated Donut hammer and automatic trip hammer. To avoid the uncertainties for example the effect of drill rod material, bore-hole diameter and sampler type, all the parameters remained similar except the hammer type. To minimize the effect of erraticness of soil strata, both the borings have been conducted within the area circumscribed by a circle of diameter no more than two feet. The blow rate of hammer has been maintained on an average of 18 blows per minute and 25 blows per minute for automatic trip hammer and Donut hammer respectively. The ratio of N values at a corresponding depth obtained from Donut hammer and automatic trip hammer has been found to vary from 1.0 to 2.0 with an average value of 1.40 as shown in Table 1.

Table 1. Compendium of the ratio of obtained “N” values.

Total No. of Data	72.00
Maximum Value	2.00
Minimum Value	1.00
Mean	1.40
Median	1.41
Interquartile Range	0.41
Standard Deviation	0.28

In the aforementioned table, the mean value is almost similar to that of median consequently the frequency distribution curve suppose to be normally distributed which has been shown in the Figure 1. Similarly in Figure 2, the box plot shows that the interquartile range is 0.41 which signifies that 50% of the total data lies within this range.

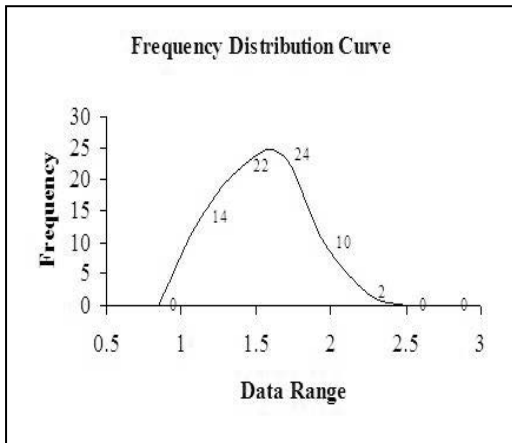


Figure 1. Frequency Distribution Curve for the Values of SPT Ratio.

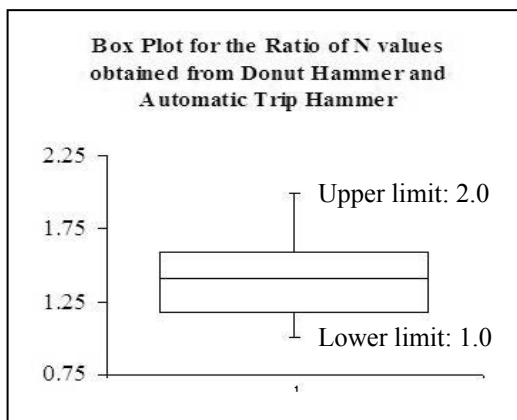


Figure 2. Box Plot for the Values of SPT Ratio

Besides the ratio of SPT values which in turns represent the ratio of energy transferred to the spoon shows a distinct behavior with depth. A plot of the ratio of N values with corresponding depth represents a different central tendency below the depth of 25 feet, near about 1.25, which rises to 1.62 above the corresponding depth as shown in Figure 3. Although all the equipments including the drill rod and split spoon remained same yet these types of variation may be specifically due to variation of energy transferred to the sampler. Despite having all other factors like soil strata, depth of boring and sampler type similar, the manually operated donut hammer provides much too inconsistent result compared to automatic trip hammer at a greater depth. At a greater depth, generally the penetration resistance has been found to increase to a considerable extent, which may have a

psychological impact to workmanship in the case of manually operated donut hammer. A plot of SPT ratio against "N" values (from Automatic Trip Hammer) as shown in Figure. 4 shows a gradual rise in central tendency along with incremental "N" values. In those locations or depths with high penetration resistance, concerned persons might be in hurry to complete the test providing less attention to regulatory parameters especially to the drop height.

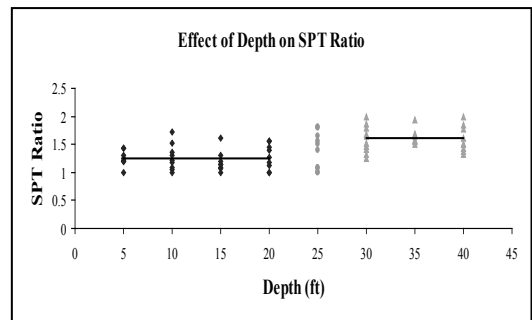


Figure 3: Effect of Depth on SPT Ratio

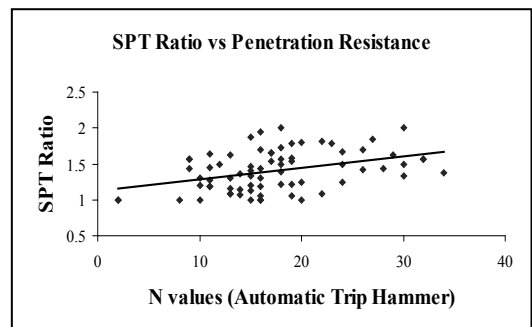


Figure 4. Effect of Penetration Resistance on SPT Ratio

Again, plotting the SPT values obtained from donut hammer against the SPT values obtained from automatic trip hammer at the corresponding depths a clear distinction between those two values can be obtained. Compared to donut hammer, experiment shows that 47.7% more energy can be transferred to the sampler by automatic trip hammer. It can be exemplified through a simple way that the values of donut hammer are almost 1.477 times more than those of automatic trip hammer as shown in Figure. 5.

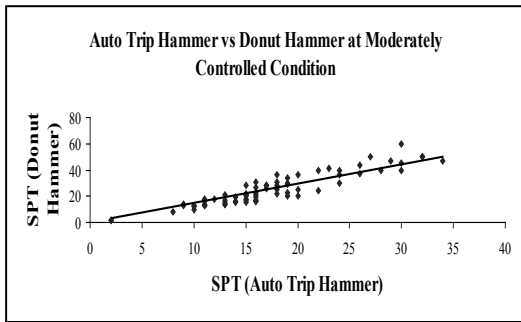


Figure 5. A Comparison of SPT Values from Donut Hammer and Automatic Trip Hammer

5. CONCLUSION:

In this paper the writer has intended to confer the discrepancies between Automatic Trip Hammer and ordinary Donut Hammer and establish an acceptable correlation between those two values. Having been concerned about the technical advantages of automatic trip hammer for example the controlled drop height and the minimized friction loss from rope-pulley system, the author has considered the “N” values from Donut hammer as an arbitrary value expressing in terms of a function of “N” values from automatic trip hammer. The conclusions include:

1. The average SPT ratio of donut hammer and automatic trip hammer has been found to rise after the depth of 20 ft. It signifies that the depth of test has a significant effect on the consistency of SPT values. Moreover the SPT ratio of donut hammer and automatic trip hammer shows an upward trend with increasing SPT values.

2. Although the boring depths have been found to influence the SPT ratio, nevertheless the author has intended to simplify the relationship in order to ease of calculation. SPT values from donut hammer, expressing these values as a function of SPT values from automatic trip hammer, have been obtained 1.477 times more than those of automatic trip hammer.

6. ACKNOWLEDGEMENT:

The observations presented here is the part of a continuous research project carried out by Soil Mechanics and Foundation Engineering Division of Housing and Building Research Institute, Bangladesh. Financial support has been obtained from the research fund of

Housing and Building Research Institute itself. The author would like to show his gratitude to all the members of soil Mechanics and Foundation Engineering Division for their relentless support to continue the research project successfully.

7. REFERENCES:

- ASTM D 1586-11, “Standard Test Method for Standard Penetration Test (SPT) and Split Barrel Sampling of Soil”
- ASTM D 4633-10, “Standard Test Method for Energy Measurement for Dynamic Penetrometers”
- De Mello, V. F. (1971), “The Standard Penetration Test,” 4th Pan-America Conf. on SMFE, San Juan, Puerto Rico (Published by ASCE), vol. 1, pp 1-86
- Gibbs H. J. and W. G. Holtz (1957), “Research on Determining the Density of Sands by Spoon Penetration Testing,” 4th ICSMEE, vol. 1, pp. 35-39
- Kovacs, W. D. and L. A. Salomen (1982), “SPT Hammer Energy Measurement,” JGED, ASCE, GT 4, April, pp. 599-620.
- Schmertmann, J. H. (1975), “The Measurement of In-Situ Shear Strength,” 7th PSC, ASCE, vol. 2, pp. 57-138.
- Youd, T. L. et al (2008), “SPT Hammer Energy Ratio versus Drop Height,” Technical Note, Journal of Geotechnical and Geoenvironmental Engineering, ASCE, vol. 134, No. 3, March 1, pp.397- 400

Test for Determining Mechanical Characteristics of Any Rocky

Aminée EL KHOURY

DEA Soil Mechanics SOIL MECHANICS ASSOCIATES, BEIRUT

Imad ESTA

DEA Soil Mechanics Civil Engineer ESIB G - TEK, BEIRUT

Jean B. ESTA

Civil Engineer ENPC SOLS RENFORCES - BEIRUT

ABSTRACT: It is difficult or impossible to assess by conventional means, static penetrometer and pressuremeter, the mechanical characteristics of embankments from any grit from the stones.

We show in this article that the use of the logs by means of correlation data used to assess Lutz module EM Ménard deformation of these materials.

1. PROBLEM

It is current, increasingly gaining ground back-filling offshore. This can be for real or promotions for achieving dock port, for example.

The embankment can be sand, clean or silty dredged sea and dumped hydraulically without compaction. It may also consist of a unit comprising from granular elements ranging from the block of stone chippings of more than 50cm diameter.

It is obvious that these embankments after installation cannot withstand static loads without significant settlements occur.

Furthermore, while in the water and, at the loose state, in particular for clean sand or polluted, they may be subjected to liquefaction where earthquakes.

To mitigate these risks can make the structures to be built on deep foundations.

The cost of these foundations is not negligible for a project, especially as they must be sized to receive, in addition to vertical loads to the structure, the effects due to negative skin friction and lateral thrust layers cowards.

It is for this reason that grew from 3 or 4 decades, technical improvements that allow either completely replace the deep foundations is to reduce the cost due to the increase in the values of the mechanical properties.

In both cases, improved or not ground, parking can be provided and it is then necessary to achieve, sustain siding with molded or secant pile walls: The calculation of stability of these structures requires knowledge of the characteristics soil mechanics and they have to support their main deformation modulus.

If , in the sand , the determination of mechanical properties is relatively easy using the Menard pressuremeter or simply static dynamic penetrometer , by cons when it comes to an all comers including means these stones become insignificant or because the dallied , behind which lies the pressuremeter cell tube is partly based on a block that does not deform and partly on sand just waiting to be deformed or that is crumbling and expanded the borehole , either because the tip penetrometer accuses a refusal on a block and cannot move , even if you have a heavy penetrometer 150 or 200kN.

For this raison we have considered two characteristic sites in Lebanon where there are embankments all comers including riprap is put in place for forty years and has undergone loads as the embankment wharf Selaata near the town of Batroun or compacted by heavy shelling as some areas reclaimed from the sea embankment on the Marina Joseph Khoury in Antelias, we decided to determine the deformation modulus Menard recording using a device Lutz drilling parameters including, depending on the depth, the speed of advance to the known constant pressure tool.

2. PROCEDURE USED

The Embankment, in its final state, is crossed by a wagon drill with an electronic apparatus for recording Lutz forward speed depending on the depth.

The operating results are based on the calculation of the settlement recommended by Menard: It calculates the average and harmonic

speed velocities obtained by cutting the ground sliced with the same values.

This gives the deformation modulus Menard by the relationship given by Lutz:

$$E_M = -\log 0.98 \log \sqrt{m} + 4.09.$$

To check if this value is a reliable loading test on a circular plate 80cm diameter is achieved by exerting an equal vertical stress at the 220kPa Operating Mode by LCPC.

According Menard compaction under load is calculated by cutting the ground plate 16 in the layers Each Having a thickness equal to the radius of the plate.

For the comparison is therefore the MOST realistic logs Lutz -have to consider 6m deep.

Furthermore the relationship linking the modulus of elasticity E obtained plate test oedometric module type.

$$E_{oed} = \frac{E(1 - \nu)}{(1 + \nu)(1 - 2\nu)}$$

ν is the Poisson's ratio to gold

$$\nu = 0.3 \quad E_{oed} = 1.35E$$

E_{oed} this unit is linked to the relationship $E_M = \alpha E_{oed}$

Where α is the coefficient equal to $1/4$ structure when it comes to rollers and $1/3$ for sand.

Consequently α should be between $2.2E_M$ and $3E_M$.

3. RESULTS

3.1. Embankment Antelias

Shelling was the carried out with a pestle 150kN repeatedly falling 15m.

As the shelling advancement speeds of 150m / h to 250m/h decreases, and effective 10 falls pestle 150kN, progress speeds vary between 50 and 100 m/h.

The operating results as shown above gives a harmonic mean speed equal to 80m / h , a pressuremeter modulus equal to 170MPa .

More over's , the tests show That the second load platform modules varies Between 270 and 300 MPa , an average of 285MPa .

In such condition $E \sim 1.7E_M$

3.2. Selaata dock

The pier was realized there forty years. The platform, 2m above sea level, is formed by a layer of concrete of 26cm thickness of granular fill up Until chipping block of more than 50cm diameter.

This embankment was therefore subjected to loads of imported or exported by broad existing industrial companies in the area various materials. It can therefore be considered as having - been compacted by the successive loads.

The operating results as shown above gives for 6 surveys, a harmonic average of the averages obtained by sampling equal to 60m / h. Fig.1.

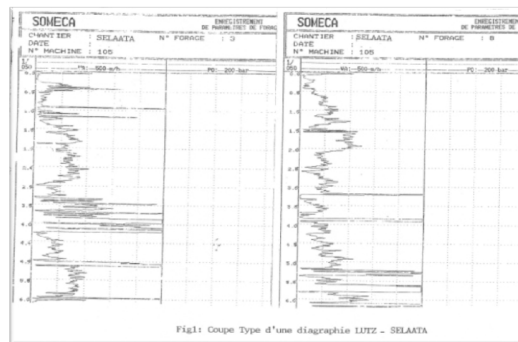


Fig.1. Type a cut logging lutz - Selaata

According To the same relationship we find $E_M = 200$ MPa.

The same locations load tests on a plate 80cm diameter gives an average of the second modules equal to 570MPa,

So here we see E that is close to $3E_M$.

The difference with the previous site probably comes from the fact on the first sandy that percentage is greater.

4. CONCLUSION

To assess the deformation modulus E_M of a medium composed of stones and granular materials, in water, logs and the correlation data Lutz are a good approach.

5. REFERENCES

- Essai de plaque - Laboratoire Central des Ponts et Chaussées.- Projet de mode opératoire. «Contrôle du compactage Détermination des modules de rigidité d'un système bicouche.»
- «Utilisation des résultats des essais pressiométriques pour le dimensionnement des fondations en Europe». International Society for Soil Mechanics and Foundation Engineering.
- Fondation rectangulaire linéairement chargée – Tassement et Contrainte – J.P. GIROUD

Laboratory and In-Situ testing for the identification of bonding parameters of GFRP pipes and soil nailing systems

Carla L. Zenti

Elas Geotecnica S.r.l.(Maccaferri Industrial Group), Segrate (MI), Italy

Andrea Bellocchio

Rocksoil S.p.A., Milan, Italy

Donatella Sterpi

Department of Civil and Environmental Engineering, Politecnico di Milano, Milan, Italy

ABSTRACT: The soil nailing is one of the most effective provisions for the control and reduction of the tunnel pre-convergence and face extrusion and its use has become integral part of modern design methods. In the years, improvements have been introduced in the technological aspects and efforts have been made to better understand the mechanical behaviour of new materials and equipments. Some innovative technical solutions are discussed in this paper, devised to improve the reinforcing action of Glass Fiber Reinforced Polymer (GFRP) pipes and of soil nails. The effectiveness of these solutions, compared with traditional ones, is assessed on the basis of laboratory and on site pull out testing.

1. INTRODUCTION

The soil nailing is one of the techniques often used for the long term reinforcement around the excavation and the temporary stabilization of the face of tunnels driven in difficult ground conditions. It is considered as one of the most economical and effective provisions for ground improvement, first introduced for the reinforcement of natural and engineered slopes (Schlosser, 1982; Juran and Elias, 1991) and later extended to other engineering applications, such as the underground excavations (Mair and Taylor, 1997). In tunnelling works, its use has become integral part of design methods, its effectiveness being recognized in the control and reduction of the tunnel pre-convergence and face extrusion (Lunardi, 2008).

In the years, efforts have been devoted to reach a better understanding of the mechanical behaviour of new materials and of equipments adopted for these techniques, that are continuously subjected to technological improvements (Zenti, 2006; Cheng et al., 2009; Kim et al., 2009). At the same time, analytical and computational procedures have been worked out, so that it is nowadays possible to take into account the mechanical reinforcing action of nailing systems at the design stage (e.g. Wong et al., 2000; Ng and Lee, 2002; Anagnostou and Serafeimidis, 2007; Oreste and Dias, 2012).

Pipes made of Glass Fibre Reinforced Polymer (GFRP) are adopted since the nineties in all the applications where GFRP's characteris-

tics could represent an advantage (Ortigao, 1996). The GFRP pipes offer high tensile strength, low unit weight, high resistance to corrosion and they can be easily removed by cutting. The latter property is particularly relevant whenever the removal of the already nailing stabilized ground mass has to take place, such as during the tunnel face advance. Moreover, the ground conditions in tunnelling are easily subjected to sudden changes, and therefore the versatility of the soil nailing technique, where length, number and pattern of nails can be easily modified during the excavation progress, represents an additional advantage.

In this paper, innovative systems for the tunnel reinforcement by nailing are described and compared with traditional ones, in particular a new GFRP corrugated pipe, which offers high bond properties due to its improved adherence surface, and a nailing technique which provides high pull out strength, due to the possibility to apply high injection pressures and to create homogeneous nails with uniform adherence. The performance of these innovative solutions is assessed on the basis of laboratory and on-site testing.

2. TECHNICAL ASPECTS ABOUT GFRP PIPES AND SOIL NAILS

Specific details are given on innovative soil nailing systems: firstly on a new kind of fibreglass pipe characterized by an external corrugated profile and secondly on a soil nail

consisting of an internal fibreglass pipe and an external geotextile sheath devised to contain the injected cement grout. Both products are patented by Elas Geotecnica S.r.L. (Segrate-MI, Italy).

2.1. Glass fibre reinforced pipes

The GFRP pipes used for soil nailing at the tunnel face are obtained through an industrial manufacturing process called “pultrusion” (Goldsworthy, 1971), that ensures to the final product a uniform distribution of perfectly aligned fibres. In general, the pultrusion of reinforced polymers is similar to the extrusion process used for metals, with the addition of tensile forces applied to the glass fibres to guarantee their alignment before the polymerisation of the matrix polyester resin.

The fibre content, usually expressed as percentage by weight or volume of reinforcing fibres with respect to the total weight or volume, influences the tensile strength of the pipe. It is therefore considered as reference parameter for the prediction of the pipe mechanical properties. In particular, a higher tensile strength is associated with a higher fibre content, according to a relation that can be assumed as roughly linear. The pultrusion process enables the production of pipes having 60-65% range in fibre content, which is almost twice the content that can be reached by other manufacturing techniques.

In addition to the tensile strength, the resistance to pull out of the GRFP pipe is another parameter used to identify the soil nail performance. In fact, in the soil nailing the pipes are driven or grouted inside drilled boreholes and remain unstressed until the soil movements (for instance those induced by the tunnel face extrusion) mobilize tensile forces which are transferred to the ground through friction along the interface. For a better performance the lateral surface of the pipe needs to be treated so to improve the adherence with the surrounding mass.

The adherence is traditionally improved by etching a spiral groove along the external surface of the pipe (Figure 1). For instance, the depth of the etching could be equal to 2 mm in a 60/40 pipe, having 60 and 40 mm respectively as external and internal diameters. A drawback of this procedure is the cutting of external glass fibres and the loss in content of continuous fibres effectively bearing tensile actions. There-

fore, the pipe tensile strength is reduced with respect to the case of pipe with a not improved adherence.

Alternatively a new product was introduced, named “Corrugated” GFRP pipe (VTR-CRG by Elas Geotecnica S.r.L.). It is obtained introducing, before the polymerisation of the resin in the production process, a phase of preforming on the aligned fibres, that creates a corrugated external profile. The depth of the transversal shrinkage is equal to 1.7 mm in the 60/40 pipe (Figure 2). In this way, the aim to improve the bonding adherence is reached, while at the same time the longitudinal continuity of the glass fibres, hence the pipe overall tensile strength, are maintained.

The fibre content by weight can be measured after heating treatment, at 800°C for 8 hours. In the case of standard pipes, with spiral groove, it is also possible to distinguish between the total content of glass and the content of glass from longitudinal continuous fibres only. Figure 3 shows the assembly of fibres after the heating treatment on the two different pipe samples: the presence of cut fibres is evident in the standard pipe while in the corrugated pipe the fibres are continuous.



Figure 1 Fibreglass reinforced pipes: 60/40 AM pipe with spiral groove

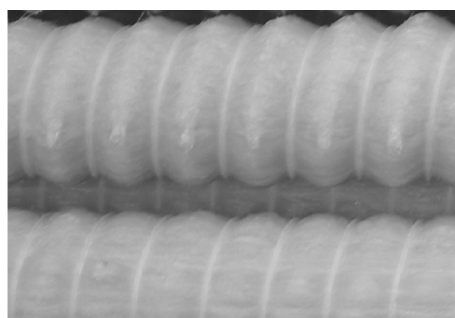
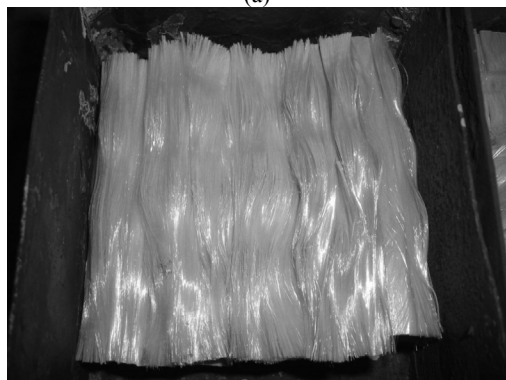


Figure 2 Fibreglass reinforced pipes: 60/40 CRG corrugated pipe



(a)



(b)

Figure 3 Glass fibre mass after heating treatment: from (a) 60/40 AM pipe with spiral groove and (b) 60/40 CRG corrugated pipe

Further details on the mechanical interaction between the two different pipes and the surrounding cement grout will be given in Section 3.1, on the basis of the pull out test results.

Another relevant consequence of the new preforming technique, with respect to the one involving the groove etching, concerns the great reduction of waste in the form of glass dust in the processing plant. In fact, in the case of preforming technique the cutting of fibres that produces the glass dust is limited to the pipe heads. This ensures a safer working environment, being the glass dust, if not properly removed by exhaust fans, highly dangerous for the workers' health during production process.

2.2. Standard and innovative soil nails

In standard soil nails used for the tunnel face reinforcement the fibreglass pipe is inserted in a previously drilled borehole, which is later filled with cement grout injected at low pressure using a small tube at the pipe side.

The innovative soil nail differs from the standard one for the presence of an external expandable geotextile sheath, which wraps the fibreglass pipe for the whole of its length and is sealed at the head and at the tip (Figure 4).

Through a small tube a low shrinkage cement grout is injected between the pipe and the sheath, so that the sheath inflates till the gap within the borehole is closed. This new system is named Pressure Element Reinforcement Ground (PERGround®, Elas Geotecnica S.r.L.). The internal pipe is the 60/40 corrugated model described in the previous Section 2.1.

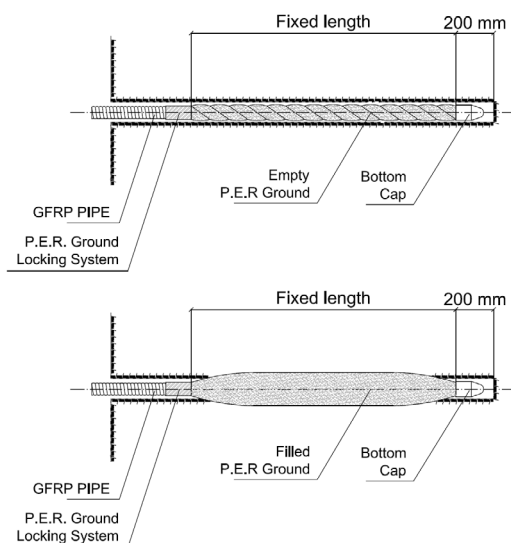


Figure 4 Innovative soil nail for the tunnel face reinforcement (PERGround, Elas Geotecnica S.r.L.)

The performance of the PERGround technique was assessed by preliminary pull out tests carried out at the face of tunnels under construction in soil and soft rock masses of various nature and conditions (Zenti et al, 2008, Renda et al., 2012). In all the tested cases, the pull out load reached values higher than those measured with standard soil nails, tested in the same construction sites to get values significant for a comparison. In some cases the pull out load was measured as almost 10 times higher, as in the case reported in Section 3.2.

To date, 24 m is the maximum length of these soil nails used in tunnelling applications. As an example of application, a documented case history concerns a tunnel being excavated in Southern Italy (max. overburden 65 m, tunnel section 150-170 m²) in highly weathered soft

rock mass and in presence of high pore water pressures (Renda et al., 2012; Sterpi et al., 2013). In the most severe conditions, the tunnel face was effectively supported by an average of 50 nails for reinforcement and 4 additional nails improved with a coaxial drain for coupled reinforcement and drainage actions. The nails had sub-horizontal direction, 20 m length and superposition of 10 m along the tunnel axis.

3. PULL-OUT TEST

Together with the tensile strength, the bonding properties of GFRP pipes and soil nails are fundamental characteristics for the design of reinforcing systems and should be assessed by both laboratory and in situ tests.

In particular, laboratory tests are necessary to identify the interaction between the GFRP pipe and the injection mixture and to highlight the possible better performance of one nail type with respect to others, under prescribed testing conditions. These can be suitably devised to investigate the influence of various factors on the nail performance. In addition, the possibility to carry out series of tests under controlled and repeatable conditions represents the basis for a commercial certification of the product. The pull out is probably the most convenient and widely used testing technique, though not the only one (Chu and Yin, 2005).

Field pull out tests are basically aimed at assessing the bonding properties in actual on site conditions. Since it is proved that the effectiveness of the reinforcement system depends also on the nature and condition of the soil being reinforced (Mair, 2008; Wong et al., 1999), the optimal design has to be based on these field tests results.

The tensile and the bond strengths are used at the design stage, in both numerical and analytical approaches. In the first case for instance, when in the mesh a distinction is made between ground mass and nails, these properties are used as mechanical parameters of the nail elements (tensile strength) and of the interface elements (bond strength). Also when the concept of “equivalent material” is assumed to simulate the presence of soil nailing in a homogeneous equivalent ground mass, the bond properties are used first to convert the mechanical action of the soil nailing in a confinement pressure exerted at the excavation face, and then to convert this confinement in an improvement of the mechanical properties (i.e. the cohesion)

of the ground mass ahead of the excavation (Grasso et al., 1989; Osgoui and Oreste, 2007; Bobet and Einstein, 2011).

3.1. Laboratory pull out tests

A first laboratory investigation was carried out in the past by applying the pull out load with a hydraulic jack. The evidence of positive results suggested to design a test set-up for standardization of this type of tests. The pull out tests were carried out with the following objectives:

- to assess the response of the reinforcing elements to a tensile load;
- to verify the achievement of a sliding condition, represented by a cumulative residual displacement at the attainment of the maximum pull-out load;
- to identify the parameters for the calculation of the adherence properties, according to standard ACI 440.3R-12.

The tested GFRP nails are constituted by CRG corrugated pipes characterized by circular hollow section of outer diameter $\varnothing_{out} = 60$ mm, internal diameter $\varnothing_{int} = 40$ mm and total length $L = 750$ mm. The hollow section of GFRP pipes was previously filled with resin to prevent breakage during the test execution.

The samples were made by placing each GFRP pipe inside a metal formwork, of 300 mm as internal diameter, 410 mm in height, and 0.8 mm in thickness, and by pouring a cement mortar. The large ratio (equal to 5) between the diameter of the grout block (300mm) and the outer diameter of the pipe (60mm), together with the reduced wall thickness of the formwork (0.8mm), allow to limit the mechanical contribution of the formwork itself to the pull out resistance, i.e. its possible confinement action.

The embedment length of the GFRP pipe inside the cement mortar block is $\ell = 300$ mm (Figure 4). The ratio between the embedment length and the outer diameter of the GFRP anchor ($\ell/\varnothing_{out}=5$) allows to approximate the adherence between the pipe and the cement mortar as a uniformly distributed effect.

The tests were carried out on a total of 6 samples: 3 tests 24 hours after casting and 3 tests 48 hours after casting. They were performed using the electromechanical testing machine Schenck (maximum load equal to 1000 kN), able to apply on the samples tensile and compression loads. For the correct positioning of the sample it was necessary to design a suitable testing framework (Figure 4).

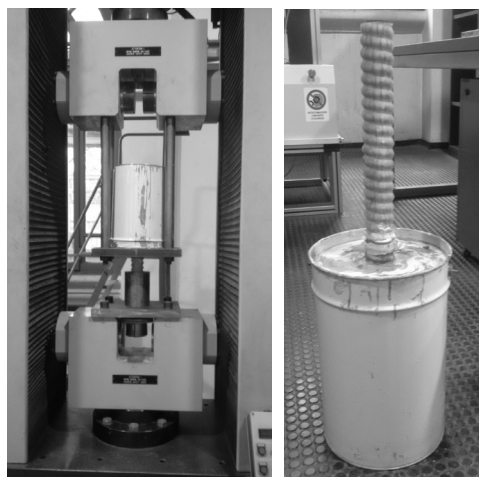
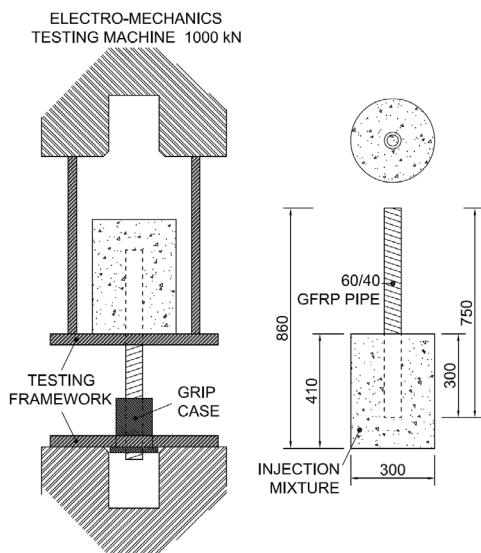


Figure 4 Sketch and pictures of the test equipment and the sample

The loading frame is constituted by four steel columns, acting as supports and vertically driving the transversal plate: this optimizes the stiffness of the frame in the loading direction.

A single type of injection mixture was used for all the GFRP pipes. The grout mixture is prepared with a water/cement ratio equal to 0.45, in particular with a dosage of 25 kg of cement, 11.25 l of water and 0.2 kg of high plasticizer. The density of mixture was found to be equal to 1883 kg/m^3 and its strength characteristics were assessed by simple compression tests on cubic specimens of 100 mm side, carried out 24 and 48 hours after casting. The results showed mean values of compression

strength equal to 6.6 N/mm^2 and 22.4 N/mm^2 , respectively 24 and 48 hours after casting.

The pull out tests were carried out as stated in section B.3 of the standard ACI 440.3R-12. Since this standard refers to fibre reinforced polymer composites bars for concrete and masonry structures, it was necessary to change the testing set up to fit: (a) the case of a fibre-glass pipe and (b) the application to the underground reinforcement. The necessary changes are related to the size of the mortar block in which the pipe is embedded and the clamping method. The free head of the GFRP pipe has been inserted in a protective steel cylinder case for gripping and application of the tensile load. This was necessary in order to extend the gripping surface, thus reducing the risk to damage the GFRP element. The pull-out tests were performed under displacement control (0.02 mm/s), with continuous load and displacement monitoring, till the complete pull out. The results (Figures 5 and 6) show that the CRG corrugated pipes offer a high pull out resistance that slightly increases with time as a consequence of the mortar hardening (24-48 h).

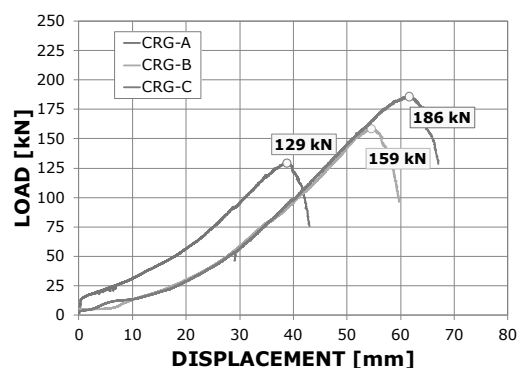


Figure 5 Laboratory pull out tests on CRG corrugated pipes after 24 hours

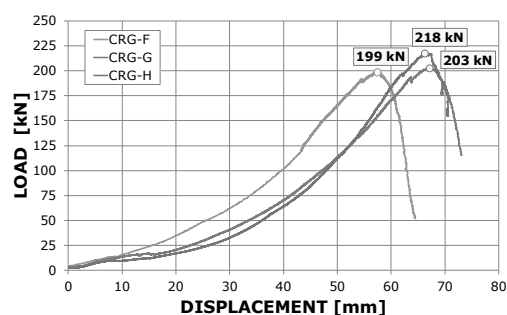


Figure 6 Laboratory pull out tests on CRG corrugated pipes after 48 hours

The maximum tangential stress at failure τ_{\max} , defined as the bond strength, can be calculated according to Equation (1)

$$\tau_{\max} = \frac{F_{\text{pull-out}}}{C_b \ell} \quad (1)$$

where: $F_{\text{pull-out}}$ is the pull-out load at failure; C_b is π times the pipe diameter; ℓ is the embedment length of the sample within the cement grout block. Considering the diameter of the tested pipes (60mm) and the embedment length (300mm), the bond strength is then evaluated assuming the maximum value of load.

Table 1. Pull-out load and bond strength

Sample	Time [h]	Load [kN]	τ – bond strength [kN/m ²]	[N/mm ²]
CRG-A	24	129	2290	2,290
CRG-B	24	159	2810	2,810
CRG-C	24	186	3295	3,295
CRG-F	48	199	3527	3,527
CRG-G	48	203	3590	3,590
CRG-H	48	218	3857	3857

In the cases tested in the past (Zenti et al., 2012), standard AM pipes led to pull out loads equal to about 50-55% of the values reached by CRG pipes, under the same testing conditions. The reason of this result lies in the different mechanical interaction between the pipe and the grout, highlighted by the fracture pattern observed after the test (Figure 7): while in the case of standard pipe the fractured zone is localized around the pipe surface, the cylindrical block of grout appearing unaffected, with the corrugated pipe the fractures extend within the surrounding grout. The particular corrugated surface allows for the activation of a compression stress in the grout, thereby providing a pull out performance better than the one with standard pipes.

3.2. In situ pull out tests

The performance of the innovative nails is shown here with reference to field tests carried out at a tunnel face in highly weathered soft ground (Figure 8). The reinforcing element is inserted and grouted into the borehole so that its head extends from the excavation face (Figure 9). The borehole axis should be driven in a direction normal to the surface, so to apply a condition of pure traction during the pull out.

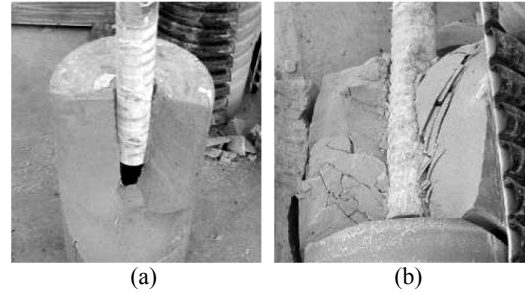


Figure 7 Fracture patterns after pull out tests: (a) standard AM and (b) corrugated CRG pipe samples

The grout is a mixture of ordinary cement, water and bentonite, in the ratio 100:60:4 by weight. The head is prepared using a threaded steel pipe, which acts as a protective case and widens the lateral surface of the nail where the load is applied, to reduce the risk of damaging.



Figure 8 Site conditions for the pull-out tests reported in Figures 9 and 10

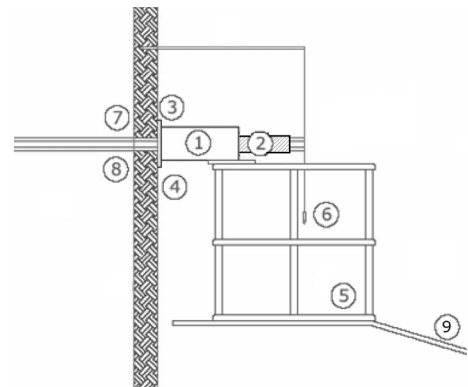


Figure 9 – In situ pull out test set up and devices: 1) hydraulic jack, 2) steel head used as a gripper, 3) stiff steel plate, 4) ball joint, 5) platform for operator, 6) plumblines, 7) reinforcing element, 8) excavation face, 9) mechanical device for platform positioning

The test takes place 24 h after injection and it follows a load controlled procedure, similar to what is prescribed for pull out tests on rock bolting (ASTM D 4435-04). Given increments of axial tensile load are applied to the nail by an electrically operated hydraulic jack and the reaction force is transferred to a stiff steel plate placed against the excavation face.

The values of pressure are controlled by an analog manometer and the displacement of the head is measured by optic differential levelling. For each load increment two measurements are made, the first at the application of the load and the second 2 min after, with constant applied load. Eventually, the nail is unloaded and, 1 min after unloading, the residual displacement is measured, to verify the occurrence of permanent sliding of the pipe along the borehole.

The results of the tests on standard GFRP pipes (AM), corrugated GFRP pipes (CRG) and innovative PERGround nails (PG) are shown in Figure 10, in terms of displacements measured 2 min after the load application.

It was observed that the tests on PERGround nails ended due to the failure of the pipes while standard GFRP pipes were pulled out without damage. PERGround nails, while undergoing minor displacements, reach a maximum load (approximately 890 kN) which corresponds to the tensile strength of the pipe. In fact, laboratory tensile tests on the same corrugated pipes, having a content of continuous longitudinal glass fibres equal to 68% by weight, resulted in a maximum tensile load equal to 900 kN.

The results confirm the better performance of corrugated pipes with respect to standard ones also in field conditions. In this case, they offered pull out loads approximately 8 times greater than those by standard pipes.

Moreover, a large additional enhancement in the nail performance is obtained with PERGround nails which result in an increase of pull out load of about 33%. This effect is likely due to the higher injection pressures, applicable during the grouting of the PERGround nail, due to the presence of the external sheath. The high pressures, up to 15 bars, induced high adherence between the nail and the soil and high pull out resistance. The external sheath confined the grout and allowed for a control of the injected volumes, even at high pressures.

Conversely, in standard soil nails the maximum allowable pressure of injection was limited (in this case up to 3 bars), to prevent soil fracturing.

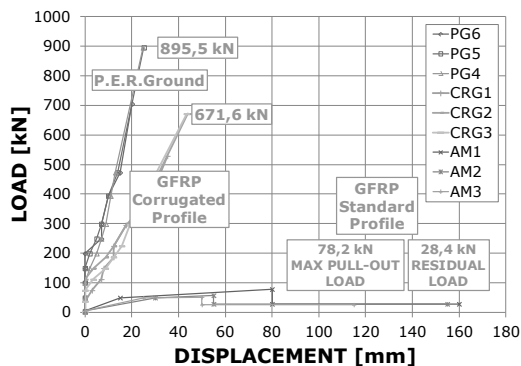


Figure 10 Results of in situ pull out tests on standard GFRP pipes (AM), corrugated GFRP pipes (CRG) and innovative PERGround nails (PG)

The observed large grout dispersion was due to the diffused weathered conditions of the ground mass. Note that also in the PERGround nails there was a loss in the fluid grout during injection, but the amount was very small and due to the water mass that seeps out from the fluid grout and soaks the geotextile sheath. An additional benefit consists in the fact that the geotextile traps the cementitious component and aids a quick setting.

The result is a highly homogeneous soil nail, characterized by high bonding properties and continuous interface adherence. These characteristics recurred in all the tested fields since the external sheath makes the final nail less affected by ground conditions (water content, soil density, presence of large voids), characteristics of the grout and quality of injection.

Nevertheless, it should be reminded that in general the nail performance and in particular the bond properties depend on the site nature and state, and that on-site testing results cannot be straightforwardly extended to other different sites. For this reason specific field testing programmes are always advisable.

4. CONCLUSION

An innovative Glass Fibre Reinforced Polymer pipe is obtained by a particular forming process that creates a corrugated external profile while avoiding, at the same time, the cutting of the glass fibres. The resulting pipe offers high bonding properties with the surrounding cement grout. Moreover, innovative systems for soft ground nailing have been described and compared with traditional ones. The new soil nailing technique provides high pull out

strength, due to the possibility to apply high injection pressures without soil fracturing and loss of grout, and to create homogeneous nails with uniform adherence. The performance of these solutions is assessed on the basis of laboratory and on-site testing.

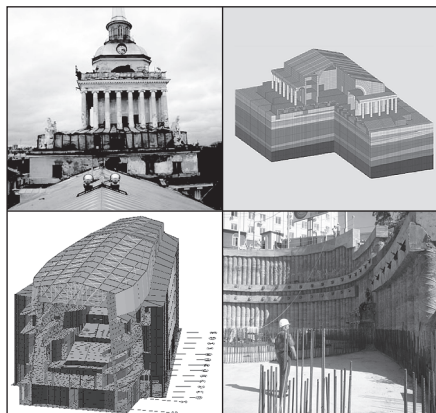
5. REFERENCES

- ACI 440.3R-12, 2012. Guide Test Methods for Fiber-Reinforced Polymer (FRP) Composites for Reinforcing or Strengthening Concrete and Masonry Structures. American Concrete Institute.
- Anagnostou, G. & Serafeimidis, K. 2007. The dimensioning of tunnel face reinforcement. *Proc. 33rd ITA AITES World Tunnel Congress WTC 2007* (Prague, Czech Republic), pp. 291–296.
- ASTM D 4435-04, 2004. Standard Test Method for Rock Bolt Anchor Pull Test. American Standard Testing Materials.
- Bobet, A. & Einstein, H.H. 2011. Tunnel reinforcement with rockbolts. *Tunnelling Underground Space Techn.*, Vol. 26, No. 1, pp. 100–123.
- Cheng, Y.M., Choi, Y., Yeung, A.T., Tham, L.G., Au, A.S.K., Wei, W.B. & Chen, J. 2009. New soil nail material – Pilot study of grouted GFRP pipe nails in Korea and Hong Kong. *J. Materials in Civil Engng.*, Vol. 21, No. 3, pp. 93–102.
- Chu, L.M. & Yin, J.H. 2005. Comparison of interface shear strength of soil nails measured by both direct shear box tests and pullout tests. *J. Geotech. Geoenv. Engng.*, Vol. 131, No.9, pp.1097–1107.
- Goldsworthy, W.B. 1971. US Patent 3556888 Pultrusion machine and method.
- Grasso, P., Mahtab, A., Pelizza, S. 1989. Reinforcing a rock zone for stabilizing a tunnel in complex formations. *Proc. Int. Congr. Progress and innovation in tunnelling*, Toronto, Vol. 2, pp.671–678.
- Juran, I. & Elias, V. 1991. Ground anchors and soil nails in retaining structures. In: *Foundation Engineering Handbook*, 2nd Edition (ed. H.Y. Fang), 868–905.
- Kim, J.-S., Lee, I.-M., Jang, J.-H. & Choi, H., 2009. Groutability of cement-based grout with consideration of viscosity and filtration phenomenon. *Int. J. Numer. Anal. Meth. Geomech.*, Vol. 33, pp. 1771–1797.
- Lunardi, P., 2008. *Design and construction of tunnels, analysis of controlled deformations in rock and soils (ADECO-RS)*, Springer.
- Mair, R.J. 2008. Tunnelling and geotechnics: new horizons. *Géotechnique*, Vol. 58, pp. 695–736.
- Mair, R.J. & Taylor, R.N. 1997. Bored tunnelling in the urban environment. *Proc. 14th Int. Conf. Soil Mech. Found. Engng.*, Vol. 4, pp. 2353–2385.
- Ng, C.W.W. & Lee, G.T.K. 2002. A three-dimensional parametric study of the use of soil nails for stabilising tunnel faces. *Computers and Geotechnics*, Vol.29, pp.673–697.
- Oreste, P.P. & Dias, D. 2012. Stabilisation of the excavation face in shallow tunnels using fibre-glass dowels. *Rock Mech. Rock Engng.*, Vol. 45, No. 4, pp. 499–517.
- Ortigao, J.A.R. 1996. FRP applications in geotechnical engineering. *Proc. ASCE 4th Materials Engineering Conference*, Washington DC, Vol.1, pp.535–544.
- Osgoui, R.R. & Oreste, P. 2007. Convergence-control approach for rock tunnels reinforced by grouted bolts, using the homogenization concept. *Geotech. Geol. Engng.*, Vol. 25, No. 4, 431–440.
- Renda, D., Grasso, P., Rizzo, F., Pinchiaroglio, L., Eusebio, A., Pescara, M., Osgoui, R., Bondanelli, L., Ballabeni, F., Aguglia, F., Zenti, C.L. & Sterpi, D. 2012. Improvement in soft ground tunnelling using an innovative technique. *Proc. Int. Symp. Advances in Ground Technology and Geo-Information – IS-AGTG*, Singapore: Research Publishing, pp.197–205.
- Schlosser, F. 1982. Behaviour and design of soil nailing. *Proc. Int. Symp. Recent Development in Ground Improvement Techn.*, pp. 399–413.
- Sterpi D., Rizzo F., Renda D., Aguglia F. & Zenti C.L. 2013. Soil nailing at the tunnel face in difficult conditions: A case study. *Tunnelling Underground Space Techn.*, Vol. 38, pp.129–139.
- Wong, H., Trompille, V., Subrin, D. & Guilloux, A. 1999. Tunnel face reinforced by longitudinal bolts: analytical model and in situ data. *Geotechnical Aspects of Underground Construction in Soft Ground*. Balkema: Rotterdam, pp. 457–462.
- Wong, H., Subrin, D. & Dias, D. 2000. Extrusion movements of a tunnel head reinforced by finite length bolts – a closed-form solution using homogenization approach. *Int. J. Numer. Anal. Meth. Geomech.*, Vol. 24, pp. 533–565.
- Zenti, C.L. 2006. *Laboratory and Field Investigation on the Behaviour of Swelling Grouts for Underground Excavation*, Ph.D. Thesis, Politecnico di Milano, Italy.
- Zenti, C.L., Sterpi, D. & Bonomi, C. 2008. Laboratory and field investigation on improved soil nails. *Proc. World Tunnel Congress WTC 2008*, Agra, India, Vol.1, pp.263–271.
- Zenti, C.L., Cassani, G. & Sterpi, D. 2012. Technical solutions for soil nails in tunnel face reinforcement and drainage. *Proc. World Tunnel Congress WTC 2012*, Bangkok, Thailand, Vol. 2 CD-ROM.



THE INSTITUTE GEORECONSTRUCTION

*architectural and structural design,
geotechnical engineering,
complex reconstruction, investigations*



The Institute "Georeconstruction" was set up 20 years ago by leading St. Petersburg geotechnical engineers and designers. Since its very foundation the Institute has been maintaining and enriching traditions and intellectual capacity of St. Petersburg school of structural design.

"Georeconstruction" has completed renaissance of the best traditions of research design institutes at a new level of construction science development. Uniting scientific research in the field of geotechnical engineering, calculations and design practice constitutes the basis of the competitive advantage of the company. Participation in large-scale international projects promotes exchange of experience of the Institute and leading national and foreign geotechnical and design companies.

Geotechnical evaluation of projects and validation of design

- Evaluation of sites' investment potential
- Site investigation
- Geotechnical calculations, design solutions
- Choice of a safe technology of works implementation
- Geotechnical calculation of construction or reconstruction impact on the adjacent buildings, underground space and underground mains
- Preparation of geotechnical validation of design documents

Geotechnical monitoring

- Development of method statements and geotechnical schedules for special works
- Adjustment of sparing technology regimes
- Deformation monitoring
- Condition monitoring of existing buildings
- Ground water level monitoring
- Vibration and acceleration monitoring in soils and structures
- Quality assessment of completed projects

Condition surveying

- Construction sites and real estate
- Historic buildings and structures

Works in congested urban environment

- Surveying
- Site investigation
- Geophysical works
- Environmental
- Geotechnical

Civil and industrial design

- Architectural design
- Construction design and engineering
- Complex development of investment validation, design and working drawings
- Design of engineering restoration of historic buildings
- Designs for construction, reconstruction and strengthening of underground structures in complicated geological conditions
- Design of dewatering and waterproofing
- Foundations for machines with dynamic loads
- Cost and technology optimization of designs
- Expert assessment of designs, design solutions

Special works

- Function of the General Designer
- Function of the Client's Engineer
- Theoretical and practical construction supervision
- Design of building and structures in frozen soils

190005, Russia, St. Petersburg
Izmaylovskiy prospekt 4
Tel./Fax: +7 (812) 316-6118, 575-3587, 251-7098
e-mail: mail@georec.spb.ru
<http://www.georec.spb.ru>

GEOIZOL Group is a leading Russian company in design, restoration and construction of underground structures.

GEOIZOL group started in 1995 as a small construction company Geoizol, initially specializing in waterproofing. In its 18 year history Geoizol has grown into a multi sector holding, consisting of the companies that work in design and underground construction, an engineering company and a machine-building plant.

GEOIZOL participates in investment and governmental projects as the General Designer, the General Contractor and a Subcontractor. The companies of GEOIZOL Group employ about 2000 people.

The head office of the company is situated in St. Petersburg. Its branches – separate subdivisions Sochi and Amurskoye – was engaged in the building projects for winter Olympic Games 2014 in the area of Krasnaya Polyana and in construction of major hydropower stations in Siberia and the Far East of Russia.

OOO GEOIZOL has executed works all over the Russian Federation from Franz-Joseph Land to the Far East, and in CIS countries, such as Tajikistan and Turkmenistan.

The company has mastered the full range of geotechnical engineering processes and gained a unique experience in construction of all types of foundations, transport construction, hydraulic engineering, expert surveying and instrumental diagnosing of structures.

OOO GEOIZOL works in the spheres of:

- Underground construction;
- Bored piling and ground anchors installation;
- Road and bridge construction;
- Construction of watertight diaphragms in rocks and incoherent soils;
- Grouting/injection methods of soil improvement, foundation and brick layer strengthening;
- Waterproofing and repair of structures (sealing and waterproofing of construction and deformation joints);
- Buildings and structures surveying and monitoring.
- Building reconstruction and restoration;
- Soil stabilization;
- Landslide and mountain slopes reinforcement with soil nails;

An important advantage of OOO GEOIZOL over the competitors is a complex approach, innovations and high quality of works. That is why major Russian and international companies have become clients and partners of OOO GEOIZOL.

OOO GEOIZOL is a member of:

- International Society of Soil Mechanics and Geotechnical Engineering
- Russian Society for Soil Mechanics, Geotechnical Engineering and Foundation Construction
- Russian Association of Restorers “Rosregionrestavratsia”
- Research society «St. Petersburg Builders Association»
- Research society «St. Petersburg Designers Association»
- Research society «St. Petersburg Surveyors Association»
- Association of St. Petersburg Road and Bridge Construction Companies “Dormost”



Geographical Distribution
of Activity

Almost each project of the company is unique. Especially challenging ones required the usage of the state-of-the-art technologies, some of which were developed and successfully applied by OOO GEOIZOL specialists::

- Diaphragm wall is a technique of construction of retaining structures for deep excavations. Vertical concrete walls are constructed under the protection of bentonite solution. This technique is effective for reconstruction of historic buildings and structures, in congested urban areas and in the proximity of utility mains;
- Semi top-down and top-down methods enable substructure and its subbasement to be built simultaneously, which allows to decrease both time and cost of the construction;
- Jet-grouting technology enables to create a secure layer of strengthened soil. Together with a retaining structure (diaphragm wall, sheet piling wall) it allows to avoid development of excessive deformations in walls of the adjacent buildings;
- Foundation underpinning using root and secant piles, including repiling of a building to the in-house root (groutinjected) piles Geoizol-MP;
- Foundation construction with Atlas piles of various diameter (screw piles with corrugated shaft) which allow to work under various soil conditions;
- Construction of Fundex bored piles of various diameters with sacrificed boot without soil extraction. Pile foundations made using this technology have a big bearing capacity. Another advantages of this technology are a possibility to use it in various soil conditions and absence of vibration in soil and structures;
- CFA technology. This method requires rebar cages to be placed into a borehole filled with concrete. The CFA technology is preferable when geological profile shows the presence of layers of hard soil;
- Bored pile construction with full length casing, the diameter of ready piles being 620–2000 mm. The advantages of this technology are the minimal impact on the neighbouring foundations, the possibility to build these piles in varying ground conditions, as well as the high bearing capacity of the constructed piles;
- Pile boring with clay drilling mud allows to carry out works in congested areas, in adjacency to the existing buildings. Drilling mud helps to further reduce negative impact on the foundations of the neighbouring buildings;
- Double Drilling System is based on the principle of soil compaction during boring. Specific design of the drilling rig enables to cut through the layers of hard soil.

The rig fleet of the company includes the equipment of the leading manufactures: Fundex, Casagrande, Hutte, Atlas (Franki), Liebherr, Enteco, Morath, Doosan, Hitachi, Kobelco, Menzi Muck, Hanix, Cubota, Mustang, Oberman, APE, Atlas Copco, Hany, Ravestein, Movax, Ingersoll Rand, Kaiser.

OOO GEOIZOL takes great pride in the works that have been done at the historical sites of St. Petersburg listed as the architectural landmarks of the city: underpinning of the foundations in the New Holland complex; reconstruction and underpinning of the foundations of the Bolshoy Menshikov Palace in Oranienbaum; The Alexander Palace in Tsarskoe Selo (Pushkin); The Alexandrinsky and Kamenny Ostrov Theatres; The General Staff Building of the State Hermitage; The Grand Ducal Burial Vault in Peter and Paul Fortress. OOO GEOIZOL has carried out the works that were unique for St. Petersburg: construction of the five-level underground parking on Komendantskaya Square; the three -level underground parkings in the historic centre of the city at 2–4, Zoologicheskoy Lane and at 74, Moika River Embankment. The company has participated in the large hydrotechnical projects: Zeiskaya hydroplant, Bureiskaya hydroplant, Viluiskaya hydroplant, Ust-Ilimskaya hydroplant, Krivopozhskaya hydroplant, Irganskaya hydroplant, Sangtudinskaya hydroplant..

Thanks to the high degree of professionalism and skills of the engineers and technical personnel, the company is able to meet various challenges, regardless of difficult environmental, climatic or geological conditions, both in new development and within the boundaries of protected historical sites.



“DIAPHRAGM WALL”

Consisting of cased secant piles 630 mm,
820 mm, with depth up to 21,5 m.
using DOUBLE ROTARY technology



Site: Collector drain “Center”, well No.14 (Timiryazeva Street, Minsk)

Cased secant piles with diameter 820mm, depth 20m in
saturated soils. Excavation of foundation pit was
carried out without dewatering.

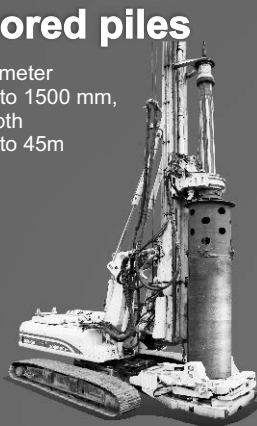


Drilling Company Delta OJSC
+7 (967) 282-7079
+7 (499) 343 81 57
+375 29 653-1976
e-mail: delta_bur@rambler.ru



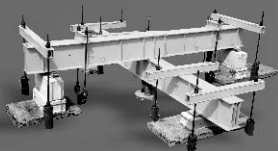
Bored piles

diameter
up to 1500 mm,
depth
up to 45m



Pile testing

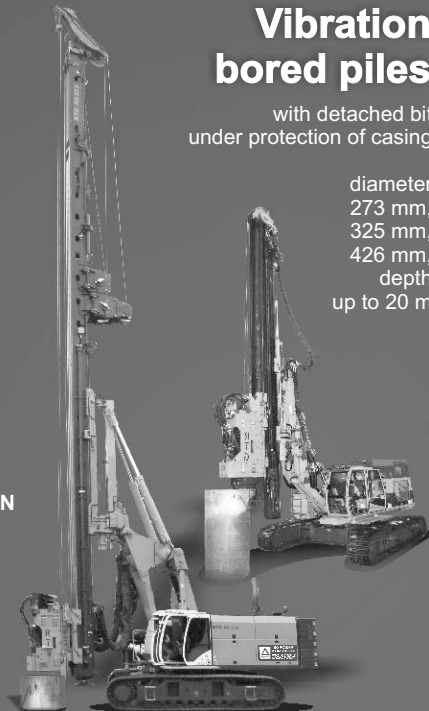
with load capacity up to 10 000 kN



Vibration bored piles

with detached bit
under protection of casing

diameter
273 mm,
325 mm,
426 mm,
depth
up to 20 m



JetGrouting



Injection anchors



Jet Grouting technology involves using high-pressure jet of cement slurry for simultaneous ground failure and mixing with cement slurry.

CFA



Construction technology of bored piles using continuous flight auger with pressurized feeding of concrete

diameter from 450 mm
up to 1000 mm,
depth up to 22 m

Double Rotary



Construction technology of bored piles using continuous flight auger and casing with simultaneous rotation in opposite directions

diameter from 630 mm, 830 mm,
depth up to 21.5 m

DDS



Construction technology of bored piles using soil rolling method (high liquid limit and fill-up soils) with pressurized feeding of concrete

diameter 400 mm, 600 mm,
depth up to 21.5 m

KARST LLC

Office 69-N, 4, letter A, Kapitanskaya st.,
St. Petersburg, 199397
tel.: +7 (812) 327 7283
fax: +7 (812) 327 7310
e-mail: office@oldcity.spb.ru
www.oldcitykarst.ru

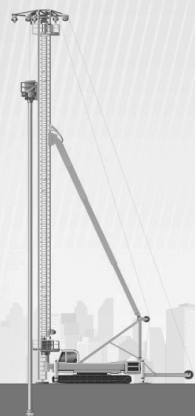
The KARST LLC Construction Company is a specialized organization, which has had a presence on the construction market for more than 20 years and performs a range of complicated geotechnical work.

The main types of work performed by the company are as follows:

- /// Design and construction of underground parking lots under challenging geotechnical conditions
- /// Arrangement of piled foundations for buildings and structures according to state-of-the-art technologies
- /// Reinforcement of building foundations (including listed buildings) by injections of cement mortar and underpinning piles
- /// Submersion of heavy steel sheet piles (including arrangement of combined walls from elements of HZ/AZ type or pipe sheet pile) and large diameter steel shells
- /// General contract for a range of zero cycle civil works (piled foundation; enclosure made from sheet piles; earth works; arrangement of monolithic reinforced concrete structures)

The company owns a large up-to-date equipment fleet required to perform above works.

KARST LLC, jointly with the Gersevanov Institute of Basements and Underground Constructions, the Kucherenko Central Research Institute of Construction and Institute of Transport Construction with the Central Scientific Research Institute of Construction, developed and implemented the corporate standard (STO 48937526-003-2013), for the design and construction of underground enclosing and load-bearing structures from steel sheet piles.



Advantages of using steel sheet piles as permanent enclosing and bearing structures in construction of underground facilities:

- /// Reduction of zero cycle works cost to 40%
- /// Reduction of construction timing to 70%
- /// Reliable hydraulic insulation of underground areas
- /// High reliability, strength and quality of steel underground structures
- /// Optimal use of land in urban development
- /// Reduced environmental impact of construction
- /// Extensive record of usage in global construction practices under urban development conditions

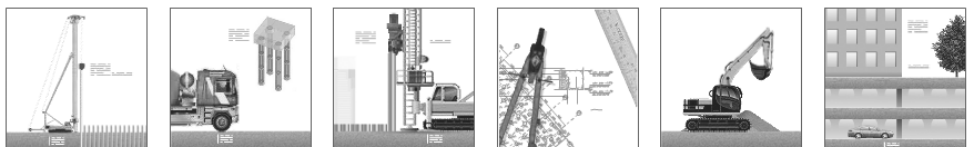
A pit may be excavated using an open method, through the installation of temporary reinforcing metal structures, or in accordance with the Top-Down method, when slabs of underground levels are arranged in a top-down pattern and serve as a bracing system for a sheet pile wall.

A wall made from steel sheet piles may serve as an external wall for underground levels of buildings or simultaneously support some loads from underground structures, serving as a part of foundation with a developed side surface.

The sheet pile wall is coupled with other structural parts of structures with the help of assemblies made with electric-arc welding; furthermore, it is possible to apply prefabricated reinforced concrete structures to support the installation of underground floor decks.

The surface of the sheet pile wall cleared of soil and then coated with a fireproof material and painted for aesthetic purposes, if required.

New effective technology for the construction of underground parking lots and structures involving the application of steel sheet piles proposed by KARST LLC provides new opportunities in the development of underground space in large cities and facilitates the implementation of the most complicated projects.



PROCEEDINGS OF THE
ISSMGE TECHNICAL COMMITTEE 207
INTERNATIONAL CONFERENCE
ON GEOTECHNICAL ENGINEERING

SOIL-STRUCTURE INTERACTION,
UNDERGROUND STRUCTURES
AND RETAINING WALLS

Volume 1

Editors – V.M. Ulitsky, M.B. Lisyuk and A.G. Shashkin
Prepress preparation for PrintHouse – E.V. Dubinin

Format 72×52/16. Offset printing. Offset paper.
Conventionally printed sheets: 12,4.
Physically printed sheets: 18. Circulation: 200.

“Georeconstruction” Institute
190005, 4 Izmaylovsky prosp., St. Petersburg, Russia
Tel./Fax: +7 (812) 316-6118, 575-3587, 251-7098
www.georec.spb.ru

Printed in “MST”
199178, 57 10-th Line of V.O., St. Petersburg, Russia
Tel./Fax: +7 (812) 325-2536, 325-2537
www.mst.spb.ru